LBL-31853
CONF-9108191 — —
UC-411

Spectroscopic Imaging, Diffraction, and Holography with X-Ray Photoemission

Report of the Workshop
at
Lawrence Berkeley Laboratory
August 14, 1991

Organized by:

C.S. Fadley, Lawrence Berkeley Laboratory and University of California at Davis
A.S. Schlachter, Lawrence Berkeley Laboratory
B. Tonner, University of Wisconsin–Milwaukee
M. Van Hove, Lawrence Berkeley Laboratory

Lawrence Berkeley Laboratory
University of California
Berkeley, California 94720

February 1992

Prepared for the U.S. Department of Energy under Contract No. DE-AC03-76SF00098

DISCLAIMER

Spectroscopic Imaging, Diffraction, and Holography with X-Ray Photoemission

Report of the Workshop

LBL--31853

DE92 009142

at

Lawrence Berkeley Laboratory

August 14, 1991

Organized by:

C.S. Fadley, Lawrence Berkeley Laboratory and University of California at Davis
A.S. Schlachter, Lawrence Berkeley Laboratory
B. Tonner, University of Wisconsin–Milwaukee
M. Van Hove, Lawrence Berkeley Laboratory

Lawrence Berkeley Laboratory
University of California
Berkeley, California 94720

This work was supported by the Director, Office of Energy Research, Office of Basic Energy Sciences, Materials Sciences Division, of the U.S. Department of Energy under Contract No. DE-AC03-76SF00098

Contents

Spectroscopic Imaging, Diffraction, and Holography with X-Ray Photoemission

Wednesday
August 14, 1991
at
Lawrence Berkeley Laboratory

⇨ The day before the ALS Annual Users' Association Meeting (August 15–16) ⇦

X-ray probes are capable of determining the spatial structure of an atom in a specific chemical state, over length scales from about a micron all the way down to atomic resolution. Examples of these probes include photoemission microscopy, energy-dependent photoemission diffraction, photoelectron holography, and X-ray absorption microspectroscopy. Although the method of image formation, chemical-state sensitivity, and length scales can be very different, these X-ray techniques share a common goal of combining a capability for structure determination with chemical-state specificity. This workshop will address recent advances in holographic, diffraction, and direct imaging techniques using X-ray photoemission on both theoretical and experimental fronts. A particular emphasis will be on novel structure determinations with atomic resolution using photoelectrons.

Organizers

Brian Tonner, U. of Wisconsin/Milwaukee
Chuck Fadley, LBL
Fred Schlachter, LBL
Michael Van Hove, LBL

For Additional Information

Brian Tonner
Department of Physics
University of Wisconsin
1900 E. Kenwood Blvd.
Milwaukee, WI 53211

Tel: (414) 229-4626
Fax: (414) 229-5589
E-Mail: TONNER@CSD4.MILW.WISC.EDU

Fred Schlachter
Advanced Light Source
MS 46-161
Lawrence Berkeley Laboratory
University of California
Berkeley, CA 94720

Tel: (415) 486-4892
Fax: (415) 486-4873
E-Mail: FRED@LBL

Spectroscopic Imaging, Diffraction, and Holography with X-Ray Photoemission

August 14, 1991
Lawrence Berkeley Laboratory
Building 66 Auditorium

-- Workshop Agenda --

Tuesday Evening, August 13:

5:00 - 7:00 P.M.	Registration	Shattuck Hotel Lobby

Wednesday, August 14:

7:45 A.M.	LBL Shuttle Bus Service	Shattuck Hotel to LBL, Bldg. 66 Auditorium
8:00	Registration Continues	Coffee in Auditorium Lobby Area

Introduction
Chair: Louis Terminello (LLNL)

8:30	Introduction to the ALS	A. S. Schlachter ALS–LBL
8:45	Spectromicroscopy and Holography in Materials Science	B. Tonner SRC
9:15	Concepts in Soft X-ray Holography	A. Szoke LLNL
9:40	BREAK	Coffee in Auditorium Lobby Area

Photoelectron Holography

10:00	From Photoelectron Diffraction to Surface Crystallography	J. J. Barton IBM T. J. Watson Research Center
10:40	Atomic-Resolution Photoelectron Holographic Crystallography	D. Saldin Univ. of Wisconsin–Milwaukee
11:20	Prospects for Advanced Photoelectron Diffraction	C. S. Fadley Univ. of California–Davis & LBL
12:00 Noon	LUNCH	LBL Shuttle Bus Service to LBL Cafeteria

-- Workshop Agenda, cont. --

Advances in Photoelectron Diffraction Theory and Experiment

Chair: Piero Pianetta (SSRL)

1:30 P.M.	Theoretical Developments in Photoelectron Diffraction	M. Van Hove LBL
1:50	Efficient Multiple-Scattering Methods in Photoelectron Diffraction	J. Rehr Univ. of Washington
2:20	Lattice-Site and Chemical-State Specific Photoelectron Diffraction	S. Chambers Boeing High Technology Center
3:00	Photoelectron Diffraction of Magnetic Ultrathin Films	J. Tobin LLNL
3:30	BREAK	

Photoemission Microscopy

4:00	Direct Imaging Photoemission Microscopy: Past, Present, and Future	E. Bauer Univ. Clausthal
4:45	High-Resolution Scanning Photoemission Microscopy	H. Ade SUNY-Stony Brook
5:30	ADJOURN	LBL Shuttle Bus Service to Shattuck Hotel
6:00–8:00	ALS Users' Association Meeting Reception	Shattuck Hotel

ADVANCED LIGHT SOURCE
USERS' ASSOCIATION ANNUAL MEETING
AUGUST 15-16, 1991*

Harald W. Ade
State University of New York
Physics Department
Stony Brook, NY 11794

Philipp A. Aebi
McMaster Univ.
IMR, 1280 Main St. West
Hamilton Ont L8S 4MI

Paul Alivisatos
UC Berkeley
Department of Chemistry
Berkeley CA 94720

David Attwood
Center for X-Ray Optics/LBL
2-400
Berkeley CA 94720

Yoshiro Azuma
Argonne National Lab.
9700 S. Cass Ave
Argonne IL 60439

Susan Barr
Argonne National Laboratory
9700 S. Cass Ave.
Argonne IL 60439

John J. Barton
IBM T.J. Watson
P.O. Box 218
Yorktown NY 10598

Ernst Bauer
Physikalische Inst. der TU Clausthal
Leibnizstrasse 4
3392 Clausthal-Zellerf., Germany

H. Raul Beguiristain
Lawrence Berkeley Laboratory
1 Cyclotron Rd. MS 2-400
Berkeley CA 94720

Jeffrey Bokor
AT&T Bell Labs
600 Mountain Ave., Rm.6E-306
Murray Hill NJ 07974

Richard R. Bott
Genecor International
180 Kimball Way
So. San CA 94080

Robert J. Burke
Rocketdyne Div. of Rockwell Int'l
6633 Canoga Ave. M/S FA60
Canoga Park CA 91301

C. Denise Caldwell
University of Central Florida
Department of Physics
Orlando FL 32816

T.A Callcott
Univ. of Tennessee
Knoxville TN 97996

Cristiano Capasso
Univ. of Wisconsin- Madison
CXRL
3731 Schneider Dr.
Stoughton WI 53589

Ronald G. Cavell
Univ. of Alberta
Dept. of Chemistry
Edmonton, CA T6G 2G2

Franco Cerrina
Center for X-ray Lithography
3731 Schneider Drive
Stoughton WI 53589

Scott A. Chambers
Boeing High Technology Center
P. O. Box 3999 MS 7J-98
Seattle, WA 98124-2499

Jie Chen
Lawrence Berkeley Laboratory
UC Davis
228 Walker Hall
Davis CA 95616

Jason H. Christiansen
UC Davis/ Applied Science
Walker Hall
Davis CA 95616

Carl W. Cork
Lawrence Berkeley Laboratory
MS 2-400
Berkeley CA 94720

* Because this workshop was held in conjunction with the ALS Users' Association Annual Meeting, a separate list of workshop participants was not prepared; however, all participants' names and addresses can be found on this list.

Bernd Crasemann
University of Oregon
Department of Physics
Eugene, OR 97403-1274

Glen Dahlbacka
Brobeck Div./Maxwell Labs. Inc.
4905 Central Ave.
Richmond CA 94804

Judy L. Dauberman
Genecor International
180 Kimball Way
So San CA 94122

David C. Eder
Lawrence Livermore Nat'l Laboratory
P.O. Box 5508 L-477
Livermore CA 94550

David L. Ederer
Natl. Inst. of Standards &Technology
A253 Physics
Gaithersburg MD 20899

Charles S. Fadley
Lawrence Berkeley Laboratory
1 Cyclotron Rd. MS 2-100
Berkeley CA 94720

Birgit Fortyr
Interatom GmbH
5060 Bergisch Gladbach 1
Friedrich-Ebert GER

Alfonso Franciosi
Univ. of Minnesota
421 Washington Ave. SE
Minneapolis MN 55455

Chalmers Frazer
14 Cherbourg Ct.
Potomac MD 20854

Leonard M. Goldman
Bechtel Corporation
P. O. Box 193965
50 Beale Street
San Francisco, CA 94119-3965

Eric D. Greene
Lawrence Berkeley Laboratory
ALS Exp. Sys. Group
1 Cyclotron Rd. MS 2-400
Berkeley CA 94720

David-Paul Gregg
Eclectic Associates
3650 Helms Avenue
Culver City CA 90232-2417

Klaus Halbach
Lawrence Berkeley Laboratory
1 Cyclotron Road
Berkeley, CA 94720

Bill Hammer
Grumman

David M. Hanson
State University of New York
Department of Chemistry
Stony Brook NY 11794-3400

William V. Hassenzahl
Lawrence Berkeley Laboratory
1 Cyclotron Rd. MS 46-161
Berkeley CA 94720

Cheryl A. Hauck
Lawrence Berkeley Laboratory
1 Cyclotron Rd. MS 16-108
Berkeley CA 94720

Philip A. Heimann
Lawrence Berkeley Laboratory
1 Cyclotron Rd. MS 2-400
Berkeley CA 94720

John Hepburn
Univ. of Waterloo
Dept. of Chemistry
Waterloo, CA N2L 3G1

R. Hewitt
Brookhaven National Labs
Exxon PRT Bldg. 510E
Upton NY 11973

R. C. Hewitt
Brookhaven National Labs
Exxon PRT Bldg. 510E
Upton N.Y. 11973

Kazuyuki Higashiyama
Lawrence Berkeley Laboratory
1 Cyclotron Rd. MS 2-100
Berkeley CA 94720

F. Himsel
IBM Research
218
Yorktown NY 10598

Adrian Ho
Adelphi Technology
285 Hamilton Ave. Ste. 430
Palo Alto CA 94301

Malcolm Howells
Lawrence Berkeley Laboratory
2-400
Berkeley CA 94720

Zdenek D. Hurych
Northern Illinois University
Department of Physics
Dekalb IL 60115

Zahid Hussain
Lawrence Berkeley Laboratory
1 Cyclotron Rd.
Berkeley CA 94720

Lou Iannielio
U.S. Dept. of Energy
Washington DC

Yves Idzerda
Naval Research Laboratory

Yves Idzerda
Naval Research Lab.
Code 6345
Washington DC 20375

Lorretta Inglehart
National Science Foundation
1800 G Street, N.W.
Washington DC 20550

Steven C. Irick
Lawrence Berkeley Laboratory
Exp. Systems Group
1 Cyclotron Rd. MS 2-400
Berkeley CA 94720

Alan Jackson
Lawrence Berkeley Laboratory
ALS Group
1 Cyclotron Rd. MS 47-112
Berkeley CA 94720

Chris J. Jacobsen
State University of New York
Physics Department
Stony Brook, NY 11794

Ken Johnson
Lawrence Berkeley Laboratory
2-400
1 Cyclotron Rd.
Berkeley CA 94720

Paul Johnson
Lawrence Berkeley Laboratory
MS 80-101
1 Cyclotron Rd
Berkeley CA 94720

Ajith Kaduwela
Lawrence Berkeley Laboratory
1 Cyclotron Rd. MS-2-100
Berkeley CA 94720

Henry C. Kapteyn
Washington State Univ.
Dept. of Physics
Pullman WA 99164-2814

Roderich Keller
Lawrence Berkeley Laboratory
1 Cyclotron Rd. MS 80-101
Berkeley CA 94720

Kwang-Je Kim
Lawrence Berkeley Laboratory
1 Cyclotron Road MS 71-259
Berkeley, CA 94720

Yong Joo Kim
Lawrence Berkeley Laboratory/MS
2-100
1 Cyclotron Rd
Berkeley CA 94720

Brian Kincaid
Lawrence Berkeley Laboratory
I Cyclotron Rd. MS 46-161
Berkeley CA 94720

Melvin Klein
Lawrence Berkeley Laboratory
Chemical Biodynamics
1 Cyclotron Rd.
Berkeley CA 94720

Joseph H. Klems
Lawrence Berkeley Laboratory
1 Cyclotron Rd. MS 90-3111
Berkeley CA 94720

Christine T. Ko
Lawrence Berkeley Laboratory
1 Cyclotron Rd. MS 2-400
Berkeley CA 94720

Masato Koike
Center for X-Ray Optics/LBL
2-400
Berkeley CA 94720

Jeffrey Kortright
Center for X-Ray Optics/LBL
2-400
Berkeley CA 94720

Manfred O. Krause
Oak Ridge National Laboratory
P.O. Box 2008, Bldg. 4500N
Oak Ridge TN 37831-6201

Glenn Kubiak
Sandia National Labs
Div. 8342
Livermore... CA 94551-0969

Henry D. Lancaster
Lawrence Berkeley Laboratory
1 Cyclotron Rd. MS 46-125
Berkeley CA 94720

Gerald Lapeyre
Montana State Univ.
Bozeman MT 59717

Thomas K. Lebrun
LURE
Centre Université de Paris-Sud,
Orsay FRA 91405 CEDEX

Patrick Len
UC Davis
Physics Dept.
Davis CA 95616

Dennis W. Lindle
NIST & UNLV
Physics A141
Gaithersburg MD 20899

Richard A. London
Lawrence Livermore Nat'l Laboratory
P.O.Box 5508 L-477
Livermore CA 94550

David L.J. Lunt
Tuscon Optical Research Corp.
210 S. Plumer
Tuscon AZ 85719

Nora B. Mansour
Argonne Nat'l Lab.
9700 South Cass Ave.
Argonne IL 60439

Steve J. Marks
Lawrence Berkeley Laboratory
1 Cyclotron Rd. MS 46-161
Berkeley CA 94720

Jay N Marx
Lawrence Berkeley Laboratory
1 Cyclotron Rd MS 46-161
Berkeley CA 94720

Dexter Massoletti
Lawrence Berkeley Laboratory
1 Cyclotron Rd. MS 46-161
Berkeley CA 94720

Wayne R. McKinney
Lawrence Berkeley Laboratory
1 Cyclotron Rd. MS 2-400
Berkeley CA 94720

Miklos E. Melczer
Lawrence Berkeley Laboratory
MS 2-400
Berkeley CA 94720

Robert H. Mellott
Knight Architects Engineers Planners
549 West Randolph Street
Chicago IL 60661

Jeffrey Moore
Lawrence Berkeley Laboratory
2-400
Berkeley CA 94720

Margaret M. Murname
Washington State Univ.
Dept. of Physics
Pullman WA 99164-2814

Art J. Nelson
Solar Energy Research Inst.
1617 Cole Blvd.
Golden CO 80401

Khanh B. Nguyen
Lawrence Berkeley Laboratory
1 Cyclotron Rd. MS 2-400
Berkeley CA 94720

David W. Niles
Solar Energy Research Inst.
1617 Cole Blvd.
Golden CO 80401

William T. Oosterhuis
U.S. Dept. of Energy
Div. Materials Sciences ER-132 GTN
Washington DC 20585

William Orme-Johnson
Massachusetts Inst. of Technology
48 Mass Ave.
Cambridge MA 02139

Douglas A. Ortendahl
UC San Francisco
Radiologic Imaging Laboratory
400 Grandview Drive
So. San CA 94080

Alex Ozeroff
Lawrence Berkeley Laboratory
1 Cyclotron Rd. MS 46-161
Berkeley CA 94720

David R. Penn
Nat'l Inst. of Standards & Tech.
Gaithersburg MD 20899

Rupert C. Perera
Lawrence Berkeley Laboratory
1 Cyclotron Rd. MS 2-400
Berkeley CA 94720

Dale L. Perry
Lawrence Berkeley Laboratory
1 Cyclotron Rd. MS 70A-1150
Berkeley CA 94720

M. Novella Piancastelli
II University of Rome "Torvergata"
Dept. of Chemical Sciences & Tech.
Rome Ital 00173

Piero Pianetta
SSRL/Stanford Univ.
Stanford CA 94309

Paul W. Plag
Ovonic Synthetic Materials Co.
1788 Northwood
Troy MI 48084

P. Venugopala Rao
Emory Univ.
Department of Physics
Rollins Research Center
Atlanta GA 30322

John Rehr
Univ. of Washington
Dept of Physics
FM-15
Seattle WA 98195

Arthur L. Robinson
Lawrence Berkeley Laboratory
1 Cyclotron Rd. MS 80-101
Berkeley CA 94720

Philip N. Ross
Lawrence Berkeley Laboratory
1 Cyclotron Rd. MS 2- 100
Berkeley CA 94720

Carolyn S. Rossington
Lawrence Berkeley Laboratory
1 Cyclotron Rd. MS 70A-3363
Berkeley CA 94720

Stephen Rothman
LBL/Research Medicine
2-400
Berkeley CA 94720

Michael Rowen
4349 Bin 99
Stanford CA 94309

Richard Sah
Brobeck Division
4905 Central Ave.
Richmond CA 94804

Dilano K. Saldin
University of Wisconsin, Milwaukee
Department of Physics
P. O. Box 413
1900 E. Kenwood Blvd.
Milwaukee, WI 53211

Mahesh G. Samant
IBM Almaden Research Center
650 Harry Road
San Jose CA 95120

Roland Savoy
Argonne National Lab
APS/362
9700 S. Cass Ave.
Argonne IL 60532

Fred Schlachter
Lawrence Berkeley Laboratory
1 Cyclotron Rd. MS 46-161
Berkeley CA 94720

Ross O. Schlueter
Lawrence Berkeley Laboratory
1 Cyclotron Rd. MS 2-400
Berkeley, CA 94720

Frank Selph
Lawrence Berkeley Laboratory
MS 80-101
1 Cyclotron Rd.
Berkeley CA 94720

David Shirley
Lawrence Berkeley Laboratory
1 Cyclotron Road
Berkeley CA 94720

Neville Smith
AT&T Bell Labs
Murray Hill NJ 07974

Donald K. Stevens
U.S. Dept. of Energy
9709 W. Bexhill Dr.
Kensington MD 20895

Joachim Stohr
IBM Almaden
650 Harry Rd.
San Jose CA 95120

Elaine W. Streets
Argonne Nat'l Lab.
9700 South Cass Ave.
Argonne IL 60439

Abraham Szoke
Lawrence Livermore National Lab
Livermore CA 94550

Ron Tackaberry
Center for X-Ray Optics/LBL
2-400
Berkeley CA 94720

Louis Terminello
Lawrence Livermore Nat. Lab.
L-268
808
Livermore CA 94550

Suntharampill Thevuthasan
Lawrence Berkeley Laboratory
1 Cyclotron Rd. MS 2-100
Berkeley CA 94720

Al Thompson
Lawrence Berkeley Laboratory/CXRO
Bldg. 2
Berkeley CA 94720

Eric Tober
UC Davis
Physics Dept.
Davis CA 95616

James G. Tobin
Lawrence Livermore Nat'l Lab
P.O. 808 L-357
Livermore CA 94550

Brian P. Tonner
University of Wisconsin
P. O. Box 413
1900 E. Kenwood Blvd.
Milwaukee, WI 53211

James Underwood
Center for X-Ray Optics/LBL
2-400
Berkeley CA 94720

John P. Unik
Argonne National Laboratory
Building 222
9700 S. Cass Ave.
Argonne IL 60439

John Vallerga
UC Berkeley
Center for EUV Astrophysics
2150 Kitredge
Berkeley CA 94720

Jan Van Elp
LBL/ UC Davis
228 Walker Hall
Davis CA 95616

Michel A. Van Hove
Lawrence Berkeley Laboratory
1 Cyclotron Rd. MS 66
Berkeley CA 94720

Michael Vella
Center for X-Ray Optics/LBL
4-230
Berkely CA 94720

Xin Wang
Lawrence Berkeley Laboratory
UC Davis
228 Walker Hall
Davis CA 95616

Z. Wang
UC Davis
Physics Dept.
Davis CA 95616

William K. Warburton
X-Ray Instrumentation Assoc.
1300 Mills St
Menlo Park CA 94025-3210

Tony Warwick
Lawrence Berkeley Laboratory
Berkeley CA 94720

Richard N. Watts
Natl. Inst. of Standards &Technology
A253 Physics
Gaithersburg MD 20899

Marvin J. Weber
Lawrence Livermore Nat'l Lab.
P.O. Box 808 L-326
Livermore CA 94550

Max Wei
Lawrence Berkeley Laboratory
1 Cyclotron Rd. MS 2-400
Berkeley CA 94720

Michael G. White
Brookhaven National Lab.
Chemistry Dept.
Upton NY 11764

Roy F. Willis
Pennsylvania State University
Department of Physics
University Park PA 16802

Herman Winick
SSRL
4349- Bin #69
Stanford CA 94305

Mervyn Wong
Lawrence Berkeley Laboratory
MS 50A-2129
1 Cyclotron Rd.
Berkeley CA 94720

Jin Wu
SSRL
Bin 69
Stanford CA 94509-0210

Jory Yarmoff
U.C. Riverside
Dept of Physics
Riverside CA 92521

Yin Yeh
UC Davis
Div. of Applied Science
Davis CA 95616

Ramon Ynzunza
UC Davis
Physics Dept.
Davis CA 95616

Ron Yourd
Lawrence Berkeley Laboratory
1 Cyclotron Rd. MS 46-161
Berkeley CA 94720

Feng Zhang
UC Davis
Physics Dept.
Davis CA 95616

Yu Zheng
Chemical Sciences Div./LBL
2-300
Berkeley CA 94720

Preface

An Advanced Light Source (ALS) workshop on "Spectroscopic Imaging, Diffraction, and Holography with X-Ray Photoemission" was held at the Lawrence Berkeley Laboratory on August 14, 1991, in advance of the fourth ALS Users' Association Annual Meeting. The workshop was one in an ongoing series with the charter to identify and explore new scientific opportunities for high-brightness, third-generation VUV and soft x-ray synchrotron light sources, in general, and the ALS, in particular. The topic reflects the rapidly advancing progress in experimental techniques based on photoelectron spectroscopy. These techniques extend the traditional chemical-state specificity of photoelectron spectroscopy that is reflected in the well-known alternate name "electron spectroscopy for chemical analysis"—or ESCA. The extensions are in two rather different directions.

In the first, photoelectron spectroscopy becomes spatially resolved photoelectron microscopy or spectroscopic imaging, by which chemically specific spectral features of inhomogeneous surfaces can be mapped with a spatial resolution eventually reaching about 100 Å. In the second, the interference between photoelectron waves that are scattered by atoms as they make their way out of the surface and those that are unscattered gives rise to angular distributions in the photoelectron intensity that can be used to obtain structural information at the atomic level. In photoelectron holography, this information takes the form of atomic-resolution images of the atoms around an emitting atom in a specific chemical state. Feasibility experiments accomplished with conventional x-ray tubes or existing synchrotron light sources well demonstrate the promise of these techniques. But it is clear that their full fruition awaits the availability of the ALS and other facilities like it, where high brightness will make it possible to perform experiments of high spectral, angular, and spatial resolution with reasonable count rates.

Spectroscopic imaging techniques fall into two broad categories: direct imaging and scanning. Ernst Bauer (Technische Universität Clausthal, Germany) reviewed the prospects for spatially resolved chemical analysis with direct imaging methods. In direct imaging, electron optics (electrostatic or magnetic lenses) or a strong solenoidal magnetic field are used to collect photoelectrons and to preserve their spatial relationship on the way to an area detector. In photoelectron microscopy, the ensemble of detected electrons of all kinetic energies generates the image. The addition of an electron-energy analyzer gives direct imaging chemical-state specificity because the image contains only electrons with kinetic energies corresponding to a specific spectral feature, such as a chemically-shifted peak. Harald Ade (SUNY-Stony Brook) provided an overview of scanning spectroscopic imaging. For scanning, it is necessary to focus the x-rays to a small spot, which is rastered across the sample (in practice, the sample is moved through the spot) to generate the image. There are several methods of focusing the x-rays with somewhat complementary strengths and weaknesses. As in direct imaging, it is

possible to do simple photoelectron microscopy by collecting all the photoelectrons or chemically specific imaging with the use of an electron-energy analyzer. At this early date, it seems likely that both the direct imaging and scanning techniques will find considerable application in the analysis of materials, surfaces, and interfaces. The ALS will be equipped with instruments of both types.

Effects due to the interference of photoelectron waves have a venerable history in synchrotron radiation. For example, the high intensity of synchrotron radiation made x-ray absorption fine structure (XAFS) spectroscopy into a practical tool for obtaining interatomic distances in both ordered and disordered materials. In XAFS, the interference between the wave emitted by an atom absorbing an x-ray photon and those scattered back toward the emitter by neighboring atoms modulates the absorption cross section, thereby giving rise to the well-known XAFS oscillations above the absorption edge. The oscillations can be Fourier-inverted to extract the radial distances between the emitter and the scattering atoms. More recently, photoelectron diffraction has been developed into a technique for obtaining detailed geometrical information about the arrangement of the scattering atoms surrounding an emitter. In a diffraction experiment, the interference between scattered and unscattered photoelectron waves creates a diffraction pattern at the detector. The detector maps the pattern by moving around the solid angle surrounding the specimen surface at fixed photon and electron energies. The resulting angular distribution of photoelectron intensity reflects the geometry of the scattering atoms. As in spectroscopic imaging, fixing the photon and electron energies selects an emitter atom in a specific chemical state. Alternatively, it is possible to map the diffraction pattern by scanning the wavelength of the photoelectron wave at a fixed angle—a technique variously called energy-dependent photoelectron diffraction or angle-resolved photoelectron fine structure (ARPEFS). To ensure that the same emitter state is excited throughout the experiment, the photon and electron energies are scanned in concert.

At the workshop, Scott Chambers (Boeing High Technology Center) demonstrated the applicability of photoelectron diffraction to the relationship between surface band bending and surface structure when selenium or tellurium are on a gallium arsenide (001) surface. In particular, selenium, which is important for surface passivation of gallium arsenide, is found several layers below the surface on arsenic sites, forming a gallium selenide arsenide layer, whereas tellurium remains at the surface. Chambers also discussed the formation of a ternary nickel gallium arsenide layer when nickel is on a gallium arsenide surface, a process that involves the interplay between interface chemistry and epitaxial regrowth. James Tobin (Lawrence Livermore National Laboratory) showed how photoelectron diffraction at low electron energies could be used to study ultrathin magnetic films of iron on copper. At low energies, photoelectron diffraction is strongly surface sensitive, thereby allowing surface alloys to be distinguished from overlayers and permitting the investigation of structure with coverage. Magnetic order can be detected by excitation of multiplet-split core states, but these experiments would be considerably enhanced by the use of electron spin detectors and circular polarization.

What makes photoelectron diffraction strongly surface sensitive at low electron energies (<200 eV) is the presence of multiple scattering—the photoelectron wave scatters from more than one atom on the way to the surface. In contrast, at high electron energies (>500 eV), the scattering is dominated by a single atom and the scattered wave tends to be concentrated in the forward direction along the axis connecting the emitter and the scattering atom, so that photoelectrons from deeper in the bulk can escape. To make a quantitative connection between diffraction patterns and atomic structure, a theoretical treatment of the scattering process is required. Michel Van Hove (Lawrence Berkeley Laboratory) provided an update of the numerous factors involved in constructing a model, such as deciding when multiple scattering must be accounted for and the possible inclusion of thermal vibrations. The computer time required to obtain structural information mounts rapidly as the number of scattering events grows, making accurate multiple-scattering calculations impractical. John Rehr (University of Washington) surveyed several methods of making approximate calculations and concluded that a method based on a separable Green's function matrix was both accurate and computationally efficient.

To obtain structural details, such as the path lengths between the emitter and scattering atoms, it is not necessary to record the entire diffraction pattern. It suffices to make selective scans to generate spectra that can be inverted to yield the structural data. In ARPEFS, for example, Fourier inversion of the energy-scanned spectrum gives information similar to that obtained with XAFS. With patience or with modern display-type analyzers, however, it is possible to make angular scans that cover much of the solid angle surrounding the specimen surface. The display-type analyzer simultaneously collects energy-selected photoelectrons in an angle-resolved mode over a large solid angle. Inversion of this two-dimensional diffraction pattern yields three-dimensional maps of the positions of the scattering atoms. In this case, the diffraction pattern plays the role of a hologram produced by the interference of the unscattered (reference) wave and the scattered waves that is then reconstructed by computer to obtain an image of the objects causing the scattering. It is important to remember, however, that this "atomic-resolution" is not to be compared with the 100-Å resolution promised for spectroscopic imaging. Photoelectron holography images are obtained by averaging over the entire illuminated area (perhaps a spot 10 micrometers in diameter) of what one hopes is a homogeneous area. It is, of course, possible in principle to conceive of a spatially resolved holography experiment with 100-Å resolution, but such a feat will require x-ray optical components with improved transmission.

To open the discussion of photoelectron holography, Brian Tonner (University of Wisconsin–Milwaukee) provided a broad overview of the present capabilities of photoelectron holography. In particular, the technique gives easily interpreted chemical-state information, provides three-dimensional images with 0.5-Å resolution (0.05 Å with modeling), can generate images of both surface and sub-surface atoms, has no need for long-range order, and is widely applicable to metals,

semiconductors, and insulators. Abraham Szoke (Lawrence Livermore National Laboratory) then gave a historical overview of the development of this technique, which dates back to 1975, summarized methods of generating holograms, and introduced the problem of reconstructing holograms. Dilano Saldin (University of Wisconsin–Milwaukee) explained in some detail the theoretical and experimental application of holography with x-ray excited Auger electrons in copper. Charles Fadley (University of California at Davis and Lawrence Berkeley Laboratory) reviewed the results of several experiments in an attempt to assess the prospects for photoelectron holography by answering such questions as: Why does holography work as well as it does, how much information can be obtained from high-angular-resolution data, how can the data be treated to reduce artifacts and improve the information content, and what are the pros and cons of electron holography at high and low electron energy? John Barton (IBM–T.J. Watson Research Center) discussed the extension of electron holography to inverse diffraction by recording three-dimensional diffraction patterns. This technique can be visualized as multiple-wavenumber holography in which several data diffraction patterns are recorded, each at a different electron energy (the photon energy moving in concert, as in ARPEFS, so that the same emitter state is excited throughout the experiment). A principal benefit is that the influence of multiple scattering and artifacts is reduced, making reconstruction of the image more straightforward.

Introduction to the Advanced Light Source

A.S. Schlachter

Lawrence Berkeley Laboratory

先進光源

THE ADVANCED LIGHT SOURCE: X-RAY BEAMS OF UNPRECEDENTED BRIGHTNESS

從未有過的量亮度的X光束

Fred Schlachter
University of California
Lawrence Berkeley Laboratory
Berkeley, California
USA

THE ADVANCED LIGHT SOURCE: OVERVIEW

- National user facility
- Provides UV and soft x-ray beams of unprecedented brightness:
  - Broadly tunable with narrow spectral features
  - Partially coherent
  - 35 psec time structure
- Utilized by researchers from industry, academic, and national laboratory communities:
  - Materials and surface science
  - Atomic and molecular physics
  - Chemistry
  - Life sciences
  - Technology
- Construction project began in late 1986
- Begin operations in spring 1993
- Construction cost — $99.5 million

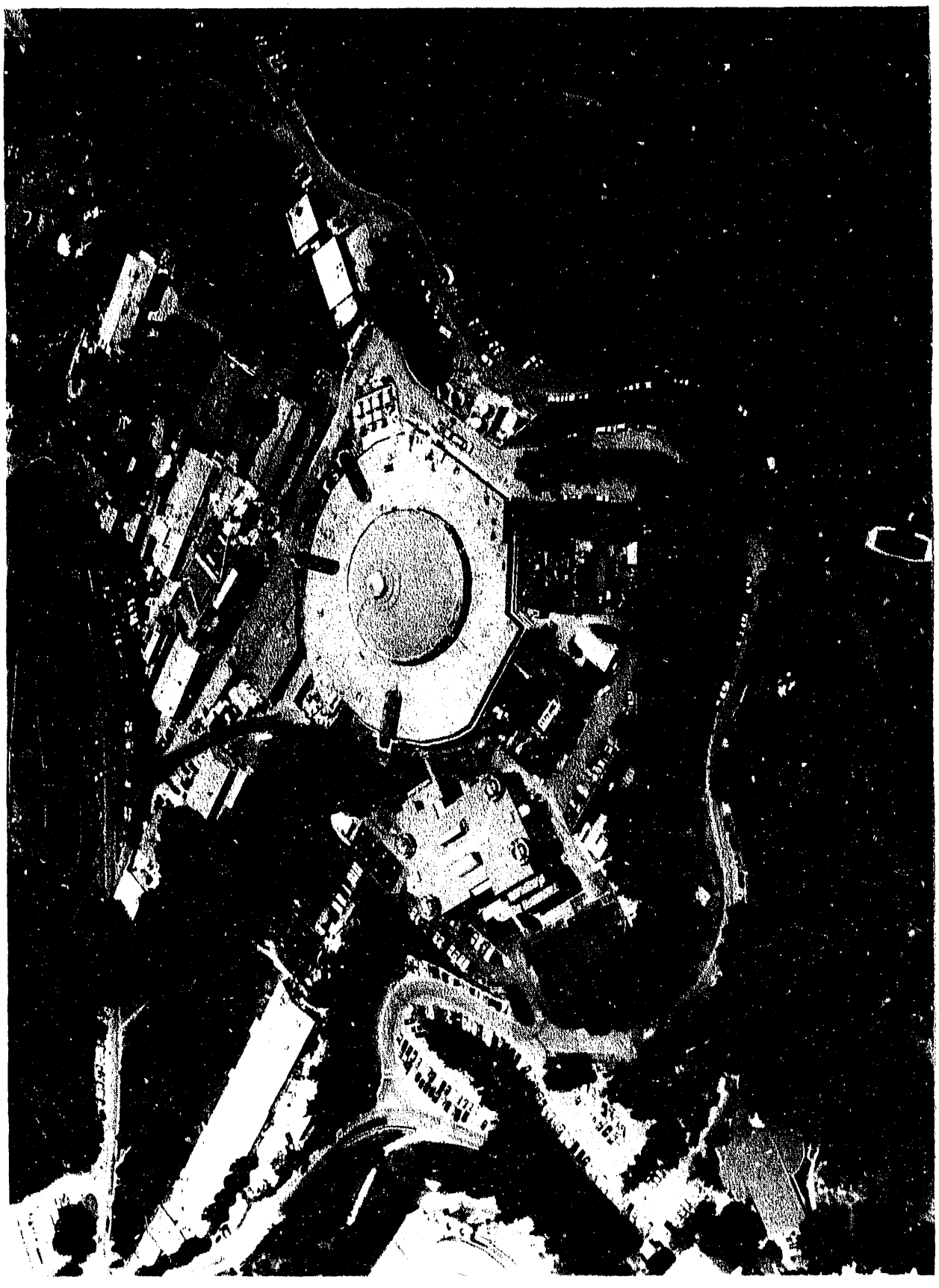

THE ALS WILL BE THE FIRST THIRD-GENERATION SYNCHROTRON-RADIATION SOURCE

ALS

- **First generation: parasitic operation at high-energy physics facilities (e.g., SSRL)**
- **Second generation: dedicated to synchrotron radiation (e.g., NSLS)**
- **Third generation: high brightness (e.g., ALS, APS)**

  - low emittance

  -long straight sections

  -permanent-magnet undulators

EVOLUTION OF SYNCHROTRON RADIATION

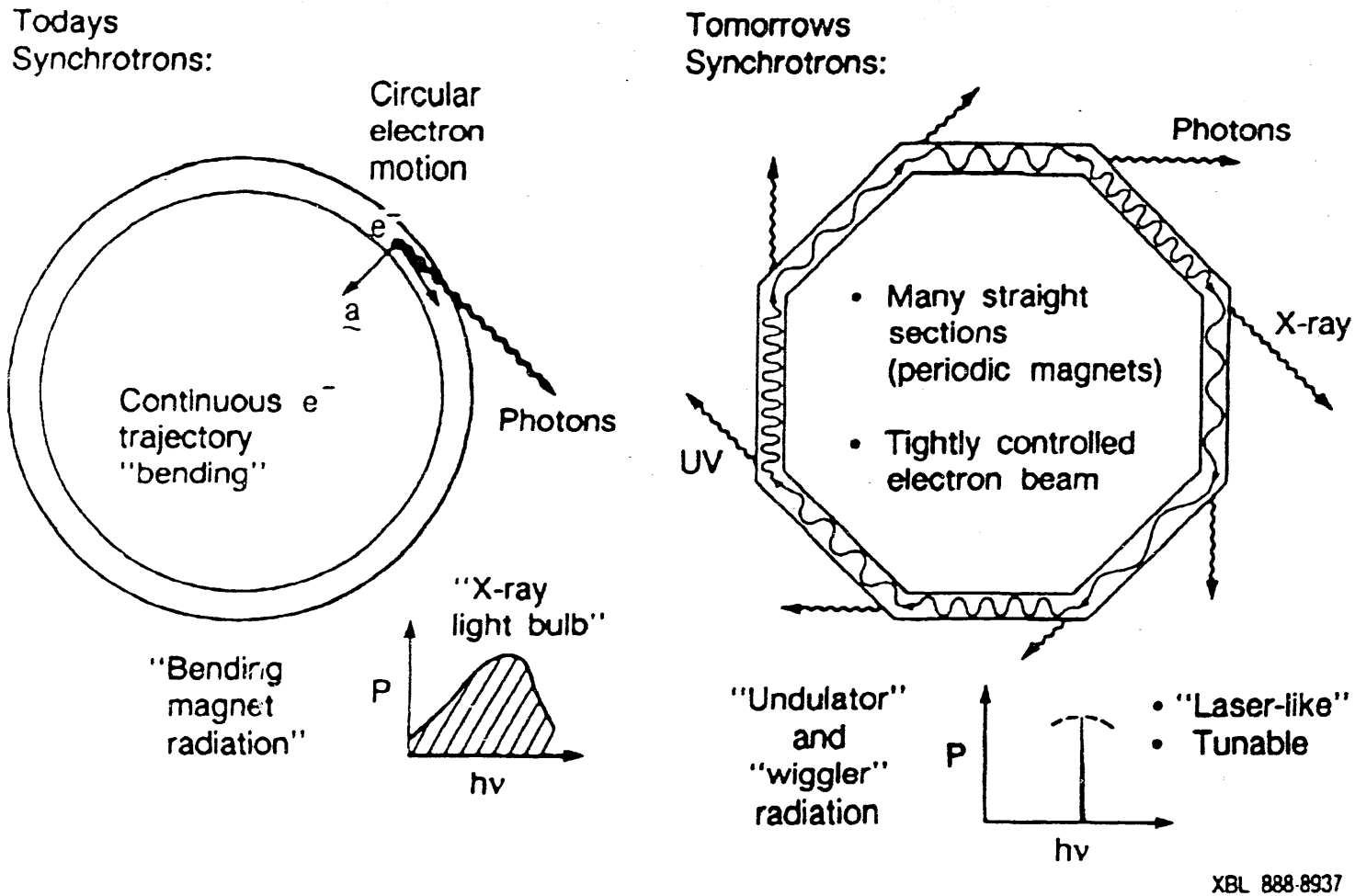

An Undulator Produces a Very Bright Beam of VUV or X Rays

- Coherent superposition of radiation from electrons bent many times in periodic permanent-magnet structure

- Properties of undulator radiation:

  — High brightness
  — Tunable photon energy
  — Partial coherence
  — High linear polarization
  — Picosecond time structure

An undulator is a tunable soft-x-ray picosecond strobe light with laser-like properties

HIGH BRIGHTNESS IS THE MAIN FEATURE OF THE ALS

- High intensity
- Ease of focussing ⇒ microscopy
- Study of tenuous targets ⇒ atomic physics, chemistry
- Element-specific sensitivity
- Coherence
- Broad tuning range
- Short pulses

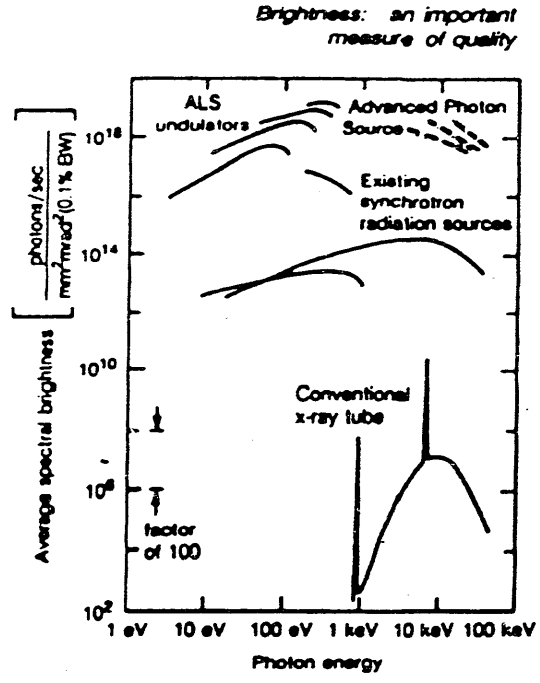

THIRD-GENERATION SYNCHROTRON-RADIATION SOURCES HAVE HIGH BRIGHTNESS

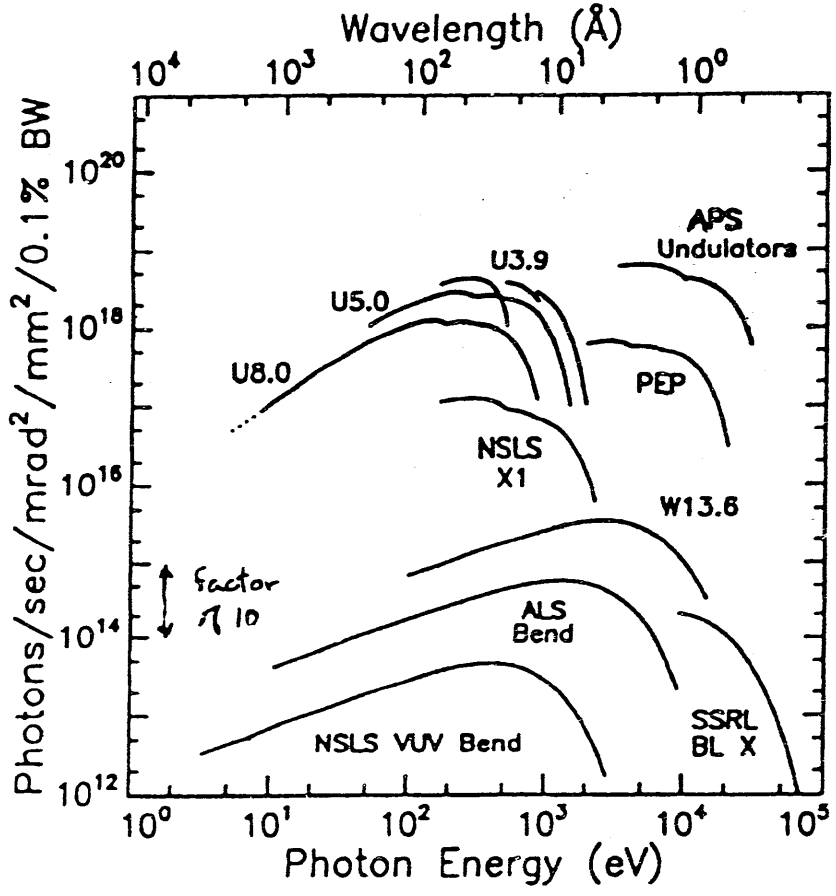

- **ALS undulators produce a beam which is a factor of 10,000 brighter than that from bend magnets**

INITIAL SCIENTIFIC PROGRAM

- Broad program
  - Photon energy: 5 eV – 10,000 eV
  - Many research disciplines
  - Researchers from many institutional settings

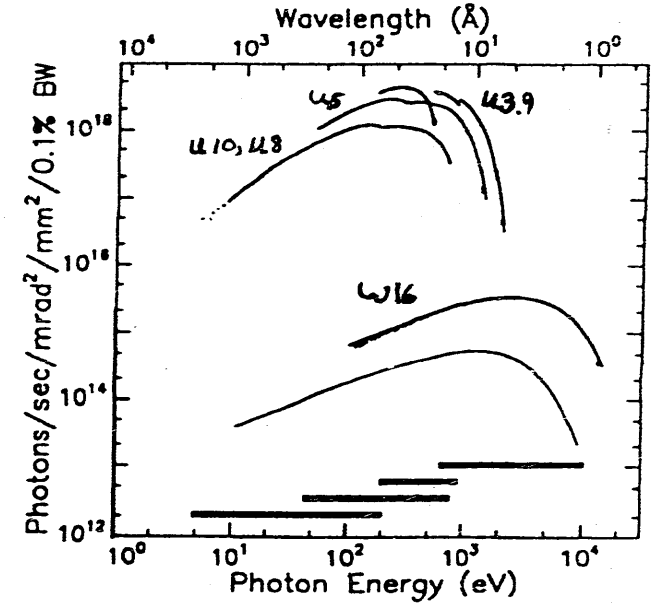

- Insertion-Device Program
  - 1 x U10 Combustion Dynamics
  - 2 x U8 Chemistry and Atomic Physics
  - 2 x U5 Surface and Materials Science
  - 1 x U3.9 X-ray Imaging and Optics
  - 2 x W16 Materials Science/Life Science

- This program will require substantial user funding to supplement ALS project funds.

- Bend-Magnet Program
  - IDTs will utilize 3 bend-magnet lines
  - Bend-magnet teams to have been approved for 4 bend-magnet lines
    - infrared
    - optics development
    - materials science
    - circularly polarized radiation

January 1896 Röntgen/Wurzburg

ATOMIC-RESOLUTION ELECTRON HOLOGRAPHY

- Image near-neighbor environment of specific chemical species in three dimensions
- Measure photoelectron diffraction pattern produced by x ray to select chemical species
- High resolution needed to resolve chemical shifts

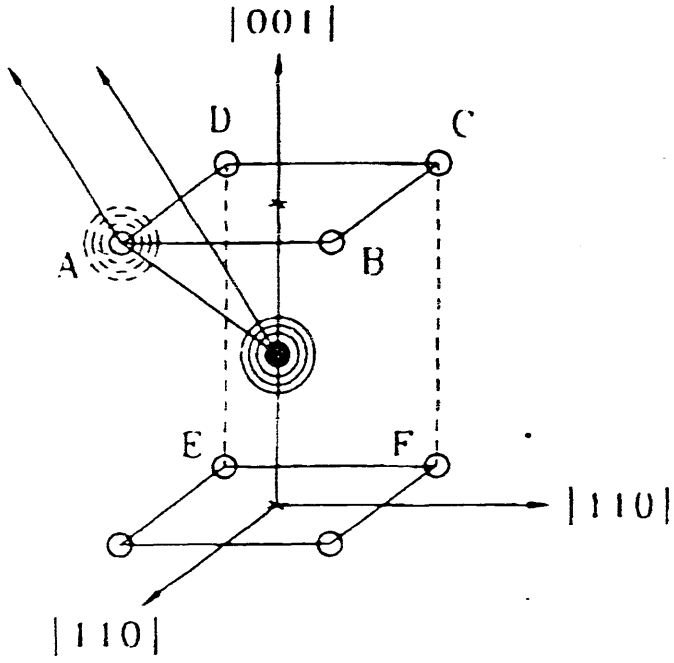

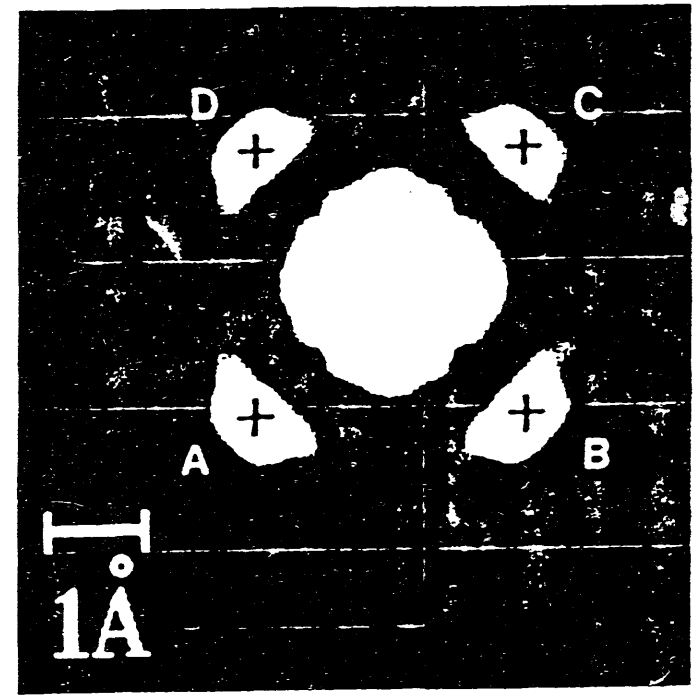

Holographic reconstruction of Cu (001)
Ref: Harp et al., *Phys. Rev. Lett.* 65, 1012 (1990); *Phys. Rev. B* 42, 9199 (1990)

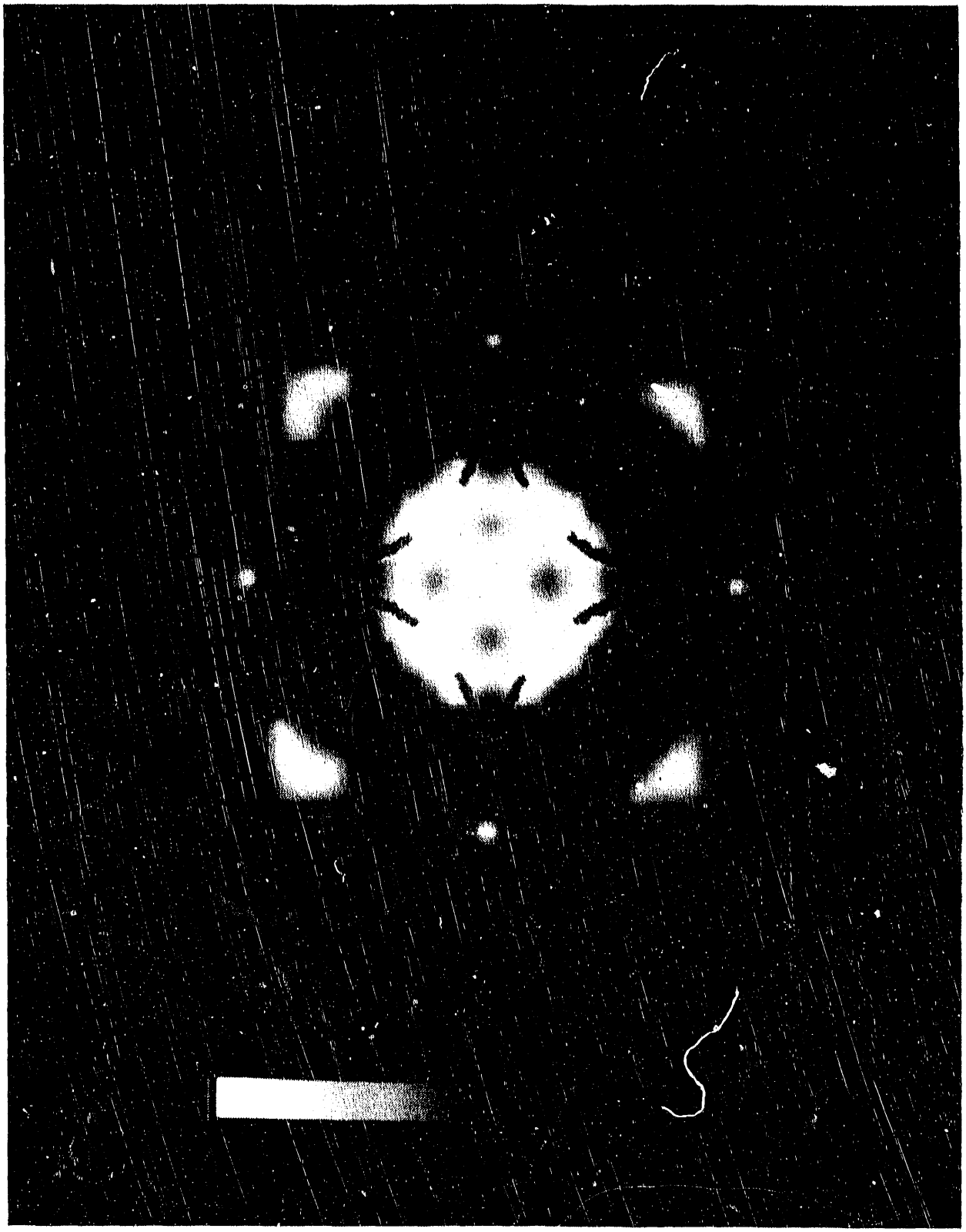

Chocolate holograms

The choice of which chocolate bar to choose may soon become more difficult with the advent of edible chocolate holograms.

Dimensional Foods, Inc., of Boston is exploring techniques to apply holograms to food, under a patent issued to company founder and president Eric Begleiter in 1987, the year the company was established.

According to *Holography News*, one technique being considered is a thermal transfer process. That process is suitable for foods such as chocolate, that may be injection-molded or poured into a mold. A reverse hologram is built into the mold as a minute relief structure resembling an embossed hologram shim. The chocolate is pressed into the relief, resulting in a hologram on the reflective surface of the chocolate.

Another technique involves a dehydration process for candy coatings. This technique reproduces diffraction grating spectral colored sugar called "Sparkle," that is under consideration for coating breakfast cereals. Other candidates are lollipops and hard candies.

If DFI's product is successful, the company is interested in licensing the technology to food manufacturers. Although initial markets are child-oriented, dealing with candy, DFI is investigating application for pressure-formed tablets produced by the pharmaceutical industry.

Photoelectron Holography and Quantitative X-Ray Photoelectron Diffraction of Surfaces and Ultrathin Films

B. Tonner

University of Wisconsin

Photoelectron Holography and Quantitative X-ray Photoelectron Diffraction of Surfaces and Ultrathin Films*

Advanced Light Source
August 14, 1991

Brian Tonner
Dept. of Physics
Univ. of Wisconsin-Milwaukee

Collaborators:

Prof. D. K. Saldin, UW-M (thy.)
G. R. Harp, Z.-L. Han,
S. Hardcastle, J. Zhang

*Supported by NSF Div. Mat. Res.

Structure of metal surfaces and thin-films by Fourier-transform Photoelectron Diffraction[†]

S. Hardcastle, Z.-L. Han, G. R. Harp, J. Zhang, X.-D. Wang, D. K. Saldin, and B. P. Tonner

- What is new about photoelectron holography?
- Physical interpretation of "images".
- Improved 'deconvolution' methods of direct imaging.
- Quantitative structure determination.

[†]Supported by NSF DMR-88-05171

Features of Photoelectron Holography

- Easily interpreted chemical-state information
- Three-dimensional "image" of atomic structure with 0.5 A resolution (direct) and 0.05 A resolution (modelled)
- Can image atoms below the surface
- Long-range order is not required
- Applies to metals, semiconductors, insulators

Method

1. Isolate region of sample by focussed X-rays or selected-area diffraction.
2. Measure 2π steradian angular-distribution of photoelectron diffraction, or *hologram*.
3. Normalize hologram to extract anisotropy function $I_{\hat{K}}$.
4. Phased two-dimensional Fourier-transform of data produces 3-dimensional structure.

$$I_K(\theta,\phi) = I_o(\theta,\phi)(1+\chi(\theta,\phi)). \tag{1}$$

$$\phi(\mathbf{r}) = \int \chi(\hat{\mathbf{K}})\, e^{i\mathbf{K}\cdot\mathbf{r}} d\hat{\mathbf{K}}. \tag{2}$$

Image function: $|\phi(\mathbf{r})|^2$

Radial image function: $|\phi(r,\hat{\mathbf{r}})|^2$

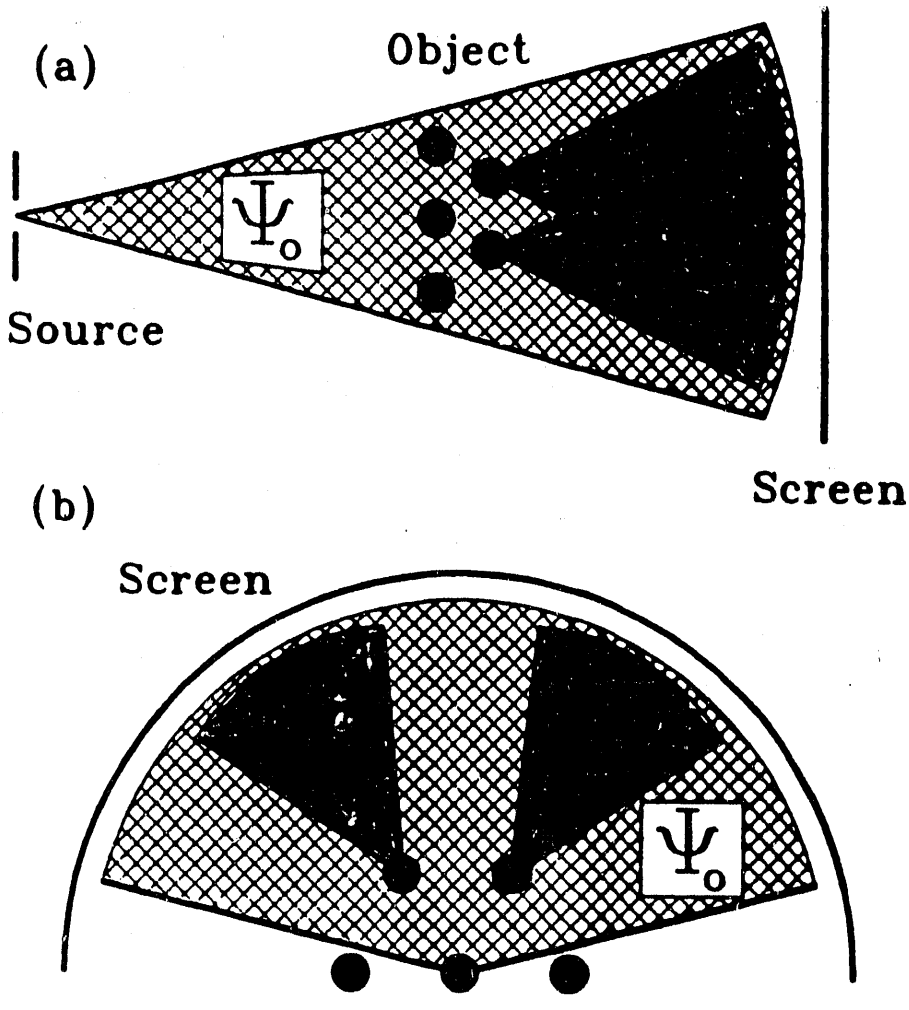
(a)
Object
Ψ_o
Source
Screen
(b)
Screen
Ψ_o

Photoemission Holography
in
Forward-scattering Geometry

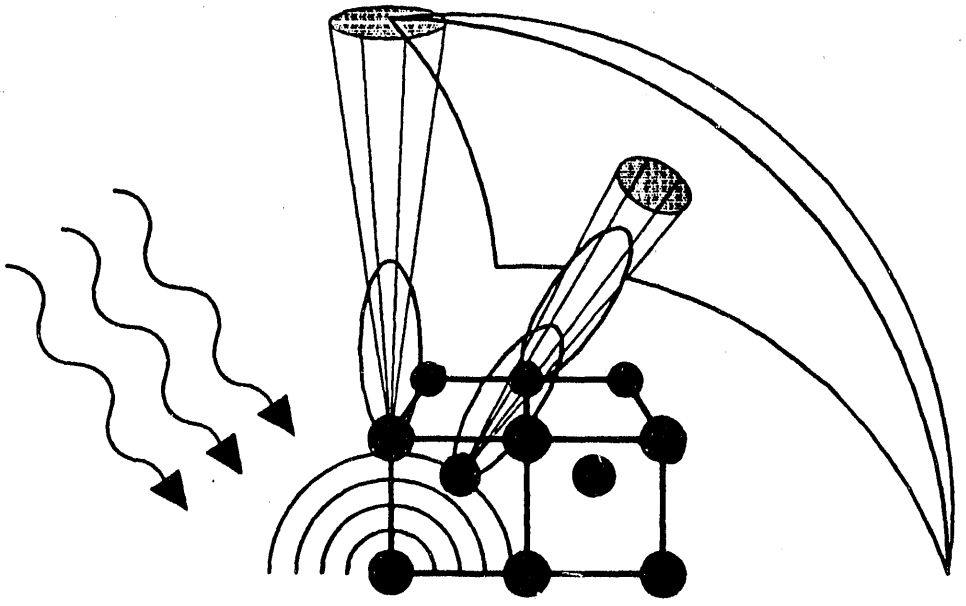

- Buried atoms
- Probes the "core"
- Distinguish emitter by chemical state

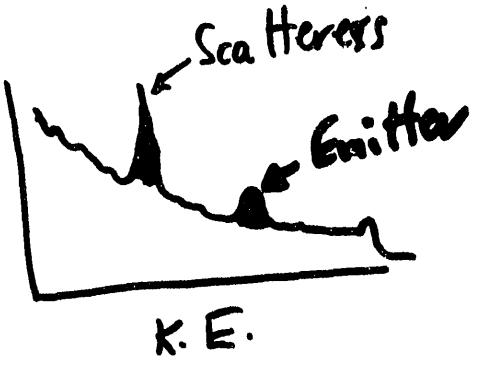

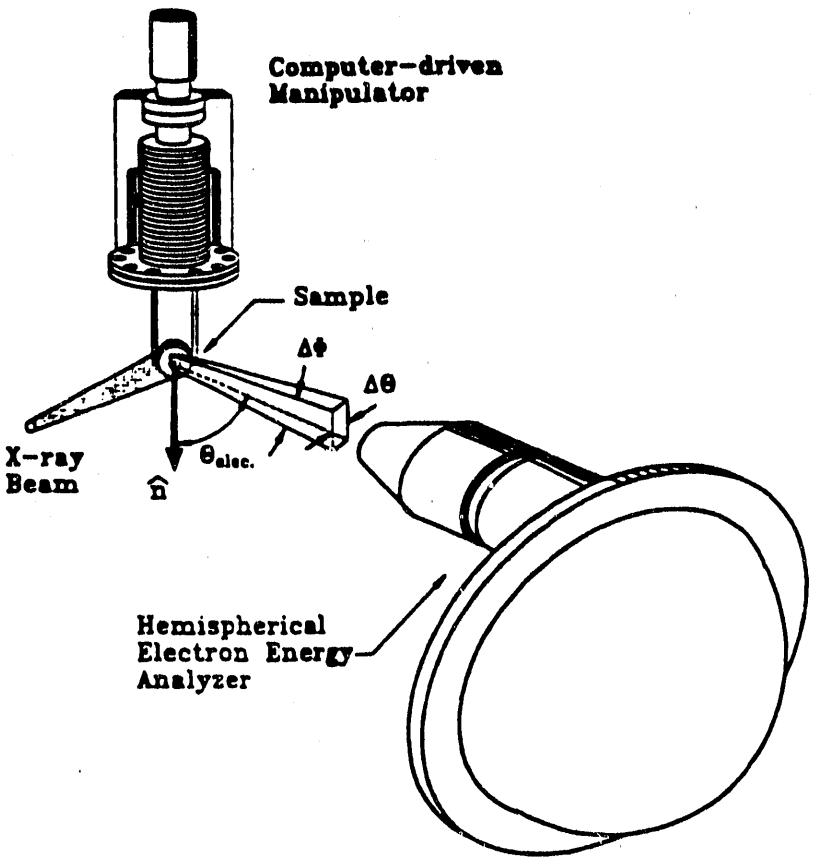

Idealization of the experimental geometry, which maintains a fixed angle between the incident X-ray beam and the ejected electron ($\Theta_{photon}+\Theta_{electron} = \Gamma = const$). For each crystal azimuth (Φ), the electron polar angle (Θ_{el}) is scanned by rotating the sample normal ($\hat{n}$). In practice, the incident X-ray beam illuminates the entire sample surface, and the detector accepts a small solid-angle ($\Delta\Theta\Delta\Phi$) around the emission direction (see text for details).

Real-space interpretation of x-ray-excited Auger-electron diffraction from Cu(001)

H. Li and B. P. Tonner*
Department of Physics and Laboratory for Surface Studies, University of Wisconsin—Milwaukee 1900 E. Kenwood Blvd., Milwaukee, Wisconsin 53211
(Received 17 August 1987)

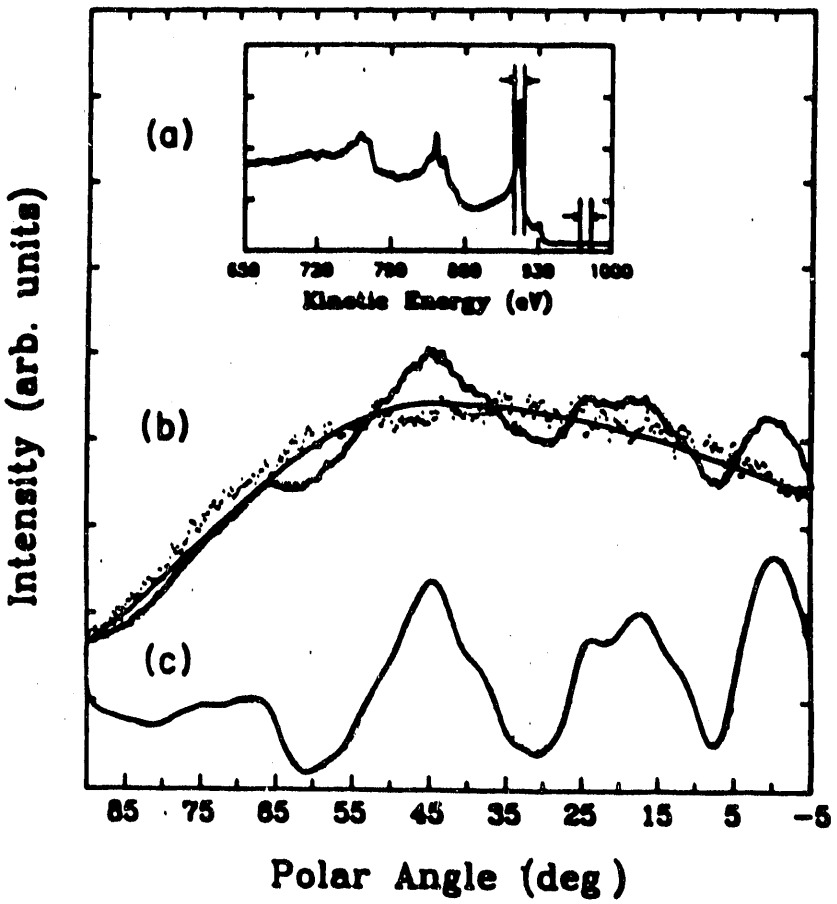

FIG. 1. Illustration of data acquisition and analysis of Auger-electron diffraction along the Cu(001) [100] azimuth. (a) Kinetic energy distribution of x-ray-excited *LVV* Auger electrons from Cu(001). The energy windows used to monitor AED at 917 eV and the background at higher energy are shown. (b) The dotted curve is the experimental background, the smooth solid curve is a theoretical fit to the experimental background. The modulated solid curve is the emission intensity from the Auger electrons. (c) Background-subtracted Auger-electron diffraction intensity, smoothed over a range of ±1.5° in polar angle.

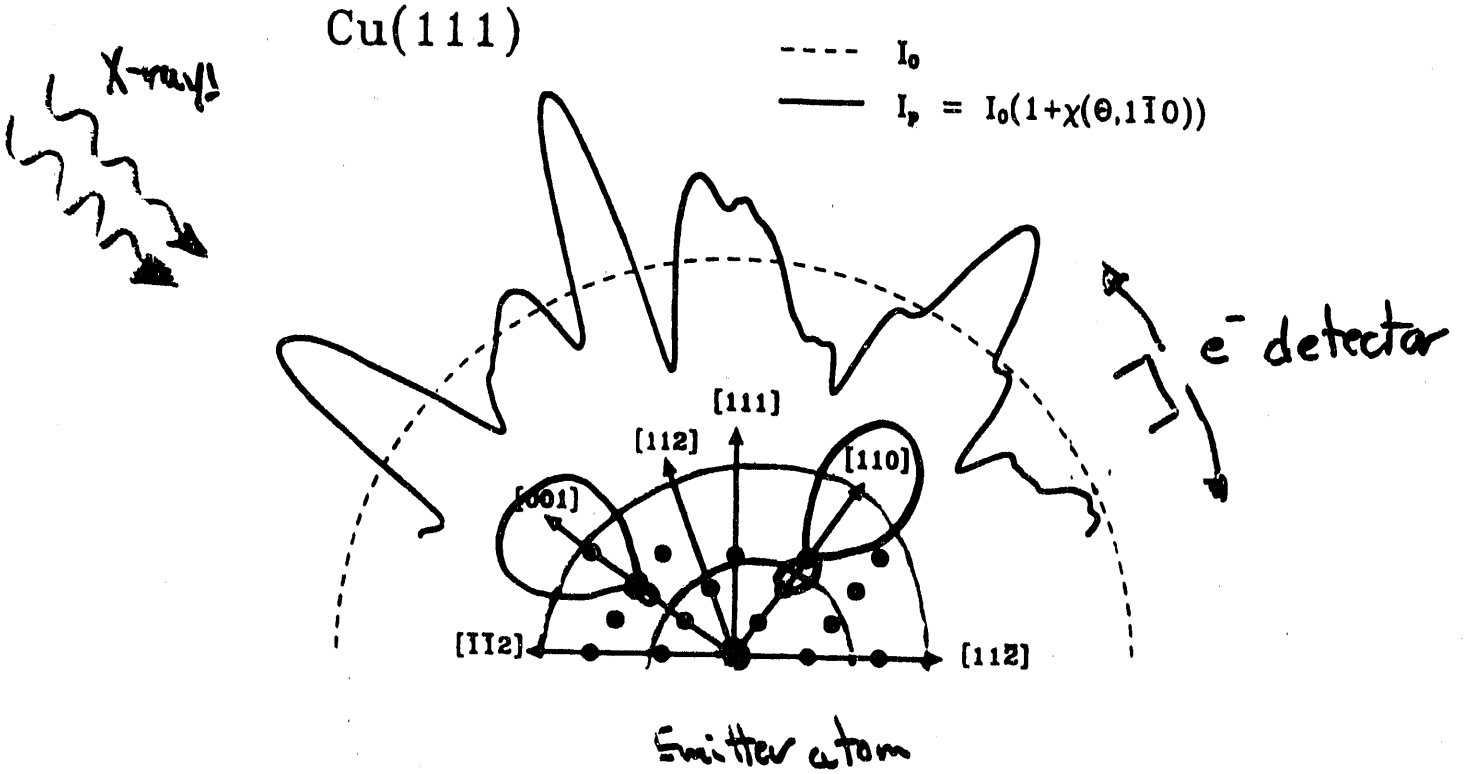
Cu(111)
X-rays
I_0
$I_p = I_0(1+\chi(\theta,1\bar{1}0))$
e⁻ detector
[111]
[112]
[110]
[001]
[$\bar{1}\bar{1}$2]
[11$\bar{2}$]
Emitter atom

fcc (111) structures

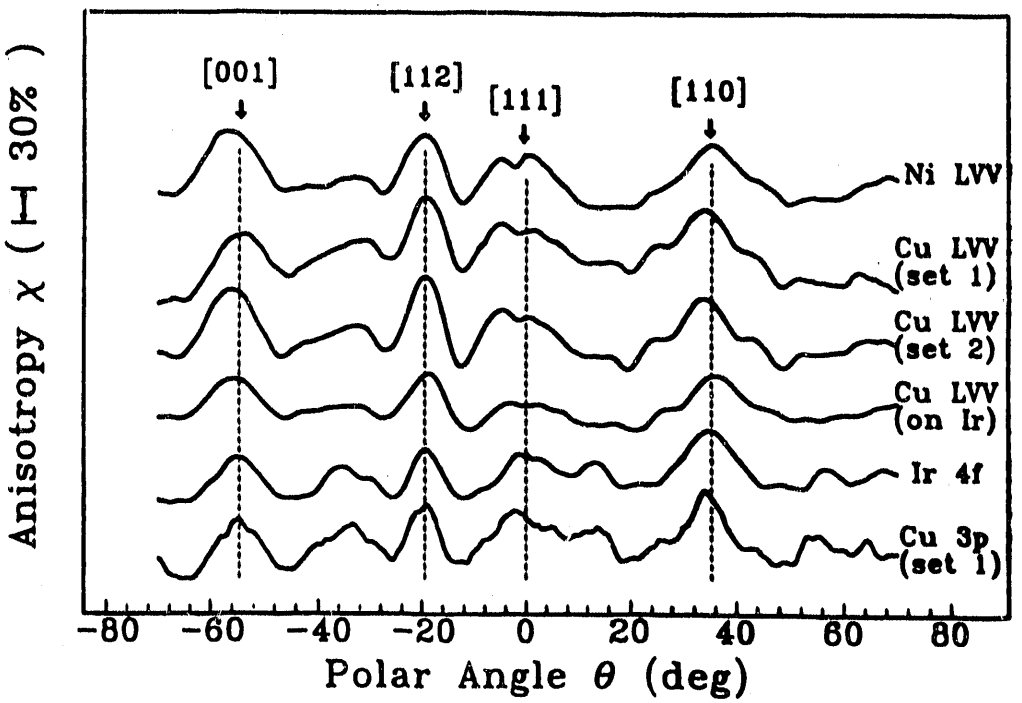

ARXPD

Structural "Fingerprinting"

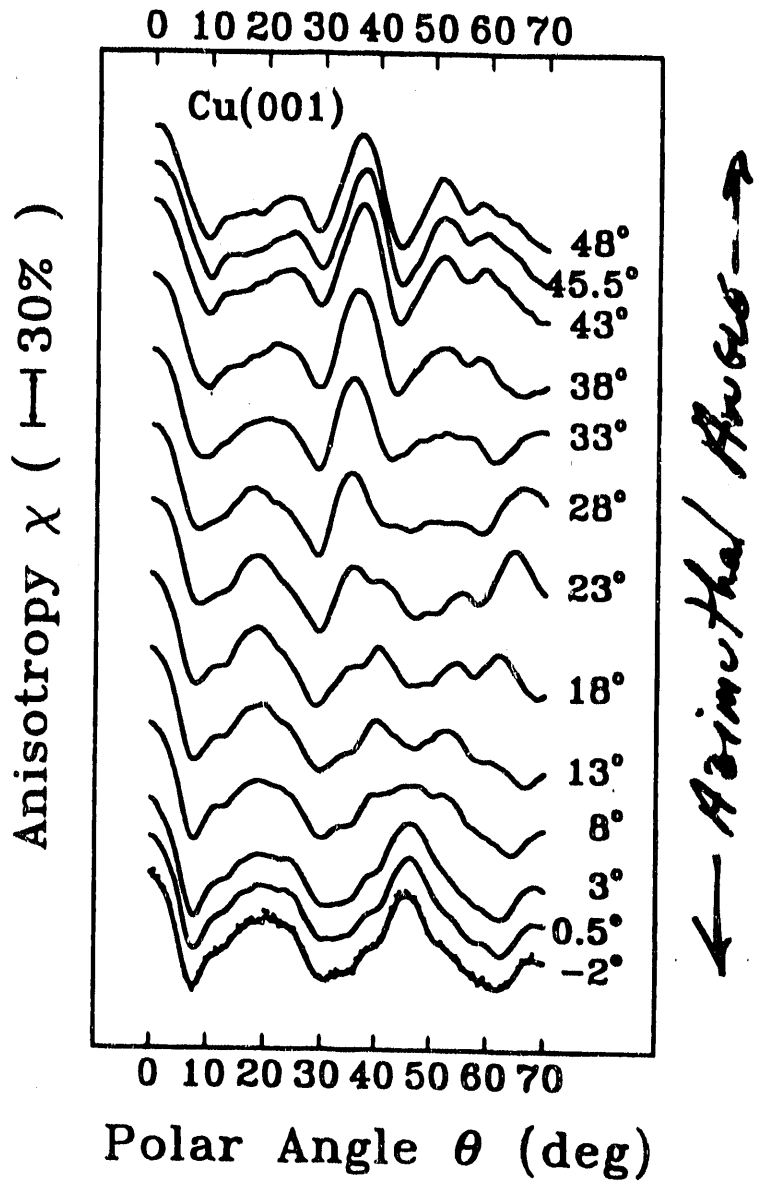
0 10 20 30 40 50 60 70
Cu(001)
48°
45.5°
43°
38°
33°
28°
23°
18°
13°
8°
3°
0.5°
−2°
Anisotropy χ (⊢ 30%)
← Azimuthal Angle →
0 10 20 30 40 50 60 70
Polar Angle θ (deg)

Cu (001)

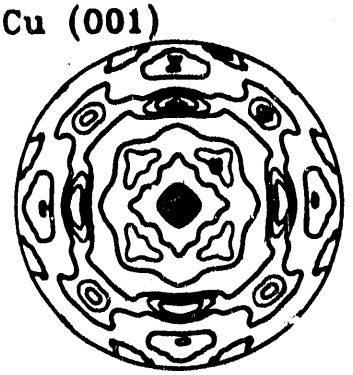

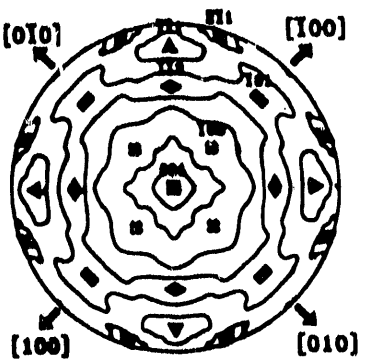

Cu(111)

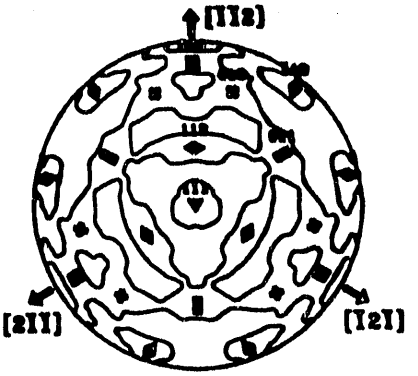

Cu(110)

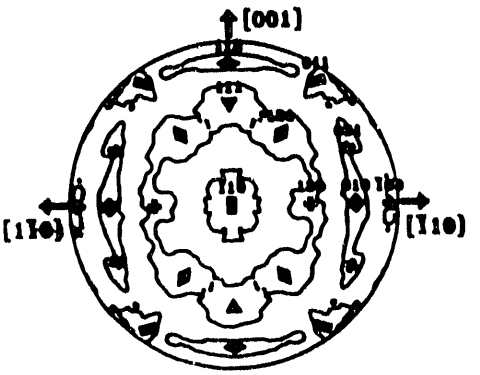

■: <100> ■: <110> ▲: <111> ♦: <211> ♦: <310>

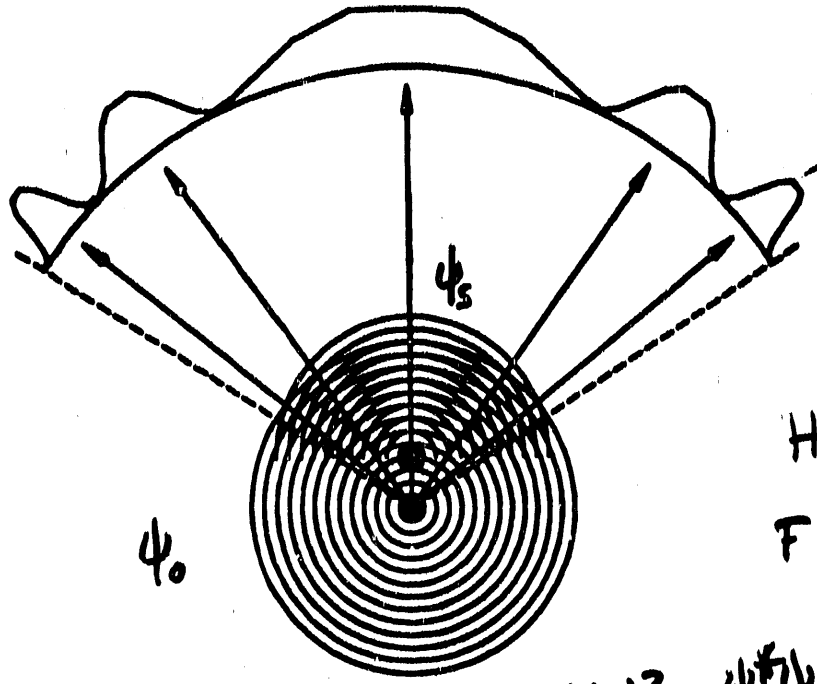

Hologram Formation

$$I(\hat{k}) = |\psi_0 + \psi_s|^2 = |\psi_0|^2 + |\psi_s|^2 + \psi_0^* \psi_s + \psi_0 \psi_s^*$$

direct twin

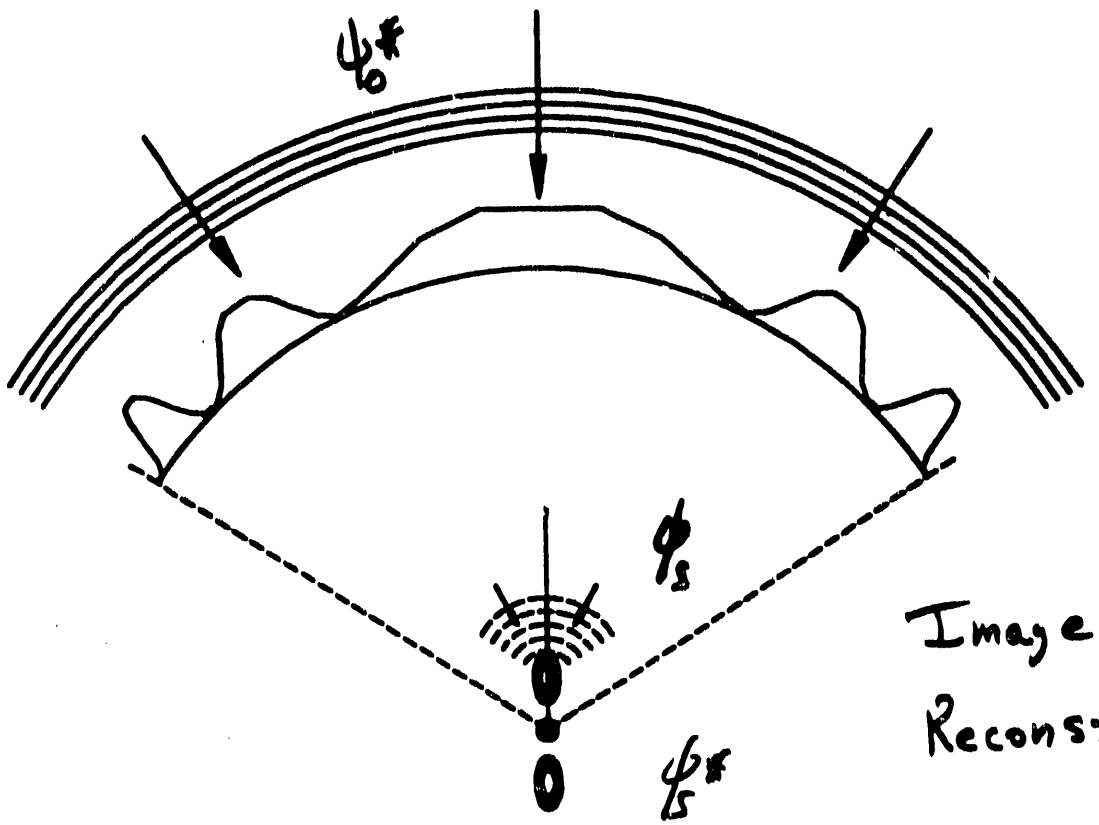

Image Reconstruction

Computer: $\int I(\hat{k})\, e^{i\bar{k}\cdot\bar{r}}\, a\hat{k} = \Psi(k, \bar{r})$

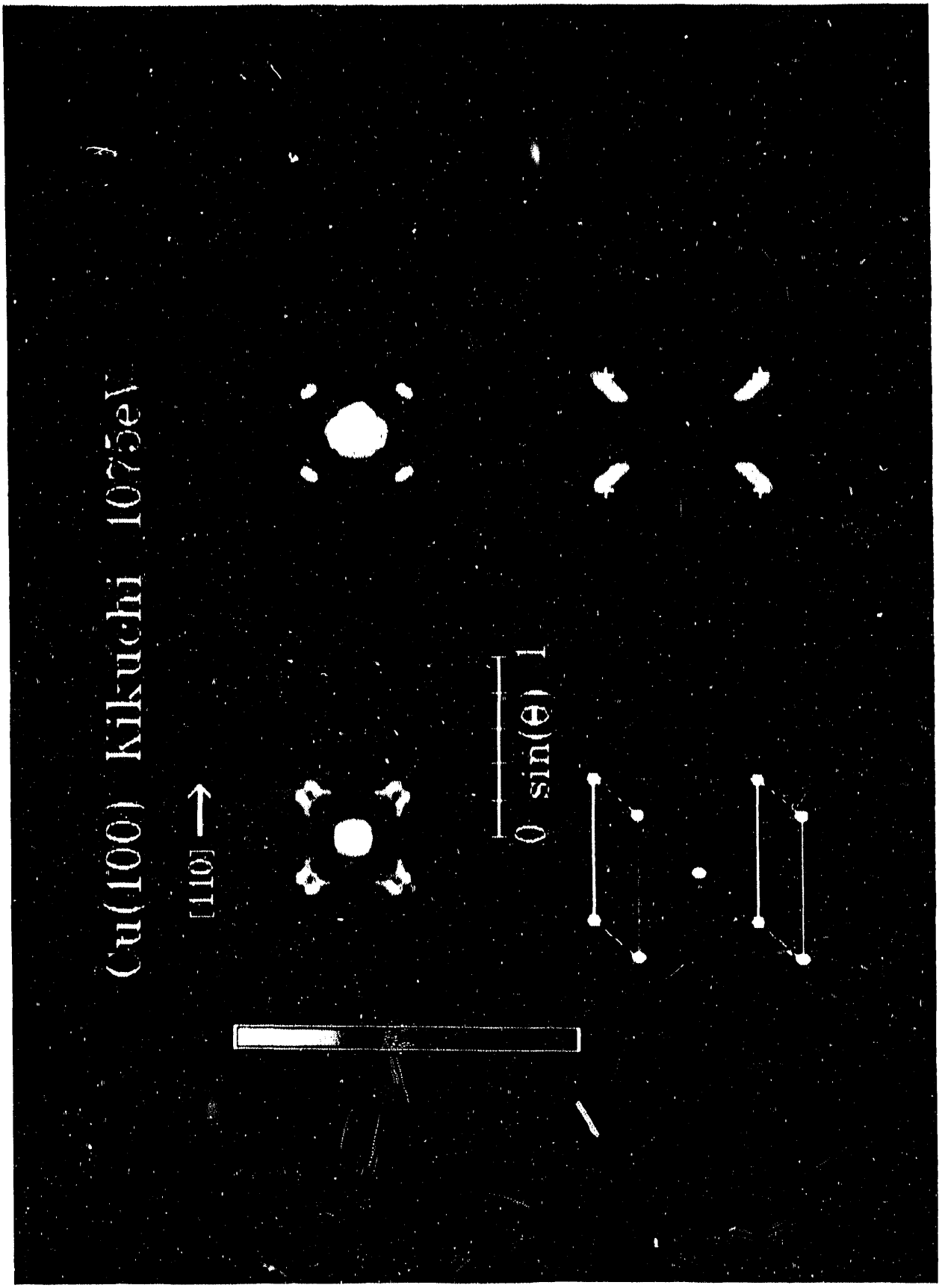
Cu(100) Kikuchi 1075eV
[110]
0 sin(θ) 1

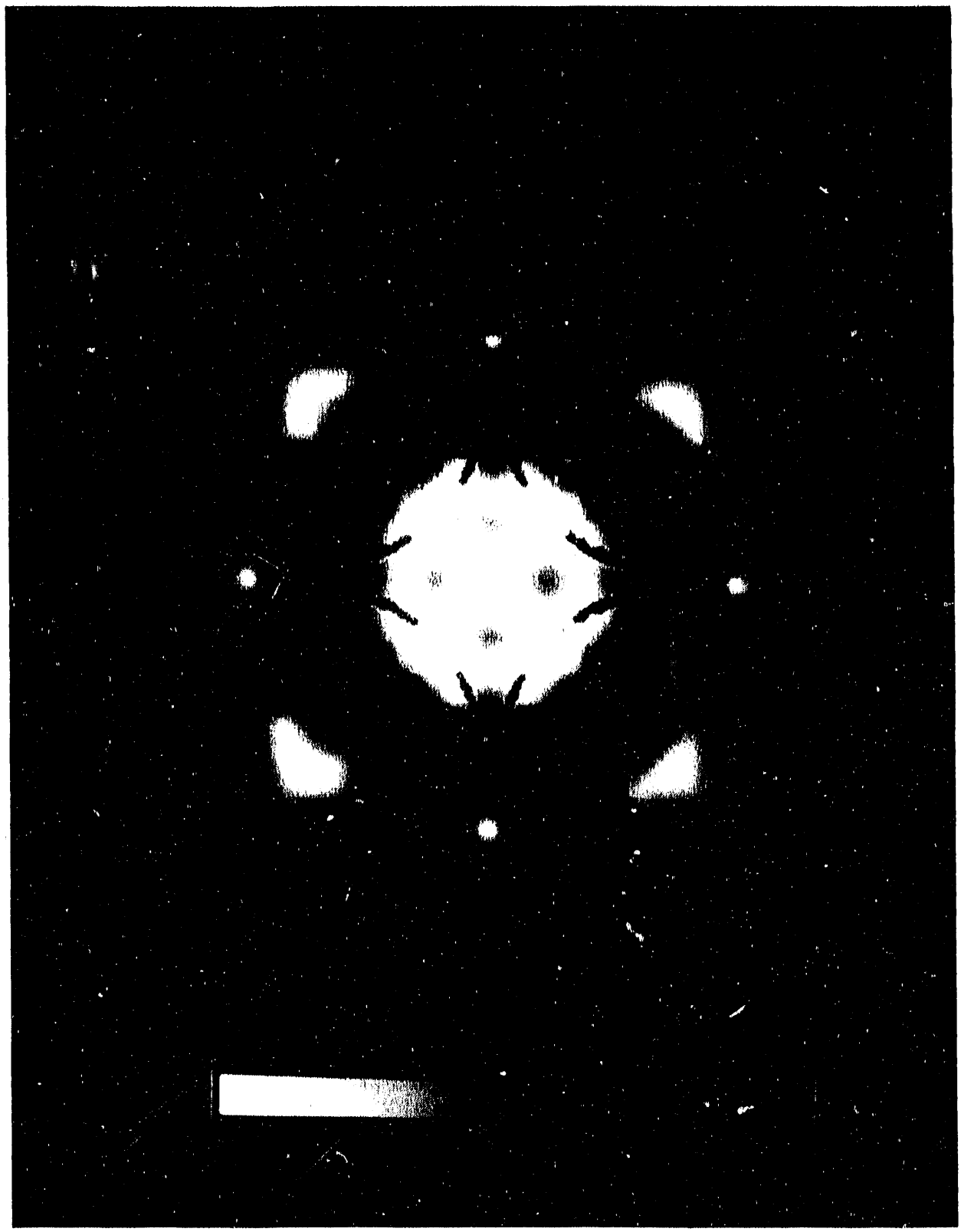

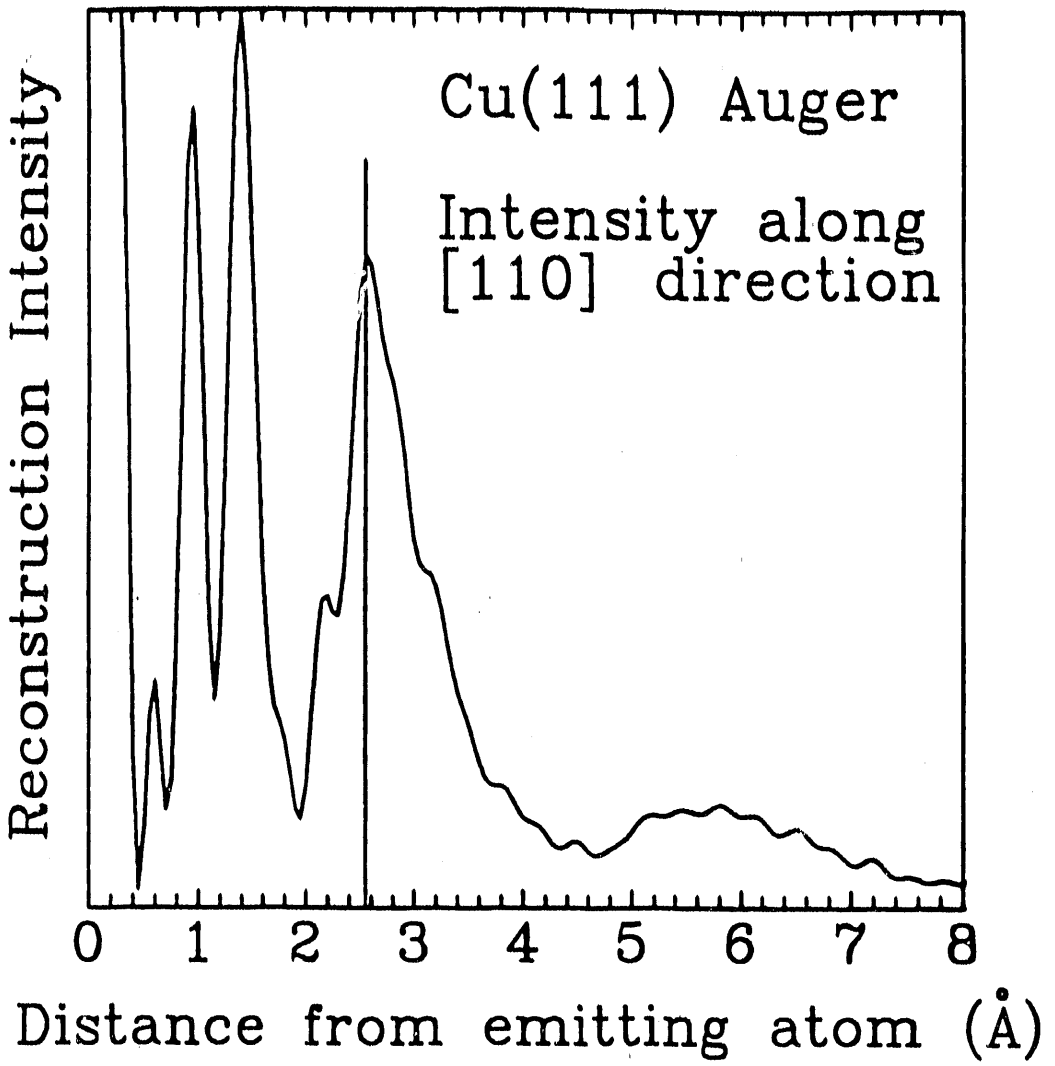

5. Intensity of the reconstruction from the Cu(111) Auger diffraction pattern, along a line in the [110] direction of the crystal, starting at the location of the emitting atom. the expected position of a nearest neighbor atom is marked by the vertical line.

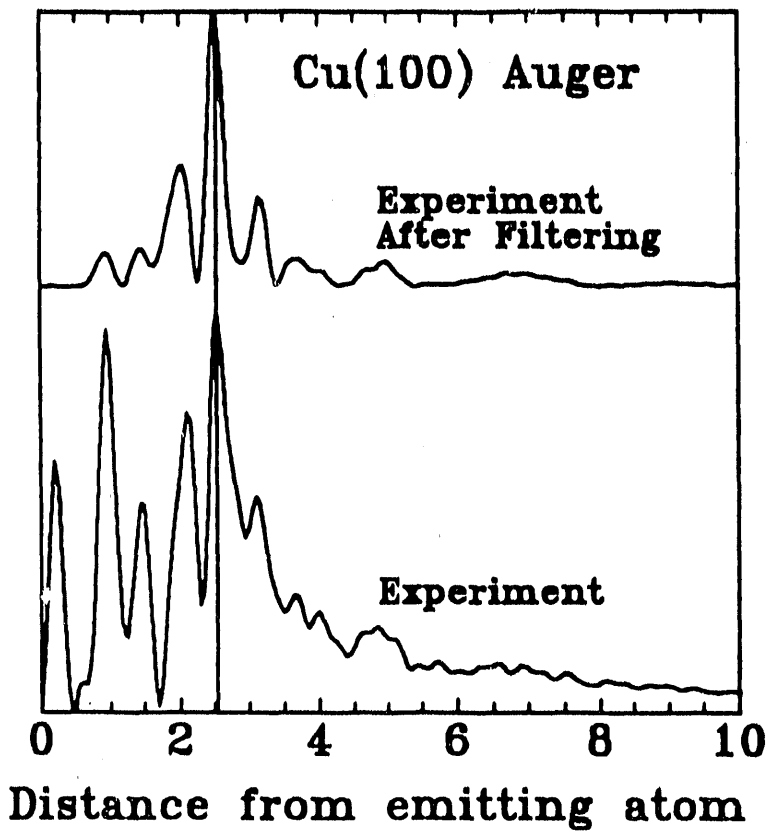
Cu(100) Auger
Experiment
After Filtering
Experiment
0
2
4
6
8
10
Distance from emitting atom (A)

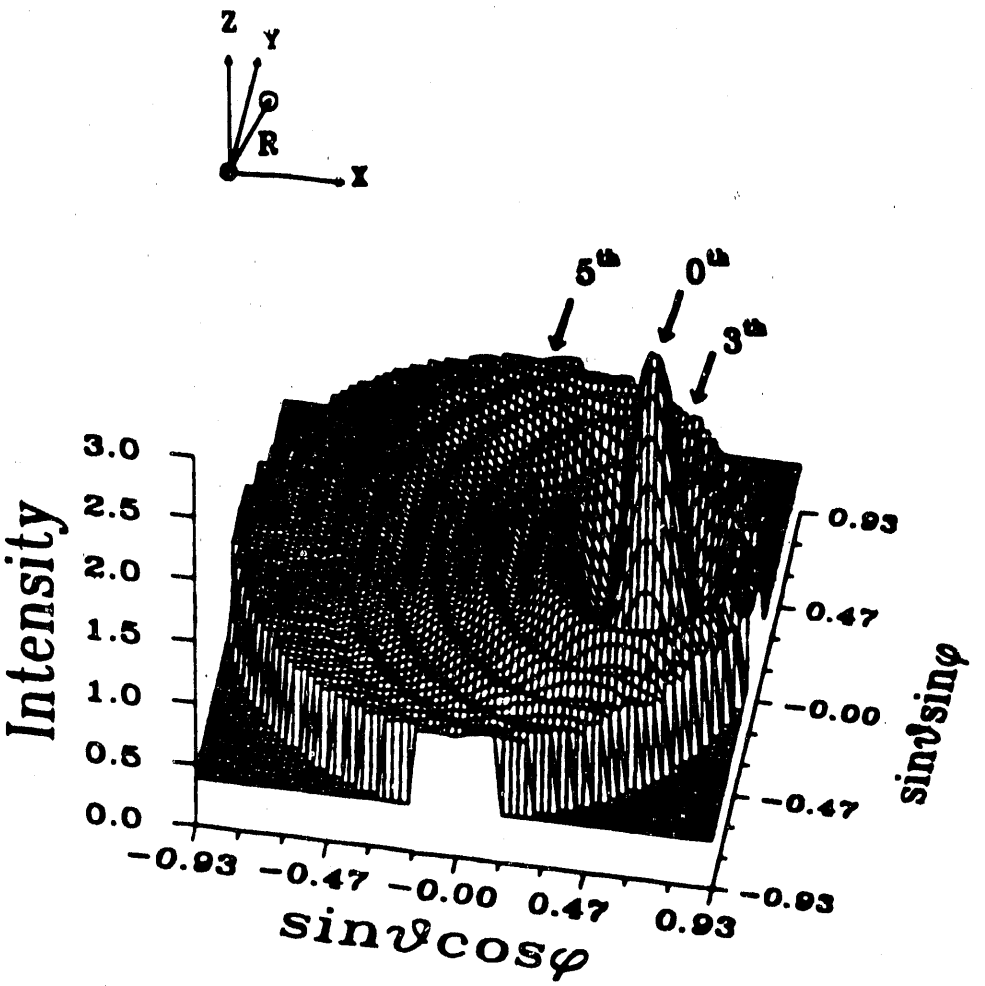

The result of scattering calculation from a chain of two atoms, which shows the zeroth-order forward-scattering along the atom chain ($\Theta = 35.3°, \Phi = 0°$) and the higher-order diffraction features around the chain. The electron energy used in the calculation is 914 eV and the distance between the atoms is 2.55$\AA$. The details of the calculation can be found in Ch. 3.

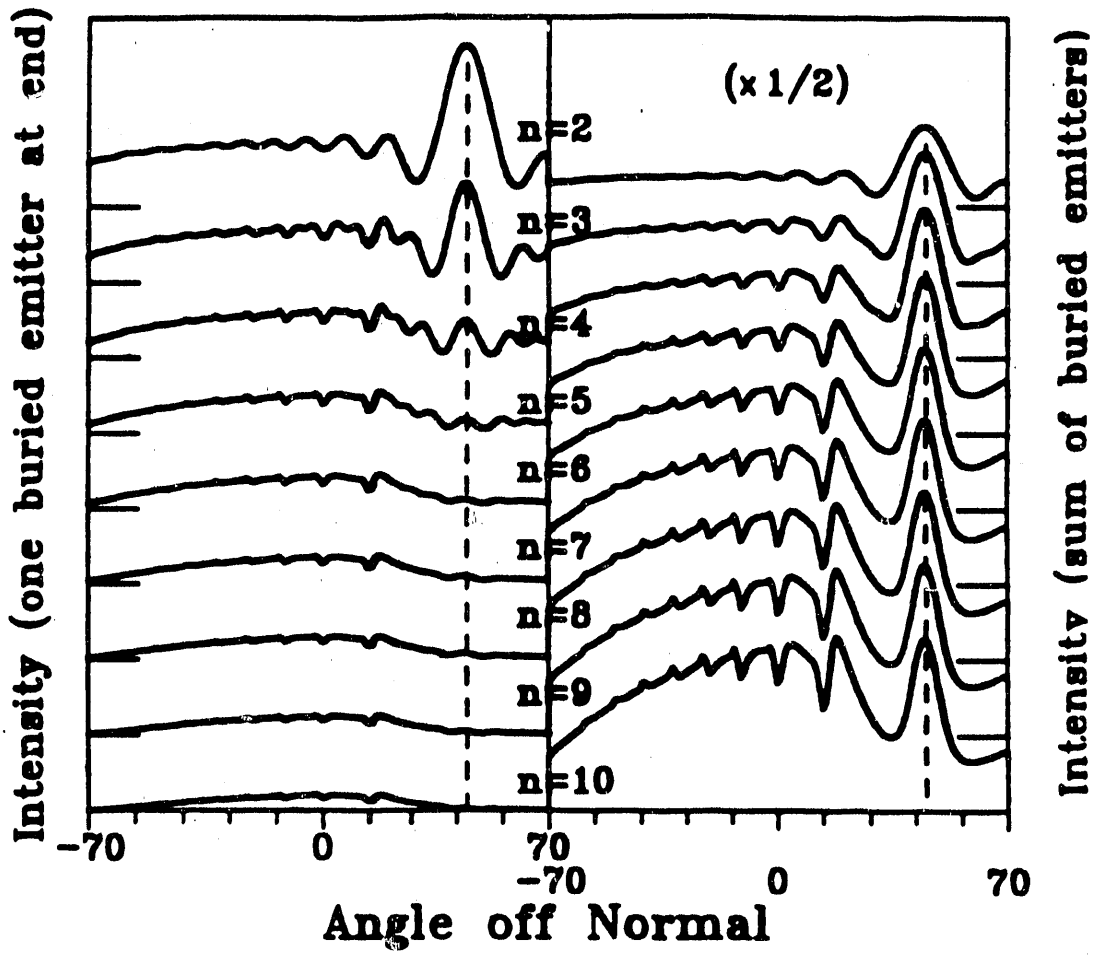

FIG 1

Tomasch & Han 91
TVBS-MSC

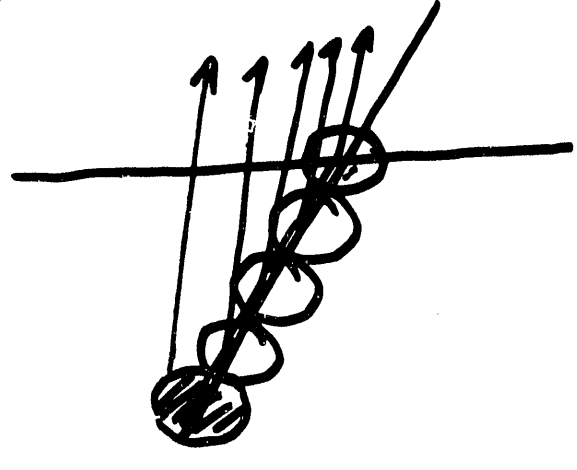

Short-Range
FS + "fringes"

Full Cluster MS

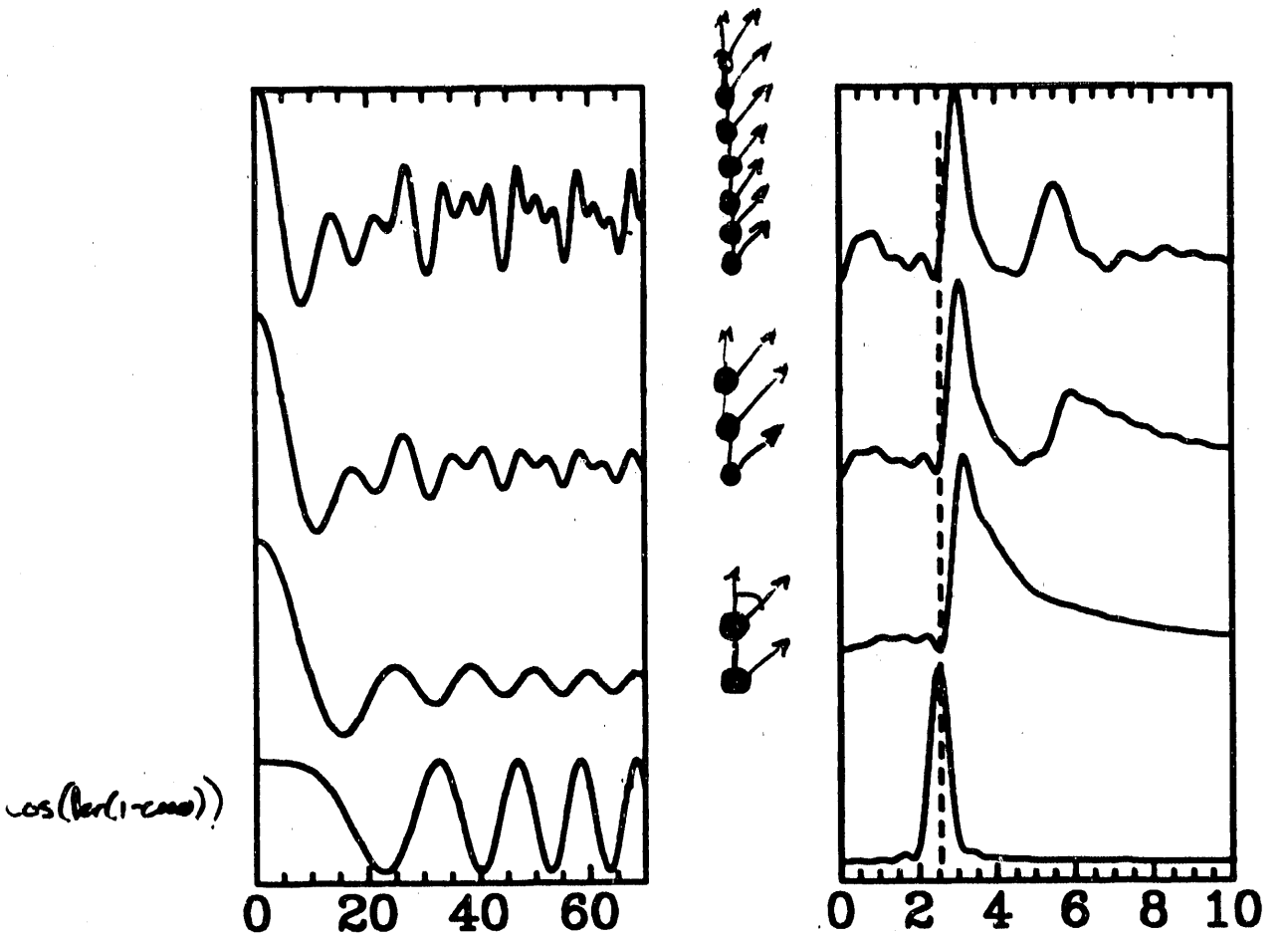

$\chi(\theta)$ F.T. $(\chi(\theta))$

$$\chi(\theta) = 2|F(\theta)| \cos(k r_j (1 - \cos\theta) + \psi(\theta_j))$$

↑ asymmetry ↑ shift

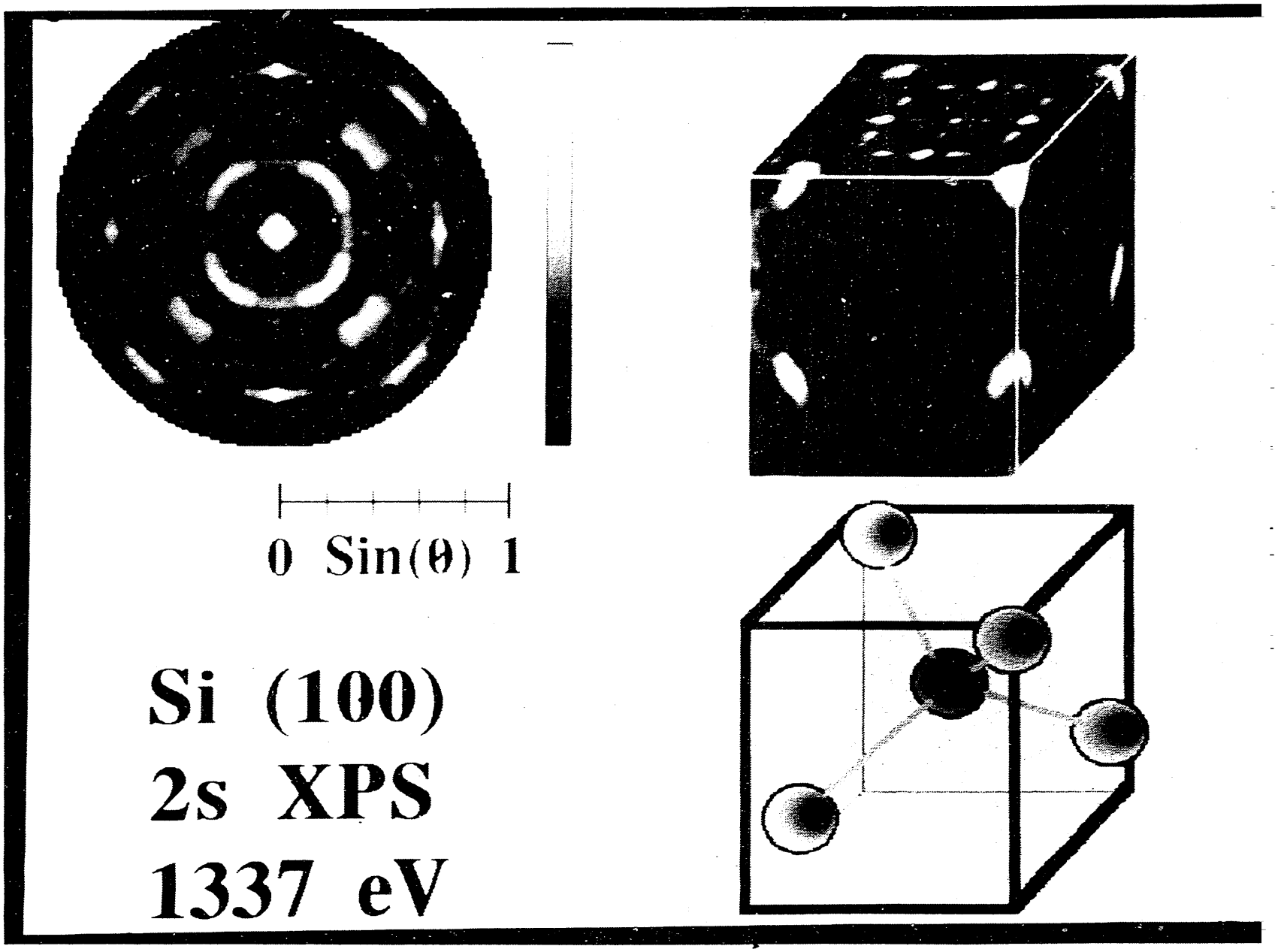
0 Sin(θ) 1
Si (100)
2s XPS
1337 eV

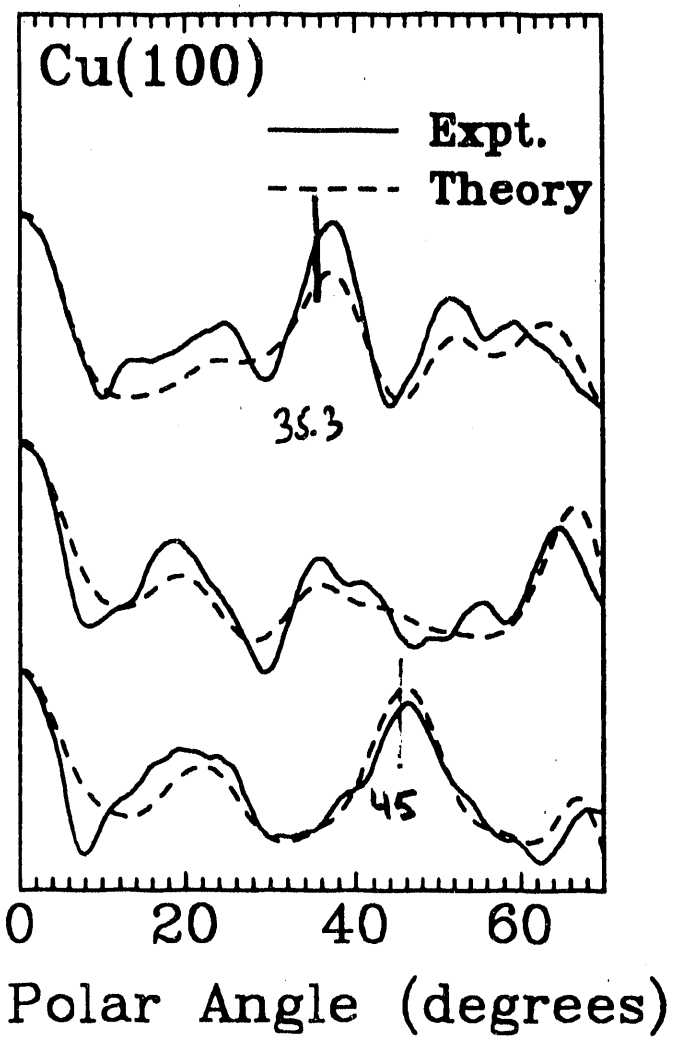
Cu(100)
Expt.
Theory
35.3
45
0
20
40
60
Polar Angle (degrees)

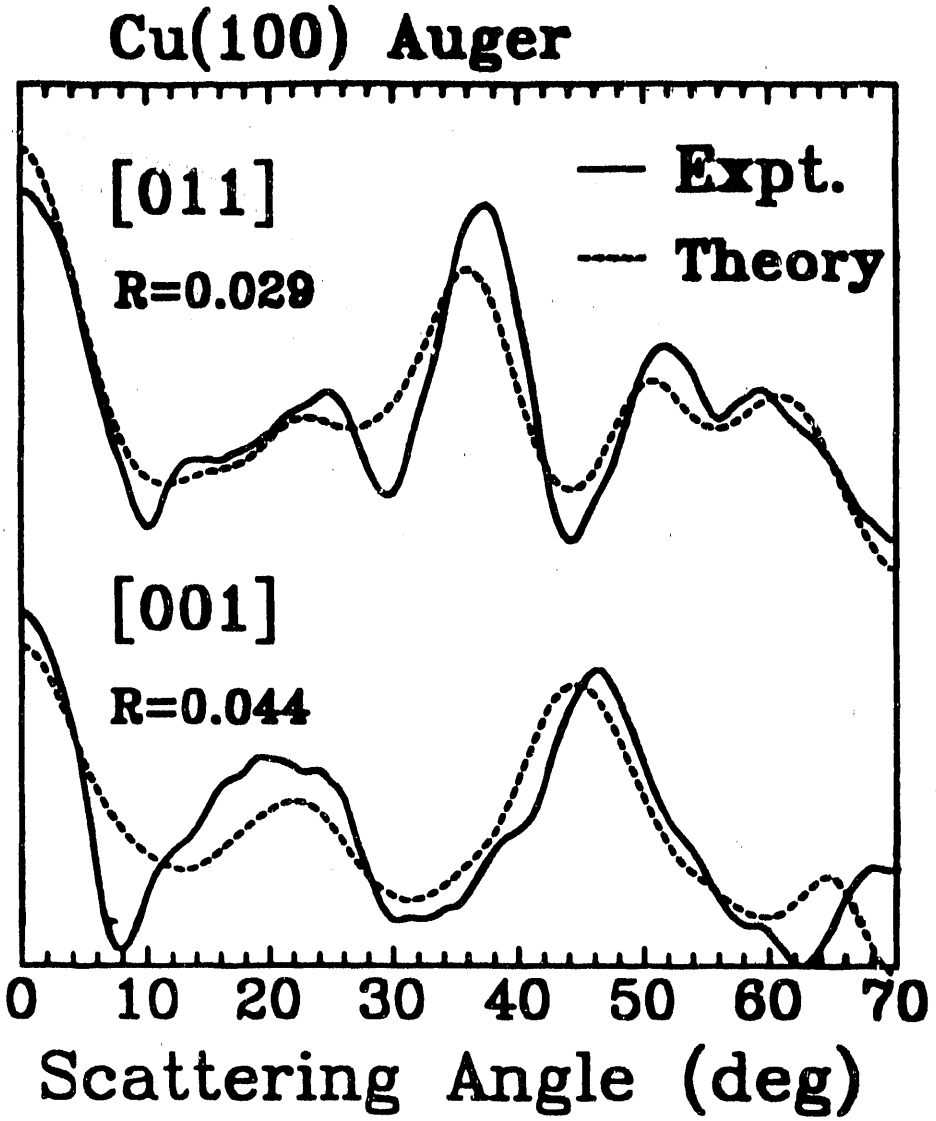
Cu(100) Auger
[011]
R=0.029
Expt.
Theory
[001]
R=0.044
0
10
20
30
40
50
60
70
Scattering Angle (deg)

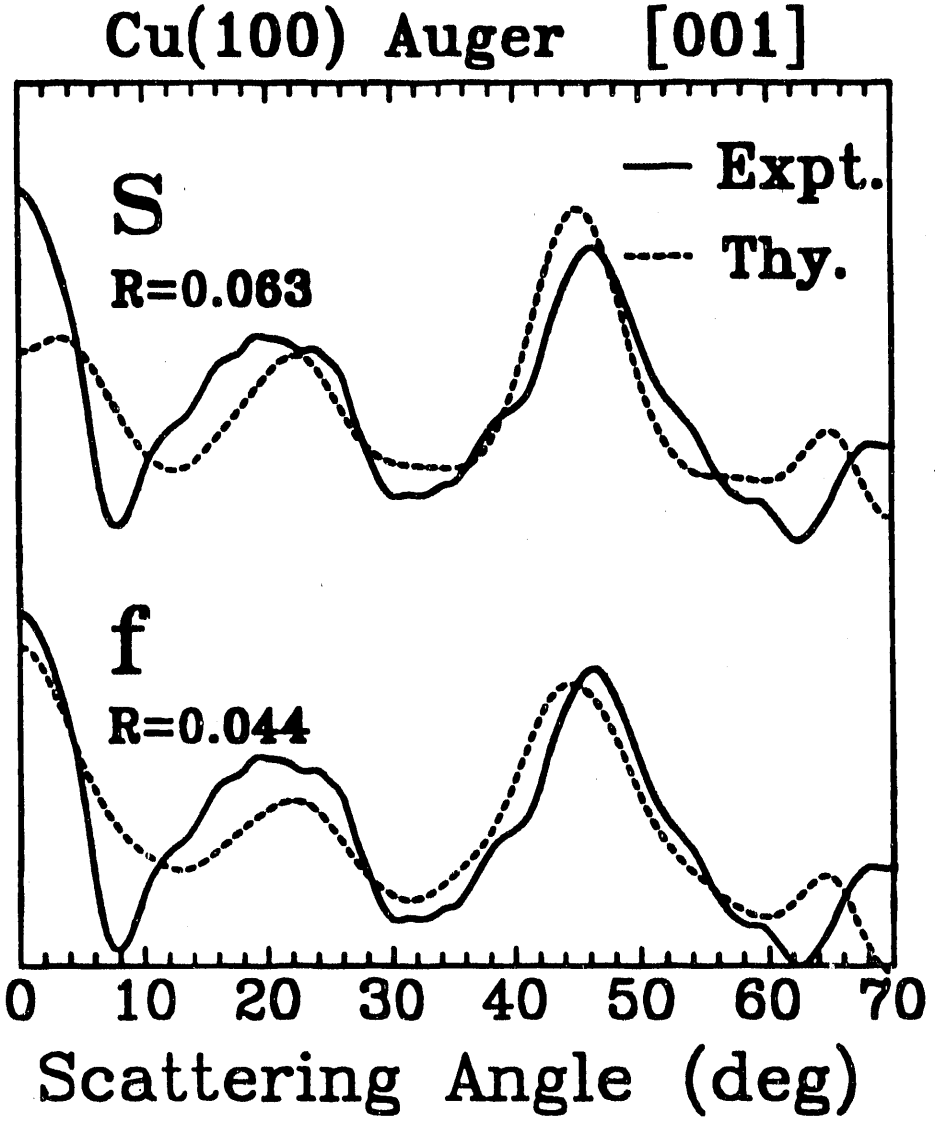
Cu(100) Auger [001]
S
R=0.063
— Expt.
---- Thy.
f
R=0.044
0 10 20 30 40 50 60 70
Scattering Angle (deg)

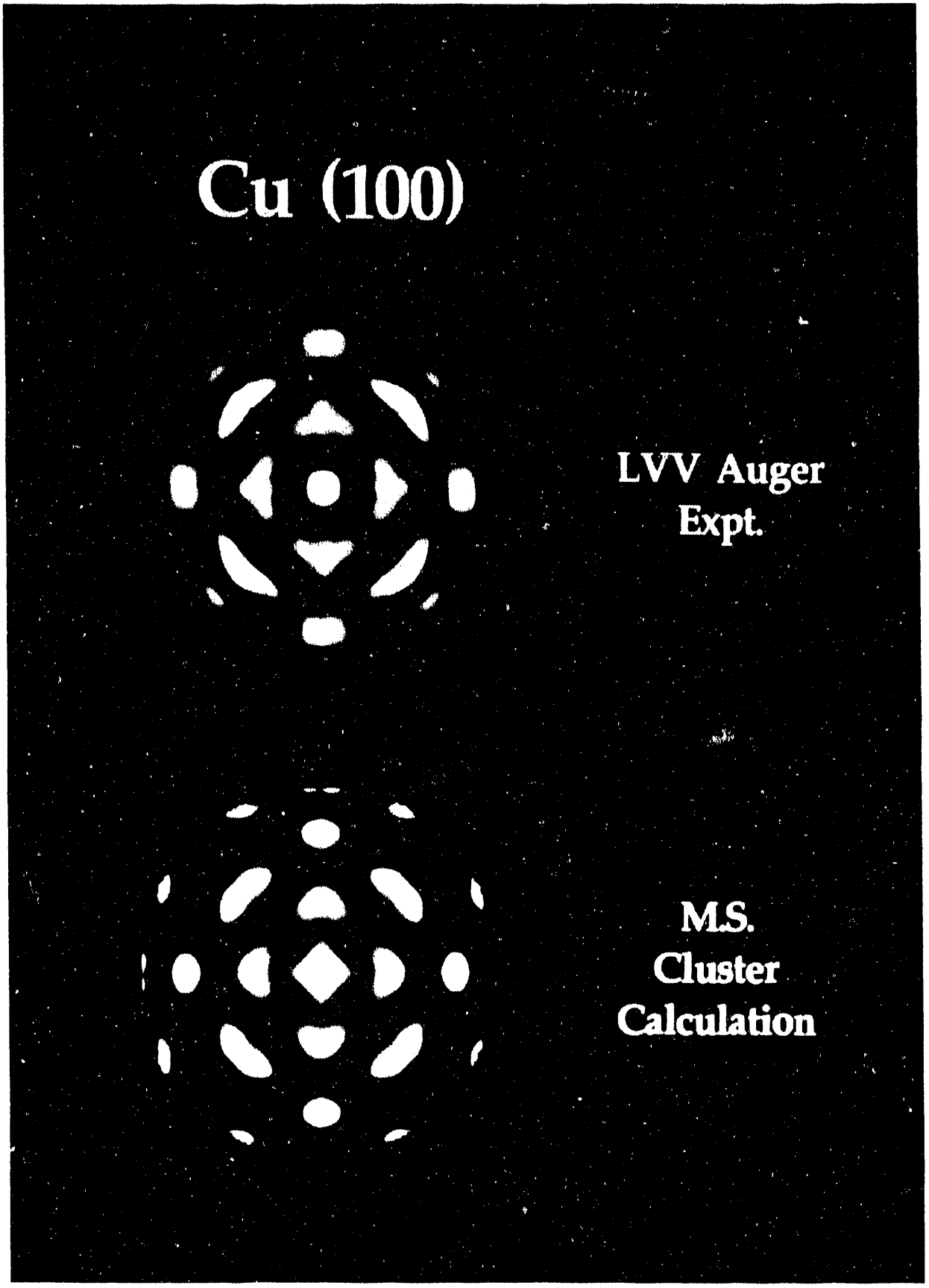
Cu (100)
LVV Auger
Expt.
M.S.
Cluster
Calculation

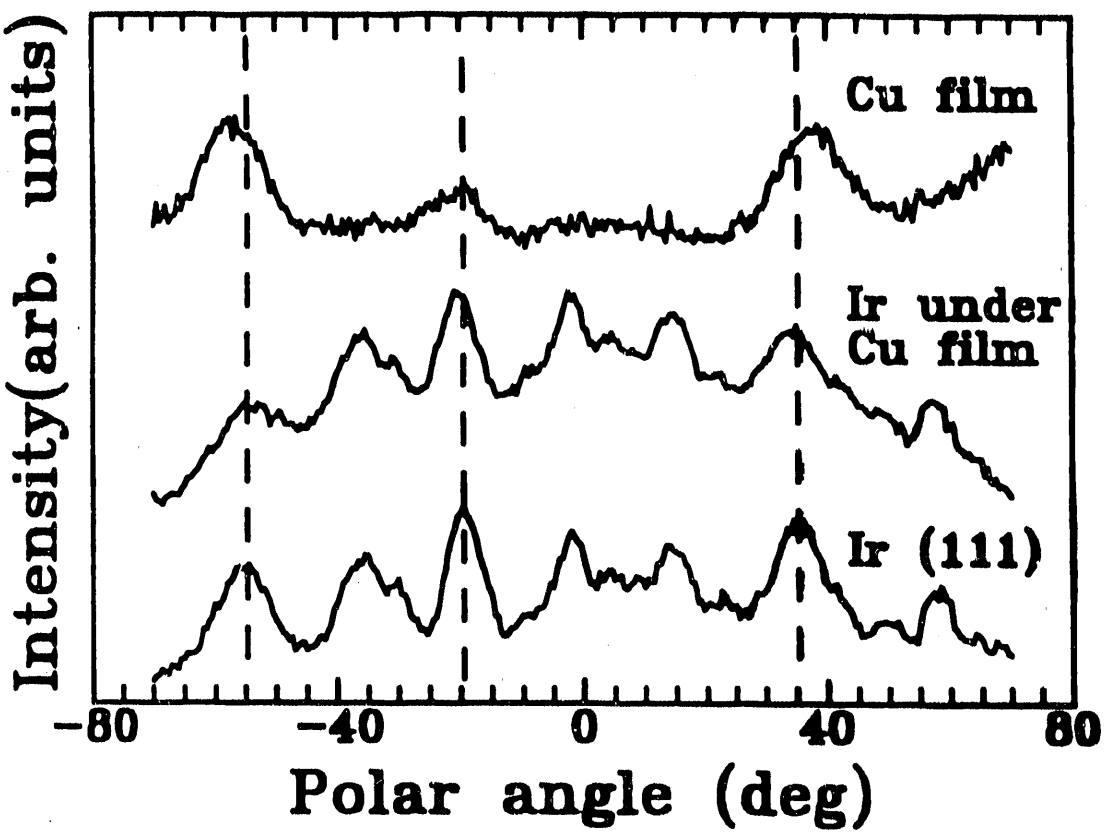
Cu film
Ir under
Cu film
Ir (111)
Intensity(arb. units)
-80
-40
0
40
80
Polar angle (deg)

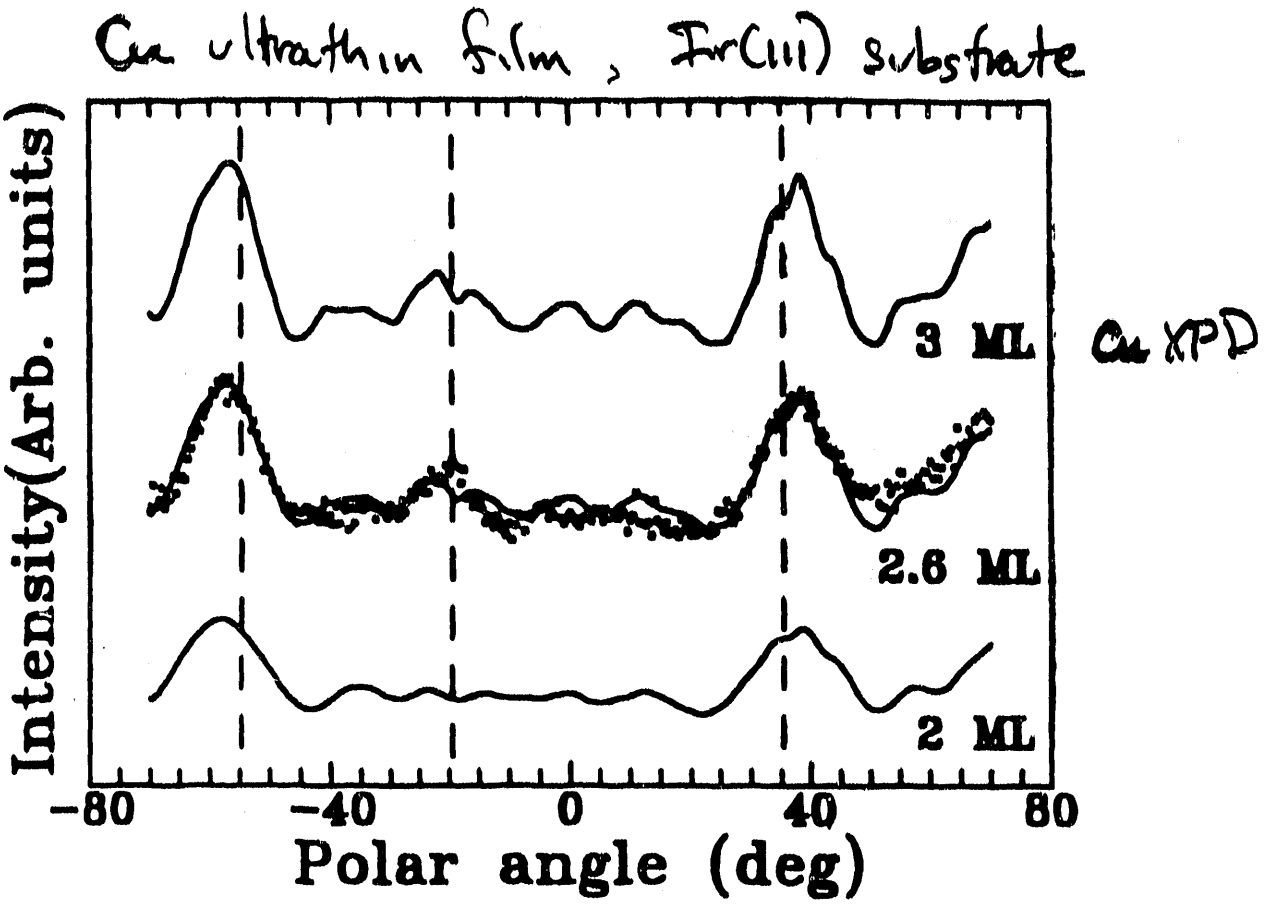
Cu ultrathin film, Ir(111) substrate
Intensity(Arb. units)
3 ML
2.6 ML
2 ML
Cu XPD
-80
-40
0
40
80
Polar angle (deg)

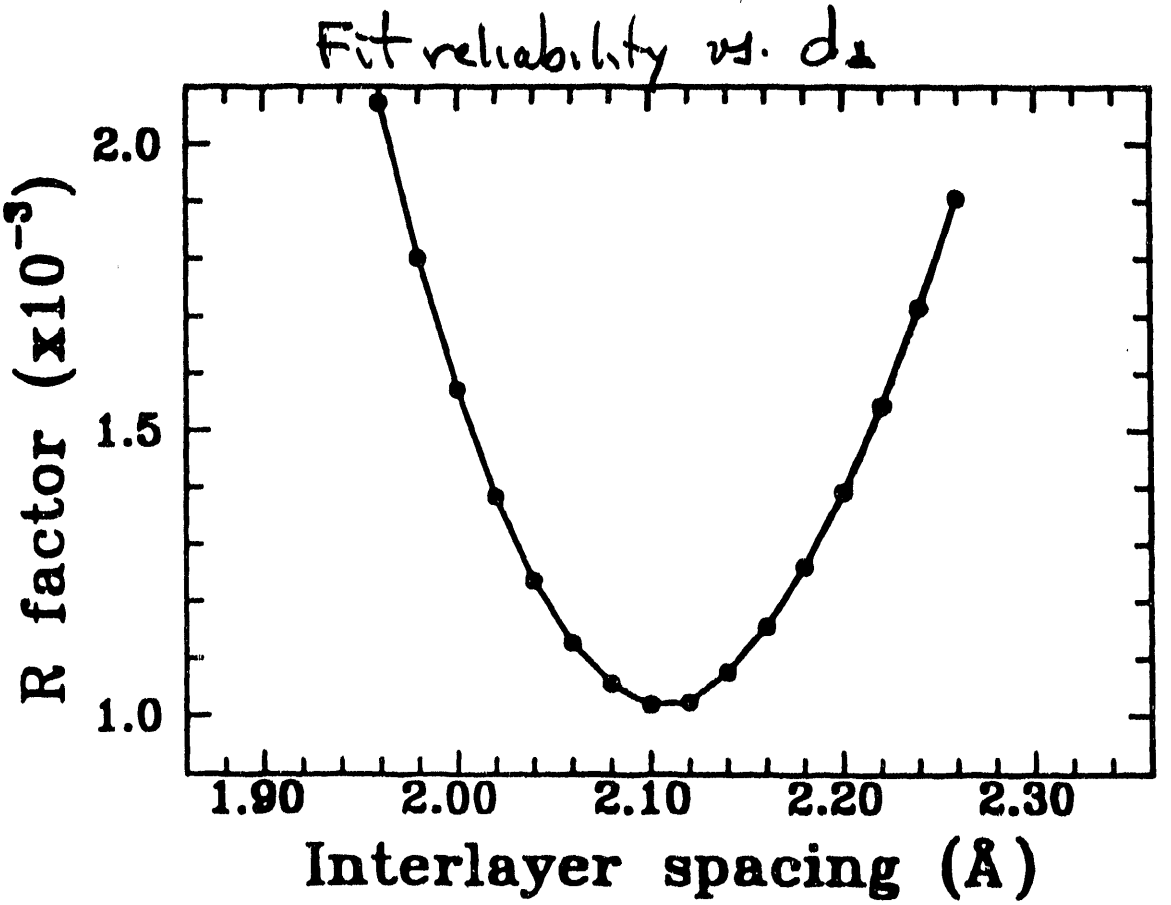
Fit reliability vs. d_1
R factor ($x10^{-3}$)
2.0
1.5
1.0
1.90
2.00
2.10
2.20
2.30
Interlayer spacing (Å)

High-resolution Photoelectron Holography

- High kinetic energy ($\approx 1keV$), $\lambda \leq 0.4\mathring{A}$.
- (Near) full hemispherical pattern.
- High angular resolution ($\approx 1^{o}$).
- Multiple energies (to suppress artifacts).
- Improved algorithms (Scattered-Wave Included F-T, SWIFT).

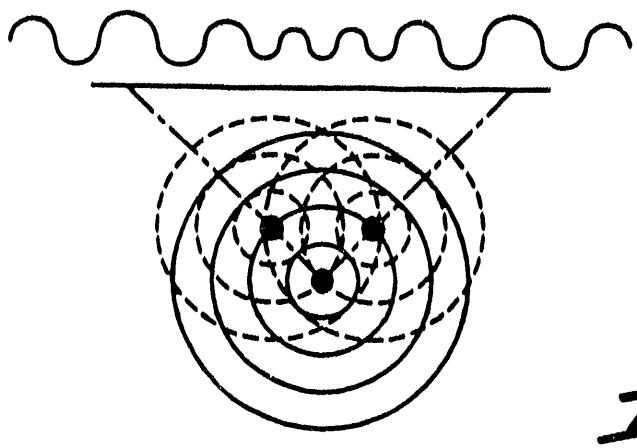

s-wave emitter,
s-wave scatterers

(a)

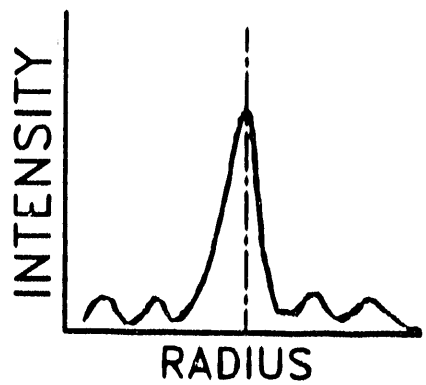

Scattered-Wave Included Fourier Transform

$$I(\vec{r}) = \int K(\vec{k}, \vec{r})\, \chi(\vec{k})\, d\vec{\sigma}$$

Derived from scattered wave

$$\psi_s(\vec{k}, \vec{r}_j) = F_k(\vec{r}_j)\, e^{i\vec{k}\cdot\vec{r}_j} e^{-i\vec{k}\cdot\vec{r}}$$

Deconvolution of Atomic Scattering Factor: Modified Fourier-transform Algorithm

$$\tilde{\phi}(\mathbf{r}) = \int \frac{1}{|f(\theta)|e^{i\psi(\theta)}} \chi(\hat{\mathbf{K}})\, e^{i\mathbf{K}\cdot\mathbf{R}} d\Omega. \qquad (10)$$

- Deconvolving only the phase removes some of the atom-shift, but leaves a large anisotropy in the atom-image intensity.
- Deconvolving both the phase and the amplitude corrects for both the atom-shift and the asymmetry, but increase the twin-image amplitude (a lot).

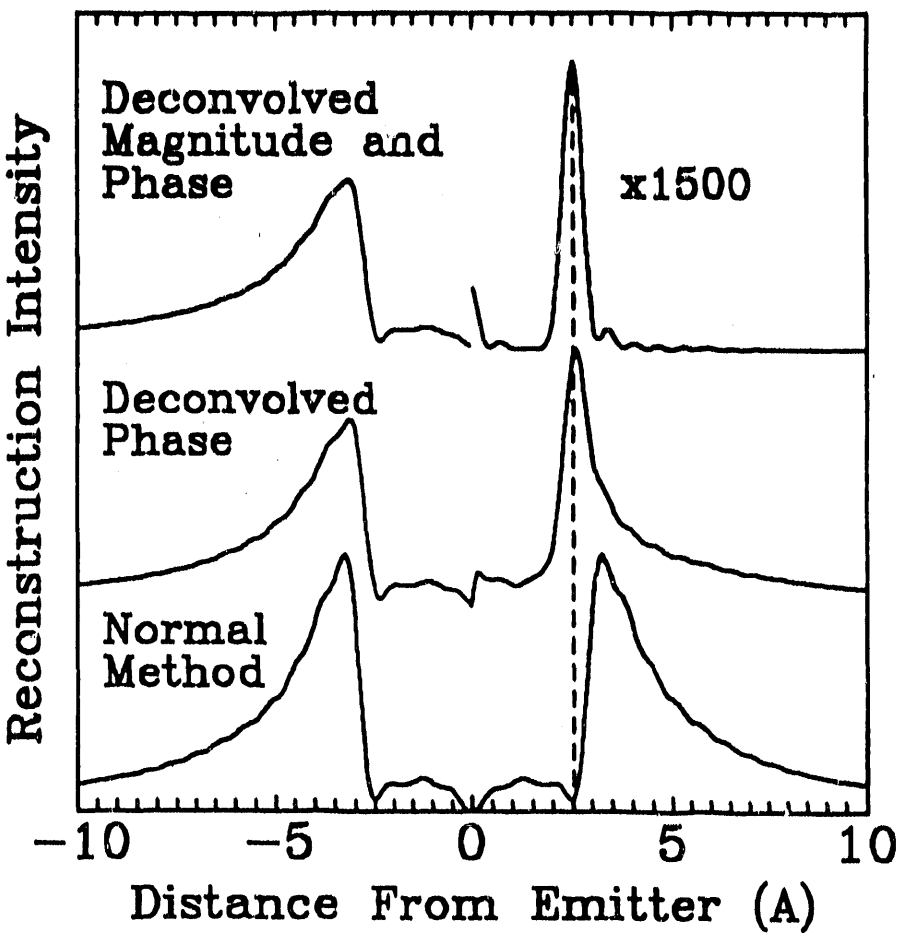

$\frac{\chi}{|f|e^{i\psi}}e^{i\vec{K}\cdot\vec{R}}$

$\frac{\chi}{e^{i\psi}}e^{i\vec{K}\cdot\vec{R}}$

$\chi e^{i\vec{K}\cdot\vec{R}}$

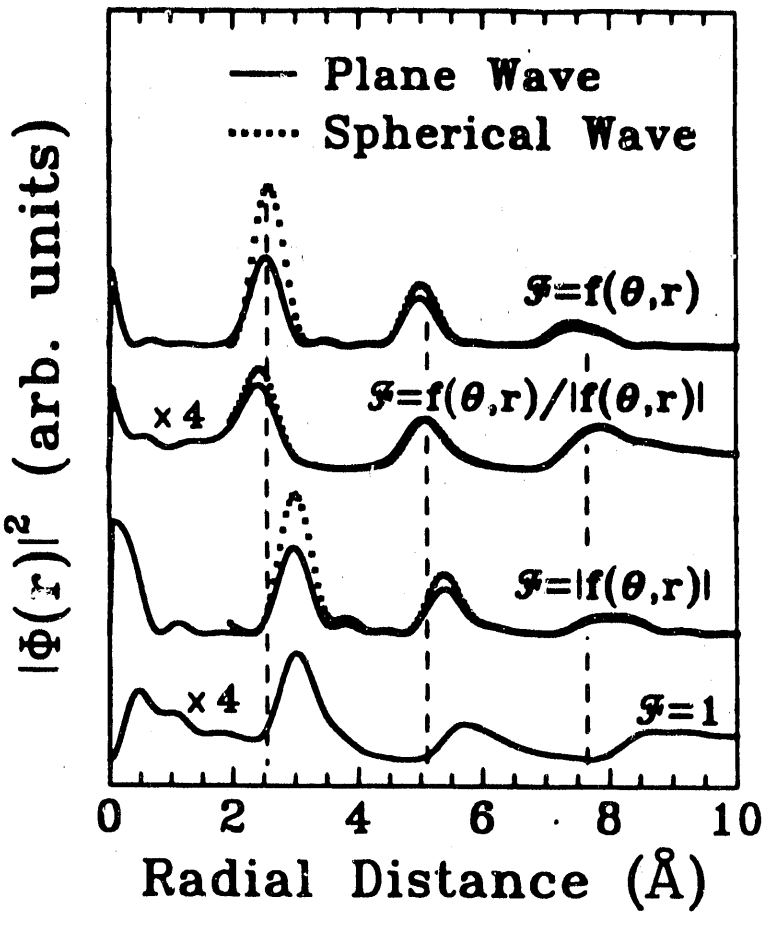

$$\Phi(\vec{r}) = \int \frac{\chi(\vec{k})}{\mathcal{F}(\vec{k},\vec{r})} e^{i\vec{k}\cdot\vec{r}}\, d\vec{k}$$

① Direct method
(no prior knowledge)

② Handles SW corrections
(r dependent $\mathcal{F}$)

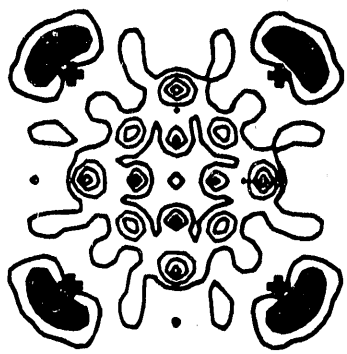

$$\int \chi(k)\, e^{i\vec{k}\cdot\vec{r}}\, d\vec{k}$$

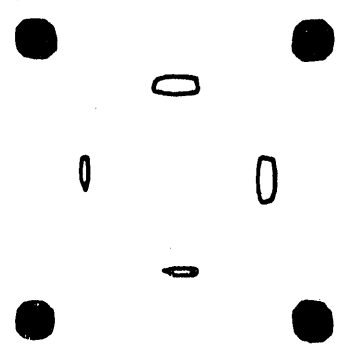

Deconvolution

$$\int \frac{\chi(k)}{\tilde{\rho}(k,r)}\, e^{i\vec{k}\cdot\vec{r}}\, d\vec{k}$$

Cu(100) bi-layer
Calculation

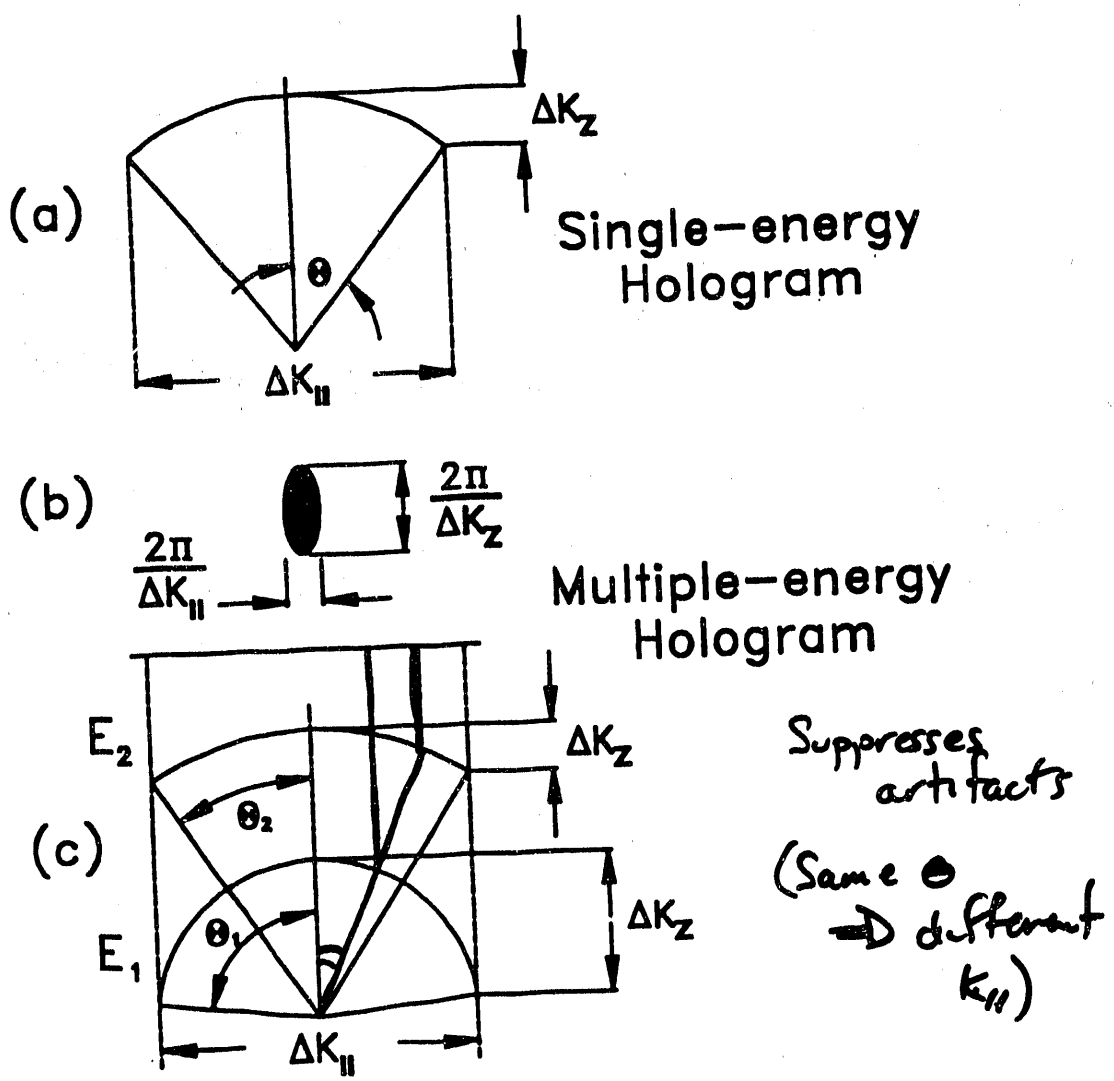
(a)
ΔK_z
Single–energy Hologram
θ
ΔK_{II}
(b)
$\frac{2\pi}{\Delta K_z}$
$\frac{2\pi}{\Delta K_{II}}$
Multiple–energy Hologram
E_2
ΔK_z
θ_2
(c)
ΔK_z
θ_1
E_1
ΔK_{II}
Suppresses artifacts
(Same θ ⇒ different k_{II})

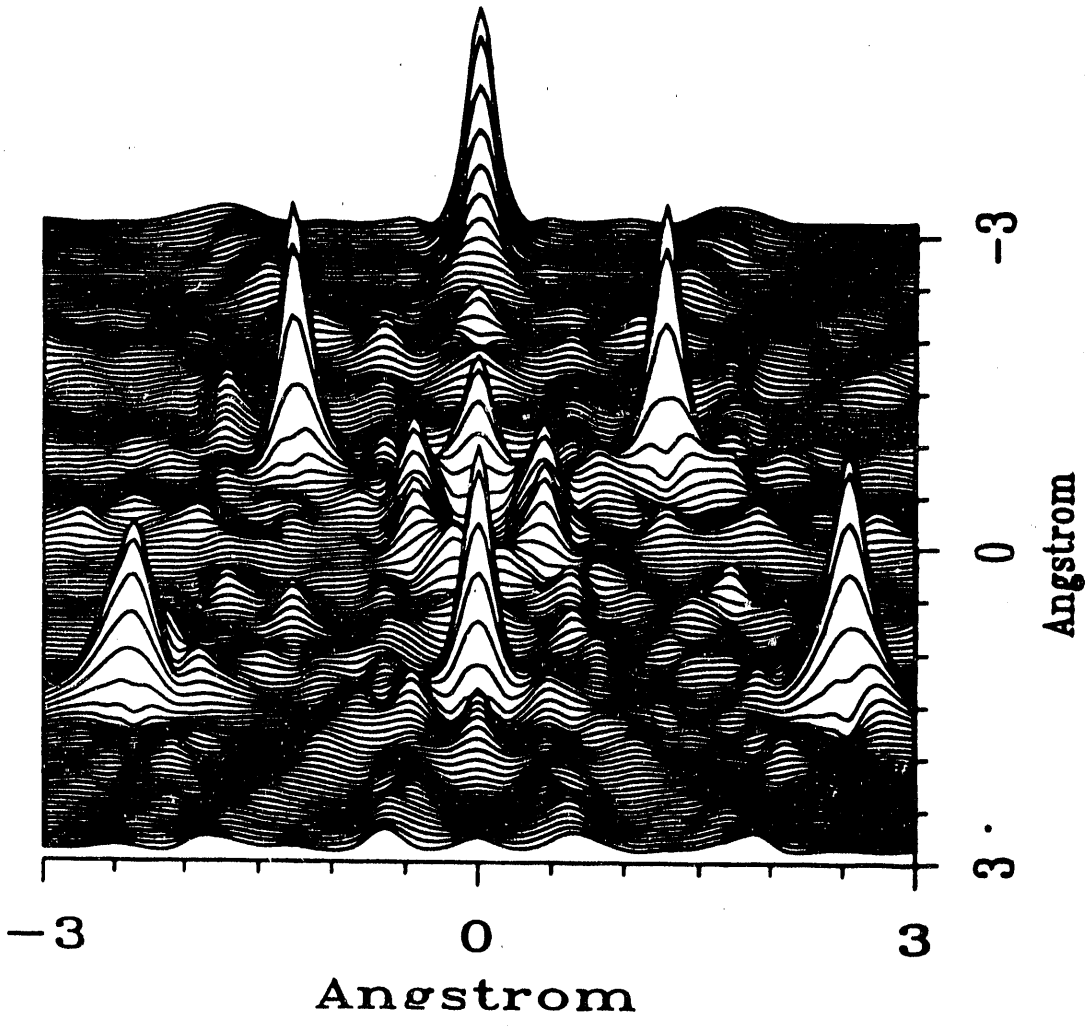

Ce(111) bi-layer
calculation
Deconvolution Image

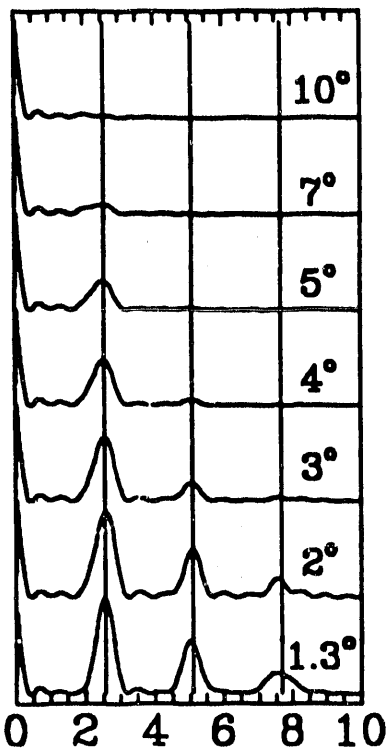

Reconstruction as Function of Angular Resolution

128 x 128 pts.

Photoemission Holography: Large distances require high angular resolution.

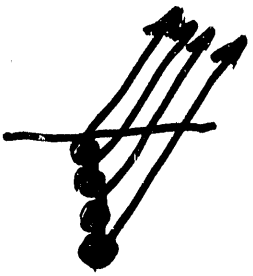

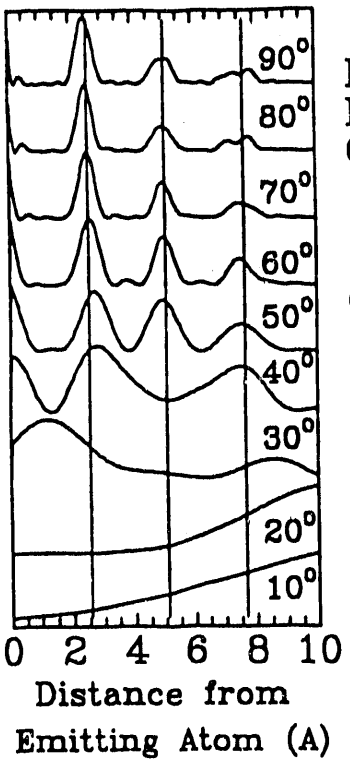

Reconstruction as Function of Collection Angle

914 (eV)

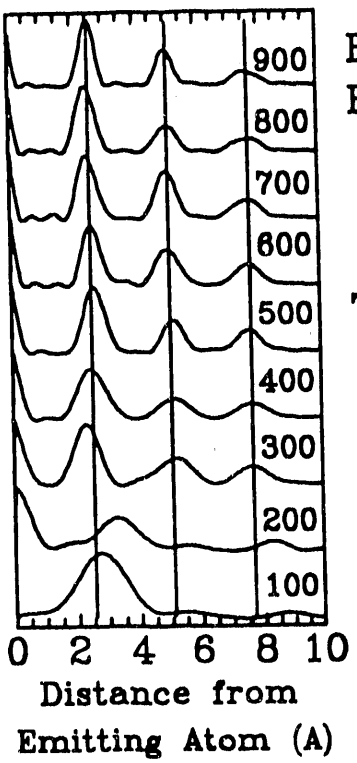

Reconstruction as Function of K.E. (eV)

70° Collection Angle

Photoemission Diffraction and Holographic Imaging

Characteristics:

- Chemical-state specific
- Surface and sub-surface atoms
- 3D atomic coordination and sites by holographic reconstruction
- Below 0.05 Angstrom accuracy with structure refinement (modelling)

Developments:

- Need high flux/small bandwidth radiation in 100-1500 eV range
- Need more efficient detectors

* Combine with SPEM

Needs for Next-generation X-ray Photoelectron Diffraction

Energy resolution of 0.1 eV	**Chemical state**
Photon energy range to 1000 eV	**Multi-energy holography**
Angular resolution of 0.1 degree	**Resolve high-frequency fringes**
Angular range of 2-pi steradian	**High accuracy in hologram**
Small spot size (few micron or less)	**Isolate small chemical domains**
High count rates	**Reduce sample exposure**

Some Aspects of X-Ray and Electron Holography

A. Szoke

Lawrence Livermore National Laboratory

SOME ASPECTS OF X-RAY AND ELECTRON HOLOGRAPHY.

ABRAHAM SZOKE

LAWRENCE LIVERMORE NATIONAL LABORATORY
AND
ROWLAND INSTITUTE FOR SCIENCE.

I./ A short historical overview.
II./ Some thoughts on the reconstruction of holograms.

A VERY SHORT HISTORICAL NOTE. (1)

HOLOGRAPHY. Gábor invented it before there were lasers.

1./ Coherent superposition of wavefronts has (most of) the missing information.
2./ Illumination with the reference beam reconstructs the object by "deconvolution".

Problems: Ordinary sources have short coherence length.
Fringes are small, of the order of λ.
Limited magnification, accompanied by distortion.

PHOTOELECTRON DIFFRACTION. Liebsch, 1974.

He realized that the first (odd) order scattering of a photoelectron contains information about the emitting atom's environment.

(Even order scattering that interferes with the photoemission produces EXAFS.)

MORE HISTORICAL NOTES. (2)

HOLOGRAPHY WITH A LOCAL REFERENCE BEAM. Szöke, 1975, 1985.

1./ The emission of a characteristic X-ray, or a potoelectron, or an Auger electron can serve as a reference beam in holography.
2./ The elastically scattered waves from neighboring objects interfere to give a hologram.

This method corrects Gábor's problems and has some more advantages.
The objects are close, no long coherence length needed.
The recorded interference fringes are large, $>>\lambda$.
Great magnification is inherent in the process.
Many similar objects, similarly oriented, (but not necessarily ordered in space) give a single hologram.

MORE HISTORICAL NOTES (3)

Methods of producing holograms (From Szöke, 1985)

	RECORDING MEDIUM	
	X-rays	electrons
Local source	Characteristic radiation	Photoelectron or Auger electron diffraction.
Scattering form a disordered array of references.	Diffuse X-ray scattering.	Diffuse LEEDS.

NEW IDEAS AND METHODS.

Explicit formulas for the reconstruction of a hologram.
(J. J. Barton, 1988)
Electrons backscattered from the lattice acting as reference.
(B. Tonner, et al., 1989)

RECONSTRUCTION OF HOLOGRAMS AND MULTIPLE SCATTERING. (1)

With acknowledgement to the work of Barton, Tong, Rehr.

1./ Single scattering, general (angle dependent, complex) scattering amplitude. We will follow Barton's derivation.

The "useful" part of the hologram is

$$\chi(\theta) = \frac{\exp(ikR)}{4\pi R} \{f_o(\theta) + \sum_n f_n(\theta)\exp[-ikr_n(1-\cos\theta)]\}$$

Using the Helmholtz - Kirchhoff intergal theorem, we get

$$U(r) = \frac{1}{2\pi R^2} \sum_n \int_S \{[f_o^*(\theta)f_n(\theta)\exp(ikr_n - ik.r_n) + cc.] \exp(-ik.r)\}$$

The reconstructed object will in general be of weird shape. If the angular dependence of $f_n(\theta)$ is known, the hologram can be corrected by multiplying it with $1/f_n(\theta)$. (This is my interpretation of the proposal by Barton and by Tong.)

An alternative interpretation is a two step process. In the first step the weird shape is reproduced, in the second the result is interpreted as a superposition of known weird shapes.

RECONSTRUCTION OF HOLOGRAMS AND MULTIPLE SCATTERING. (2)

2./ Multiple scattering, general considerations.

The propagation of the electron, or the X-ray in the medium can be described by an integral equation.
In X-ray diffraction it is called the dynamical theory. (Darwin, Ewald, Laue, beginning cca. 1915.)
In quantum mechanics it is called the Lippmann - Schwinger equation.
For discrete scatterers the integral reduces to a sum.

3./ Multiple scattering, isotropic (s-wave) point scatterers.

The Green's function for the propagation of the electron is

$$G(\mathbf{R},0;E) = \frac{\exp(ikR)}{4\pi R} + \sum_{n\neq 0} \frac{\exp(ik|\mathbf{R}-\mathbf{r}_n|)}{4\pi R} V_n \frac{\exp(ik|\mathbf{r}_n|)}{4\pi|\mathbf{r}_n|}$$

$$+ \sum_{n\neq m \; m\neq 0} \frac{\exp(ik|\mathbf{R}-\mathbf{r}_n|)}{4\pi R} V_n \frac{\exp(ik|\mathbf{r}_n-\mathbf{r}_m|)}{4\pi|\mathbf{r}_n-\mathbf{r}_m|} V_m \frac{\exp(ik|\mathbf{r}_m|)}{4\pi|\mathbf{r}_m|} + \ldots$$

The series can be resummed by singling out the last scatterer

$$G(\mathbf{R},0;E) = \frac{\exp(ikR)}{4\pi R}\left[1+\sum_{n\neq 0}\frac{\exp(-ik|r_n|)}{4\pi|r_n|}V_n\frac{\exp(ik|r_n|)}{4\pi|r_n|} + \sum_{n\neq m\neq 0}\frac{\exp(-ik|r_n|)}{4\pi|r_n|}V_n\frac{\exp(ik|r_n-r_m|)}{4\pi|r_n-r_m|}V_m\frac{\exp(ik|r_m|)}{4\pi|r_m|}+\ldots\right]$$

$$+\sum_{n\neq 0}\frac{\exp(ik|\mathbf{R}-r_n|)}{4\pi R}V_n\left[\frac{\exp(ik|r_n|)}{4\pi|r_n|}+\sum_{m\neq n\ m\neq 0}\frac{\exp(ik|r_n-r_m|)}{4\pi|r_n-r_m|}V_m\frac{\exp(ik|r_m|)}{4\pi|r_m|}+\ldots\right]$$

The general form of the series is the same as for single scattering

$$G(\mathbf{R},0;E) = \frac{\exp(ikR)}{4\pi R}\{f_o(\theta) + \sum_n f_n(\theta)\exp[-ikr_n(1-\cos\theta)]\}$$

The first term, $f_o(\theta)$, is the angle, and energy dependent factor for EXAFS. The second term changes the phase, and intensity of atom n in its reconstruction, but it does not move its position.

This is the "theory of fog". The first layer of scatterers is seen clearly, the images of the deeper layers are attenuated severely even if there are no losses.

RECONSTRUCTION OF HOLOGRAMS AND MULTIPLE SCATTERING. (4)

4./ Discrete scatterers, but general scattering.

Rehr has derived a formula that treats this case. It is also similar in form to the single scattering case, but both $f_0(\theta)$ and $f_n(\theta)$ depend strongly on the scattering by the other atoms.

The only real hope I have that an iterative algorithm will converge to the correct solution.

Recent work by Barton and by Tong propose to use holograms at various electron energies to arrive at better estimates. These can also be used the same way.

From Photoelectron Diffraction to Surface Crystallography

J.J. Barton

IBM T.J. Watson Research Center

c(2x2)S/Ni(001)

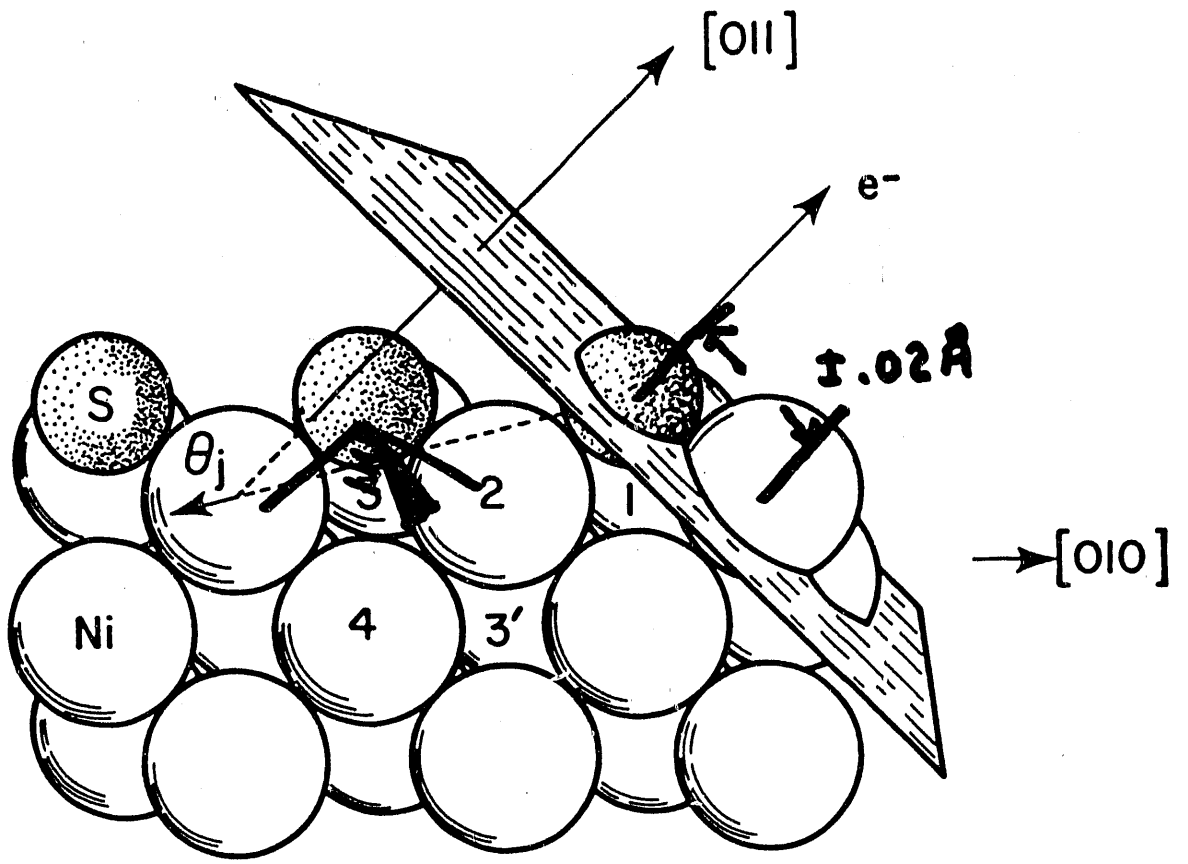

XBL 853-8008

Surface Structure:

Site : Direct

Bond Length: Accurate.

From Photoelectron Diffraction To Surface Crystallography

Point-Source Electron Diffraction

- **Geometrical Phase Terms.**
- **Direct crystallography.**

Experimental Design

- **2D angles + 1D wavenumber.**
- **Medium Energies.**

Will It Work?

- **The Problem of the Auger Holes**
- **Multiple Scattering w/o Partial Waves**

w/ Lou Terminello, LLNL

Role Of Photons

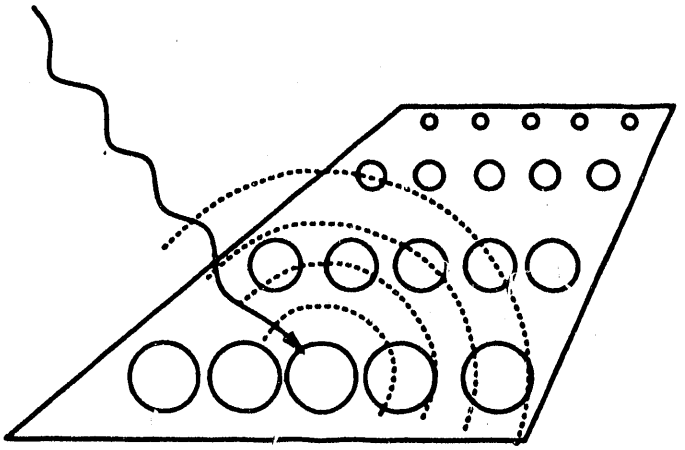

One Photon,
One Atom,
One Photoelectron.

Photon Coherence Not Relevant.

Photons Select Source Atoms.

Resolution Determines Averaging.

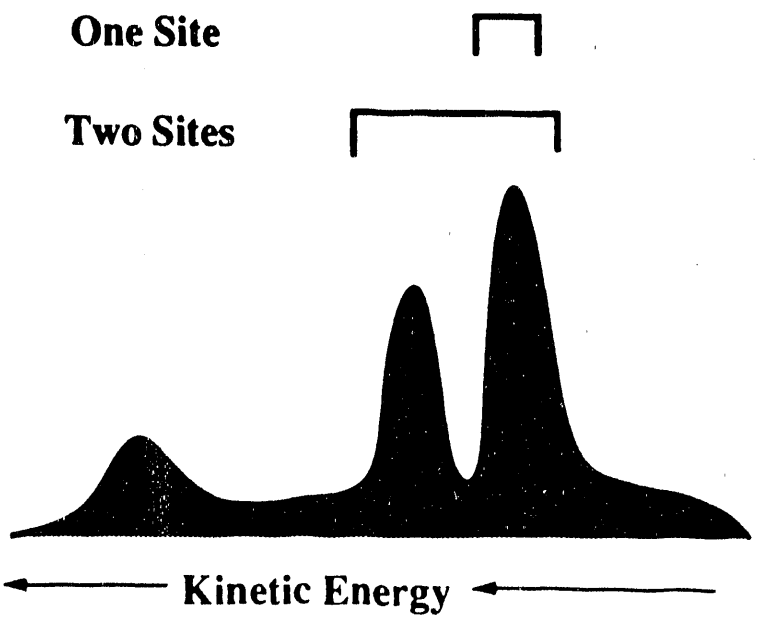

Surface Site Crystallography

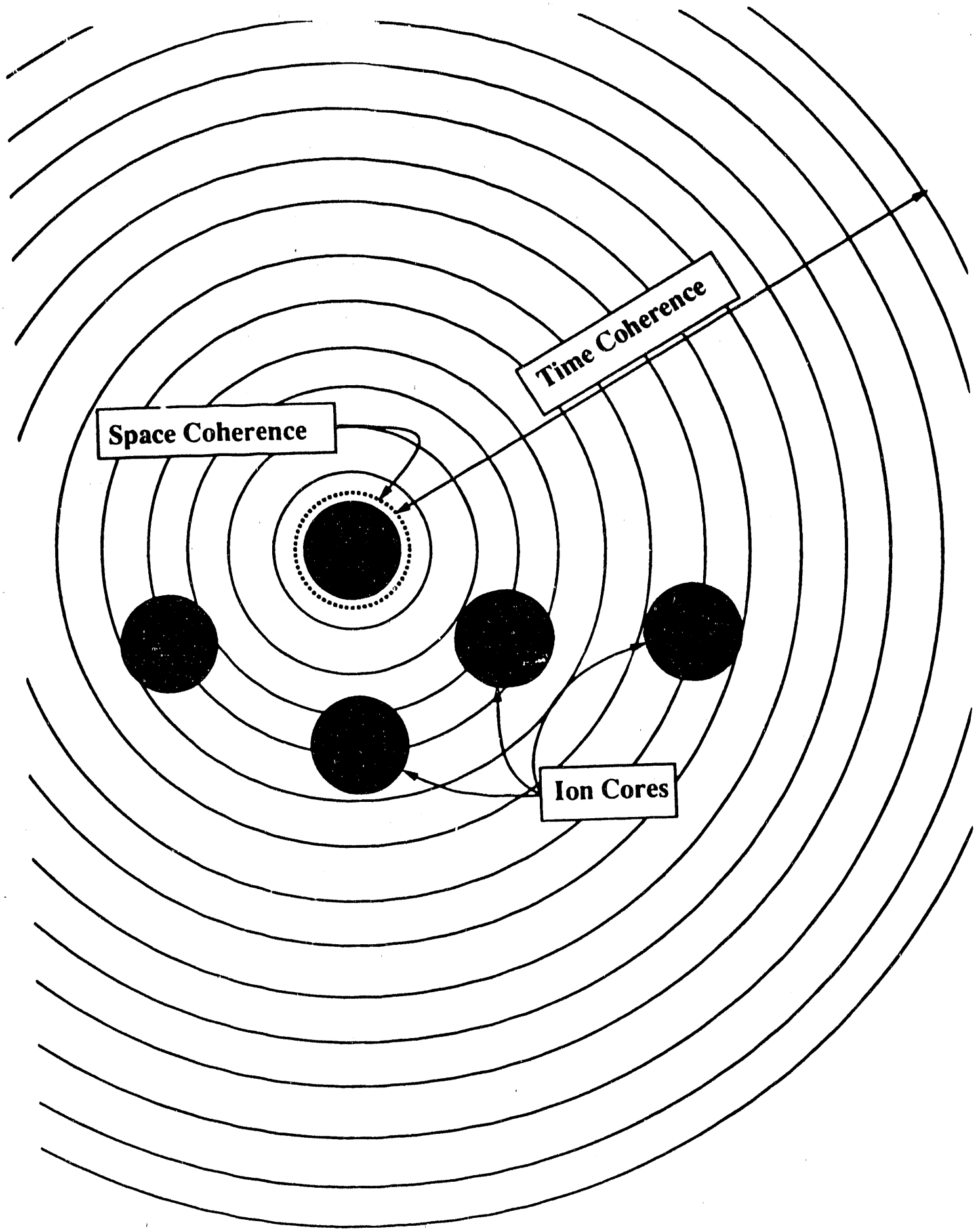
Time Coherence
Space Coherence
Ion Cores

Interference Oscillations

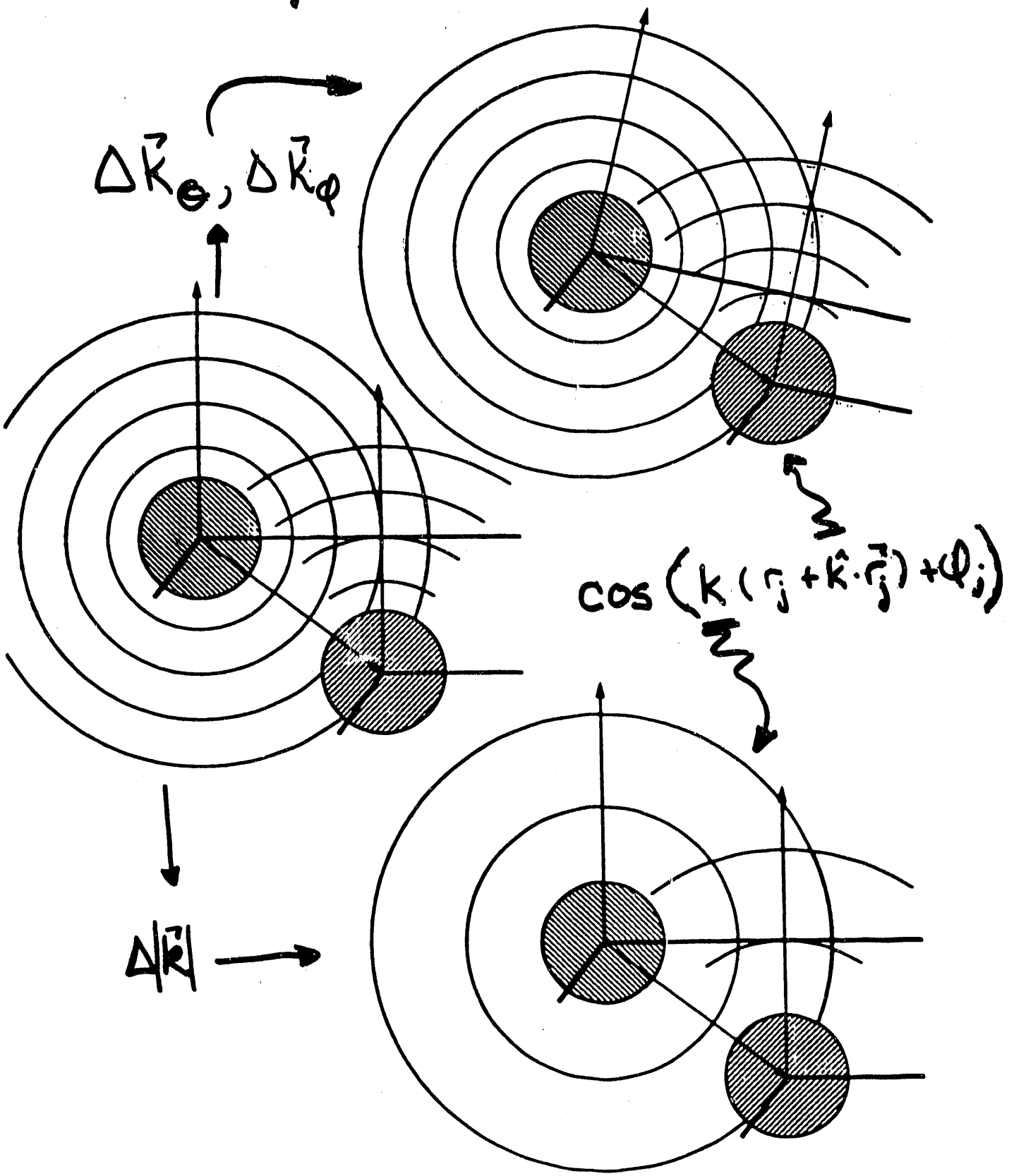

Scattering Factor Methods.

Separate Geometry from Potential

↓ Phase ↓ Amp.

Plane wave approx. $\tilde{F} \rightarrow f(\theta)$

C. Fadley.

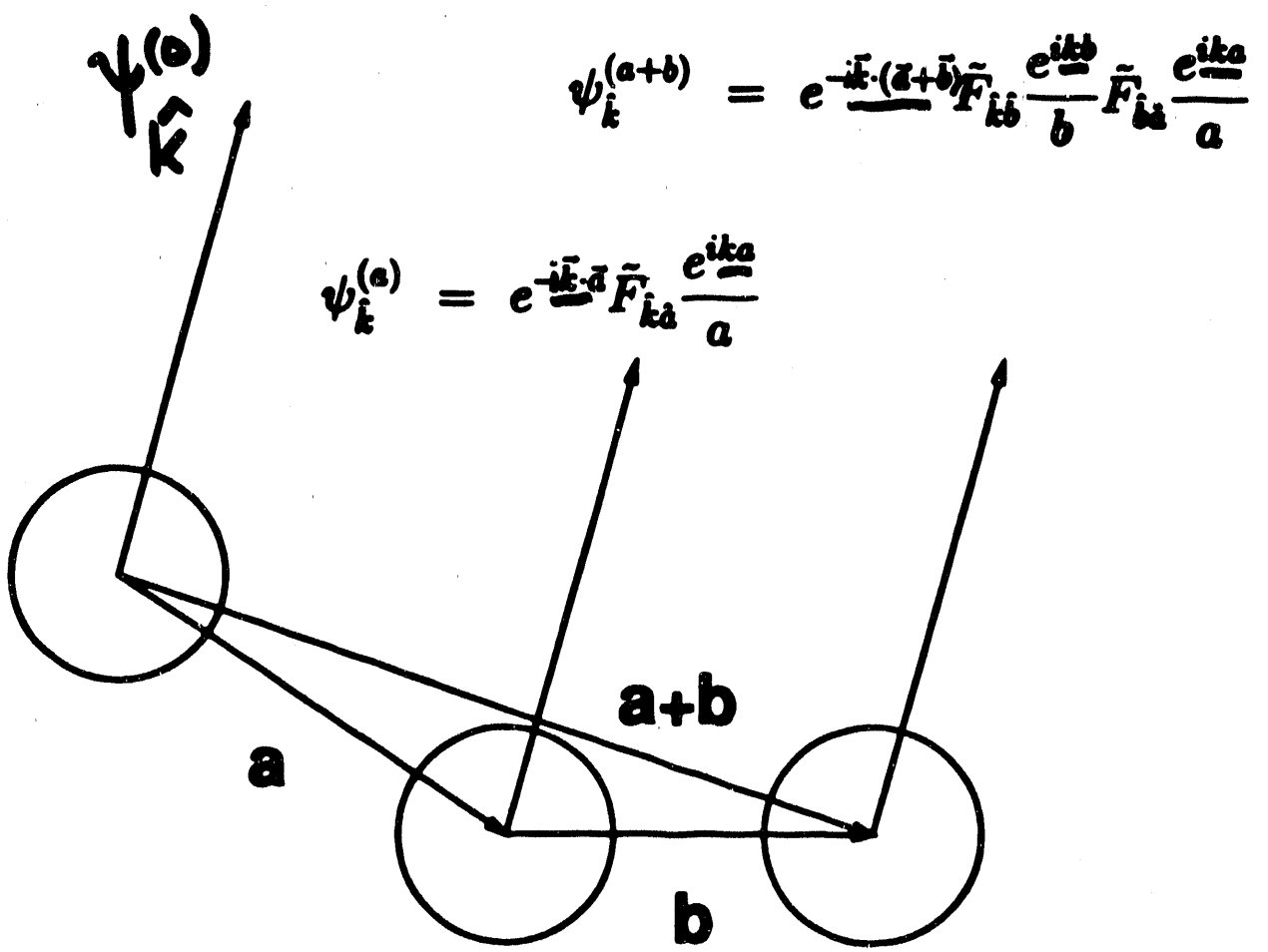

Geometrical Phase Terms

$$I(\vec{k}) = \Psi_{\vec{k}}^{*}\Psi_{\vec{k}}$$

$$\Psi_{\vec{k}} = \psi_{\vec{k}}^{(0)} + \sum_{a}\psi_{\vec{k}}^{(\vec{a})} + \sum_{a}\sum_{b}\psi_{\vec{k}}^{(\vec{a}+\vec{b})} + \ldots$$

$$I(\vec{k}) = |\tilde{F}_0|^2 +$$

$$\sum_{a}\tilde{F}_0^{*}\frac{\tilde{F}_{\hat{k}\hat{a}}}{a}e^{ik(a-\hat{k}\cdot\vec{a})} +$$

c.c. +

$$\sum_{a}\sum_{b}\tilde{F}_0^{*}\frac{\tilde{F}_{\hat{k}\hat{b}}}{a}\frac{\tilde{F}_{\hat{b}\hat{a}}}{b}e^{ik(a-\hat{k}\cdot\vec{a})}e^{ik(b-\hat{k}\cdot\vec{b})} +$$

c.c +

$\ldots$(multiple − scattering) +

$$\sum_{a'}\frac{\tilde{F}_{\hat{k}\hat{a}'}^{*}}{a'}\sum_{a}\frac{\tilde{F}_{\hat{k}\hat{a}}}{a}e^{-ik(a'-\hat{k}\cdot\vec{a}')}e^{ik(a-\hat{k}\cdot\vec{a})} +$$

$\ldots$(cross − terms)*

All terms have same form.

Only geometry (applies to all electron sources)

Oscillatory in k and $\hat{k}$.

Angle Resolved Photoemission Extended Fine Structure

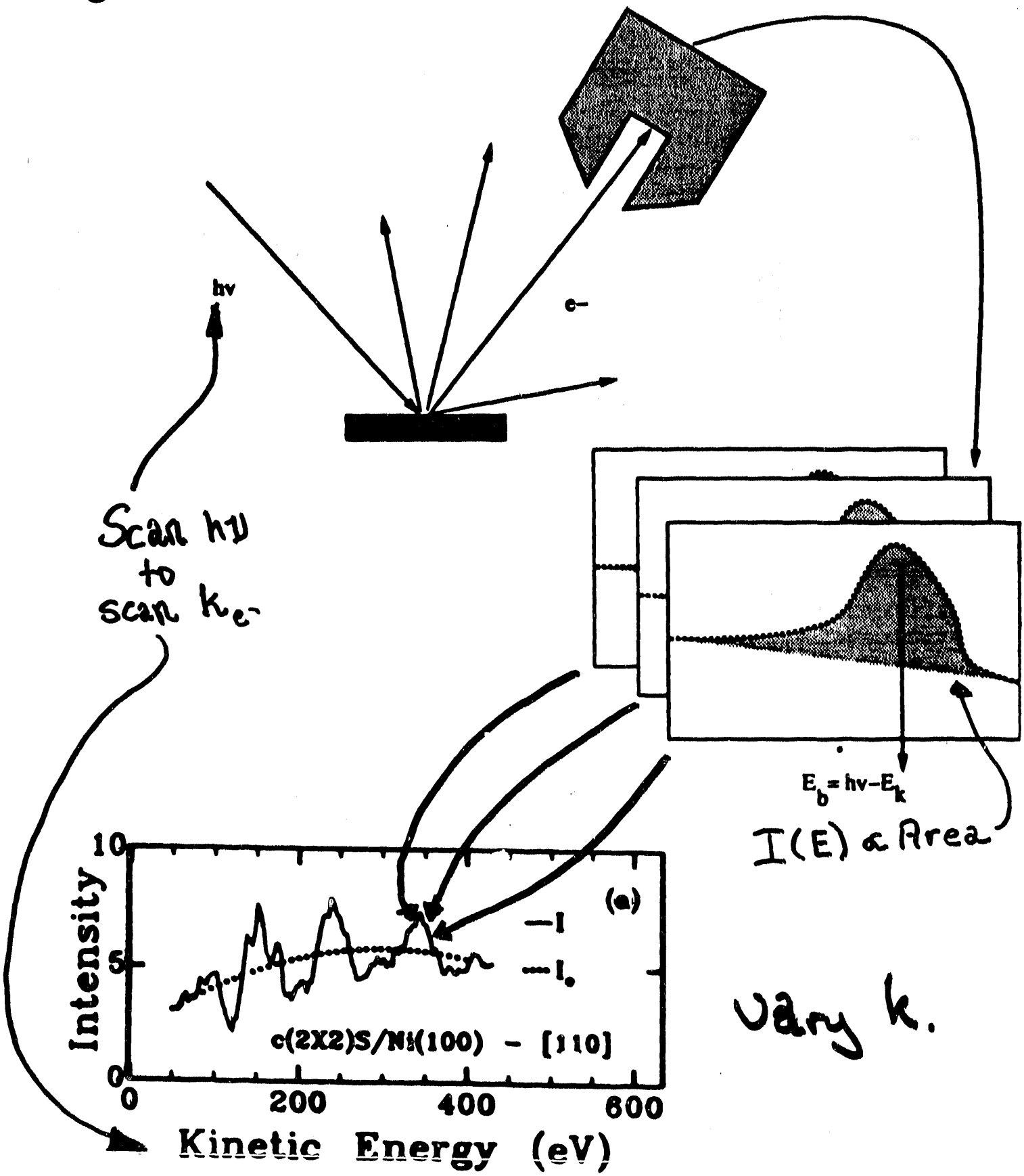

Angle Resolved Photoemission Extended Fine Structure

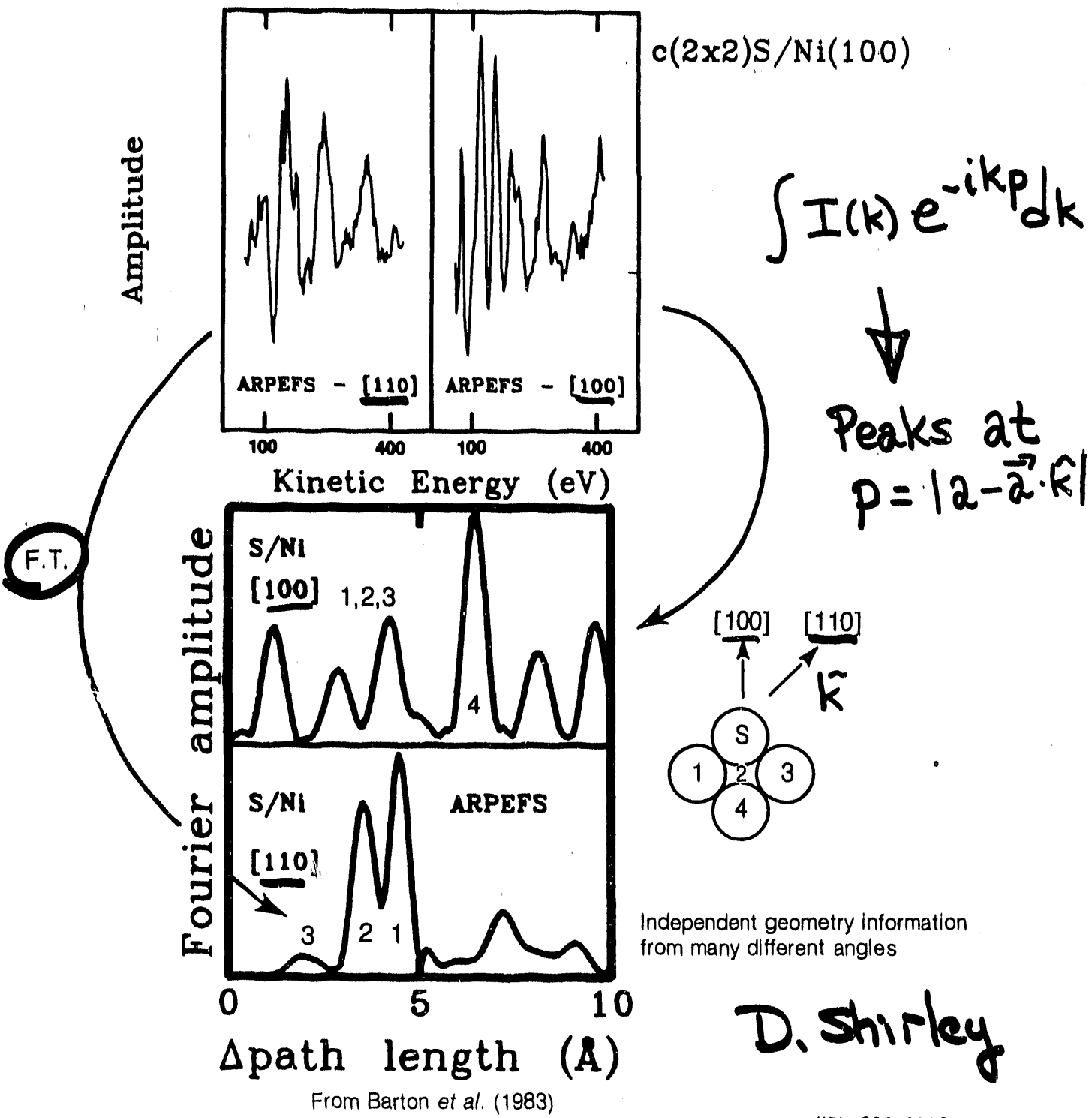

From Barton *et al.* (1983)

$$\int I(k)\, e^{-ikp}\, dk$$

$$\Downarrow$$

Peaks at $p = |a - \vec{a}\cdot\hat{k}|$

Independent geometry information from many different angles

D. Shirley

XBL 834-9336

	Experiment	Stationary Phase Integral	Peak
1D	ARPEFS	$\int dk\, e^{ik(a-\vec{a}\cdot\hat{k})} e^{-ikr'}$	$P[r' - \lvert a - \vec{a}\cdot\hat{k}\rvert]$
2D	Holography	$\iint dk_x dk_y\, e^{ik(a-\vec{a}\cdot\hat{k})} e^{ik\vec{r}\cdot\hat{k}}$	$e^{ika} P[\vec{r} - \vec{a}]$
3D	Inverse Diffraction	$\int dk \iint dk_x dk_y\, e^{ik(a-\vec{a}\cdot\hat{k})} e^{-ik(r'-\vec{r}\cdot\hat{k})}$	$P'[r' - a] P[\vec{r} - \vec{a}]$

$\int I(k) e^{-ikr'} dk$ extracts all $|a - \vec{a}\cdot\hat{k}|$ oscillations.

1) Too many
   - multiple Scat.
   - Sums & Diff.
2) Still indirect
   - $\vec{a} \rightarrow |a - \vec{a}\cdot\hat{k}|$

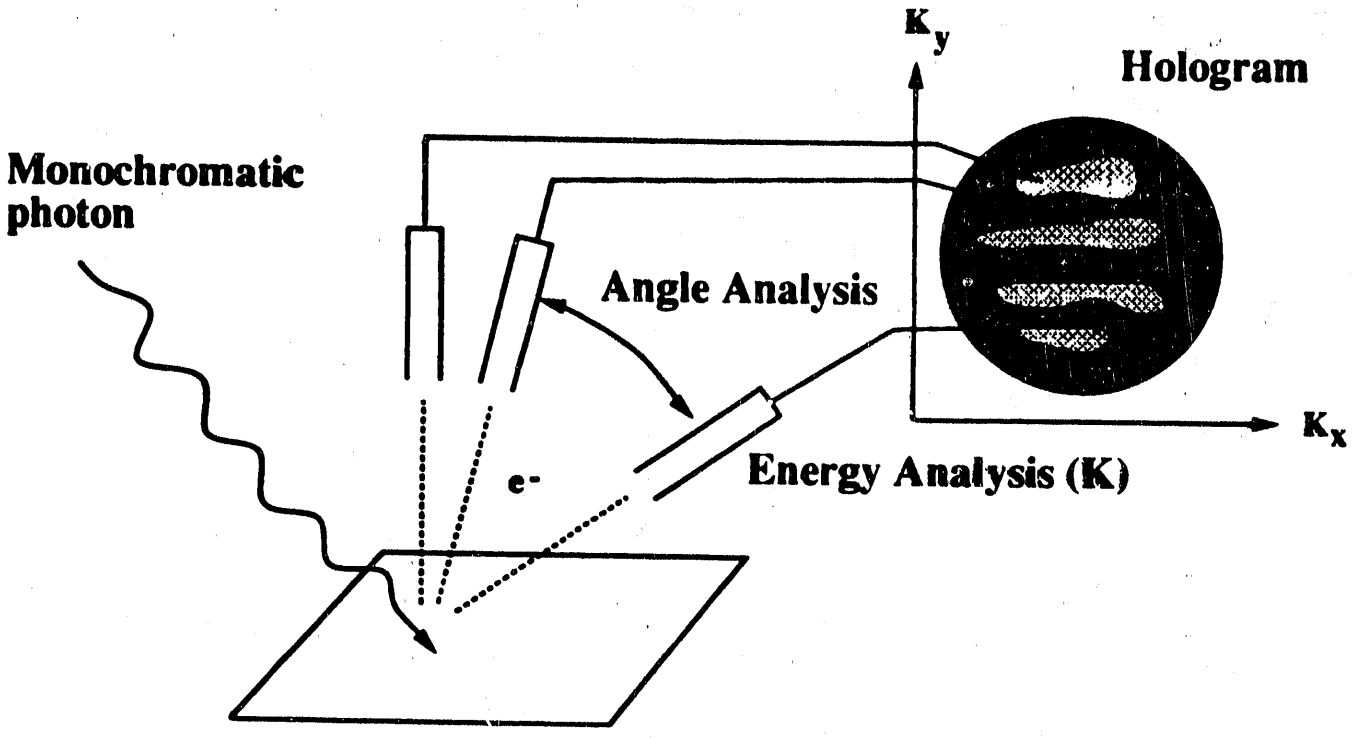

Photoelectron Measurement (K)

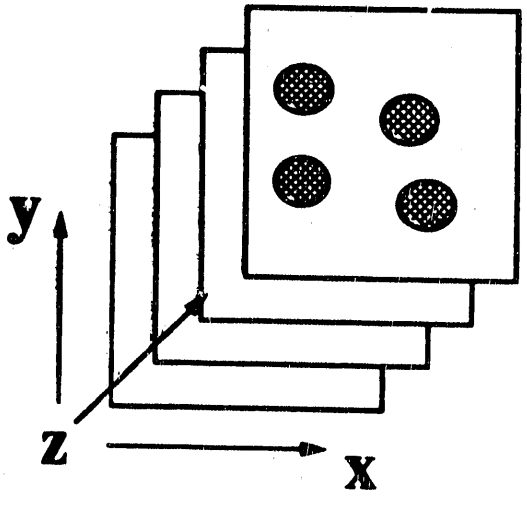

3-D Image

A. Szoke: Photoelectr for Holograph

Holographic Reconstruction (R)

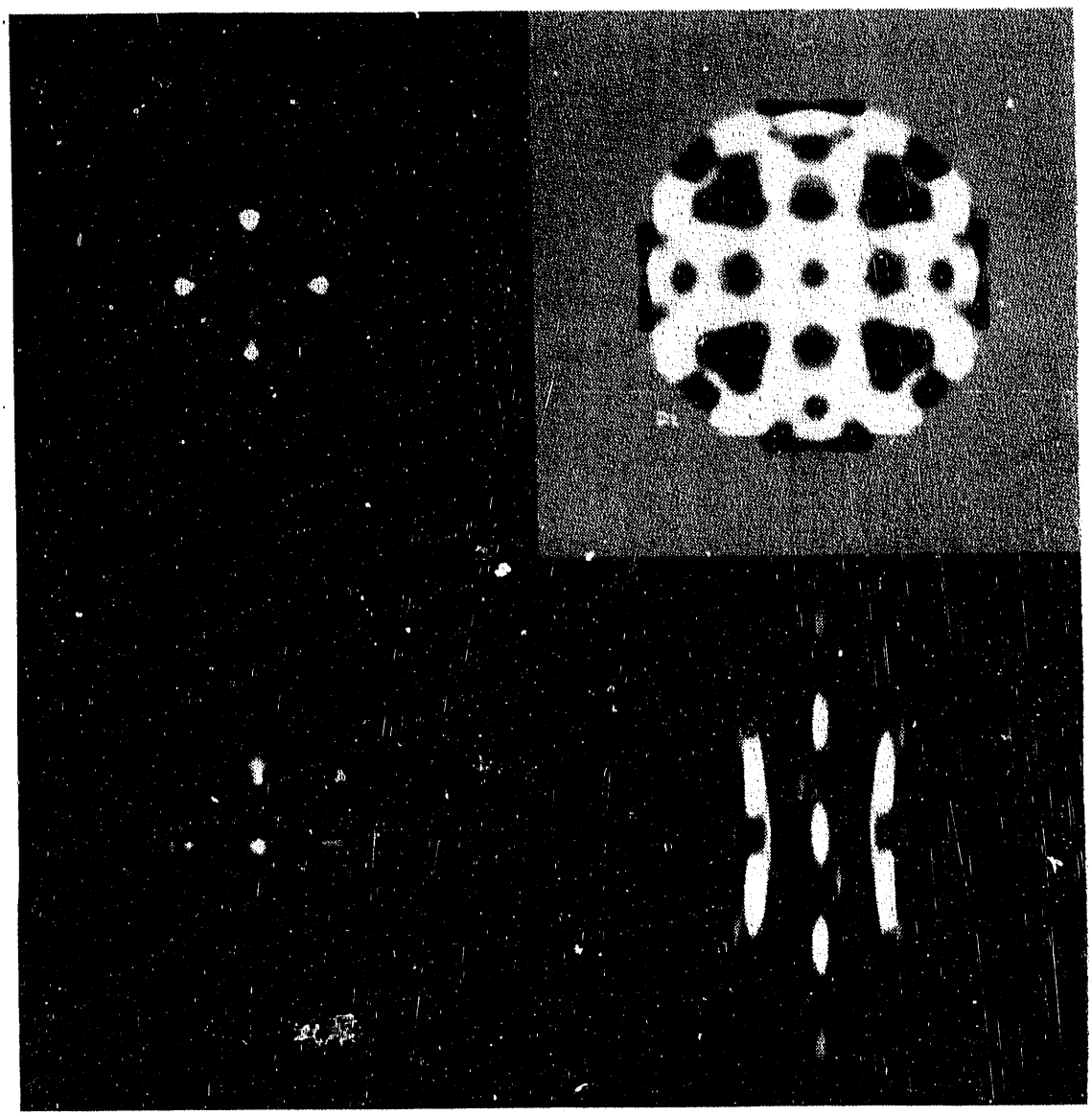

Theory S/Ni(100) k = 12Å

$\int_A e^{ikk\cdot r} dr$ is peaked at $r=0$

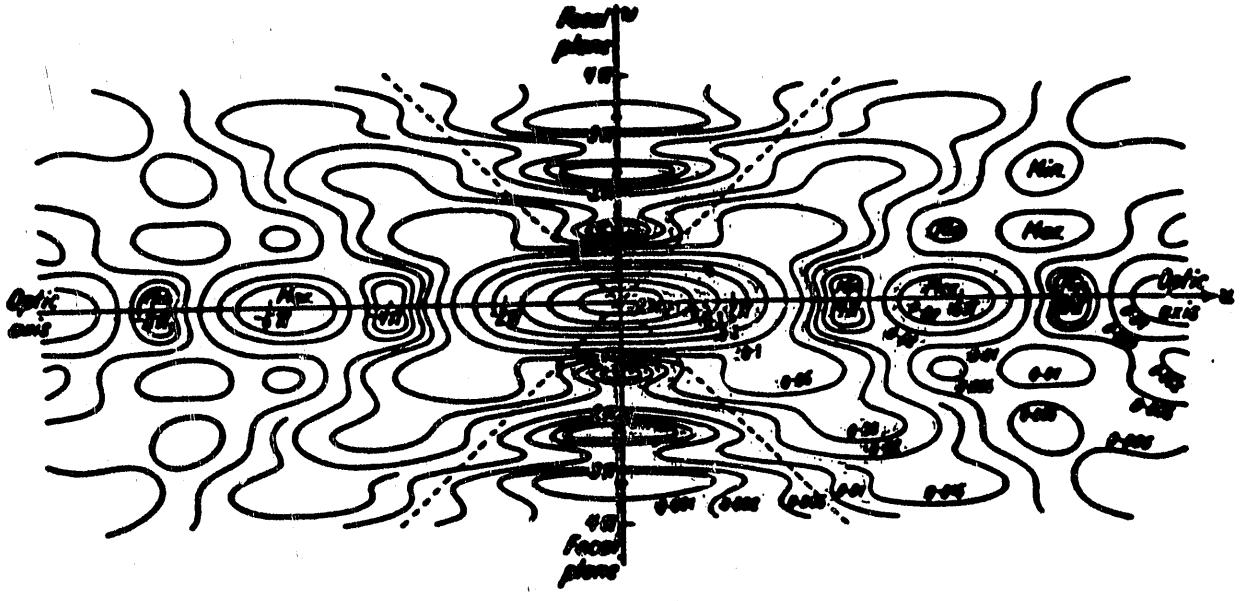

Isophotes [contour lines of the intensity $I(u,v)$] in a meridional plane near focus of a converging spherical wave diffracted at a circular aperture. The intensity is normalized to unity at focus. The dotted lines represent the boundary of the geometrical shadow. When the figure is rotated about the u-axis, the minima on the v-axis generate the AIRY dark rings.

[Adapted from E.H. LINFOOT AND E. WOLF, Proc. Phys. Soc. B 69, 823 (1956).]

Born & Wolf

	Experiment	Stationary Phase Integral	Peak
1D	ARPEFS	$\int dk\, e^{ik(a-\vec{a}\cdot\hat{k})}e^{-ikr'}$	$P[r' - \lvert a - \vec{a}\cdot\hat{k}\rvert]$
2D	Holography	$\iint dk_x dk_y\, e^{ik(a-\vec{a}\cdot\hat{k})}e^{ik\vec{r'}\cdot\hat{k}}$	$e^{ika}P[\vec{r'} - \vec{a}]$
3D	Inverse Diffraction	$\int dk \iint dk_x dk_y\, e^{ik(a-\vec{a}\cdot\hat{k})}e^{-ik(r'-\vec{r'}\cdot\hat{k})}$	$P'[r' - a]P[\vec{r'} - \vec{a}]$

$\iint I(\vec{k})\, dk_x dk_y\, e^{ik\vec{r}\cdot\hat{k}}$ extracts all $\vec{a}$ oscillations

1) Too many
   - twins
   - ghosts
   - multiple
2) Direct!

Inverse Diffraction from Multiple Wavenumber Photoelectron Holography

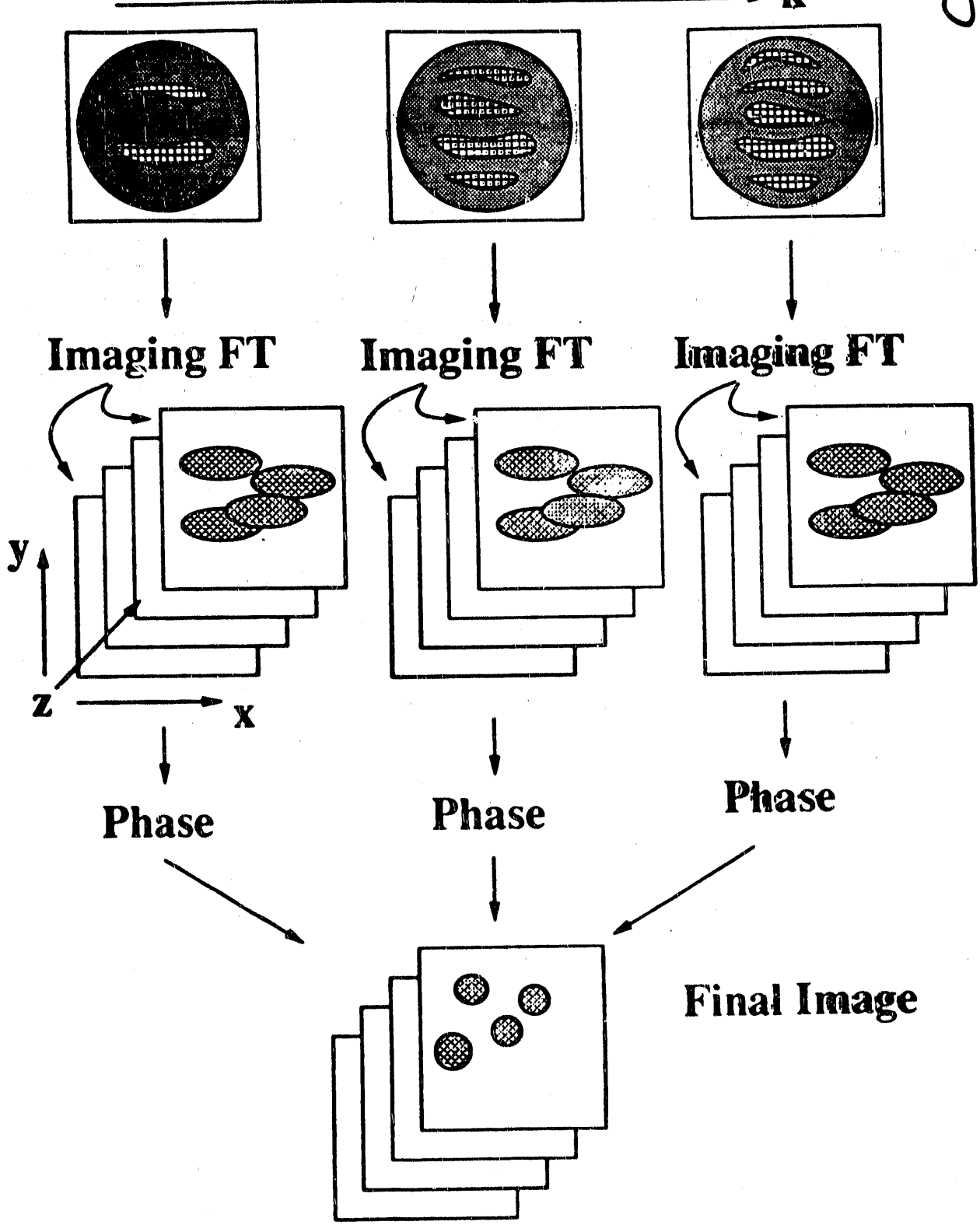

	Experiment	Stationary Phase Integral	Peak
1D	ARPEFS	$\int dk\, e^{ik(a-\vec{a}\cdot\hat{k})} e^{-ikr'}$	$P[r' - \lvert a - \vec{a}\cdot\hat{k}$
2D	Holography	$\iint dk_x dk_y\, e^{ik(a-\vec{a}\cdot\hat{k})} e^{ik\vec{r'}\cdot\hat{k}}$	$e^{ika} P[\vec{r'} - \vec{a}]$
3D	Inverse Diffraction	$\int dk \iint dk_x dk_y\, e^{ik(a-\vec{a}\cdot\hat{k})} e^{-ik(r'-\vec{r'}\cdot\hat{k})}$	$P'[r' - a]P[\vec{r'} -$

$\int dk \iint dk_x dk_y\, I(\vec{k})\, e^{-ik(r'-\vec{r'}\cdot\hat{k})}$

extracts oscillations with $\vec{a}$ and $|\vec{a}|$.

1) Single Scattering!
   - No Twins
   - Less Ghosts
   - Less Multiple Scat.

2) Direct!

Experimental Design Issues

Goals:

- **Direct → Site.**
- **Accurate → 0.02Å.**

Requirements:

- **Measureable**
  - **Low or Medium Energies** 100 - 300eV
  - **Simultaneous 2D**
- **Resolvable Site (2Å)**
  - **Multiple Medium Energies**
- **Accurate (0.02Å)**
  - **Precise relative emission angles.**
  - **Precise relative amplitudes.**
  - **More accurate theory.**

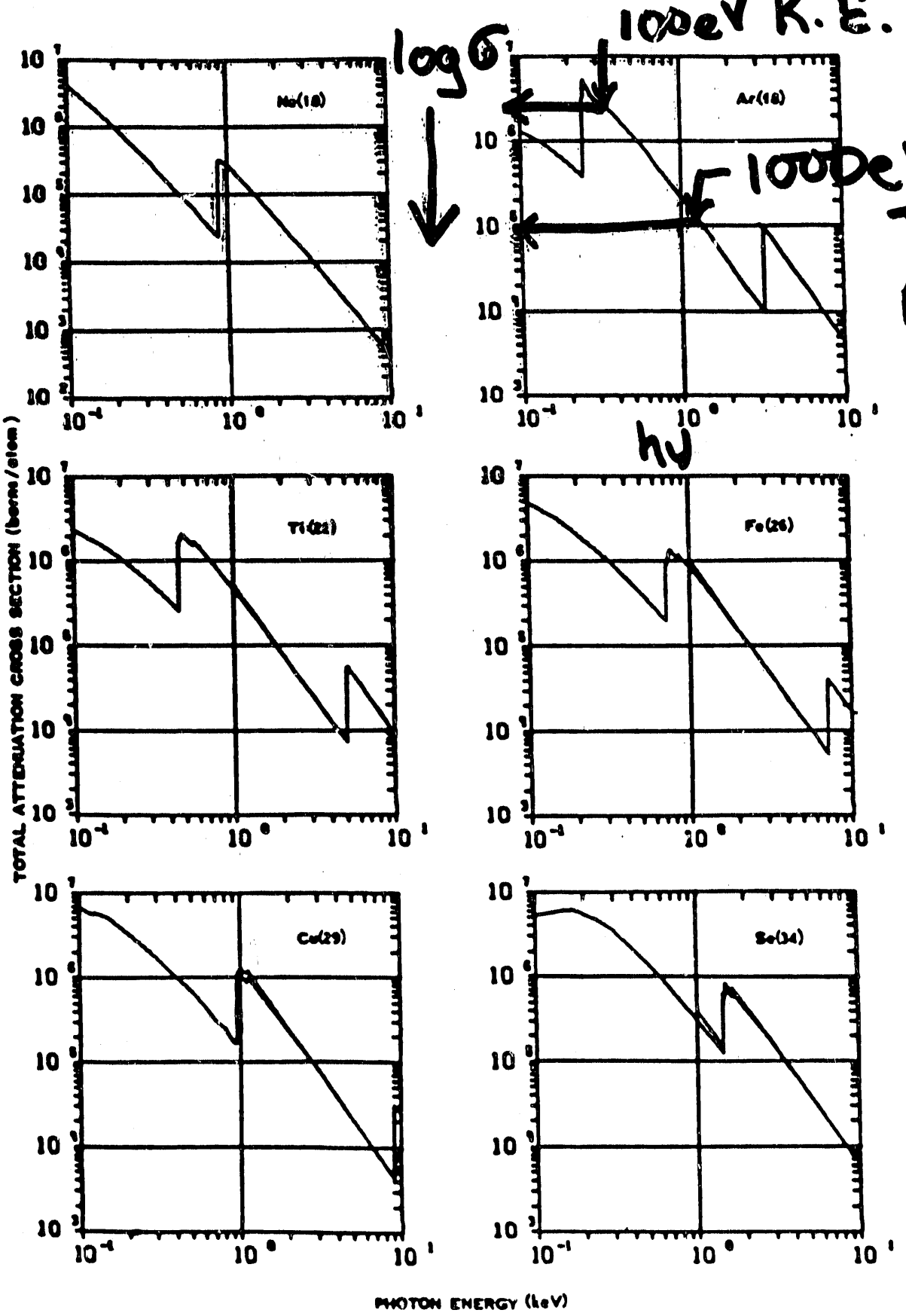

APHS. Computer plots. 0.1 keV $\leq h\nu \leq$ 1 – 10 keV from theory; 1 keV $\leq h\nu \leq$ 10 keV from least-squares fit to experimental data. In regions of overlap the calculated curves are to be preferred.

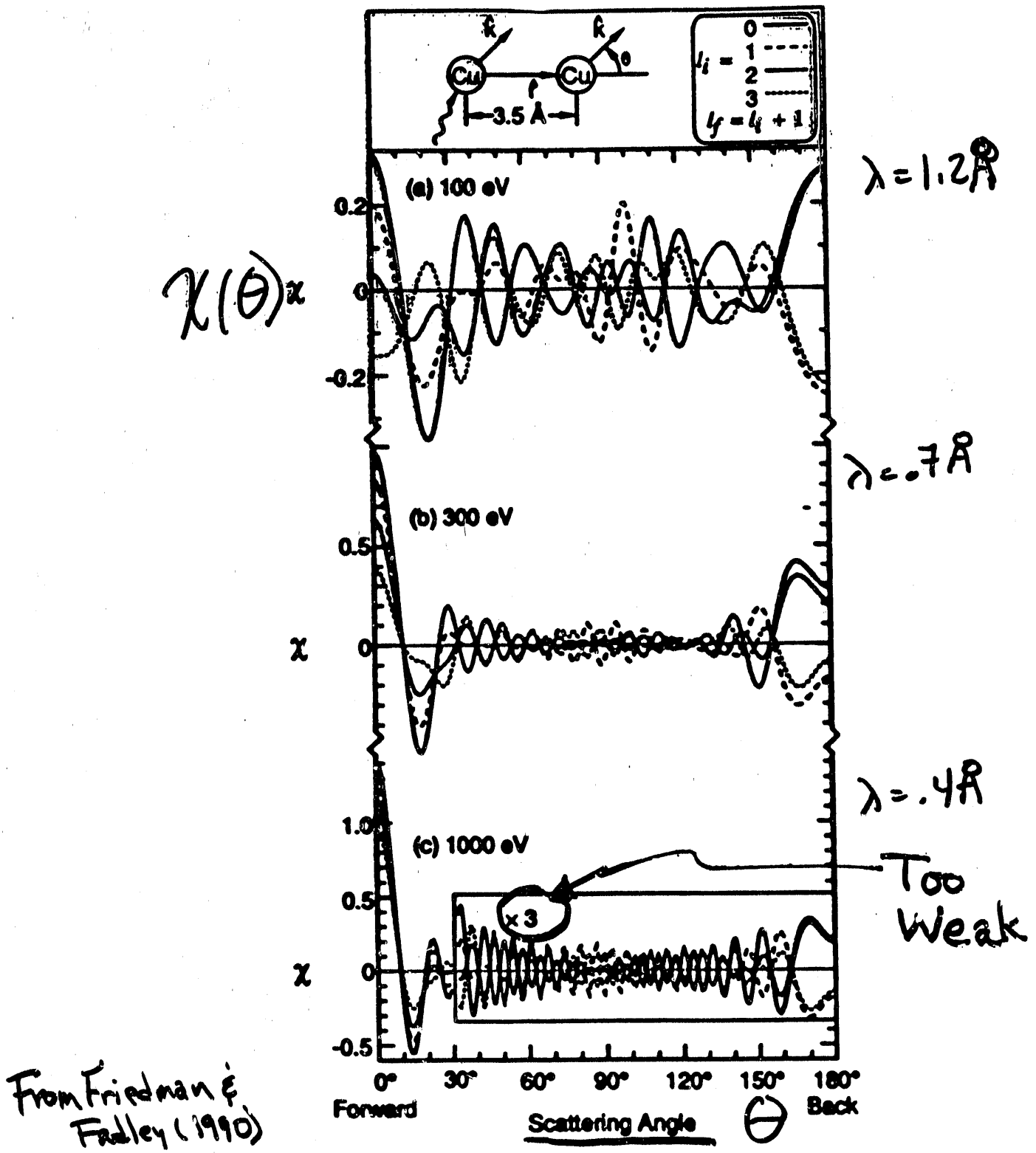

From Friedman & Fadley (1990)

The photoemission intensity calculated for a Cu-Cu photoemitter-scatterer system as a function of scattering angle. The radiation is unpolarized (sum of two perpendicular polarizations) and incident perpendicular to the $\hat{k}, \hat{r}$ plane. Curves are shown for initial-state angular momentum l_i ranging from $l_i = 0$ to 3, and electron kinectic energies of 100 eV, 300 eV, and 1000 eV. Only the $l_i \rightarrow l_i + 1$ channel is included. The intensity I is normalized to the primary-wave intensity I_0 as the quantity $X \equiv (I - I_0)/I_0$.

Display Type Spectrometer

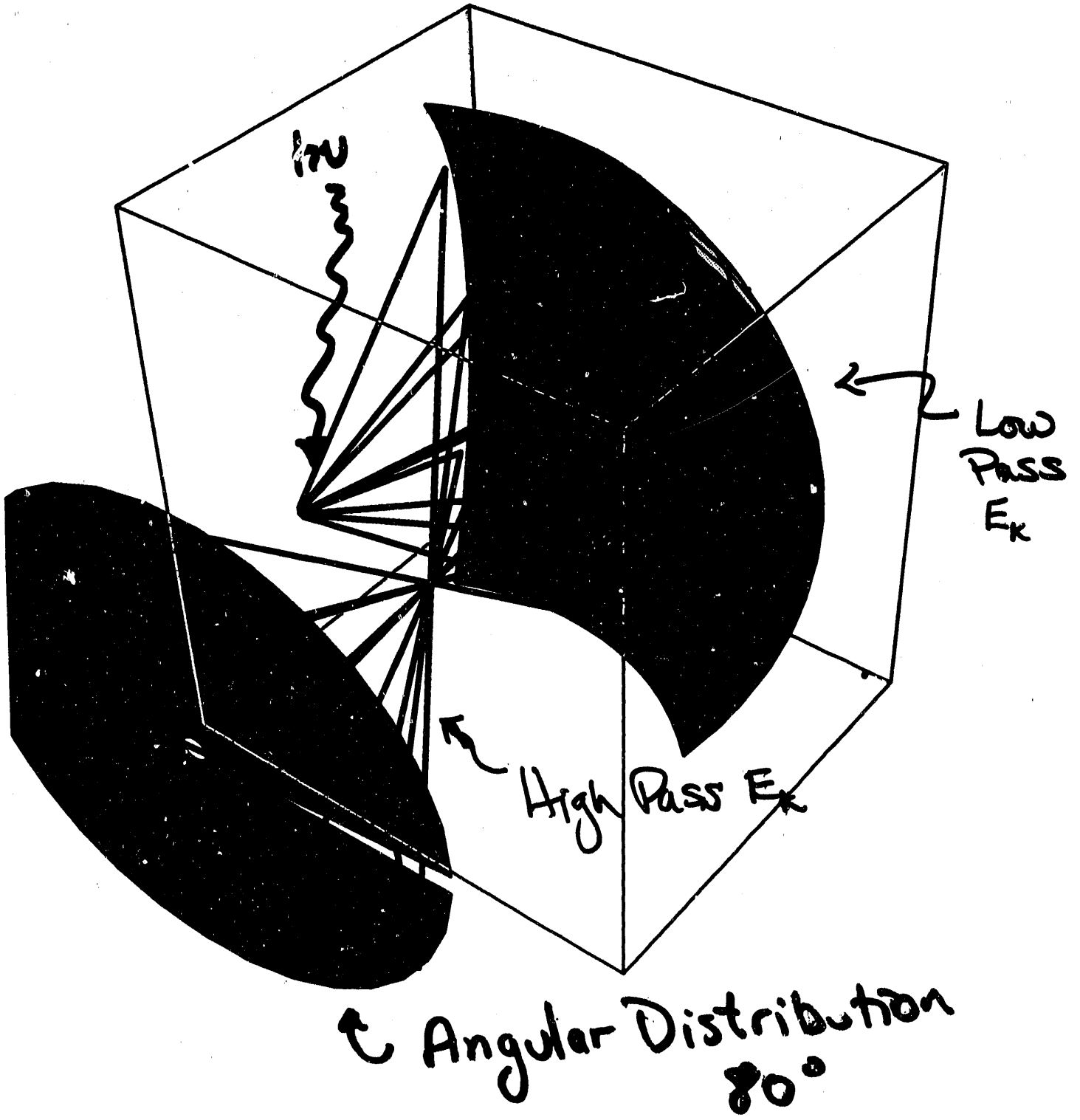

Angle Correction

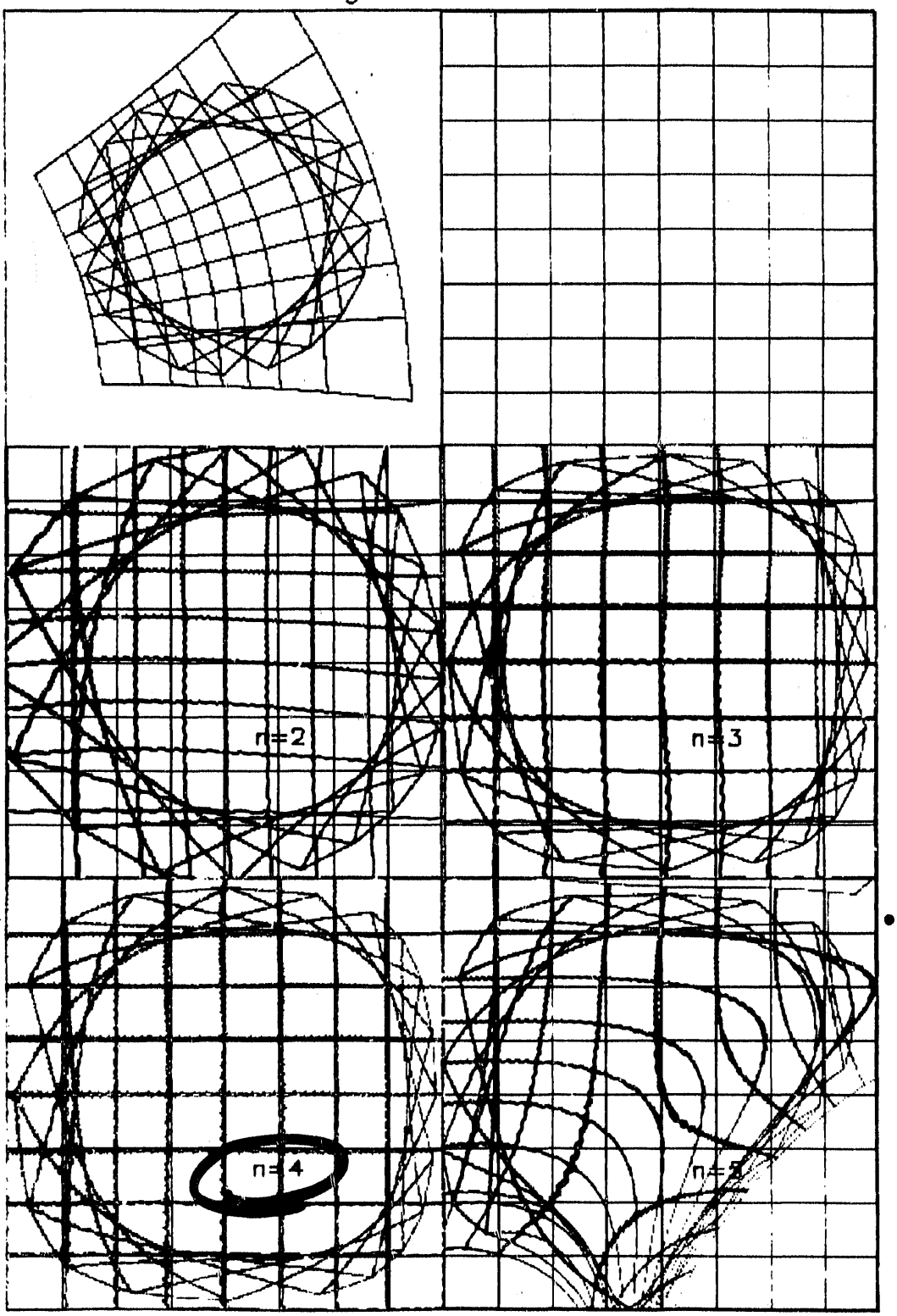

Polynomial (order n)

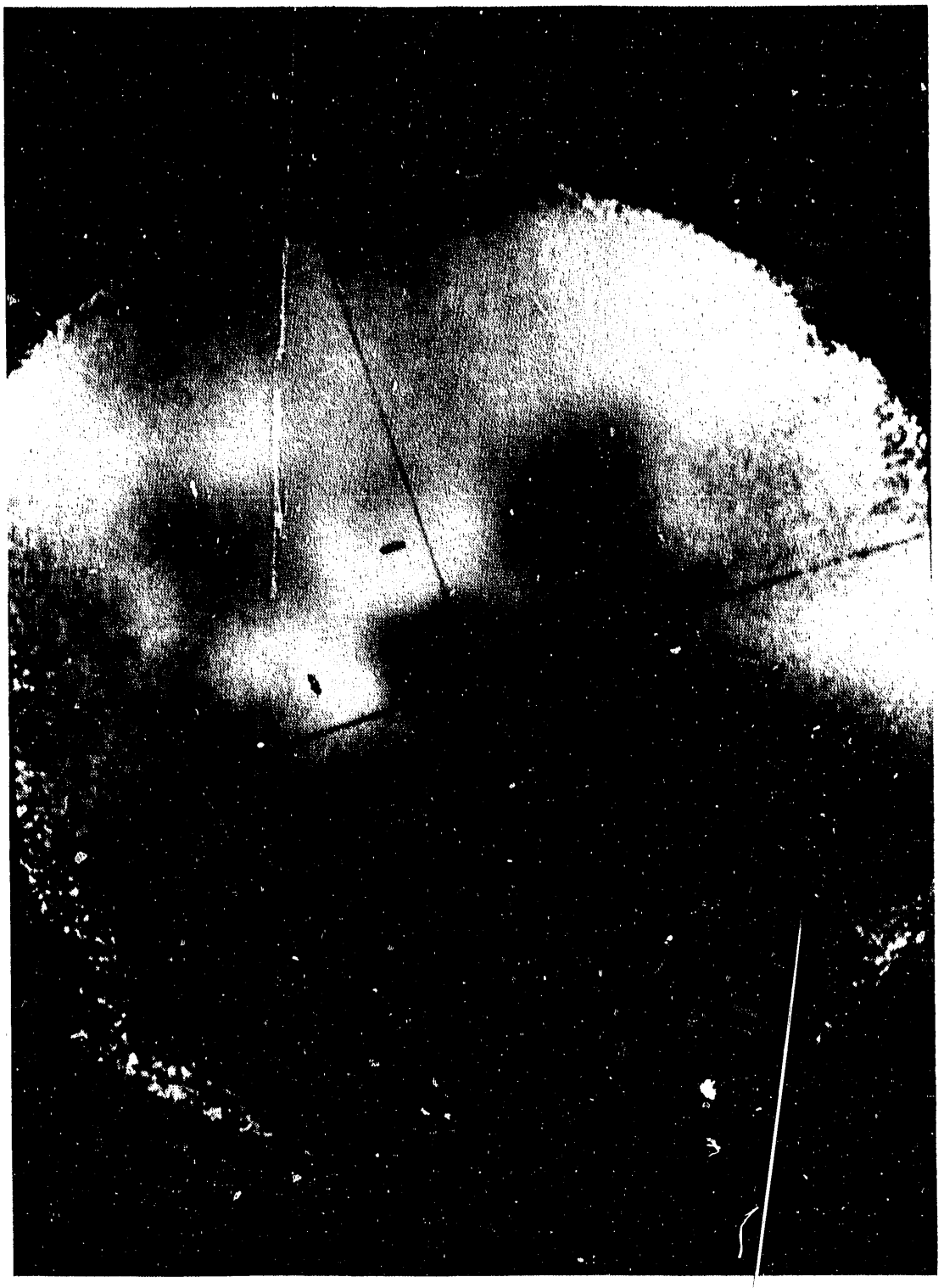

Cl/Cu(001)FFT

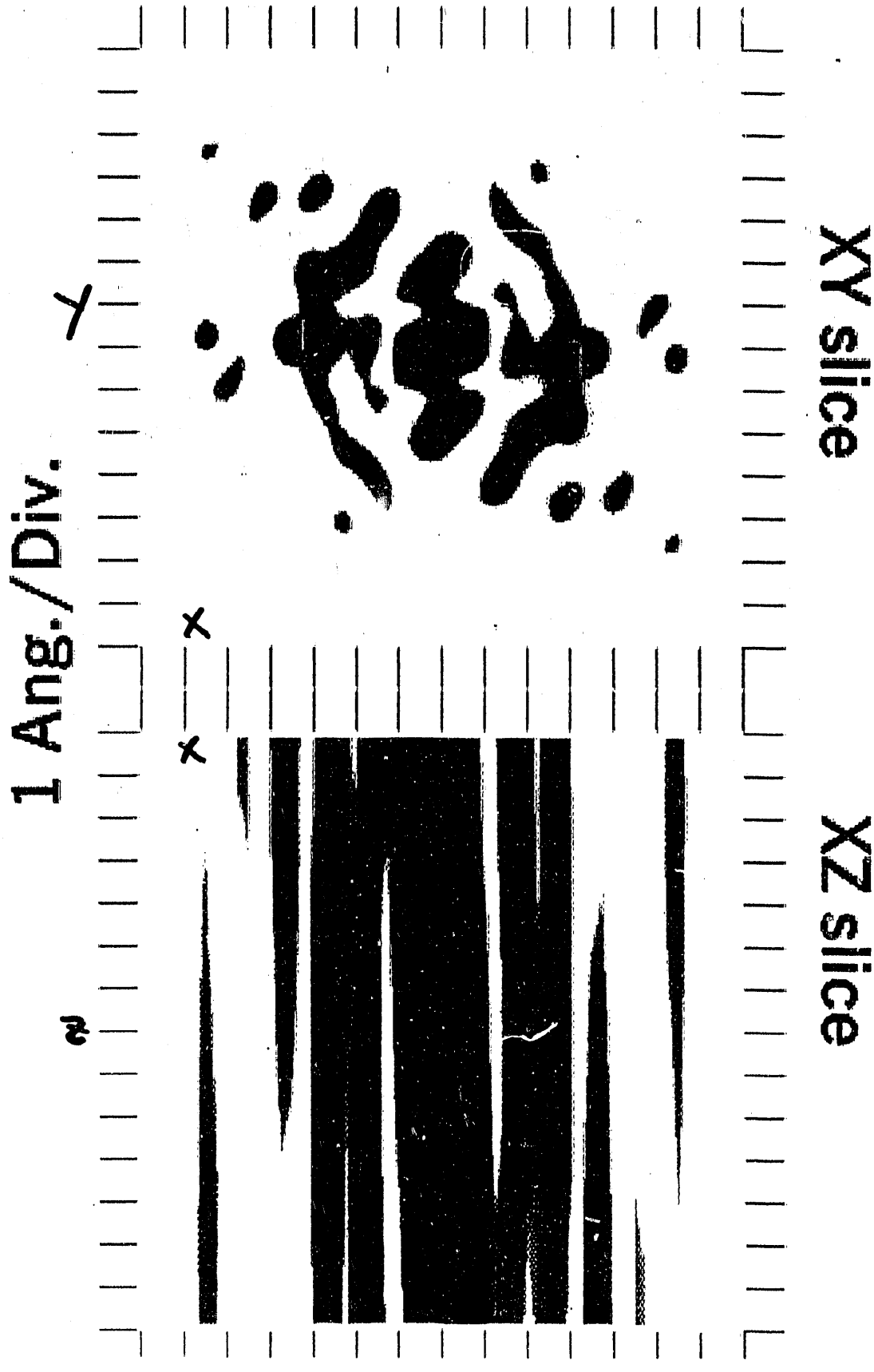

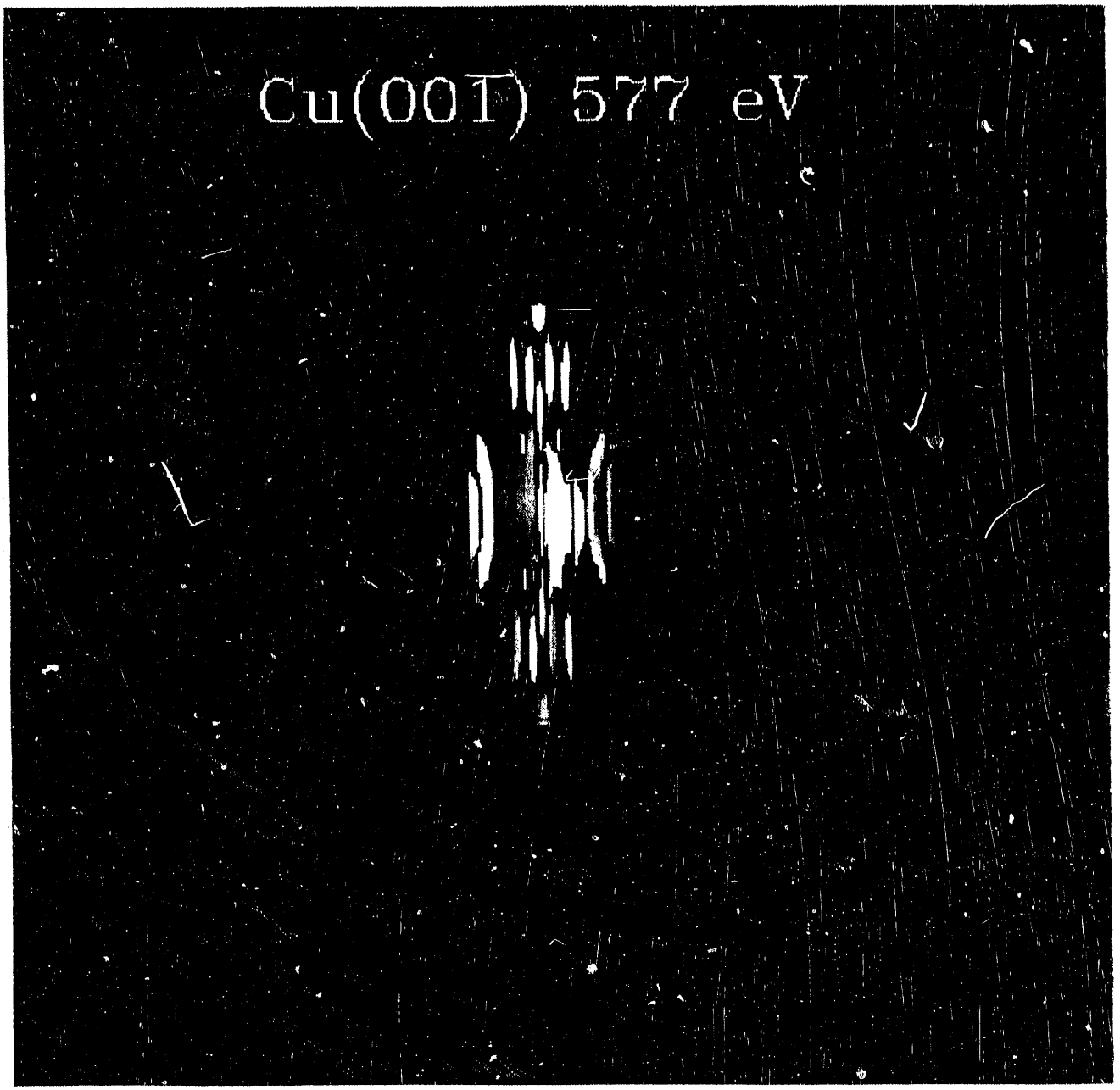
Cu(00$\bar{1}$) 577 eV

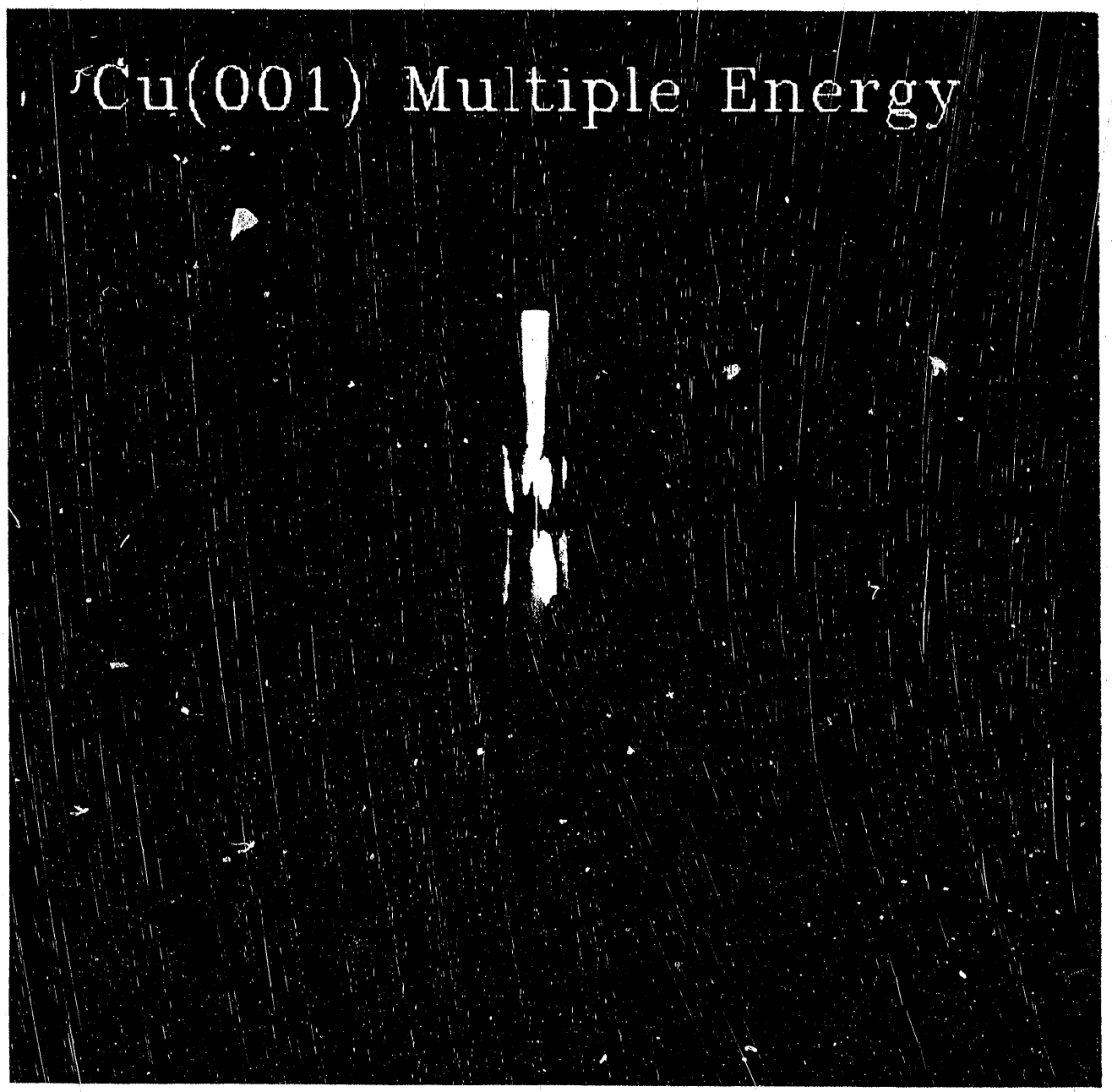
Cu(001) Multiple Energy

Experimental Prognosis

Setup Complicated:

- Synchrotron Radiation.
- 2D Analyzer.
- Angle Calibration.
- High-Capacity Computing System.
- 3D Data Analysis Software.

Use Straightforward:

- No time-dependent calibration.
- No mechanical motions.
- Electron energy only variable.
- Insensitive to macroscopic vibration.
- Insensitive to sample position.
- Ten holograms at 1/10 as much time.
- Direct analysis to 3D images of surface sites!

Will It Work?

Cannot just "Try It and See"

- Accuracy Criterion?
- Limitations Intrinsic?

Do We Understand Electron Scattering?

- Yes, but...
- Problem of the Auger Holes (D. Frank, A. Hubbard, et al.).

Theoretical Best Inversion.

- Inverse Diffraction.
- Angular Spectrum of Plane Waves.

Cu(100) 56 eV

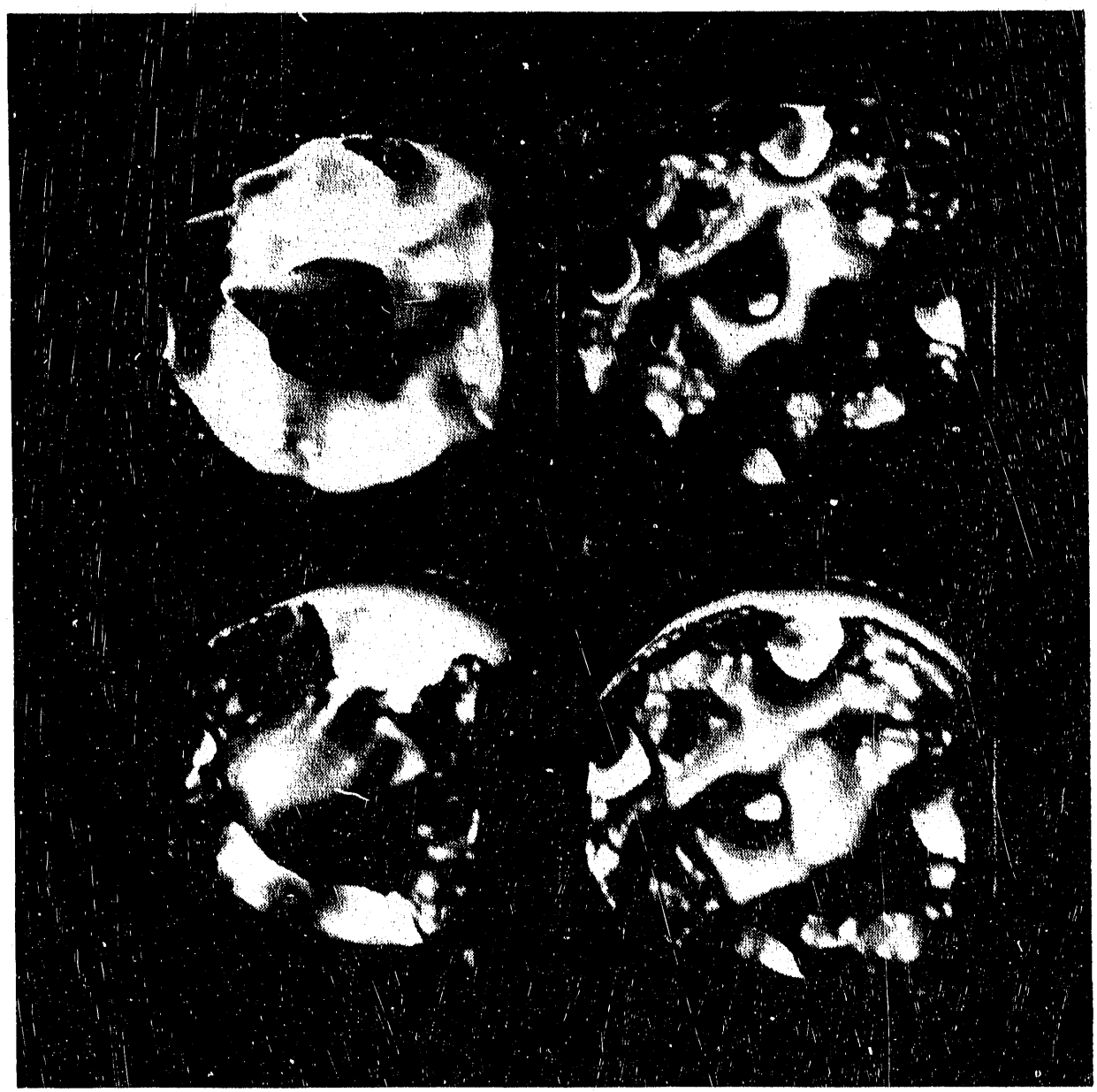

Curved Source Waves.

- Effects appear when $l(l+1)/kr$ is not small.
- Photoemission selection rules:

$$\begin{aligned} l_{\max} &= l_i + 1 \\ l_f &= l_{\max}, l_{\max} - 2 \end{aligned}$$

For example, Cu 3p, $l_f = 2, 0$.

- Auger selection rules:

$$\begin{aligned} l_{\max} &= l_i + l_1 + l_2 \\ l_f &= l_{\max}, l_{\max} - 2, \ldots \qquad (l_f > 0) \end{aligned}$$

For example, Cu 3p3d3d ($M_{23}N_{45}N_{45}$), $l_f = 5, 3, 1$.

$l=0$ vs $l=3$

↑ Peaks ↓ Dips ?

Source Wave Angular Momentum via Effective Potential.

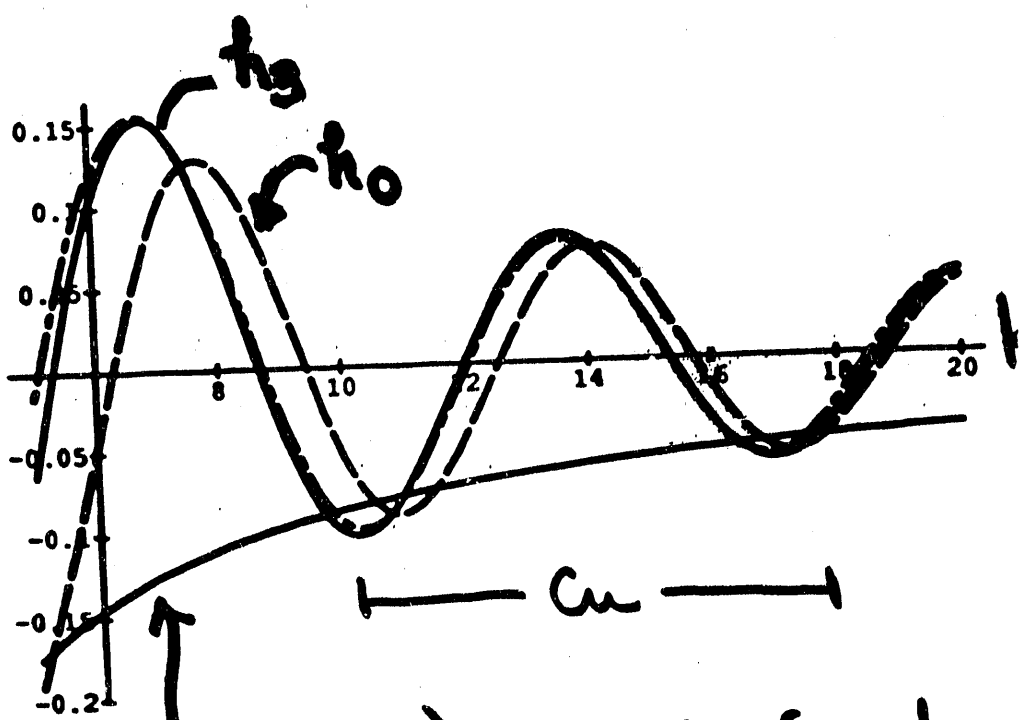

$\frac{\ell(\ell+1)}{r^2}$ centrifugal potential

$h_3 \sim h_0(k'r)$

$$k' = \int_{\ell+1/2}^{r} \sqrt{k^2 - \frac{(\ell+1/2)^2}{r^2}}\, dr \approx \alpha k + \beta$$

Cu 56eV

Two Atom $\chi(\theta)$

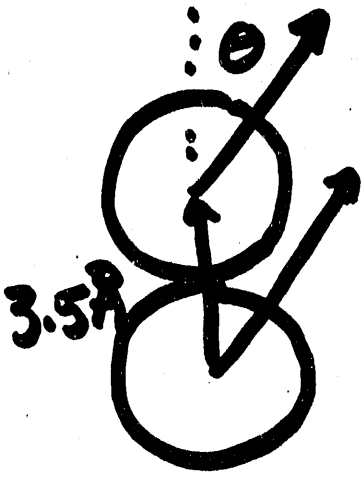

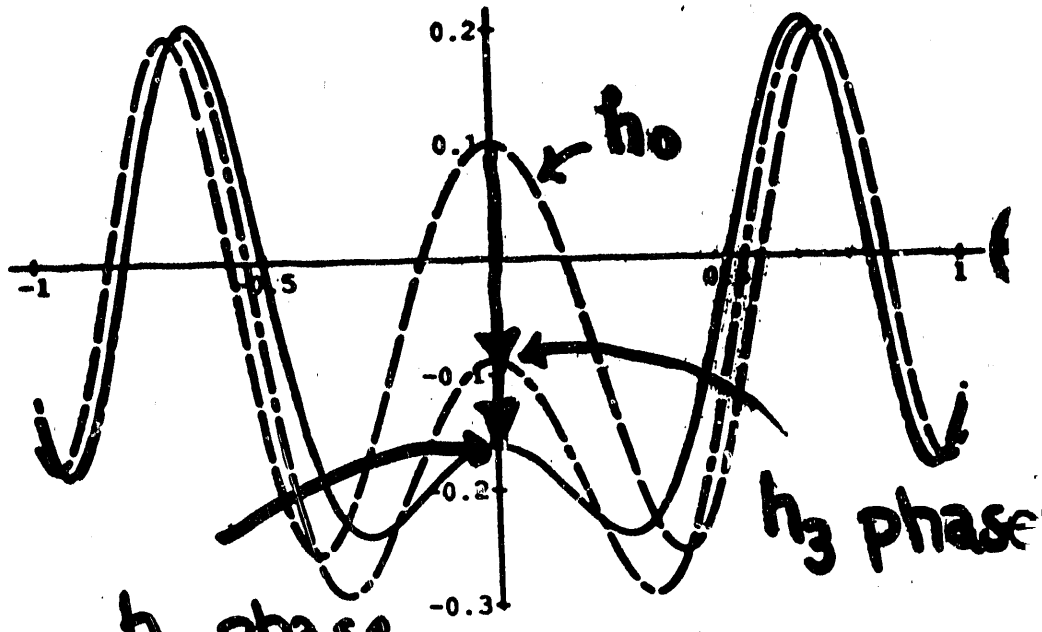

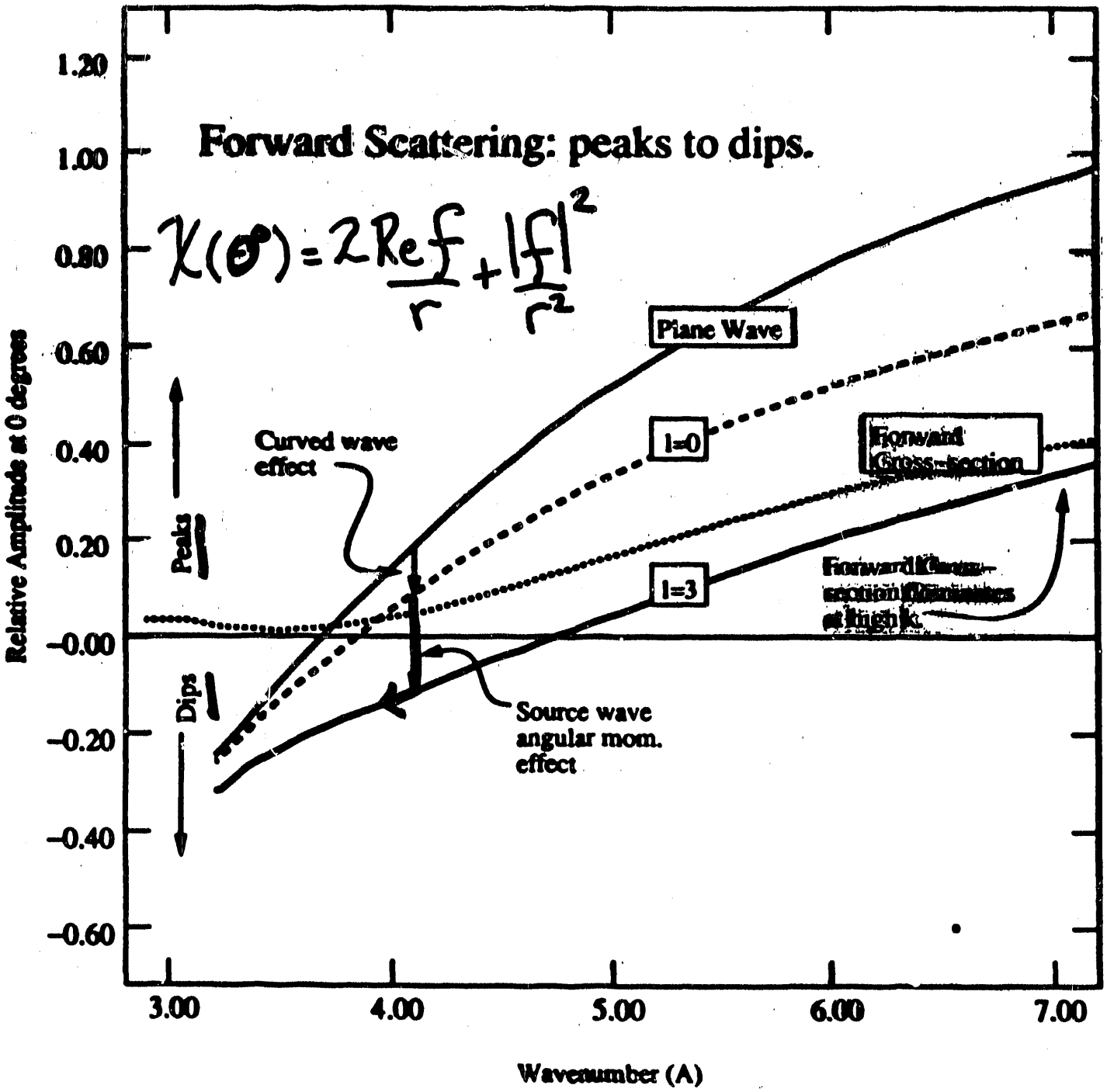
Forward Scattering: peaks to dips.
$\chi(\theta) = 2\mathrm{Re}\frac{f}{r} + \frac{|f|^2}{r^2}$
Plane Wave
l=0
l=3
Forward Cross-section
Curved wave effect
Source wave angular mom. effect
Peaks
Dips
Relative Amplitude at 0 degrees
1.20
1.00
0.80
0.60
0.40
0.20
-0.00
-0.20
-0.40
-0.60
3.00
4.00
5.00
6.00
7.00
Wavenumber (A)

Electron Mutiple Scattering in Angular Spectrum Representation

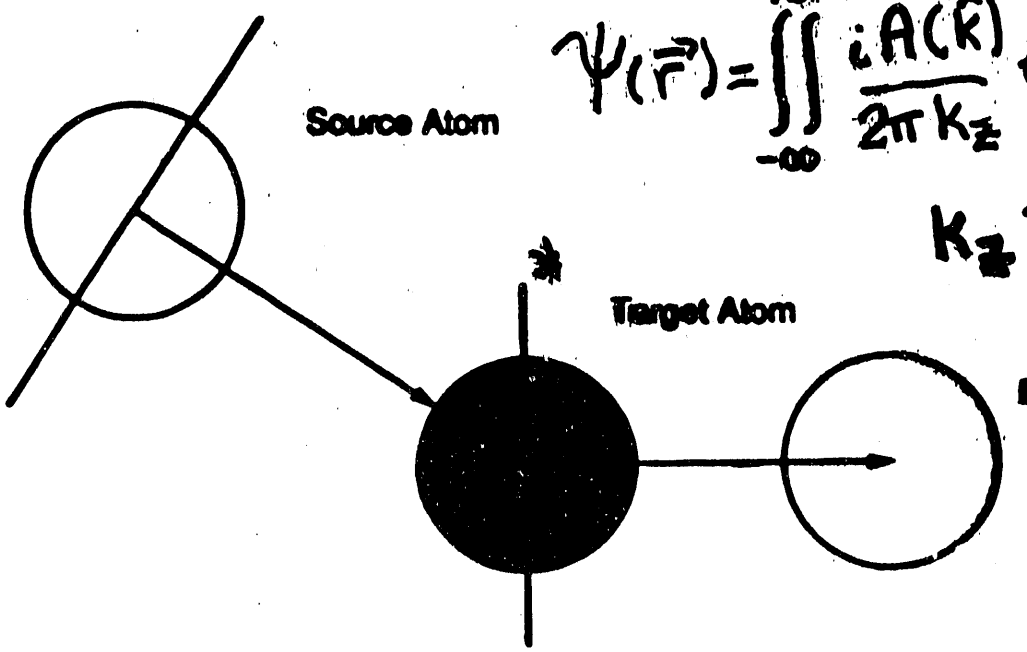

$$\psi(\vec{r}) = \iint_{-\infty}^{+\infty} \frac{iA(k)}{2\pi k_z} e^{ik\hat{k}\cdot\vec{r}}\, dk_x dk_y$$

$k_z = |\vec{k}| = k$ fixed

1. Two dimensional FT of Source (= Angular Spectrum!)
2. Scatter individual plane waves.*
3. Integrate scattered waves –> Scattered Angular Spectrum.

* Scattered wave $\vec{k}$ w.r.t. rotated axis.

c 2 × 2 S/Ni(100) δ1s Theory k = 12 Å

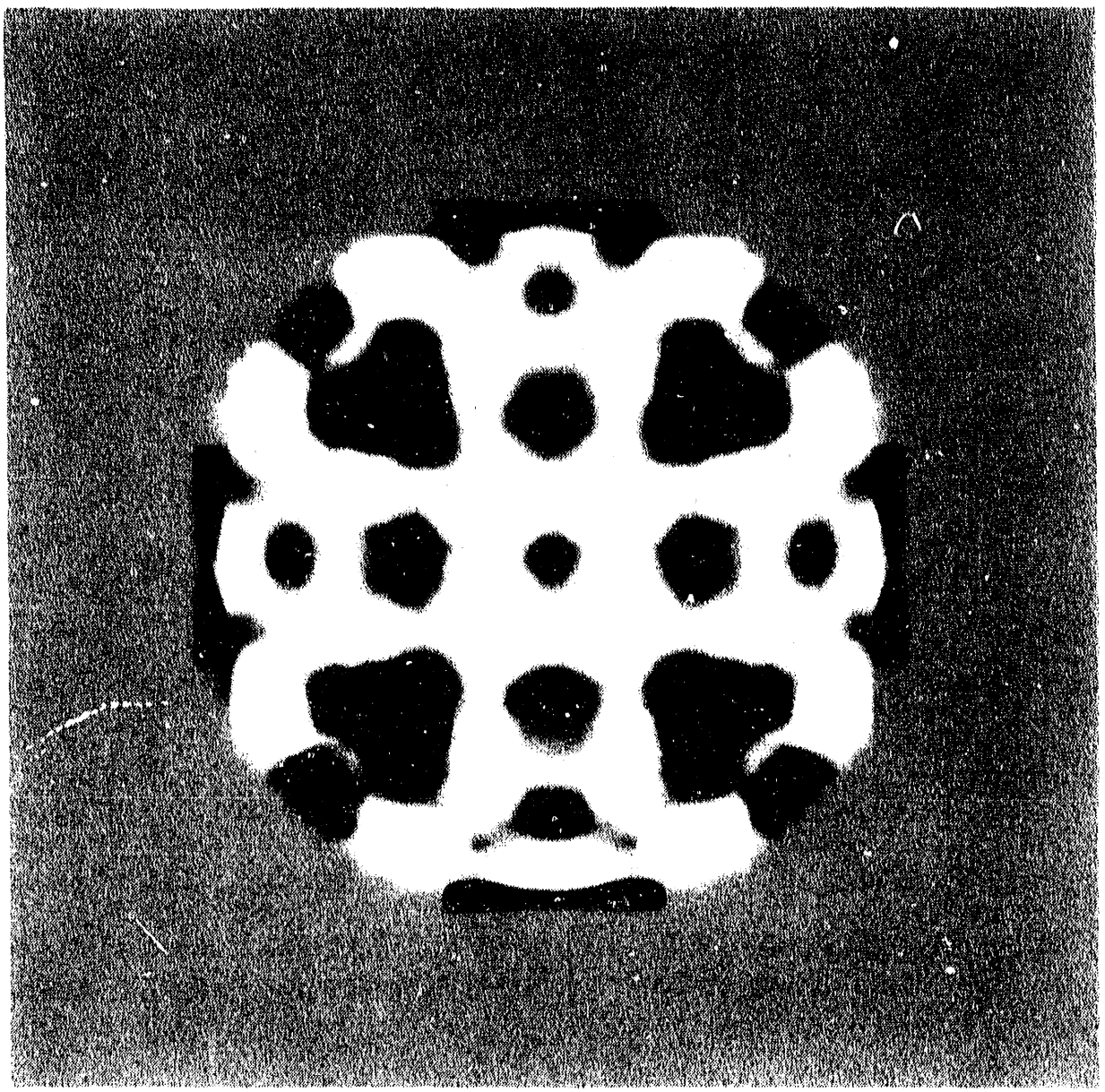

Holographic Crystallography

D. Saldin

University of Wisconson–Milwaukee

Holographic Crystallography

D. K. Saldin

Collaborators

B. P. Tonner

G. R. Harp

Z. L. Han

B. L. Chen

X. Chen

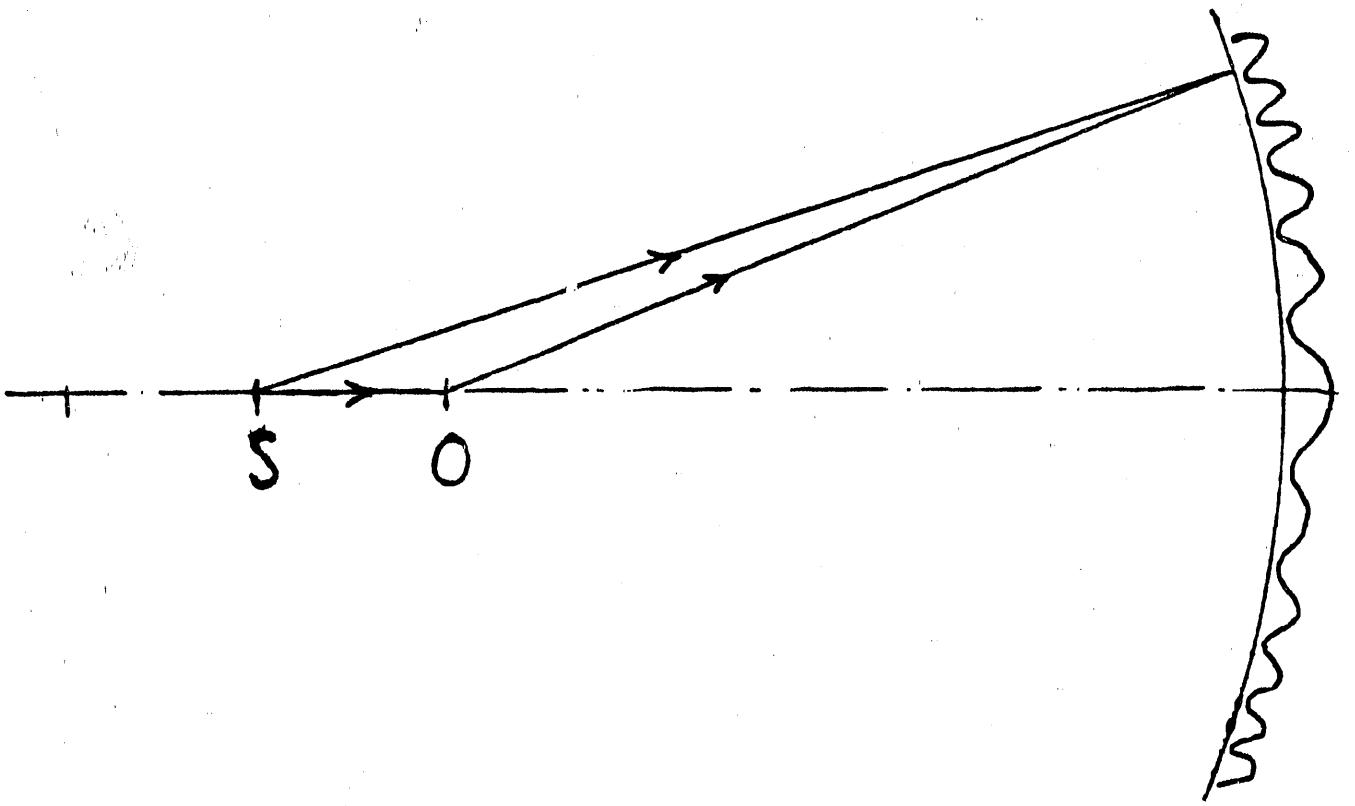

ZONE PLATE HOLOGRAM

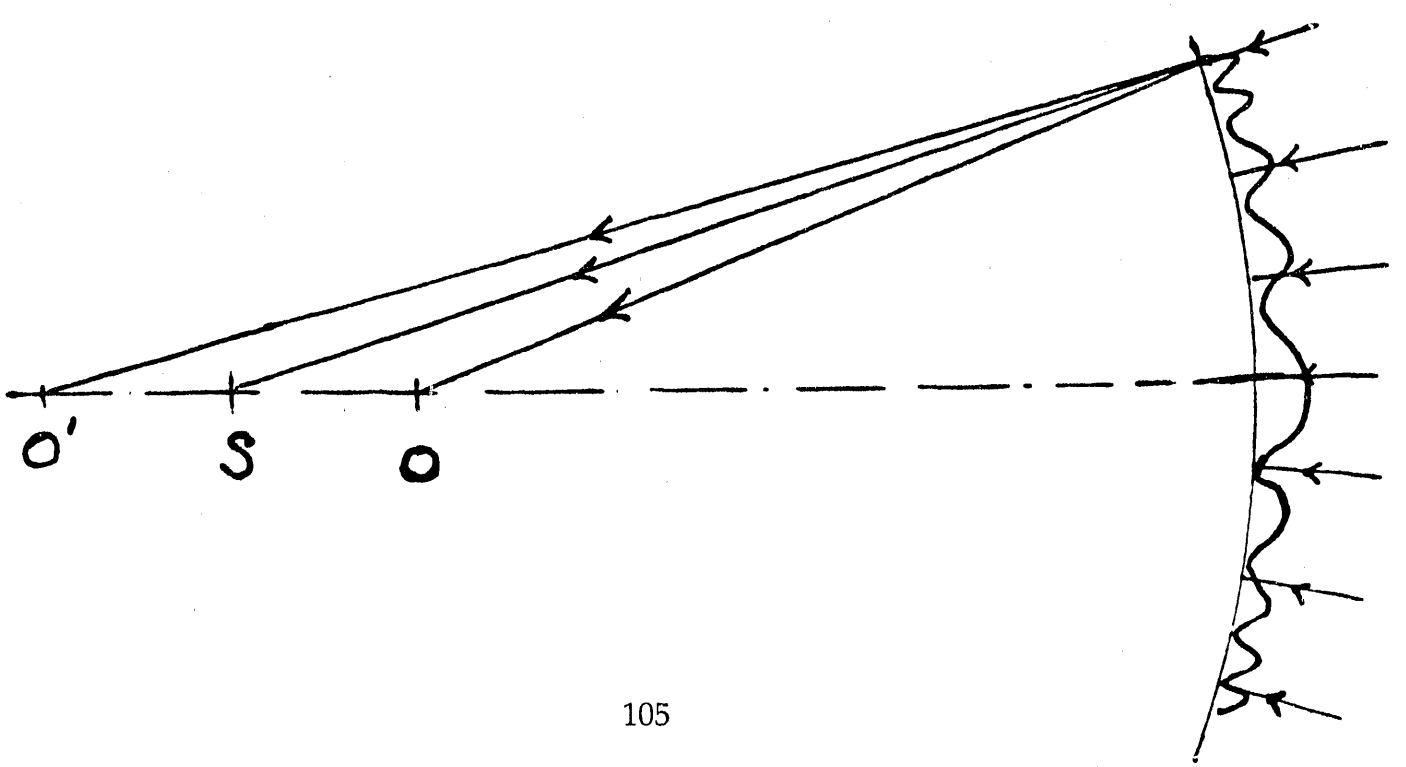

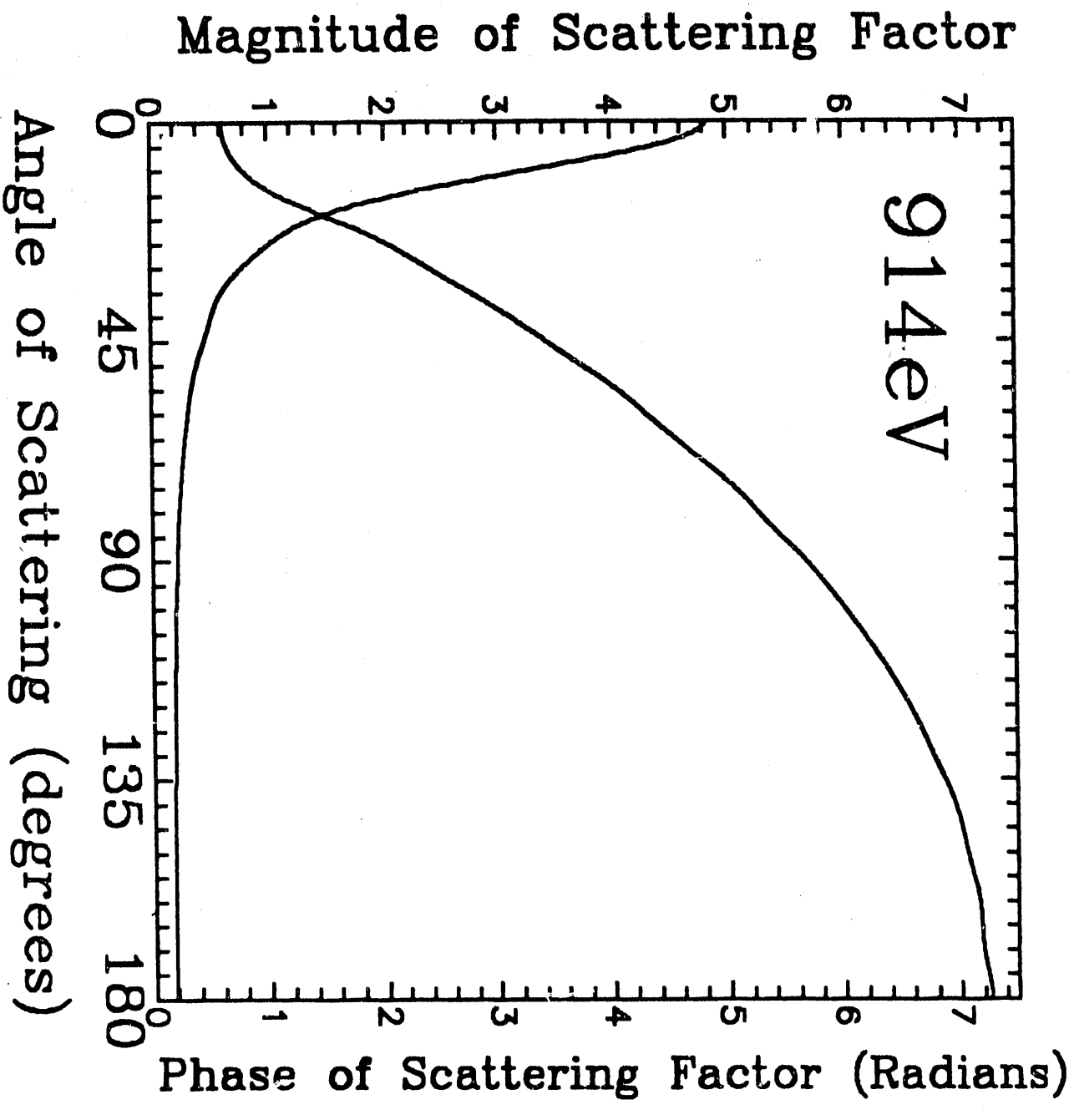
Magnitude of Scattering Factor
0
1
2
3
4
5
6
7
914eV
Angle of Scattering (degrees)
0
45
90
135
180
Phase of Scattering Factor (Radians)

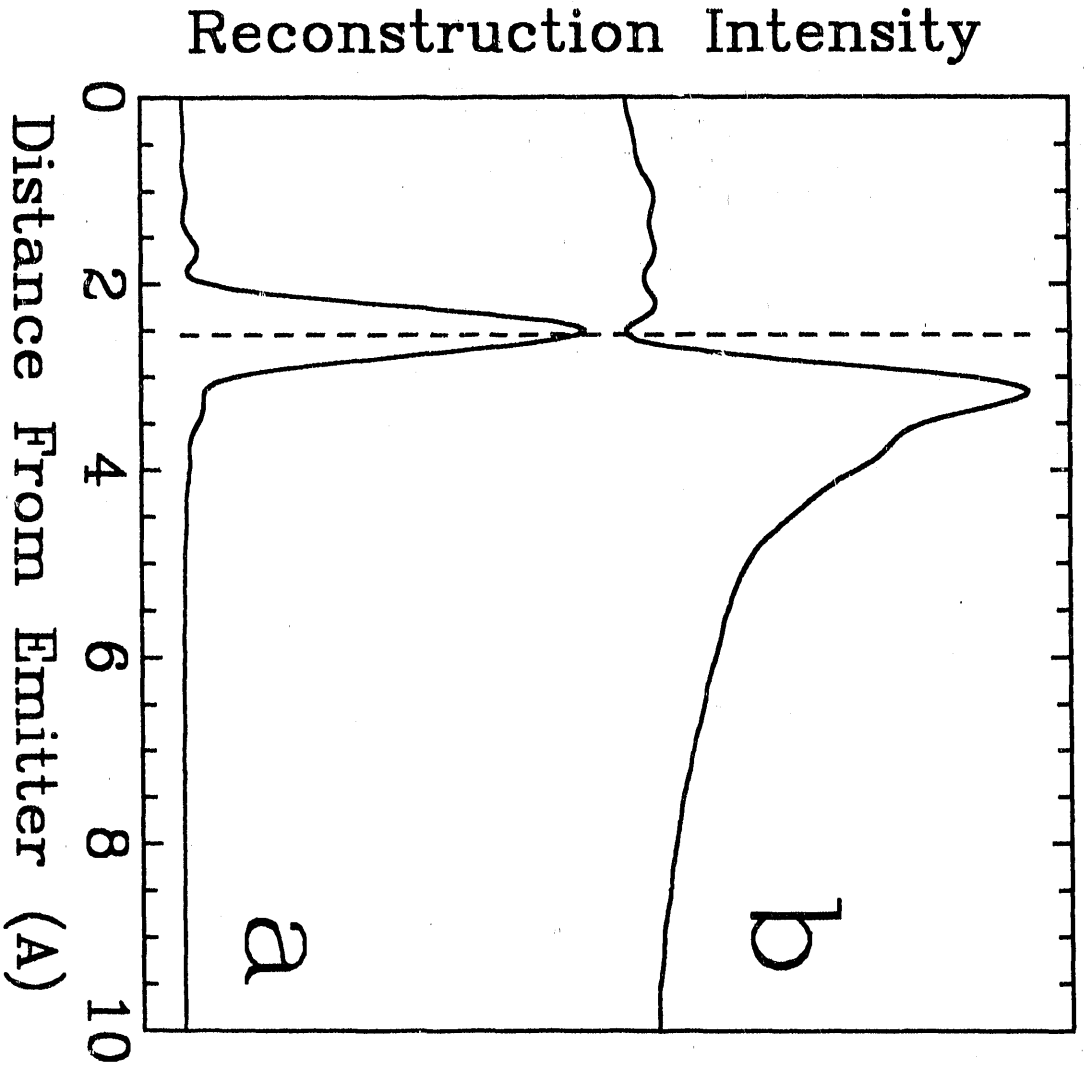
Reconstruction Intensity
Distance From Emitter (A)
0
2
4
6
8
10
a
b

Detected Intensity

$$I(\underline{k}) = \left| 1 + \sum_i f(\hat{\underline{k}}.\hat{\underline{r}}_i) \exp\{i(kr_i - \underline{k}.\underline{r}_i)\}/r_i \right|^2$$

$$= 1 + \sum_i |f(\underline{k}.\hat{\underline{r}}_i)|^2/r_i^2 + \sum_i f^*(\hat{\underline{k}}.\hat{\underline{r}}_i) \exp\{(\underline{k}.\underline{r}_i - kr)\}/r_i$$

$$+ \sum_i f(\underline{k}.\hat{\underline{r}}_i) \exp\{-i(\underline{k}.\underline{r}_i - kr_i)\}/r_i + \cdots$$

Helmholtz-Kirchoff algorithm

$$A(\underline{r}) = \int I(\underline{k}) e^{-i\underline{k}.\underline{r}} d\hat{\underline{k}}$$

the terms linear in f^* and f give:

$$A(\underline{r}) = \cdots + \sum_i \frac{e^{-ikr_i}}{r_i} \int f^*(\underline{k}.\hat{\underline{r}}_i) e^{i\underline{k}.(\underline{r}_i - \underline{r})} d\hat{\underline{k}}$$

$$+ \sum_i \frac{e^{ikr_i}}{r_i} \int f(\underline{k}.\hat{\underline{r}}_i) e^{-i\underline{k}.(\underline{r}_i + \underline{r})} d\hat{\underline{k}} + \cdots$$

This gives peaks at $r = \pm r_i$ only if $f(\underline{k}.\hat{\underline{r}}_i)$ is slowly varying with $\hat{\underline{k}}$.

Scattering factor deconvolution

$$A(\underline{r}) = \int \frac{I(\underline{k})}{f^*(\underline{k}.\underline{r})} e^{-i\underline{k}.\underline{r}} d\hat{\underline{k}}$$

THIS GIVES GOOD STATIONARY PHASE CONDITION AT $\underline{r} = \underline{r}_i$ but not at TWIN, $\underline{r} = -\underline{r}_i$

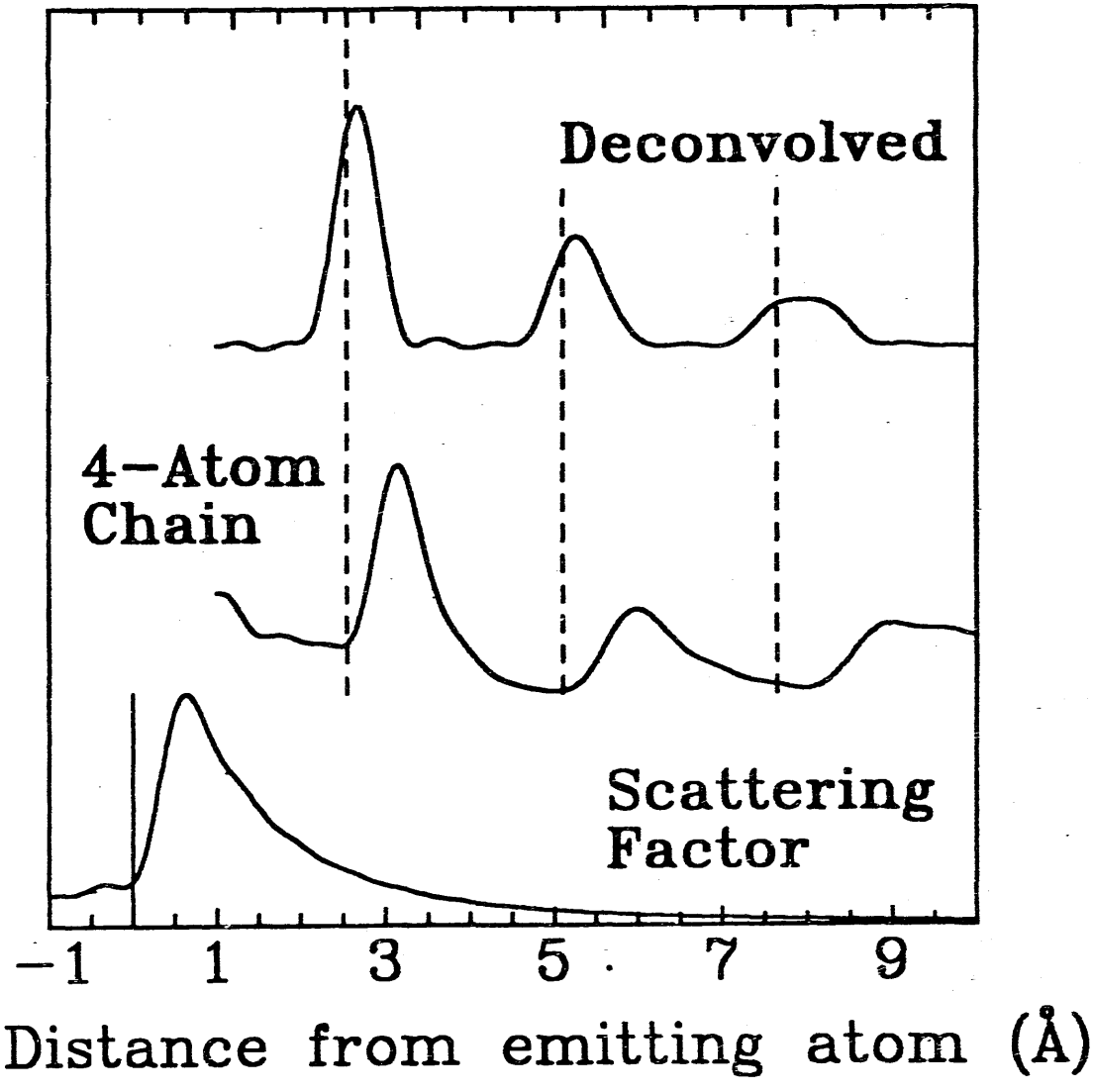
Deconvolved
4-Atom
Chain
Scattering
Factor
-1
1
3
5
7
9
Distance from emitting atom (Å)

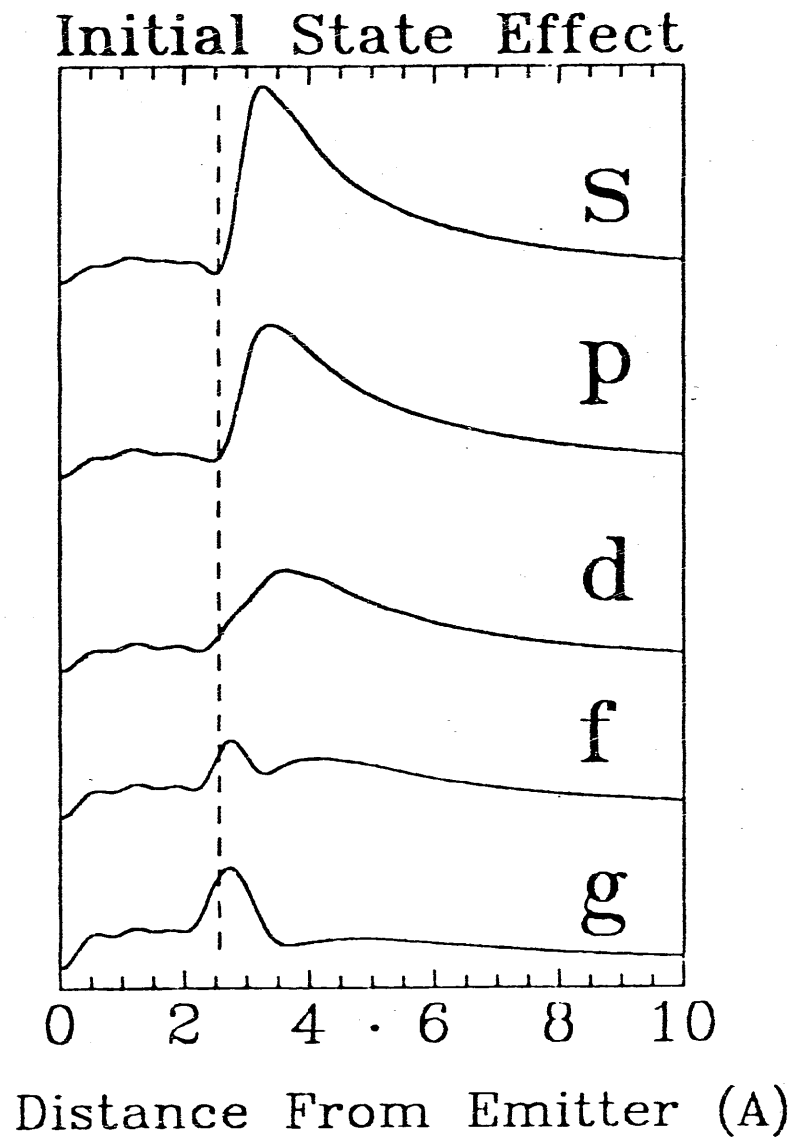
Initial State Effect
s
p
d
f
g
0
2
4
6
8
10
Distance From Emitter (A)

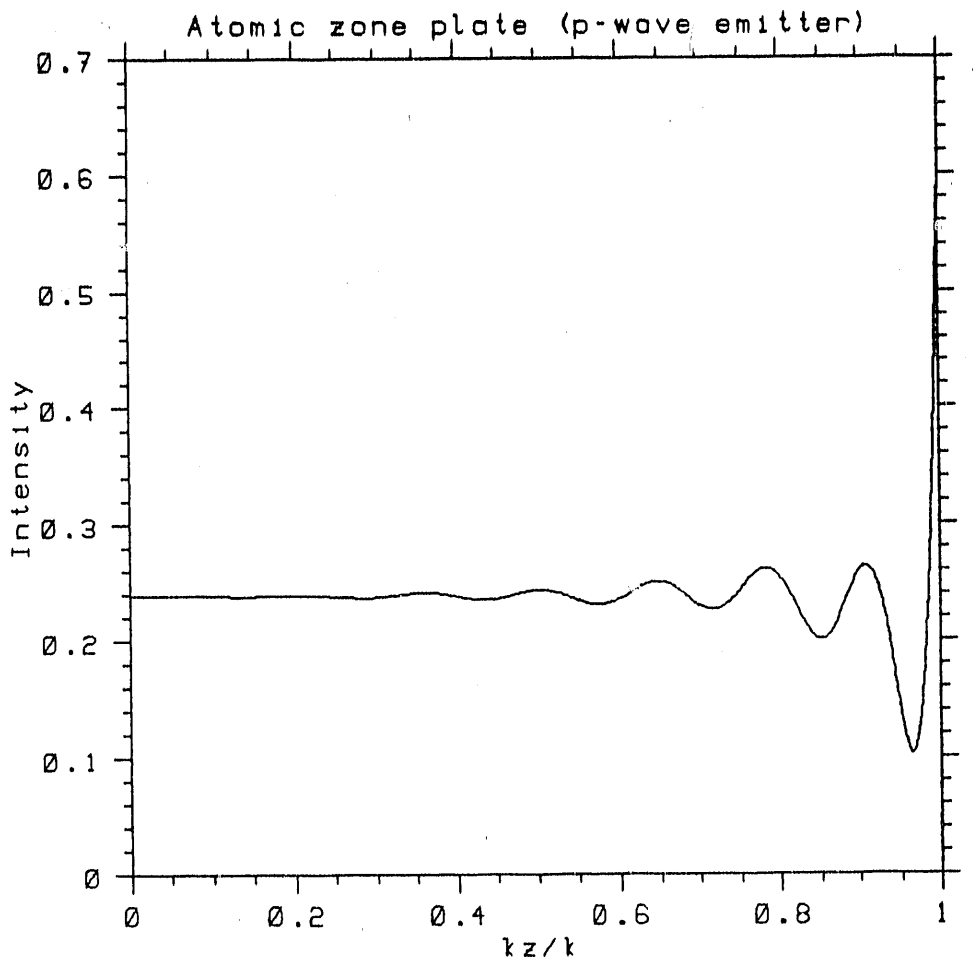
Atomic zone plate (p-wave emitter)
Intensity
0.7
0.6
0.5
0.4
0.3
0.2
0.1
0
0
0.2
0.4
0.6
0.8
1
kz/k

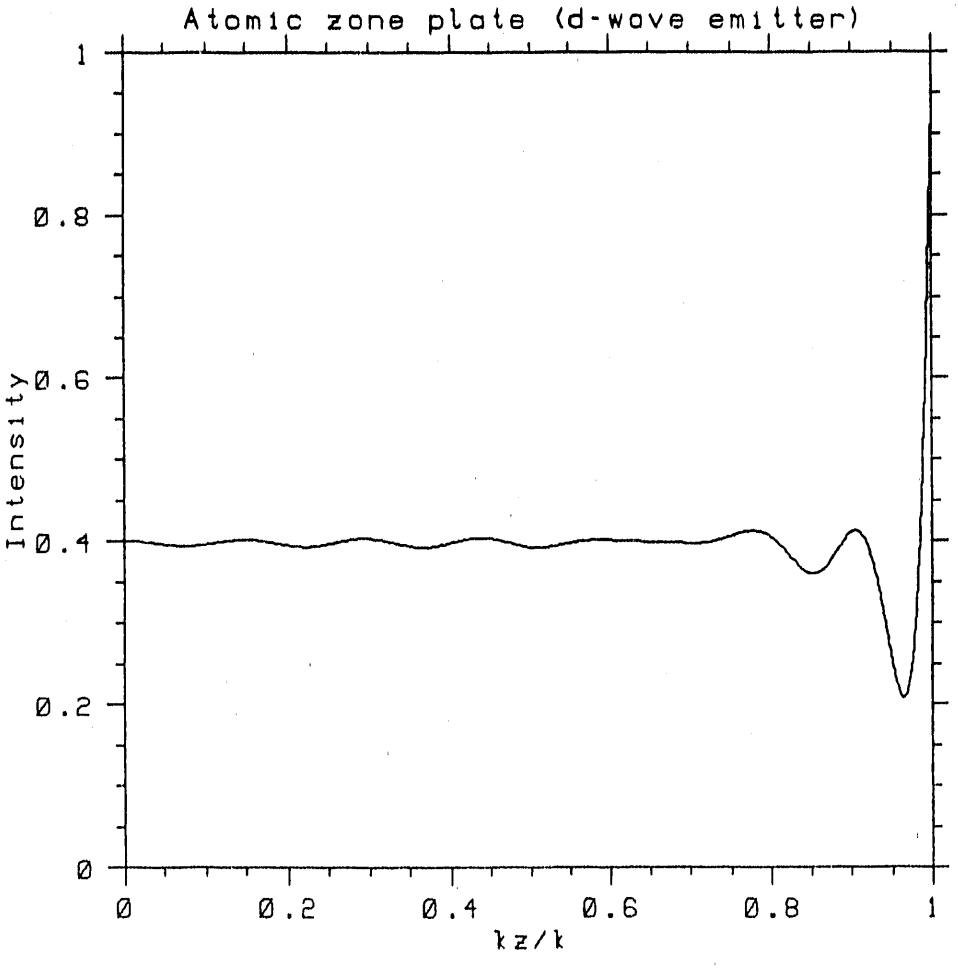
Atomic zone plate (d-wave emitter)
Intensity
1
0.8
0.6
0.4
0.2
0
0
0.2
0.4
0.6
0.8
1
kz/k

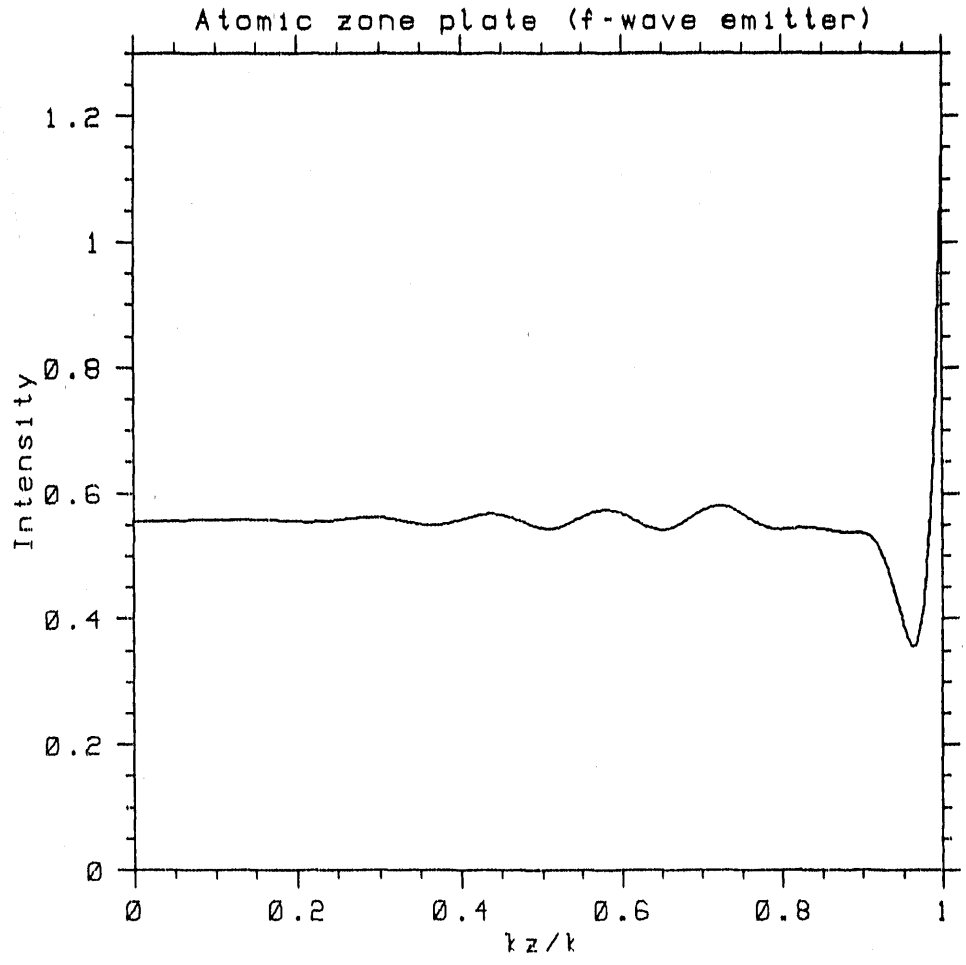
Atomic zone plate (f-wave emitter)
Intensity
1.2
1
0.8
0.6
0.4
0.2
0
0
0.2
0.4
0.6
0.8
1
kz/k

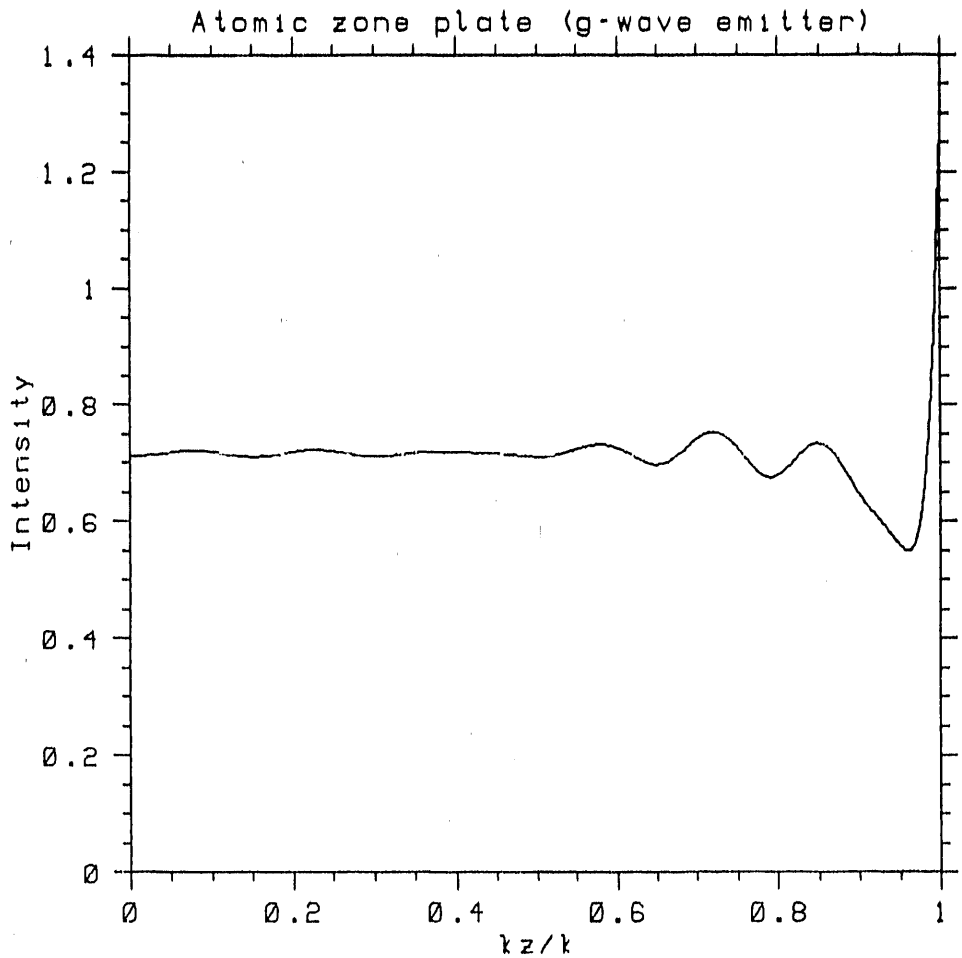
Atomic zone plate (g-wave emitter)
Intensity
1.4
1.2
1
0.8
0.6
0.4
0.2
0
0
0.2
0.4
0.6
0.8
1
kz/k

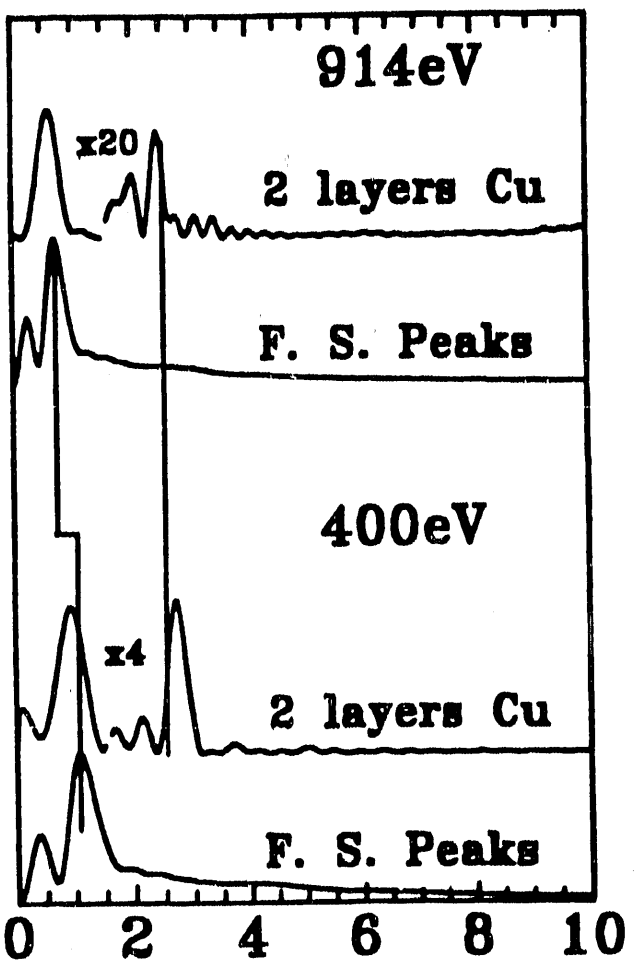
914eV
x20
2 layers Cu
F. S. Peaks
400eV
x4
2 layers Cu
F. S. Peaks
0
2
4
6
8
10
Distance From
Emitting Atom (Å)

Rotating polar axis

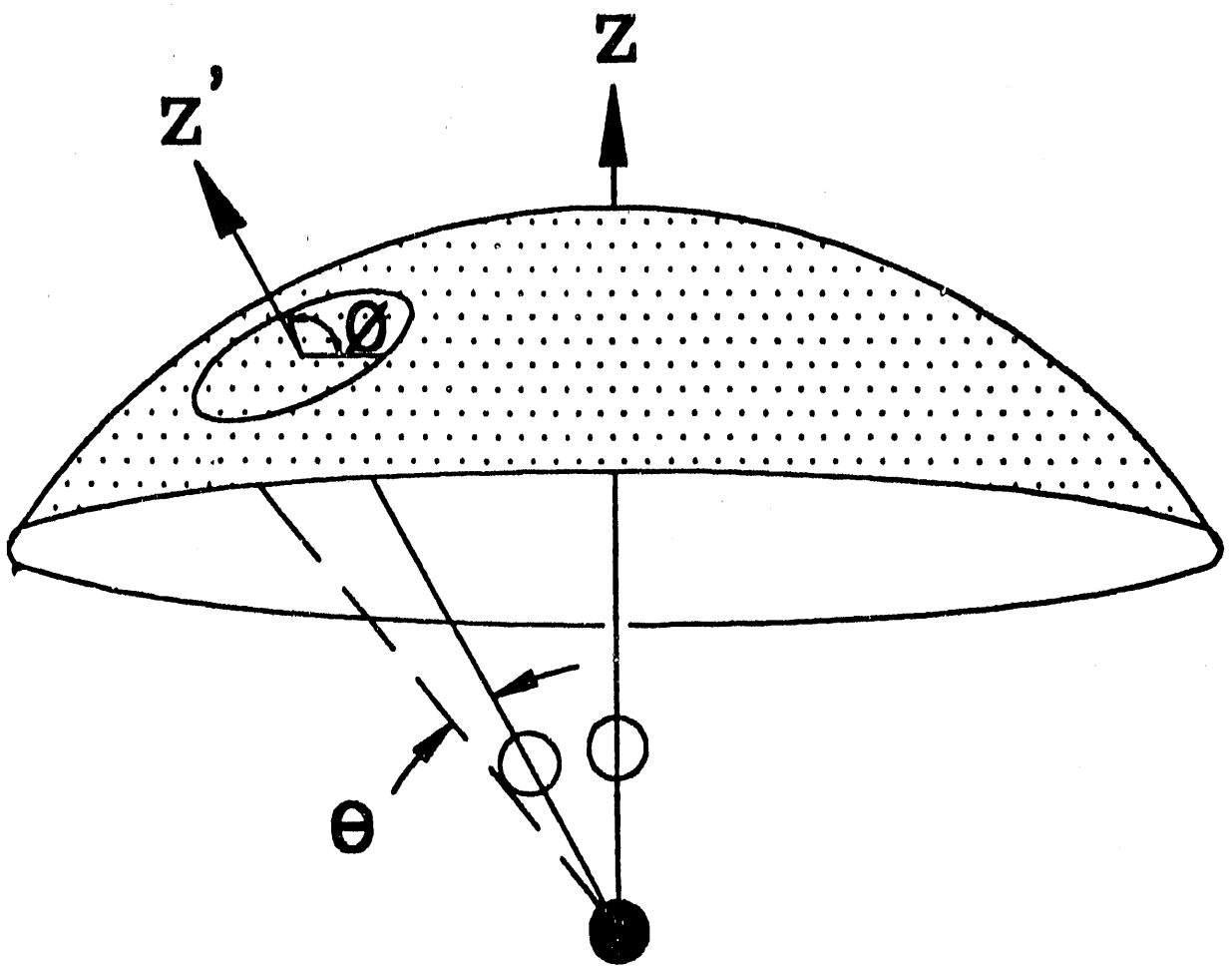

Radial image function (RIF)

In general, a polar axis (z') may be chosen in the direction of the RIF currently being considered.

From $A(\underline{r}) = \iint I(k_x, k_y)\, e^{-i \underline{k} \cdot \underline{r}}\, dk_x\, dk_y$

$$A(z') = -\int \{ I(k_{z'}, \phi)\, d\phi \}\, e^{-i k_{z'} z'}\, dk_{z'}$$

$$= -\int J(k_{z'})\, e^{-i k_{z'} z'}\, dk_{z'}$$

where $J(k_{z'}) = \int I(k_{z'}, \phi)\, d\phi$

Thus the RIF is a 1-D F.T. of the azimuthally integrated intensity as a function of $k_{z'}$.

Cu(100) 2-layer film

Neighboring forward scattering peak.

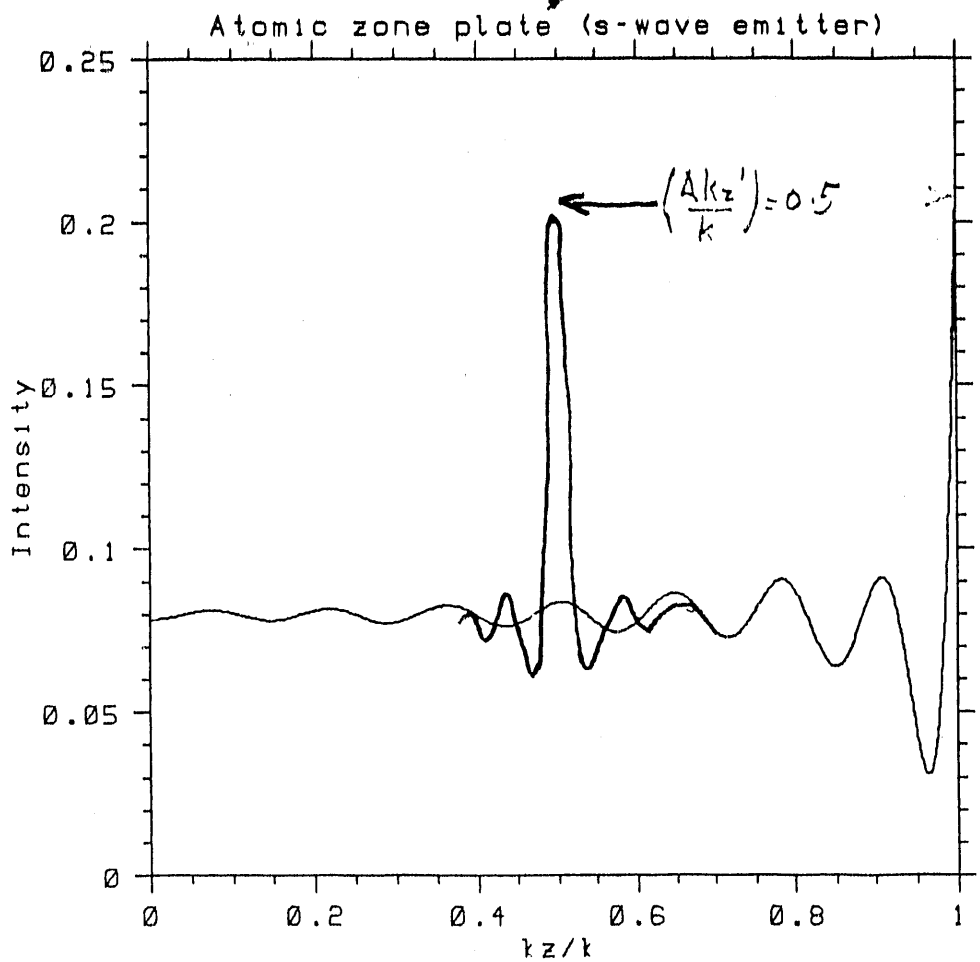

$$A(z') = \int I(k_z') e^{-i k_z' z'} dk_z'$$

"Frequency" $= z_a = \frac{2\pi}{\Delta k_z'} = \frac{2\pi}{(0.5)k}$

$$= \begin{cases} 1.2\,\text{Å} & \text{for } E = 400\text{ eV} \\ 0.8\,\text{Å} & \text{for } E = 914\text{ eV} \end{cases}$$

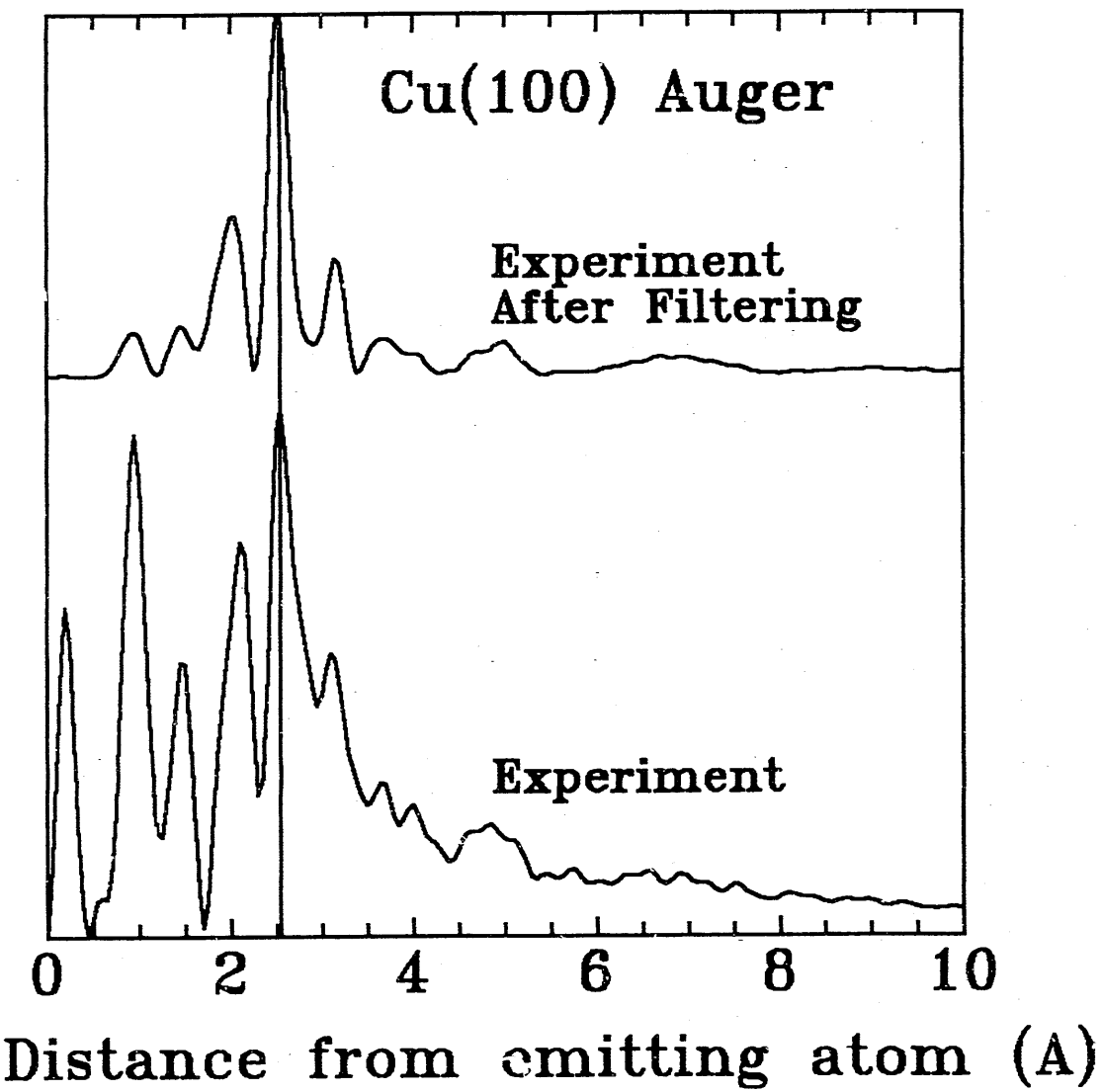
Cu(100) Auger
Experiment
After Filtering
Experiment
0
2
4
6
8
10
Distance from emitting atom (A)

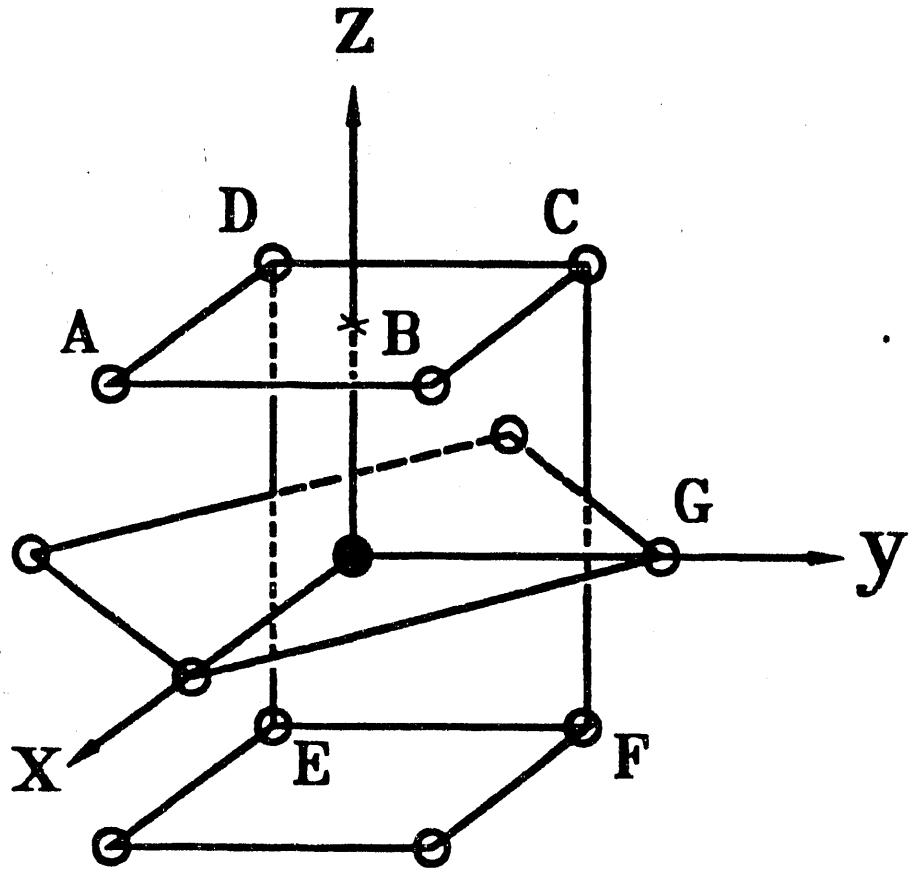
Z
D
C
A
B
G
y
X
E
F

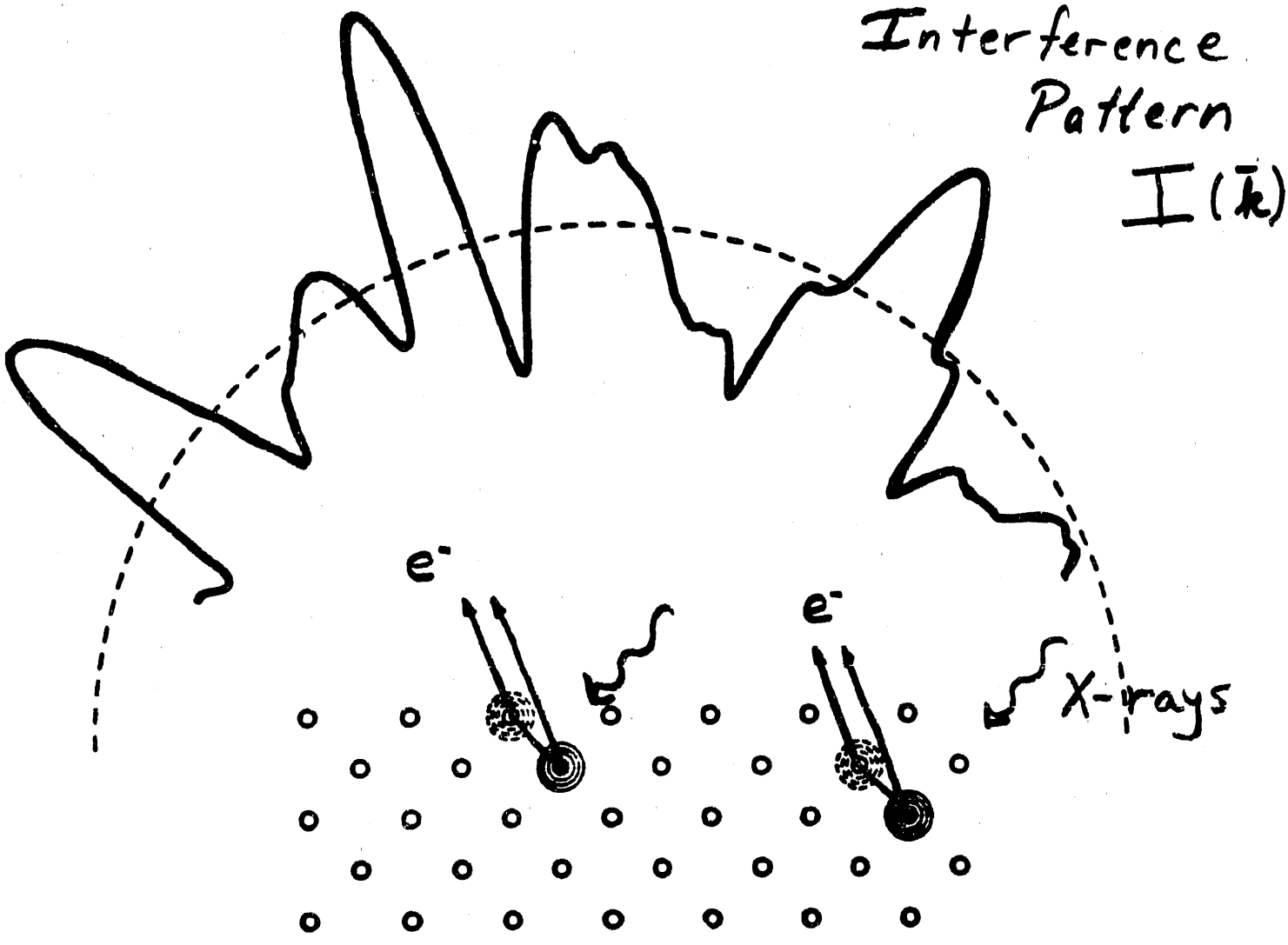
Interference
Pattern
I(k)
e⁻
e⁻
X-rays

"Onion-Skin" Algorithm

D. K. Saldin and J. B. Pendry,
Surface Sci., **162**, 941 (1985)

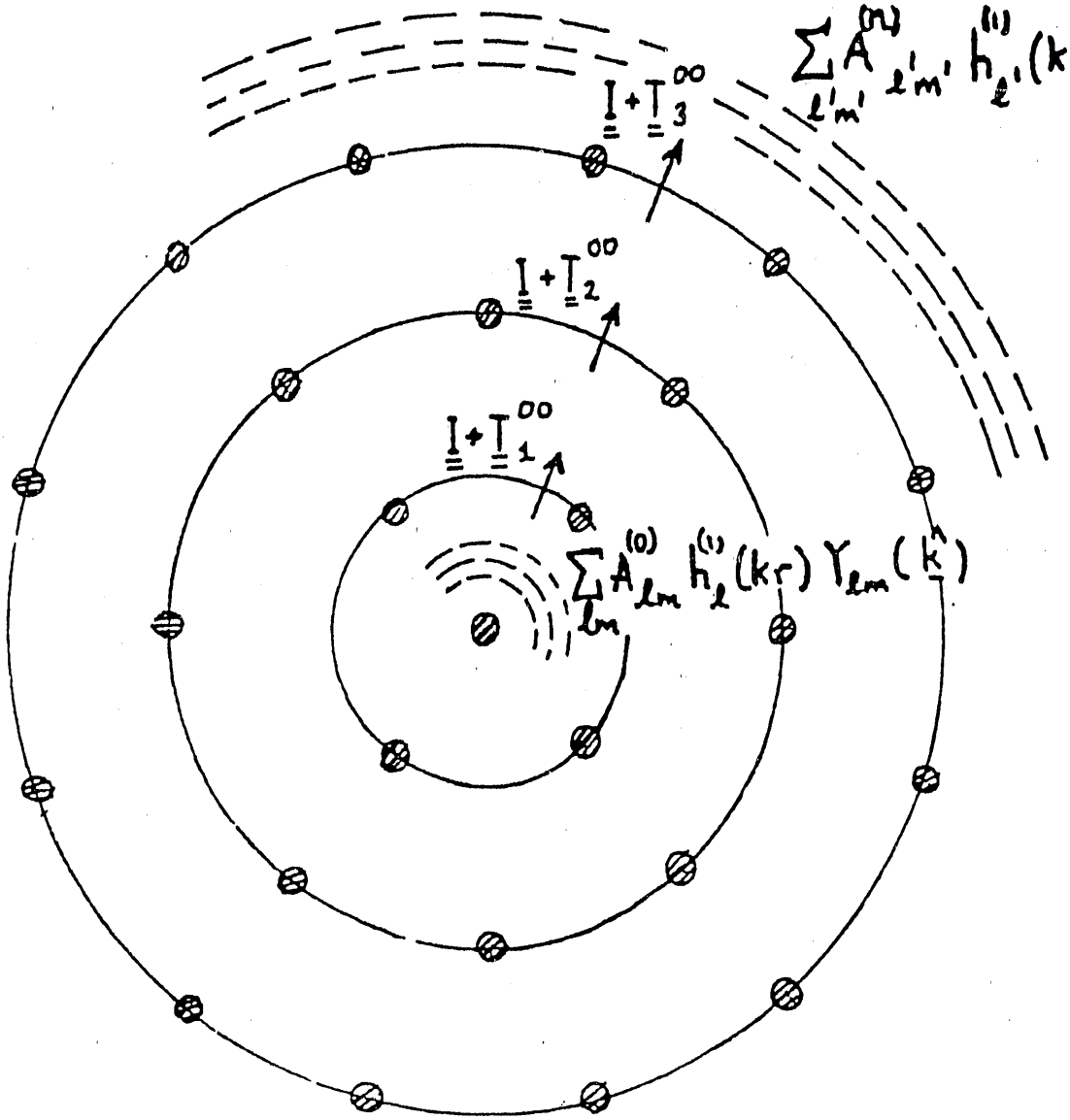

$$\underline{\underline{A}}^{(n)} = \underline{\underline{A}}^{(0)} \underline{\underline{S}}^{(n)}$$

$$\underline{\underline{S}}^{(0)} = \underline{\underline{I}} \quad ; \quad \underline{\underline{S}}^{(k+1)} = \underline{\underline{S}}^{(k)} \left(\underline{\underline{I}} - \underline{\underline{T}}^{0I}_{k+1} \underline{\underline{J}}^{I0}_{k}\right)^{-1} \left(\underline{\underline{I}} + \underline{\underline{T}}^{00}_{k+1}\right)$$

$$\underline{\underline{J}}^{I0}_{0} = \underline{\underline{t}}_c \quad ; \quad \underline{\underline{J}}^{I0}_{k+1} = \underline{\underline{T}}^{I0}_{k+1} + \left(\underline{\underline{I}} + \underline{\underline{T}}^{II}_{k+1}\right) \underline{\underline{J}}^{I0}_{k} \left(\underline{\underline{I}} - \underline{\underline{T}}^{0I}_{k+1} \underline{\underline{J}}^{I0}_{k}\right)^{-1} \left(\underline{\underline{I}} + \underline{\underline{T}}^{00}_{k+1}\right)$$

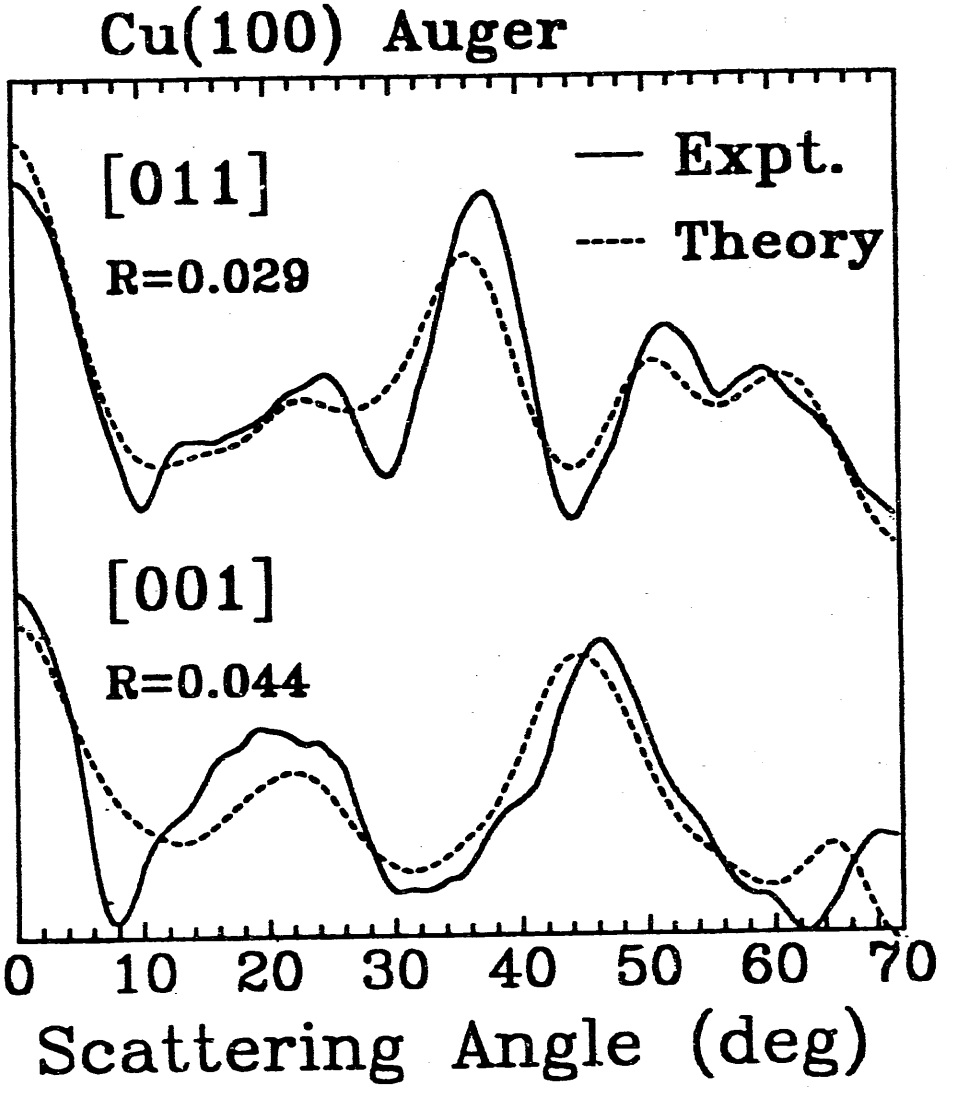
Cu(100) Auger
[011]
R=0.029
Expt.
Theory
[001]
R=0.044
0
10
20
30
40
50
60
70
Scattering Angle (deg)

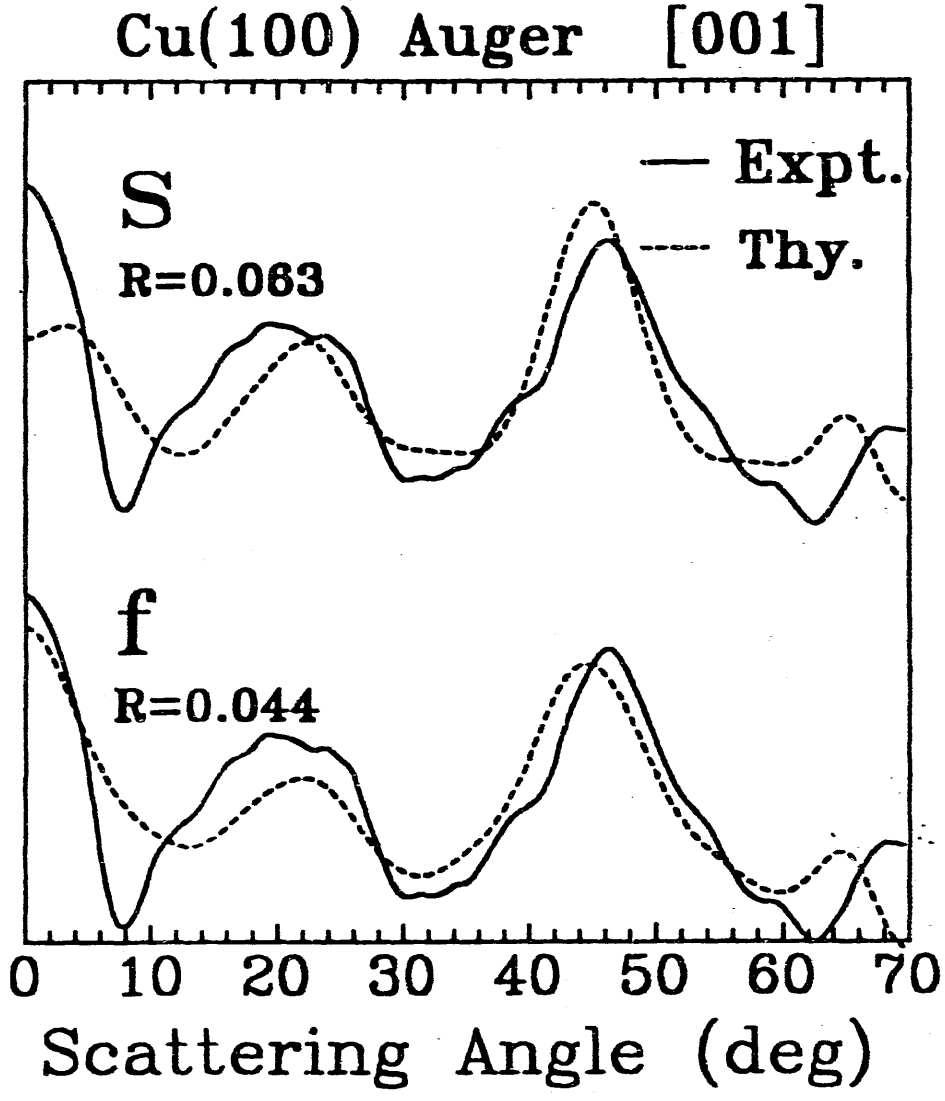
Cu(100) Auger [001]
— Expt.
---- Thy.
S
R=0.063
f
R=0.044
0 10 20 30 40 50 60 70
Scattering Angle (deg)

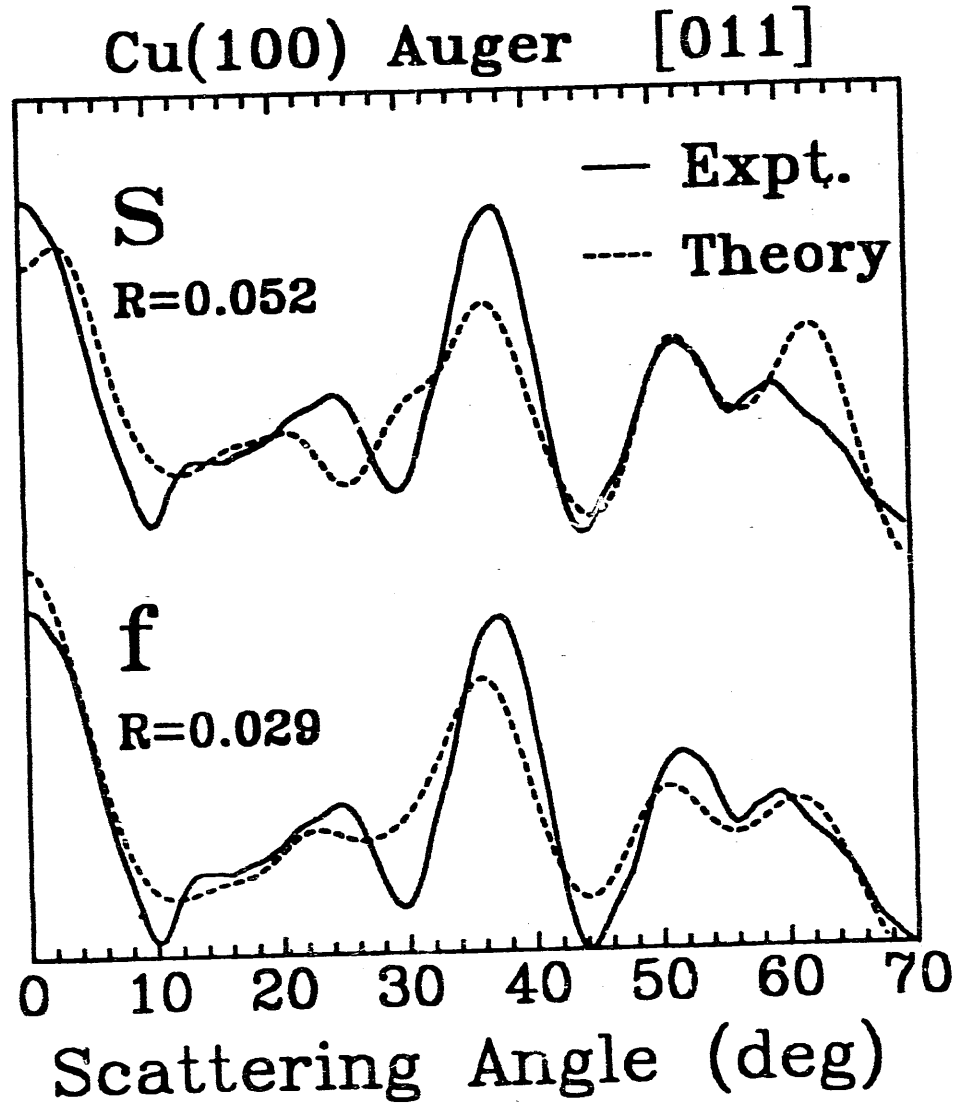
Cu(100) Auger [011]
— Expt.
---- Theory
S
R=0.052
f
R=0.029
0 10 20 30 40 50 60 70
Scattering Angle (deg)

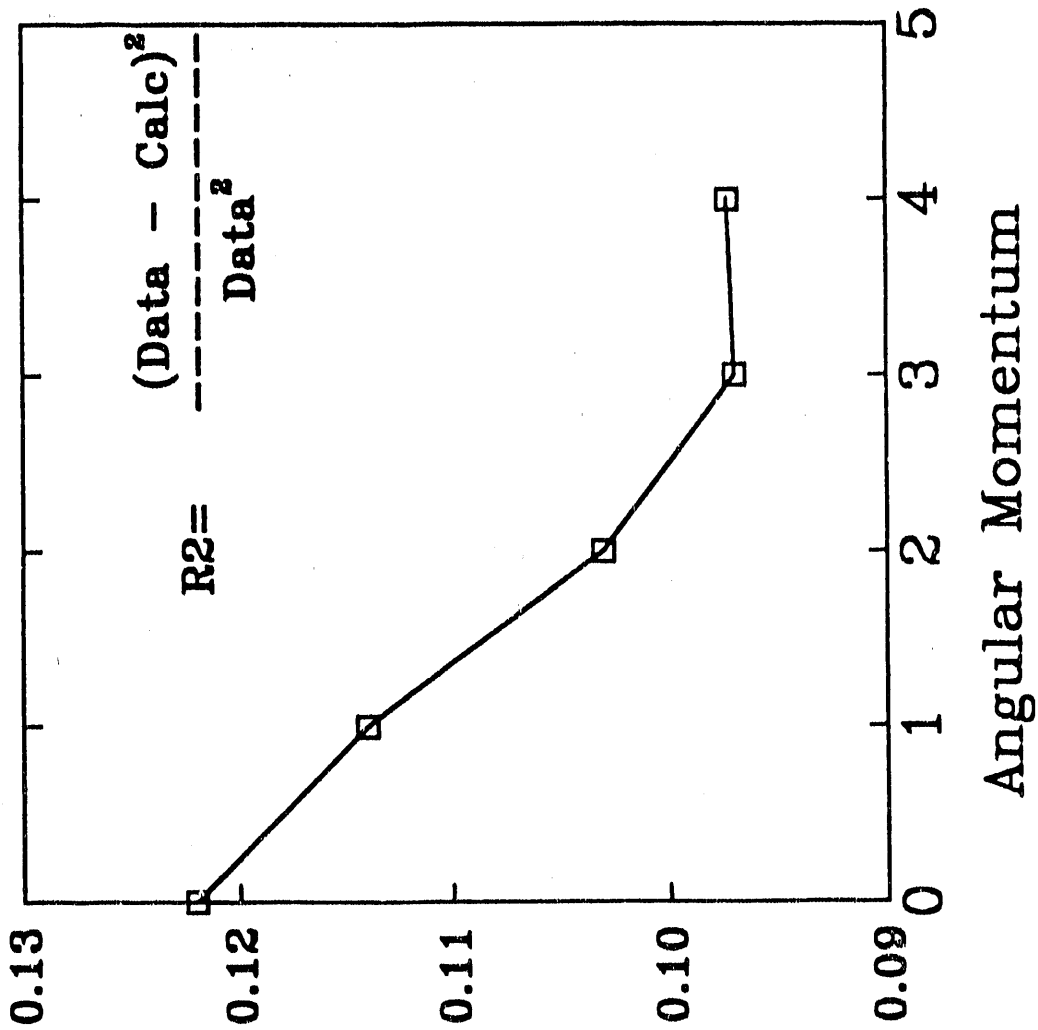
R2= (Data - Calc)² / Data²
0.13
0.12
0.11
0.10
0.09
0
1
2
3
4
5
Angular Momentum

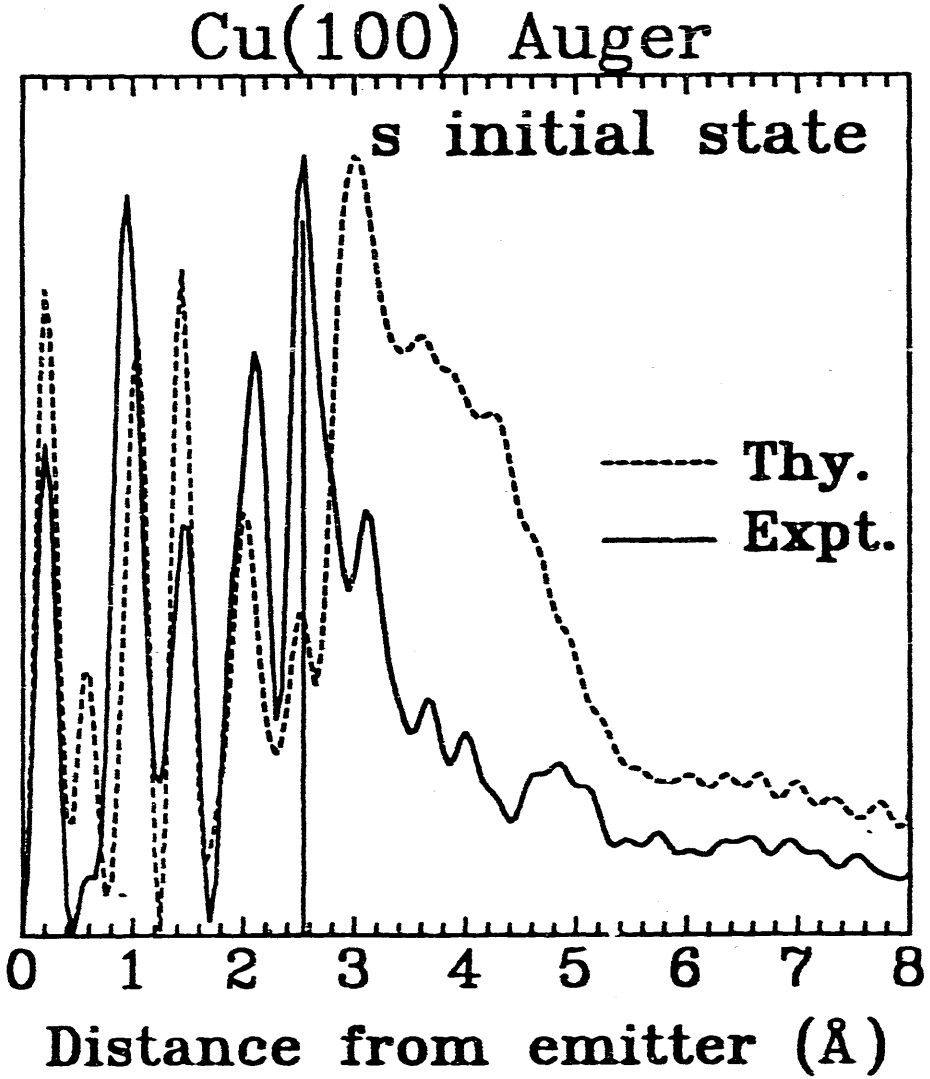
Cu(100) Auger
s initial state
Thy.
Expt.
0
1
2
3
4
5
6
7
8
Distance from emitter (Å)

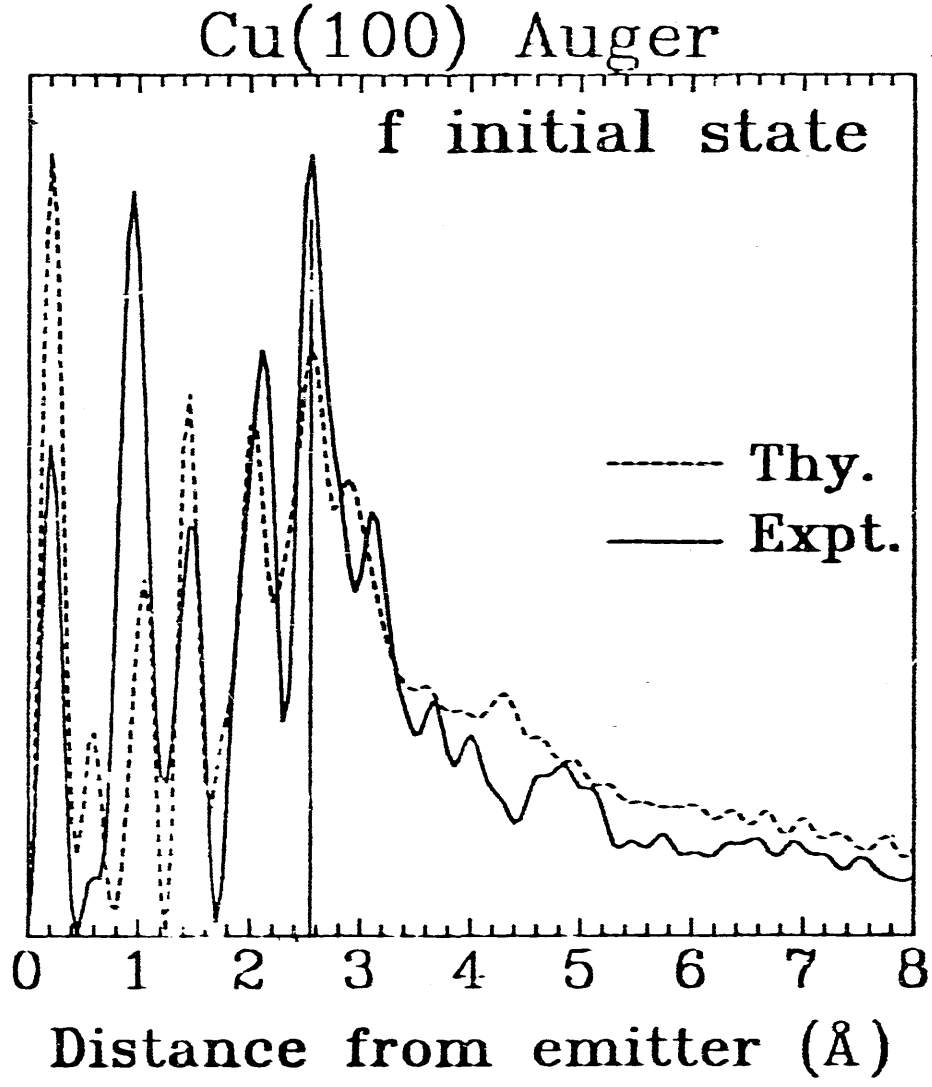
Cu(100) Auger
f initial state
Thy.
Expt.
0
1
2
3
4
5
6
7
8
Distance from emitter (Å)

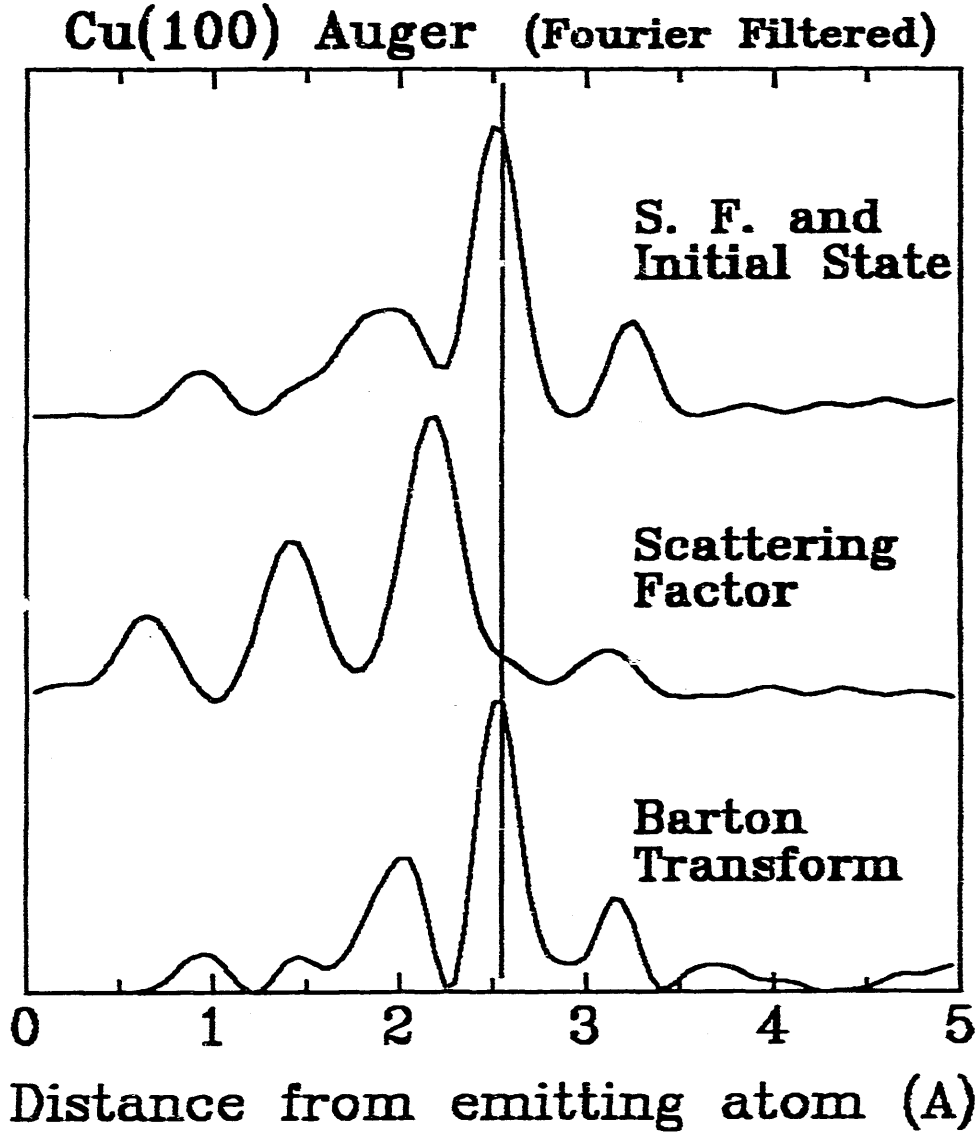
Cu(100) Auger (Fourier Filtered)
S. F. and
Initial State
Scattering
Factor
Barton
Transform
0
1
2
3
4
5
Distance from emitting atom (A)

Prospects for Advanced Photoelectron Diffraction

C.S. Fadley

University of California at Davis
and
Lawrence Berkeley Laboratory

PROSPECTS FOR ADVANCED PHOTOELECTRON DIFFRACTION

S. THEVUTHASAN[+], G.S. HERMAN, T. TRAN, Y.J. KIM, R.S. SAIKI, F. ZHANG[+]

UNIV. OF HAWAII

A.P. KADUWELA, M. VAN HOVE, C.S. FADLEY[+]

LAWRENCE BERKELEY LAB.

([+] ALSO UNIV. OF CALIF.-DAVIS)

- PHOTOELECTRON-/AUGER- HOLOGRAPHY: WHY DO THEY WORK AS WELL AS THEY DO? HOW MUCH BETTER CAN WE MAKE THEM?
- HIGH ANGULAR RESOLUTION DATA: HOW MUCH MORE INFO. DOES IT CONTAIN?
- TEMPERATURE-DEPENDENT STUDIES OF:
  - SURFACE PHASE TRANSITIONS
  - MAGNETIC SHORT-RANGE ORDER- WITH e^- SPIN RESOLUTION

SUPPORTED BY: D.O.E.-L.B.L.
O.N.R.
N.E.D.O.-M.I.T.I. (JAPAN)

SOME FUNDAMENTALS:

- ATOM-SPECIFIC PROBE
- SHORT-RANGE-ORDER PROBE:
  - LARGELY FIRST 3-5 SPHERES, BUT
  - SOME INFO. OUT TO ~10-15 Å
- VERY SHORT TIME SCALE OF $\sim 10^{-17}$ SEC
  (CF. MÖSSBAUER @ $\sim 10^{-7}$ SEC
  INELASTIC n^0 SCATT. @ $\sim 10^{-12}$ SEC
  2-e^- CAPTURE BY d @ $\sim 10^{-16}$ SEC)
- RATHER WELL DESCRIBED FOR $\gtrsim$ 200 eV BY SINGLE-SCATTERING MODEL, WITH MULTIPLE SCATTERING* EFFECTS POSSIBLE IN LOW-INDEX ROWS AND @ LOWER ENERGIES.
- HIGH-ENERGIES $\gtrsim$ 500 eV $\Rightarrow$
  - FORWARD-SCATTERING DOMINANT
  - MORE BULK SENSITIVITY
- LOW-ENERGIES $\lesssim$ 200 eV $\Rightarrow$
  - FORWARD- AND BACK-SCATTERING
  - MORE SURFACE SENSITIVE
  - MAGNETIC SCATTERING EFFECTS (EXCHANGE, SPIN-ORBIT) BECOME IMPORTANT

---

* TONG ET AL., BARTON + SHIRLEY, VAN HOVE ET AL., OUR GROUP

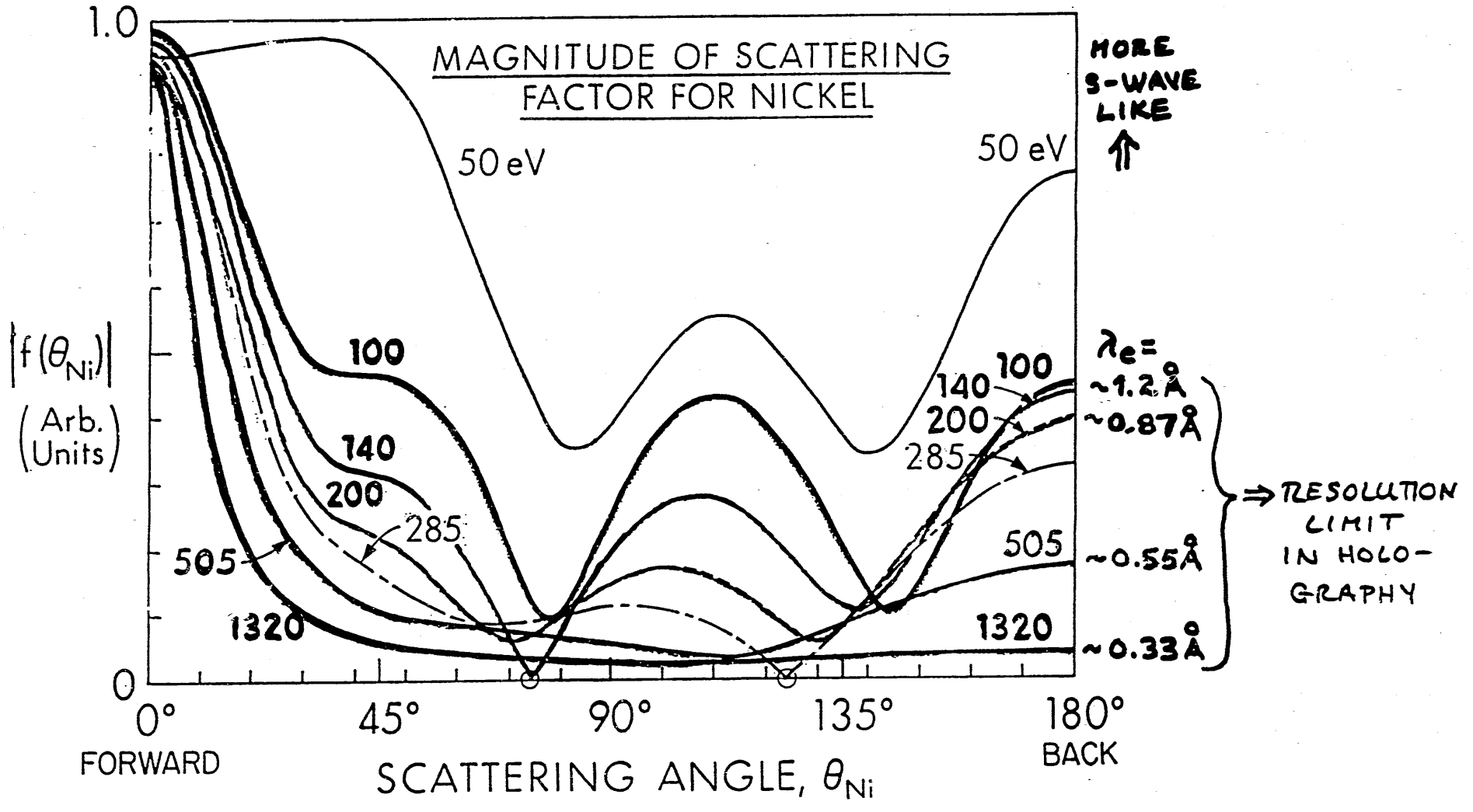
MAGNITUDE OF SCATTERING FACTOR FOR NICKEL
1.0
0
50 eV
50 eV
100
140
200
285
505
1320
100
140
200
285
505
1320
MORE S-WAVE LIKE
λ_e =
~1.2 Å
~0.87 Å
~0.55 Å
~0.33 Å
⇒ RESOLUTION LIMIT IN HOLOGRAPHY
$|f(\theta_{Ni})|$
(Arb. Units)
0°
FORWARD
45°
90°
135°
180°
BACK
SCATTERING ANGLE, θ_{Ni}

FROM SINGLE-SCATTERING THEORY:

(E. G., P. R. B 22, 6085 ('80); P. R. B 27, 781 ('83))

$$I(\vec{k}) \propto \left|\phi_0 + \sum_j \phi_j\right|^2, \quad \sum_j \text{ ON FINITE CLUSTER},$$

$$\propto |\phi_0|^2 + \sum_j (\phi_0^* \phi_j + \phi_0 \phi_j^*) + \sum_j \sum_{j'} \phi_j^* \phi_{j'}.$$

IF $\phi_j \phi_{j'}^*$ SMALL W.R.T $\phi_0^* \phi_j + \phi_0 \phi_j^*$, A NECESSARY CONDITION FOR SIMPLE HOLOGRAPHY:

$$I(\vec{k}) \propto \underbrace{F_0^2}_{\| \; I_0} + 2F_0 \sum_j |F_j(\theta_j)| \cos\left[\underbrace{kr_j(1-\cos\theta_j)}_{\text{PATH LENGTH DIFFERENCE}} + \underbrace{\psi_j(\theta_j, k)}_{\text{SCATTERING PHASE}}\right]$$

$$\boxed{\chi(\vec{k}) = \frac{I(\vec{k}) - I_0}{I_0^{1/2}} \propto \left\{ \text{" " " " " "} \right\}}$$

WITH: $F_0 = (\hat{\varepsilon}\cdot\hat{k}) \exp(-L_0/2\Lambda_e)$

= amplitude of direct wave $= I_0^{1/2}$

$$|F_j(\theta_j)| = (\hat{\varepsilon}\cdot\hat{r}_j)\frac{|f_j(\theta_j)|}{r_j} W_j(\theta_j) \exp(-L_j/2\Lambda_e)$$

= amplitude of scattered wave

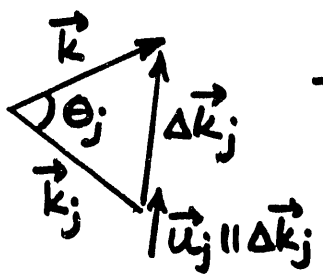

$$W_j = \exp(-\Delta k_j^2 \overline{u_j^2})$$

$$= \exp(-2k^2(1-\cos\theta_j)\overline{u_j^2})$$

LIKE EXAFS/SEXAFS, BUT THERE:

- ADD CENTRAL ATOM PHASE SHIFT
- $\phi_j \Rightarrow \pi$ FOR ALL SCATTERERS
- cos ⇒ sin IN ANGLE INTEGRATION
- $\hat{\varepsilon}\cdot\hat{r}_j/r_j \Rightarrow \hat{\varepsilon}\cdot\hat{r}_j/r_j^2$ IN OUT/BACK PATHS

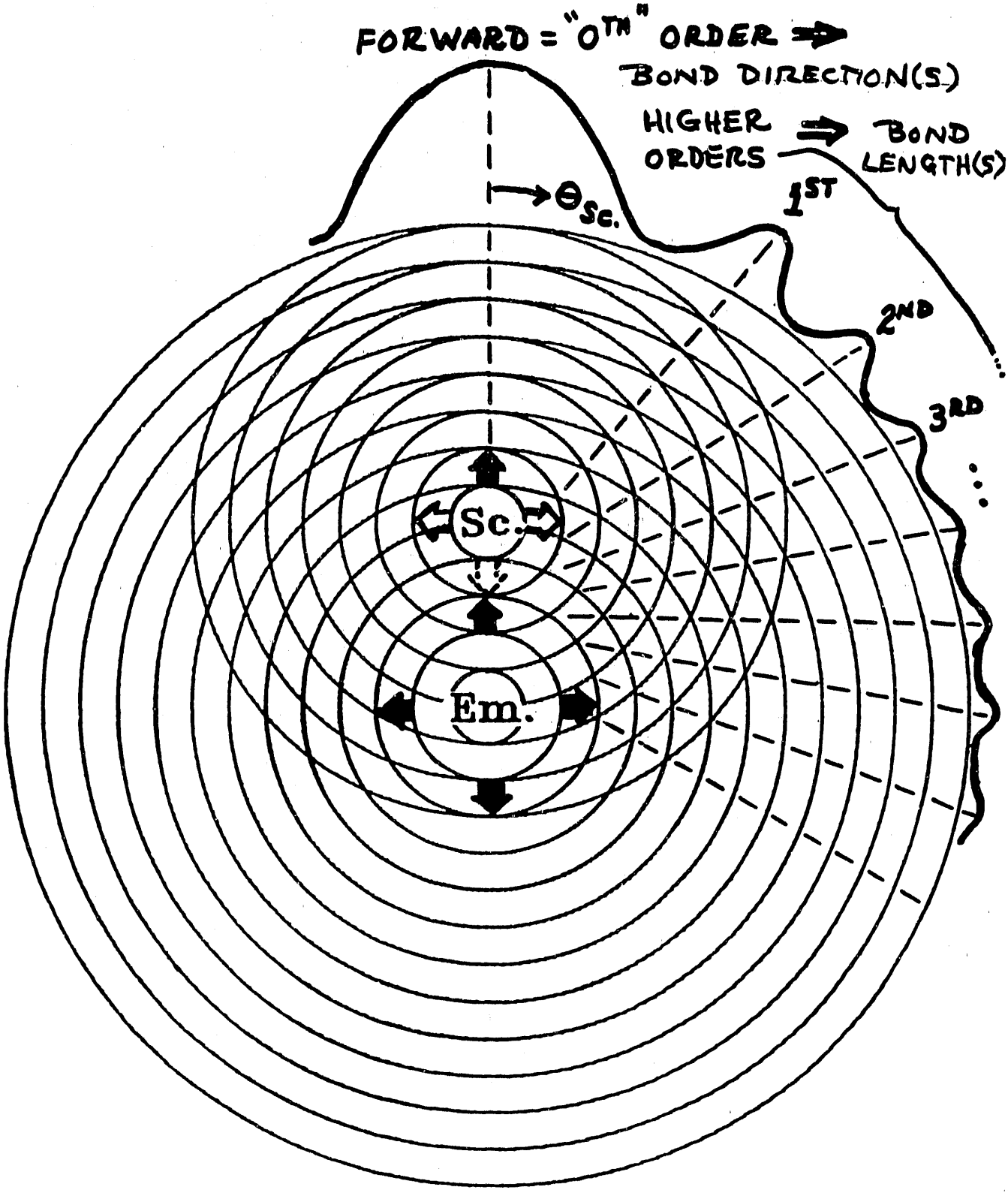

IN REAL CASE, ORDERS FROM:

$$2\pi n = k r_{Sc.}(1-\cos\theta_{Sc.}) + \Psi_{Sc.}(\theta_{Sc.})$$

PATH LENGTH DIFF. SCATT. PHASE SHIFT

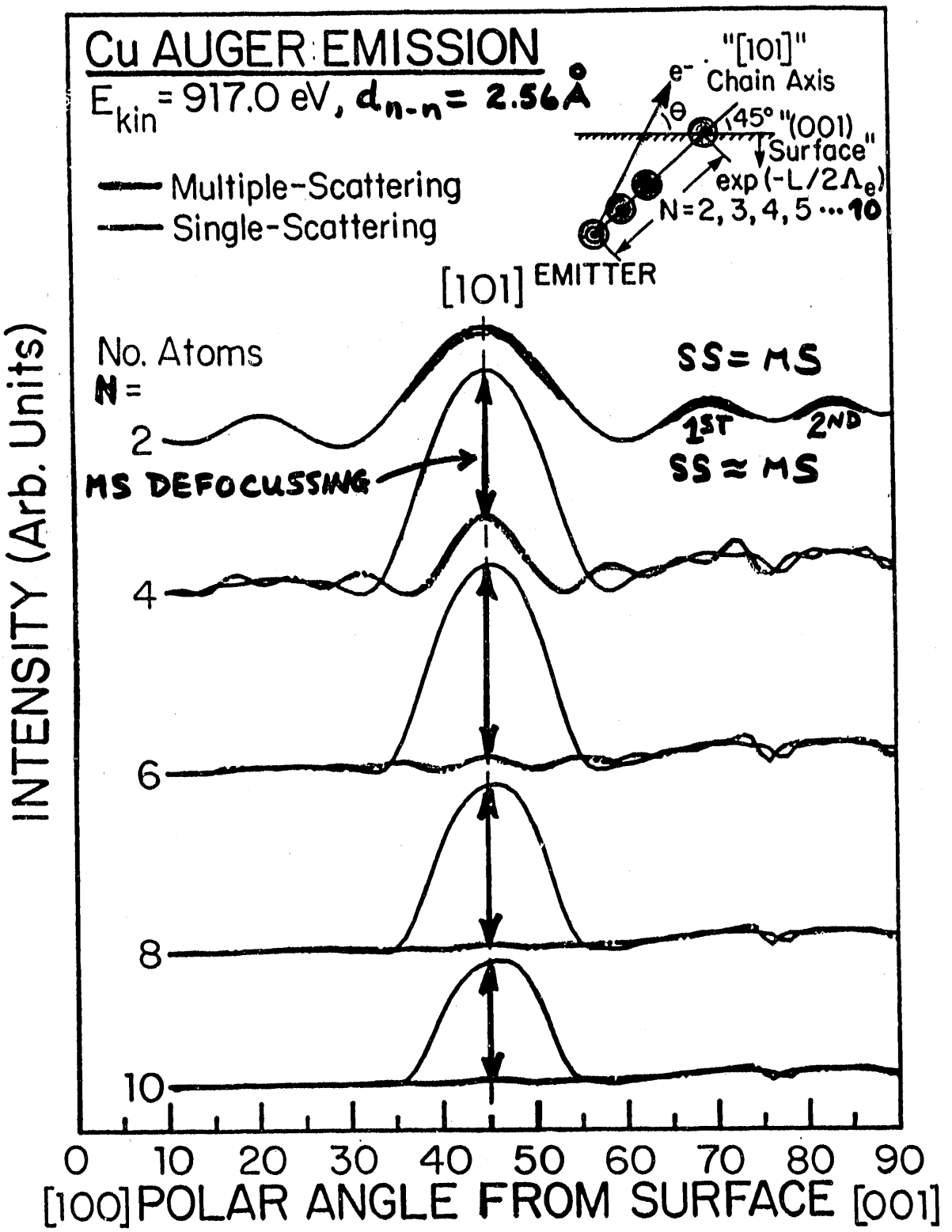

KADUWELA ET AL., PHYS. SCRIPTA 41, 948 ('90)
REHR, ALBERS, PHYS. REV. B 41, 8139 ('90)

(b) SOME MULTIPLE SCATTERING EFFECTS

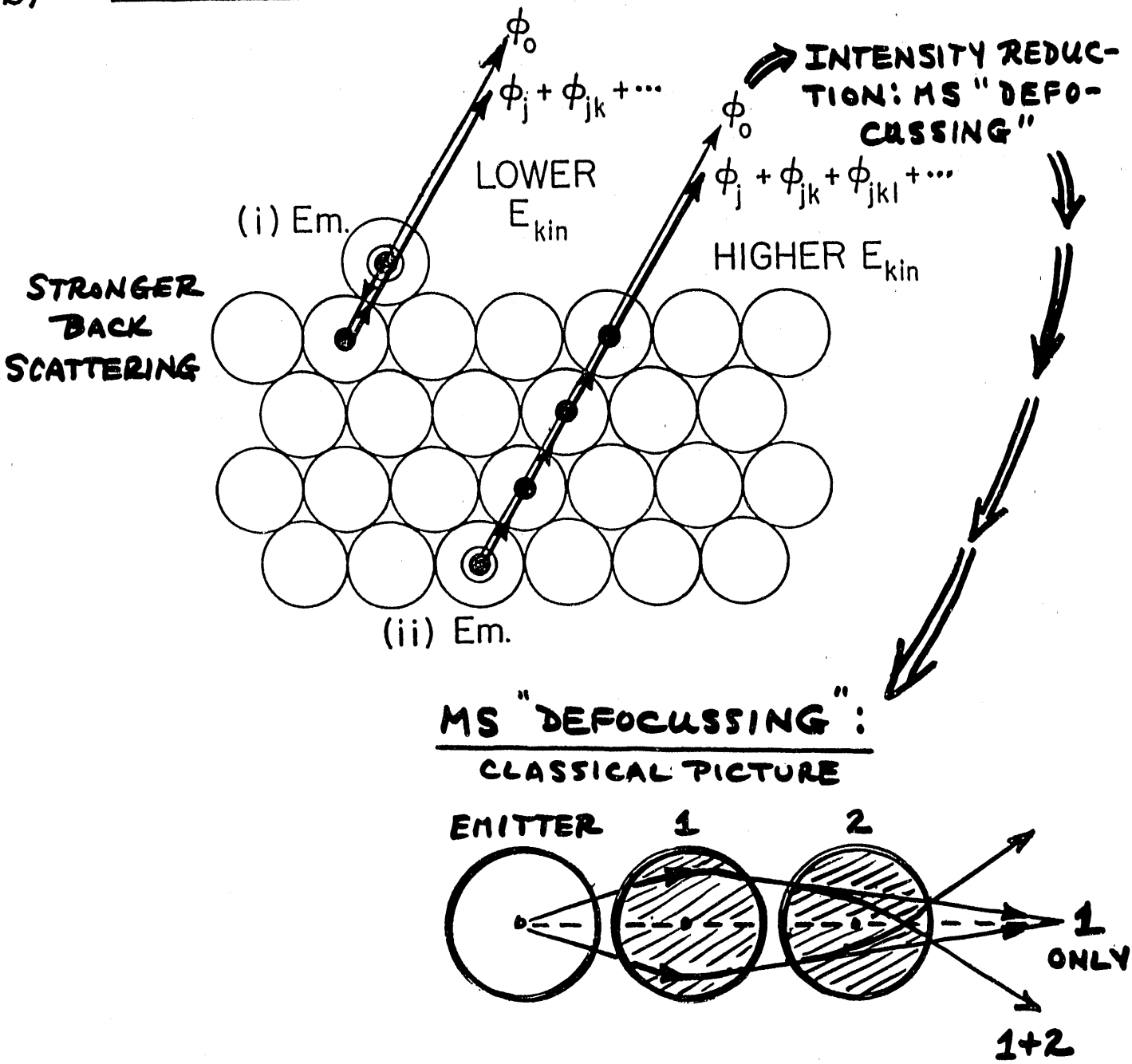

MS "DEFOCUSSING": CLASSICAL PICTURE

CALCS. BY: TONG ET AL.
BARTON, VAN HOVE ET AL.
OUR GROUP

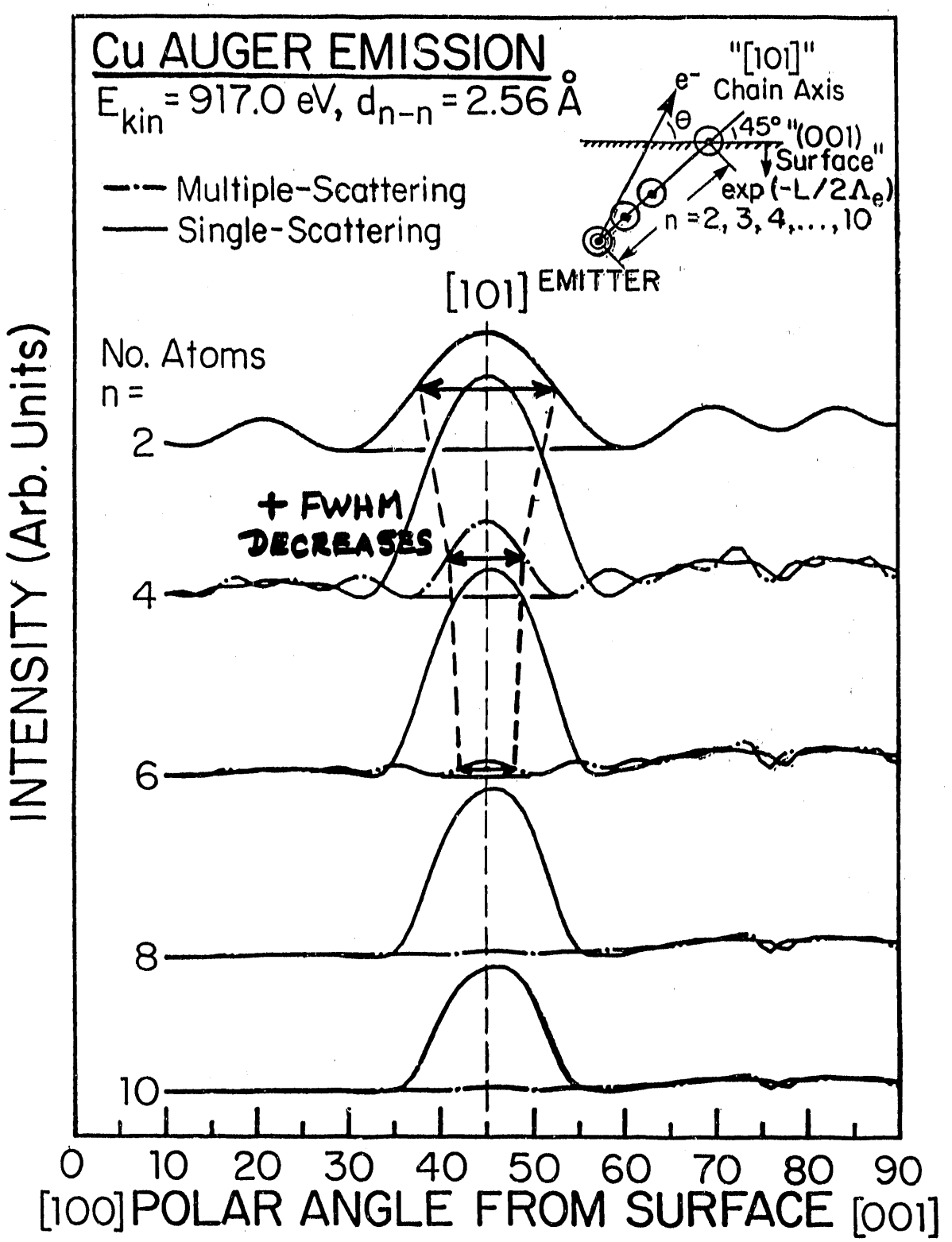
Cu AUGER EMISSION
E_{kin} = 917.0 eV, d_{n-n} = 2.56 Å
Multiple-Scattering
Single-Scattering
"[101]"
Chain Axis
e⁻
θ
45°
"(001)
Surface"
exp(-L/2Λe)
n = 2, 3, 4, ..., 10
[101] EMITTER
No. Atoms
n =
2
4
6
8
10
+ FWHM
DECREASES
INTENSITY (Arb. Units)
0 10 20 30 40 50 60 70 80 90
[100] POLAR ANGLE FROM SURFACE [001]

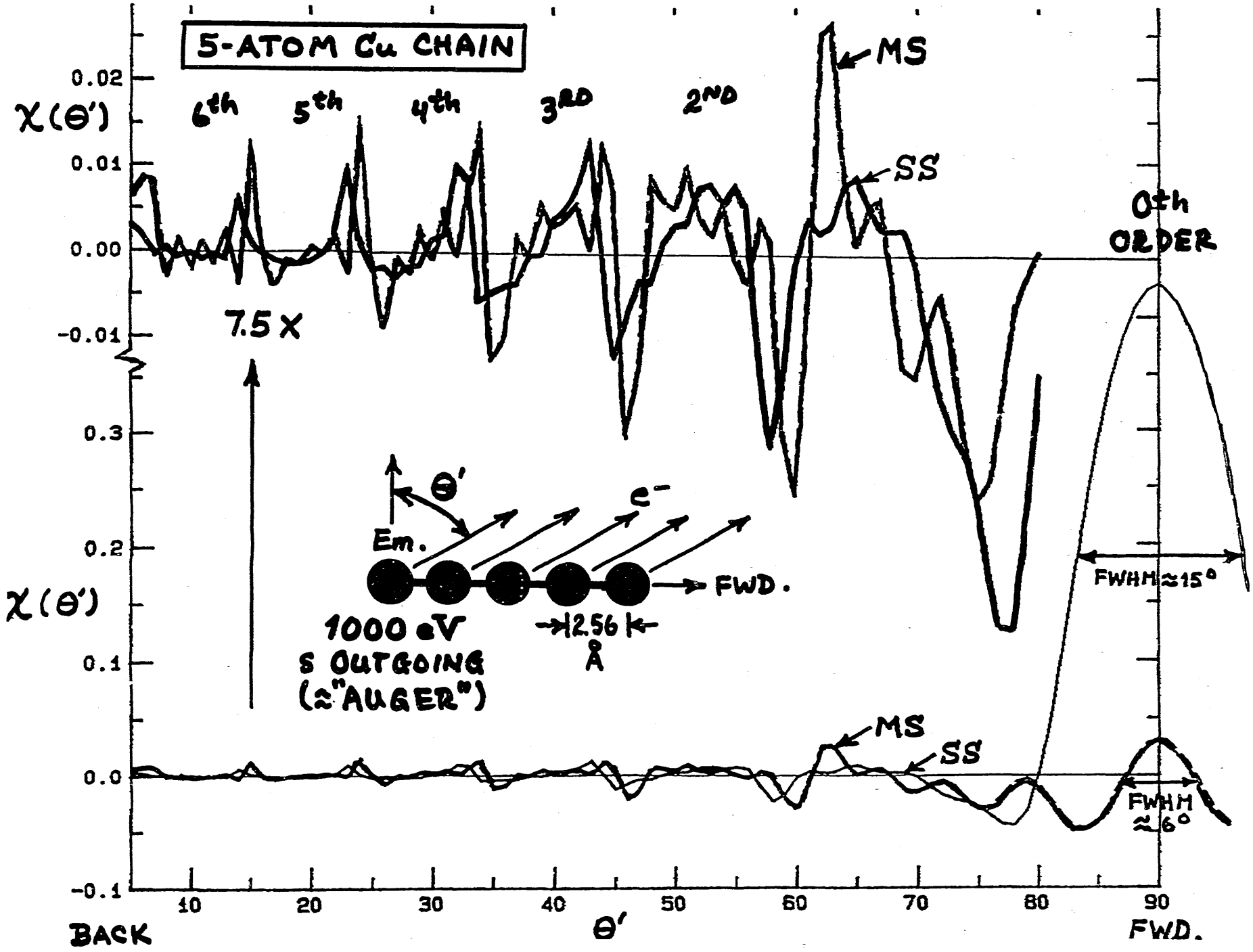
5-ATOM Cu CHAIN
6th
5th
4th
3RD
2ND
MS
SS
0th ORDER
χ(θ')
0.02
0.01
0.00
-0.01
7.5 X
0.3
0.2
0.1
0.0
-0.1
θ'
Em.
e⁻
FWD.
1000 eV
S OUTGOING
(≈"AUGER")
→2.56←
Å
FWHM≈15°
FWHM ≈6°
10
20
30
40
50
60
70
80
90
BACK
θ'
FWD.

$\chi(k_x, k_y)$ FOR Si2p EMISSION FROM Si(111): ~1387 eV

$\alpha = 174°$

EXPERIMENT:

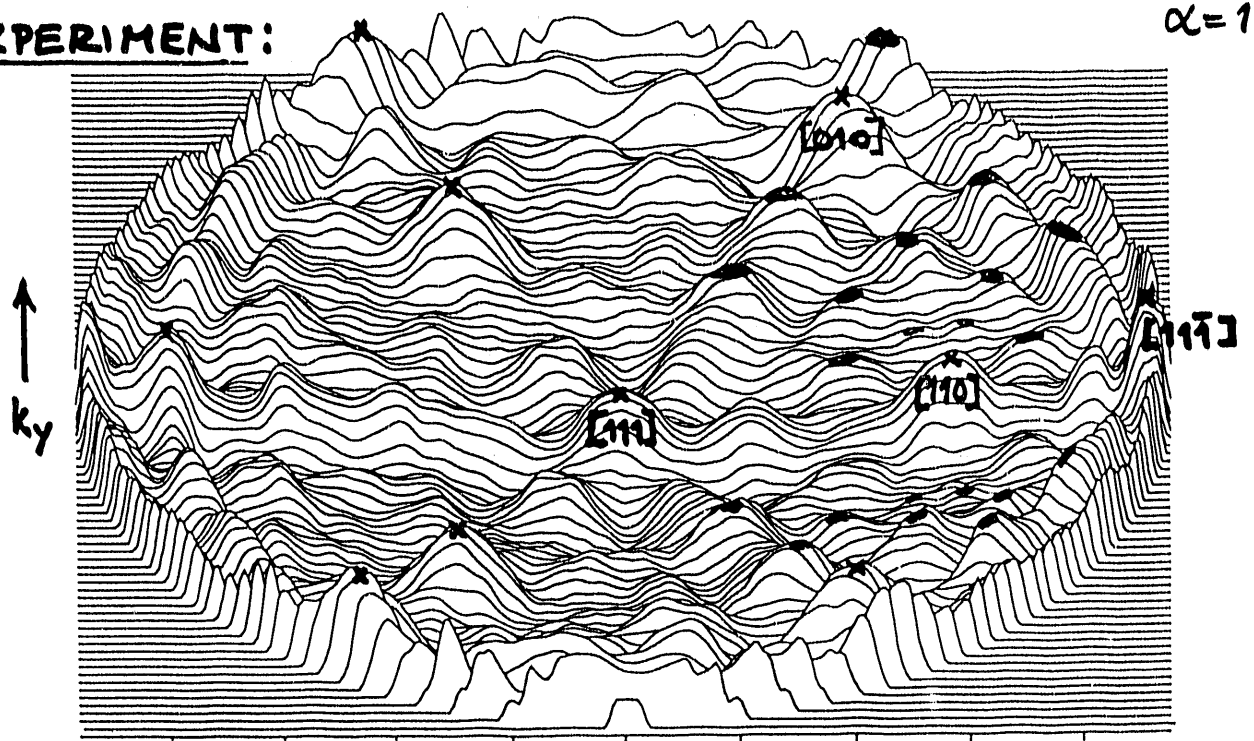

SS THEORY:

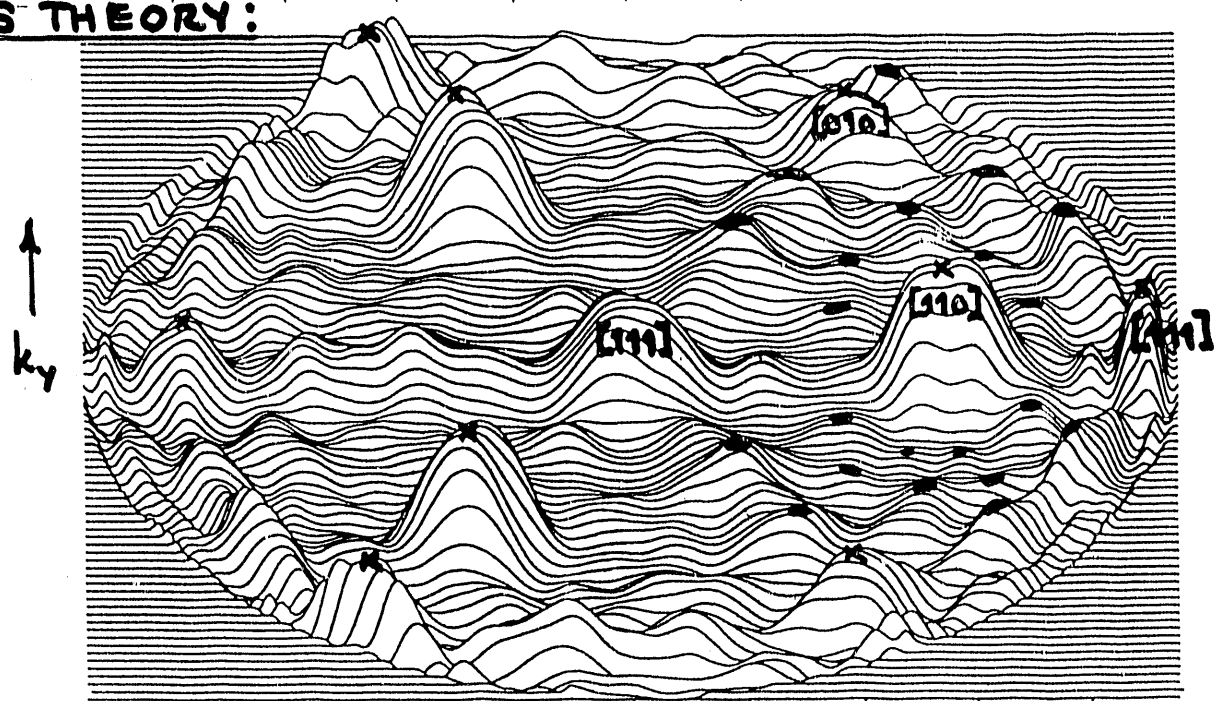

16 12 8 4 0 -4 -8 -12 -16

$k_x(\text{Å}^{-1})$

0 20 40 60 80 120 ... 180

α (°) = OPENING ANGLE OF HOLDER.

ELECTRON EMISSION HOLOGRAPHY

Synthetic Image Reconstruction

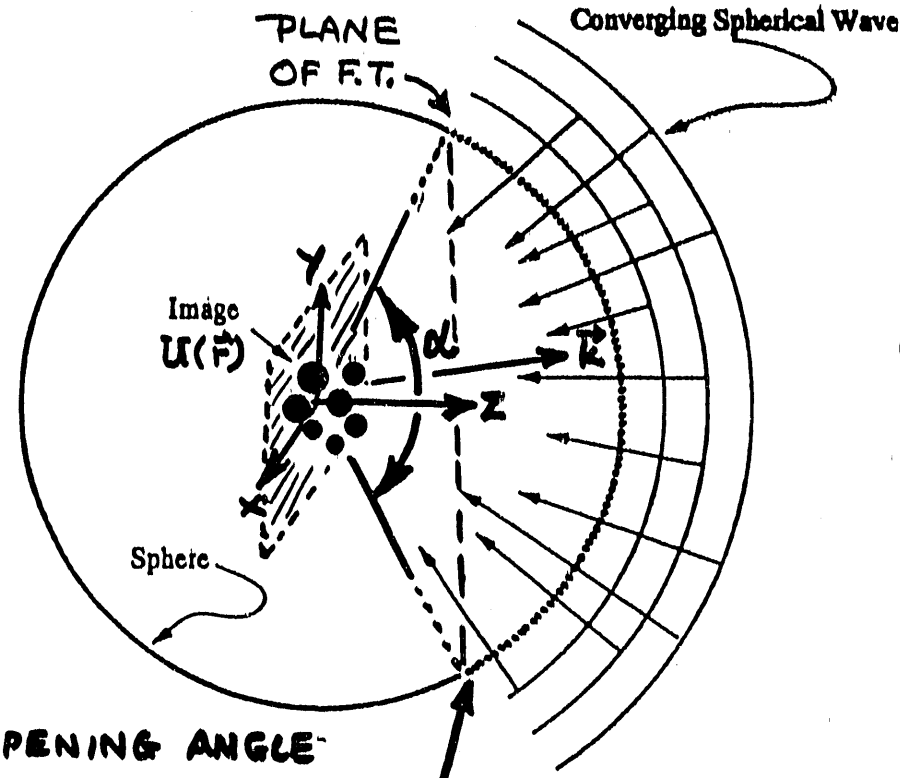

- SZÖKE, AIP CONF. PROC. 147 (1986)
- BARTON, PHYS. REV. LETT. 61, 1356 ('88)

α = OPENING ANGLE

$$\chi(k_x, k_y, k_z) = \frac{I(k_x, k_y, k_z) - I_0}{I_0^{1/2}}$$

UNSCATT. REF.

$$\approx \sum_j^{\text{SCATT.}} |F_j(\theta_j)| \cos\{kr_j(1-\cos\theta_j) + \psi_j(\theta_j)\}$$

$|F_j(\theta_j)|$: SCATT. AMPLITUDE (SS→MS)

$kr_j(1-\cos\theta_j)$: PATH LENGTH DIFFER

$\psi_j(\theta_j)$: SCATT. PHASE SHIFT (SS→MS)

RESOLUTION:

$$|\Delta x| = |\Delta y| = \frac{0.6\lambda_e}{\sin(\alpha/2)} \; ; \; |\Delta z| \approx \frac{2.0\lambda_e}{\sin^2(\alpha/2)}$$

IMAGE:

$$U(\vec{r}) = U(x,y,z) \propto \left| \iint_S \chi(\vec{k})\, e^{-i\vec{k}\cdot\vec{r}}\, d\sigma \right|$$

$$\propto \left| \iint \chi(\vec{k})\, e^{ik_z z}\, e^{ik_x x}\, e^{ik_y y}\, dk_x\, dk_y \right|$$

= 2 DIM. F.T.

THE BASIC EQUATIONS:

$$I(\vec{k}) \propto \left| \overbrace{\phi_0}^{\text{UNIF.}} + \overbrace{\sum_j \phi_j}^{\text{SCATT}} \right|^2$$

$$\propto |\phi_0|^2 + \sum_j (\phi_0^* \phi_j + \phi_0 \phi_j^*) + \sum_j \sum_k \phi_j \phi_k^*$$

WITH $\phi_0 = F_0(\vec{k}) e^{i\vec{k}\cdot\vec{r}}$

$\phi_j = F_j(\vec{k}) e^{i\vec{k}\cdot(\vec{r}-\vec{r}_j)}$

F's MAY INCLUDE: MATRIX ELEMENTS, INELASTIC ATTEN., e^{ikr_j}, f_{SW}, D.W., M.S.

$$I(\vec{k}) \propto |F_0|^2 + \sum_j \{F_0^* F_j e^{-i\vec{k}\cdot\vec{r}_j} + F_0 F_j^* e^{i\vec{k}\cdot\vec{r}_j}\}$$

$$+ \sum_j \sum_k \{F_j^* F_k e^{i\vec{k}\cdot(\vec{r}_j - \vec{r}_k)} + F_j F_k^* e^{i\vec{k}\cdot(\vec{r}_k - \vec{r}_j)}\}$$

$$\chi(\vec{k}) \propto \underbrace{\sum_j \{F_0^* F_j e^{-i\vec{k}\cdot\vec{r}_j} + F_0 F_j^* e^{i\vec{k}\cdot\vec{r}_j}\}}$$

SIMPLE HOLOGRAM → FT PEAKS AT $\pm \vec{r}_j$

$$+ \underbrace{\sum_j \sum_k \{F_j^* F_k e^{i\vec{k}\cdot(\vec{r}_j - \vec{r}_k)} + F_j F_k^* e^{i\vec{k}\cdot(\vec{r}_k - \vec{r}_j)}\}}$$

SELF HOLOGRAM → FT PEAKS AT $\pm(\vec{r}_j - \vec{r}_k) \equiv \pm \Delta\vec{r}_{jk}$?

...PLUS EFFECTS DUE TO NON-CONSTANT $F_0(\vec{k})$ AND $F_j(\vec{k})$ IN FT ?

... PLUS EFFECTS DUE TO MULTIPLE SCATT?

METHODOLOGY:

- SS + MS FULL SPHERICAL-WAVE CALCULATIONS WITH GENERAL CODE USING REHR-ALBERS METHOD: S-OUTGOING ("AUGER"); EXACT $\ell \to \ell \pm 1$ PHOTOEMISSION; IDEAL WEAK $S \to S$ OUT SCAT.
- IMAGES PRODUCED BY USUAL FOURIER TRANSFORM (BARTON):

$$|FT| = W(x,y,z) = \left| \int\int [\chi(\vec{k}) e^{ik_z z}] e^{ik_x x} e^{ik_y y} dk_x dk_y \right|$$

- IMAGE IMPROVEMENT BY:
  - CUTTING FULL HOLOGRAM ANGLE α ($\leq 180°$) TO ELIMINATE FORWARD SCATT. PEAKS

  - ELIMINATING FORWARD SCATT. PEAKS BY GAUSSIAN FACTOR:

$$1 - \exp(-0.691\,\delta^2/\gamma^2)$$

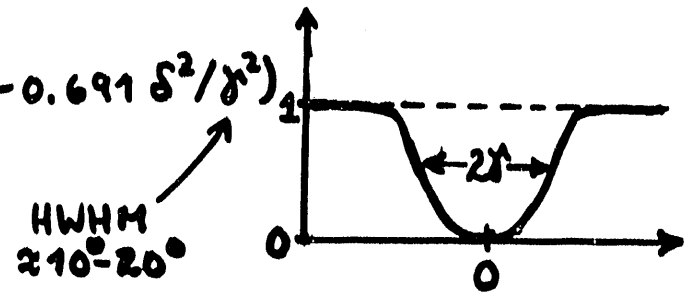

HWHM ≈ 10°-20°

- USE OF SCATTERED-WAVE INTEGRAL FOURIER TRANSFORM (SWIFT) METHOD OF SALDIN ET AL.:

$$|SWIFT| = W'(x,y,z) = \left| \iint \frac{[\chi(\vec{k}) e^{ik_z z}]}{F(k, \hat{k}\cdot\hat{r}, v)} e^{ik_x x} e^{ik_y y} dk_x dk_y \right|,$$

// SPHERICAL-WAVE $f_{sw}(k, \hat{k}\cdot\hat{r}, v)$ FOR NOW,

WITH REQUIREMENT THAT $|f_{sw}|$ NOT GO BELOW SOME THRESHOLD (= SWIFT') AS % OF $|f_{sw}|_{MAX}$ FOR PROBLEM

ARE POSITIONS, PEAK SHAPES IMPROVED WITH SWIFT' CORRECTIONS?

- USING ONLY PART OF FULL HOLOGRAM TO ISOLATE CERTAIN ATOMS AND REDUCE REAL/TWIN OVERLAP.

  IS SWIFT' CORRECTION MORE EFFECTIVE?

- DOING PHASED SUMMATION OF IMAGES AT SEVERAL ENERGIES (BARTON) WITH AND WITHOUT SCATTERED-WAVE CORRECTION:

$$U''(x,y,z) = \left| \sum_i e^{-ik_i r} (FT)_i \right|, \quad i = 1,2,\ldots n \text{ ENERGIES}$$

OR

$$U'''(x,y,z) = \left| \sum_i e^{-ik_i r} (SWIFT')_i \right|.$$

ARE TWINS + MS EFFECTS REDUCED?

SELF-INTERFERENCE EFFECTS:

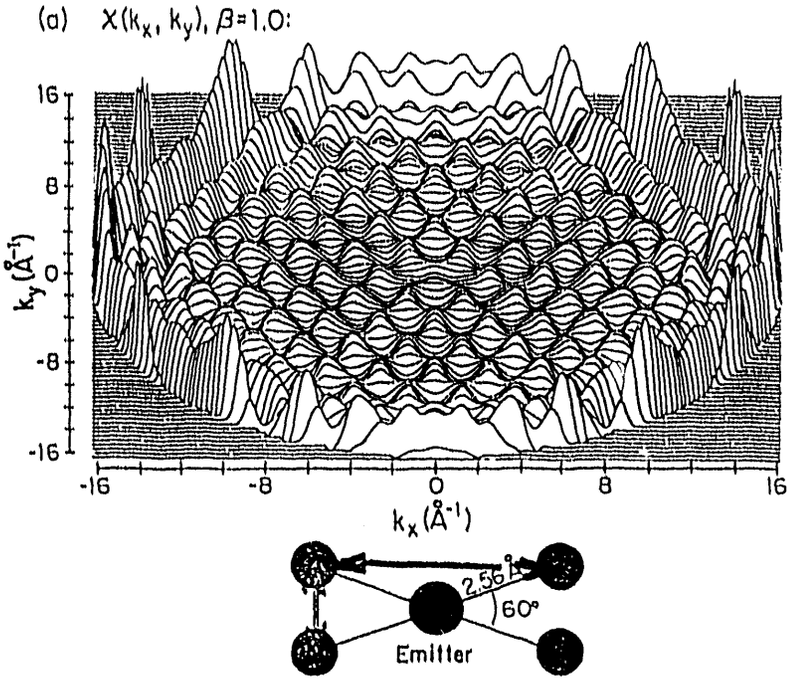

$$\Psi = \Phi_0 + \beta \sum_j \Phi_j$$

↑ VARIABLE PARAMETER

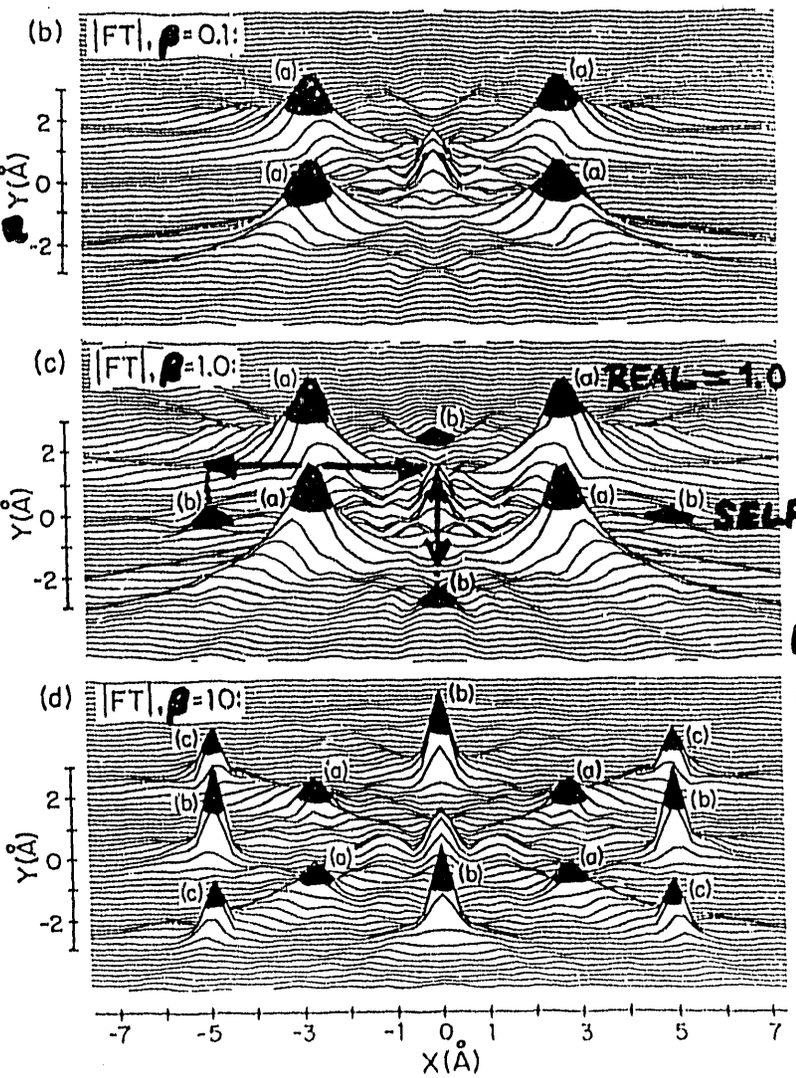

ACTUAL SCATT. STRENGTH

MAY BE IMPORTANT AS WEAKER FEATURES!

THEVUTHASAN ET AL., P.R.L., 7/22/91

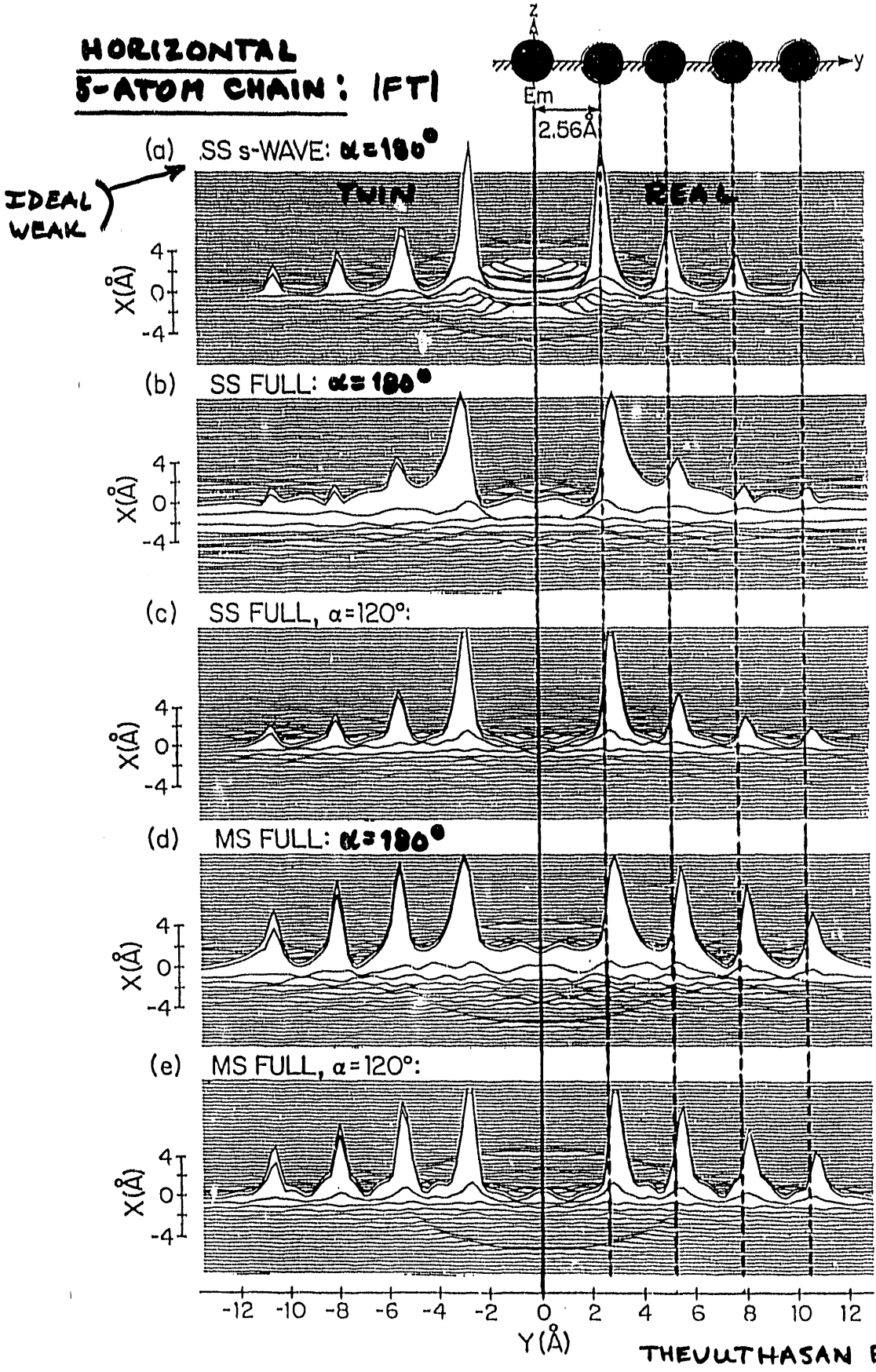

THEULTHASAN ET AL.,
P.R.L., 7/22/91

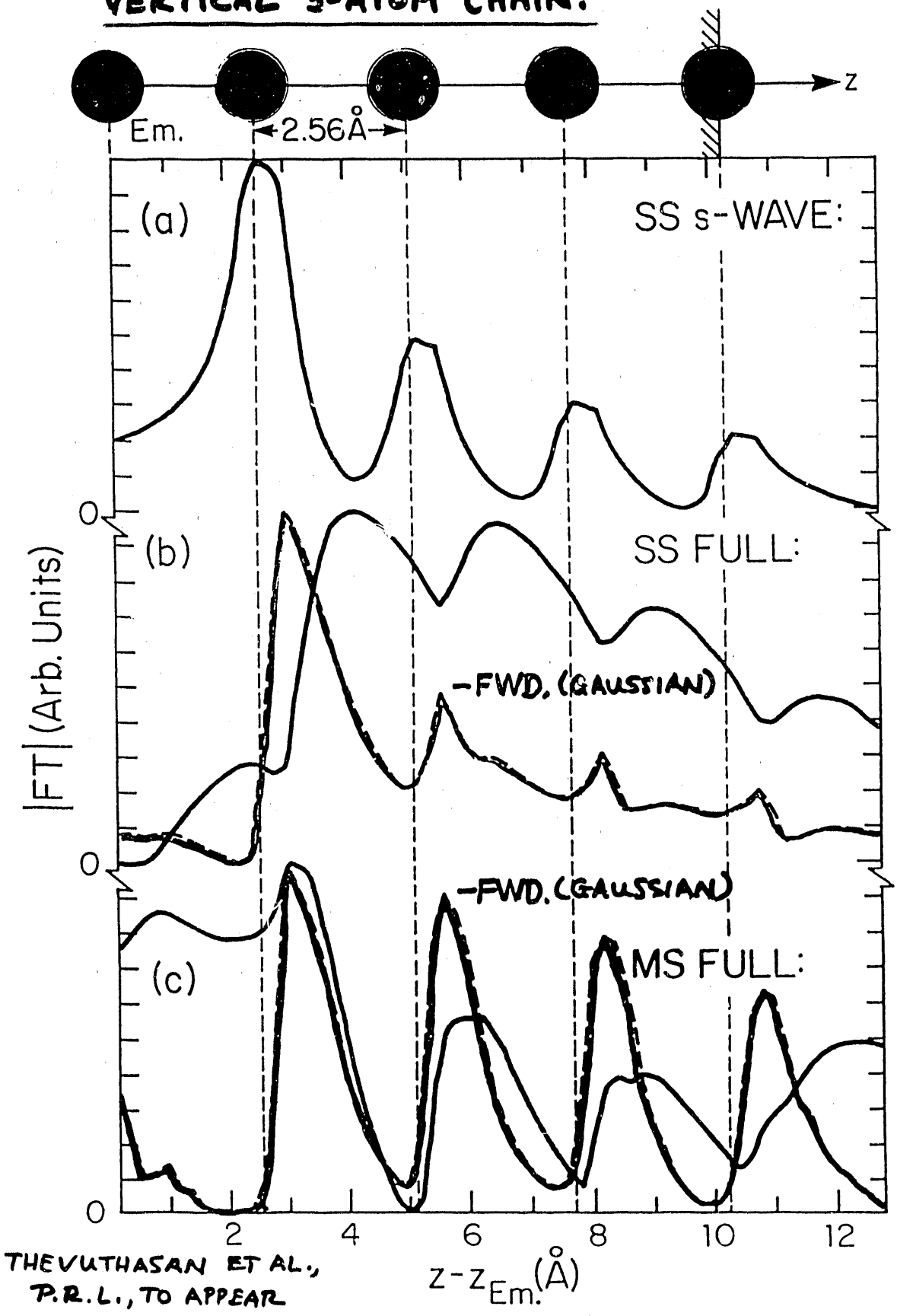
VERTICAL 5-ATOM CHAIN:
z
Em.
2.56Å
(a)
SS s-WAVE:
(b)
SS FULL:
-FWD. (GAUSSIAN)
(c)
-FWD. (GAUSSIAN)
MS FULL:
|FT| (Arb. Units)
0
0
0
2
4
6
8
10
12
z - z_Em. (Å)
THEVUTHASAN ET AL.,
P.R.L., TO APPEAR

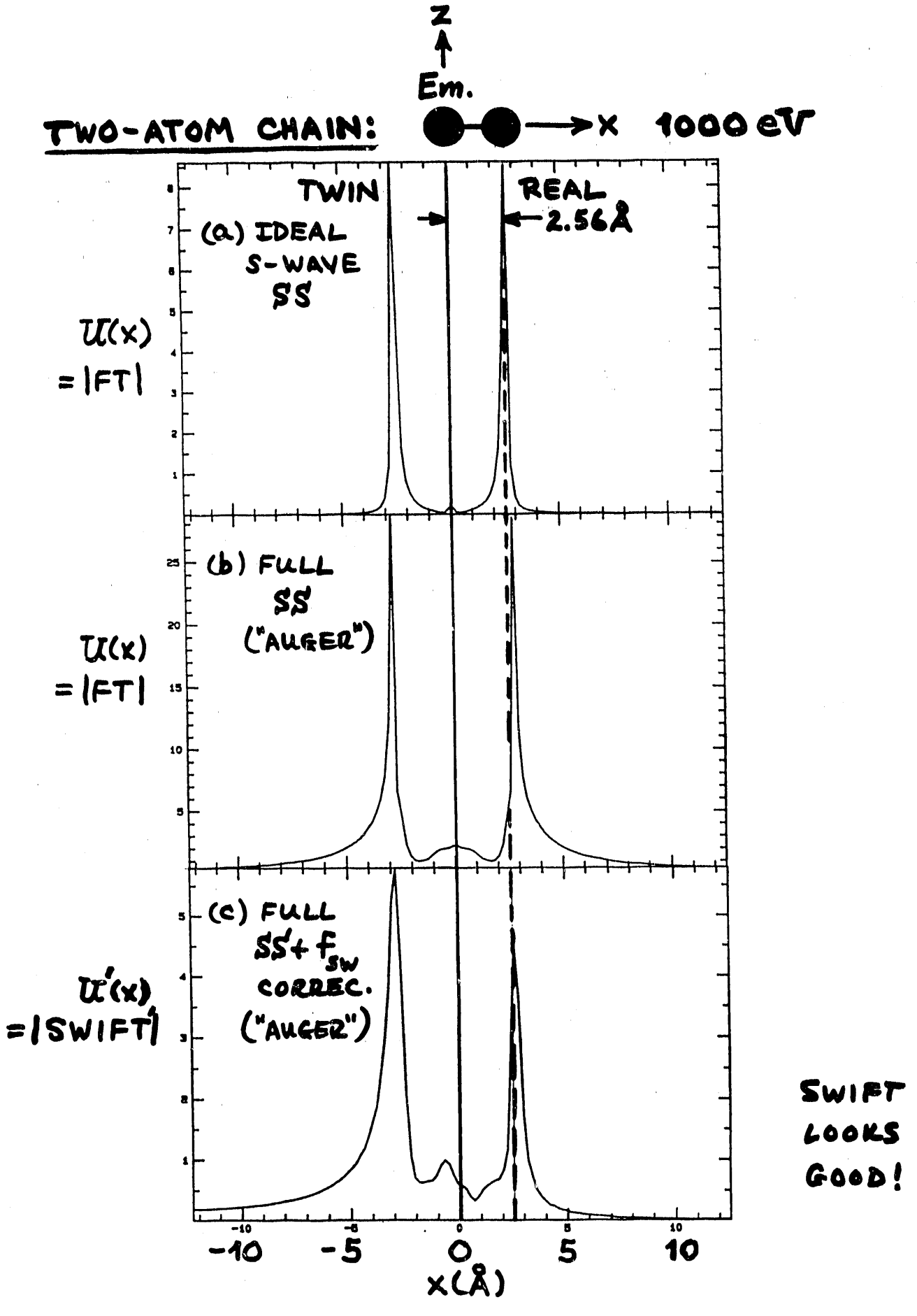
TWO-ATOM CHAIN:
z
Em.
x
1000 eV
TWIN
REAL
2.56Å
(a) IDEAL S-WAVE SS
U(x) = |FT|
(b) FULL SS' ("AUGER")
U(x) = |FT|
(c) FULL SS' + f_sw CORREC. ("AUGER")
U'(x) = |SWIFT'|
-10
-5
0
5
10
x(Å)
SWIFT LOOKS GOOD!

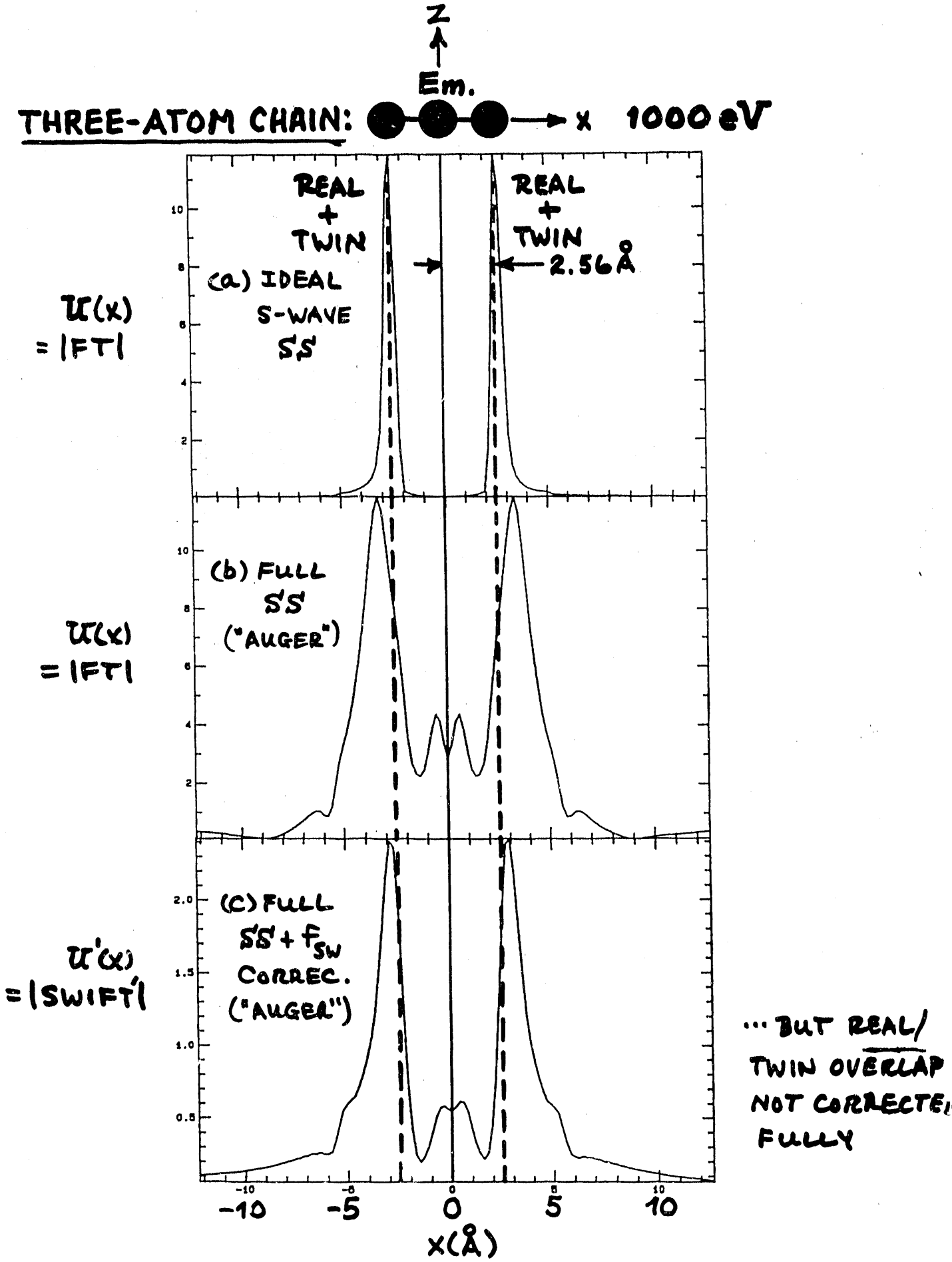
Z
Em.
THREE-ATOM CHAIN:
x 1000 eV
REAL + TWIN
REAL + TWIN
2.56 Å
(a) IDEAL S-WAVE SS
U(x) = |FT|
(b) FULL SS ("AUGER")
U(x) = |FT|
(c) FULL SS + f_{SW} CORREC. ("AUGER")
U'(x) = |SWIFT'|
... BUT REAL/TWIN OVERLAP NOT CORRECTED FULLY
-10
-5
0
5
10
x(Å)

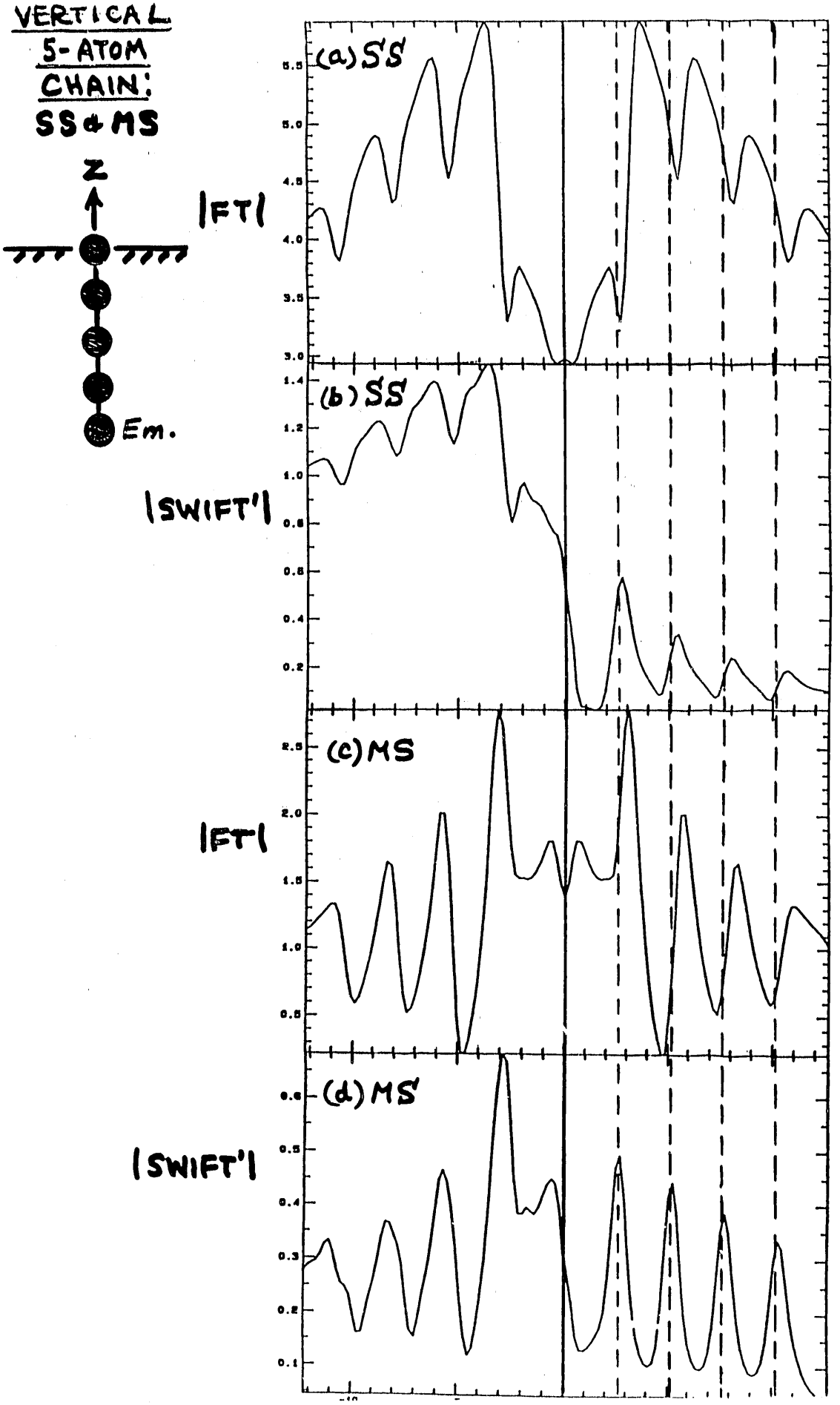
VERTICAL
5-ATOM
CHAIN:
SS & MS
z
Em.
|FT|
(a) SS
|SWIFT'|
(b) SS
|FT|
(c) MS
|SWIFT'|
(d) MS

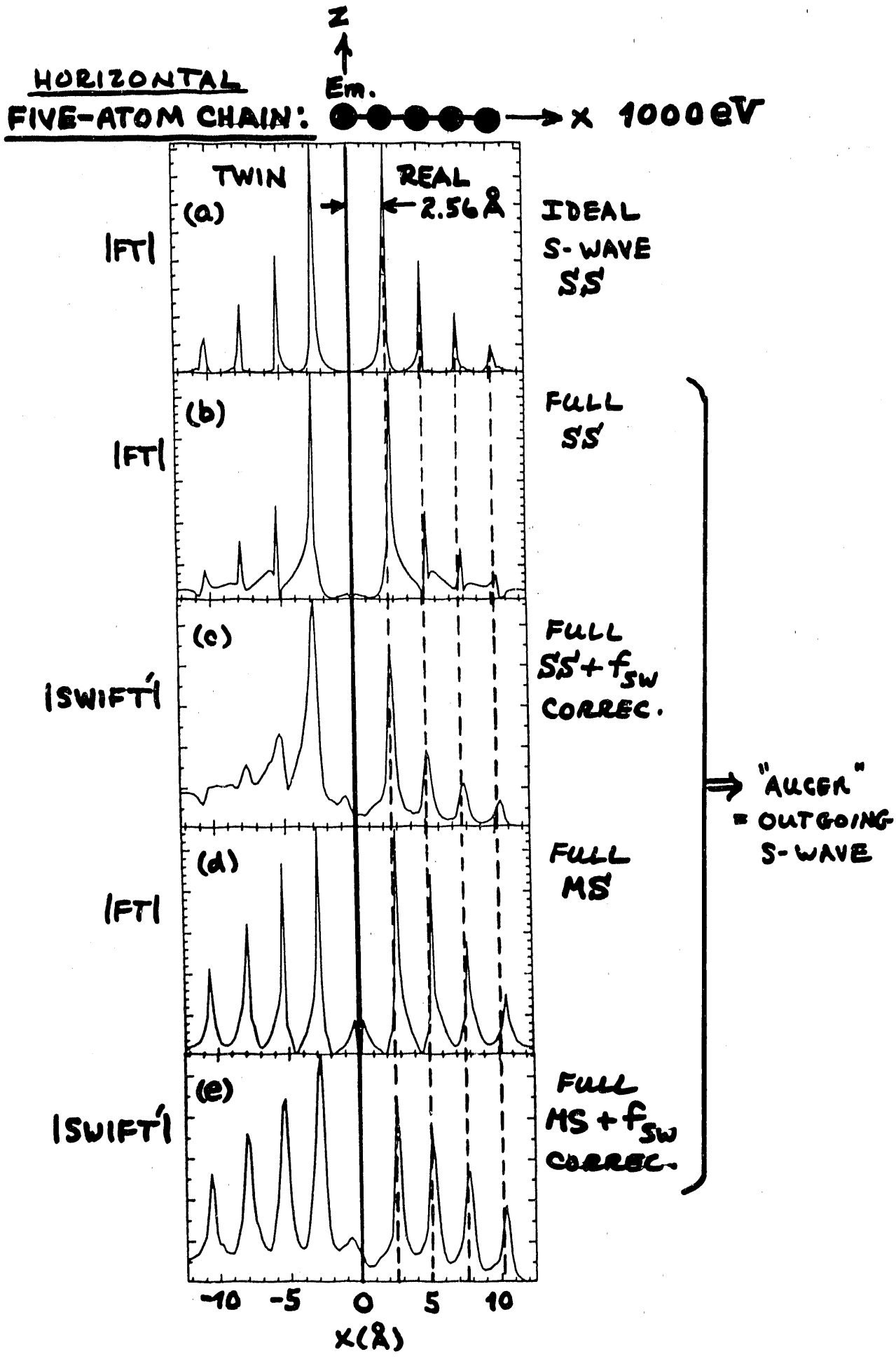
z
Em.
HORIZONTAL
FIVE-ATOM CHAIN:
× 1000eV
TWIN
REAL
2.56Å
(a)
IDEAL
S-WAVE
SS
|FT|
(b)
FULL
SS
|FT|
(c)
FULL
SS + f_{SW}
CORREC.
|SWIFT'|
⇒ "AUGER"
= OUTGOING
S-WAVE
(d)
FULL
MS
|FT|
(e)
FULL
MS + f_{SW}
CORREC.
|SWIFT'|
-10
-5
0
5
10
x(Å)

HORIZONTAL
5-ATOM CHAIN
MS

$$\left|\sum_i e^{-ik_i|x|}(FT)_i\right|$$

$$\left|\sum_i e^{-ik_i|x|}(SWIFT')_i\right|$$

$$\left|\sum_i e^{-ik_i|x|}(FT)_i\right|$$

$$\left|\sum_i e^{-ik_i|x|}(SWIFT')\right|$$

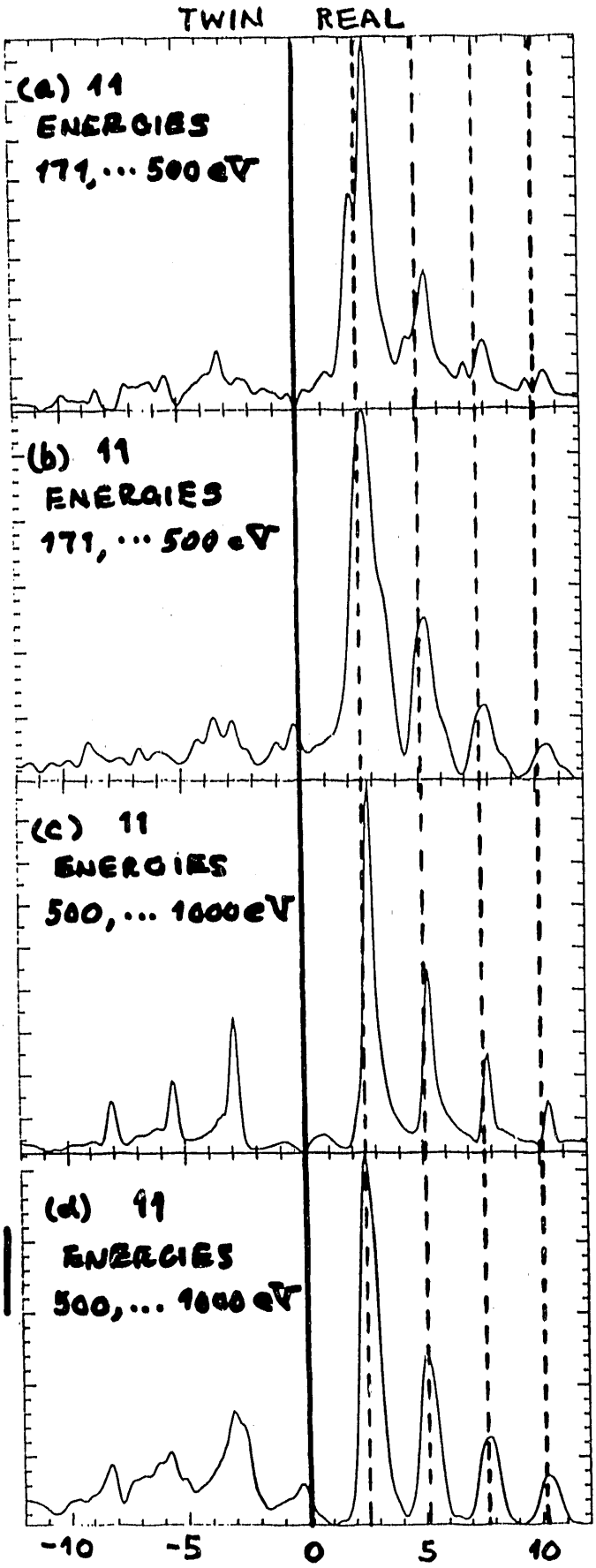

TWIN SUPPRESSION GOOD AT LOWER ENERGIES, BUT REAL IMAGE BETTER AT HIGHER

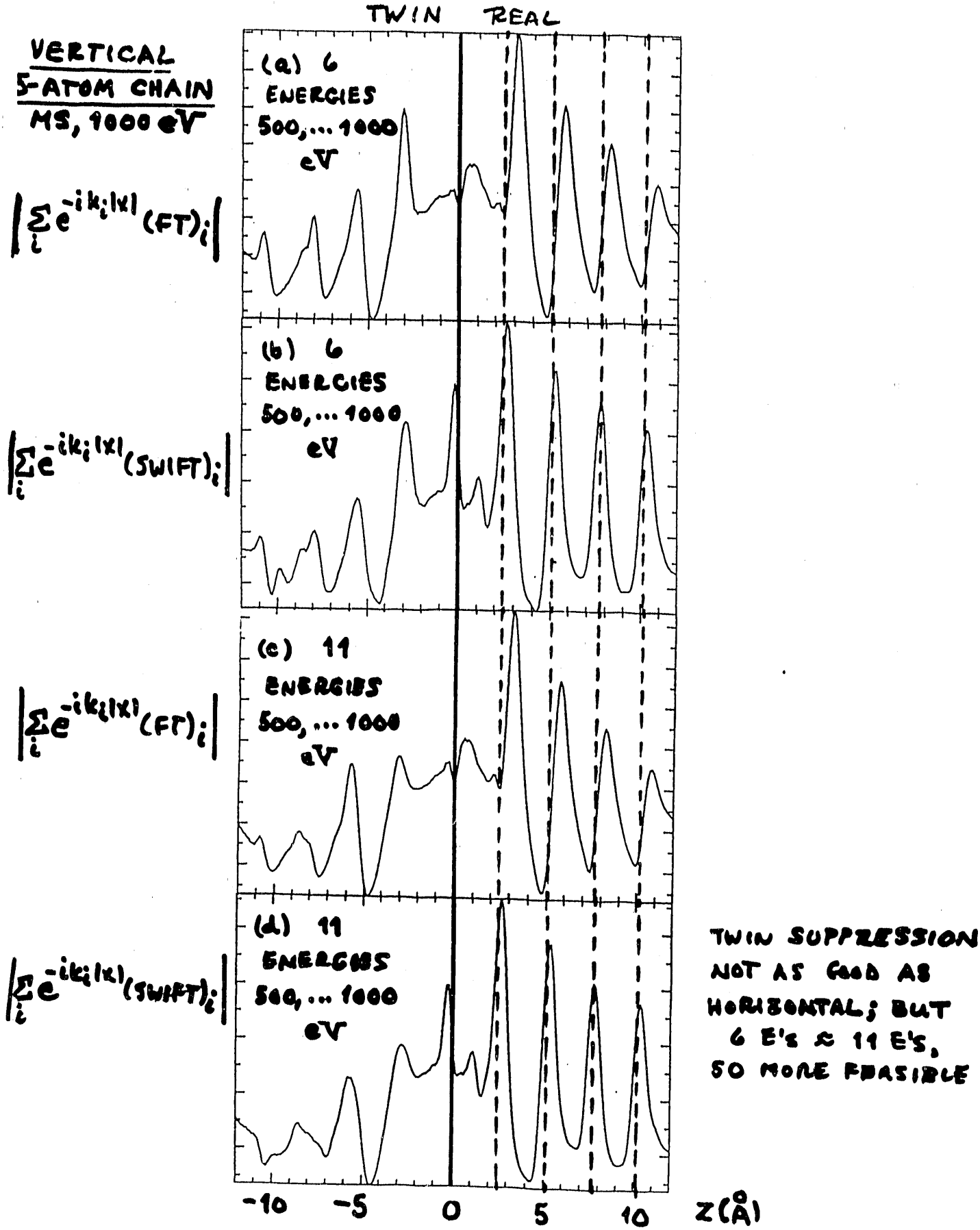

TWIN SUPPRESSION NOT AS GOOD AS HORIZONTAL; BUT 6 E's ≈ 11 E's, SO MORE FEASIBLE

S-OUTGOING VS. PHOTOEMISSION

THEORY:
$\chi(k_x, k_y)$
FOR S EMISS.
FROM 9-ATOM
S CLUSTER

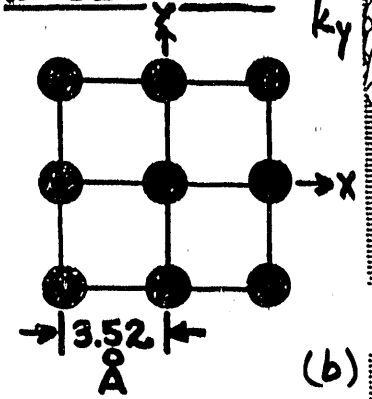

⇒ c(2×2)S/
Ni(001)
E_{kin} = 1085 eV

(a) k_y

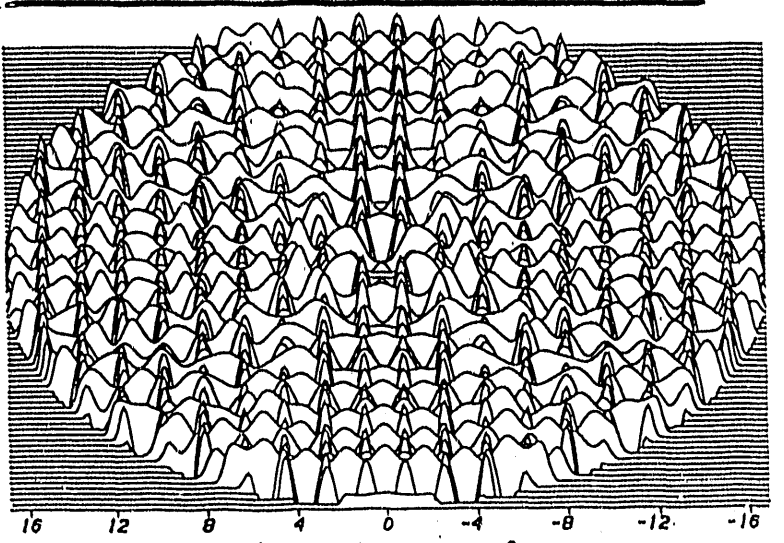

IDEAL
S-WAVE
SS

(b) k_y

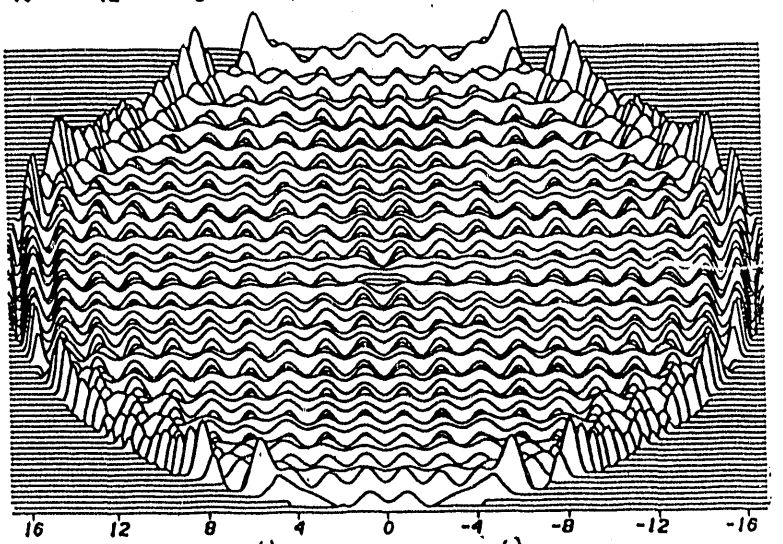

OUTGOING
S-WAVE
("AUGER"),
FULL
SS

(c) k_y

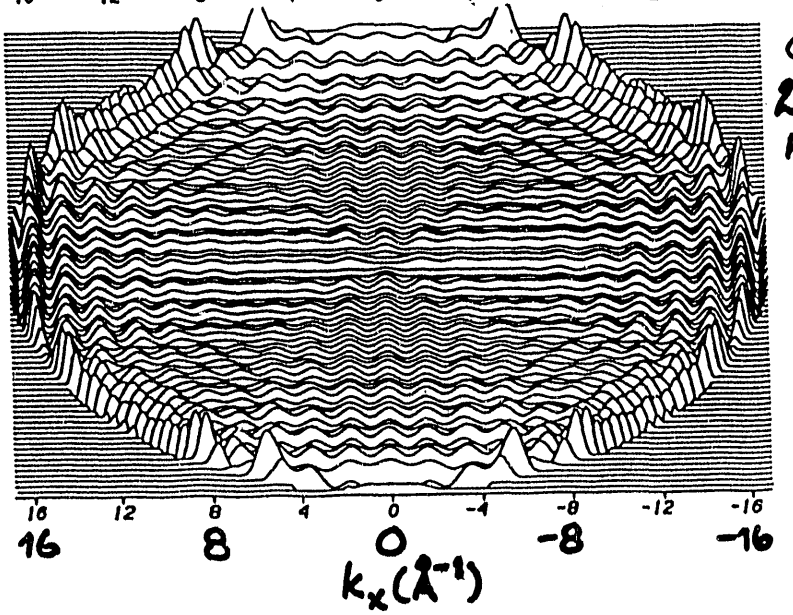

OUTGOING
$2p \rightarrow s+d$,
FULL SS

THEORY: |FT| FOR S' EMISS. FROM 9-ATOM CLUSTER

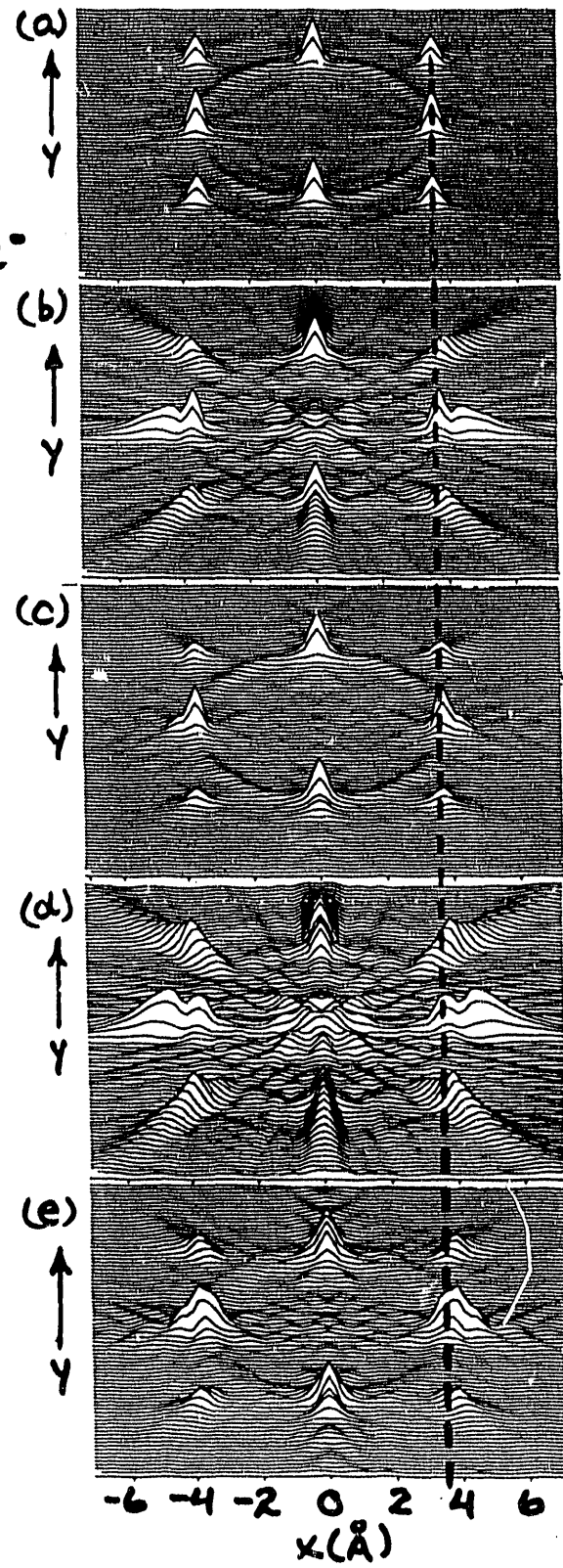

IDEAL S-WAVE SS'

OUTGOING S-WAVE FULL SS' $\alpha = 178°$

" " " " $\alpha = 120°$

OUTGOING $2p \rightarrow s + d$, FULL SS' $\alpha = 178°$

" " " " " $\alpha = 120°$

PHOTOELECTRONS INHERENTLY WORSE, UNLESS CORRECTED FOR ϕ_0, ϕ_i ANISOTROPY

XPD FROM A HIGH-z ADSORBATE - S/Ni(001)

S2p, Ekin = 1085 eV

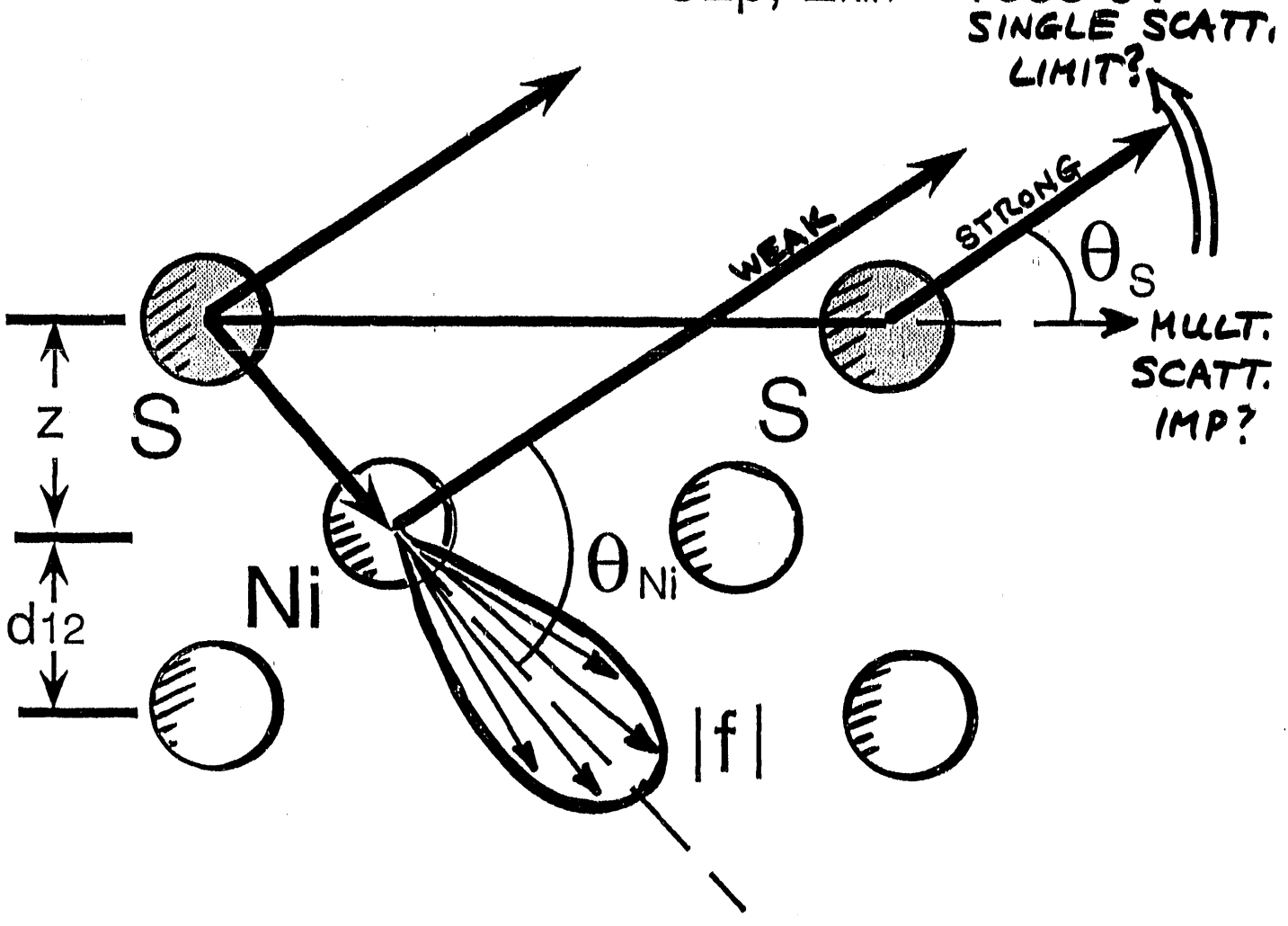

Info. from substrate requires large θ-scattering
∴ Weaker effect

Does high angular resolution data permit determining z? ... And d_{12}?

SAIKI, ET AL., TO BE PUBL.

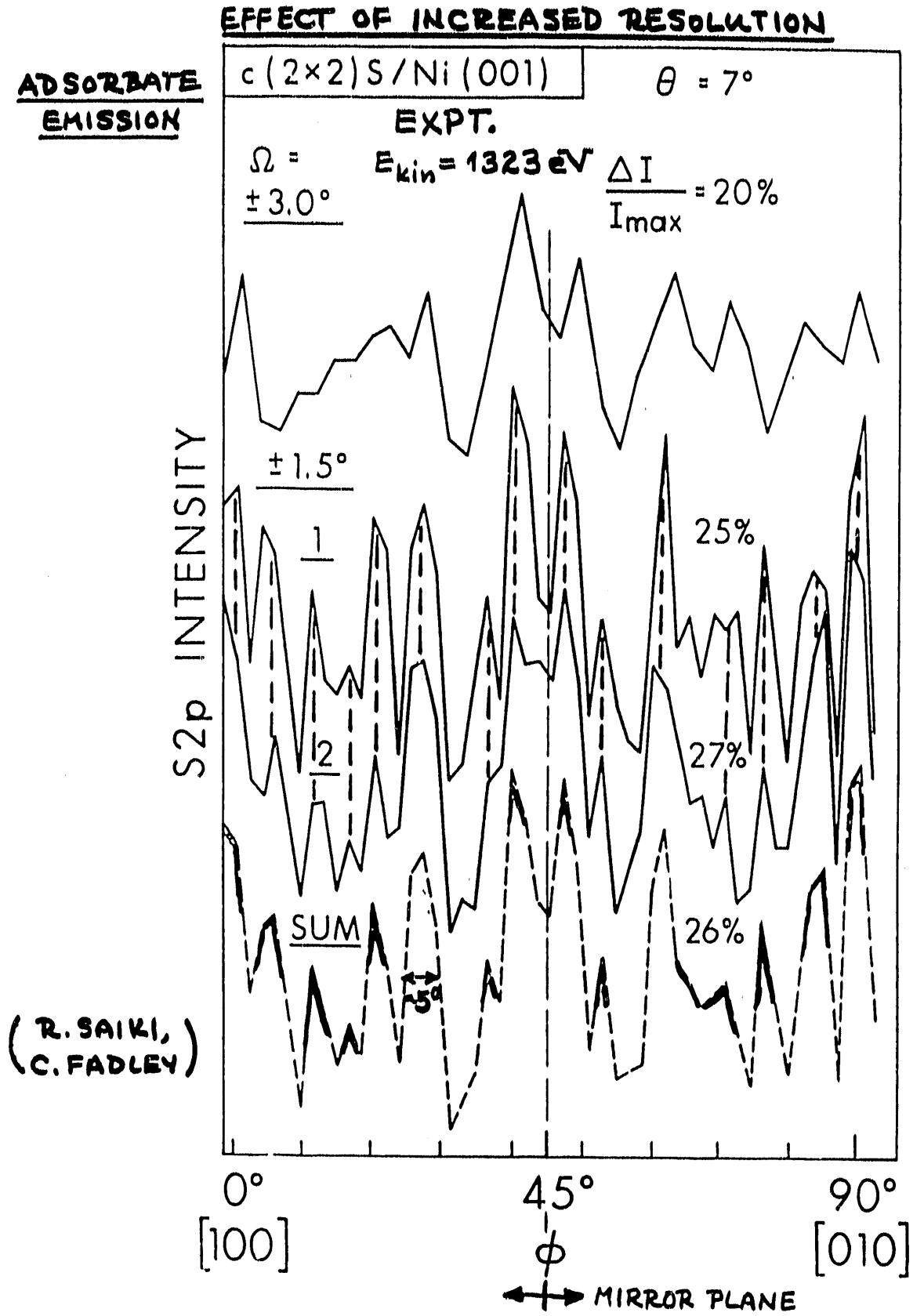
EFFECT OF INCREASED RESOLUTION
ADSORBATE EMISSION
c(2×2)S/Ni(001)
θ = 7°
EXPT.
Ω = ±3.0°
E_kin = 1323 eV
ΔI / I_max = 20%
±1.5°
1
2
SUM
25%
27%
26%
5σ
S2p INTENSITY
0°
[100]
45°
φ
90°
[010]
MIRROR PLANE
(R. SAIKI, C. FADLEY)

FINAL EXPT. / THEORY COMPARISON:

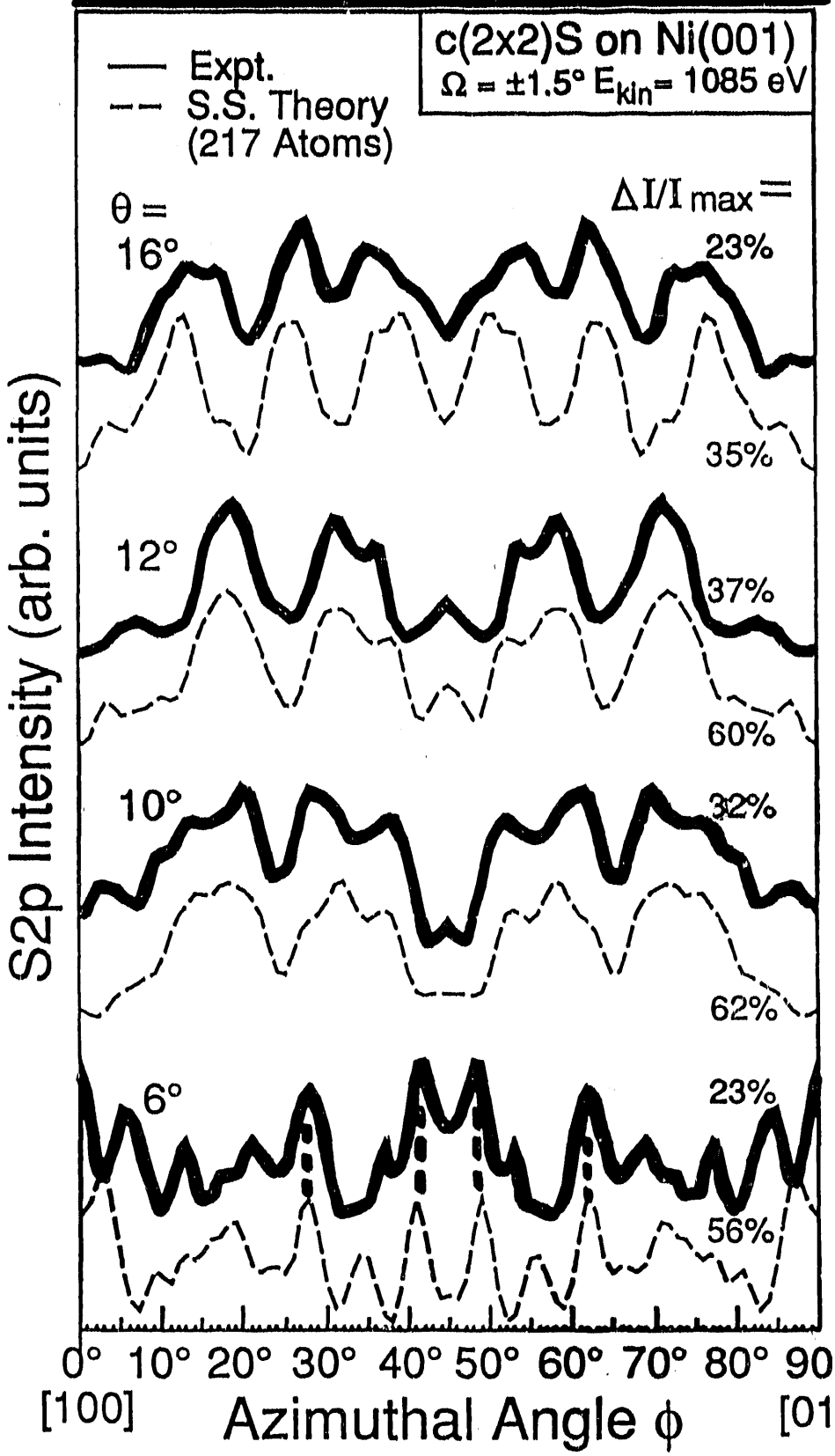

$z = 0.75$ Å
$d_{12} = 1.86$ Å

R-FACTOR ANALYSIS ("CLASSIC")

SOME MS EFFECTS AT LOWEST ANGLE?

Effect of Ni Substrate Interplanar Expansion

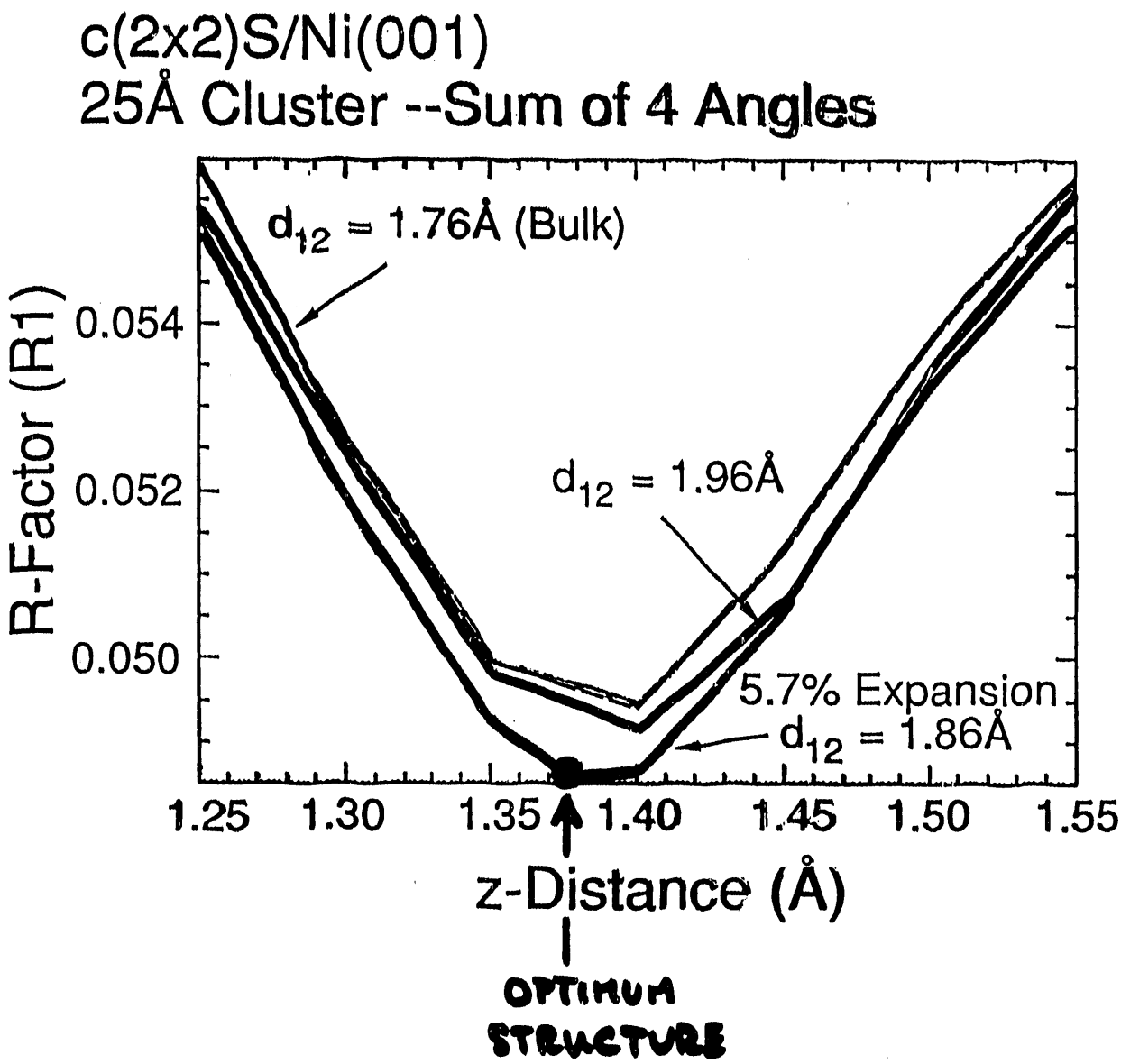

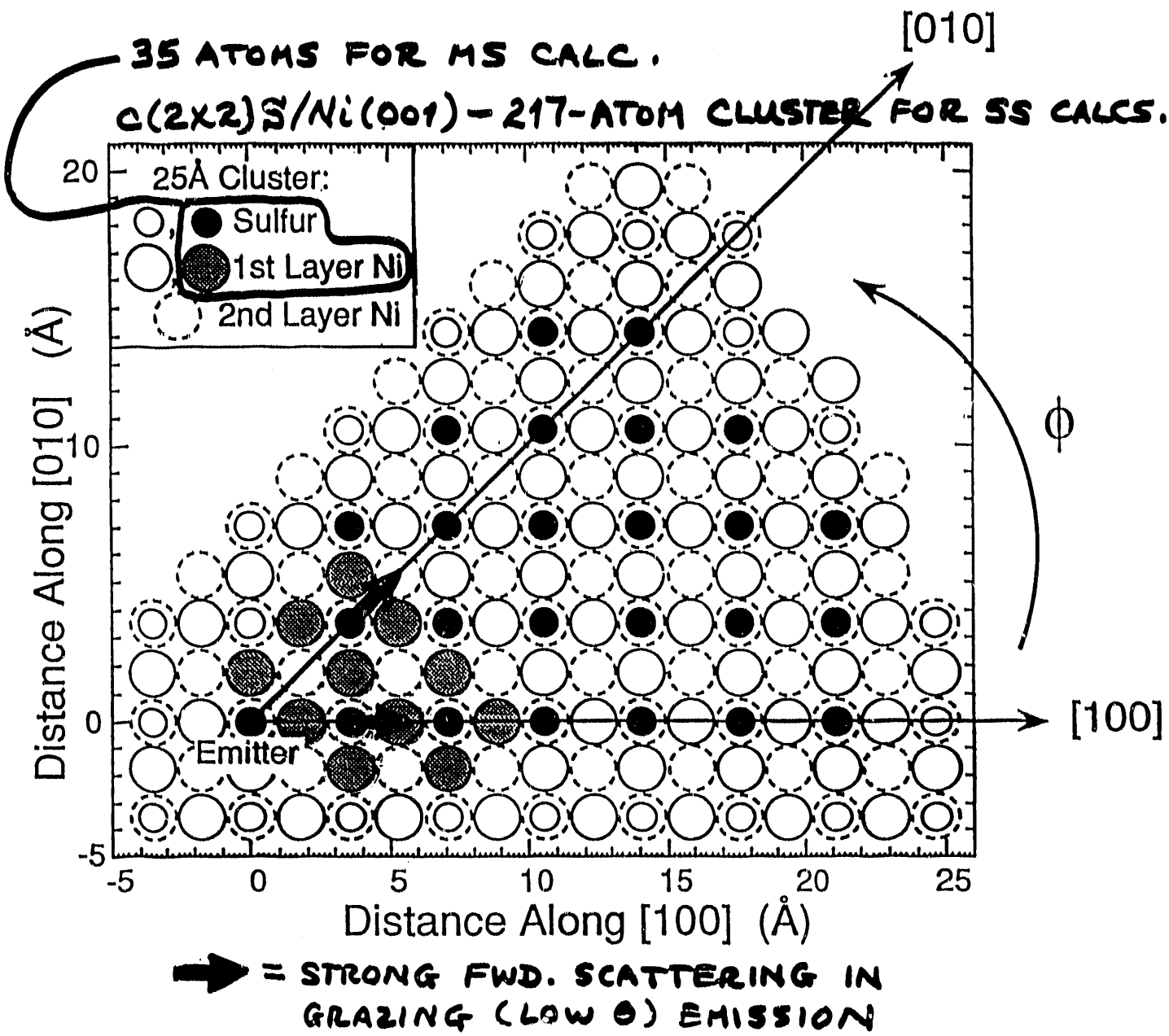
35 ATOMS FOR MS CALC.
c(2x2)S/Ni(001) - 217-ATOM CLUSTER FOR SS CALCS.
[010]
25Å Cluster:
Sulfur
1st Layer Ni
2nd Layer Ni
Distance Along [010] (Å)
Distance Along [100] (Å)
Emitter
[100]
ϕ
= STRONG FWD. SCATTERING IN GRAZING (LOW θ) EMISSION

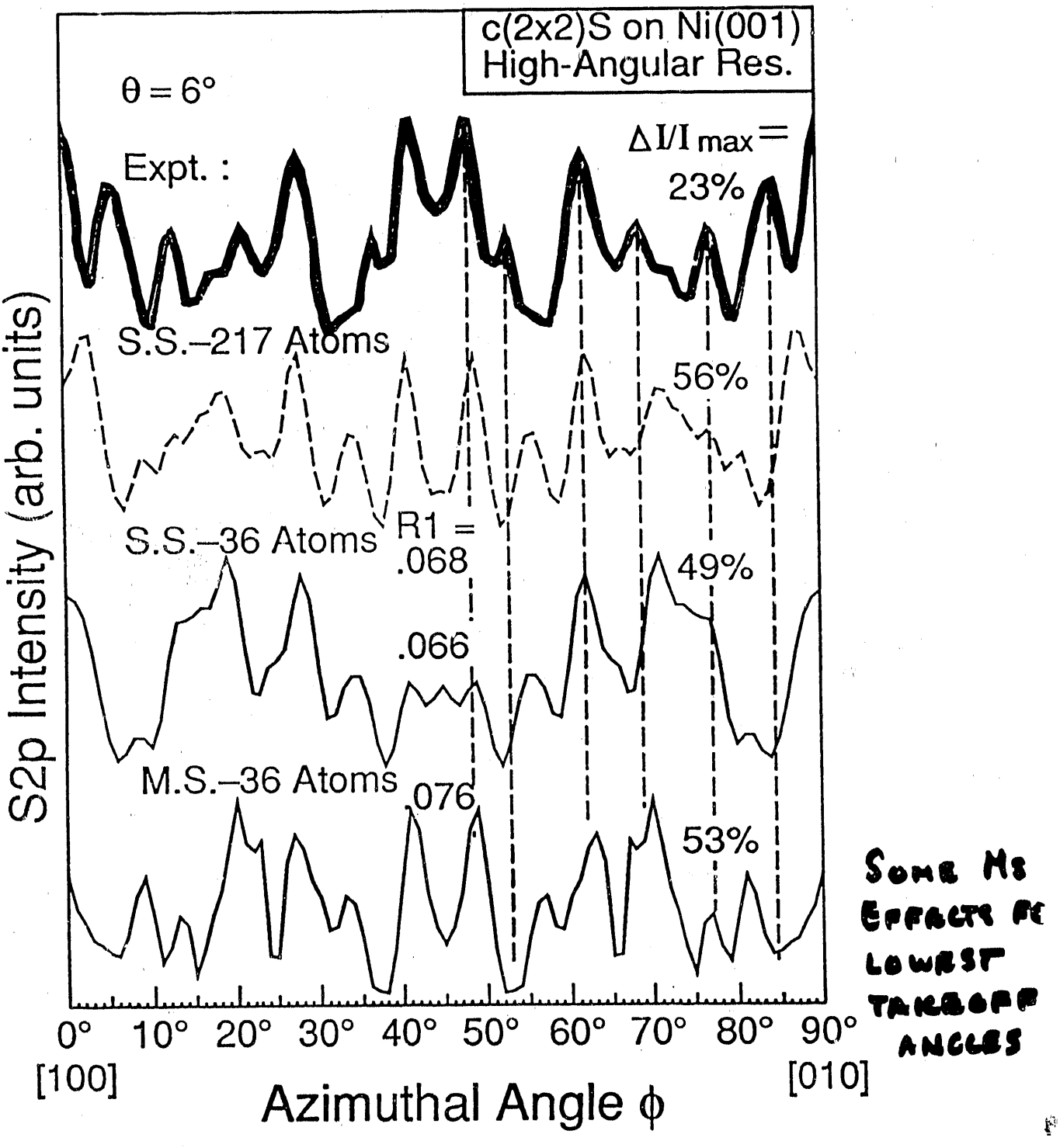
c(2x2)S on Ni(001)
High-Angular Res.
θ = 6°
Expt. :
ΔI/I max =
23%
S.S.–217 Atoms
56%
S.S.–36 Atoms
R1 =
.068
49%
.066
M.S.–36 Atoms
.076
53%
S2p Intensity (arb. units)
0° 10° 20° 30° 40° 50° 60° 70° 80° 90°
[100]
[010]
Azimuthal Angle ϕ
SOME MS EFFECTS AT LOWEST TAKEOFF ANGLES

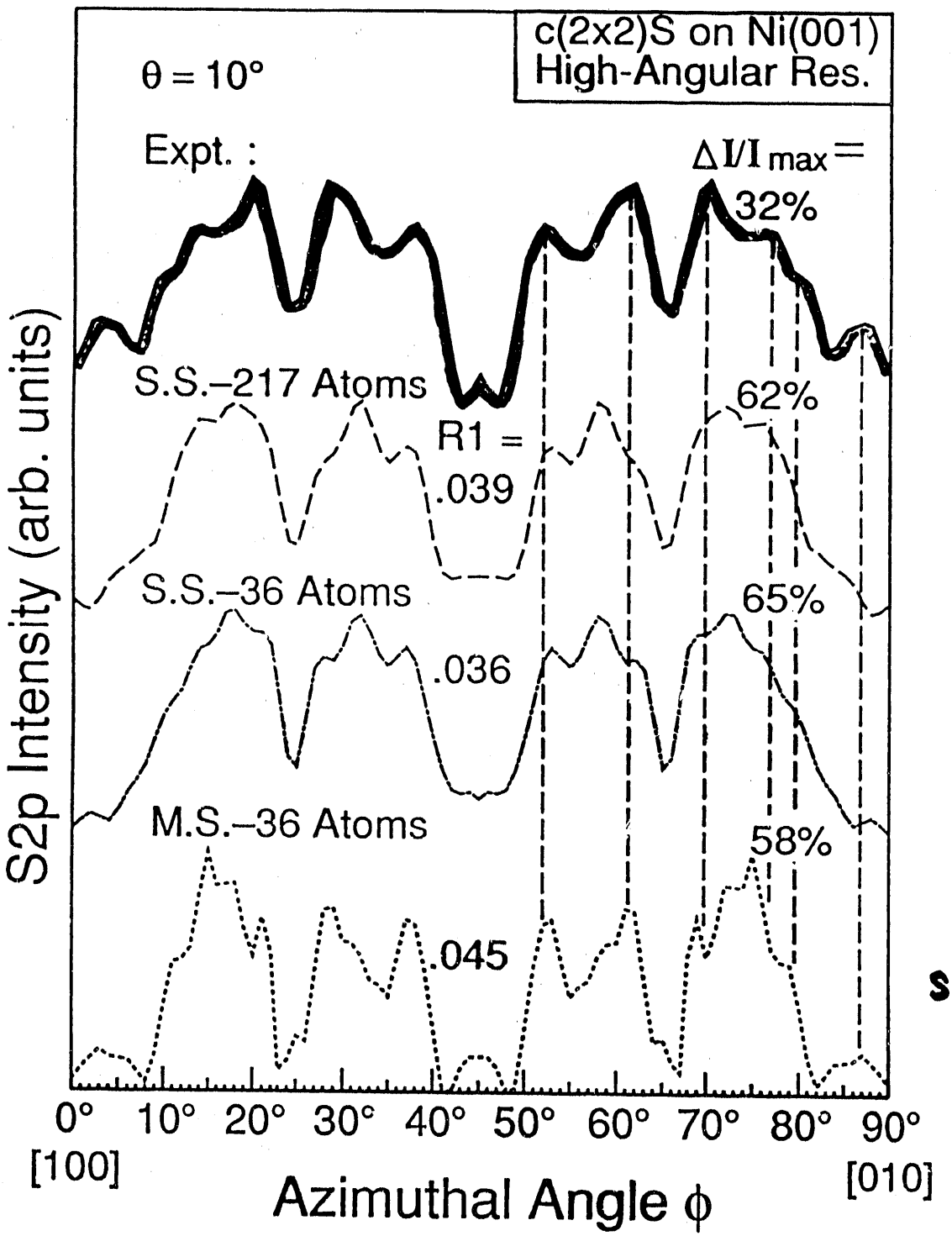
c(2x2)S on Ni(001)
High-Angular Res.
θ = 10°
Expt. :
ΔI/I max =
32%
S.S.–217 Atoms
R1 =
.039
62%
S.S.–36 Atoms
.036
65%
M.S.–36 Atoms
.045
58%
S2p Intensity (arb. units)
0° 10° 20° 30° 40° 50° 60° 70° 80° 90°
[100]
[010]
Azimuthal Angle ϕ

SS ≈ MS

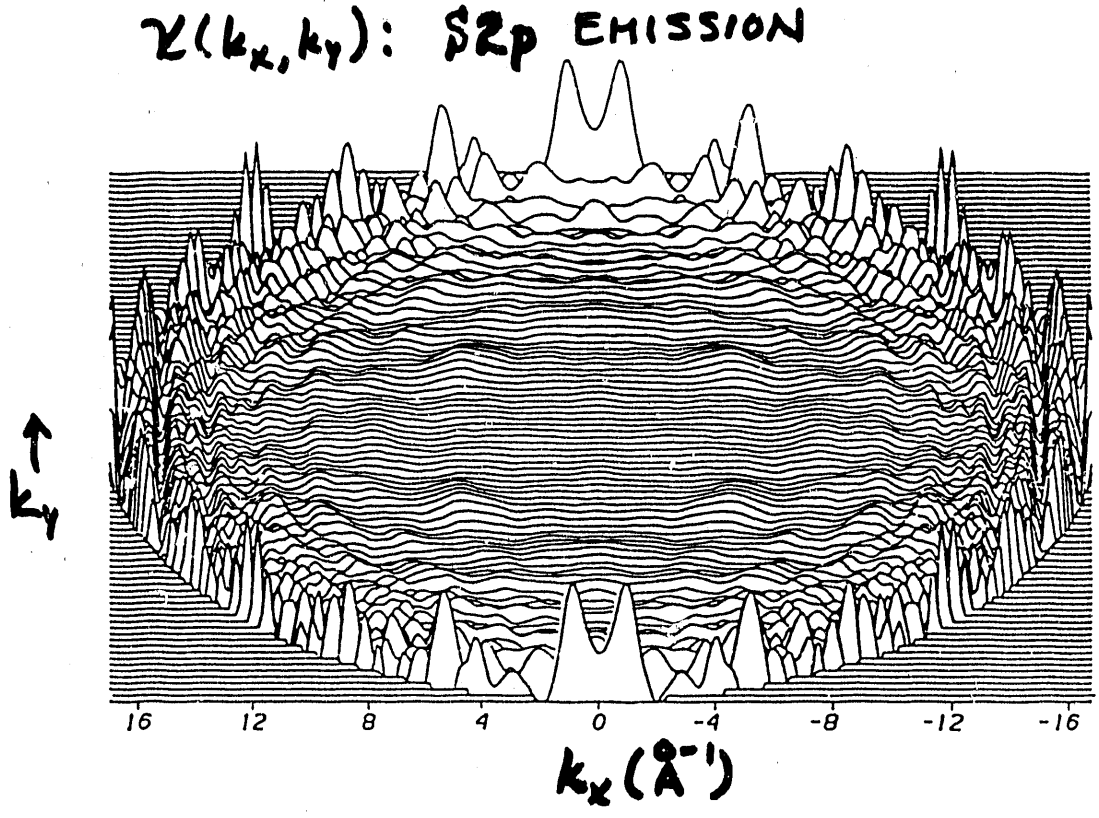
I(kx,ky): S2p EMISSION
ky
16
12
8
4
0
-4
-8
-12
-16
kx (Å-1)

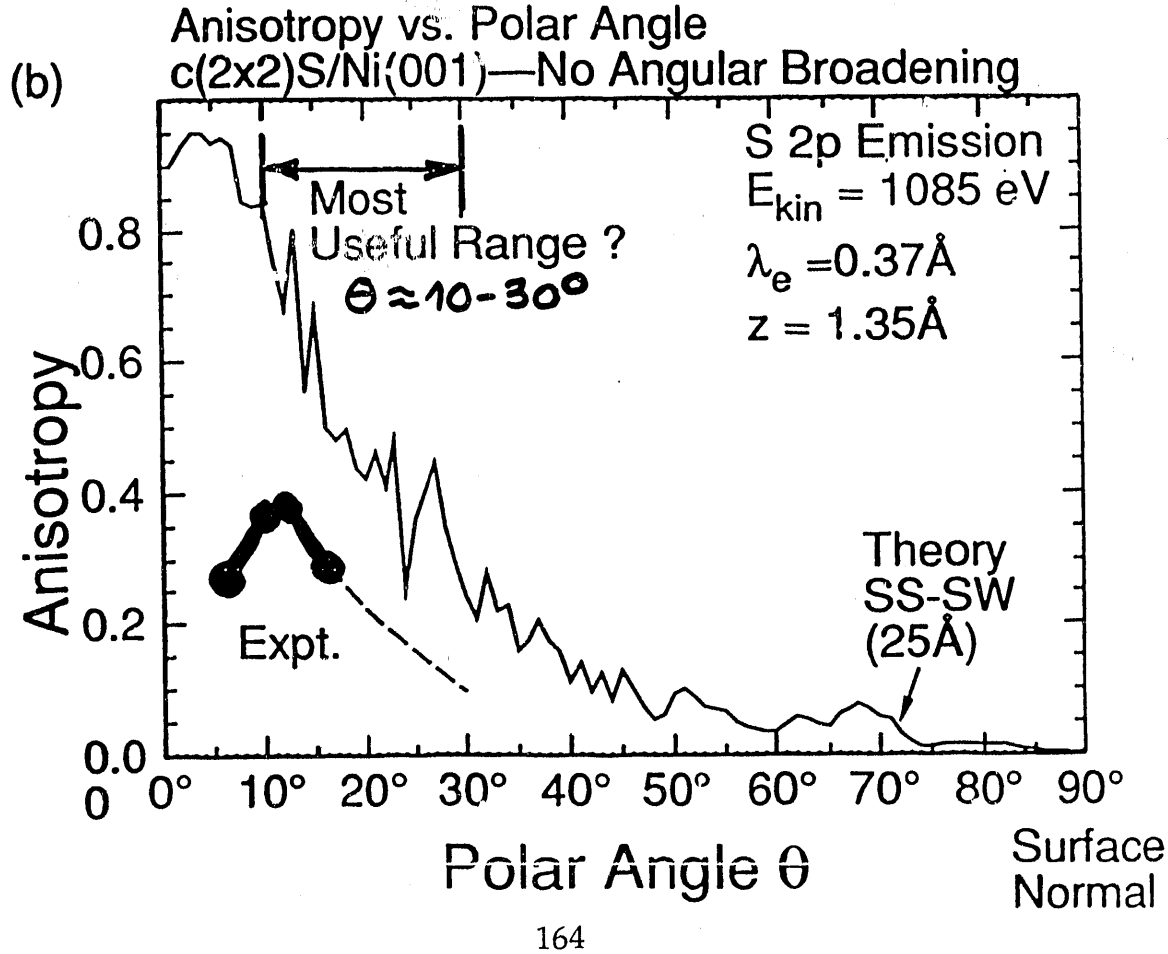
(b)
Anisotropy vs. Polar Angle
c(2x2)S/Ni(001)—No Angular Broadening
S 2p Emission
Ekin = 1085 eV
λe =0.37Å
z = 1.35Å
Most
Useful Range ?
θ≈10-30°
Anisotropy
0.0
0.2
0.4
0.6
0.8
Expt.
Theory
SS-SW
(25Å)
0
0°
10°
20°
30°
40°
50°
60°
70°
80°
90°
Polar Angle θ
Surface
Normal

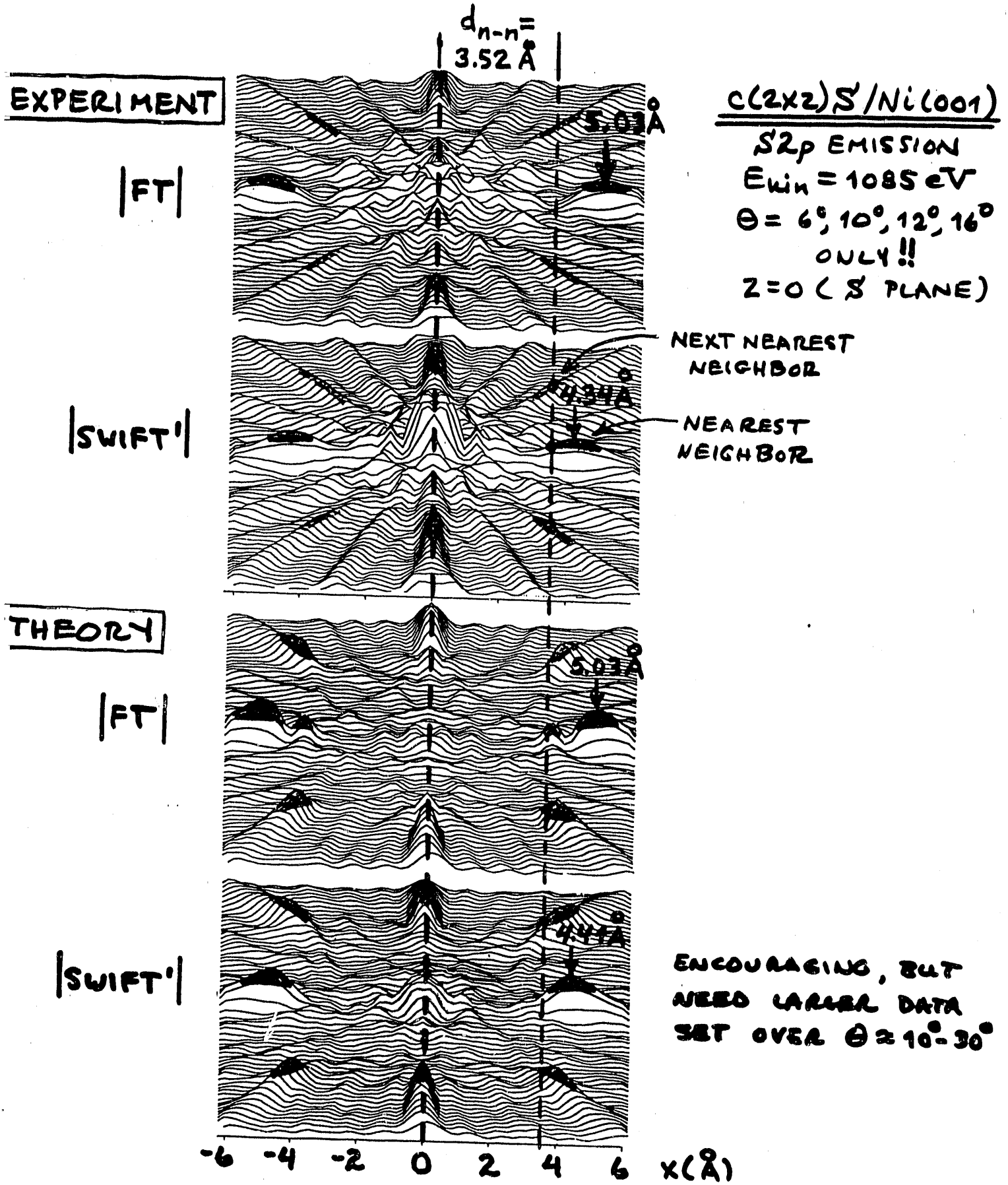

C(2x2)S/Ni(001)

S2p EMISSION

E_{kin} = 1085 eV

θ = 6°, 10°, 12°, 16° ONLY!!

Z=0 (S PLANE)

ENCOURAGING, BUT NEED LARGER DATA SET OVER θ ≈ 10°-30°

C(2x2)S/Ni(001): z=0

THEORY

$\Theta = 10\text{-}30^\circ$ ONLY

(a) FULL HOLOGRAM, |FT|

(b) " " , |SWIFT|

(c) RIGHT 1/2 OF HOLOG., |FT|

⇒ ELIMINATES TWIN/REAL OVERLAP

(d) " " " " , |SWIFT|

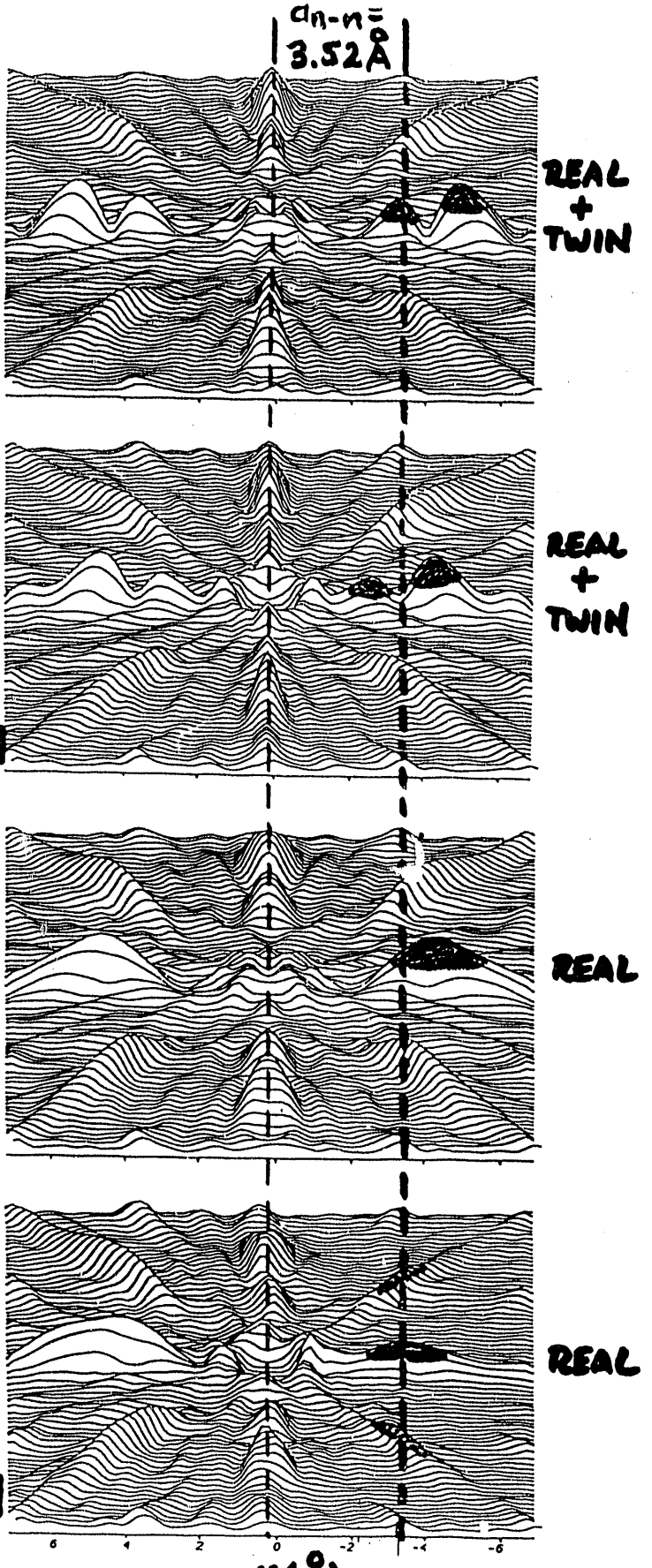

⇒ CORRECTING ONLY A PART OF HOLOGRAM MAY IMPROVE IMAGES!

Si(111):

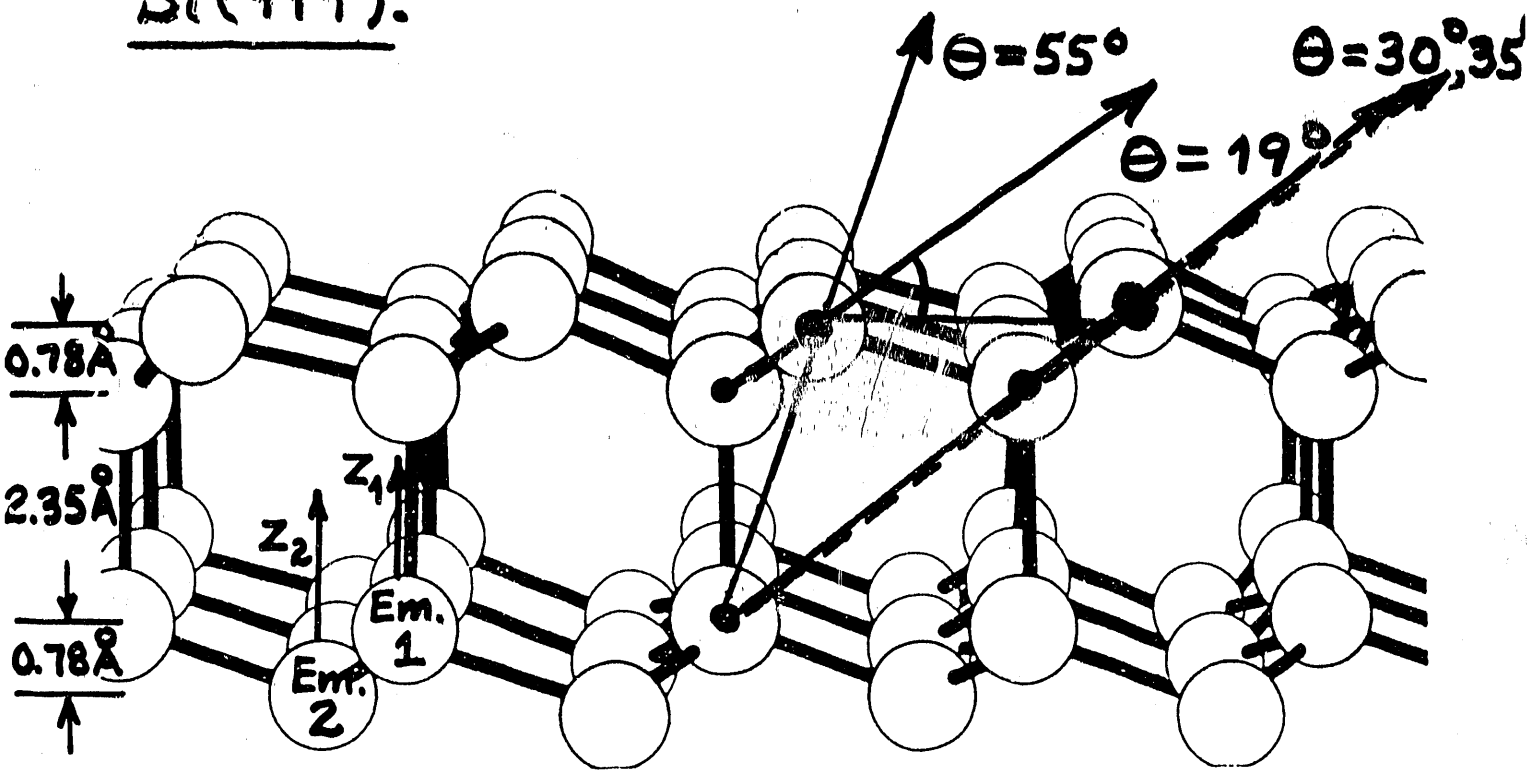

$\chi(k_x, k_y)$ FOR Si 2p FROM Si(111):
1387 eV
$\alpha = 174^\circ$

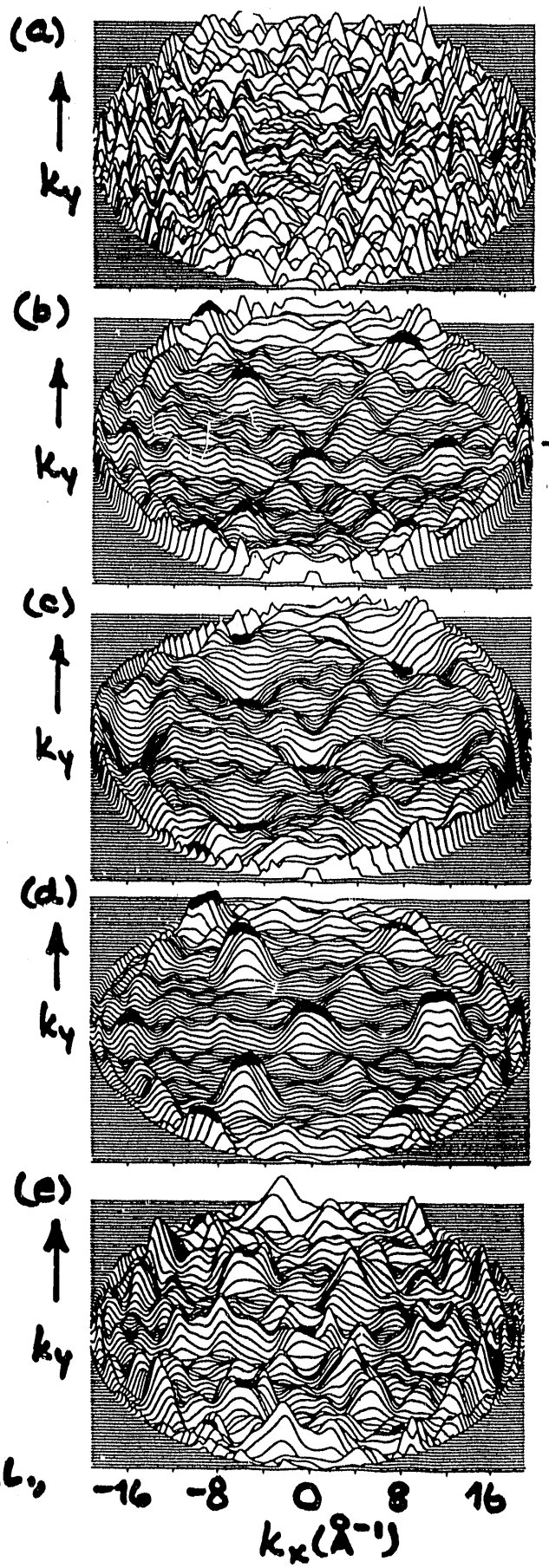

THEORY: IDEAL S-WAVE SS'

EXPT.

EXPT. − FWD. SCATT. PEAKS

THEORY: FULL p EMISSION SS'

THEORY: FULL p EMISSION SS' − FWD. SCATT. PEAKS

HERMAN ET AL., TO BE PUBL.

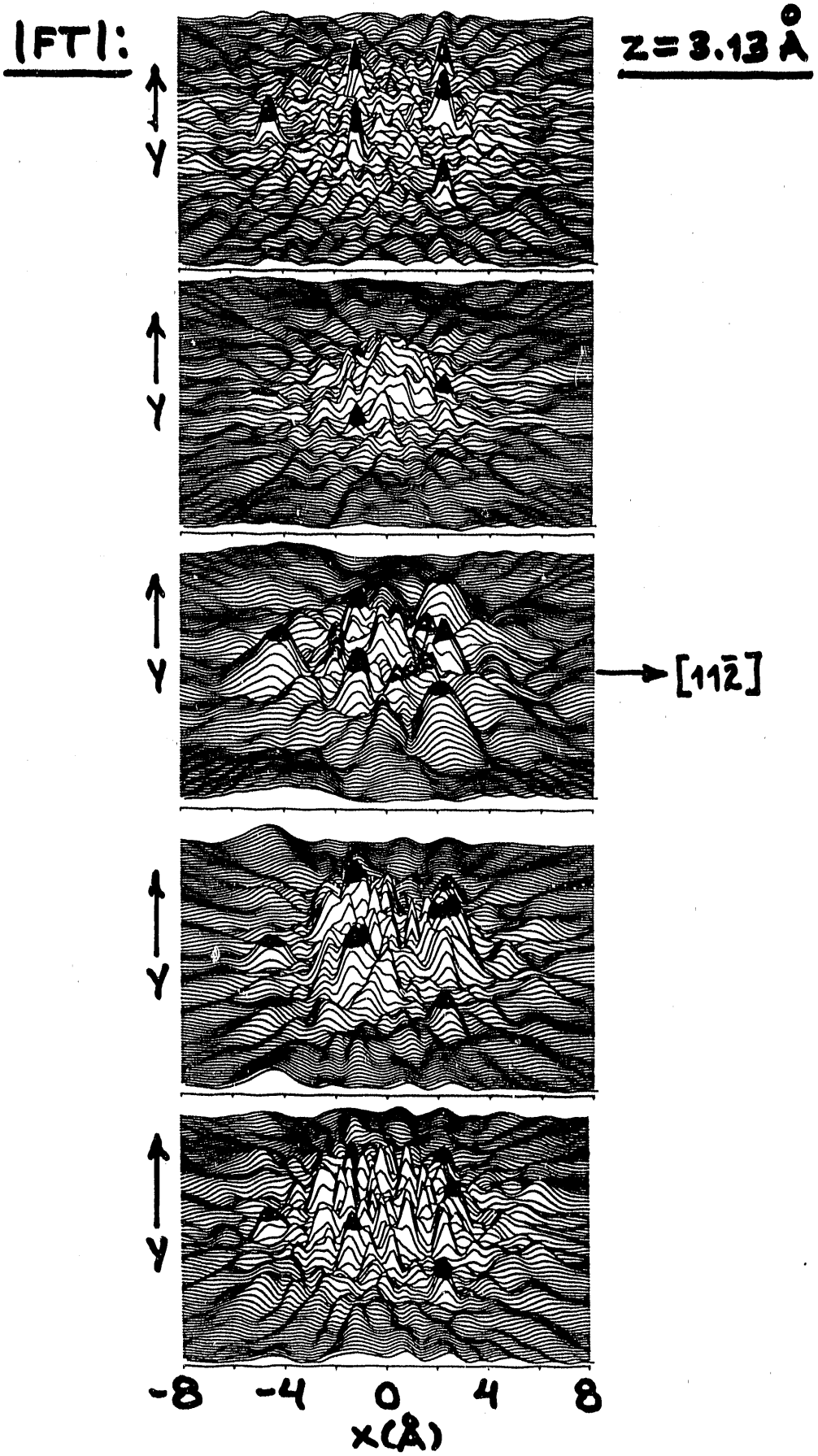
|FT|:
z = 3.13 Å
Y
Y
Y
[11$\bar{2}$]
Y
Y
-8
-4
0
4
8
x(Å)

Si(111) - Si2p : FT @ 2 = 3.13Å

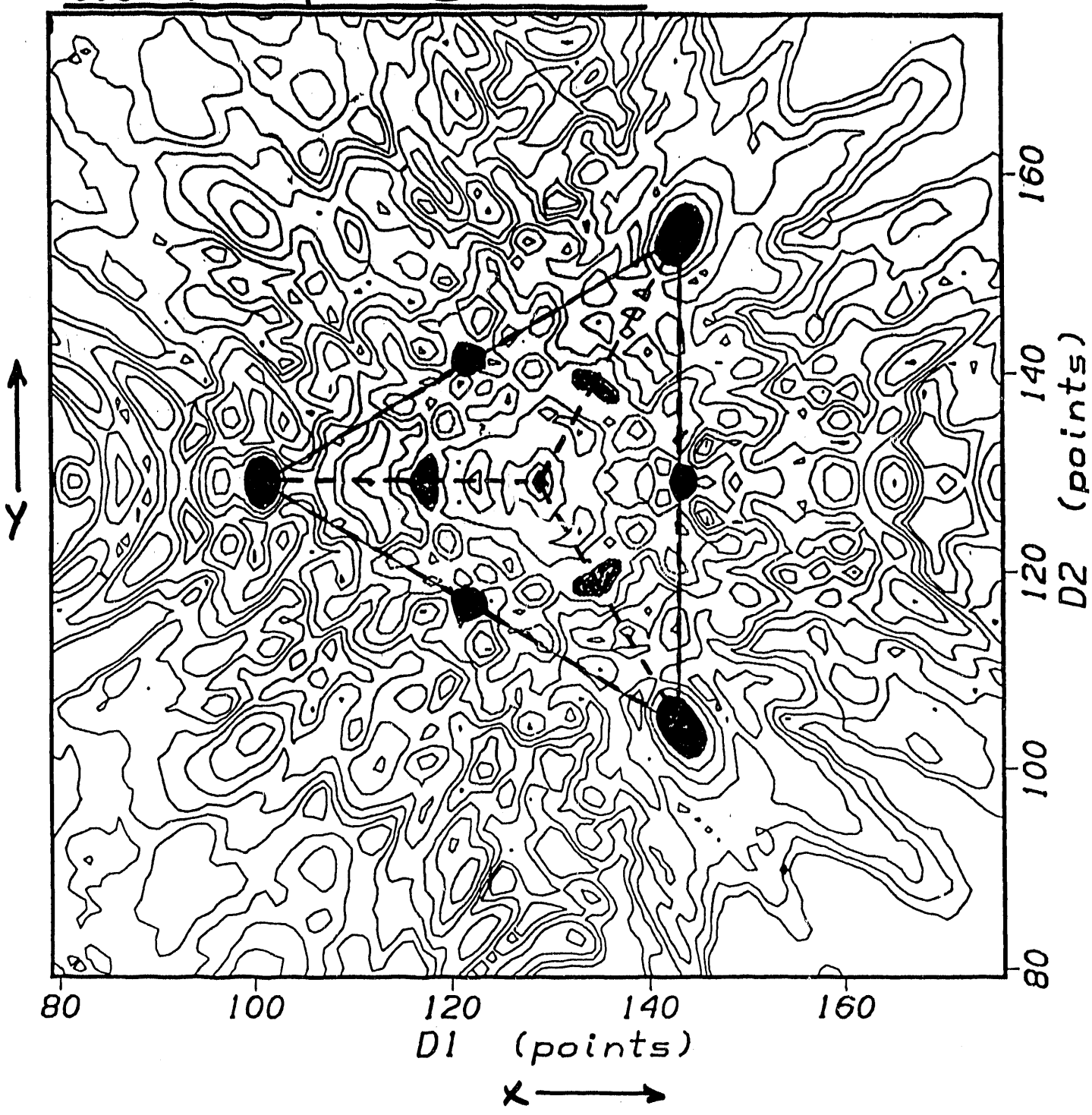

CENTER TO CORNER = 4.65Å (CF. 4.42Å IN Si)

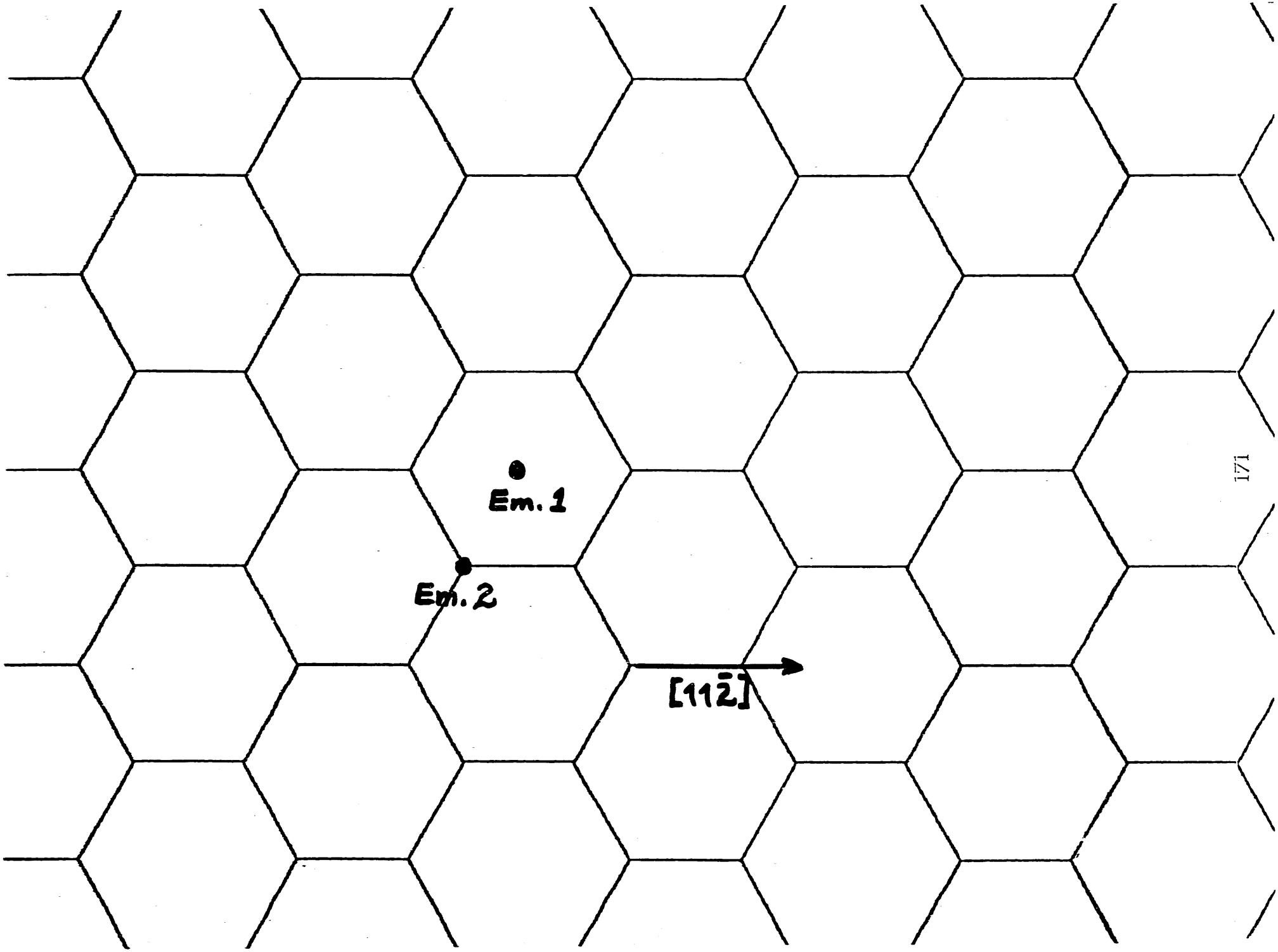
Em. 1
Em. 2
[11$\bar{2}$]

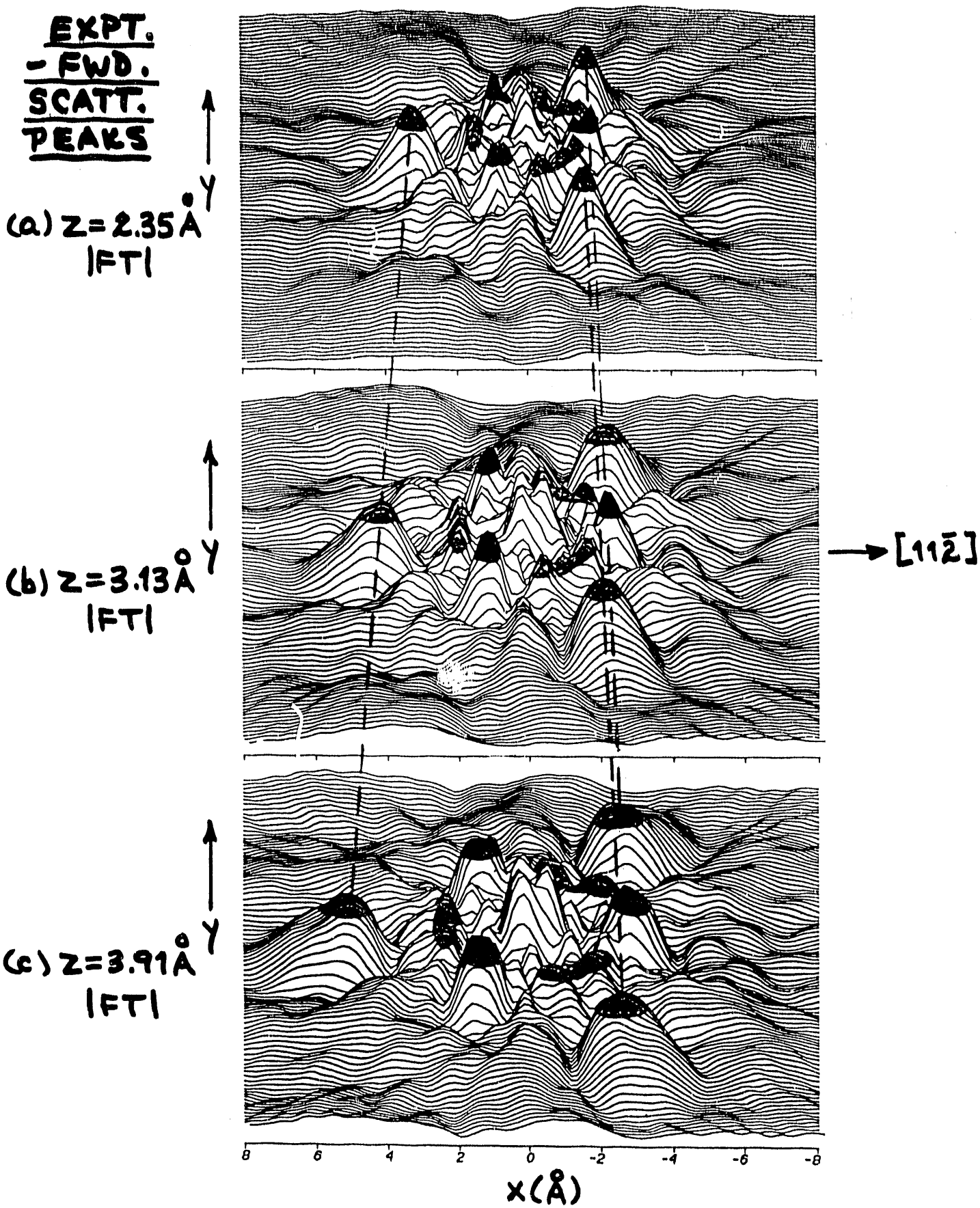
EXPT.
- FWD.
SCATT.
PEAKS
(a) Z = 2.35 Å
|FT|
Y
(b) Z = 3.13 Å
|FT|
Y
[11$\bar{2}$]
(c) Z = 3.91 Å
|FT|
Y
8
6
4
2
0
-2
-4
-6
-8
x(Å)

Si(111) AND $\sqrt{3}$ Ag/Si(111): LATERAL POSITION OF FT PEAK RELATIVE TO EMITTER

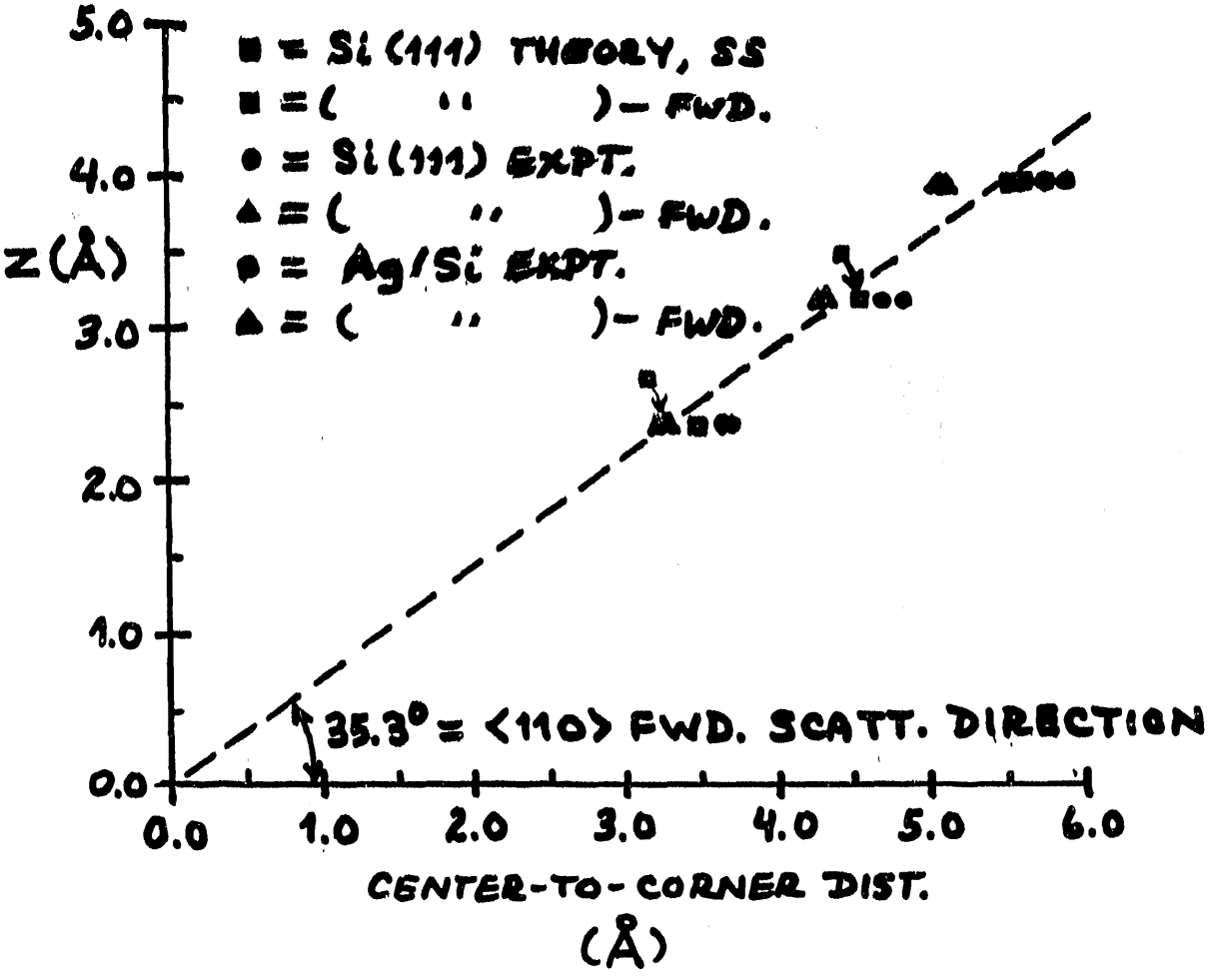

⇒ IMAGE ELONGATED ALONG FWD. SCATT. DIRECTION (AS IN METALS)

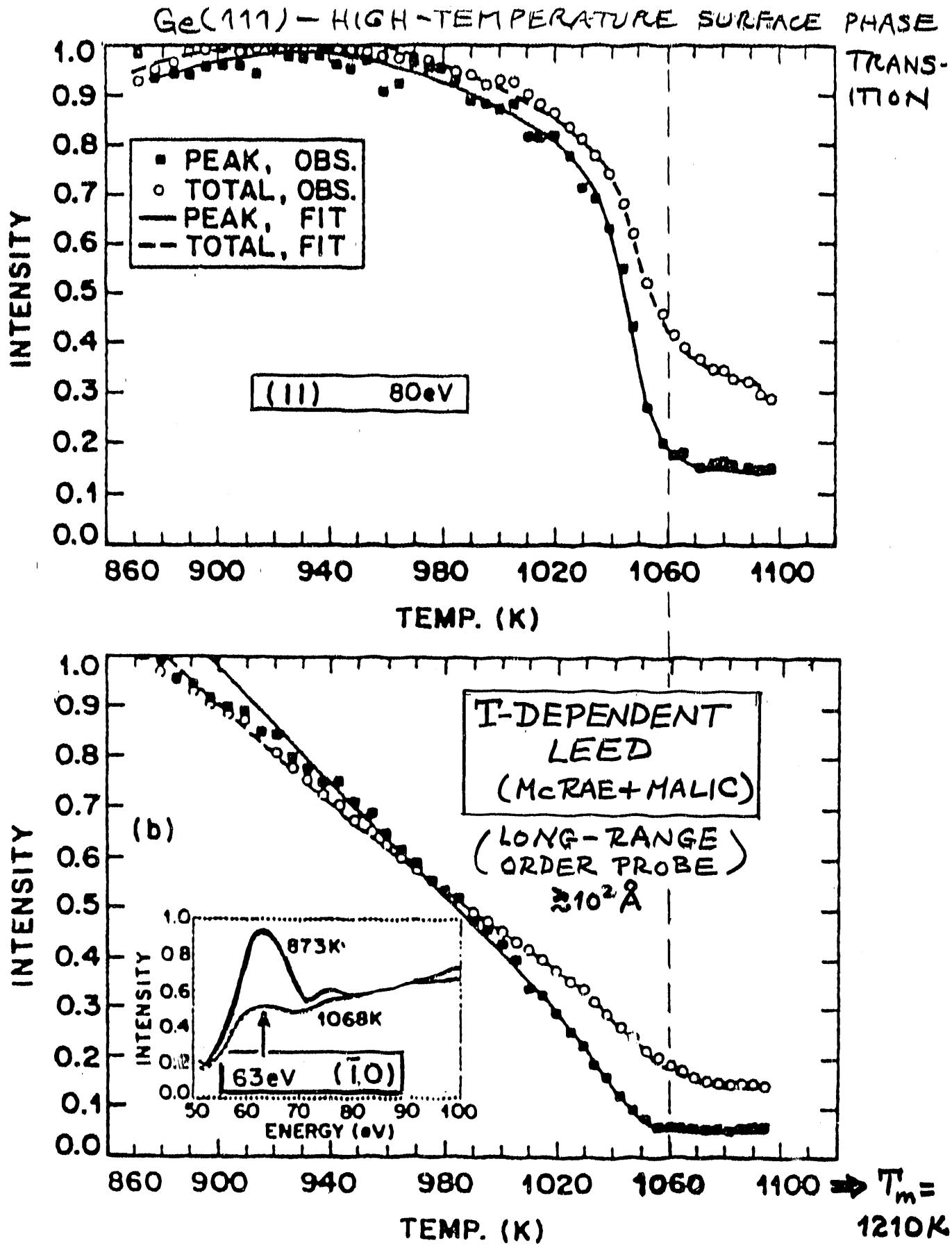

E.G. McRae and R.A. Malic, Phys. Rev. B 38, 13163 (1988)

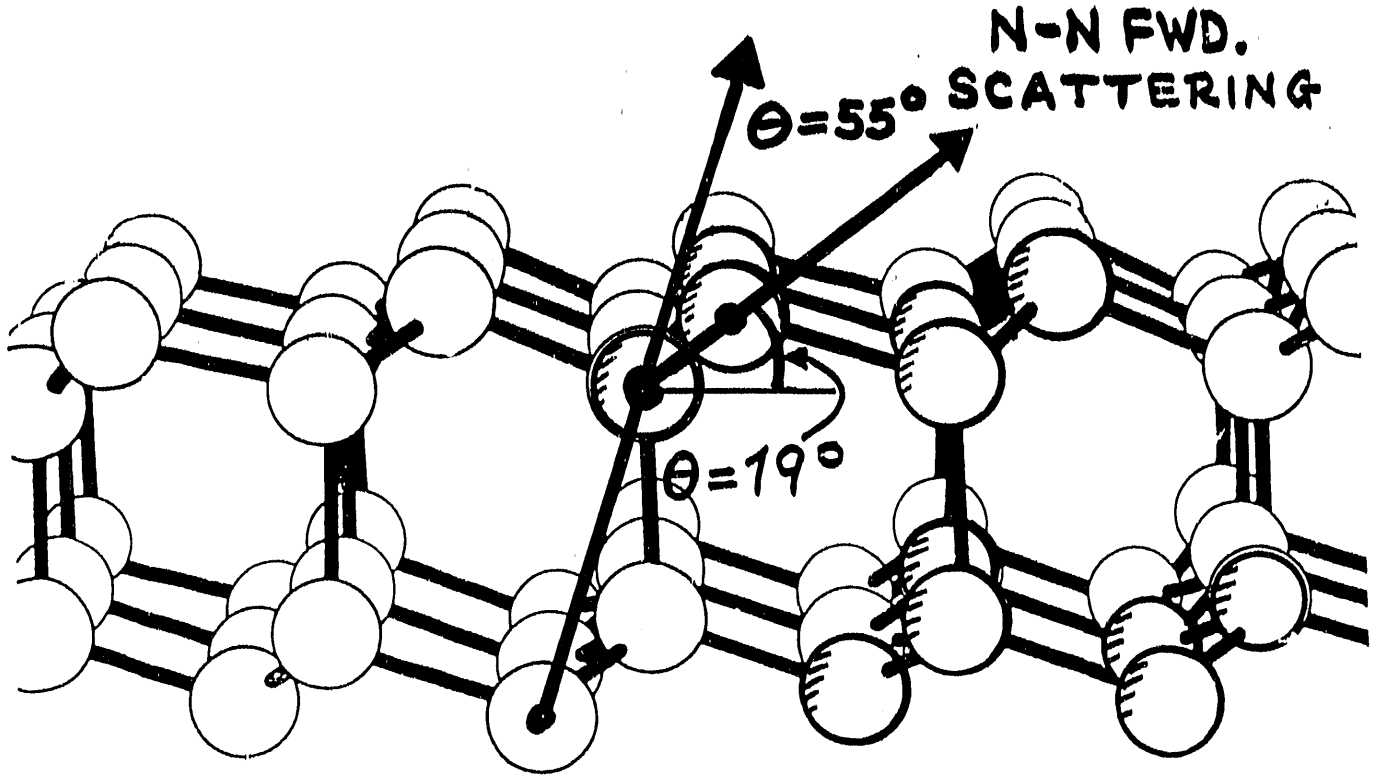

Ge(111) - (1x1) ⇒
(2×8) RECONSTRUC-
TION

Melting point = 1210.4 K

Density of solid at Tm = 5.22 g/cm^3

Density of liquid at Tm = 5.53 g/cm^3

5.6% COMP.

(Solid-to-liquid linear compression of 1.9%)

A Proposed Model:

T < 1050 K

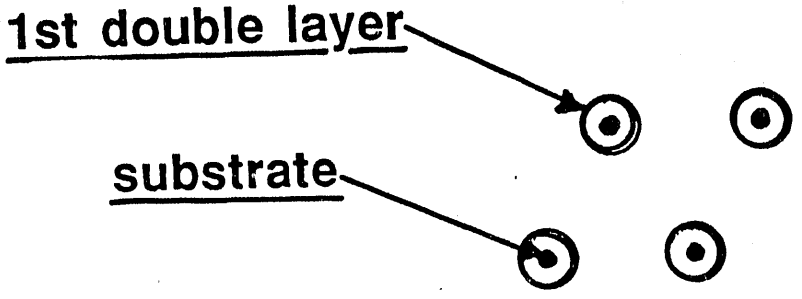

T > 1050 K

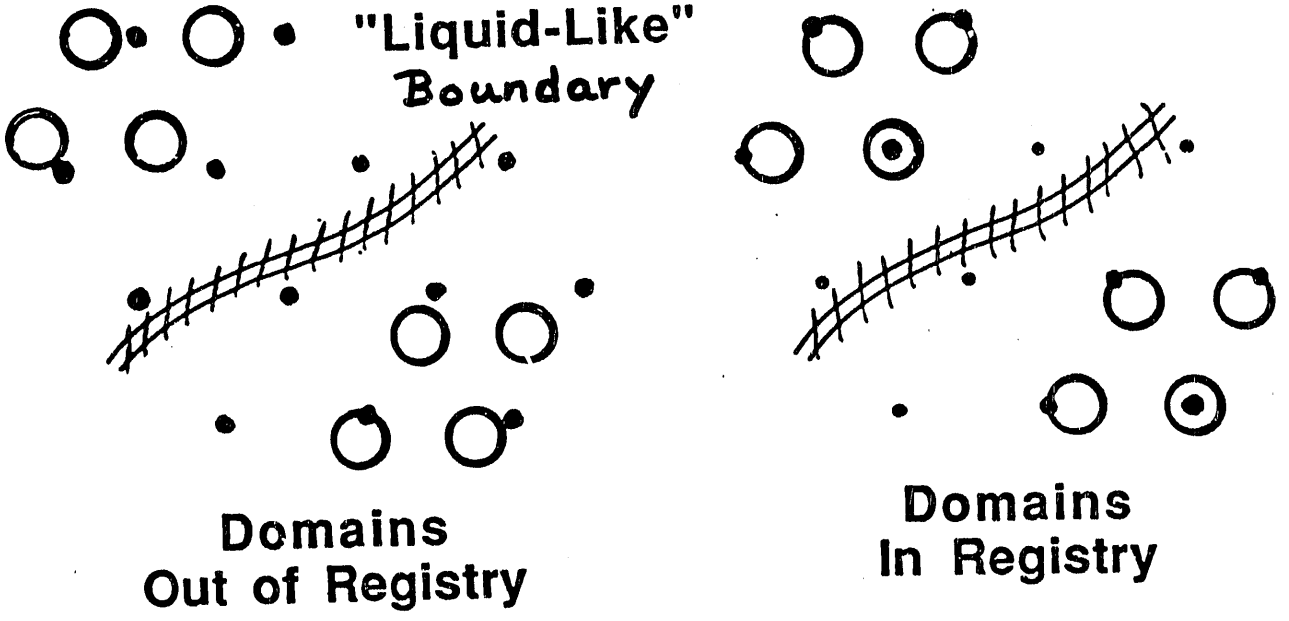

E.G. McRae and R.A. Malic, Phys. Rev. B 38, 13163 (1988)

Does this involve also solid to liquid compression?

Azimuthal Data, θ = 19°

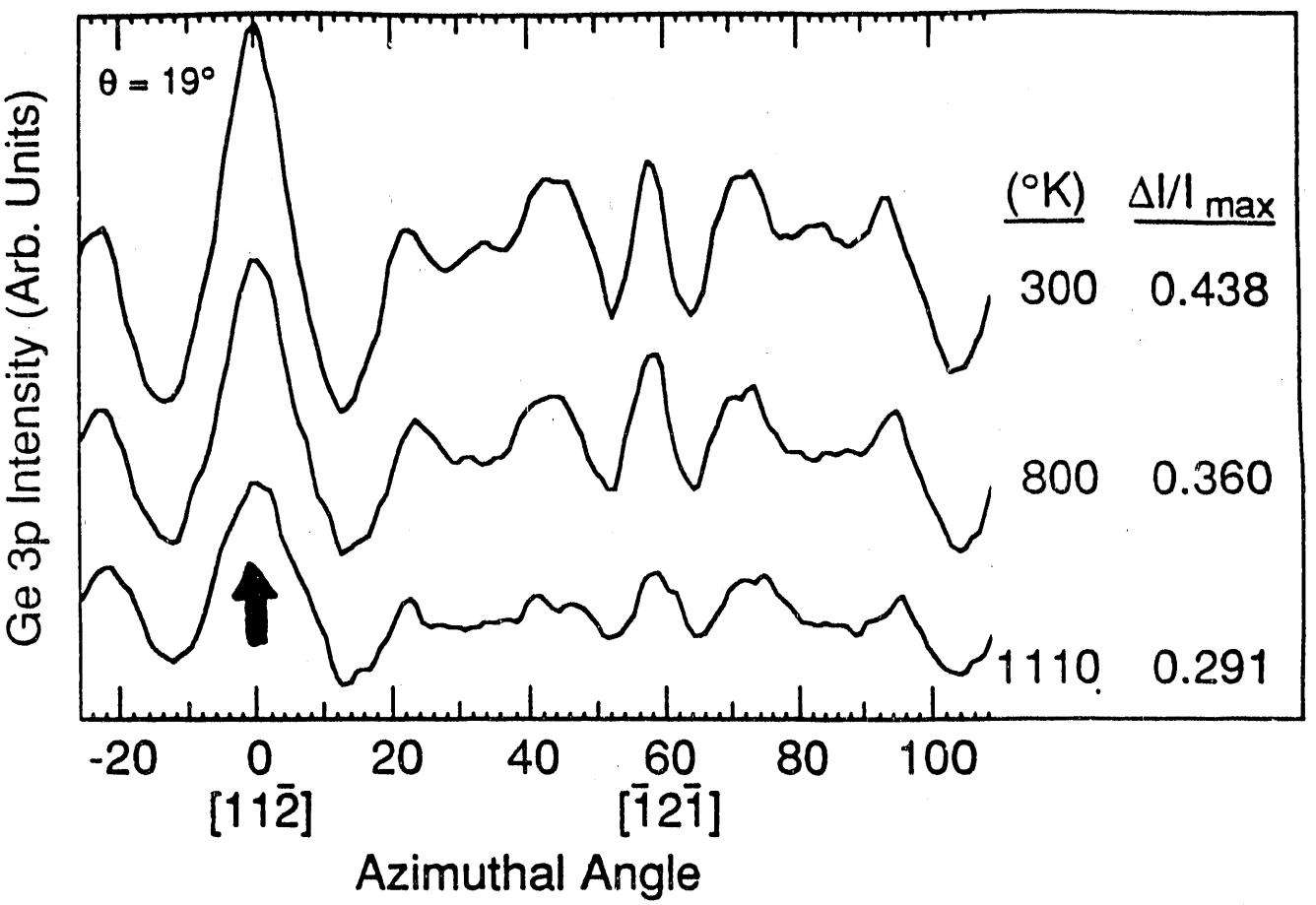

TRAN ET AL.,
TO BE PUBL.

Temperature Dependence of Forward-Scattering Peak

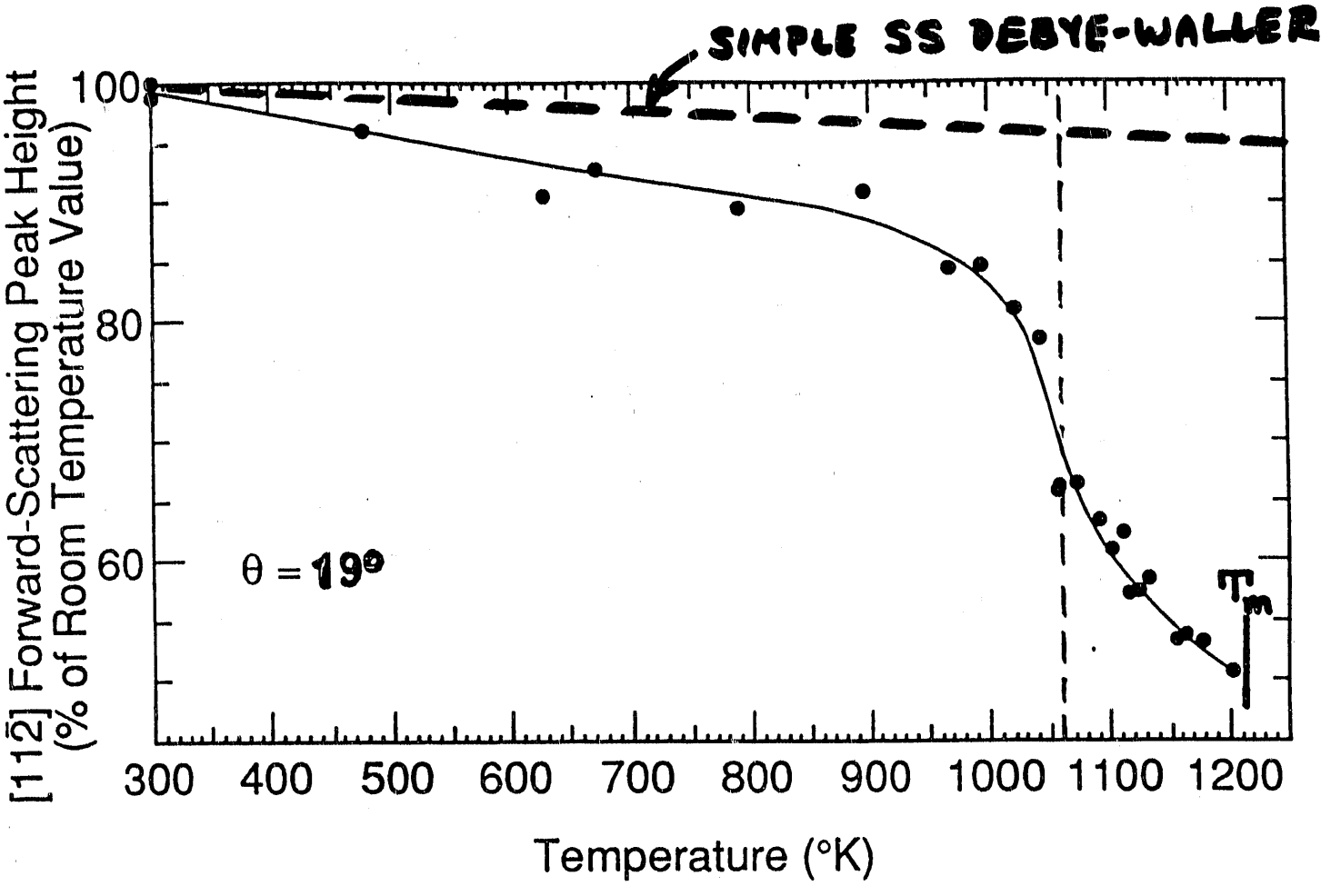

Temperature Dependence of Forward-Scattering Peak

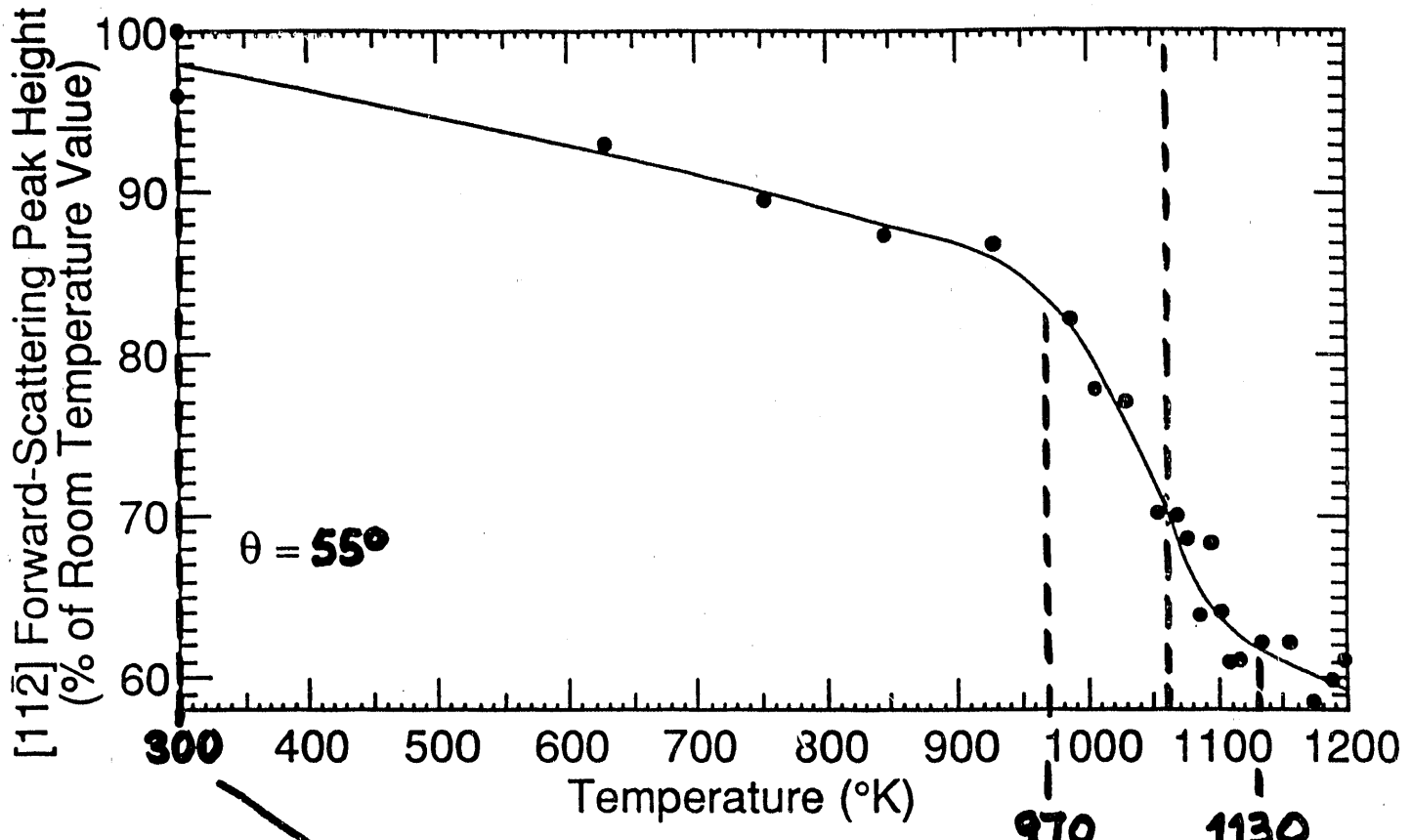

⇒ INDICATES TRANSITION INVOLVING SEVERAL DOUBLE LAYERS

PLUS FULL "HOLOGRAMS" AT 3 T's

Projection of $\chi(\underline{k})$ Onto k_x-k_y Plane

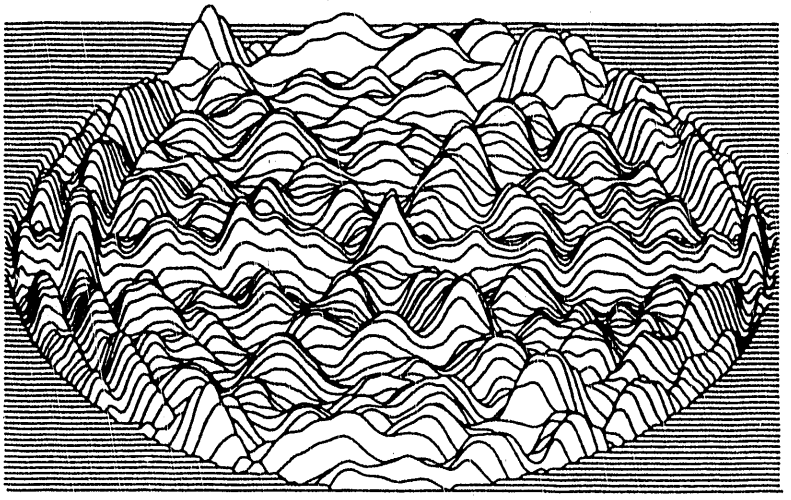

$\chi(k_x,k_y)$
Experiment, RT:
300K

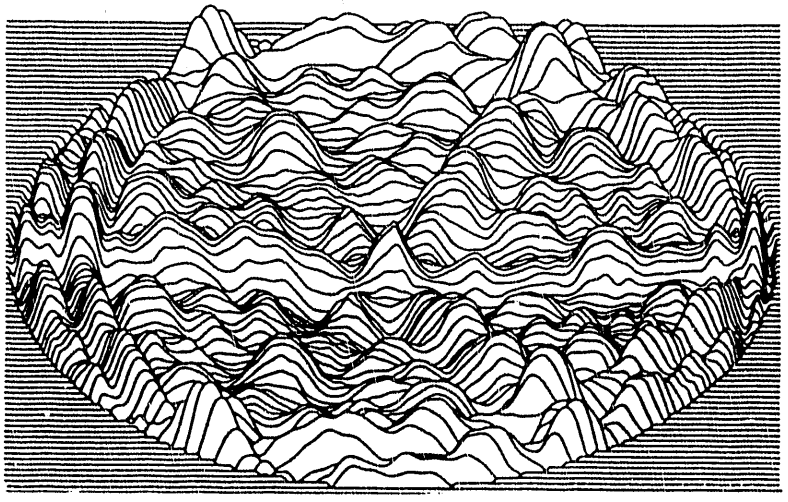

$\chi(k_x,k_y)$
Experiment, MT
970K

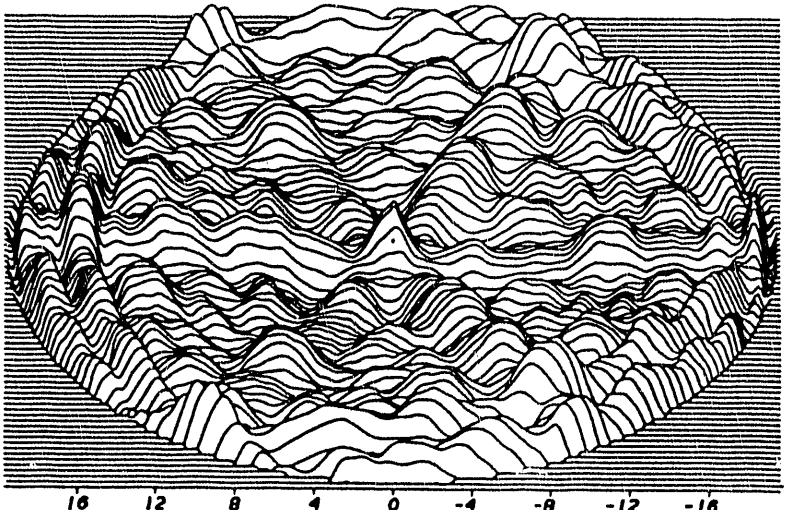

k_y

$k_x(\text{Å}^{-1})$

$\chi(k_x,k_y)$
Experiment, HT:
1130K

Horizontal FT Contour Plots

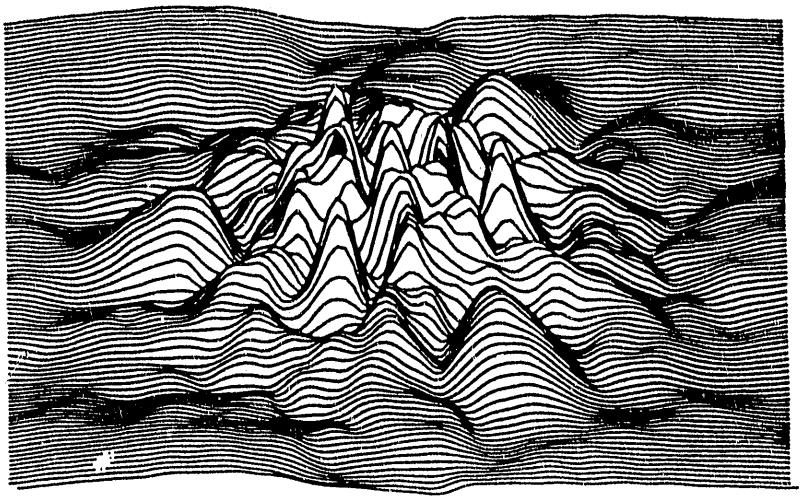

|FT|, Experiment
HWHM = 7.5Å
Z = 3.27Å, RT =
300K

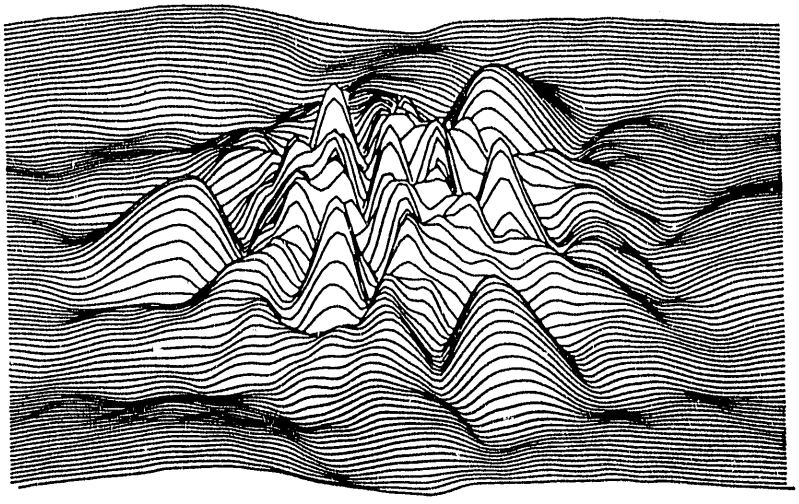

|FT|, Experiment
HWHM = 7.5Å
Z = 3.27Å, MT =
970K

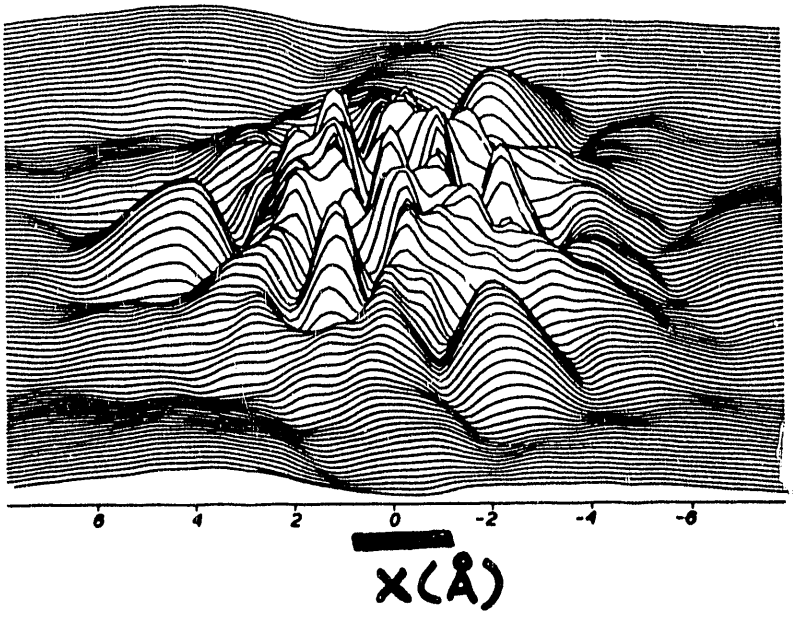

Y

|FT|, Experiment
HWHM = 7.5Å
Z = 3.27Å, HT =
1130K

⇒ SAME MEAN INTER-LAYER BOND ANGLES

A POSSIBLE MODEL:

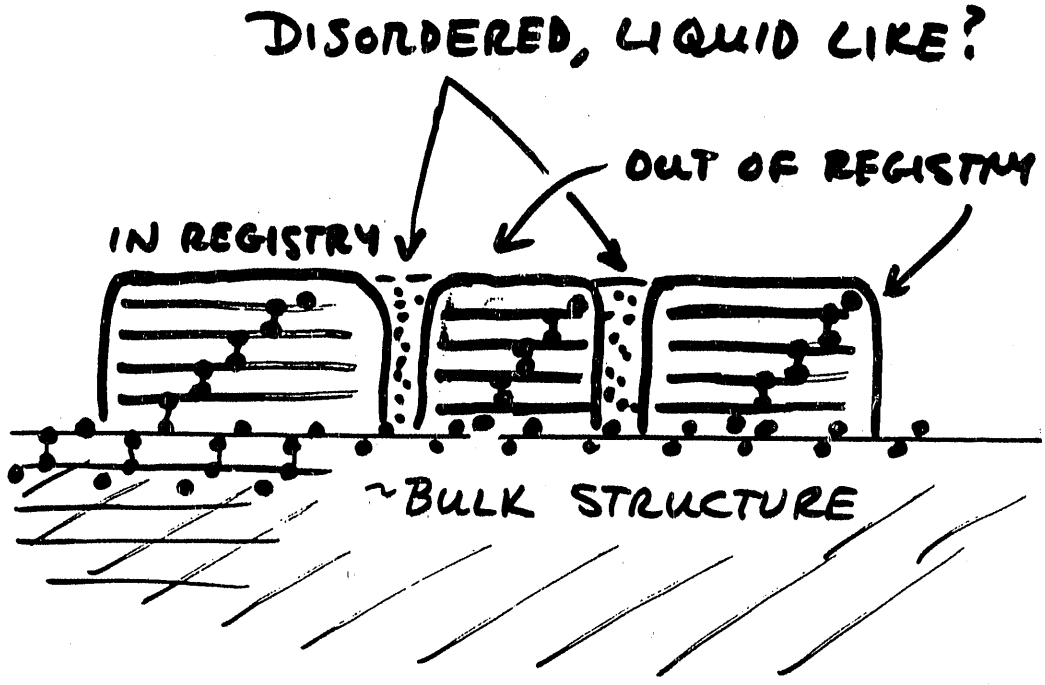

- DOMAINS $\leq$ 50 Å IN SIZE
- THICKNESS $\geq$ 3-5 DOUBLE LAYERS
- LATERAL + VERTICAL COMPRESSION
  $\Rightarrow$ LIQUID DENSITY

CONCLUSIONS / FUTURE PROSPECTS

ϕ BARTON
* TONNER, SALDIN ET AL
+ OUR GROUP

- HOLOGRAPHIC FOURIER TRANSFORMS[ϕ] OF EXPERIMENTAL DATA FOR Cu(001)[*], Cu(111)[*], c(2×2)S/Ni(001)[+], Si(111)[+], & Ge(111)[+] SHOW PEAKS ~ AT NEAR-NEIGHBOR POSITIONS, BUT SHIFTED OUTWARD AND ELONGATED ALONG SCATTERING DIRECTIONS, AS EXPECTED FROM THEORY
  THEORETICAL SS + MS SIMULATIONS SHOW THAT:
- FOR HIGHER ENERGIES ≳ 500 eV ⇒ STRONG FORWARD SCATTERING:
  - HIGHER-ORDER DIFFRACTION FEATURES VERY KINEMATICAL[+]
  - MS ALONG ATOMIC CHAINS SUPPRESSES SCATTERING ANISOTROPY ⇒ BETTER IMAGES[+]
- SELF-INTERFERENCE EFFECTS MAY BE PRESENT AT ~15-20% OF NEAREST-NEIGHBOR PEAKS[+] REMOVING FWD. SCATT. PEAKS IMPROVES IMAGE CONTRAST + PEAK SHAPE IN BOTH EXPT. + THEORY[+]: REDUCE OPENING ANGLE OR USE GAUSSIAN ELIMINATION
- SCATTERED-WAVE INCLUDED FOURIER TRANSFORM (SWIFT') METHOD[*] WORKS WELL, BUT TWIN OVERLAP PROBLEM: USE PART OF HOLOGRAM?[+]
- SUMMING IMAGES AT SEVERAL (~10) ENERGIES[ϕ] WITH SWIFT' IMPROVES PEAK POSITIONS,[*†] AND FOR SOME GEOMETRIES/LOWER ENERGIES, ALSO REMOVES TWINS (…AND MS?)[ϕ+]
- PHOTOELECTRON ANISOTROPY IN $\phi_0 = \phi_{REF}$ AND $\phi_j = \phi_{OBJECT}$ YIELDS WORSE IMAGES THAN ISOTROPIC "AUGER-LIKE" EMISSION ⇒ SWIFT" CORRECTION NEEDED?
- ENCOURAGING, BUT NEED MORE EXPTS. + TESTING!

	LOW ENERGY ~100-300 eV	HIGH ENERGY ~500-1500 eV
SS vs MS	MS OVER LARGER ANGLE RANGE −	MS ALONG FWD. − CHAINS; ~SS + ELSEWHERE
SCATT. FACTOR	MORE ISOTROPIC, + MORE S-LIKE, BACKSCATT. INFORMATION +	STRONG FWD. + PEAK-USEFUL! BUT BAD IN HOLOGRAPHY −
ULTIMATE RESOLUTION	$\propto \lambda_e$ − WORSE	$\propto \lambda_e$ + BETTER
PHOTO e^- CROSS SECTION	HIGHER +	LOWER −
TOTAL SCATT. FACTOR	HIGHER→ LARGER + EFFECTS	LOWER→ LESS SELF-INT. + + MS +
INELASTIC ATTEN.	MORE SURF. SENSITIVE	MORE BULK SENSITIVE
MAGNETIC SCATT?	YES +	NO −

- PHOTOELECTRON DIFFRACTION CAN BE USED TO STUDY NEAR-SURFACE PHASE TRANSITIONS IN BOTH POSITIONAL ORDER AND SHORT-RANGE MAGNETIC ORDER (USE OF CIRCULARLY-POLARIZED RADIATION WILL PERMIT GOING BEYOND SIMPLE MULTIPLETS).

Theoretical Developments in Photoelectron Diffraction

M. Van Hove

Lawrence Berkeley Laboratory

Theoretical Developments in Photoelectron Diffraction

M.A. Van Hove

Center for Advanced Materials
Materials Sciences Division
Lawrence Berkeley Laboratory
Berkeley

Collaborators:

J.J. Barton	IBM (Yorktown)	ED theory
C.S. Fadley	Berkeley	holography
K. Heinz	U. Erlangen	FF exp.
A. Kaduwela	Berkeley	holography theory
K. Müller	U. Erlangen	FF exp.
S. Thevuthasan	Berkeley	holography theory
M.-L. Xu	U. Toronto	ED and DLEED theory

Funding:

DOE
DOE Supercomputer
ARO
IBM Postdoc Fellowship (J.J. Barton)

INTRODUCTION

Purpose:

summarize:

theoretical state of the art
in electron emission from surfaces

address:

some physical principles
that underlie the formation of holograms

BASICS OF ELECTRON EMISSION

Types of electron emission:

- photoelectrons

  matrix element well known (if single-channel emission)

  element specific

- Auger electrons

  matrix element poorly known,
  but approximately s-wave at E > 300 eV

  element specific

- Kikuchi (inelastic) electrons

  matrix element poorly known, except for phonon losses

  not element specific

- MEED (elastic) electrons

  matrix element well known

  not element specific

Electron energy range:

- 300 - 1500 eV

Measurement:

- scanned angle (ARXPD, ARAES,...)
- scanned energy (PhD, ARPEFS,...)

Structure information:

- interference between direct and scattered paths
- forward focusing (forward scattering)

  Fadley, Egelhoff, ...

Osterwalder et al

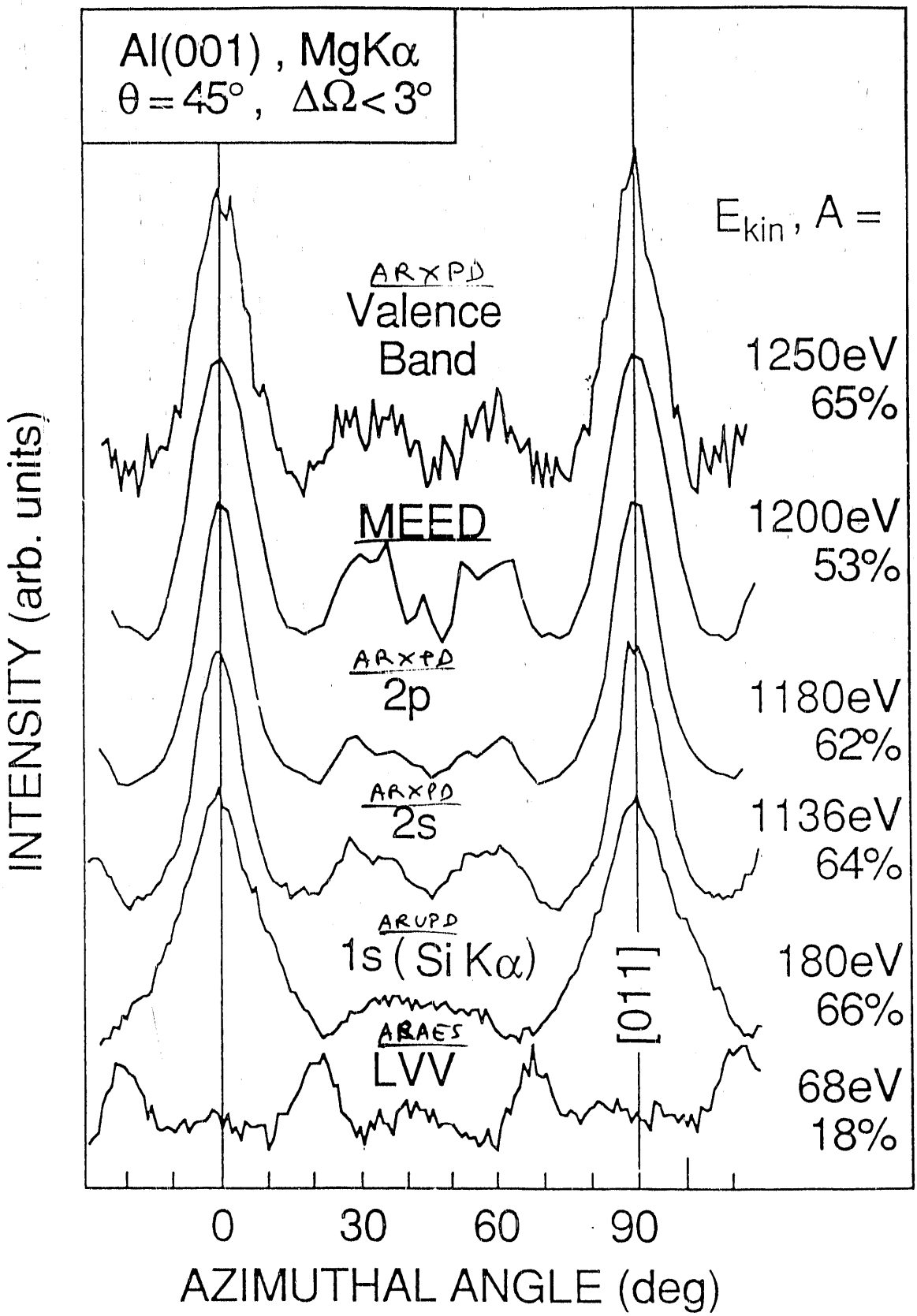

THEORY

Physical ingredients:

- **muffin-tin model**
- **inelastic mean free path**
- Debye-Waller factor ?

Form of scattering wave:

- **plane wave vs. spherical wave**

  plane wave simpler

Role of multiple scattering:

- **single vs. multiple scattering**

  single scattering much simpler

Validity of approximations:

- **single and plane-wave (SSPW) scattering valid in favorable cases**

  what is accuracy of such (non-holographic) structure determination?

- **multiple and spherical-wave (MSSW) scattering often needed**

  for aligned atoms (forward focusing)

  for interference features

  what is accuracy of such (non-holographic) structure determination?

ATOMIC SCATTERING AMPLITUDE

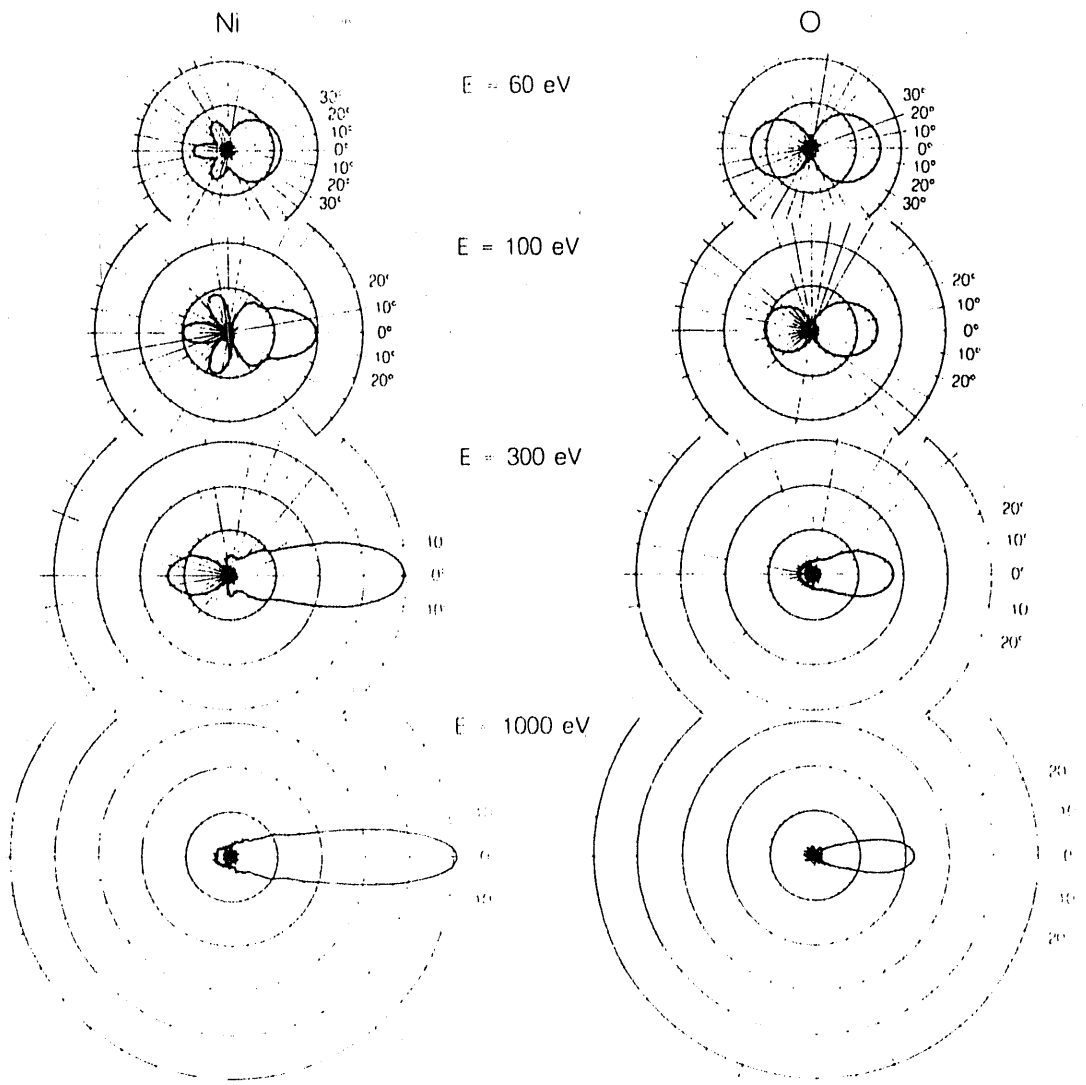

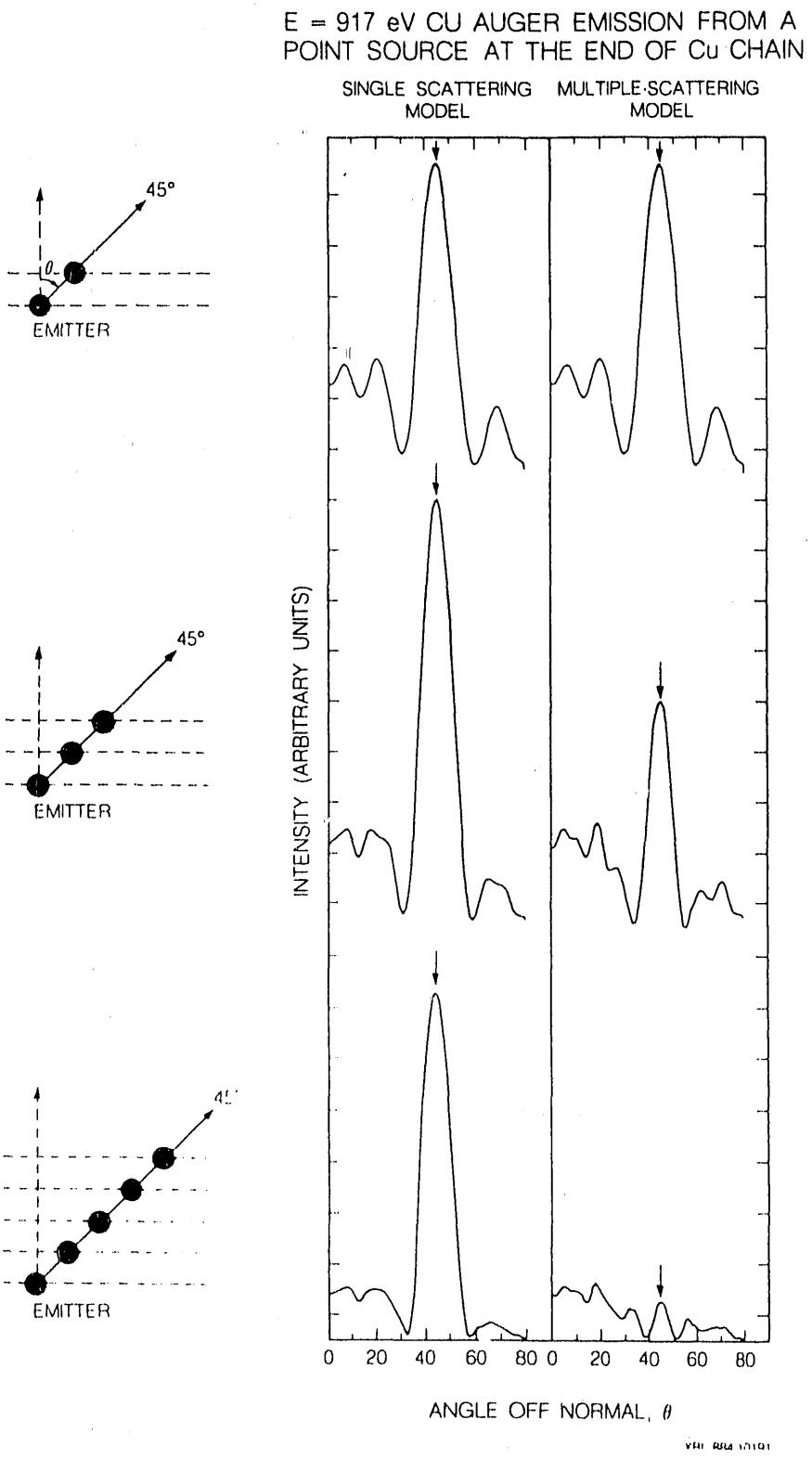
E = 917 eV CU AUGER EMISSION FROM A POINT SOURCE AT THE END OF Cu CHAIN
SINGLE SCATTERING MODEL
MULTIPLE-SCATTERING MODEL
45°
θ
EMITTER
45°
EMITTER
EMITTER
INTENSITY (ARBITRARY UNITS)
0 20 40 60 80 0 20 40 60 80
ANGLE OFF NORMAL, θ

forward focusing

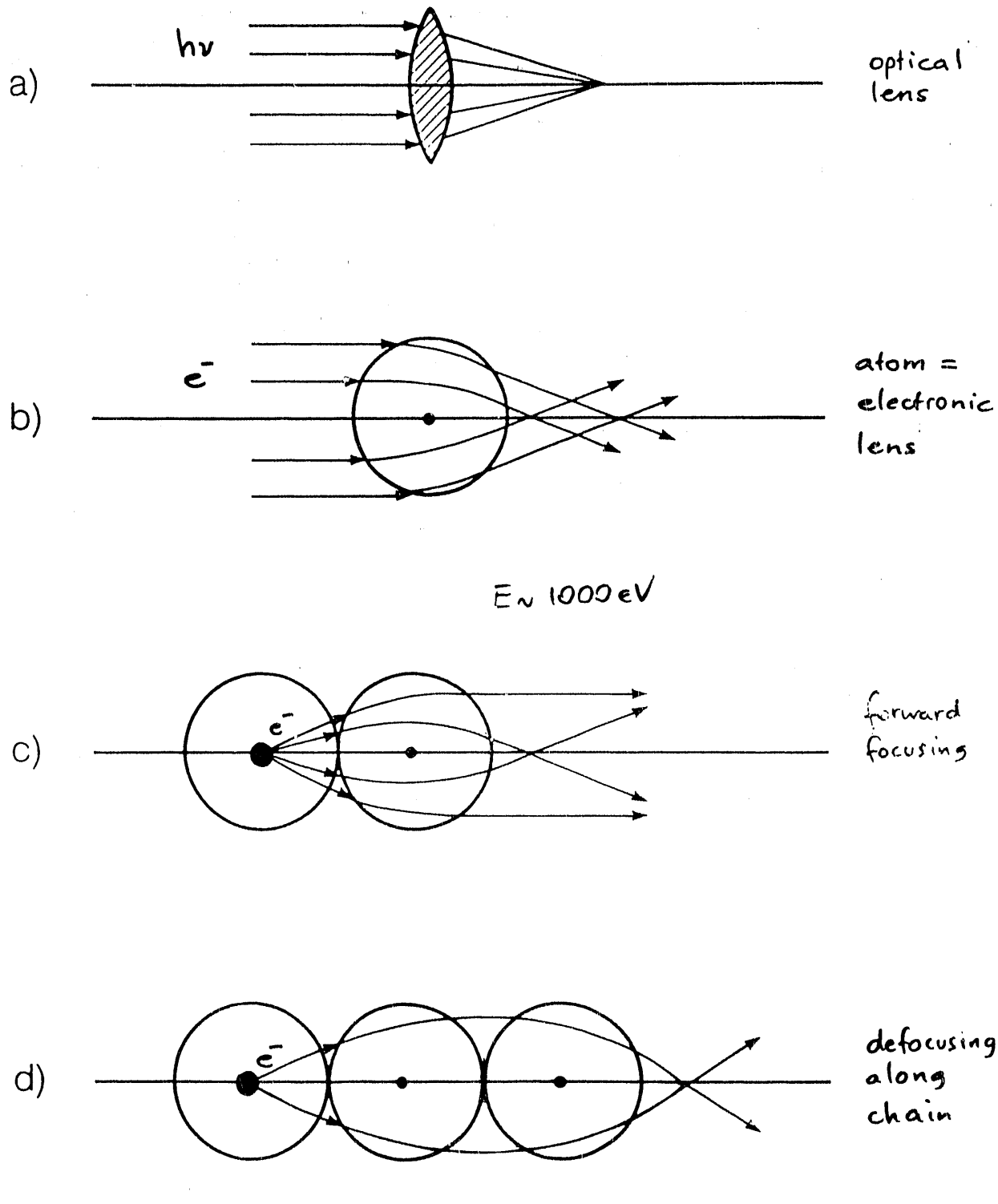

XBL 884-10187

MSSW implementations:

common physical ingredients, but slightly different mathematical treatments

<u>cluster approach</u>

- Taylor-Series Magnetic-Quantum-Number Expansion (TS-MQNE)

  Barton and Shirley, Van Hove

- separable Green's function matrix method

  Rehr and Albers, Fadley et al

- Reduced Angular Momentum Expansion (RAME)

  Fritzsche, Rennert

- concentric shells (XANES-like)

  Saldin et al

<u>slab approach</u>

- layer stacking (LEED-like)

  Tong et al

AN ISSUE

Thermal vibrations:

Debye-Waller factor

distant source (MEED, LEED, XRD, etc.):
average of diffracted amplitudes over configurations

nearby point source (ARPES, ARAES, XAFS, etc.):
average of diffracted intensities over configurations

both averages give same Debye-Waller factor (Rehr - XAFS)

DW factor sharpens forward focusing peak, with no height loss;

counter to observation, e.g. Pb, CO (Bonzel et al):
peak broadens and weakens!

BUT: DW assumes:

rms vibration amplitude $\sqrt{<u^2>}$ << wavelength λ

examples:

$\sqrt{<u^2>} \approx 0.10$ Å *(bulk Ni) -* 0.25 Å *(bulk Pb, -CO) at RT*

$300 < E < 1000$ eV $\rightarrow 0.7 > \lambda > 0.4$ Å

SO: $\sqrt{<u^2>} \approx \lambda$ and DW breaks down!

EFFECT: forward focusing peak must be smeared out, not sharpened!

→ *no forward focusing in electron microscopy:*
$\lambda \approx 0.03 - 0.01$ Å $<< \sqrt{<u^2>}$

straight averaging over configurations

Fadley, Kaduwela, Van Hove: CO / Fe (100)

other complication: correlated vibrations

Fadley et al

Surf. Sci. 199, L419 (1988)

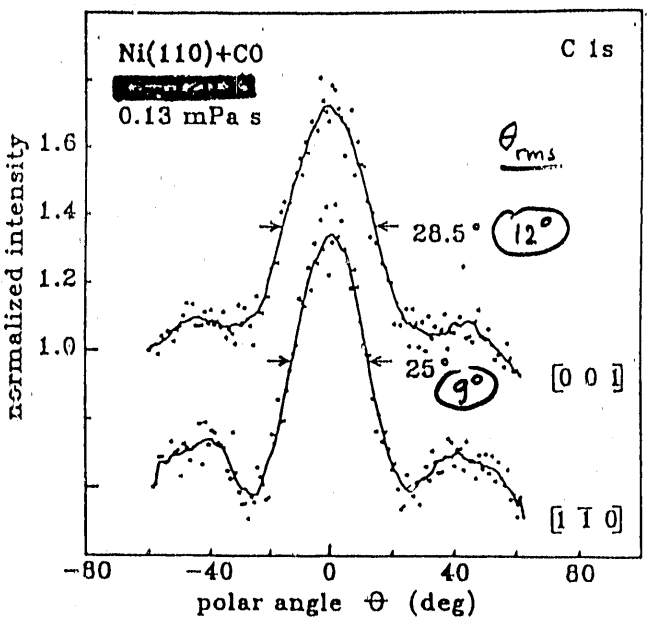

Polar angle dependence of C 1s normalized intensities for a low CO coverage on Ni(110). Two perpendicular azimuths along [001] and [1$\bar{1}$0] directions are shown. The numbers indicate the FWHM of the main forward scattering peak.

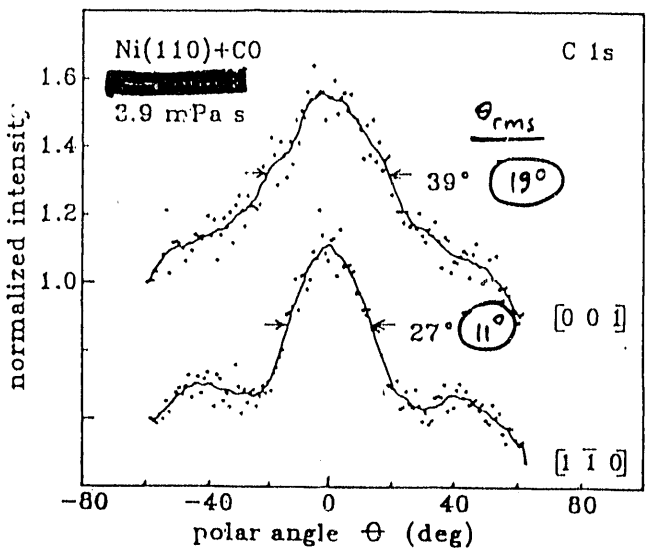

Same as in fig. 2 but for CO adsorption at 300 K.

θ_{rms} from calibration by Fadley et al

JVST A8, 2489 (1990)

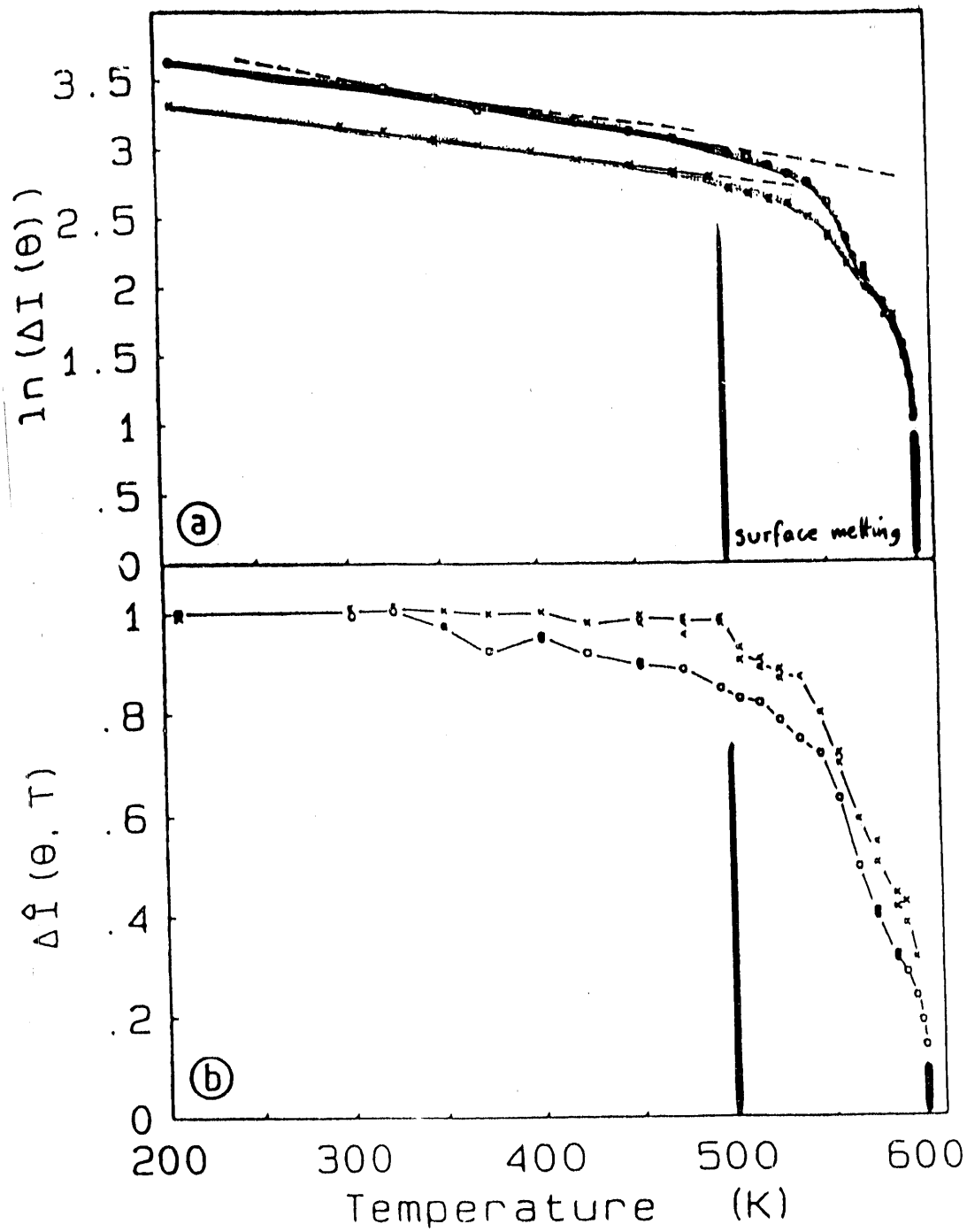

(a) Plot of ln $\Delta I(\Theta,T)$ vs temperature for the peak at $\Theta = 45°$ in [110] (□) and $\Theta = 54.7°$ in [001] direction (×). (b) For Debye-Waller effects corrected intensity distribution $\Delta\hat{I}(\Theta,T)$ vs temperature for the two peaks in (a).

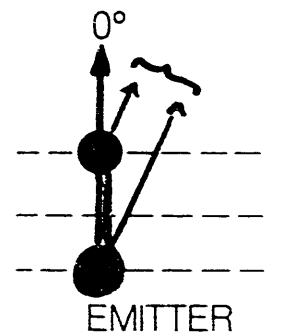

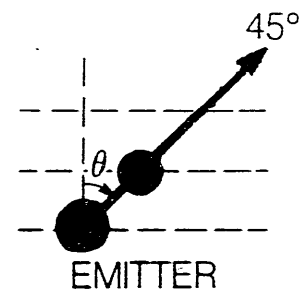

Cu ELECTRON EMISSION FROM A POINT SOURCE AT THE END OF Cu CHAIN

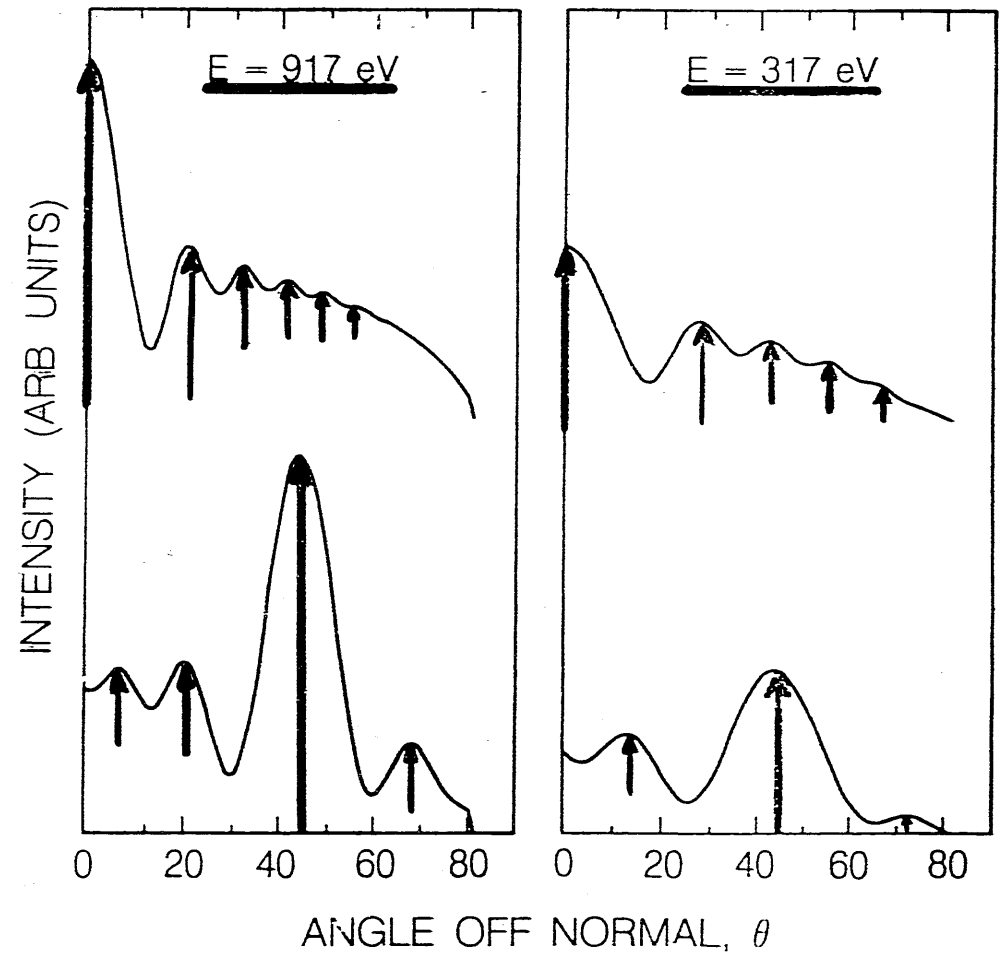

XBL 884-10189

Fe_5CO cluster

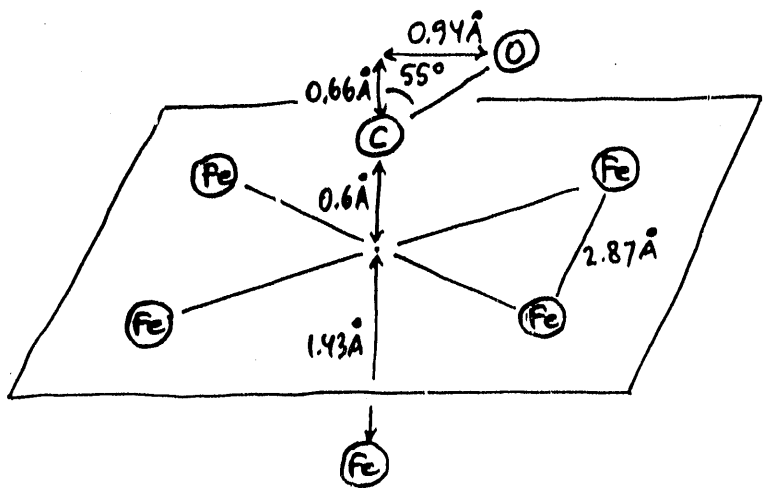

treatment of vibrations
C emission from Fe_5CO cluster

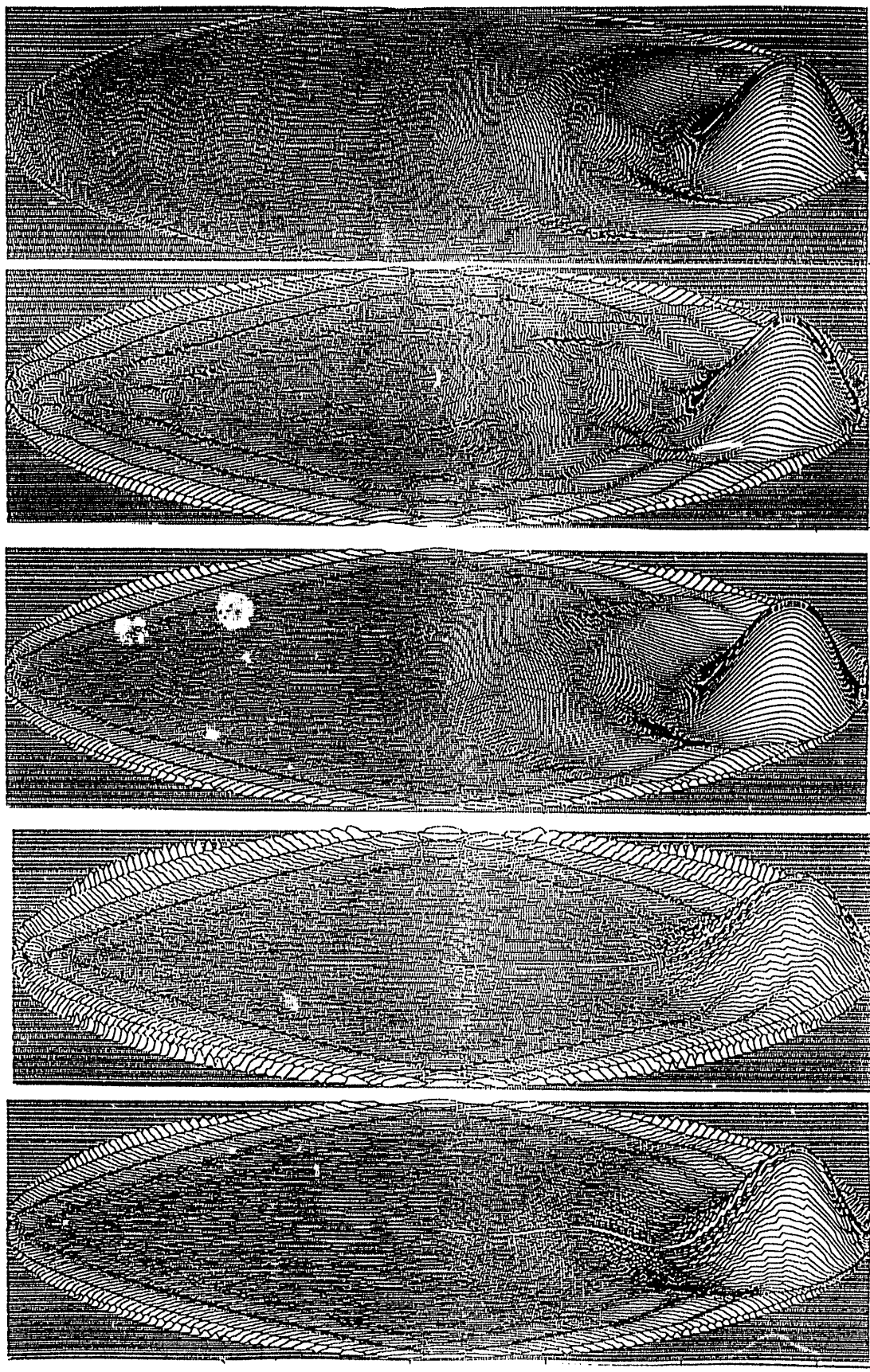

Kaduwela et al

ANOTHER ISSUE

Meaning of Fourier transform in electron holography:

assume weighted and phased distribution $S(\mathbf{R})$ of s-wave point sources, emitting amplitude $A(\mathbf{k},\mathbf{R})$ at large R, excluding all scattering:

(this mimicks multiple scattering as extra sources)

$$A(\mathbf{k},\mathbf{R}) \approx \frac{e^{ikr}}{R} \iiint d^3R\, S(\mathbf{R})\, e^{-i\mathbf{k}.\mathbf{R}}$$

then, inversely:

$$S(\mathbf{R}) \approx \iiint d^3k\, A(\mathbf{k},\mathbf{R})\, e^{i\mathbf{k}.\mathbf{R}}$$

SO: Fourier transform of non-scattered amplitude is point-source distribution

- this is ideal goal of holography

BUT: electron holography uses intensity $I(\mathbf{k},\mathbf{R})$:

$$S'(\mathbf{R}) \approx \iiint d^3k\, I(\mathbf{k},\mathbf{R})\, e^{i\mathbf{k}.\mathbf{R}}$$

i.e.:

image = effective point source distribution $S'(\mathbf{R})$,
such that $S'(\mathbf{R})$ reproduces "amplitude" $A' = I$,
where I is actual hologram

SO: electron holography yields an effective point source distribution $S'(\mathbf{R})$, that compensates for:

- using I, not A (giving twin and self-images)
- phase shifts, including forward focusing
- multiple scattering
- finite integration domain
- etc...

example:

forward focusing:

causes effective source at focus
and no image at nucleus of scatterer

Efficient Multiple-Scattering Methods in Photoelectron Diffraction and XAFS

J. Rehr

University of Washington

Efficient Multiple-Scattering Methods in Photoelectron Diffraction & XAFS

collaborators - R.C. Albers (Los Alamos)
- S.I. Zabinsky, Jose Mustre (UW)
- C.S. Fadley, A. Kaduwela, D. Friedman (U. Hawa

support - U.S. D.O.E.

Goal: Fast, accurate calculations of P.D., XAFS, AES, etc

PD:

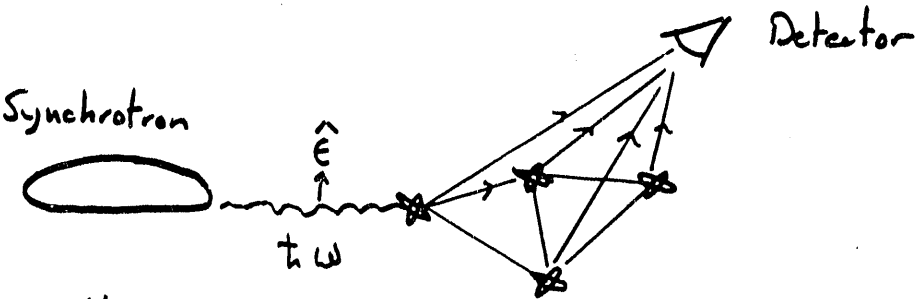

$$\frac{d\sigma}{d\Omega} \sim \left| \sum_{L,N}^{\text{paths}} G^{N}_{00,L} \langle L | \hat{\epsilon} | c \rangle \right|^2$$

Talk:
1) Introduction - "Angular Momentum Disease"
Practical IMPOSSIBILITY of calculating $G^{N}_{00,L}$
2) Approximations: (cures)
Spherical Wave Approximation SWA
Magnetic Quantum Number Expansion MQNE
Scattering Matrices SM
3) Why does it work?

1. Introduction - Multiple Scattering Expansion

$G^N_{00,L}$ N-leg propagator

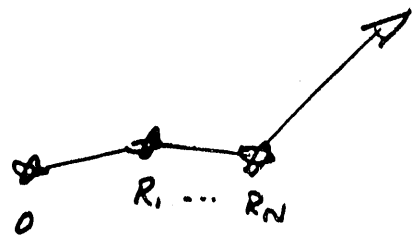

$$G^N_{00,L} = G_{00,L_N}(\bar{R}_N - \bar{R}_N)\, t_{L_N}(R_N)\, G_{L_N L_{N-1}}(\bar{R}_N - \bar{R}_{N-1}) \cdots t_{L_1}(R_1)\, G_{L_1 L}(\bar{R}_1)$$

matrix product

Ingredients: — $G_{LL'}(\bar{R})$ free propagator

⊗ $t_L \delta_{LL'}$ t-matrix

$t_\ell = e^{i\delta_\ell} \sin\delta_\ell$

Angular Momentum Disease

$L = \ell, m$ $\quad \ell \tilde{<} kR_{mt}$ $\quad 2 < k < 20\,\text{Å}^{-1}$ $\quad R_{mt} \sim 1.2$ $\Rightarrow \ell_{max} \tilde{=} 25$

$-\ell < m < \ell$

Matrix Dimension: $\ell_{max} \cdot (2\ell_{max}+1) \sim 10^3$

Storage $\sim L^2 \sim 10^6$

CPU $\sim L^3 \sim 10^9 \times$ # paths

$\Rightarrow$ IMPOSSIBLE to calculate high order paths at <u>high</u> energy.

2. Approximations - CURES (?)

Spherical Wave Approximation (SWA)

J.R. - Albers - Natoli-Stern (1986)

$$G_{LL'}(\bar{R}) = c \int \frac{d^3k}{(2\pi)^3} \frac{Y_L^*(\hat{k})\, Y_{L'}(\hat{k})\, e^{i\vec{k}\cdot\vec{R}}}{E - \frac{1}{2}k^2 + i0^+}$$

LARGE # $kR \Rightarrow$ small angles

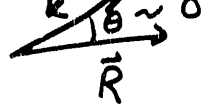

$$\cong \text{saddle-point} \quad 4\pi \frac{e^{ikR}}{kR} Y_L^*(\hat{R})\, Y_{L'}(\hat{R})\, C_\ell(kR)\, C_{\ell'}(kR)\, J_0\left(\frac{\ell\ell'}{kR}\right)$$

- separable! ($J_0 \approx 1$)
  ℓ, ℓ' uncoupled

C_ℓ = "spherical correction factor to Hankel fn"

$$C_\ell \cong \left(1 + \frac{\ell(\ell+1)}{2(kR)^2}\right)^{1/2} e^{i\frac{\ell(\ell+1)}{2kR}}$$

(SWA)

$$h_\ell^+ = i \frac{e^{-\ell\, ikR}}{kR} C_\ell(kR)$$

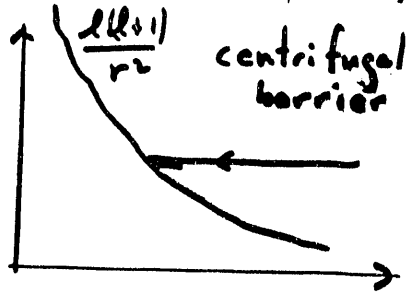

LARGE $\frac{\ell(\ell+1)}{2kR}$ phase shift due to centrifugal barrier

Result: Matrix product →

product of "curved wave scattering amplitudes"

$$G\, t_N\, G\, t_{N-1}\, G \cdots t_1\, G \rightarrow$$

$$f(\infty, R_N\, \theta_N)\, f(R_N\, R_{N-1}\, \theta_{N-1}) \cdots f(R_0\, R, \theta)$$

$$f(R\, R'\, \theta) = \frac{1}{k} \sum_{\ell}{}' (2\ell+1)\, t_\ell\, P_\ell(\cos\theta)\, \underbrace{C_\ell(kR)\, C_\ell(kR')}$$

curved wave correction

- Simplicity of PWA!
- Fair to Good approximation to full spherical-wave
  - Sagurton et al (1986)

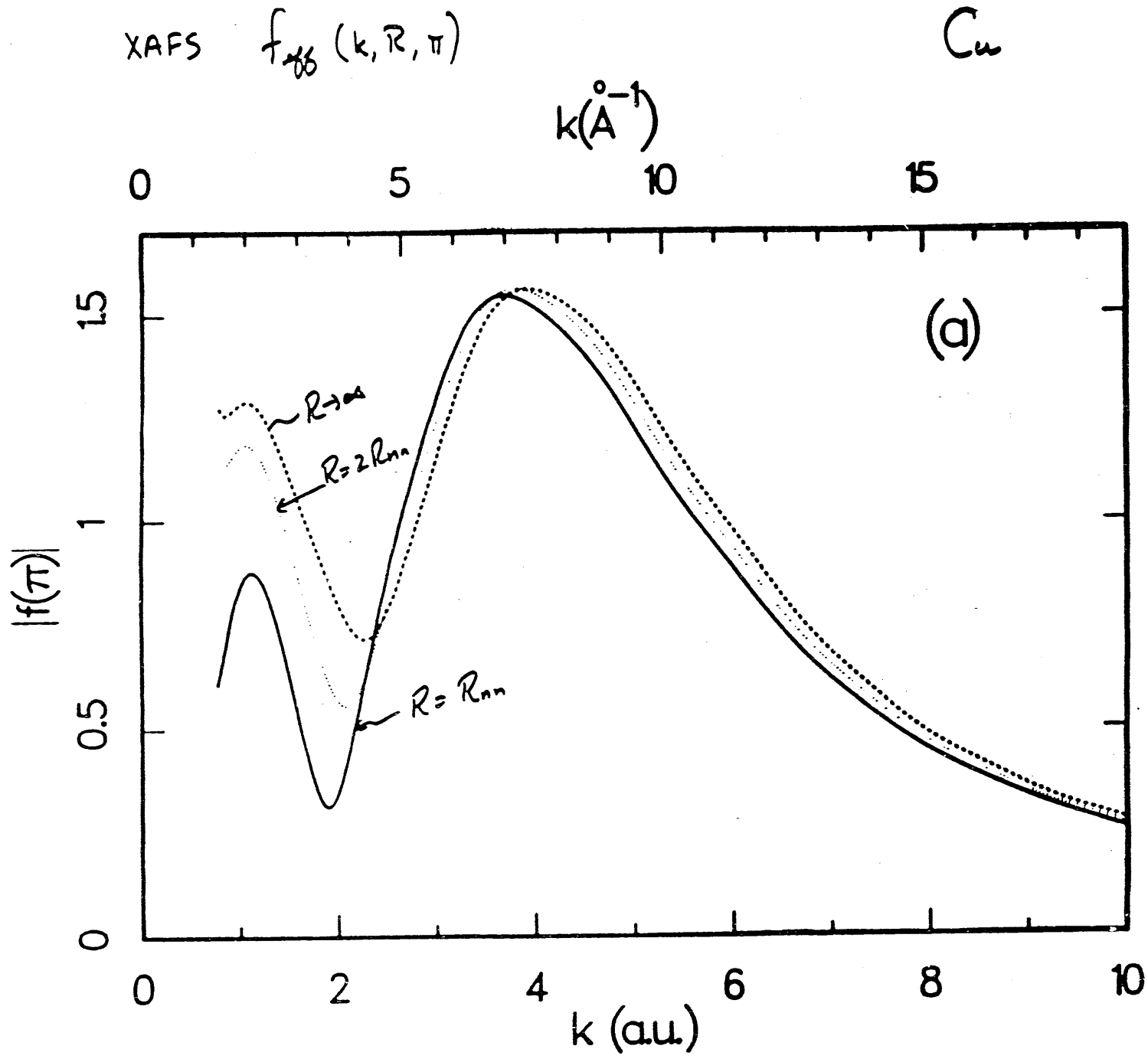
XAFS $f_{eff}(k, R, \pi)$
Cu
k(Å^{-1})
0
5
10
15
(a)
$R=\infty$
$R=2R_{nn}$
$R=R_{nn}$
|f(π)|
0
0.5
1
1.5
0
2
4
6
8
10
k (a.u.)

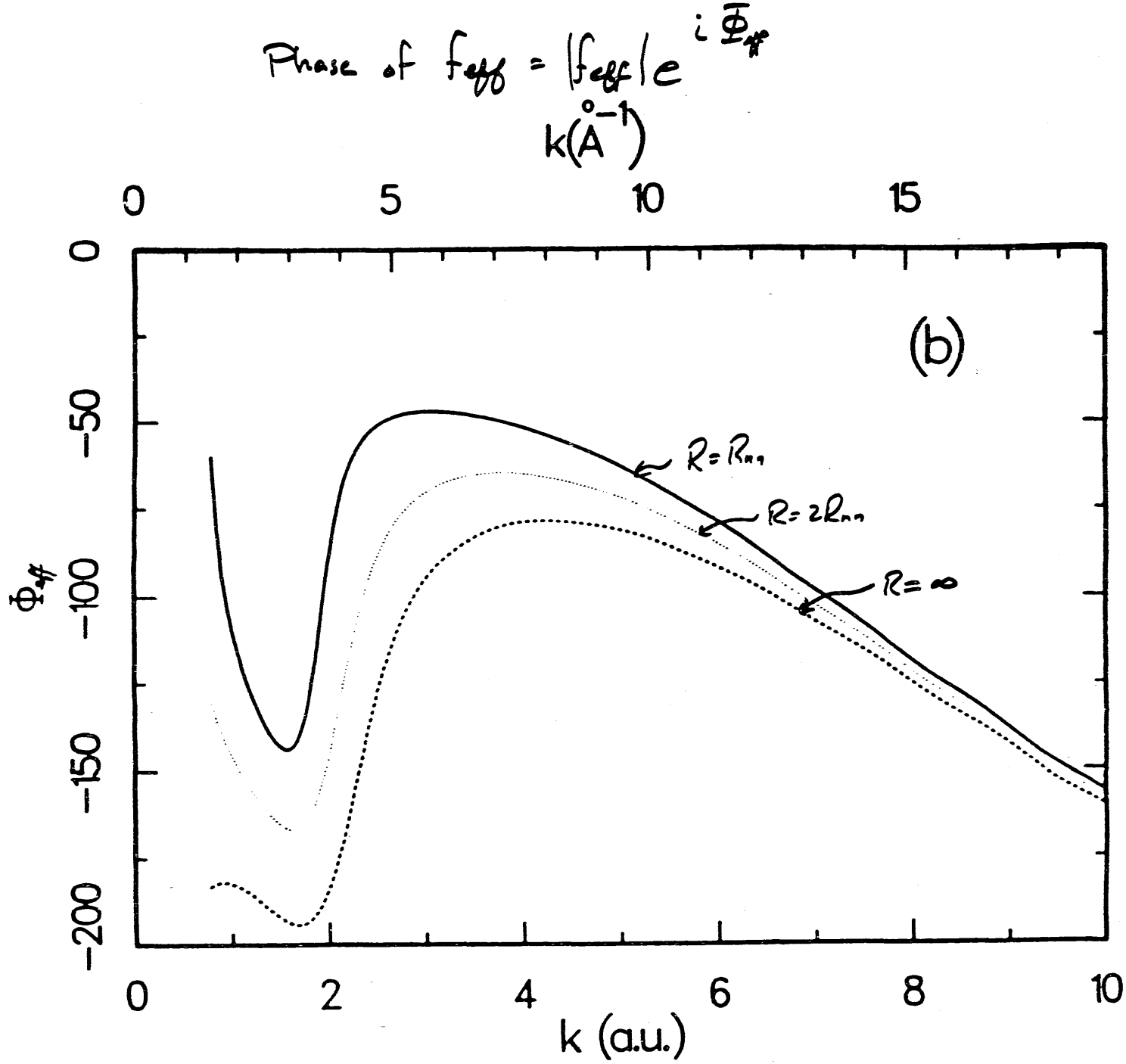
Phase of $f_{eff} = |f_{eff}| e^{i\Phi_{eff}}$
k(Å^{-1})
0
5
10
15
(b)
R = R_{nn}
R = 2R_{nn}
R = ∞
Φ_{eff}
0
−50
−100
−150
−200
0
2
4
6
8
10
k (a.u.)

M. Sagurton E Bullock R Saiki A. Kaduwela
C. Brundle C. Fadley & J. R. Phys Rev B 33 2207 (86)

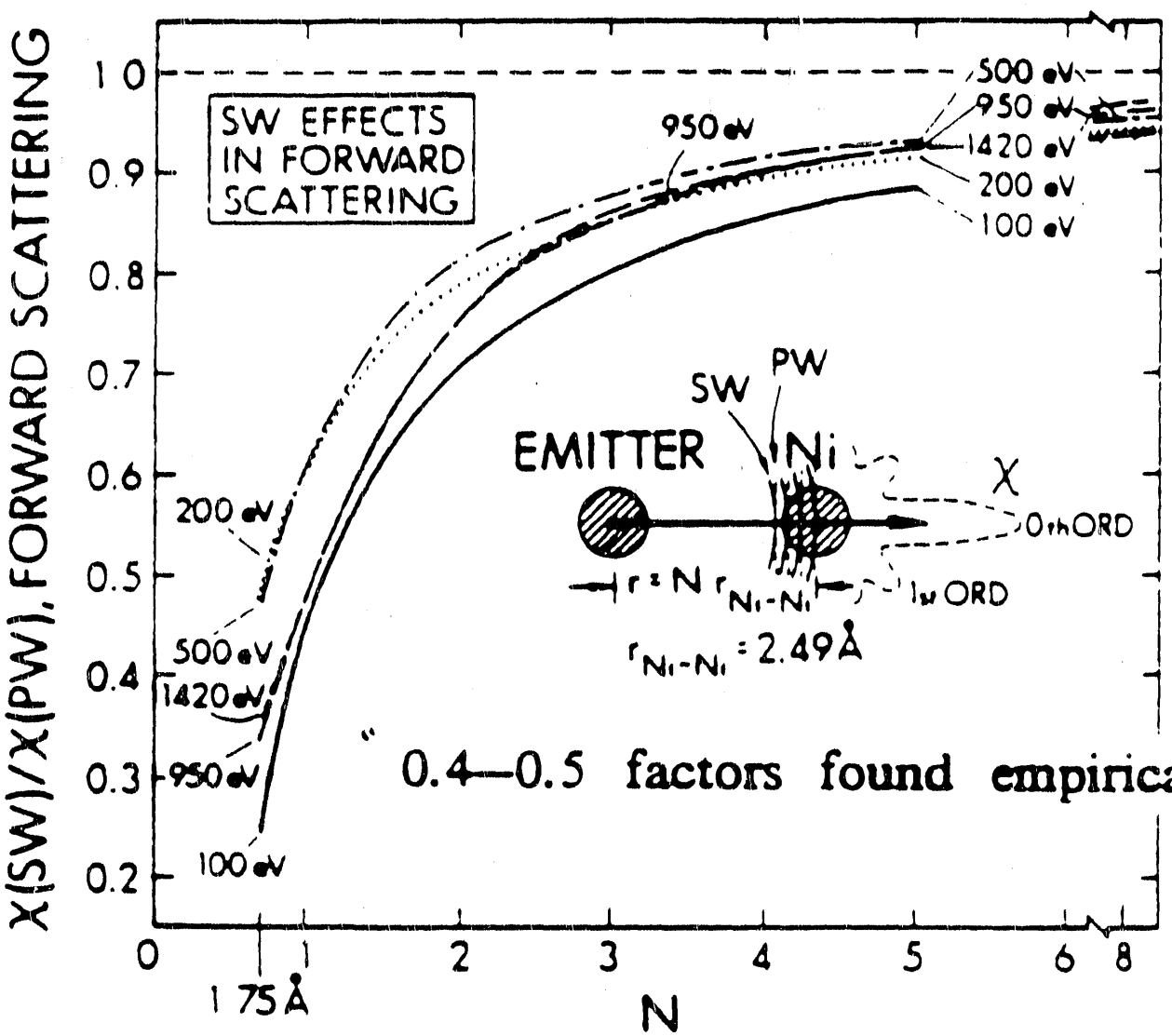

"0.4—0.5 factors found empirically."

Theoretical forward scattering ($\theta_{Ni}=0°$) ratios of χ(SW)/χ(PW) are shown as a function of scatterer distance from 1.75 to 19.92 Å and for energies of 100—1420 eV.

(SWA) Spherical Wave Approx $C_\ell \sim \left(1 + \frac{\ell(\ell+1)}{2(kR)^2}\right)^{1/2} e^{i\frac{\ell(\ell+1)}{2kR}}$

Spherical wave effects in photoelectron diffraction χ

(M. Segurton, E. Bullock
R. Saiki, A. Kaduwela
C. Brundle, C Fadley
+ J.R.
Phys Rev B 33, 2207 (86)

$$\chi = \frac{I - I_0}{I_0}$$

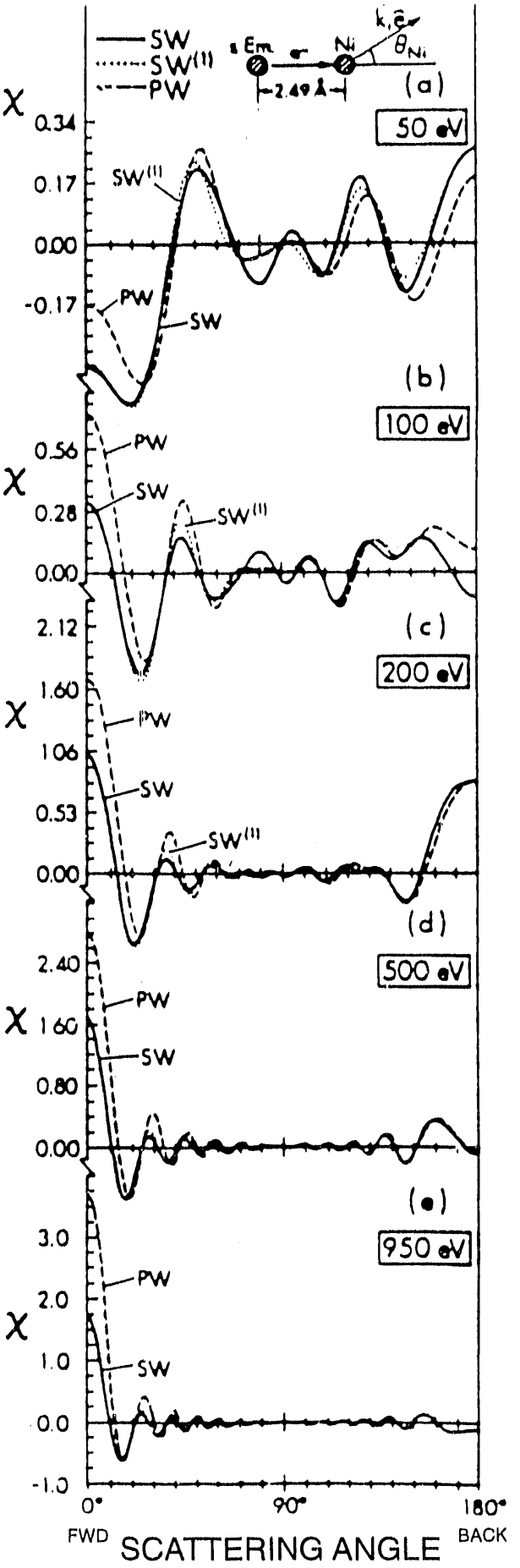

SW(1) - SWA
Spherical Wave Approx
of J.R., R. Albers,
E. Stern, C. Natoli

SW - exact spherical wave

PW - plane wave

B. Small m- expansion — MQNE Barton Shirley
— RAMF Fritzsche
Trick rediscovered many times! etc.

Note: Only small m contribute to $G_{lm\,l'm'}(\vec{R})$
if $\vec{R} \parallel \hat{z}$. $G \sim \frac{e^{ikR}}{kR} Y^*_{lm}(\hat{R})\, Y_{lm}(\hat{R})$

∴ Rotate bonds // $\hat{z}$ axis

$$Y_L \to \sum_\mu' R^l_{m\mu}\, Y_{l\mu}$$

↑ Rotation matrix

⇒

$$G_{LL'}(\vec{R}) = \sum_\mu' R^l_{m\mu}\, G_{l\mu\,l\mu}(R\hat{z})\, R^{l'}_{\mu m'}$$

$$G_{l\mu\,l\mu'}(R\hat{z}) = \sim \frac{e^{ikR}}{kR}\, G^{\mu}_{ll'}(kR)\, \delta_{\mu\mu'}$$

"z-axis propagator"

→ ALMOST-CURE

$l(2l+1) \to l\cdot(2\mu+1) \tilde{<} 5 l_{max} \sim 10^2$

$\mu \tilde{<} 2$

Problem reduced to CRAY hours! 100×100 matrices!

Danos & Maximon (1965)

Many of our results are contained in the literature. They are, however, not easily available. As a matter of fact, we found the references only after having rederived most of them. The characteristic of being hidden was re-emphasized in that an additional genealogic tree of references was called to our attention[12] after having submitted the paper to the Editor. It is very likely that still further references exist in the literature. - going back to Rayleigh 1890's

J.R. + R. Albers (1990)

Our method is based on a new separable representation of the free Green's-function matrix elements $G_{L,L'}(\rho)=\langle L,\mathbf{R}|G|L',\mathbf{R}'\rangle$, where $\rho=k(\mathbf{R}-\mathbf{R}')$. These propagator (or translation operator) matrix elements $G_{L,L'}$ also appear in the addition formula for the translation of screened spherical waves[13-15] as well as in multiple-scattering expansions.[1-2,15] The theory of such functions has an extensive, if relatively obscure literature; a historical survey is given in Ref. 13. Like other researchers in this area, we have occasionally found some of our results in the literature only after having first worked them out independently by ourselves.

Impt. References: R. Nozawa J. Math Phys 7, 1841 (1966)
** J. Barton & D. Shirley Phys Rev A 32, 1019 (85) etc.
V. Fritzsche & P. Rennert Phys Stat Sol 135, 49 (86)

C. Scattering Matrix

J.R. + R. Albers Phys. Rev. B41, 8139 (1990)

EXACT Separable representation (J.R.)

$$G_{LL'} = \frac{e^{ikR}}{kR} \sum_{\lambda} \tilde{\Gamma}_{L,\lambda} \Gamma_{L'\lambda}$$

"cut diagram"

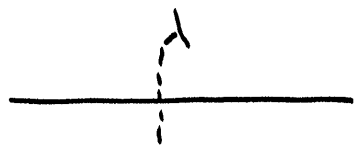

$\Rightarrow$

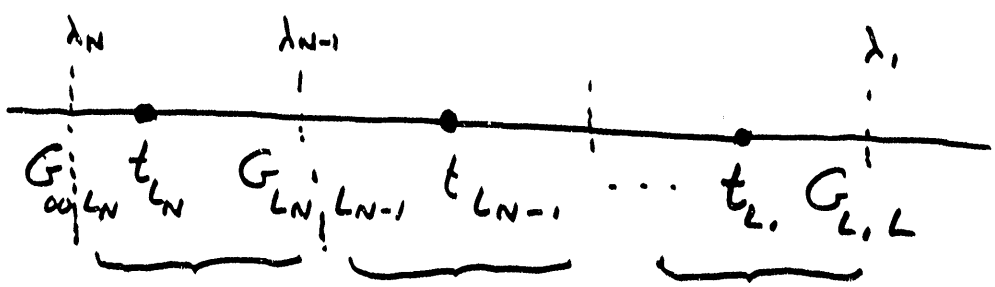

$$G^N_{00L} \equiv G_{0\lambda_N} t_{L_N} G_{L_N,\lambda_{N-1}} t_{L_{N-1}} \cdots t_{L_1} G_{L_1,L}$$

$$= \tilde{\Gamma}_{00,\lambda_N} F_{\lambda_N \lambda_{N-1}} F_{\lambda_{N-1}\lambda_{N-2}} \cdots F_{\lambda_2 \lambda_1} \Gamma_{\lambda_1,L}$$

$$\boxed{F_{\lambda\lambda'} = \sum_L{}' t_L \Gamma_{L\lambda} \tilde{\Gamma}_{L\lambda'}}$$

$\Gamma_{L\lambda} \sim \frac{1}{(kR)^\lambda}$

$\Gamma_{L0} \sim C_\ell Y_L(\hat{R})$

JR + Albers : $\lambda \tilde{<} 6$ for convergence!

$\Rightarrow$ CURE 6x6 matrices

< A. Kaduwela, D. Friedman & C. Fadley
U. Hawaii preprint, 1991

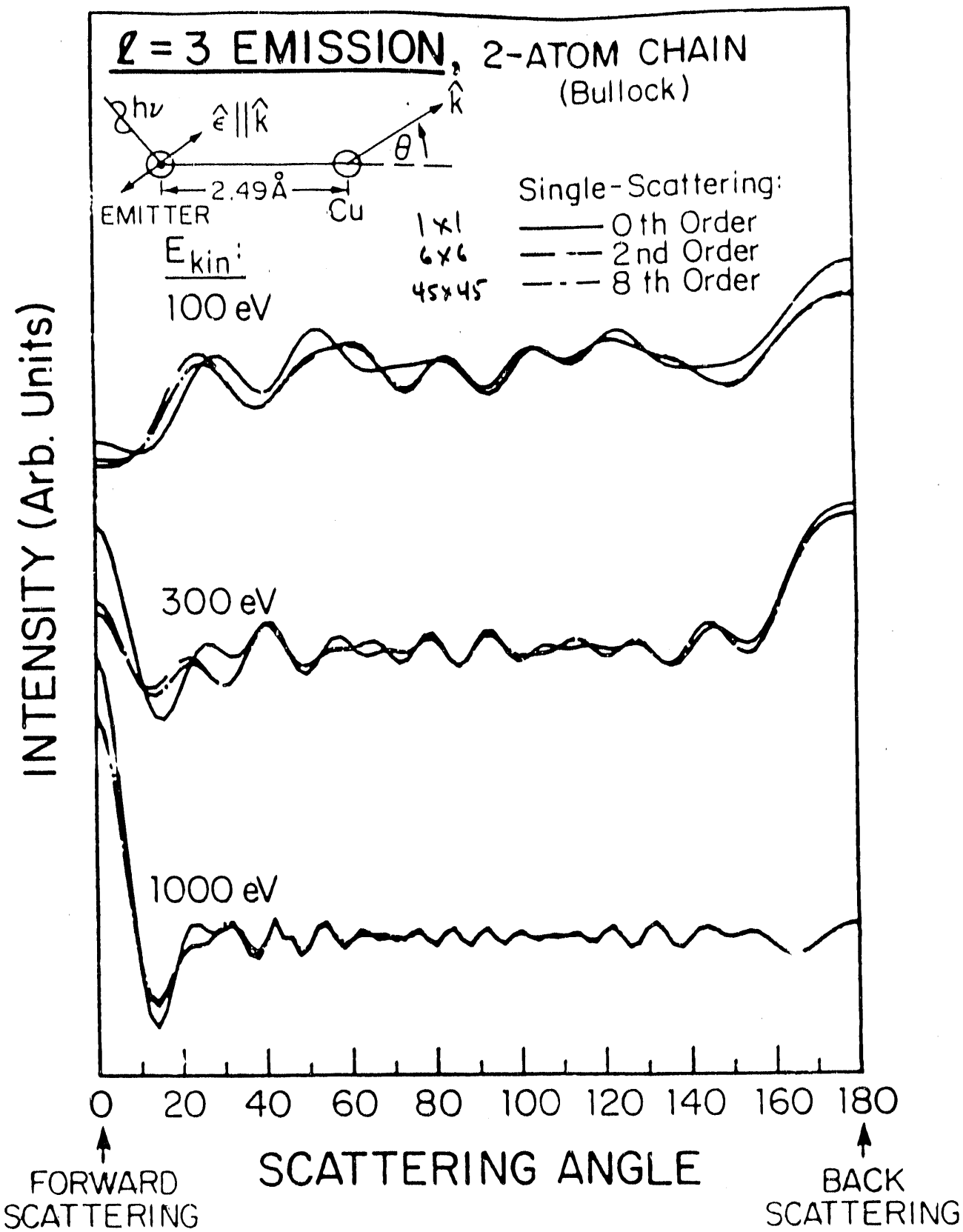

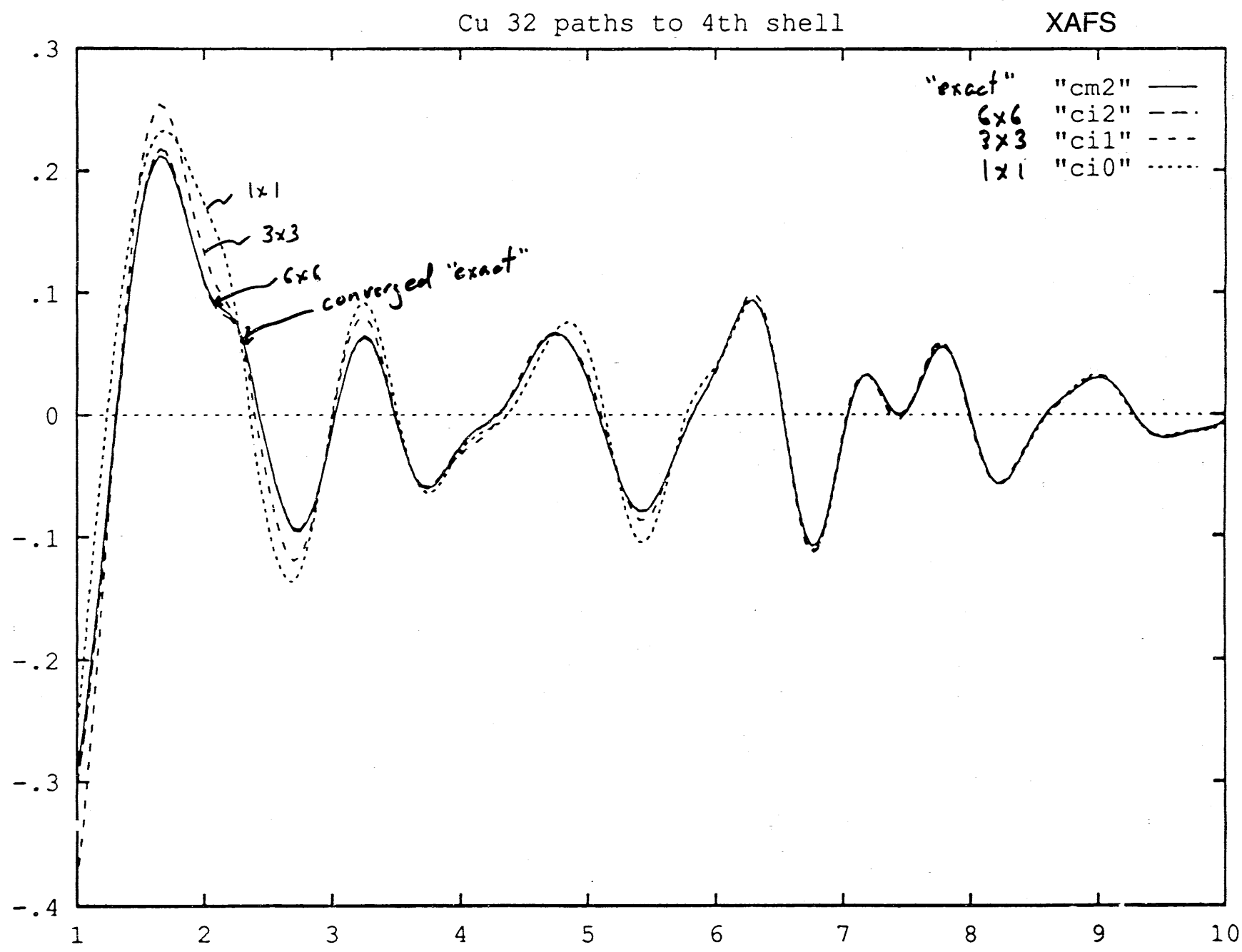
Cu 32 paths to 4th shell
XAFS
"exact" "cm2"
6x6 "ci2"
3x3 "ci1"
1x1 "ci0"
1x1
3x3
6x6
converged "exact"
.3
.2
.1
0
-.1
-.2
-.3
-.4
1
2
3
4
5
6
7
8
9
10

< A. Kaduwela D. Friedman C. Fadley
U. Hawaii preprint 1991

ARPEFS

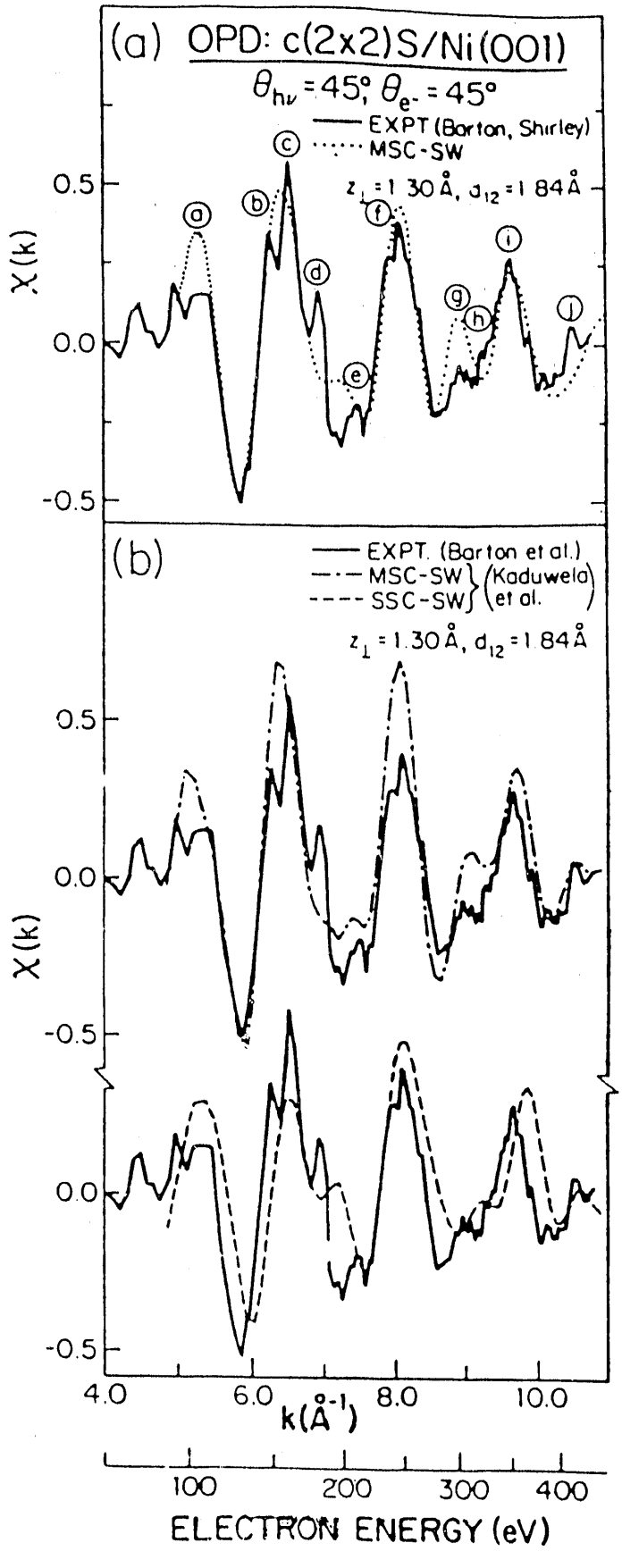

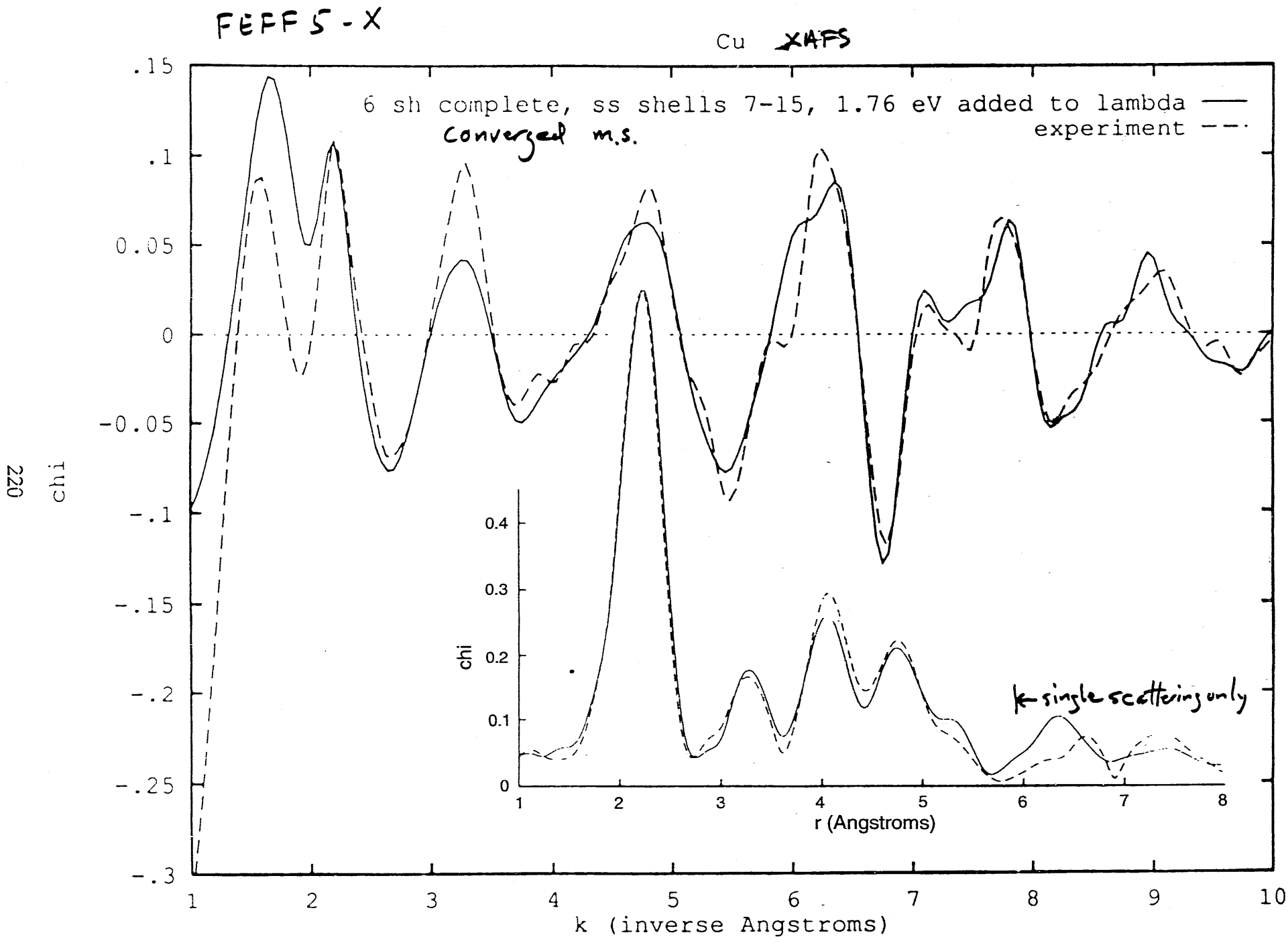
FEFF 5 - X
Cu XAFS
6 sh complete, ss shells 7-15, 1.76 eV added to lambda
converged m.s.
experiment
chi
k (inverse Angstroms)
r (Angstroms)
k-single scattering only

Results: Cu XAFS 32 paths < 4th shell

4 single scattering 

9 double scattering 

19 triple scattering 

	Method	CPU (SUN-SPARC I)	Accuracy
A.	SWA	-	< 20%
		FAST	Fair accuracy

B. MQNE / RAME

m = 1	1399 s	~ 5%
m = 2	3288 s	~ 0.1%
m = 3	8600 s	converged
	SLOW	v. accurate

C. Scattering Matrix

3 x 3	214 s	5%
6 x 6	308 s	< 1%
10 x 10	512 s	~ 0.1%
	FAST	ACCURATE

3. Why does the Separable Approximation work?

Fritzsche: - expect LARGE errors in Scattering Matrix at high energy!

- "instability"

Our analysis:

i) Fritzsche is partly right -

- terms in separable expansion converge slowly - if at all! $\sim C_\ell \frac{\ell\ell+1}{kR}$

ii) Fritzsche is partly WRONG -

- C_ℓ's $\Rightarrow$ Fresnel convergence
  $\Rightarrow$ large ℓ cutoff!

Approximation gets better with increasing energy!

third shell, k=20 inv Ang

Forward scattering

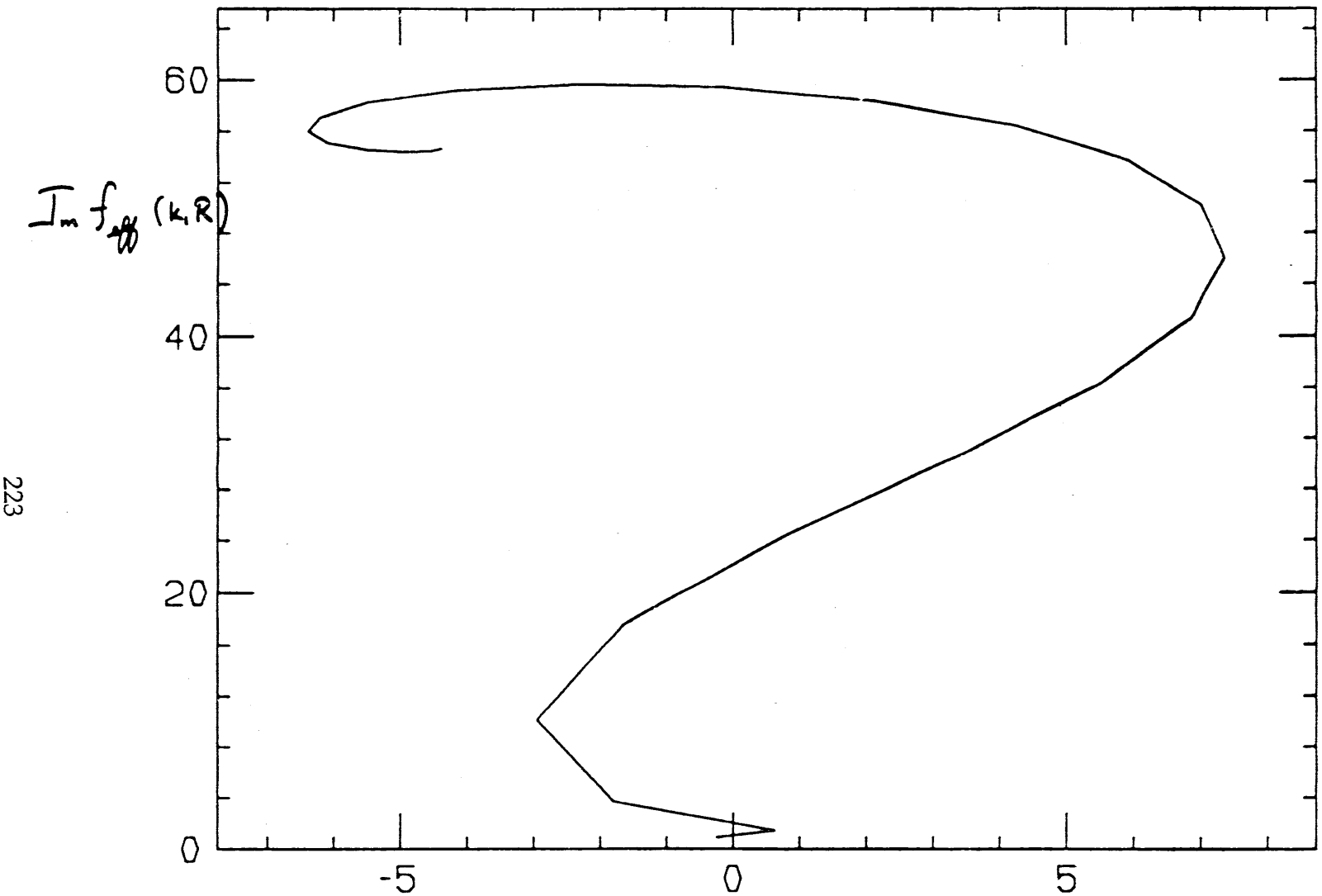

Partial sums

$$f_{eff} = \sum_{l}' (2l+1)\, t_l\, C_l^2(kR), \quad 0 \le l \le 20$$

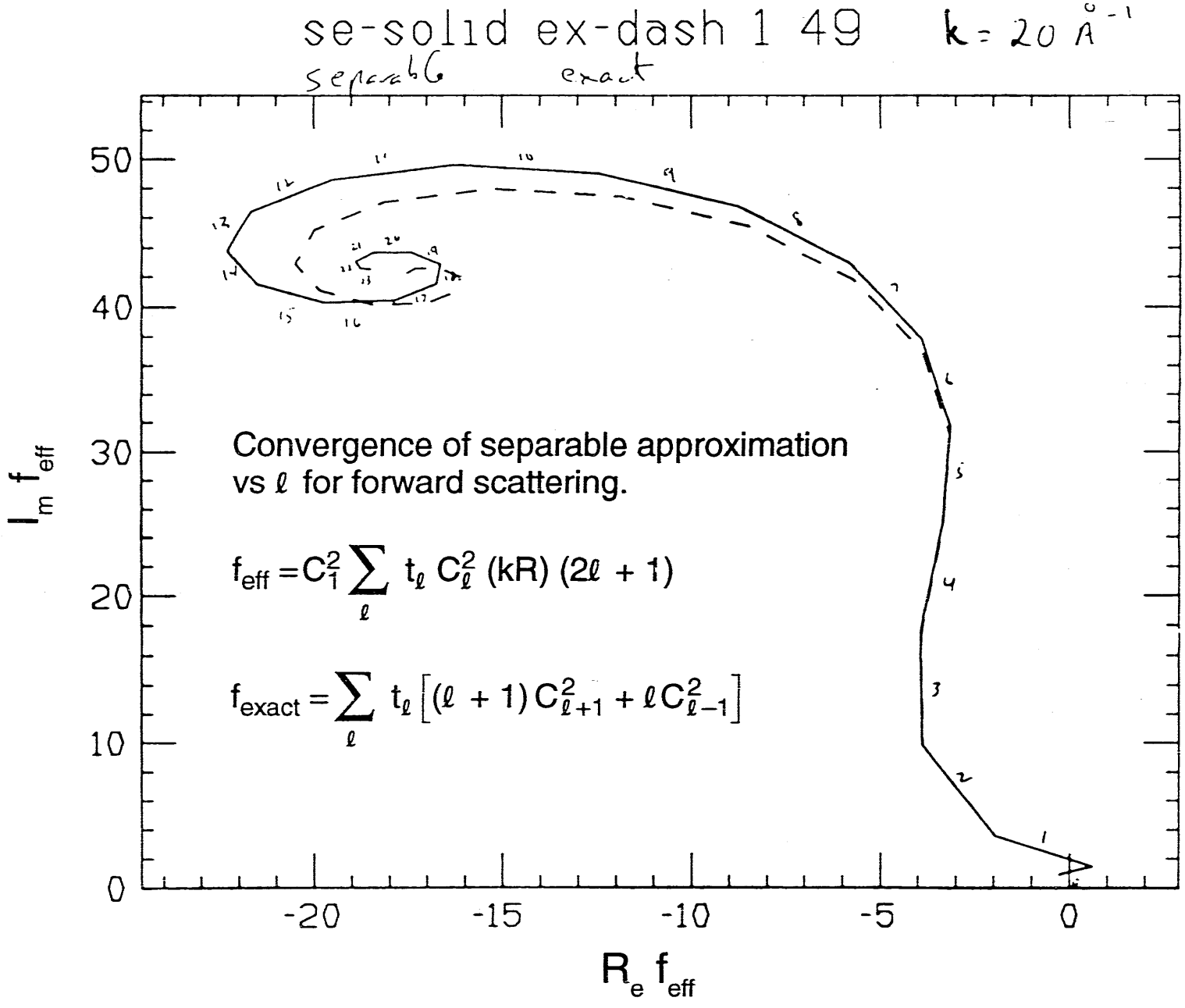
se-solid ex-dash 1 49 k = 20 Å⁻¹
separab exact
Convergence of separable approximation
vs ℓ for forward scattering.
$f_{eff} = C_1^2 \sum_\ell t_\ell C_\ell^2 (kR)(2\ell + 1)$
$f_{exact} = \sum_\ell t_\ell \left[(\ell + 1) C_{\ell+1}^2 + \ell C_{\ell-1}^2\right]$
$I_m f_{eff}$
$R_e f_{eff}$
50
40
30
20
10
0
-20
-15
-10
-5
0

Conclusions

1) SWA — Fast ✓, fair approximation

2) MQNE — Slow, Accurate ✓

3) S-Matrix — Fast ✓, Accurate ✓ CURE!

- 6×6 matrices
- order of magnitude faster than MQNE
- 2 orders of magnitude faster than exact
- can calculate arbitrarily high order paths

" Results obtained using this new separable Green's function matrix approach are in very good agreement with other MS methods and with experiment."

A. Kaduwela Ph.D. Thesis U. Hawaii 1991

4) Fritzsche's "instability" NOT a problem.

Lattice-Site- and Chemical-State-Specific Photoelectron Diffraction

S. Chambers

Boeing High-Technology Center

Lattice-site- and Chemical-state-specific X-ray Photoelectron Diffraction

Scott A. Chambers
Boeing High Technology Center
Seattle, Washington

Outline

I. Site-specific XPD

A. Se/GaAs(001)

B. Te/GaAs(001)

Issue -- Relationship between surface band bending and surface structure

II. State-specific XPD

A. Ni/GaAs(001)

Issue -- Interplay between interface chemistry and epitaxial regrowth

XPD

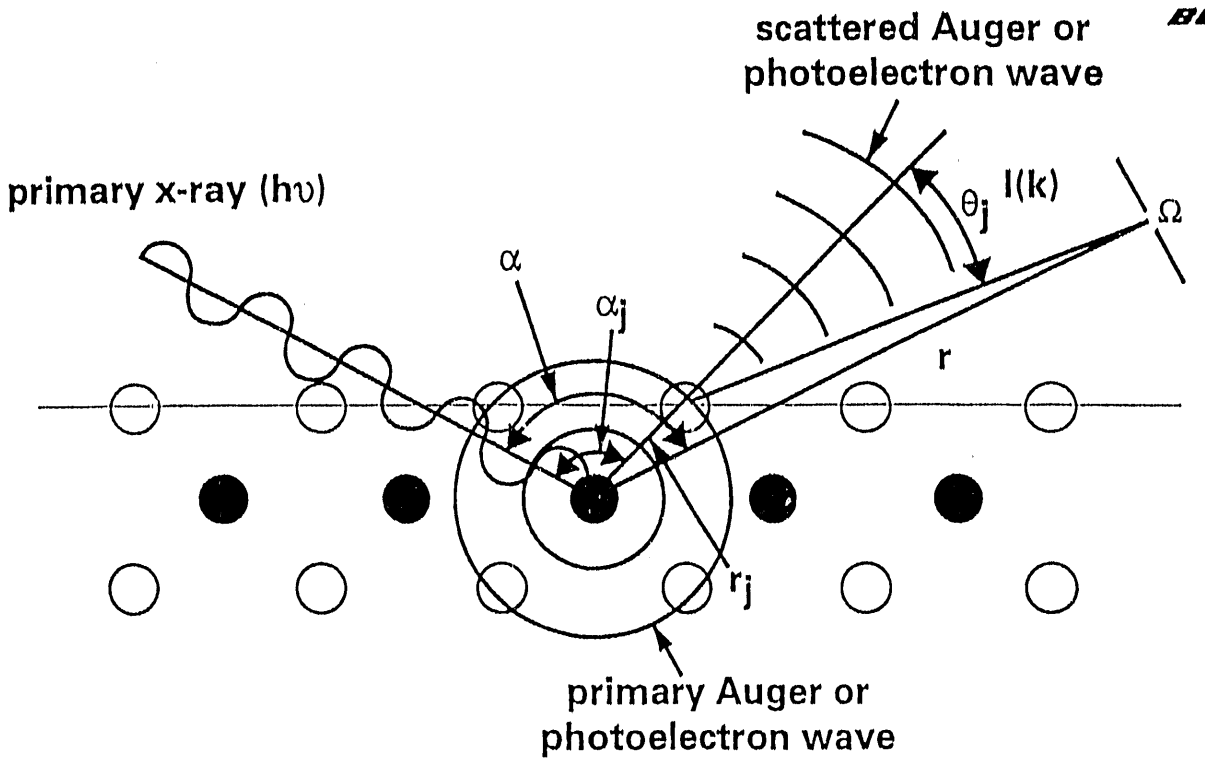

$$I(k) \propto \left| \psi_o (r,\alpha) + \sum_j \psi_j(r_j,\alpha_j,\theta_j) \right|^2$$

Fermi-level Pinning

$$\Phi_m < \Phi_s$$

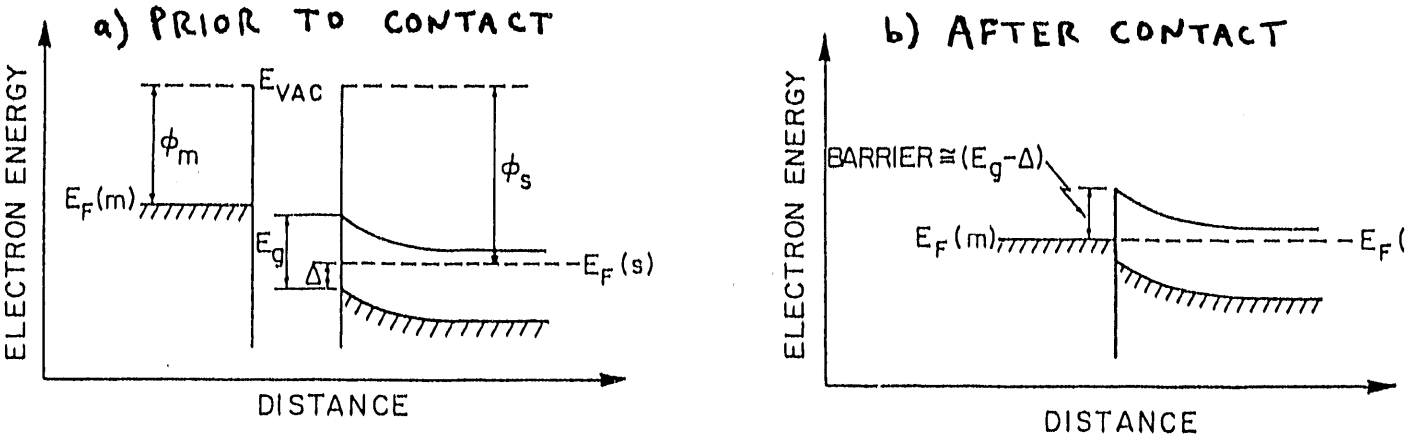

TAKEN FROM, INTRODUCTION TO APPLIED SOLID STATE PHYSI

BY RICHARD DALVEN - PLENUM, N.Y. (1980)

SITE-SPECIFIC XPD

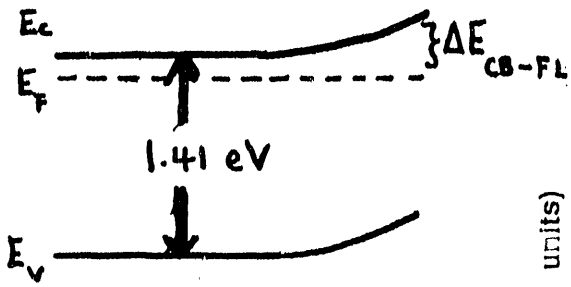

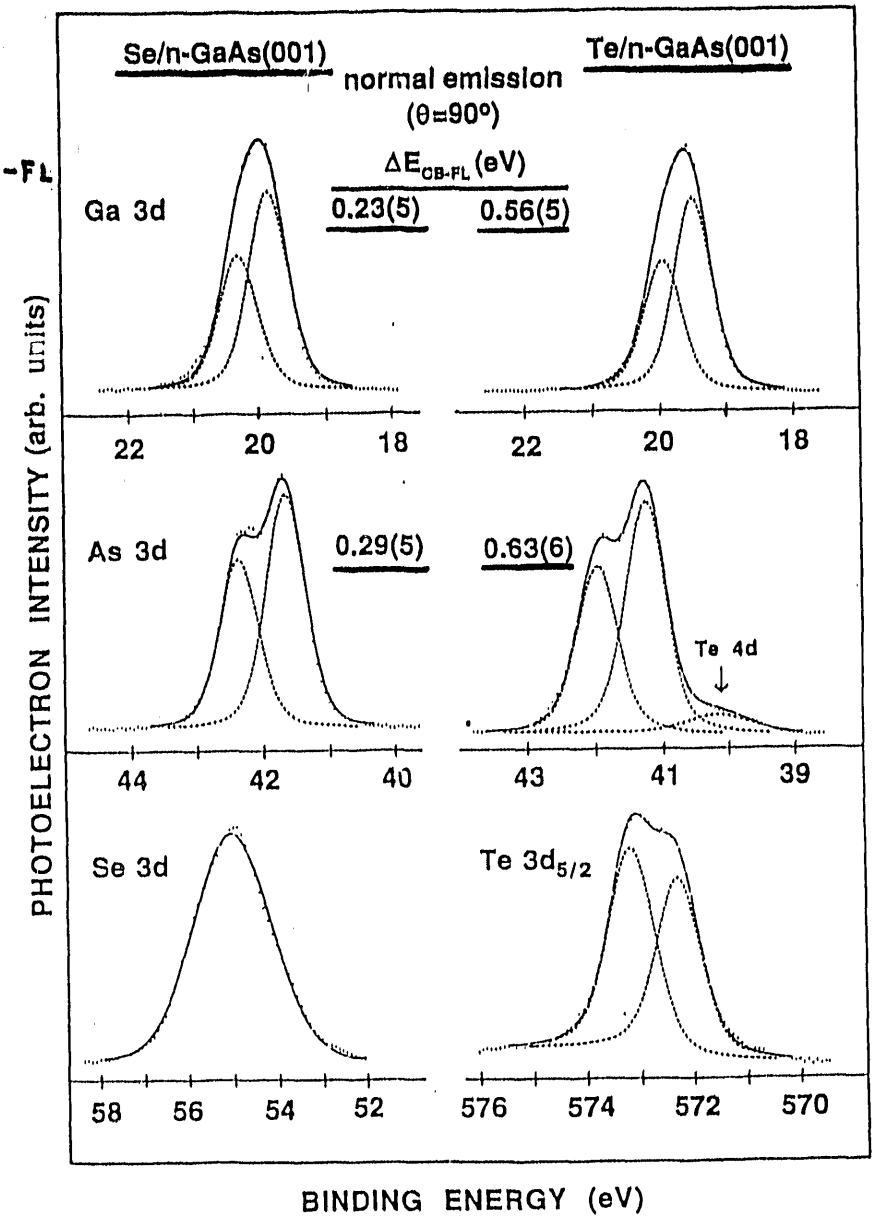

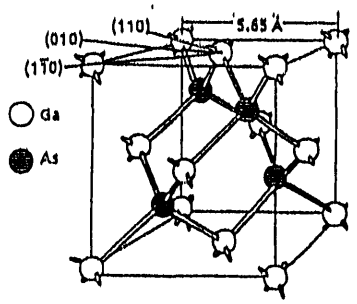

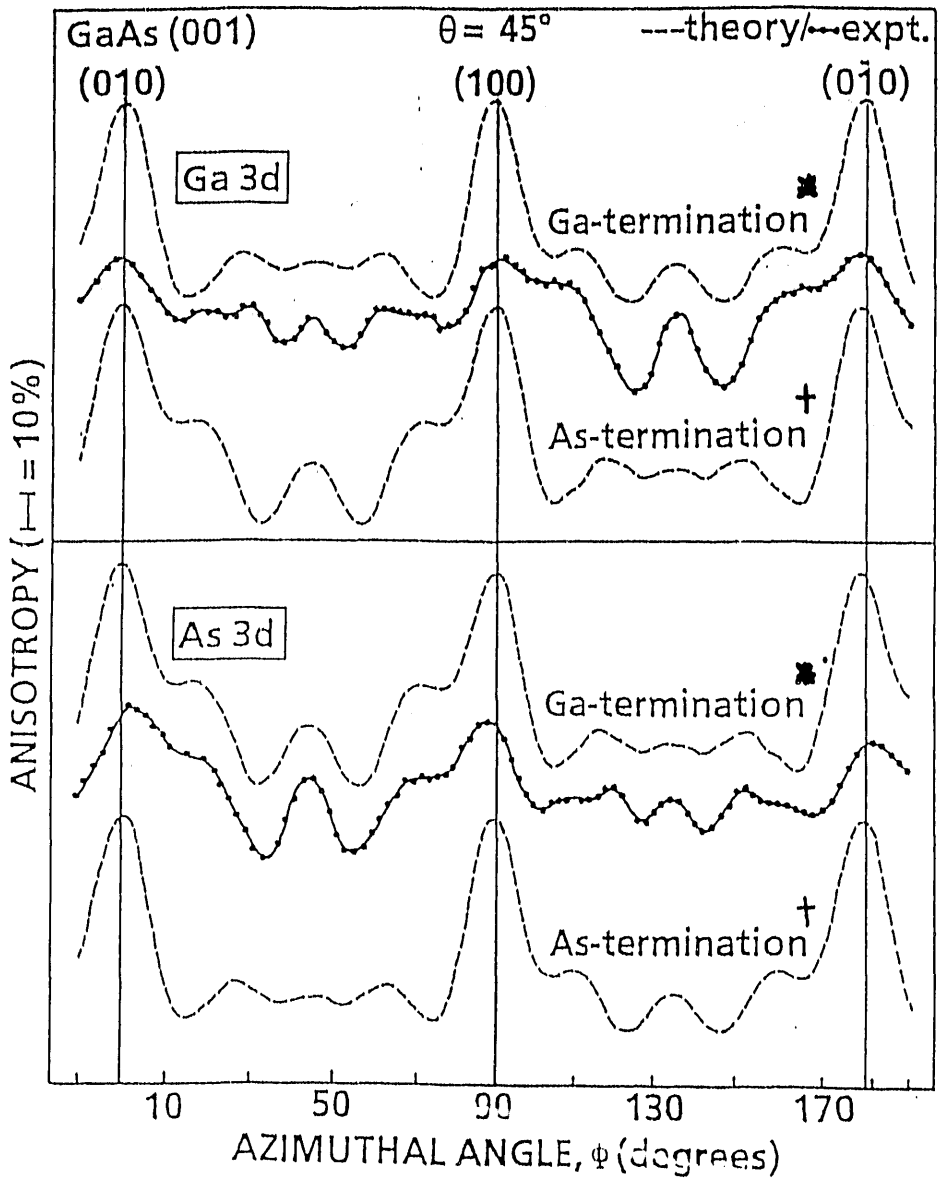

* - Ga IN LAYERS 1, 3, 5...

+ - As IN LAYERS 1, 3, 5...

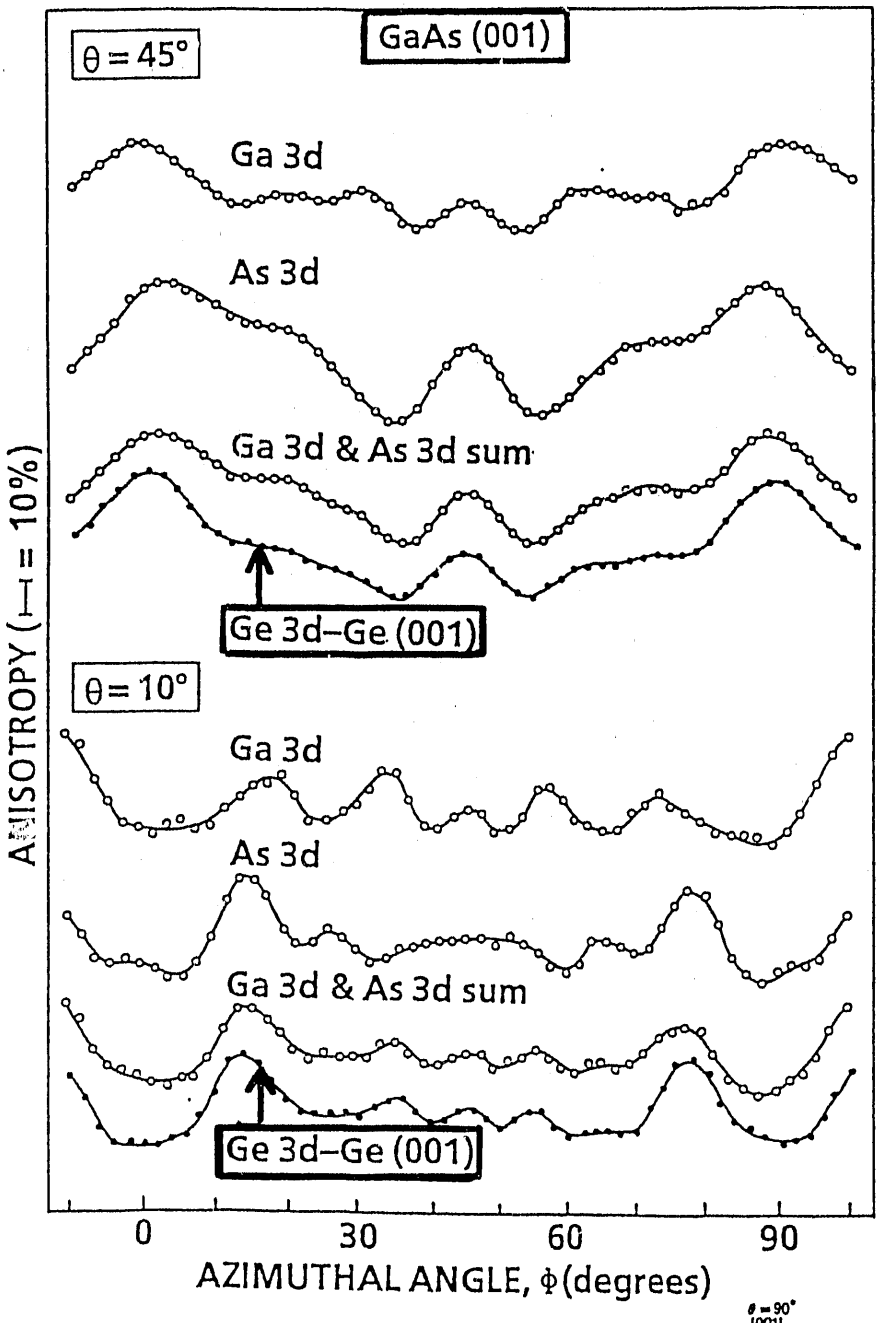

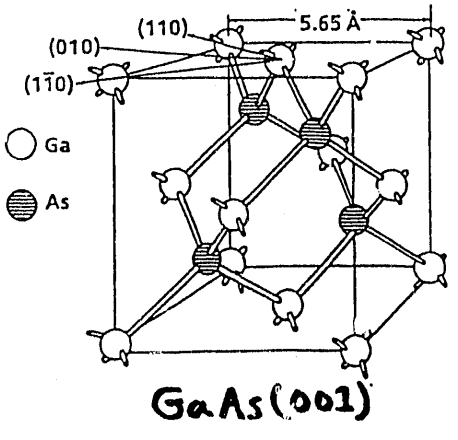

GaAs(001)

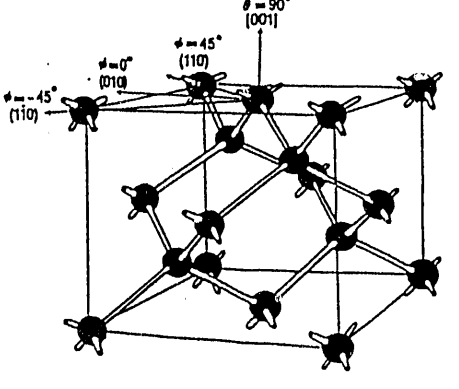

Ge(001)

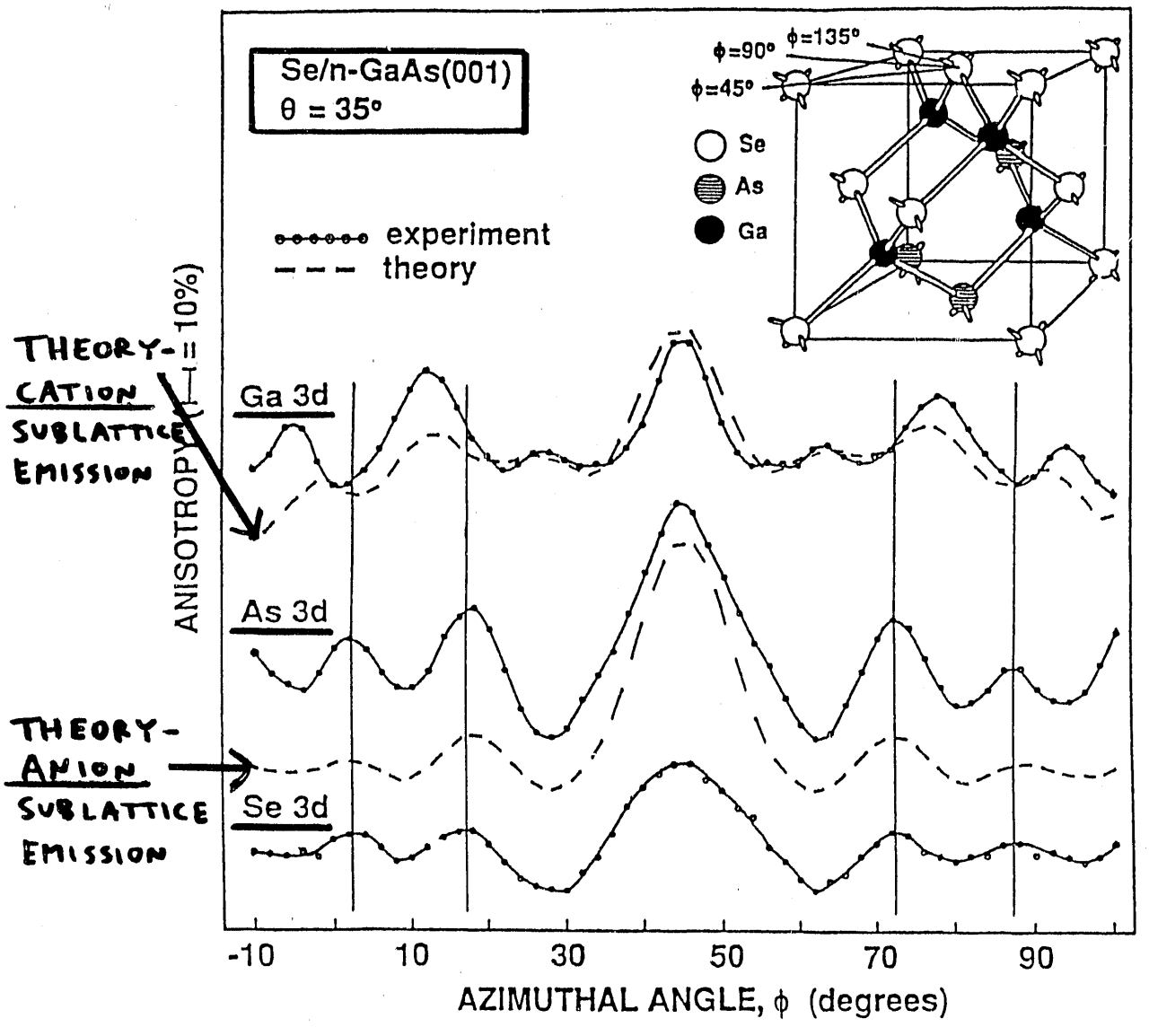

$GaAs(001) + Se \rightarrow GaSe_xAs_{1-x}/GaAs(001) + As$

CHAMBERS & SUNDARAM APL 57, 2342 (1990)

a = Se/GaAs(001) b = Te/GaAs(001)

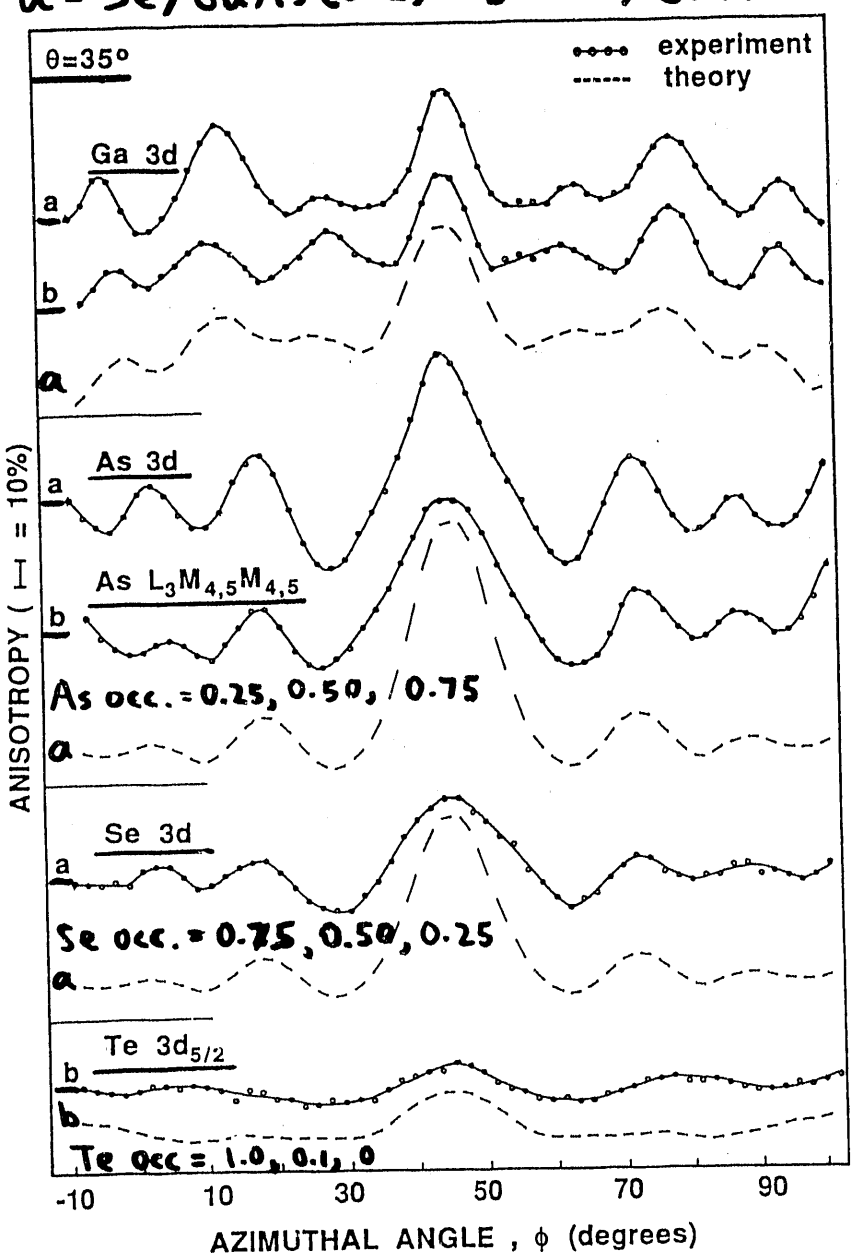

CHAMBERS & SUNDARAM, JVST B

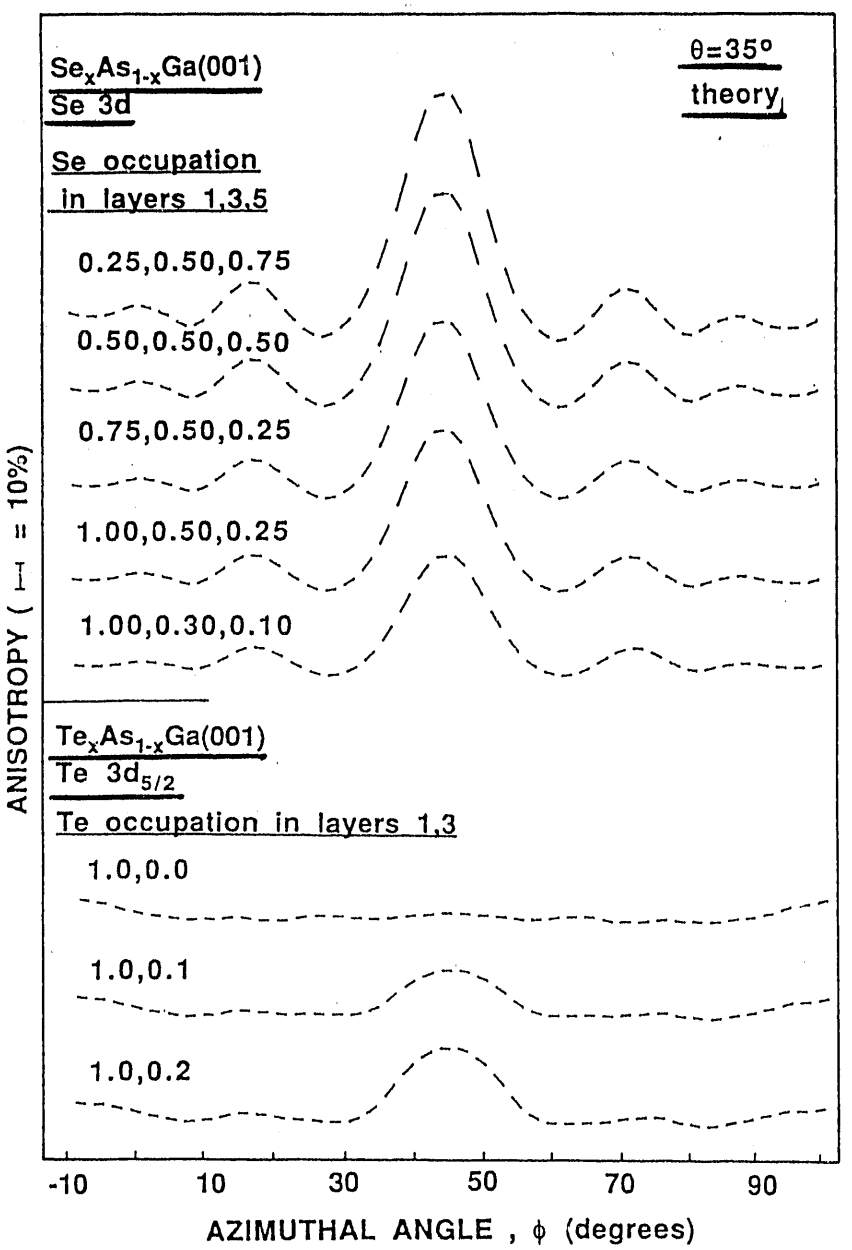
$Se_xAs_{1-x}Ga(001)$
Se 3d
θ=35°
theory
Se occupation
in layers 1,3,5
0.25,0.50,0.75
0.50,0.50,0.50
0.75,0.50,0.25
1.00,0.50,0.25
1.00,0.30,0.10
$Te_xAs_{1-x}Ga(001)$
Te $3d_{5/2}$
Te occupation in layers 1,3
1.0,0.0
1.0,0.1
1.0,0.2
ANISOTROPY (⊢ = 10%)
-10
10
30
50
70
90
AZIMUTHAL ANGLE , ϕ (degrees)

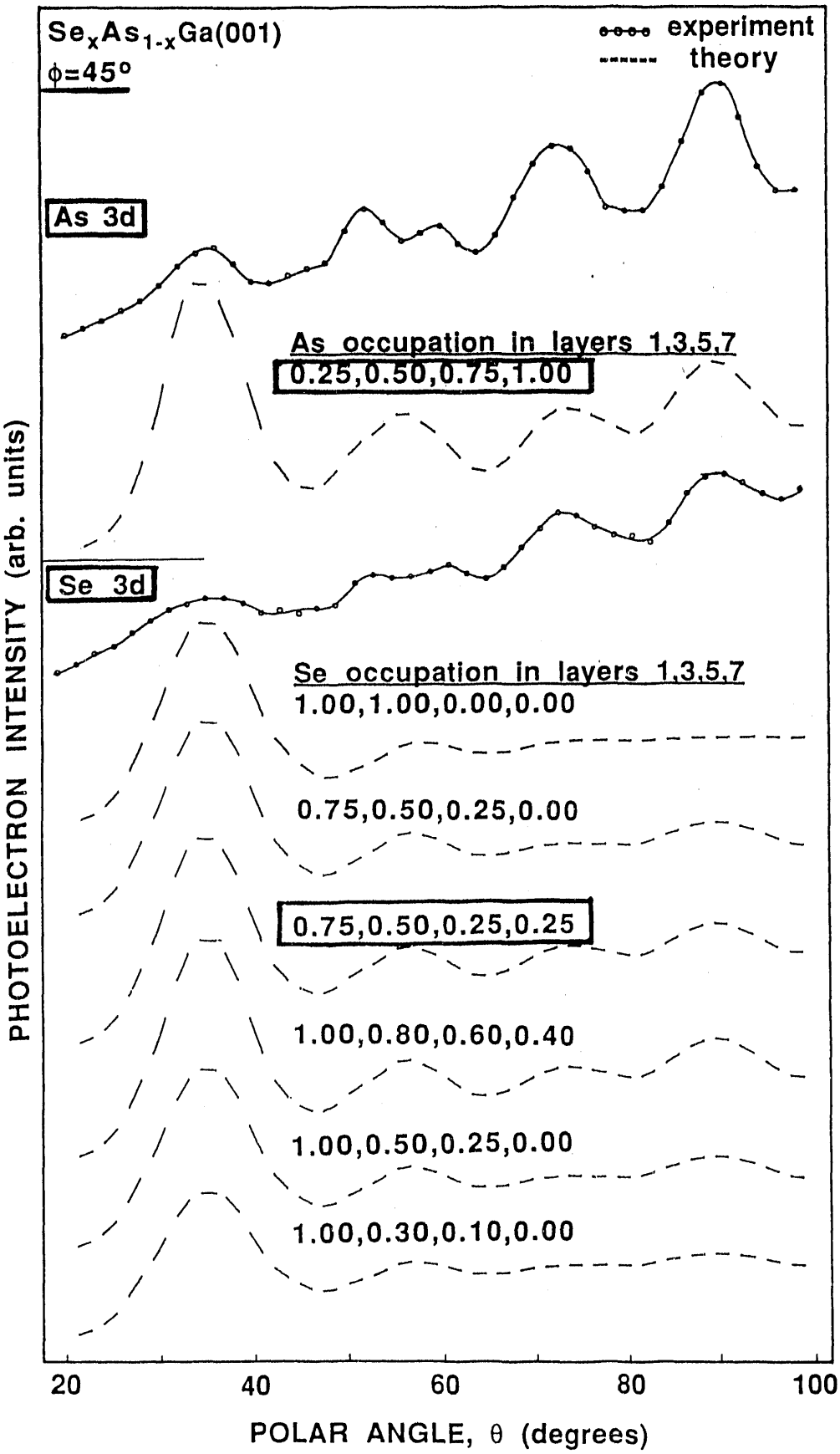
Se$_x$As$_{1-x}$Ga(001)
ϕ=45°
experiment
theory
As 3d
As occupation in layers 1,3,5,7
0.25,0.50,0.75,1.00
Se 3d
Se occupation in layers 1,3,5,7
1.00,1.00,0.00,0.00
0.75,0.50,0.25,0.00
0.75,0.50,0.25,0.25
1.00,0.80,0.60,0.40
1.00,0.50,0.25,0.00
1.00,0.30,0.10,0.00
PHOTOELECTRON INTENSITY (arb. units)
20
40
60
80
100
POLAR ANGLE, θ (degrees)

$$GaAs(001) + Se \longrightarrow GaSe_xAs_{1-x}/GaAs(001)$$

$$GaAs(001) + Te \longrightarrow Te/GaAs(001)$$

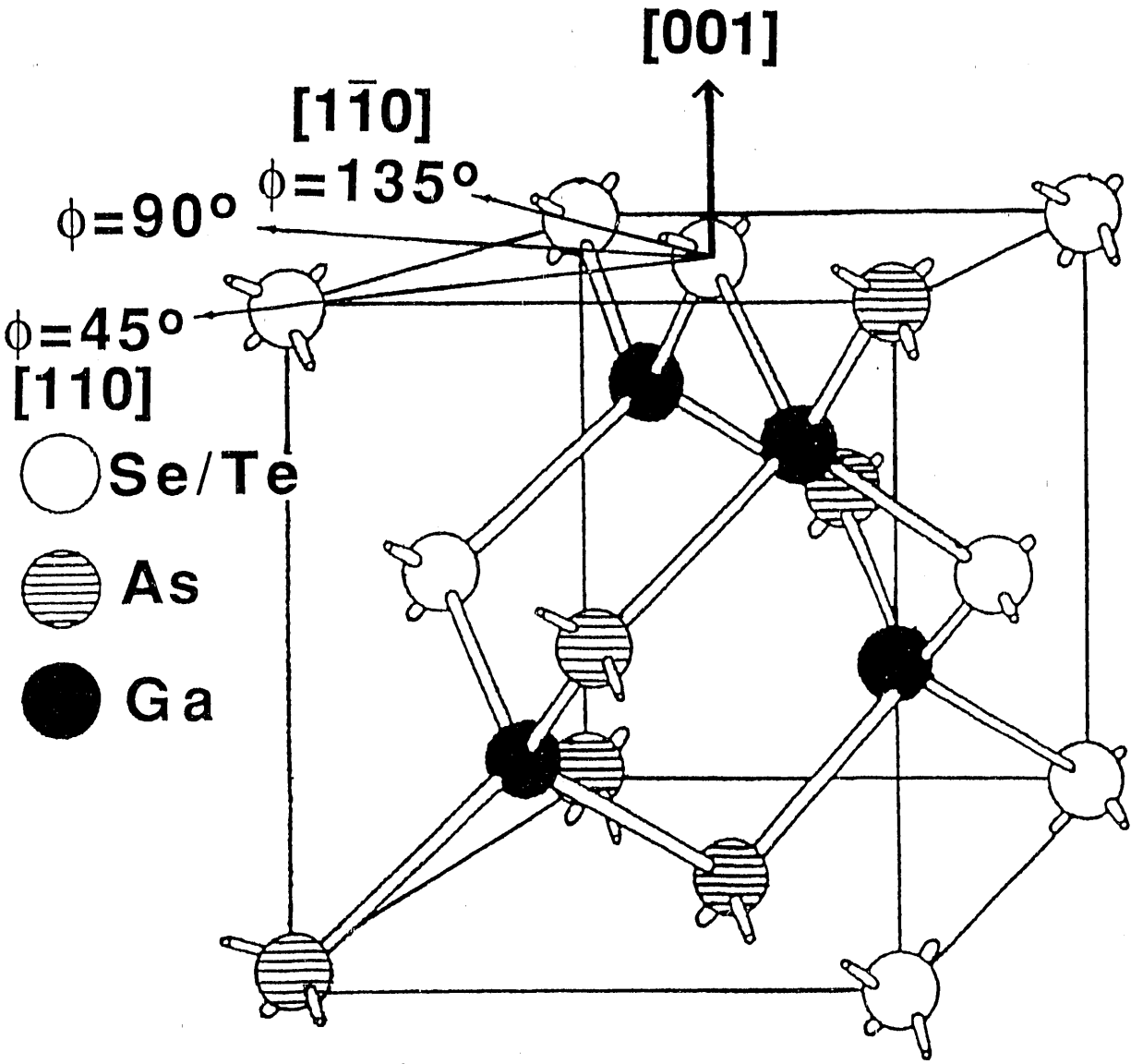

LAYER	1	3	5	7	9
Se	0.75	0.50	0.25	0.25	0
Te	1.00	0.10	0	0	0

THREE POSSIBLE CAUSES OF SURFACE ELECTRONIC PASSIVATION--Se/GaAs(001)

1. Elimination of Ga & As dangling bond states

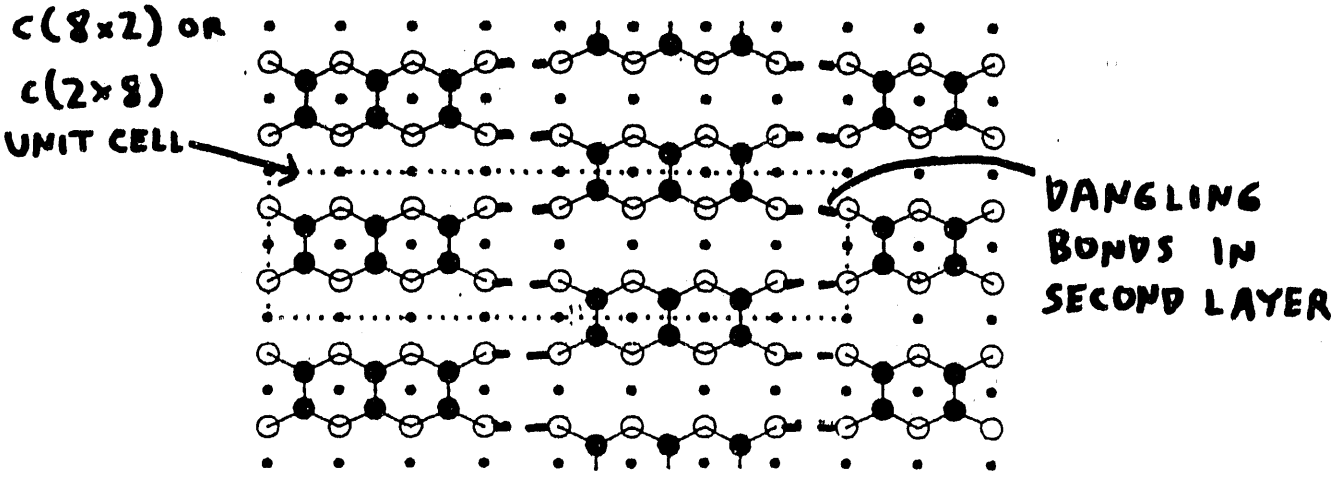

2. Low gap state density at the surface

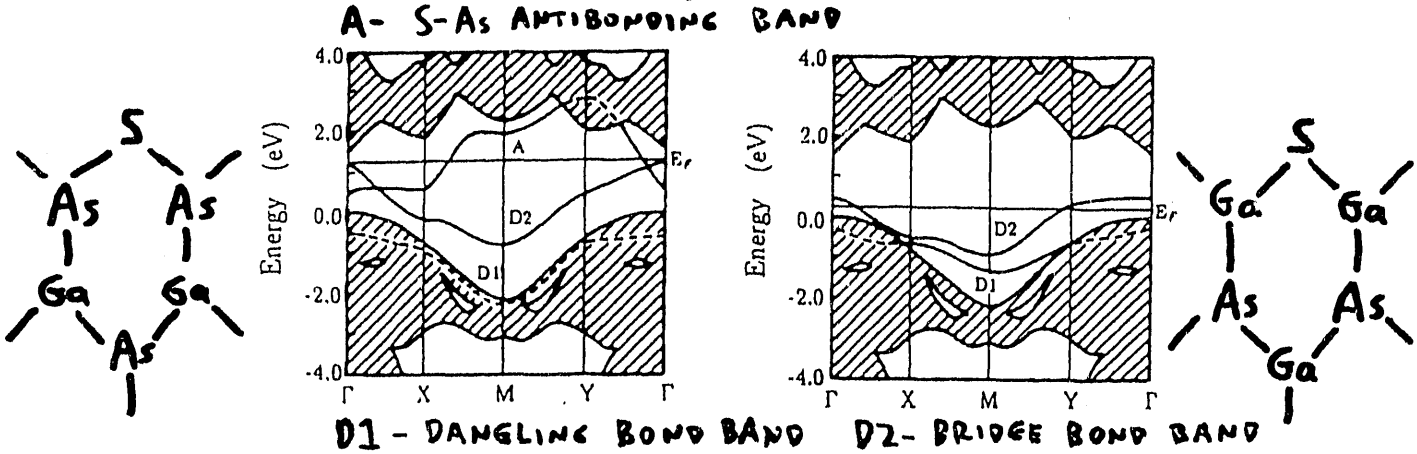

T. Ohno and K. Shiraishi, Phys. Rev. B42, 11194 (1990)

3. Delta doping at the surface

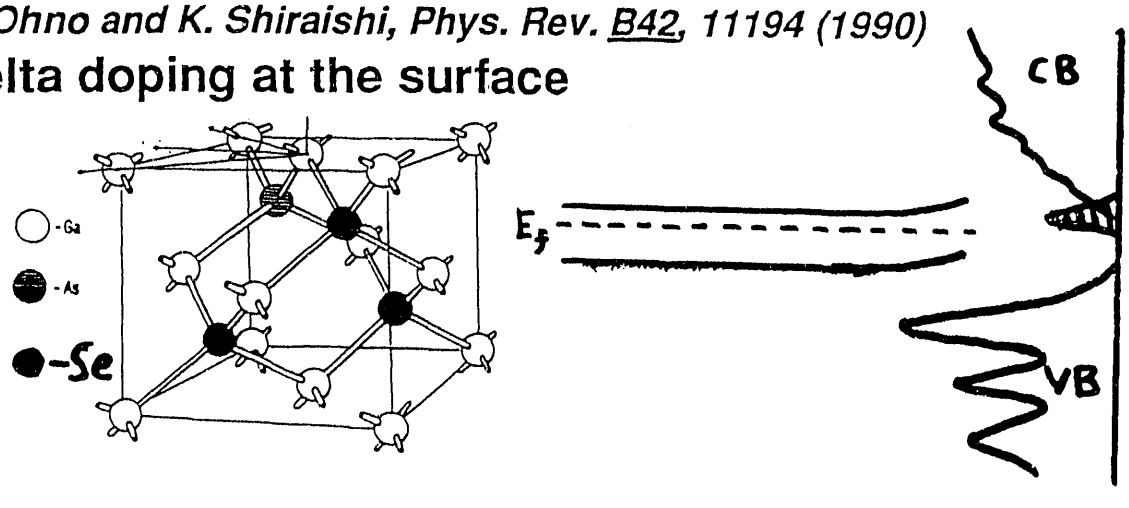

Ni:Al/GaAs(001)

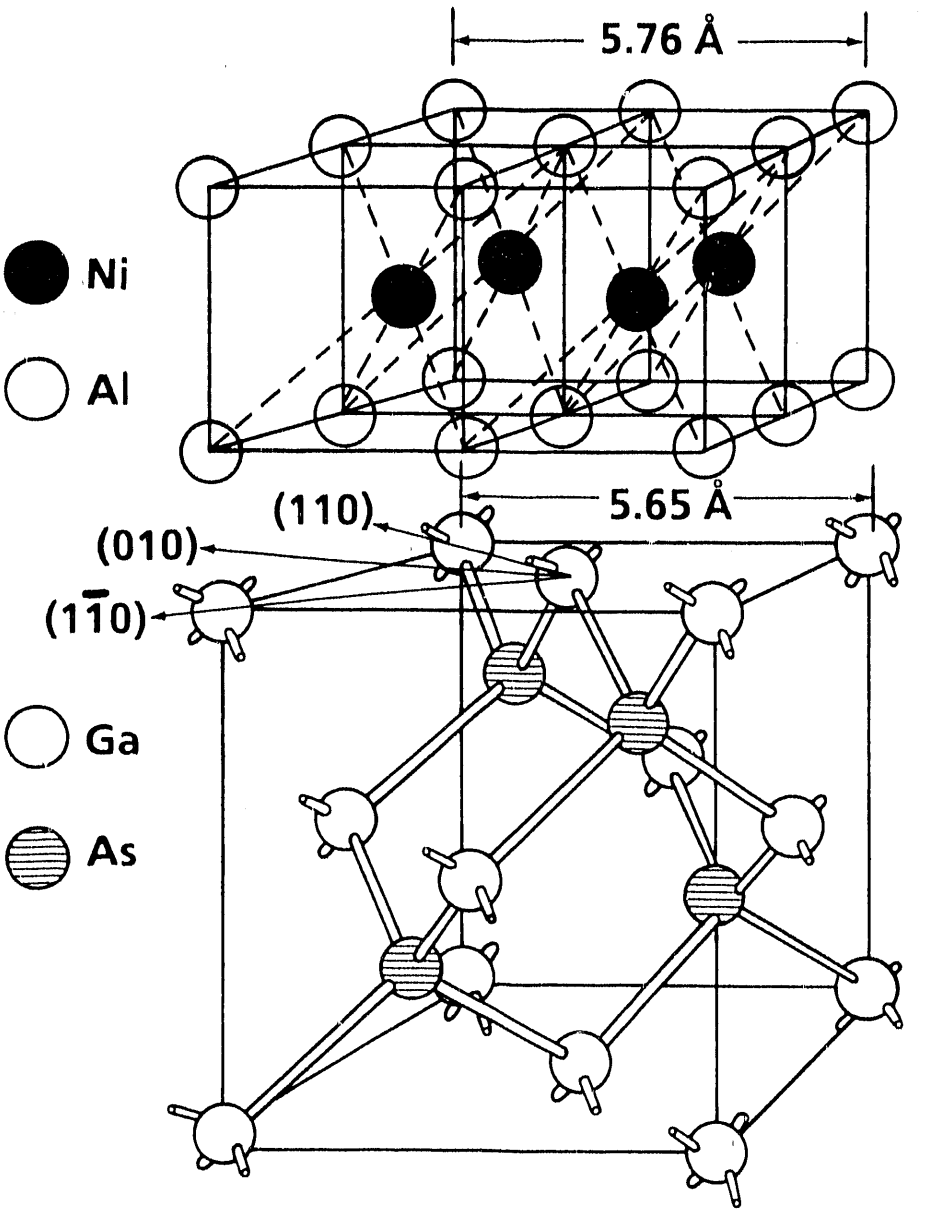

(~ 2% LATTICE MISMATCH)

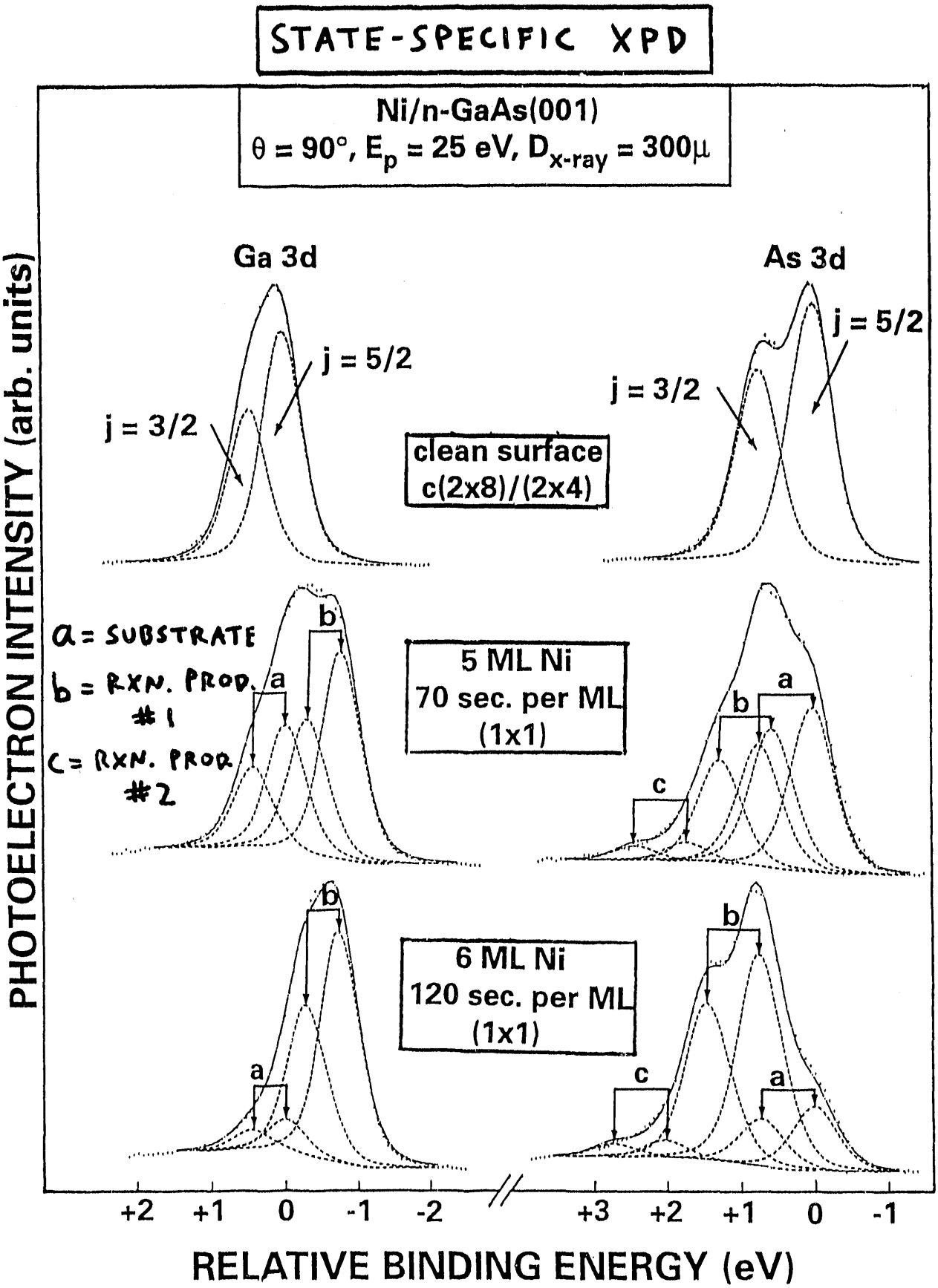
STATE-SPECIFIC XPD
Ni/n-GaAs(001)
θ = 90°, E_p = 25 eV, D_x-ray = 300μ
Ga 3d
As 3d
j = 5/2
j = 3/2
clean surface
c(2x8)/(2x4)
a = SUBSTRATE
b = RXN. PROD. #1
c = RXN. PROD. #2
5 ML Ni
70 sec. per ML
(1x1)
6 ML Ni
120 sec. per ML
(1x1)
PHOTOELECTRON INTENSITY (arb. units)
+2 +1 0 -1 -2
+3 +2 +1 0 -1
RELATIVE BINDING ENERGY (eV)

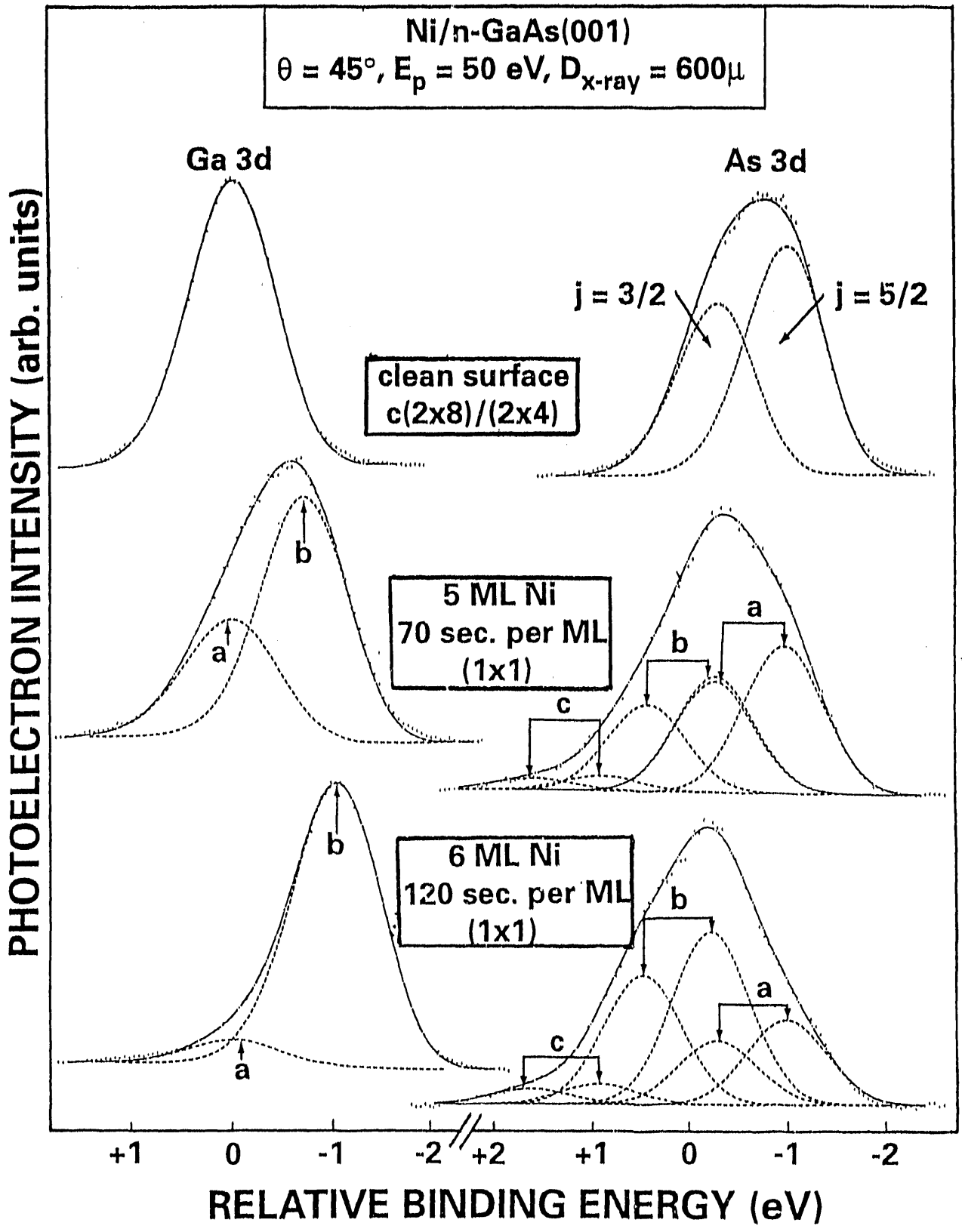
Ni/n-GaAs(001)
θ = 45°, E_p = 50 eV, D_x-ray = 600μ
Ga 3d
As 3d
j = 3/2
j = 5/2
clean surface
c(2x8)/(2x4)
5 ML Ni
70 sec. per ML
(1x1)
6 ML Ni
120 sec. per ML
(1x1)
a
b
c
PHOTOELECTRON INTENSITY (arb. units)
+1
0
-1
-2
+2
RELATIVE BINDING ENERGY (eV)

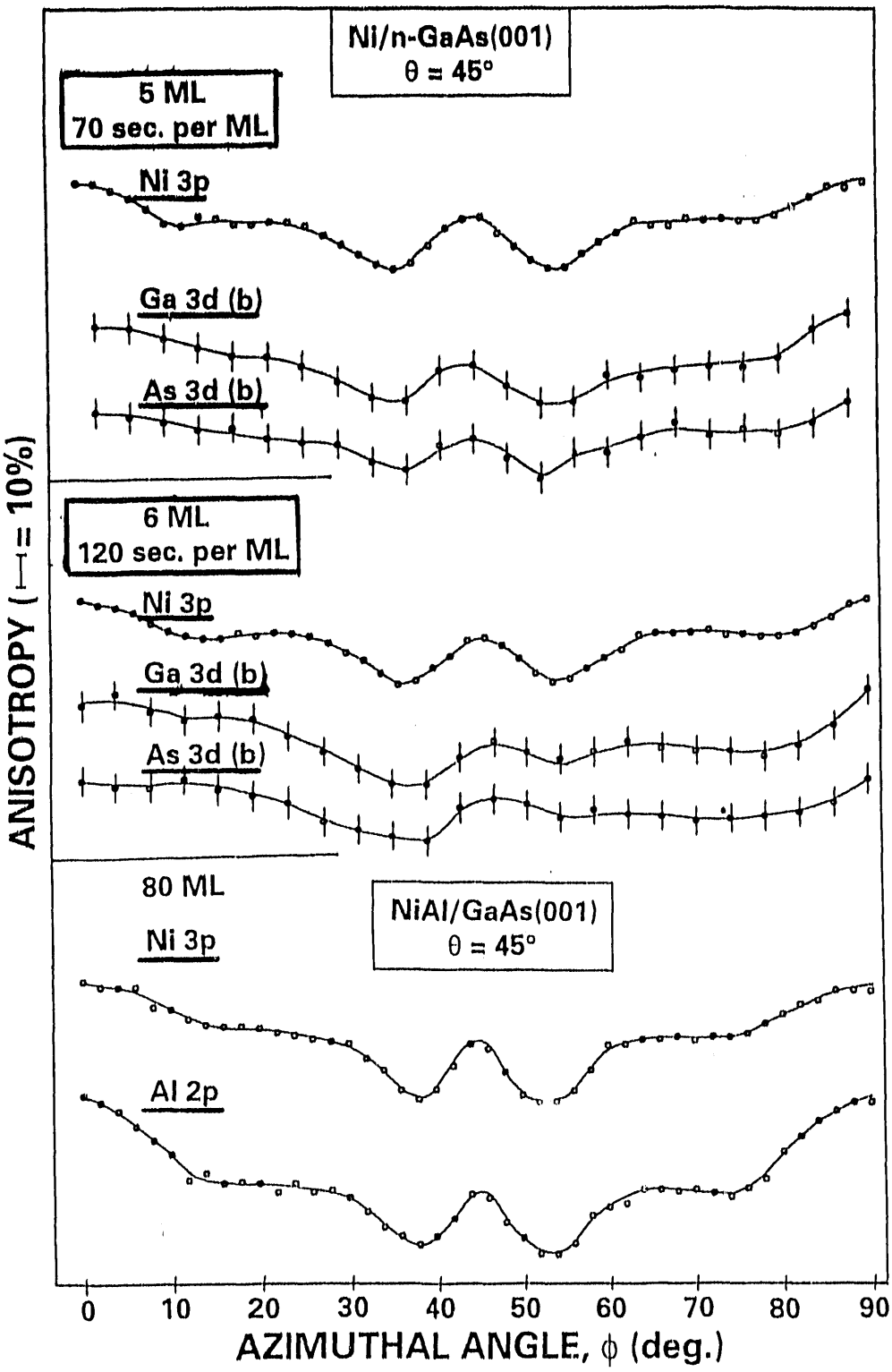
Ni/n-GaAs(001)
θ = 45°
5 ML
70 sec. per ML
Ni 3p
Ga 3d (b)
As 3d (b)
6 ML
120 sec. per ML
Ni 3p
Ga 3d (b)
As 3d (b)
80 ML
NiAl/GaAs(001)
θ = 45°
Ni 3p
Al 2p
ANISOTROPY (⊣⊢ = 10%)
0
10
20
30
40
50
60
70
80
90
AZIMUTHAL ANGLE, ϕ (deg.)

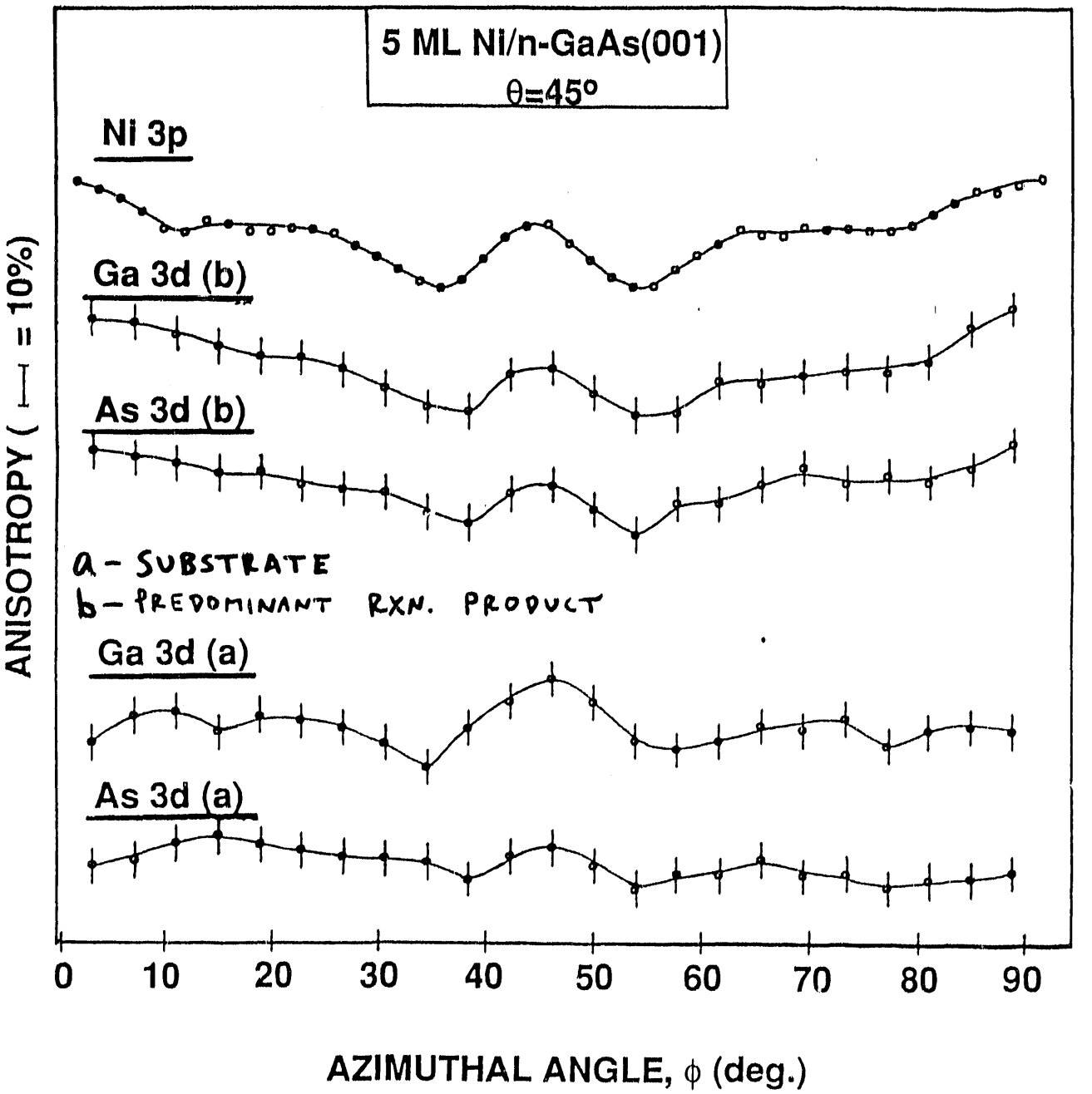
5 ML Ni/n-GaAs(001)
θ=45°
Ni 3p
Ga 3d (b)
As 3d (b)
a - SUBSTRATE
b - PREDOMINANT RXN. PRODUCT
Ga 3d (a)
As 3d (a)
ANISOTROPY (⊣ = 10%)
0
10
20
30
40
50
60
70
80
90
AZIMUTHAL ANGLE, ϕ (deg.)

$Ni_{\sim 0.5}Ga_{\sim 0.3}As_{\sim 0.2}/GaAs(001)$

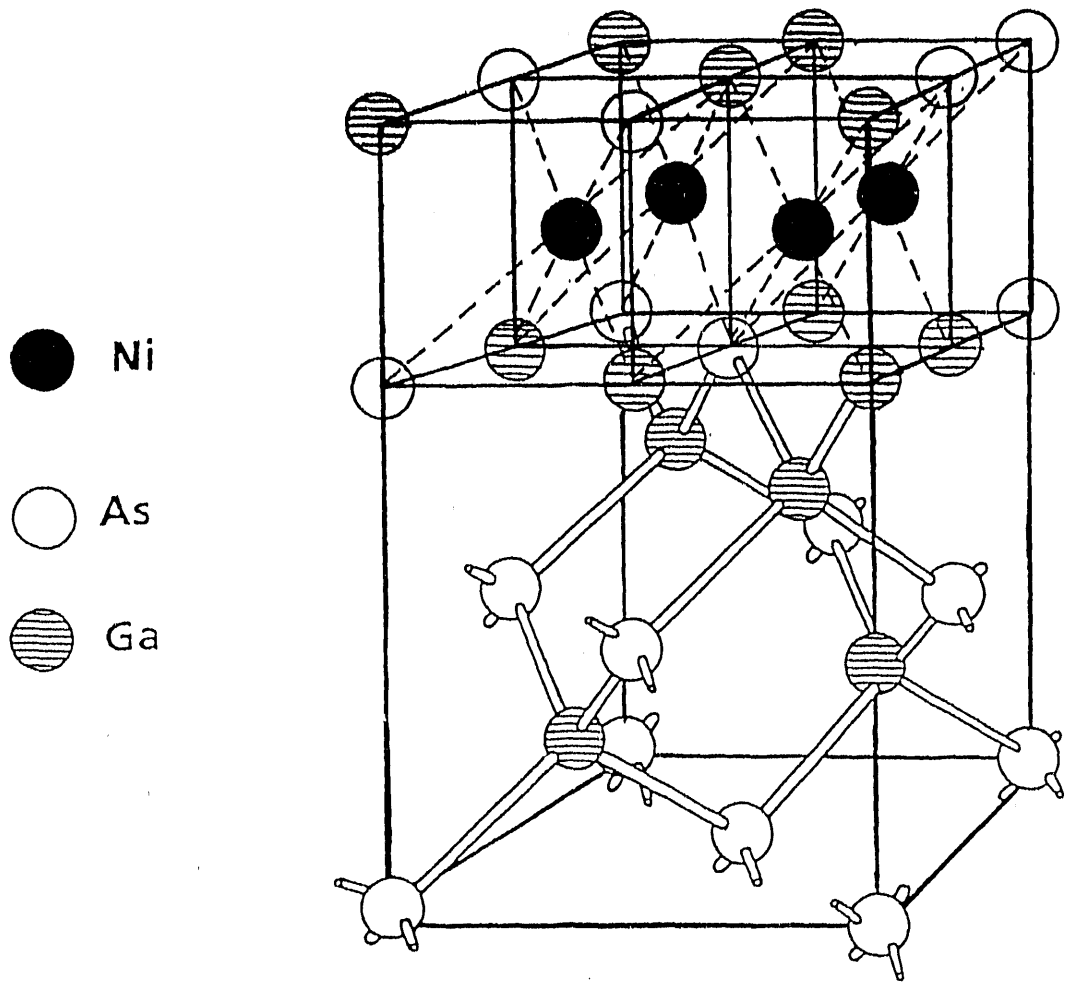

Conclusions and Future Directions

1. Site-specific XPD works provided the sites possess different symmetries with respect to specimen crystal axes (i.e. zincblende).

2. State-specific XPD works provided the chemical shifts are large enough to be reasonably resolved.

3. State-specific XPD can be done with monochromatic lab x-ray sources, but it is very slow. High total energy resolution (~0.2-0.3 eV), high photon energy (>~ 1 keV), and high intensity (ALS!) required for more rapid data acquisition and lower statistical uncertainties in measured anisotropies.

Photoelectron Diffraction of Magnetic Ultrathin Films

J. Tobin

Lawrence Livermore National Laboratory

Photoelectron Diffraction of Magnetic Ultrathin Films

James G. Tobin
Lawrence Livermore National Laboratory

Goal: Determination of both the local Geometric and Magnetic Structures

Collaborators:
G. D. Waddill, LLNL
S. Y. Tong, U. Wisc. - Milwaukee
X.-Q. Guo, U. Wisc. - Milwaukee
M. K. Wagner, U. Wisc. - Madison

Photoelectron Diffraction of Magnetic Ultrathin Films

- Review of energy dependent photoelectron diffraction
- Two regimes: multiple scattering (low KE) and single scattering (high KE)
- Lower energies - advantages and difficulties

1. Strong surface sensitivity
   Distinguish overlayers from surface alloys
2. Magnetic Structure

Energy Dependent Photoelectron Diffraction

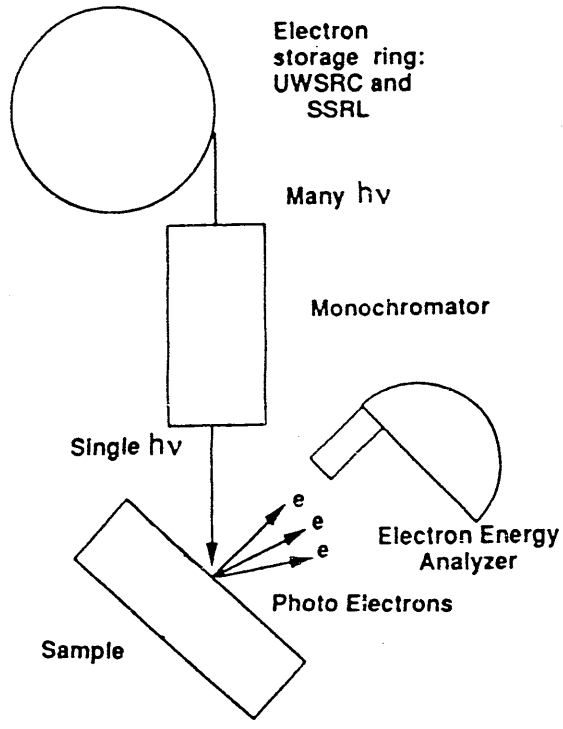

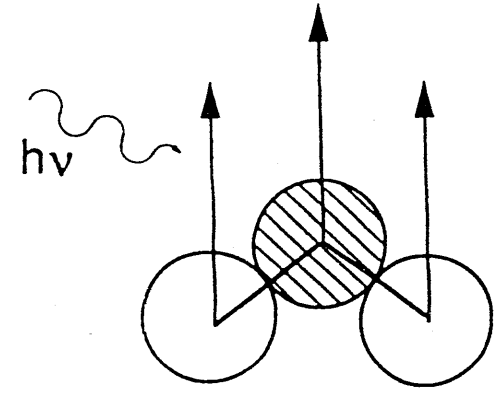

$$KE = h\nu - B^F + V_o - \phi$$

Energy Dependent Photoelectron Diffraction

Early study of Se/Ni(001)

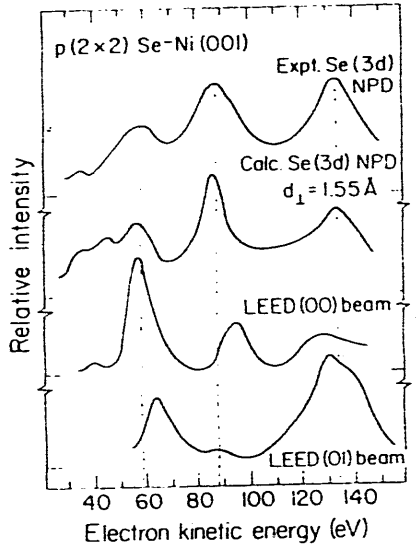

Kevan et al.
PRB 20, 4133 (1979)

Wider energy ranges and Fourier transforms

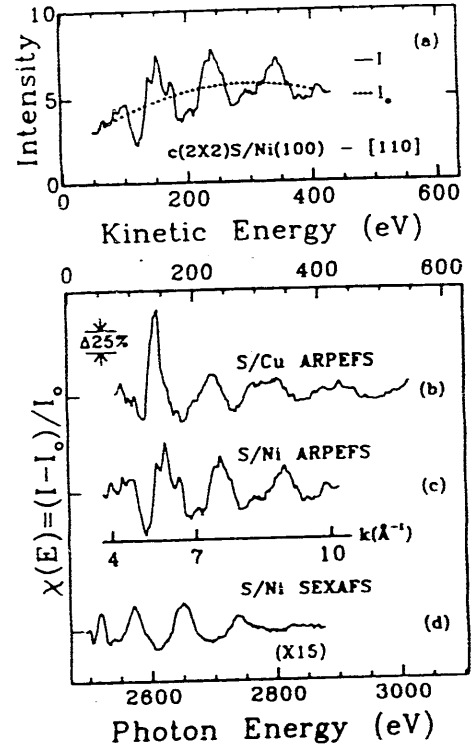

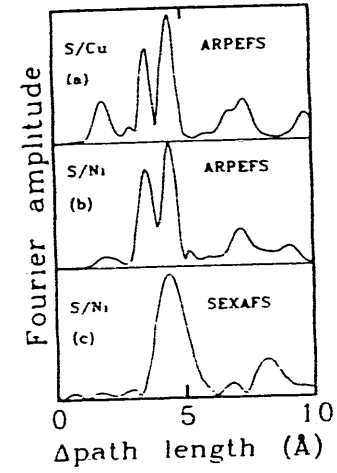

Barton et al., PRL 51, 272 (1983).

Energy Dependent Photoelectron Diffraction

Searchlight effect using 180° back scattering

S(is) cross section of S/Cu(001) at various emission angles

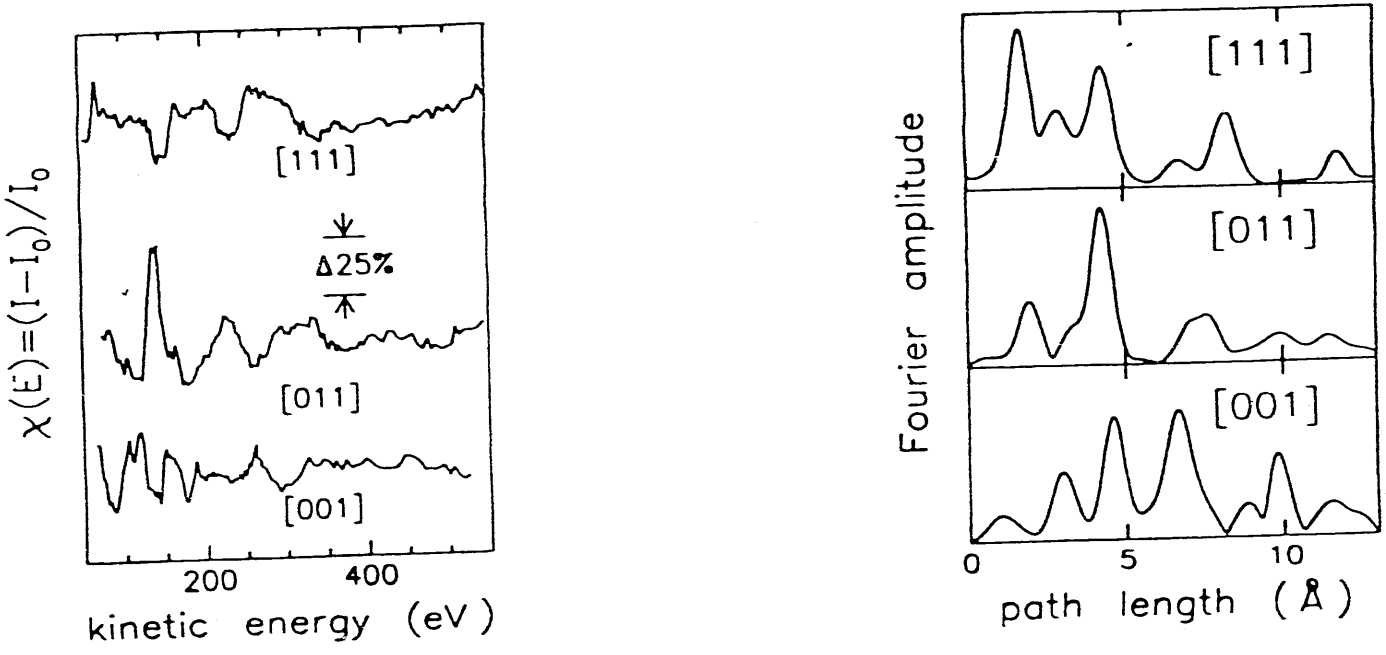

C. C. Bahr et al., PRB 35, 3773 (1987)

Photoelectron Diffraction

Two Regimes: (1) Multiple Scattering (low KE)

(2) Single Scattering and Forward Focussing (high KE)

Multiple Scattering Theory

Reverse Leed: Li, Lubinsky and Tong, PRB 17, 3128 (1978)

Cluster: Barton and Shirley, PRB 32, 1906 (1985);
Barton, Xu and Van Hove 37, 10475 (1988)

Single Scattering Theory

C. S. Fadley, Prog. in Surf. Sci. 16, 275 (1984).

PHOTOELECTRON DIFFRACTION OF BIMETALLIC SURFACES

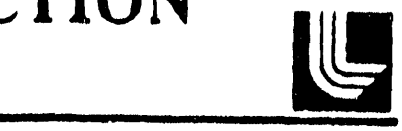

Surface Sensitivity and Elemental selectivity

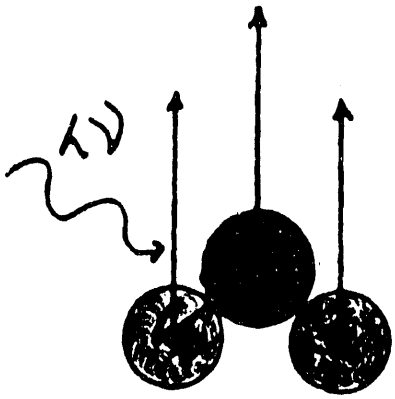

Photoelectrons scattering off of neighbors.

Au/Cu (001)

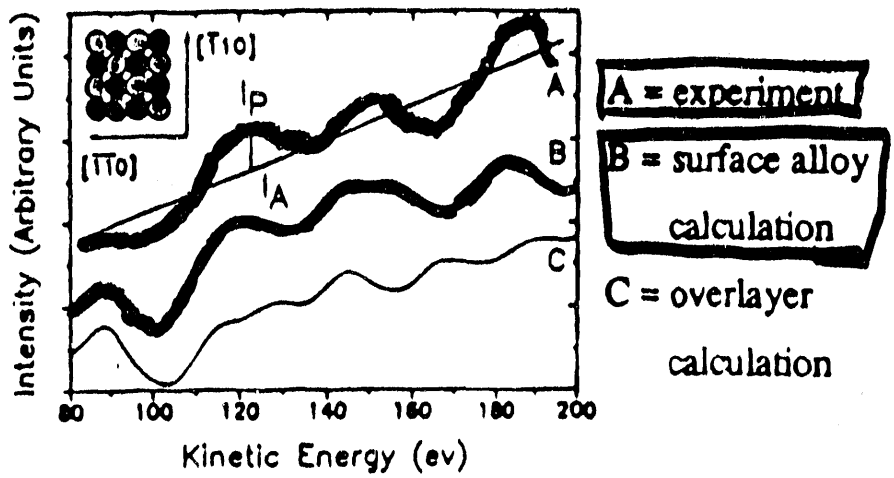

Diffractions causes modulations in cross section vs. kinetic energy.

(1) Distinguish a surface alloy from an overlayer and
(2) Study variations in structure as a function of coverage.

Experiment: Tobin, et al.
Theory: S. Y. Tong, et al.

Magnetic Ultrathin Films

1. Geometric Structure - Fe3p Phctoelectron diffraction
   a) FCC Fe site
   b) wider KE range

2. Magnetic Structure - Spin dependent photoelectron diffraction
   a) multiplet split 3s
   b) circular polarized x-rays

Fe/Cu (001) Cores

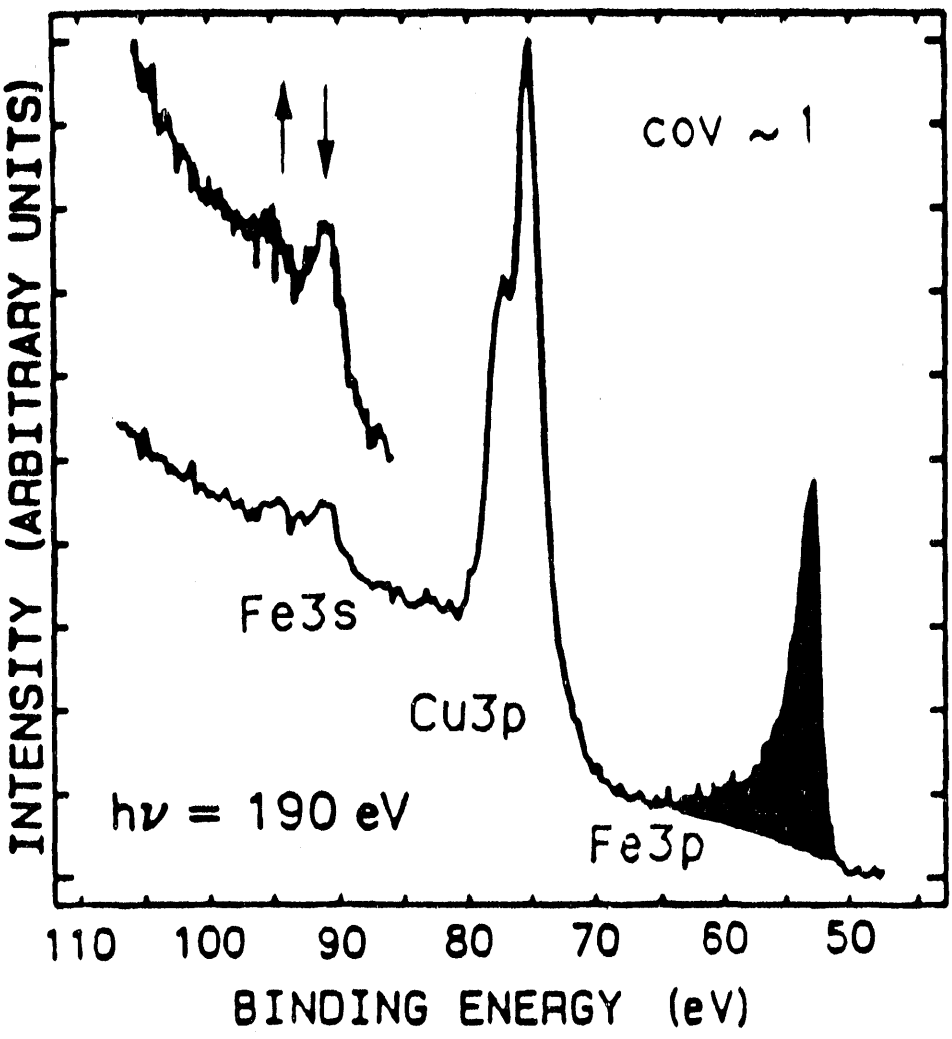

Photoelectron Diffraction of Fe 3p

→ Multiplet Splitting & Spin-Orbit Splitting Produce Asymmetry

NPD Fe/Cu(001) 3P CROSS SECTION

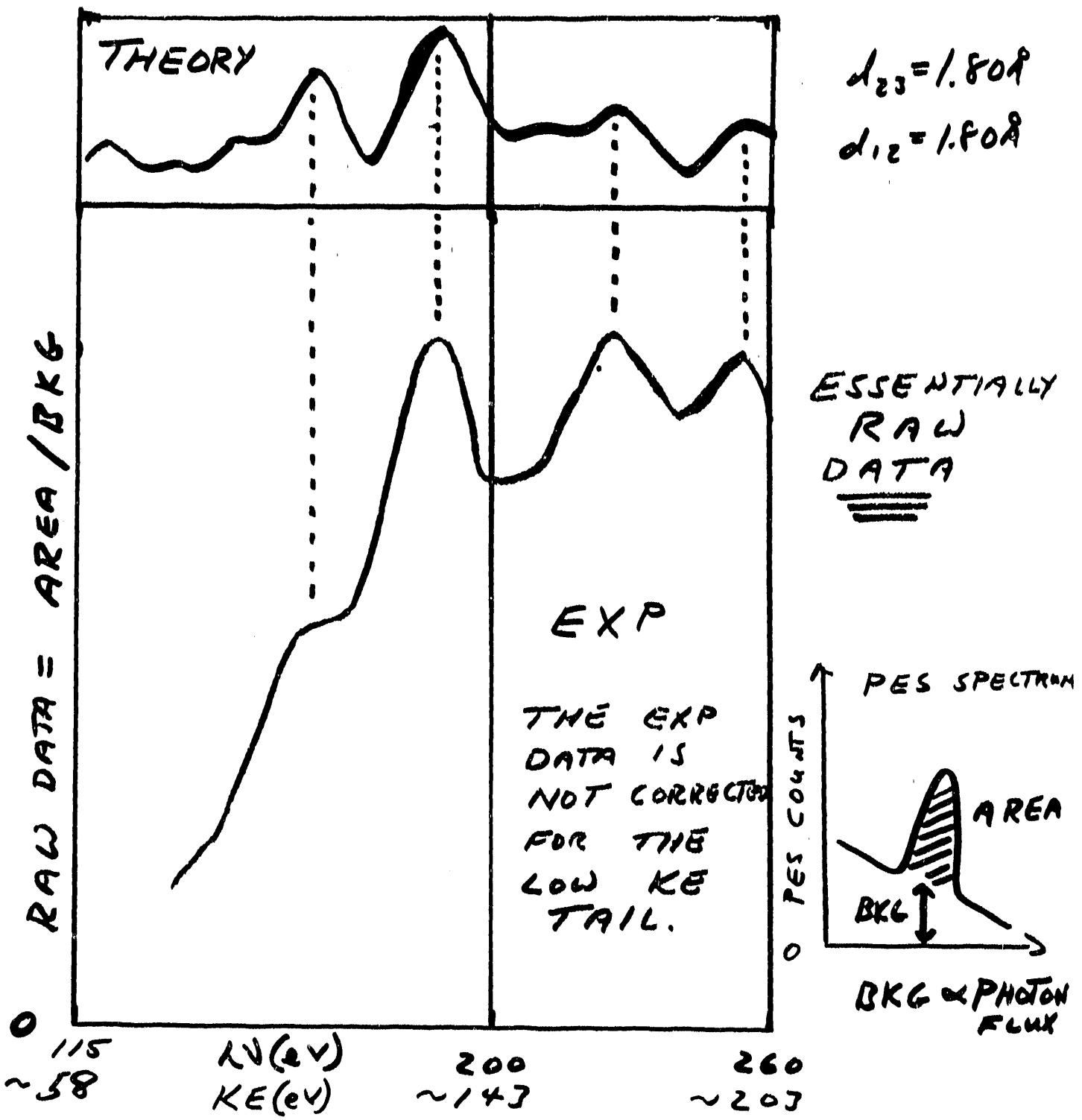

Fe/Cu(001)
Four Fold Hollow Model FCC - (001)

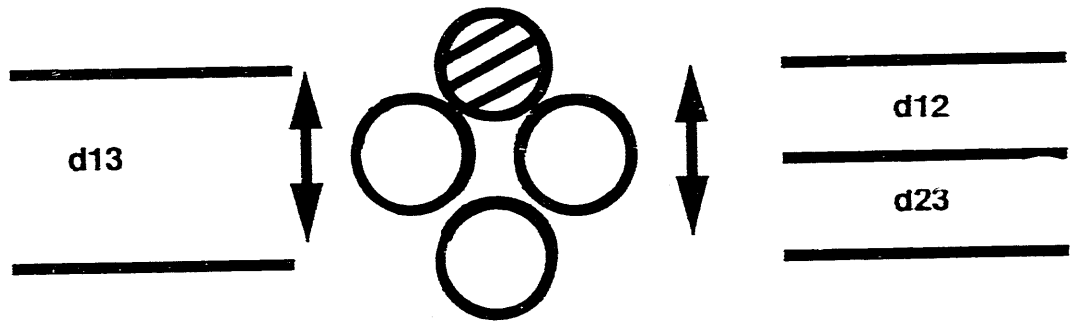

d13 = d12+d23

d13 = 3.60 Å

1. d_{12} uncertain

2. Composition (Fe vs. Cu) unknown

   [used monolayer, bilayer and trilayer of Fe on Cu (001)]

Fe/Cu (001) Photoelectron Diffraction

Why are we sensitive to $d_{13} = d_{12} + d_{23}$?

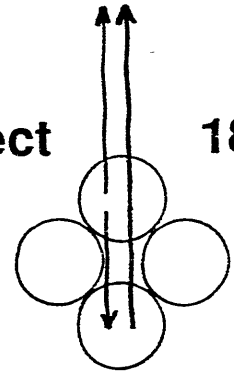

Direct 180° backscattered

NORMAL EMISSION

How can we measure d_{12}?

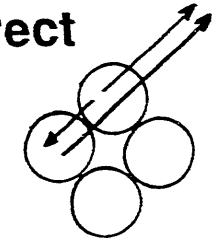

Direct 180° backscattering

OFF-NORMAL EMISSION ~45°

Scattering amplitude vs. angle, at low KE.

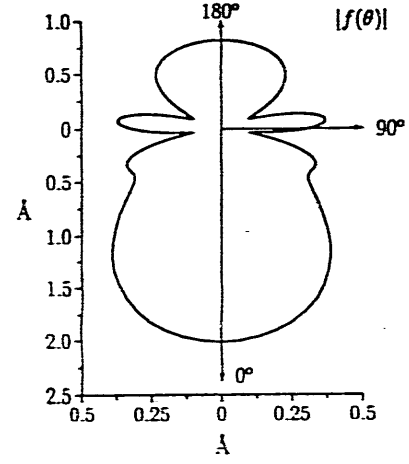

Fe 3p Photoelectron Diffraction

Consistent with FCC structure, d_{13} = 3.60Å

Need to determine

1. d_{12}
2. Elemental nature of nearest neighbors (overlayers vs. clusters vs. alloying...)
3. Accuracy to $\lesssim \pm$ .05Å

Solutions

1. Wider hν range
2. σ vs KE at 45° emission to test d12
3. Multiplet split photoelectron diffraction
   → Fe 3s ←
   Spin dependence + Local magnetic ordering

Wider Photon Energy Range: Preliminary Analysis

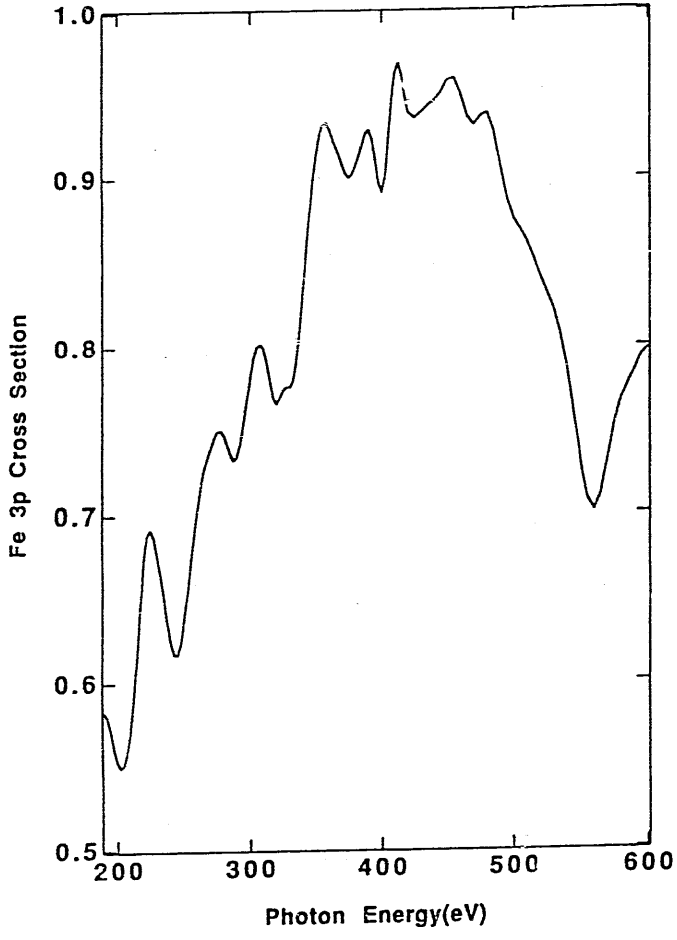

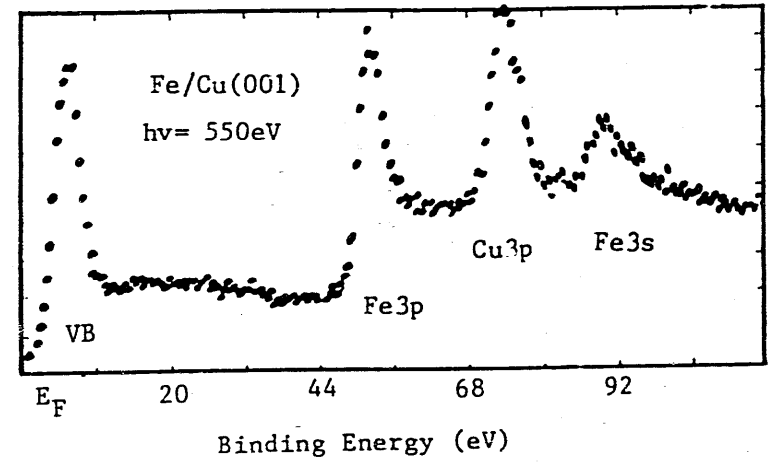

Magnetic Structure: Spin Dependent Photoelectron Diffraction

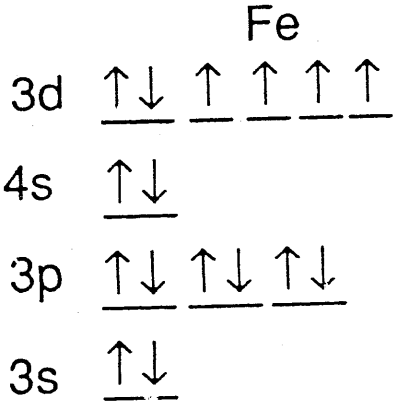

1. **Multiplet split 3s intrinsic spin resolution**

2. **Circular polarization at SSRL on the UC/LLNL PRT SGM beamline**

PHOTOELECTRON SPECTROSCOPY
SPIN RESOLUTION

Fe

3d ↑↓ ↑ ↑ ↑ ↑

4s ↑↓

3p ↑↓ ↑↓ ↑↓

3s ↑↓

← Origin of magnetism: alignment of spins.

- **Spin Polarization**

  Problem: low efficiency of detector (10^{-4}) in photoemission

  Solution: intense sources, e.g. undulators

- **Intrinsic Spin Resolution: Multiplet Splitting** } THIS WORK

  ~ 1 "ML" Fe/Cu (001)

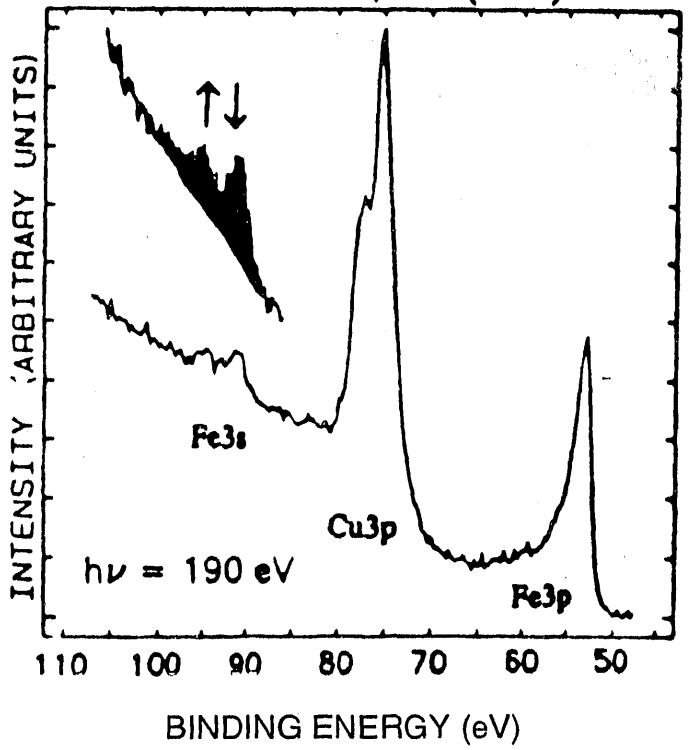

CARBONE et al
Z. PHYS. B 79, 325 (1990)
HILLEBRECHT et al
PHYS. REV. LETT. 65, 2450 (1990)
BULK Fe

Use the 3s to do photoelectron diffraction.

Fe3s Peaks

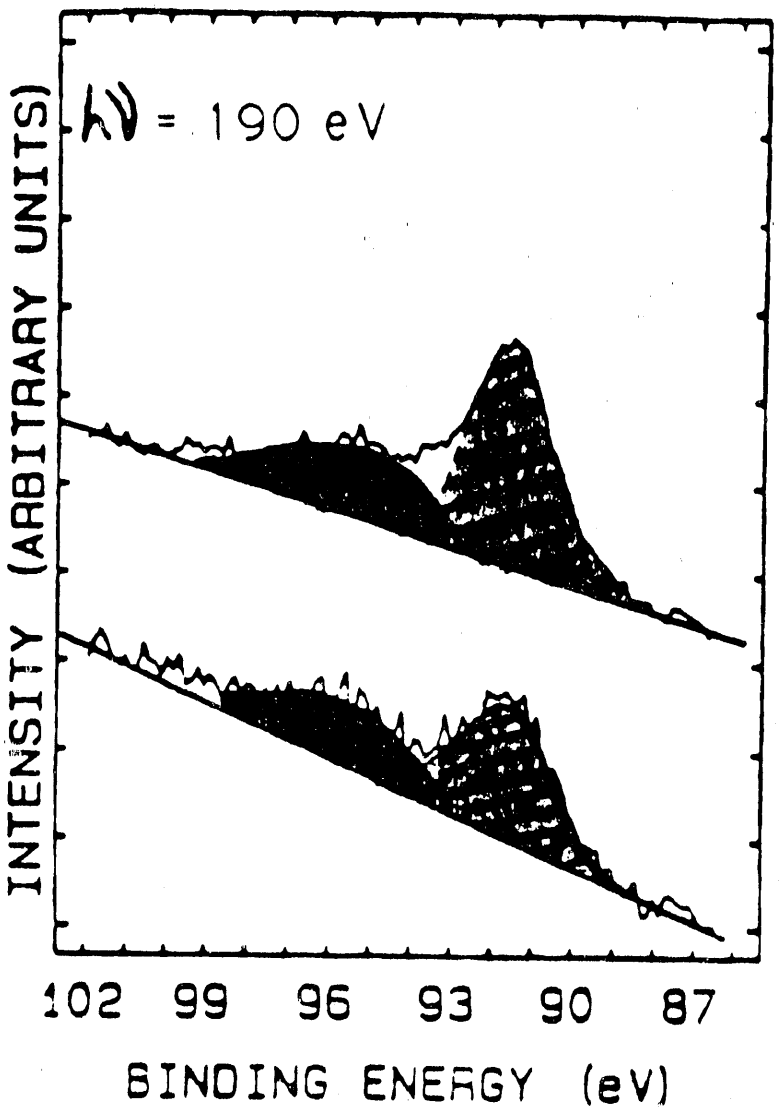

Coverage

1 5/8

3/4

$\Delta B^F \approx 3.8$ eV
Approximately

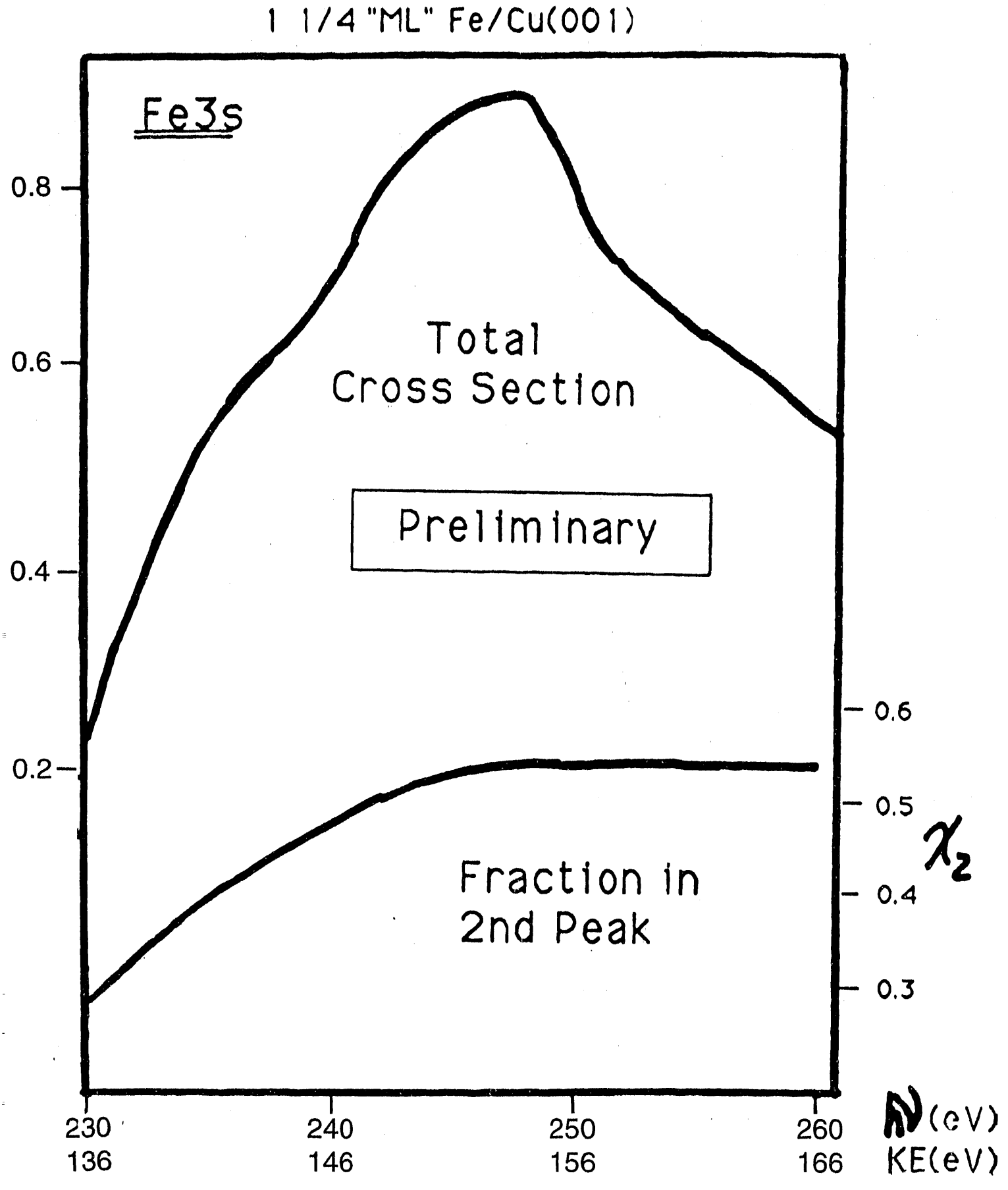
1 1/4 "ML" Fe/Cu(001)
Fe3s
0.8
0.6
0.4
0.2
Total
Cross Section
Preliminary
Fraction in
2nd Peak
0.6
0.5
0.4
0.3
χ_2
230
136
240
146
250
156
260
166
hν (eV)
KE(eV)

Nanoscale Magnetics

Demonstration of circular polarization capability of the UC/LLNL SGM beamline at SSRL by Jo Stohr et al of IBM on July 15,

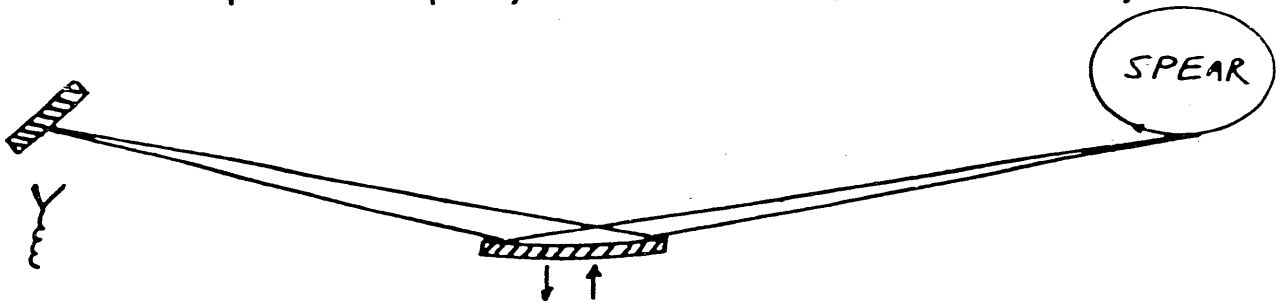

Move mirror to sample above or below plane of ring: elliptically polarized x-rays, right and left handed.

X-ray Circular Dichroism of Co/Pd multilayers

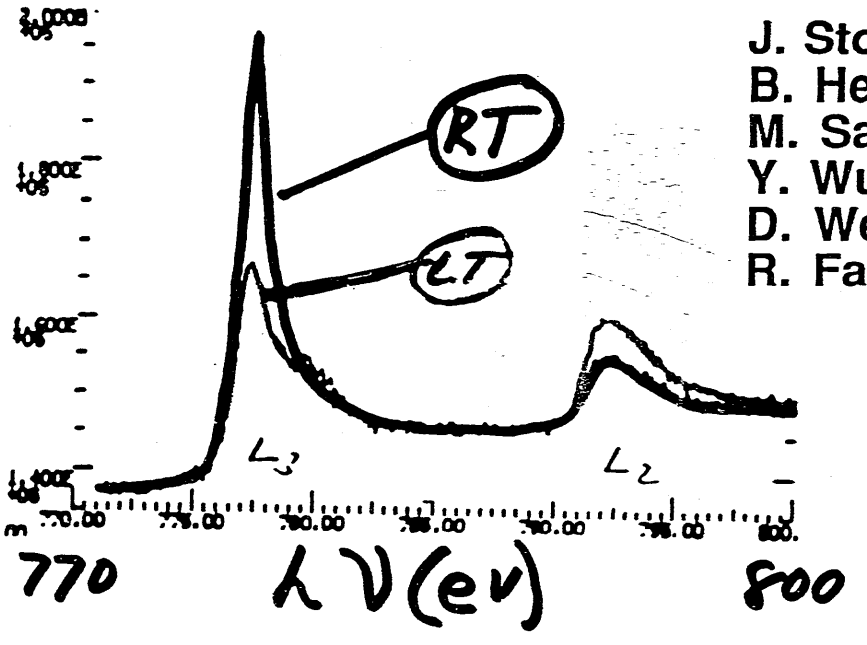

J. Stohr
B. Hermsmeier
M. Samant
Y. Wu
D. Weller
R. Farrell

Near Edge X-ray Absorption Fine Structure: NEXAFS
Transition: 2p → Empty 3d

Next: Via the LLNL/IBM/SSRL collaboration, we will implement a more sophisticated capability.

Photoelectron Diffraction of Magnetic Ultrathin Films

Fe/Cu (001)

Geometric Structure

- FCC site for Fe
- Wider KE range should help specify structure
  eg. Fourier transform for nearest neighbors

Magnetic Structure

- Multiplet split 3s
- Circular polarization

Direct Imaging Photoemission Microscopy: Past, Present, and Future

E. Bauer

Technische Universität Clausthal

DIRECT IMAGING

PHOTOEMISSION MICROSCOPY:

PAST, PRESENT AND FUTURE

UHV

CATHODE LENS SYSTEMS

MATERIALS SCIENCE

PAST: DISCHARGE LAMPS

↓

FUTURE: SYNCHROTRON RADIATION

COLLABORATORS (CHRONOLOGAL):

G. TURNER, W. TELIEPS, M. MUNDSCHAU, W. SWIECH, L. VENEKLASEN, G. MARX, M. ALTMAN, H. PINKVOS, G. LILIENKAMP

Goal:

Chemical Analysis

Indirect Analysis

in

PEEM LEEM

via

$\Delta\phi$ LEED

Examples:

Cu/Mo(110) 2d Mo carbide/Mo(110)

3d η''-Cu_3Si / Si(111)

Direct Analysis

chemical { composition $S(E_{char})$; environment ΔE_{core}

E_{char} = { $h\nu - E_i$ Photoelectron XPEEM ; E_{kke} = $E_h - E_k - E_e$ Augerelectron AEEM

by

microspectroscopy spectromicroscopy

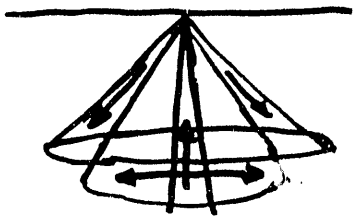

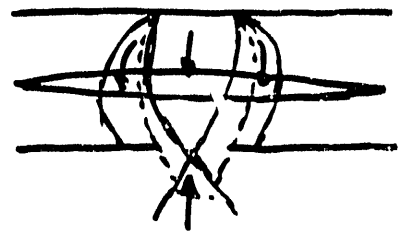

sequential parallel

Transmission $T \approx 10\%$ $T = ?$

(Energy analyzer) (cathode lens + energy filter)

$$S+B \sim T$$

$$N \sim (S+B)^{1/2}$$

$$\frac{S}{N} \sim T^{1/2} - \alpha B T^{-1/2}$$

Direct (non-scanning) Surface Microscopy with characteristic X-ray photo electrons "XPEEM"

Why? ① Disadvantages of scanning

- Sequential image acquisition
- Stringent photon focussing requirements
- Large local specimen load
- Extreme long time mechanical stability of complete system

② Chemical information complementary to structural " obtained by Low Energy Election Microscopy (LEEM)

LEEM → XPEEM / AEEM (Auger)

↓

XPEEM as an extension of LEEM

Spectromicroscopy

$T = ?$ ⟶ Electron optics (I)

Signal, Background? (Noise) ↗ Emission process (from atoms) (II)

↘ Illumination (III)

(I) - (III)

↓

Qualitative analysis (IV)

↓

Quantitative analysis (V)

(Emission process from condensed matter)

(I) Electron optics

Assumption:

Quality (Transmission T, Resolution δ) limited by aberrations of acceleration field of cathode lens (not by aberrations of energy filter or other components of system)

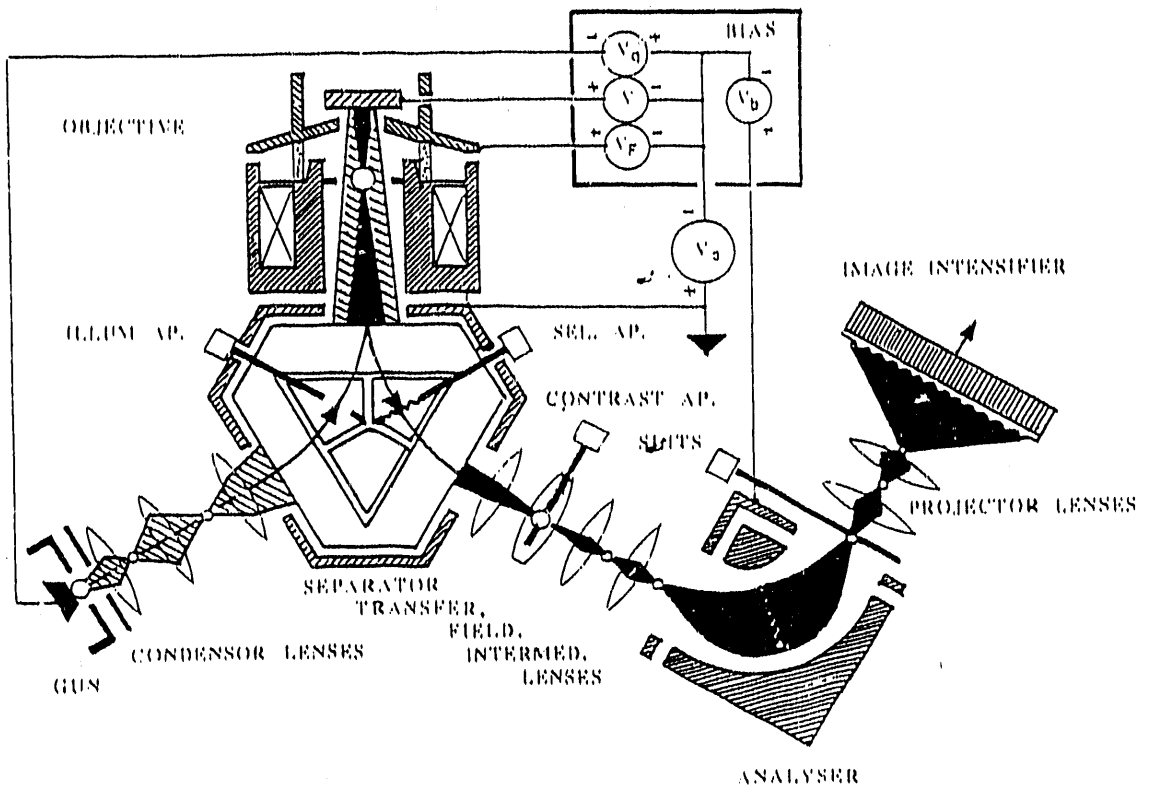
BIAS
OBJECTIVE
ILLUM. AP.
SEL. AP.
CONTRAST AP.
SLITS
IMAGE INTENSIFIER
PROJECTOR LENSES
SEPARATOR
TRANSFER,
FIELD,
INTERMED.
LENSES
CONDENSOR LENSES
GUN
ANALYSER

Approximation : homogeneous field

$$\delta^2 = \delta_c^2 + \delta_s^2 + \delta_d^2$$

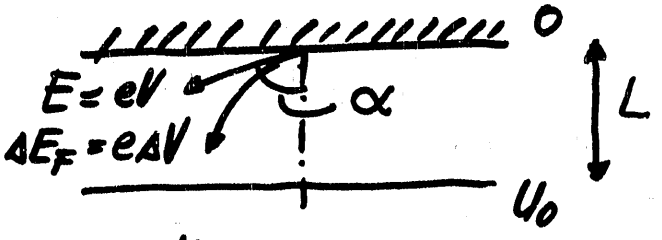

$$\delta_c = \varepsilon \sin\alpha$$

$$\delta_s = \rho \sin^3\alpha$$

$$\delta_D = \frac{0.6\,\lambda}{\sqrt{\rho}\sin\alpha}$$

$$\underline{I = I_0 \cos\alpha}$$

$$\varepsilon = \frac{\Delta V}{U_0} \qquad \delta = \frac{r}{L}$$

$$\rho = \frac{V}{U_0} \qquad \lambda = \frac{\Lambda}{L}$$

$$\Lambda = \frac{h}{\sqrt{2emU_0}}$$

$$T = \sin^2\alpha \, \frac{\Delta E_F}{\overline{\Delta E}} = \sin^2\alpha \; \varepsilon e U_0 / \overline{\Delta E}$$

$$Q_n = \frac{T^n}{\delta^2} = Q_n(\alpha, \varepsilon, \rho) \stackrel{!}{=} \text{Max}$$

A) Strong signal (LEEM) : T of no concern → $n = 0$

$\alpha^0_{opt}(\varepsilon, \rho)$ ε_{opt} for $\varepsilon \to 0$ $r_0(\Delta V, V)$ $T_0(\Delta V, V)$

B) Weak signal : $n = 1$

$\alpha^1_{opt}(\rho)$ $\varepsilon^1_{opt}(\rho)$ $r_1(V)$ $T_1(V)$

C) Very weak signal (XPEEM, AEEM) : $n = 2$

$\alpha^2_{opt}(\varepsilon, \rho)$ ε_{opt} for $\varepsilon \to 1$ $r_2(\Delta V, V)$ $T_2(\Delta V, V)$

$n > 2$: No optimum α, ε

Homogeneous Field

Transmission $\underline{T}$

Resolution $\underline{r} = \delta \cdot L$

for optimum aperture

and $\Delta E_F = 1eV$

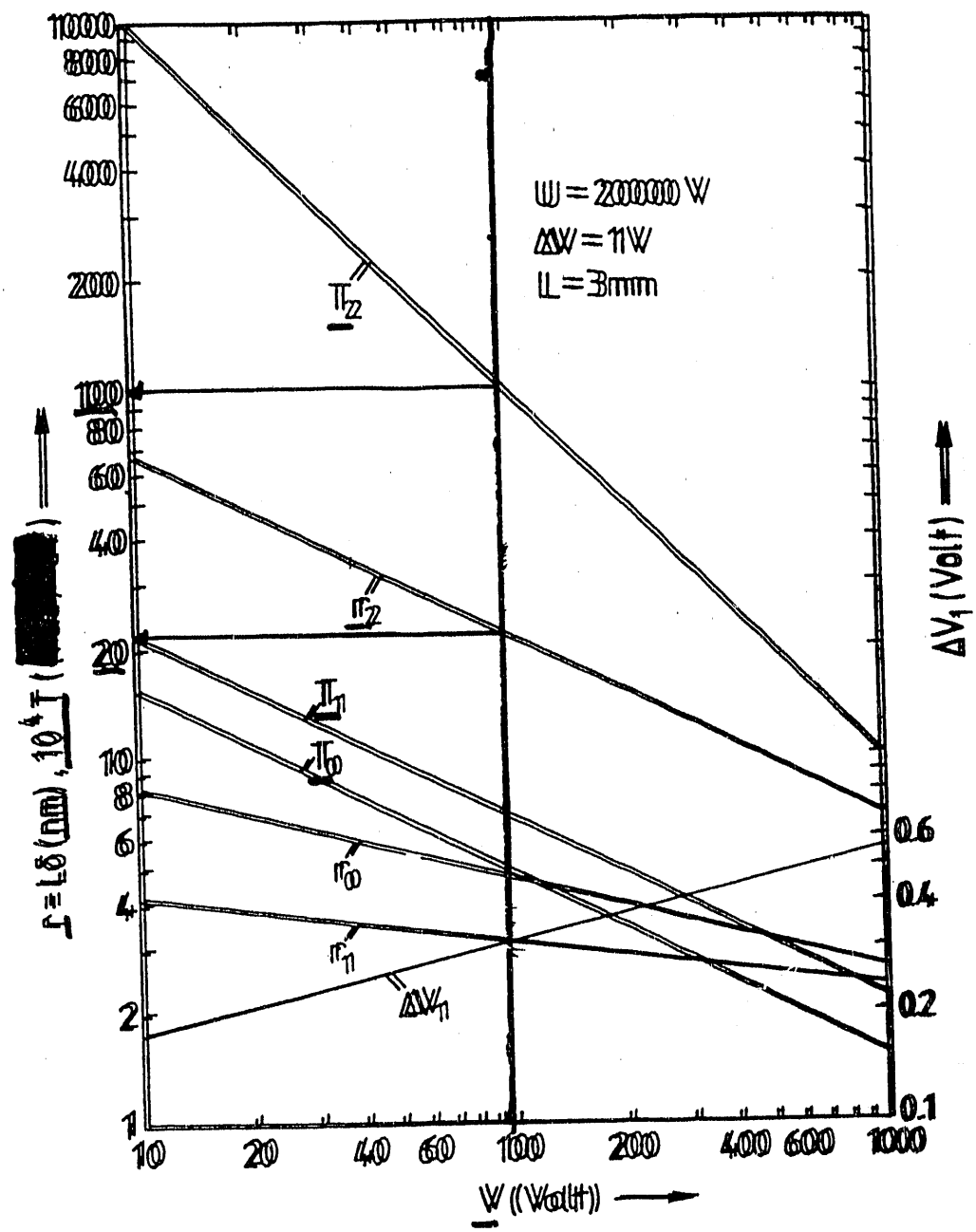

Homogeneous Field
Transmission T
Resolution r
for optimum aperture
and E = 100 eV

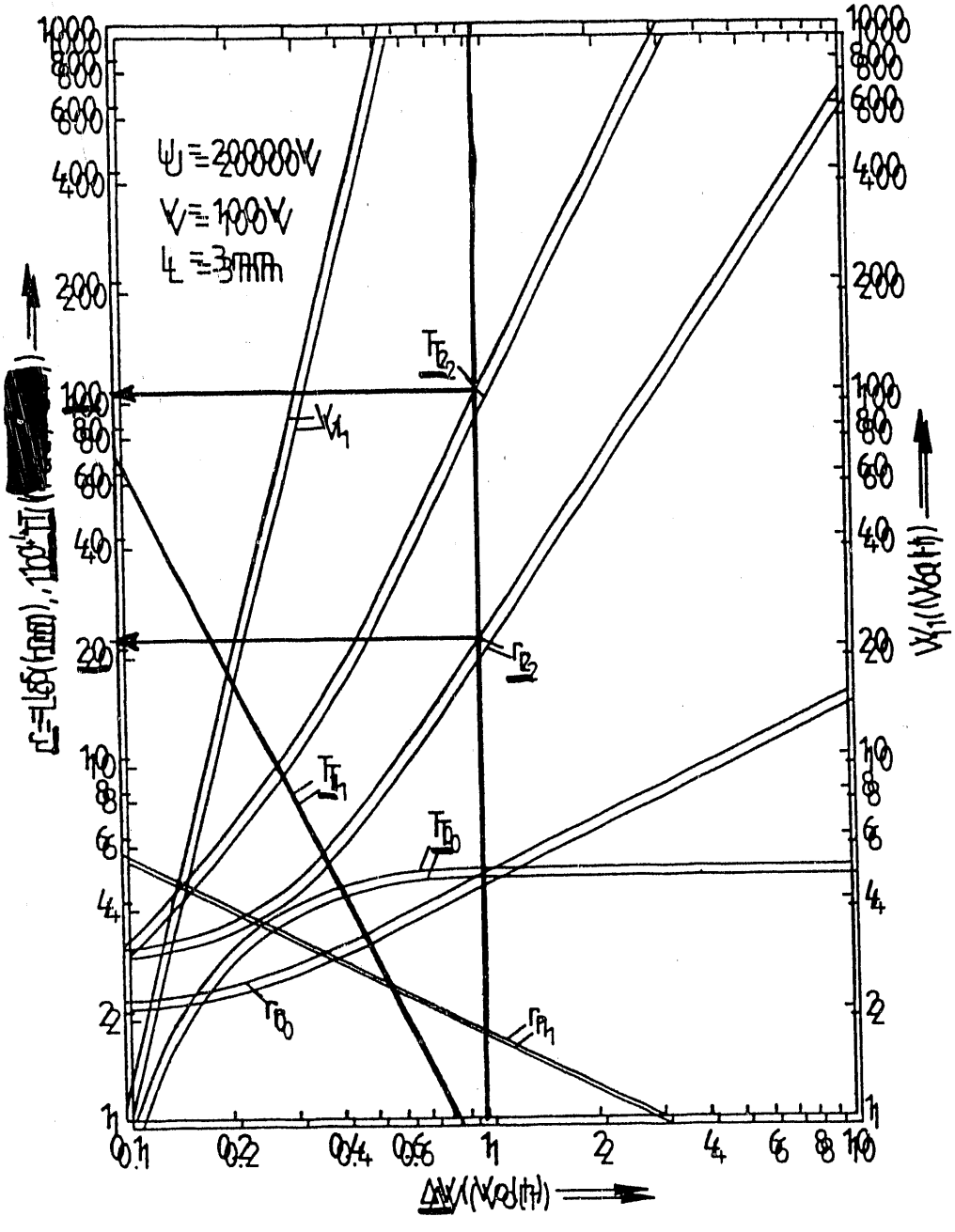

Q_1 for $\overline{\Delta E} = \Delta E_F$

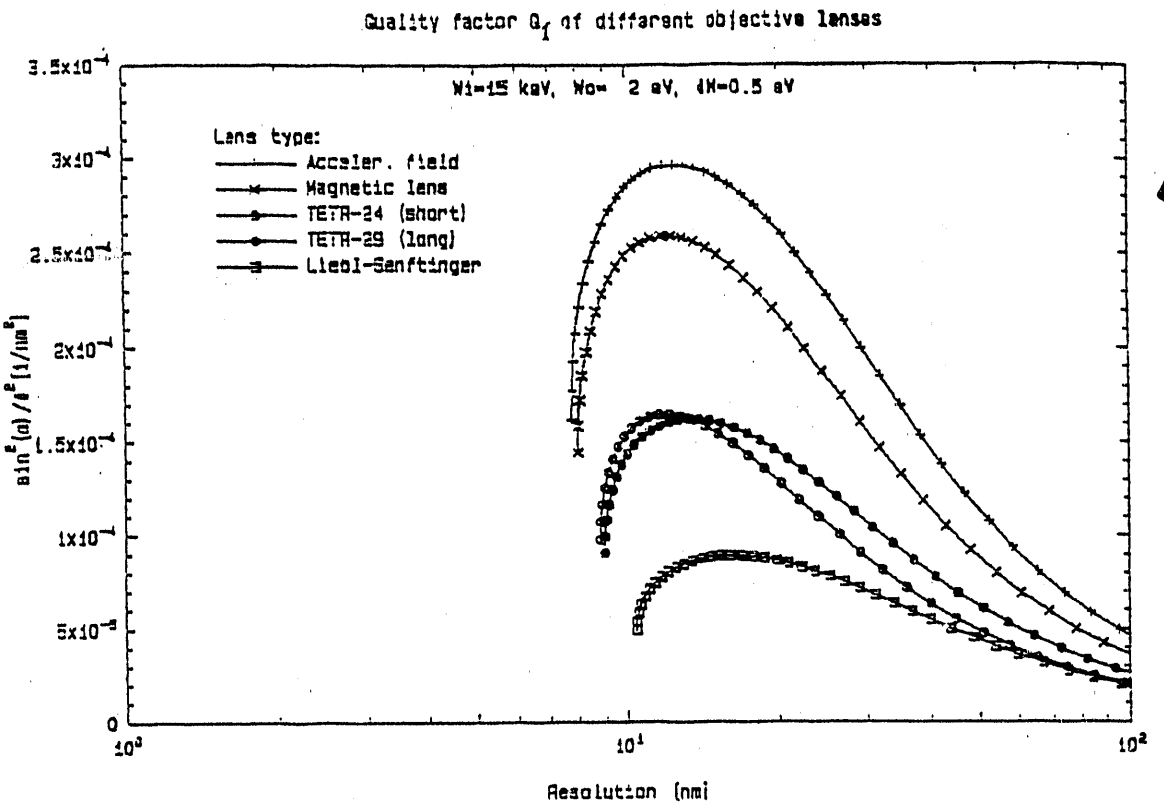

$E_0 = 2eV$

$\Delta E = 0.5eV$

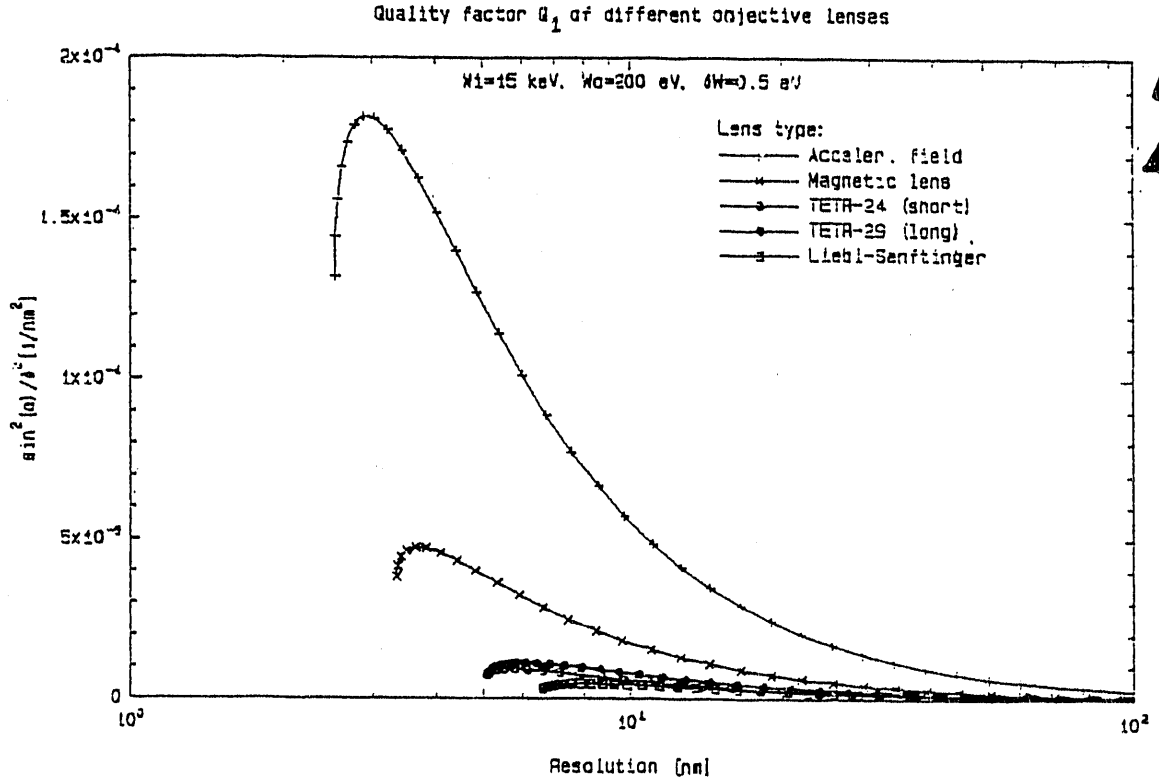

$E_0 = 200eV$

$\Delta E = 0.5eV$

(II) Emission process

Requirements

(1) Energy

(a) Background

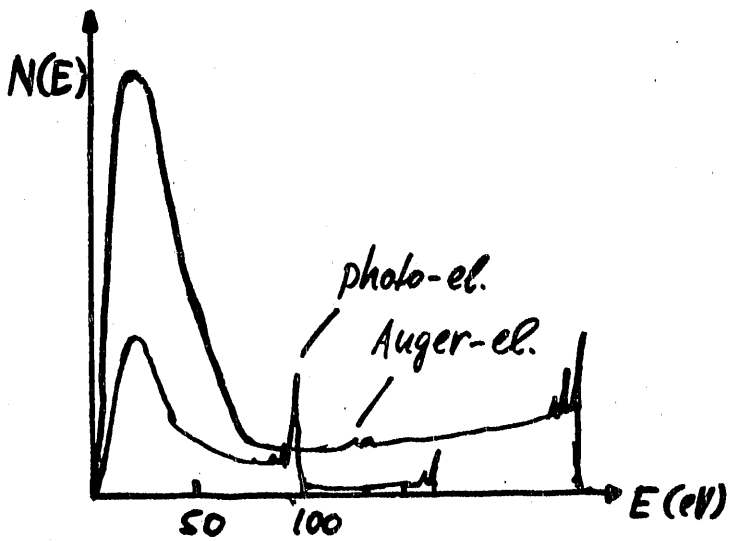

(b) Escape depth

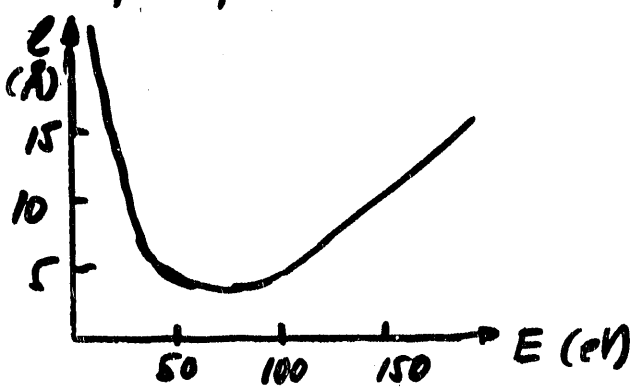

$\rightarrow E_{char}^{opt} \approx$ 50 - 150 eV, e.g. 100 eV

XPEEM: $h\nu \approx E_i$ + 100 eV, not Mg K_α, Al K_α!
→ tuneable source: synchrotron

AEEM: low energy transitions (> 50 eV), not high " " !

② Intensify
ionization cross-sections

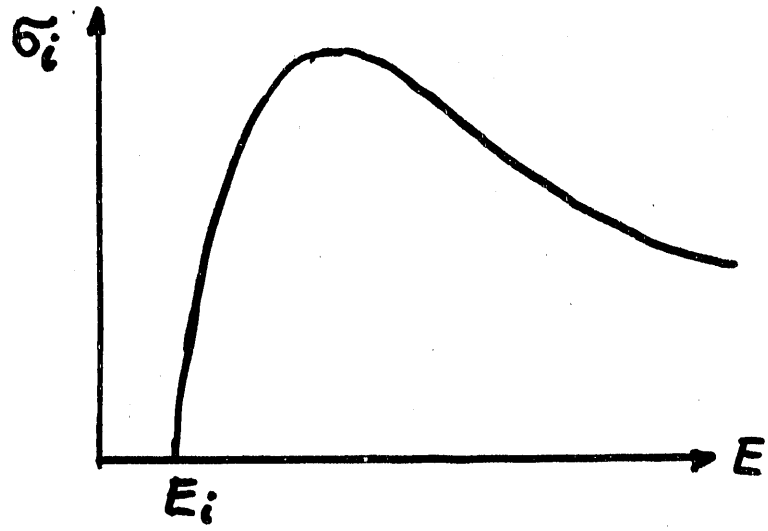

$\sigma_{i,opt}^{x}$ compatible with condition ①
for most $100 eV \lesssim E_i \lesssim 1000 eV$

$\sigma_{i,opt}^{e}$ at $E_p \approx 3\text{-}4\ E_i$
condition not important because of
slow σ_i-decrease above σ_i^{max} in
condensed matter (backscattering!)

↓

E_p fixed at ≈ 1 keV for
low energy transitions

Comparisons

	electrons	photons

Maximum ionization cross-sections (in 10^{-22} m^2)

		calc.	exp.
K-shell			
C	0.31	0.9	0.7
N	0.18	0.7	0.66
O	0.10	0.5	0.57
L_{23}-shell			
P	2.25	5	4
S	1.5	5	4.1
Cl	1.2	5	3.6

↓

Photons 3-4 times more effective than electrons

2nd reason for photons: lower background

		AEEM	XPEEM
①	$\frac{S}{B}$	small	large
②	peak width	large ($\approx$ 10 eV)	small ($\lesssim$ 1 eV)

↓

XPEEM is far superior to AEEM for same excitation flux density on surface

(III) Illumination

Light source

Flux $\approx 10^{15}$ photons/s/0.1% bandwidth

Source size $\simeq 10^{-2}$ mm^2

Transfer from source to specimen

Demagnification x 10

Monochromacy : XPEEM : 0.5 - 1 eV

AEEM : uncritical

Assumed losses : factor 10^3

Specimen

Illuminated area : 10^4 μm^2

Flux density : XPEEM $\approx 10^{22}$ photons/m^{2}s

AEEM $\approx 10^{24}$ "

(10% bandwidth)

(IV) Qualitative Analysis

Example: Ag/Si

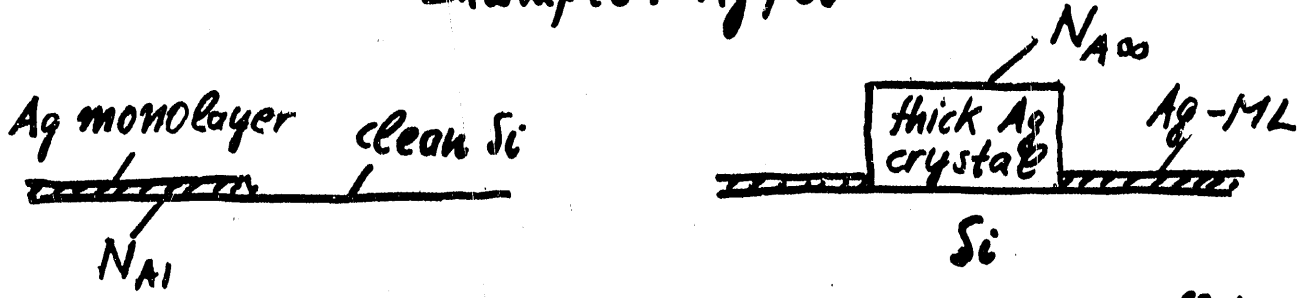

XPEEM $E_{char} = 100\,eV$ $(h\nu = 484\,eV)$ $n = 10^{22}/m^2s$

AEEM $E_{M_{45}VV} \approx 350\,eV$ $(E_p \approx 1.5\,keV)$ $n = 10^{24}/m^2s$

Feature recognition when signal difference

- $\Delta S \gtrsim 5N = 5(\overline{S+B})^{1/2}$ Rose criterion

Signal from object region with area

$r^2 = (L\delta)^2 = 500\,nm^2 \approx (22\,nm)^2$ for $T = 10^{-2}$:

- $S = n(L\delta)^2 N_A \sigma_A T$

$N_{Al} \approx 8 \times 10^{18}$ atoms/m^2

$N_{A\infty} = \dfrac{N_{Ag(111)}}{1 - \exp(-d_{111}/\ell)} \approx 40 \times 10^{18}$ atoms/m^2

$\sigma_A = 3.5 \times 10^{-22}\,m^2$

$S_{Al} \approx 1.4 \times 10^2$ e/s

$S_{A\infty} \approx 7 \times 10^2$ e/s

LEEM

I_0 5 nA in 6 µm $\phi \hat{=} \frac{36\pi}{4} \times 10^{-12}\,m^2 \approx 25 \times 10^{-4}$

$R = 60\% \rightarrow I = \frac{3 \times 10^{-9}}{1.6 \times 10^{-19}} \approx 2 \times 10^{10}$ e/s in "

$I_{in\ 500\,nm^2} = \frac{500 \times 10^{-18}}{25 \times 10^{-12}} 2 \times 10^{10}$ e/s $= 4 \times 10^5$ e/s

8 µm ϕ, 30% R $\rightarrow 1 \times 10^5$ e/s

Background

clean Si: scaled from Mg K_α (1254 eV) to 484 eV excitation via $\sigma_i(h\nu)$:

$B_{Si} \approx 1.25 \times 10^2$ e/s

Ag monolayer: $B_{Al} \approx B_{Si}$

thick Ag crystal: $B_{A\infty} \approx 0$

↓

① Ag monolayer island recognition

$\Delta S_{min} \approx 5\left[\frac{1}{2}(S_{Al} + B_{Si} + B_{Si})\right]^{1/2} \approx \underline{70}$ vs

$\Delta S_{exp} = S_{Al} + B_{Si} - B_{Si} \approx \underline{140}$

1 s → 10 s $\quad \Delta S_{exp} \approx \underline{1400}$ vs $\Delta S_{min} \approx \underline{220}$

② thick Ag crystal recognition

$\Delta S_{min} \approx 5\left[\frac{1}{2}(S_{A\infty} + S_{Al} + B_{Si})\right]^{1/2} \approx \underline{110}$ vs

$\Delta S_{exp} = S_{A\infty} - (S_{Al} + B_{Si}) \approx \underline{535}$

V. Quantitative Analysis

Detectable $\Delta N_A = N_A - N_A'$

at a given average density

$$\bar{N}_A = \frac{1}{2}(N_A + N_A')$$

in integration time τ

N_A	$N_{A'}$
S_A	$S_A' = S_A + \Delta S_A$
B	B'

assume $B = B'$

$$\Delta N_A \triangleq \Delta S_A = \Delta\theta\, S_{A1}$$

θ coverage

S_{A1} monolayer signal

Recognition condition

$$\Delta S_A \geqq k\,(S_A + B + S_A' + B')^{1/2} \longrightarrow$$

$$\Delta\theta_{min} \approx k\sqrt{2}\,\frac{\sqrt{B+S_A}}{S_{A1}}$$

$\Delta\theta_{min}$ for $S_A \approx S_{A1}$, 22×22 nm^2 pixel, $k = 5$

τ (sec)	XPEEM $S_{A1} = 140$, $B = 125$	AEEM $S_{A1} = 240$, $B \approx 900$
1	0.92	1.05
10	0.27	0.32
100	0.08	0.10
1000	0.03	0.03

↓

Quantitative analysis possible with

$\delta \approx 20$ nm, $\tau = 100 - 1000$ s, $\Delta\theta = 0.10 - 0.03$ ML.

Auger electron angular distributions

$M_{45}VV$

1 ML Ag on Si(111)

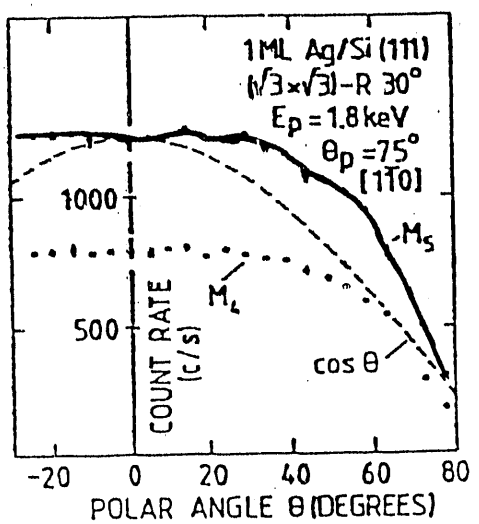

a

Ag(111)

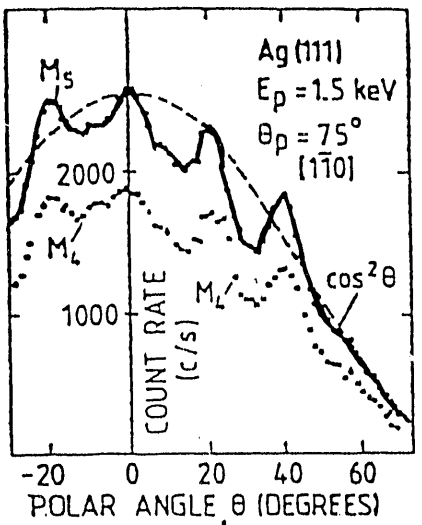

b

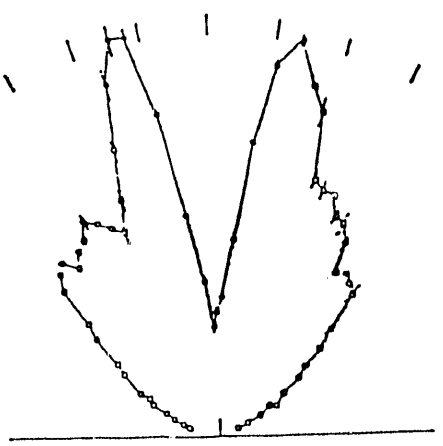

c

Cu (100)

$M_{23}VV$

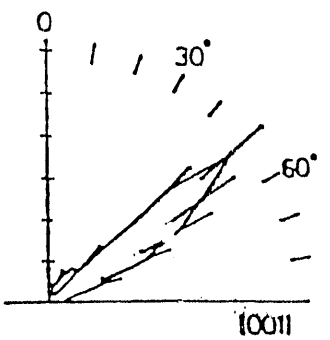

d

½ ML Se on Ni (100)

$M_{45}VV$

Auger electron and photo electron backdiffraction can cause mayor problems because of small angular acceptance of system

Ag-ML on Si :	OK
thick Ag (111) :	≈ OK
Cu (100) :	not OK
Se ½ ML on Ni (100) :	not OK

Nevertheless

Direct chemical imaging appears very promising, in particular in combination with

LEEM
LEED
and
UV-PEEM

Recent Developments in Undulator-Based Scanning Photoemission Microscopy

H. Ade

State University of New York–Stony Brook

Recent Developments in Undulator-Based Scanning Photoemission Microscopy

X1-SPEM (NSLS, BNL, USA)

Harald Ade, Cheng-Hao Ko, and Janos Kirz
Steven L. Hulbert and Erik D. Johnson
Erik Anderson, Dieter Kern

MAXIMUM (SRC, Wisconsin, USA)

Franco Cerrina et al.

Ellipsoidal Ring Mirror SPEM (DESY, Hamburg, FRG)

Christoph Kunz et al.

Outline

- Motivation for spectromicroscopy. What can we learn?
- Approaches to spectromicroscopy, microprobe devices.
- Requirements on the source.
- X1-SPEM, instrument details
- First results, present status
- Future outlook: spatial, energy, and time resolution

Why X-Ray Photoemission Microscopy?

- Photoemission/Soft X-Ray Spectroscopies are

  Very Powerful Techniques for Studying

  - Chemistry at Surfaces
  - Geometric and Electronic Structure

- Until Recently, Not Much Lateral Resolution
  - Require Model System (PES)
  - Robust Systems (electron probes: SAM, STEM, etc.)

- Many Systems of Interest Are Inhomogeneous and/or e-Beam Sensitive
  - Oxides/Oxyhydroxides
  - Catalytic Systems
  - Thin Film/Thin Film Growth (polymers esp.)
  - Semiconductor Devices
  - Interfaces, Co-polymers

- PEM Contains More Information than SAM: Primary Photoelectron Peaks and AUGER Peaks (can use Auger parameter)

- XANES Mode for Certain Elements

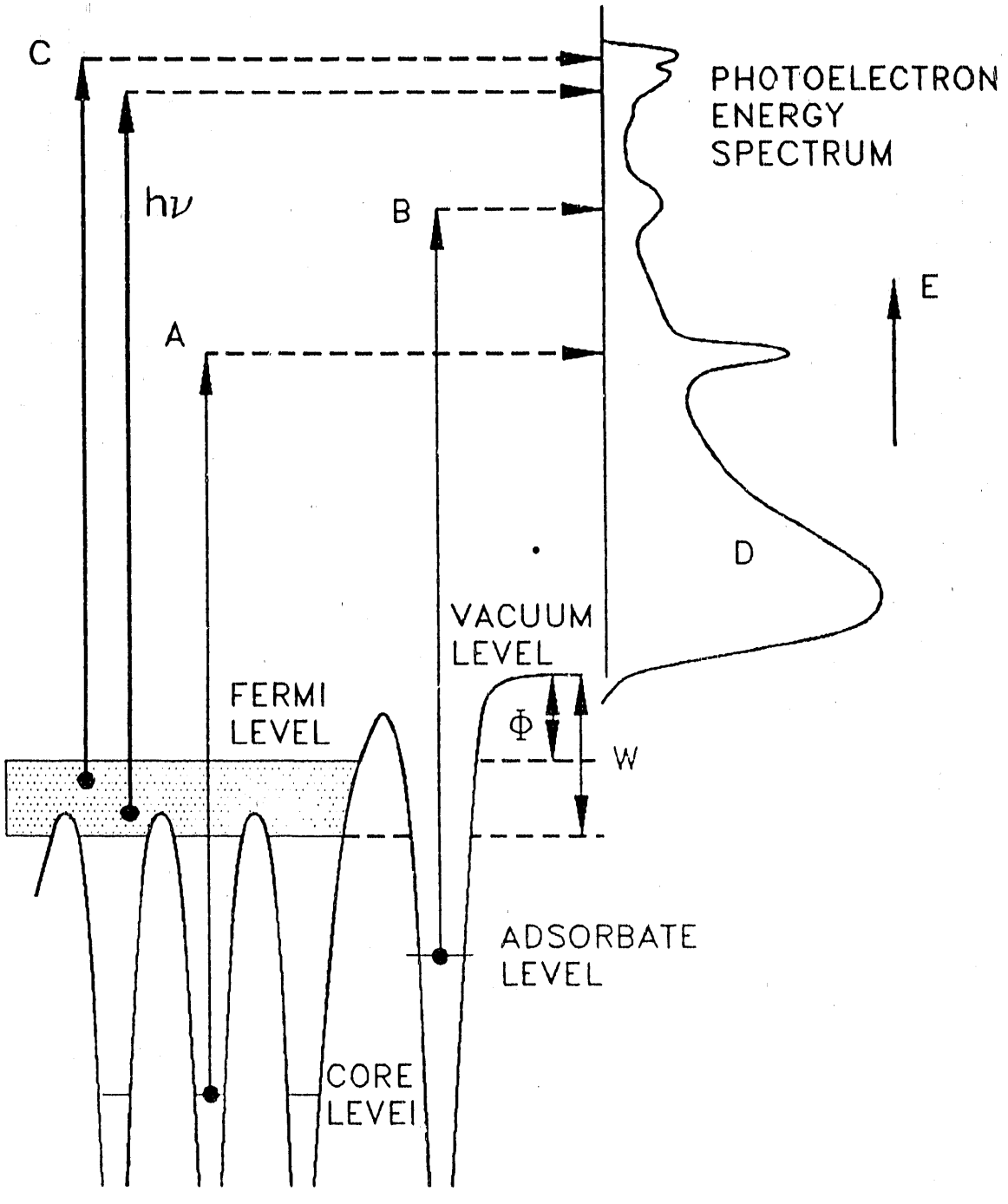

Auger decay of core hole

Chemical Shifts

tri fluoro methyl acrylate

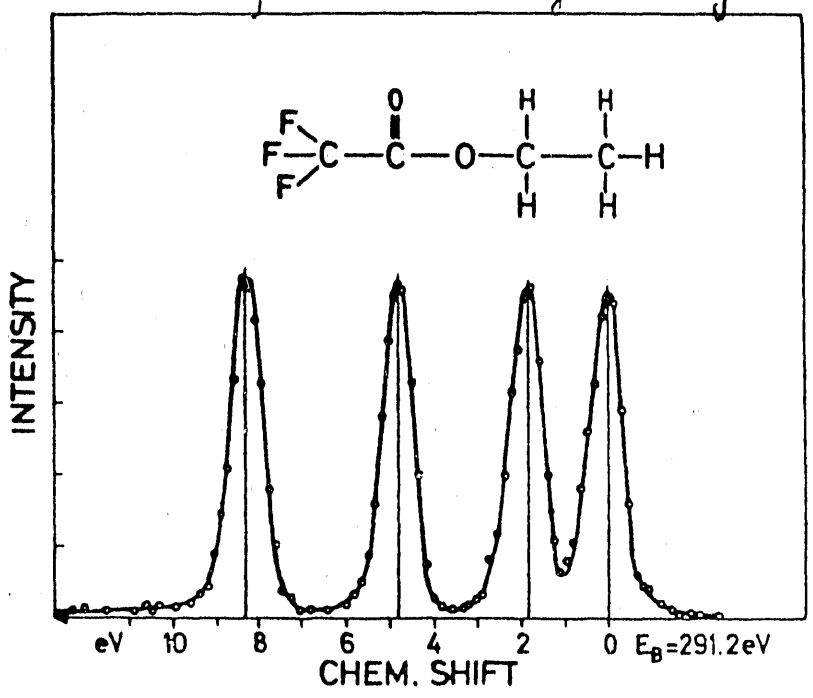

K. Siegbahn et al.

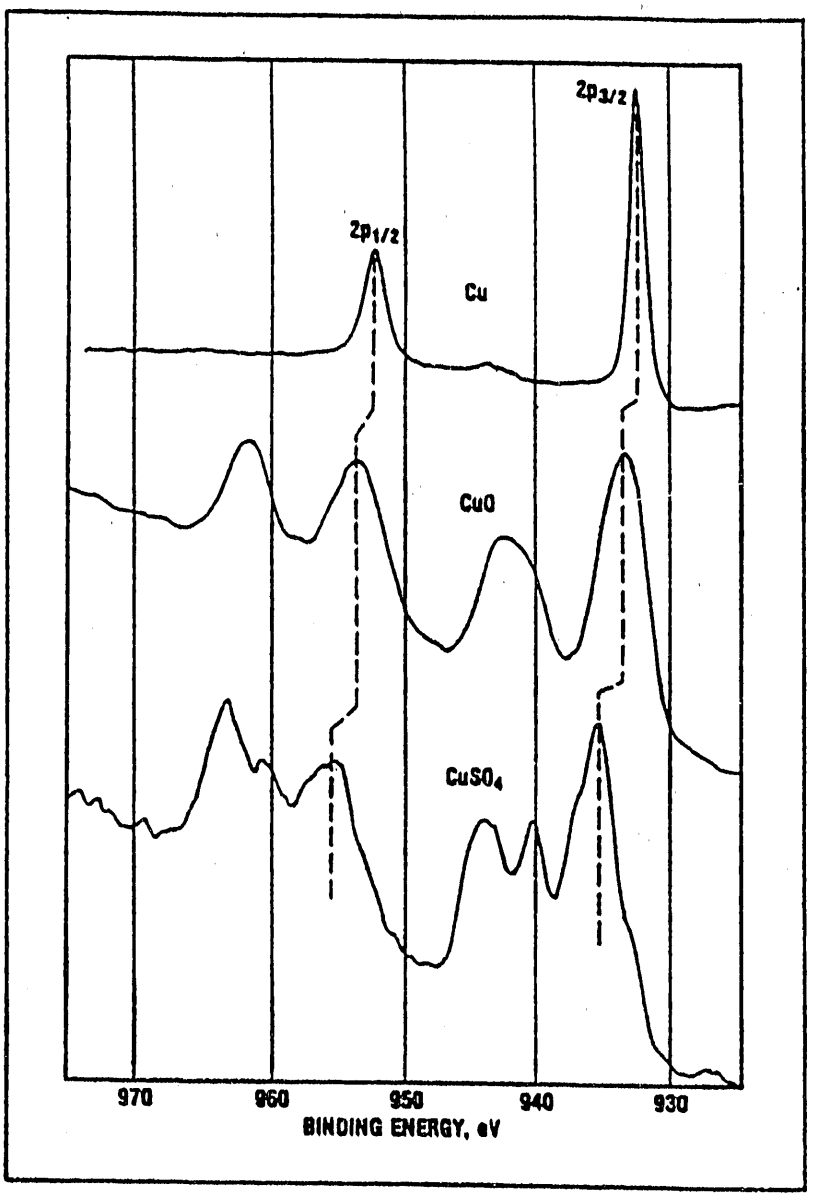
2p3/2
2p1/2
Cu
CuO
CuSO4
970
960
950
940
930
BINDING ENERGY, eV

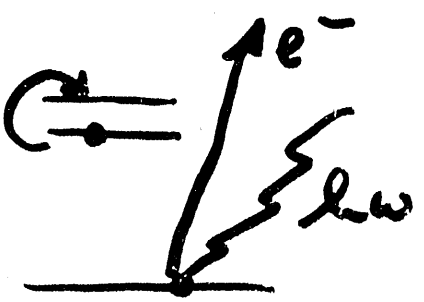
e⁻
hω

Approaches to Spectromicroscopy

Image e- (Electron Optical Instruments):

- electro-static (Bauer-Telieps, Tonner micro-XANES)

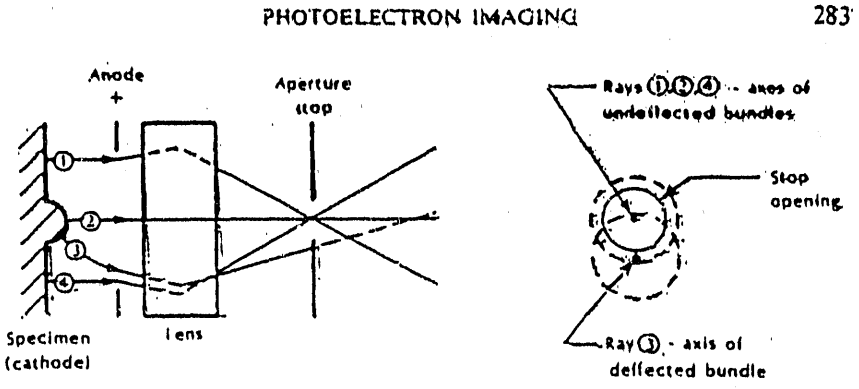

- magneto-static (Beamson, Pianetta)

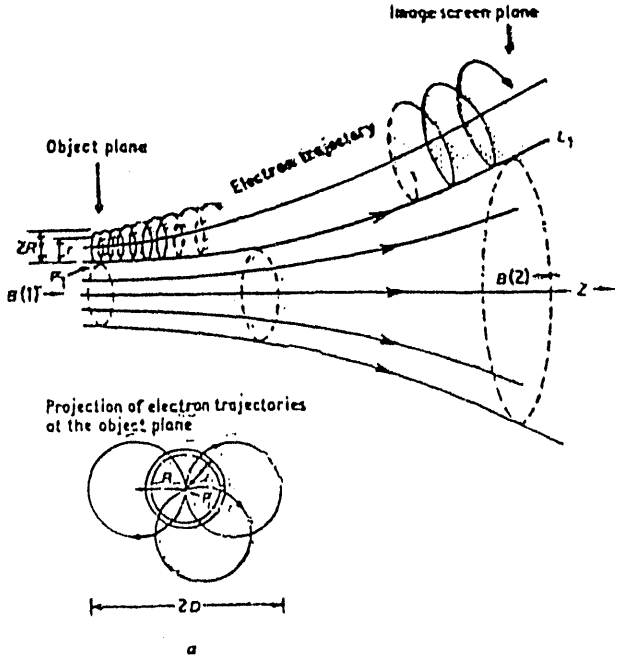

Focus X-rays (Microprobe Instruments):

- **normal incidence multilayer Schwarzschild (F.Cerrina)**

potentially very high spatial resolution

stiff limit (3mm) ≈ 6mm

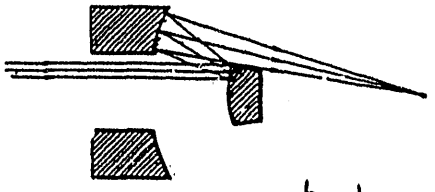

f + f(λ)
WD few cm

but only few % BW tunability

Figure 1. 0.3 N.A. Schwarzschild objective

presently hν < 280 eV

- **grazing incidence ellipsoid (Kunz)**

20 eV → 2000 eV f + f(λ)

inefficient beam 95% obstructed (radius)

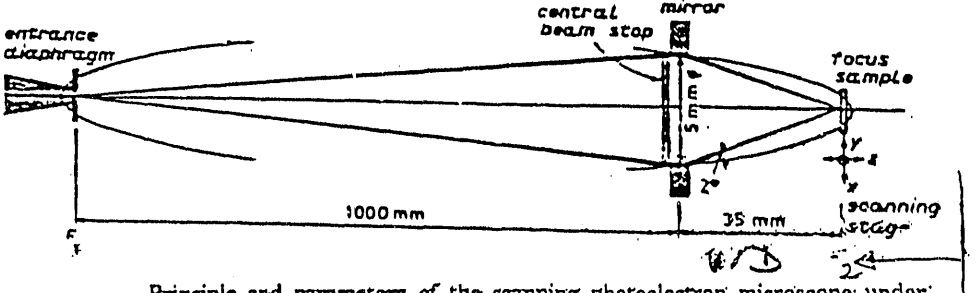

Principle and parameters of the scanning photoelectron microscope under construction at HASYLAB. F_1, F_2 are the foci of the elliptical mirror.

Central obstruction → more flux into outer lobes of Airy pattern

- **zone plate (SPEM)**

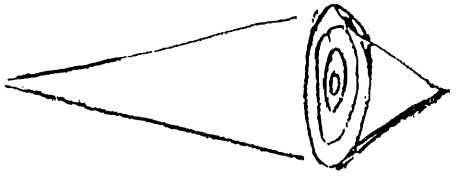

~100 eV → ~2000 eV
tunable over ~15% BW (so far)

$f \propto E \left(\propto \frac{1}{\lambda}\right)$

WD ≈ 1-2 mm

Diffraction limited resolution

$$d \propto \frac{\lambda}{2\,N.A.}$$

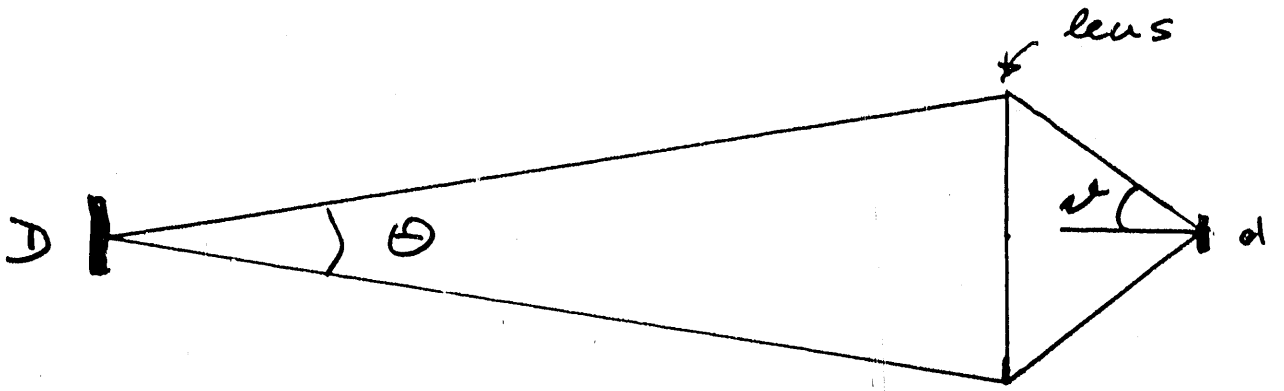

for small angles $\alpha \propto N.A.$

$$\xrightarrow{(1)} \quad 2\alpha d \propto \lambda$$

Liouville's Theorem (conservation of photon phase space)

$$D\theta = 2\alpha d \propto \lambda$$

∴ for smallest possible probe size need to limit the accepted source phase space to about λ i.e. need coherent illumination

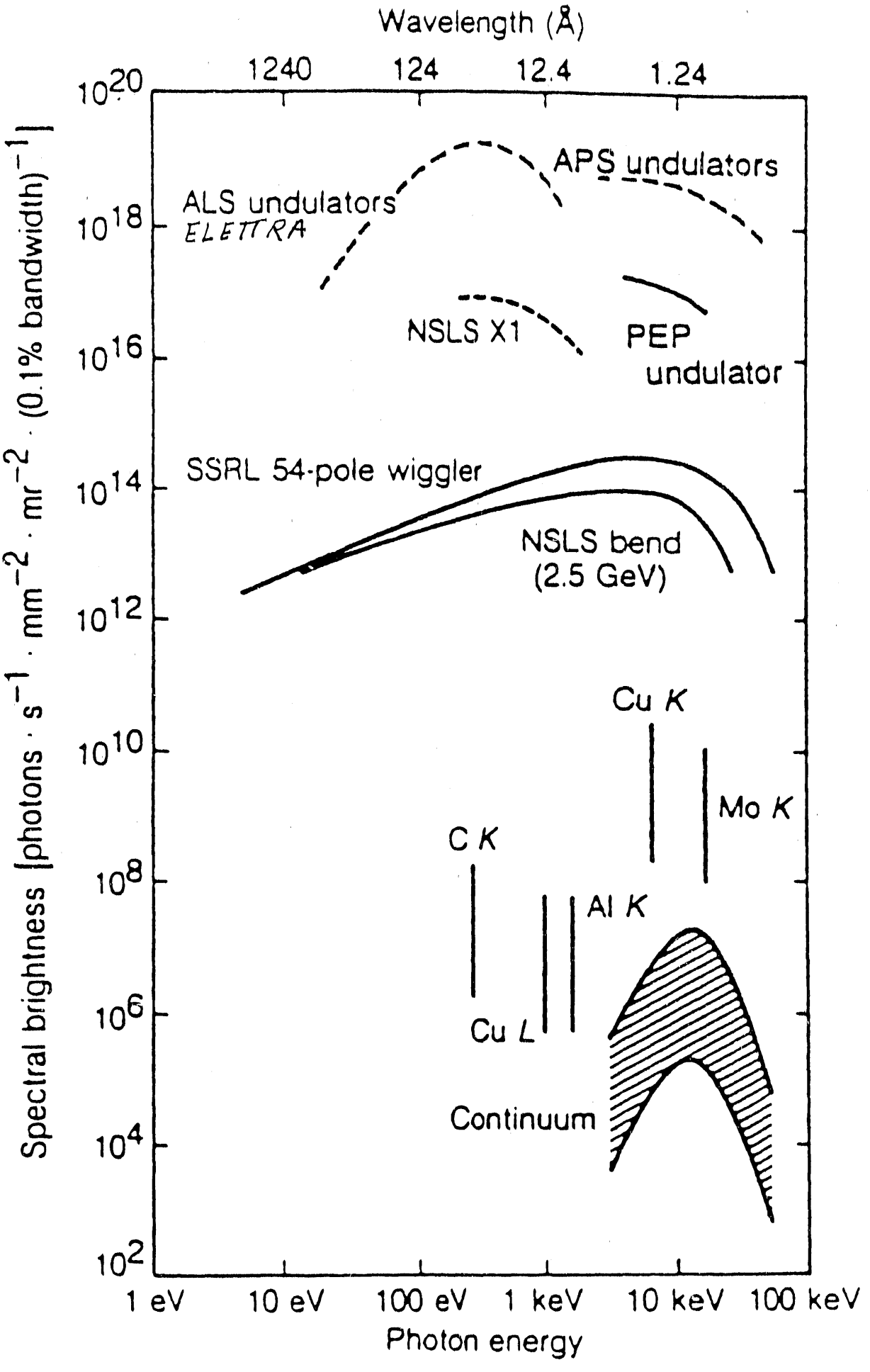
Wavelength (Å)
1240
124
12.4
1.24
10^{20}
10^{18}
10^{16}
10^{14}
10^{12}
10^{10}
10^{8}
10^{6}
10^{4}
10^{2}
Spectral brightness [photons · s^{-1} · mm^{-2} · mr^{-2} · (0.1% bandwidth)$^{-1}$]
ALS undulators
ELETTRA
APS undulators
NSLS X1
PEP
undulator
SSRL 54-pole wiggler
NSLS bend
(2.5 GeV)
Cu K
Mo K
C K
Al K
Cu L
Continuum
1 eV
10 eV
100 eV
1 keV
10 keV
100 keV
Photon energy

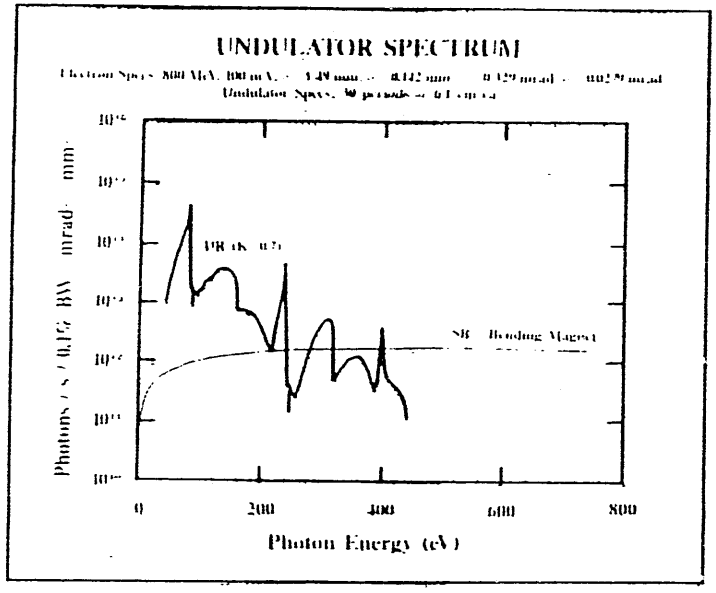

Scanning Soft X-ray Microscope (MAXIMUM)

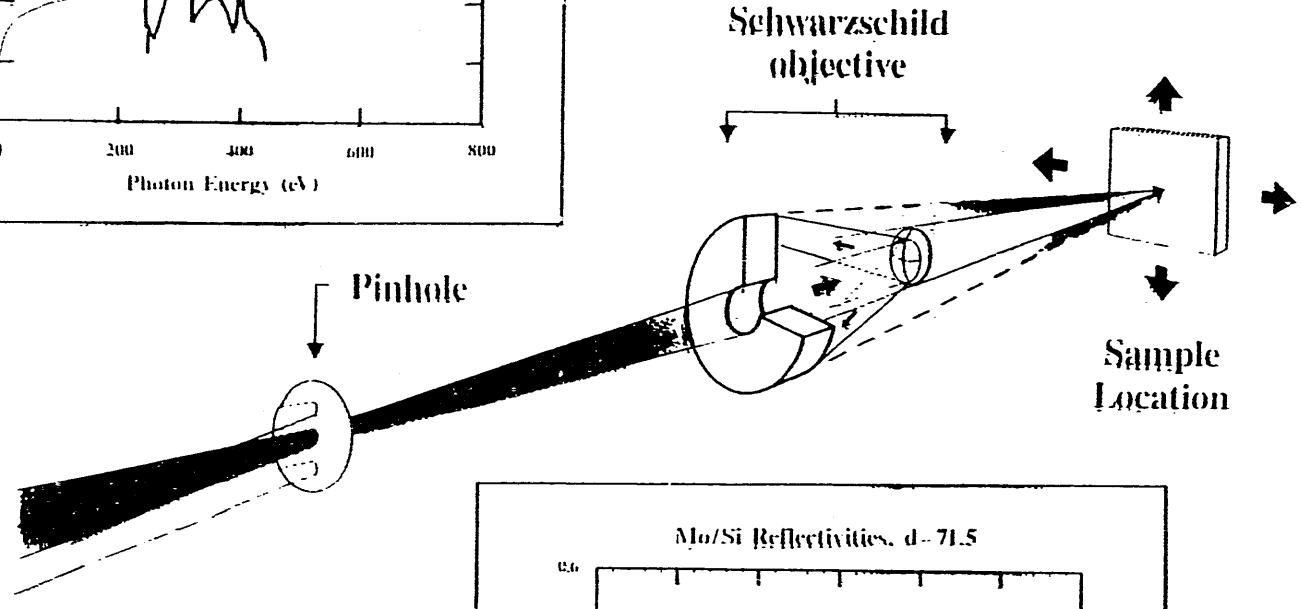

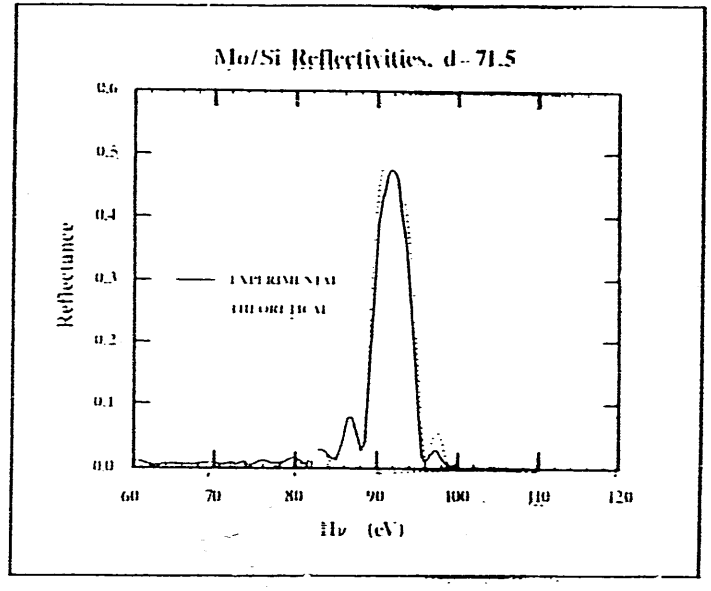

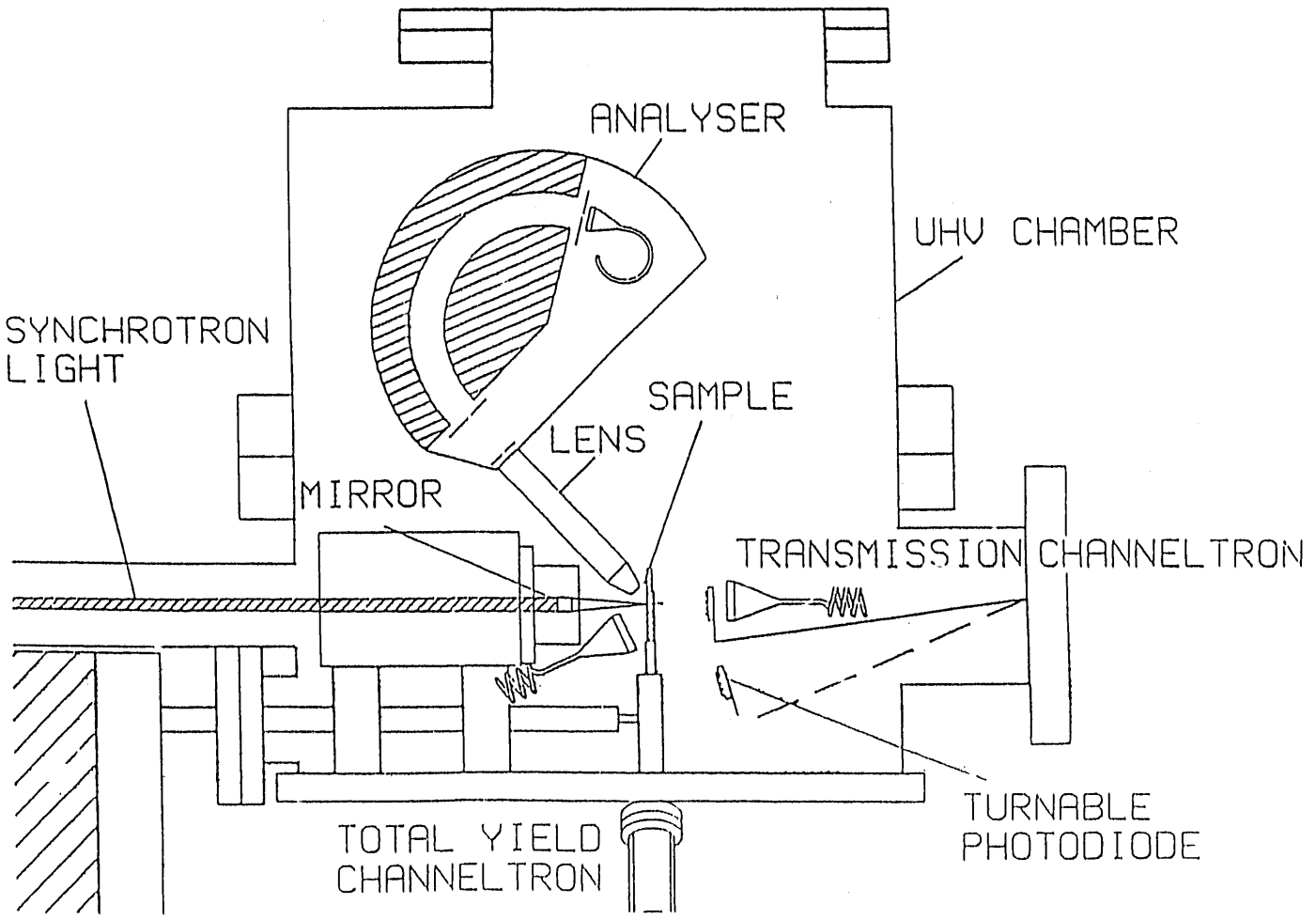
ANALYSER
UHV CHAMBER
SYNCHROTRON
LIGHT
SAMPLE
LENS
MIRROR
TRANSMISSION CHANNELTRON
TURNABLE
PHOTODIODE
TOTAL YIELD
CHANNELTRON

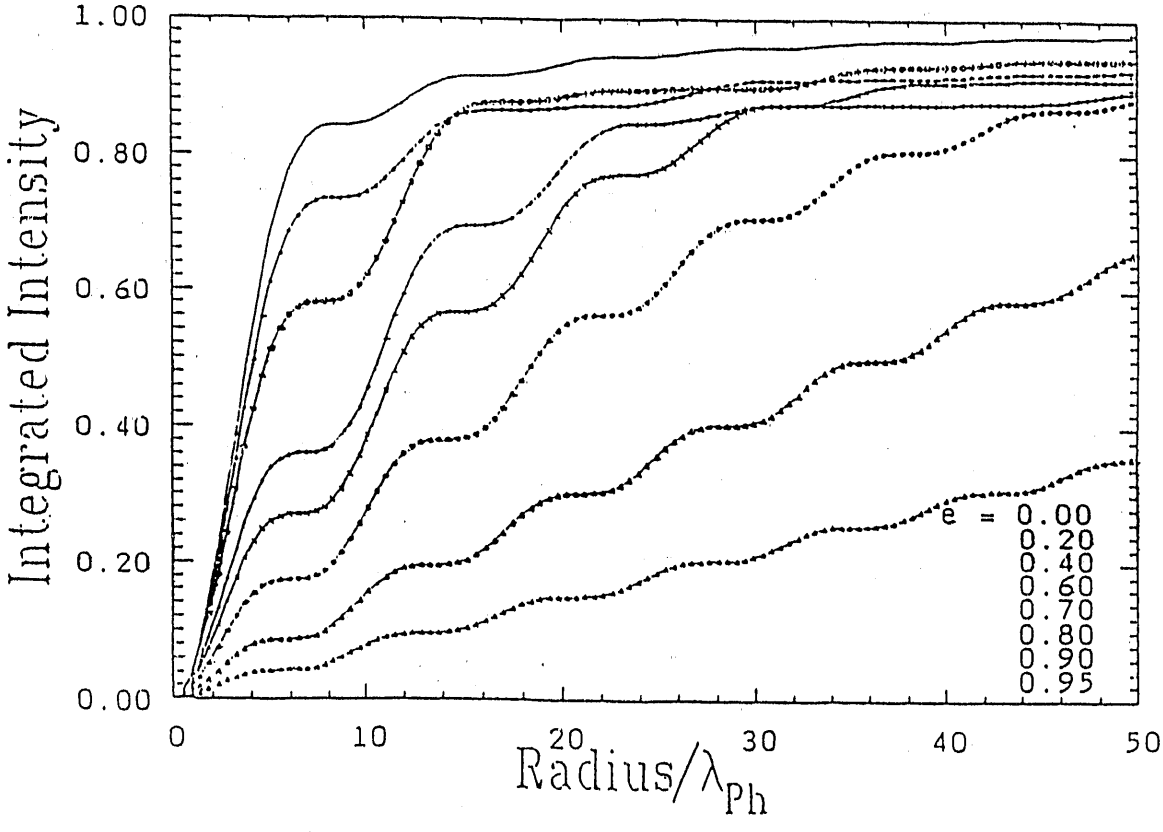
1.00
0.80
0.60
0.40
0.20
0.00
Integrated Intensity
0
10
20
30
40
50
Radius/λ_{Ph}
e = 0.00
0.20
0.40
0.60
0.70
0.80
0.90
0.95

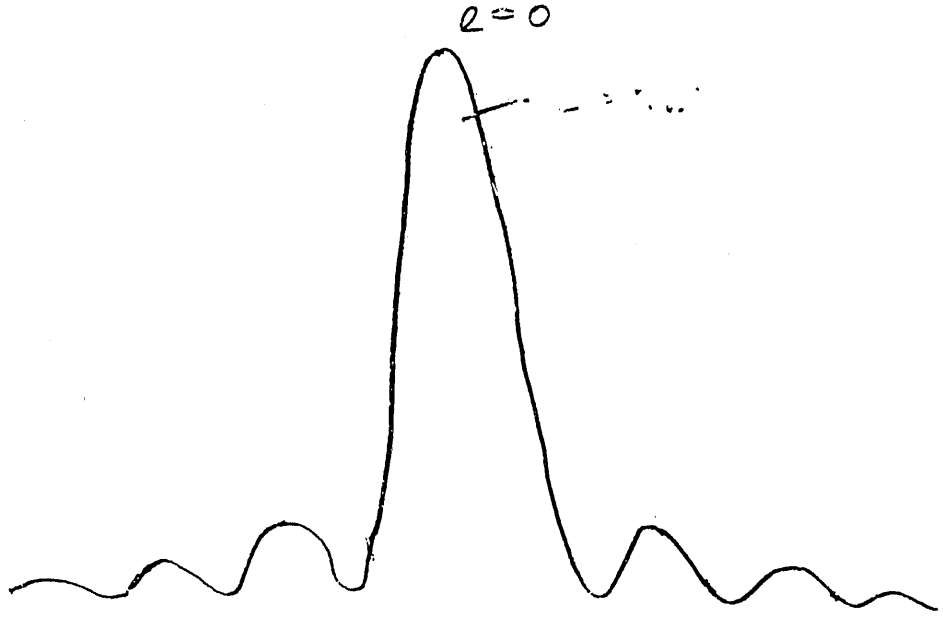
e = 0

KUNZ ET AL.

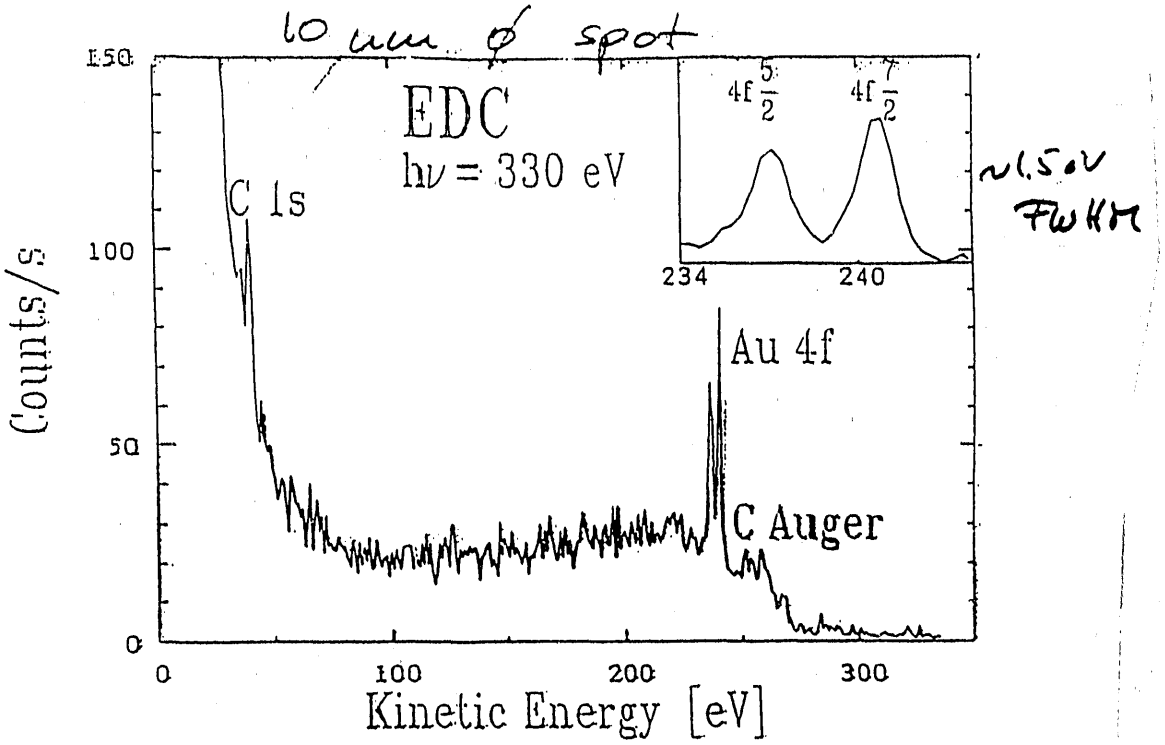
10 mm ϕ spot
EDC
hν = 330 eV
C 1s
Au 4f
C Auger
4f 5/2
4f 7/2
234
240
≈1.5eV FWHM
Counts/s
Kinetic Energy [eV]
0
50
100
150
0
100
200
300

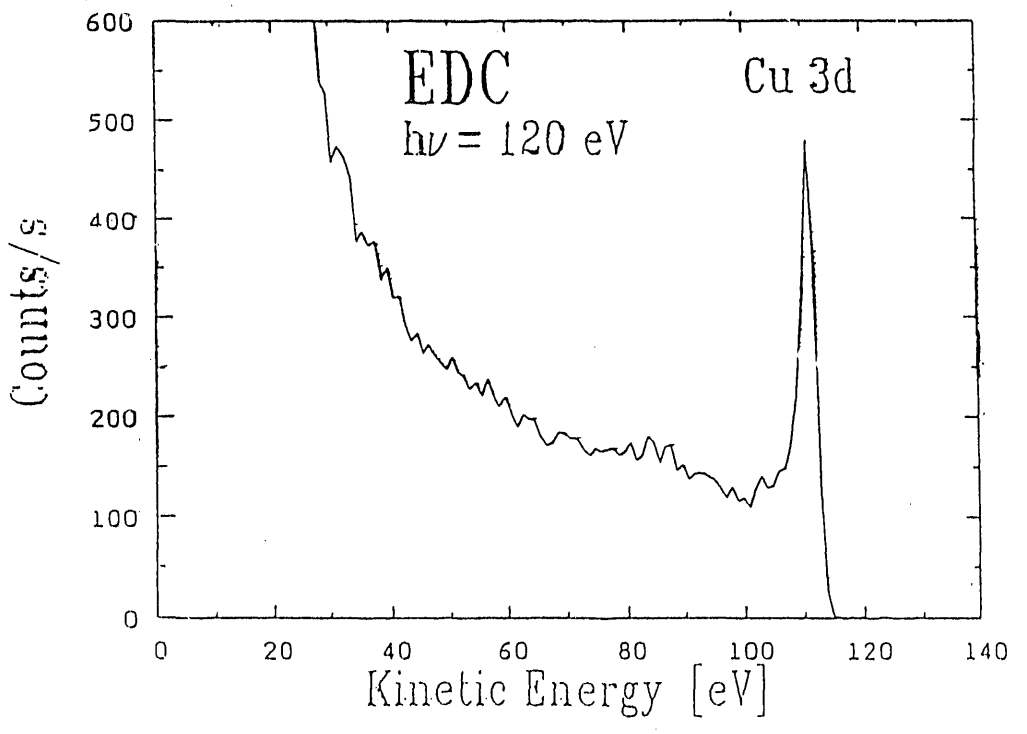
EDC
hν = 120 eV
Cu 3d
Counts/s
Kinetic Energy [eV]
0
100
200
300
400
500
600
0
20
40
60
80
100
120
140

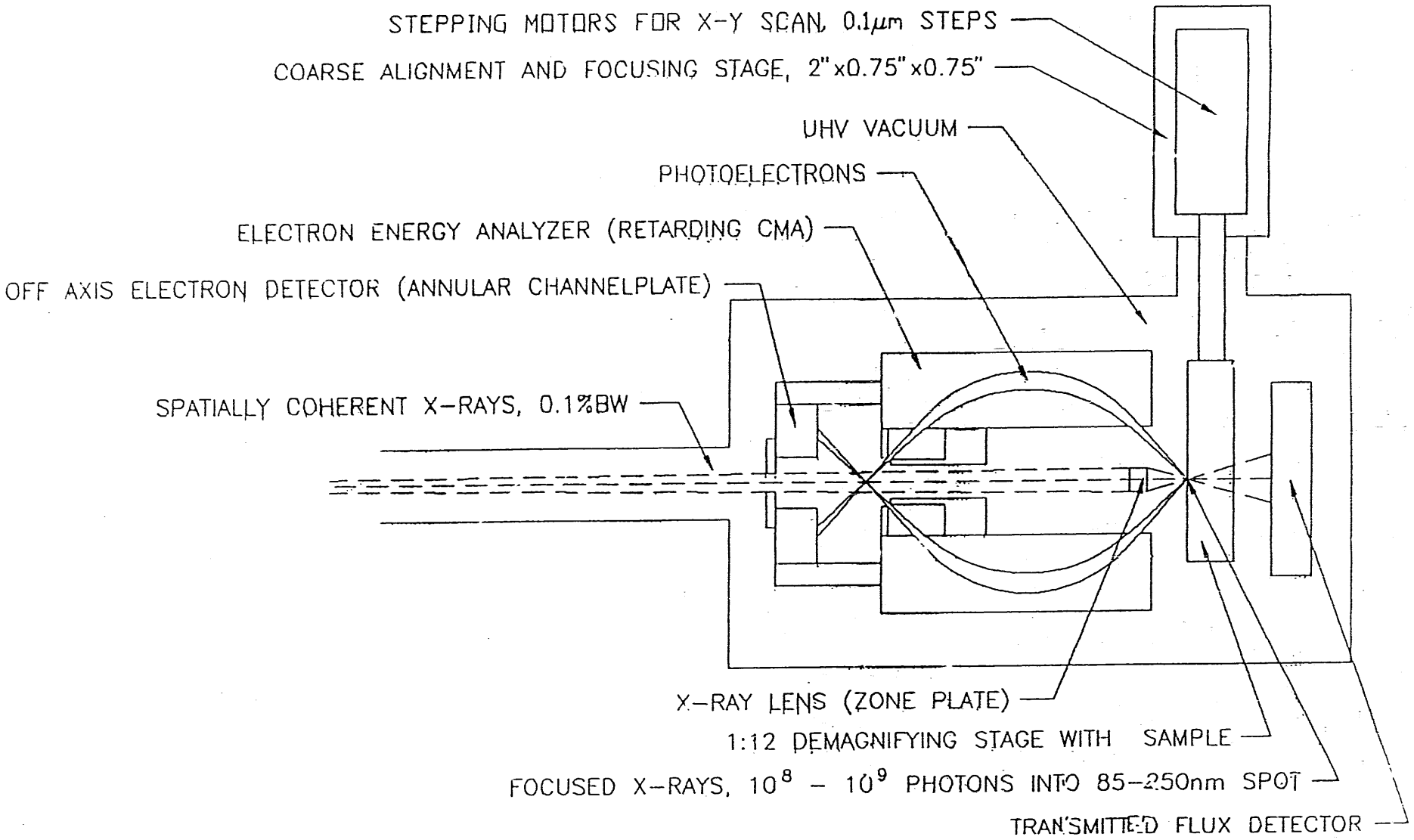
STEPPING MOTORS FOR X-Y SCAN, 0.1μm STEPS
COARSE ALIGNMENT AND FOCUSING STAGE, 2"x0.75"x0.75"
UHV VACUUM
PHOTOELECTRONS
ELECTRON ENERGY ANALYZER (RETARDING CMA)
OFF AXIS ELECTRON DETECTOR (ANNULAR CHANNELPLATE)
SPATIALLY COHERENT X-RAYS, 0.1%BW
X-RAY LENS (ZONE PLATE)
1:12 DEMAGNIFYING STAGE WITH SAMPLE
FOCUSED X-RAYS, 10^8 - 10^9 PHOTONS INTO 85-250nm SPOT
TRANSMITTED FLUX DETECTOR

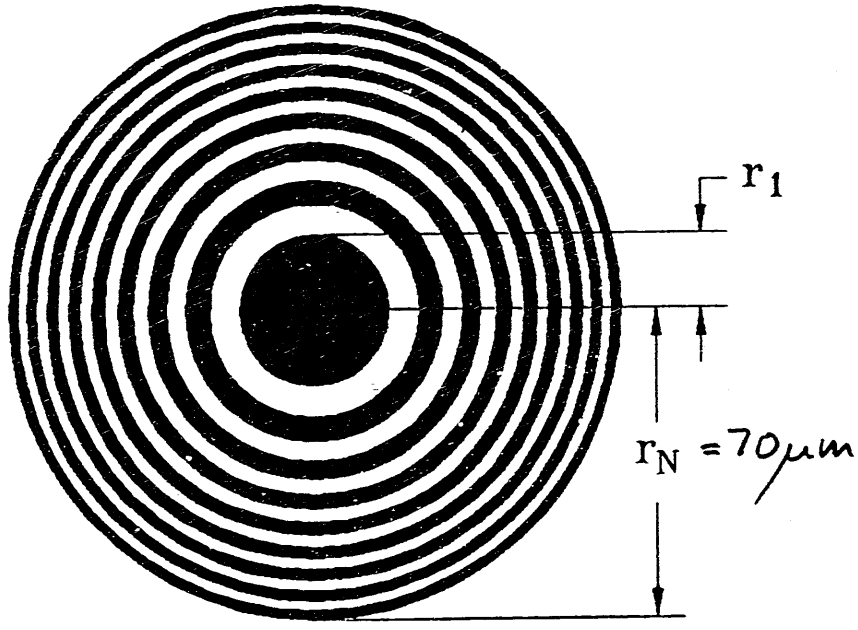

$\delta_1 \leftarrow \frac{\lambda}{2\,N.A}$

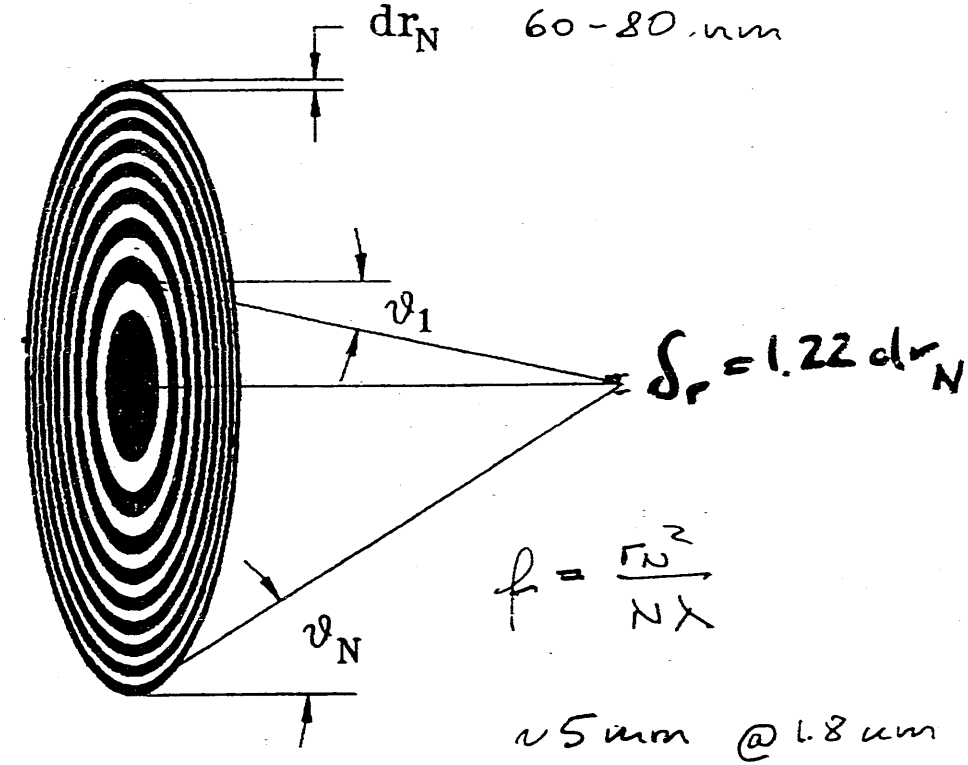

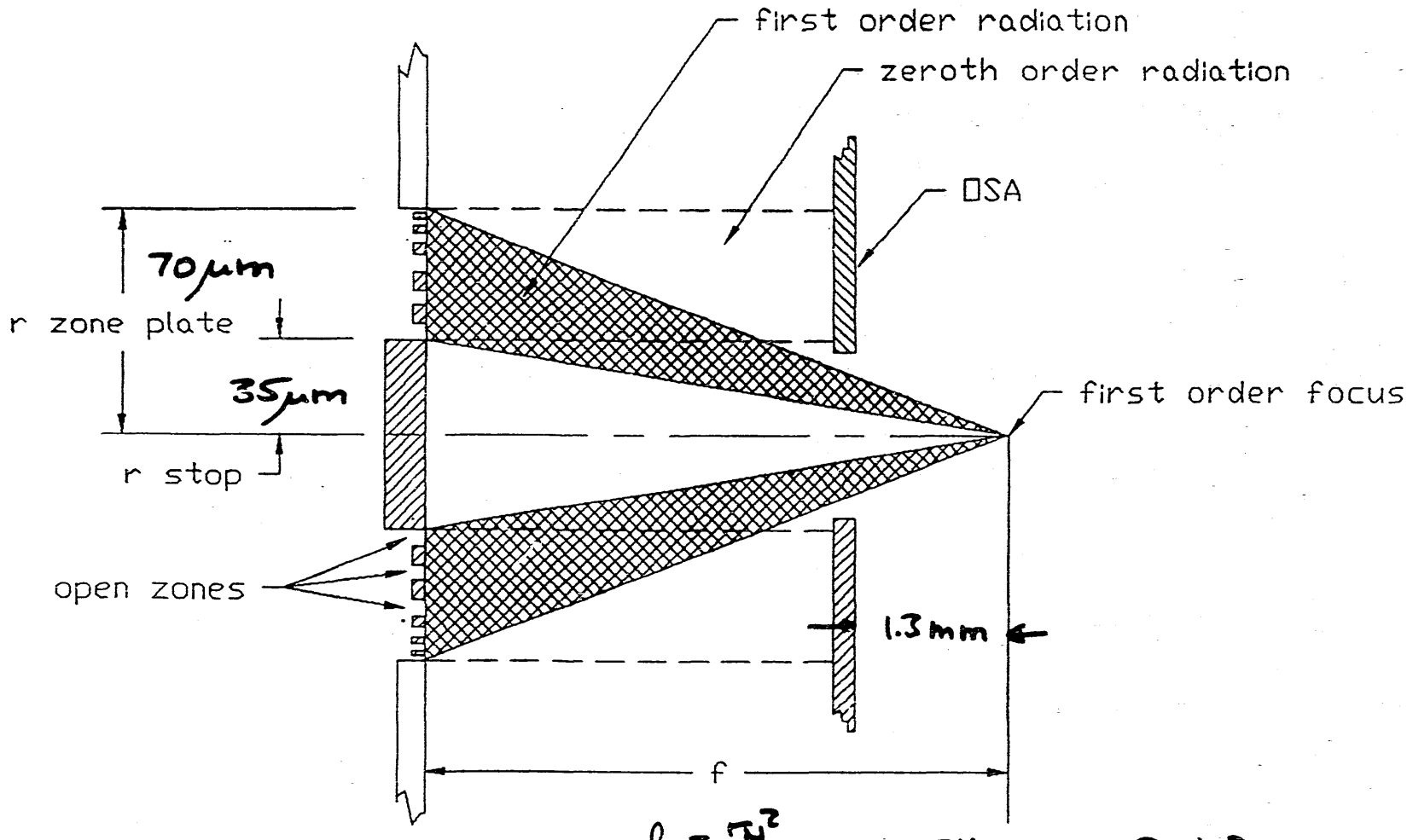
first order radiation
zeroth order radiation
OSA
70μm
r zone plate
35μm
r stop
first order focus
open zones
1.3mm
f
$f = \frac{\pi r^2}{N\lambda}$ → 5.4mm @ 1.8nm

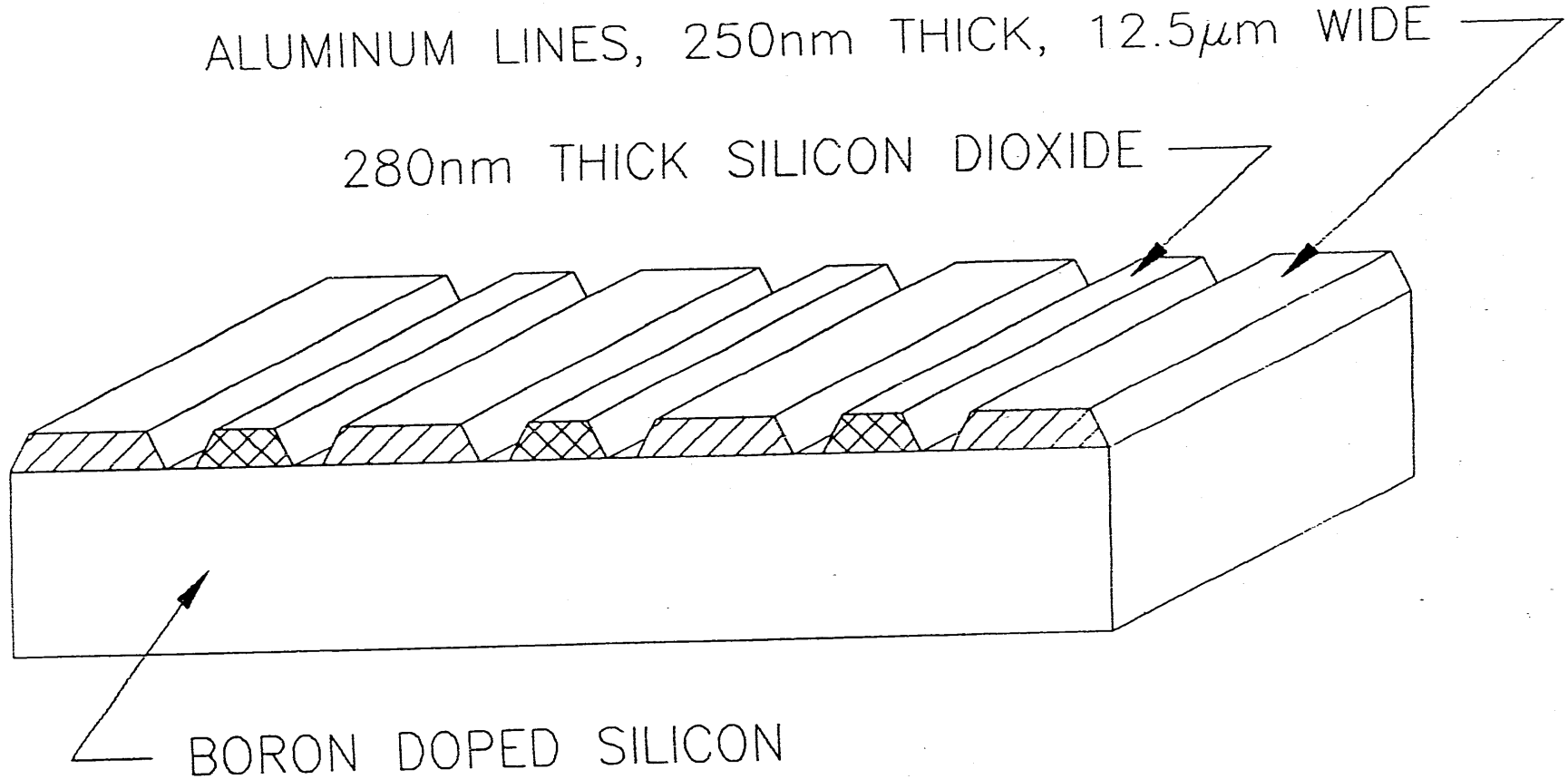
ALUMINUM LINES, 250nm THICK, 12.5μm WIDE
280nm THICK SILICON DIOXIDE
BORON DOPED SILICON

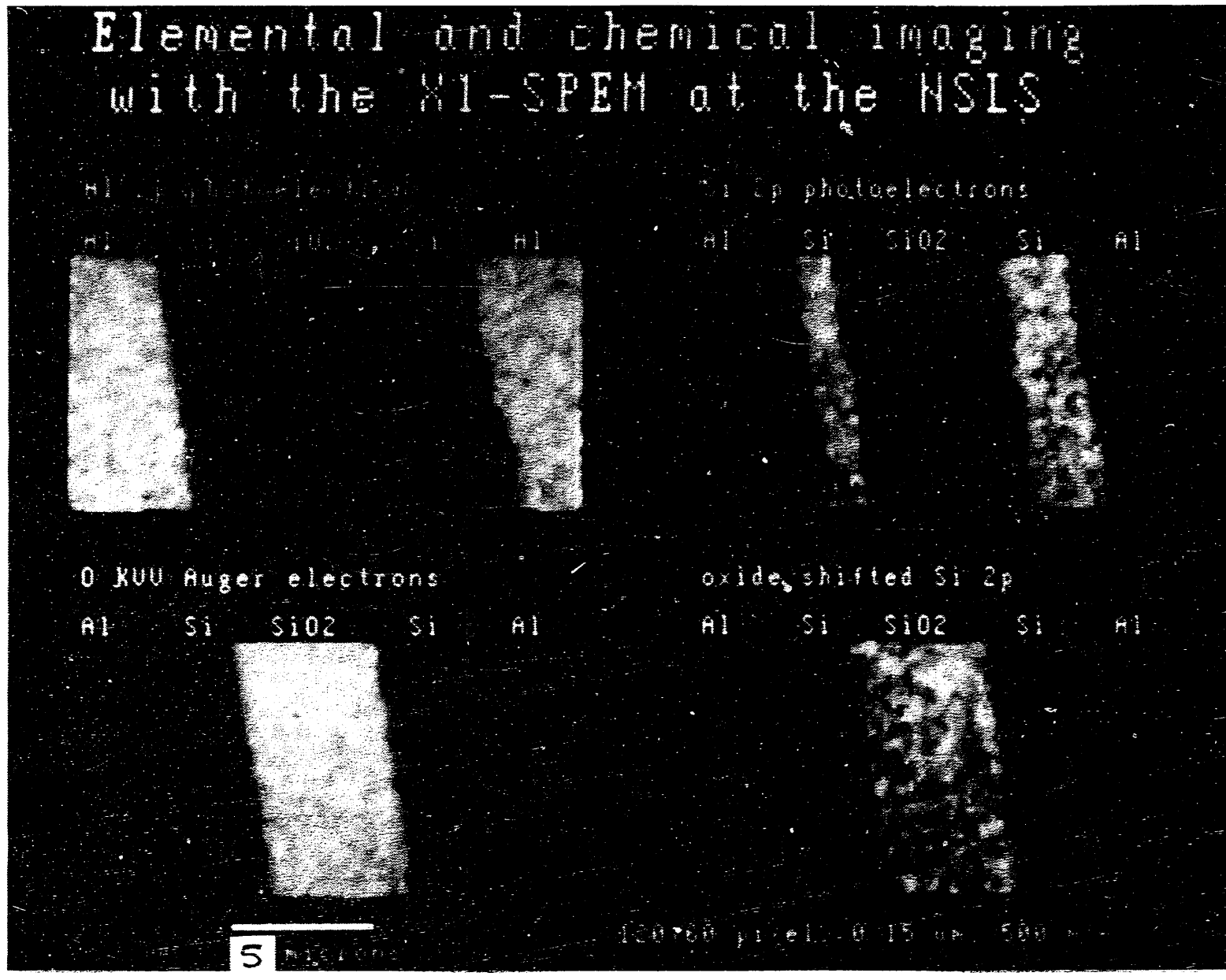
Elemental and chemical imaging
with the X1-SPEM at the NSLS
Si 2p photoelectrons
Al Si SiO2 Si Al
O KVV Auger electrons
Al Si SiO2 Si Al
oxide shifted Si 2p
Al Si SiO2 Si Al
5

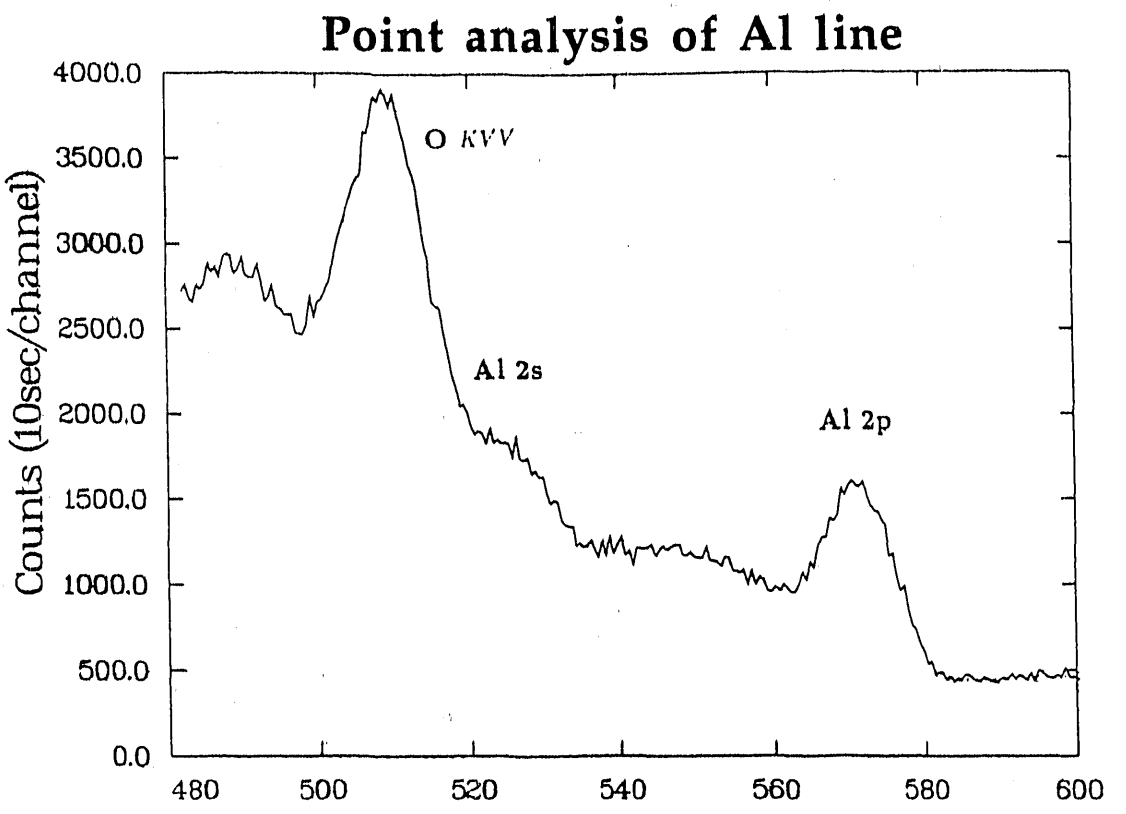
Point analysis of Al line
Counts (10sec/channel)
4000.0
3500.0
3000.0
2500.0
2000.0
1500.0
1000.0
500.0
0.0
O KVV
Al 2s
Al 2p
480
500
520
540
560
580
600

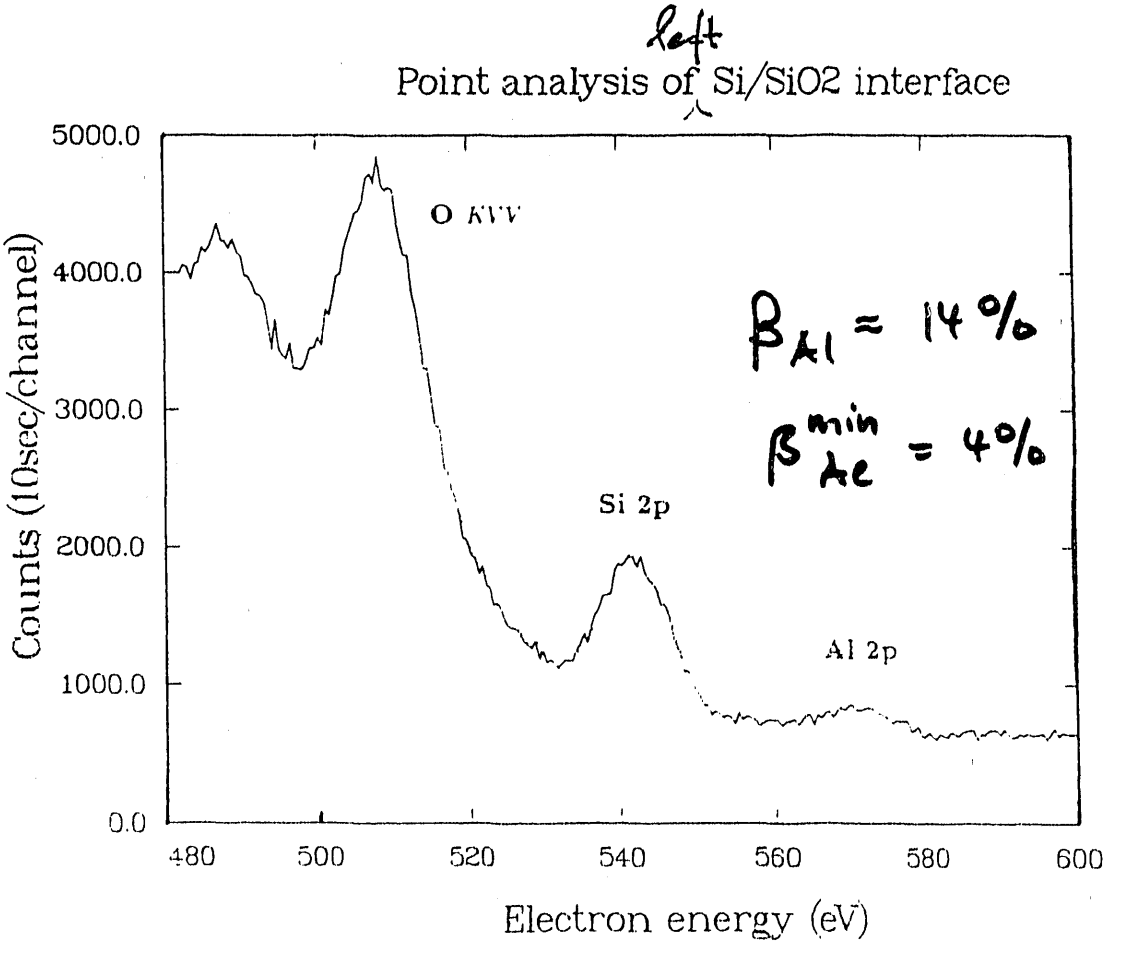
left
Point analysis of Si/SiO2 interface
Counts (10sec/channel)
5000.0
4000.0
3000.0
2000.0
1000.0
0.0
O KVV
Si 2p
Al 2p
$\beta_{Al} = 14\%$
$\beta_{Ac}^{min} = 4\%$
480
500
520
540
560
580
600
Electron energy (eV)

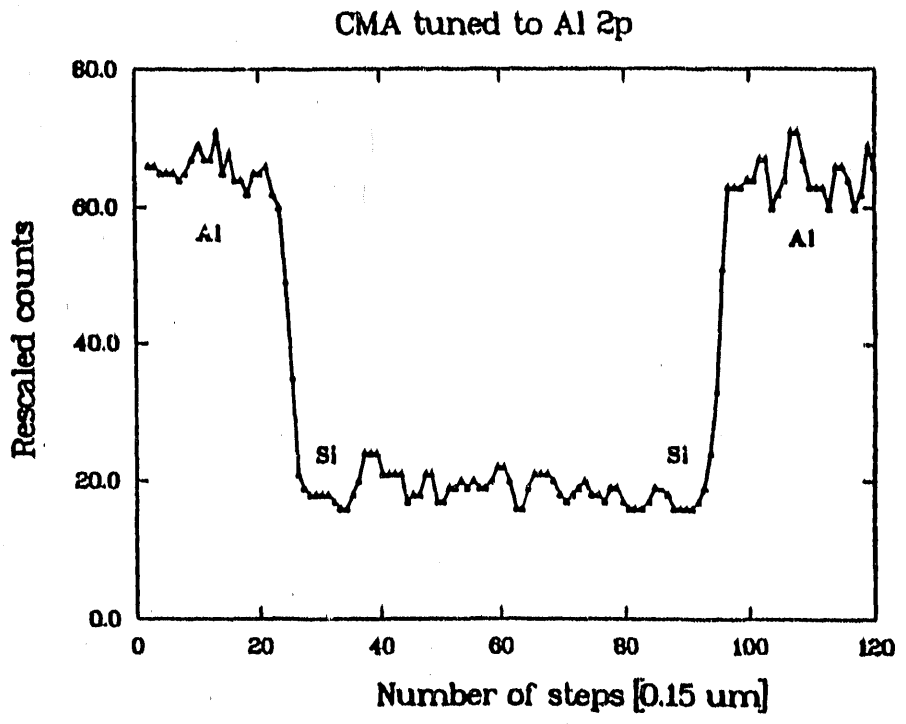
CMA tuned to Al 2p
Rescaled counts
Number of steps [0.15 um]
Al
Si
Si
Al
60.0
40.0
20.0
0.0
0
20
40
60
80
100
120

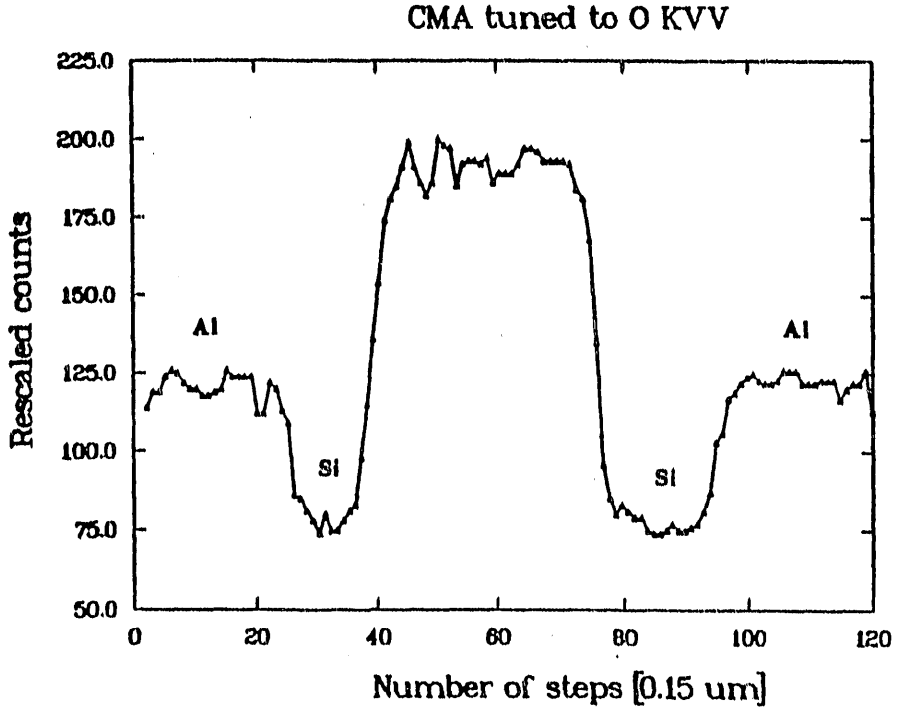
CMA tuned to O KVV
Rescaled counts
Number of steps [0.15 um]
Al
Si
Si
Al
225.0
200.0
175.0
150.0
125.0
100.0
75.0
50.0
0
20
40
60
80
100
120

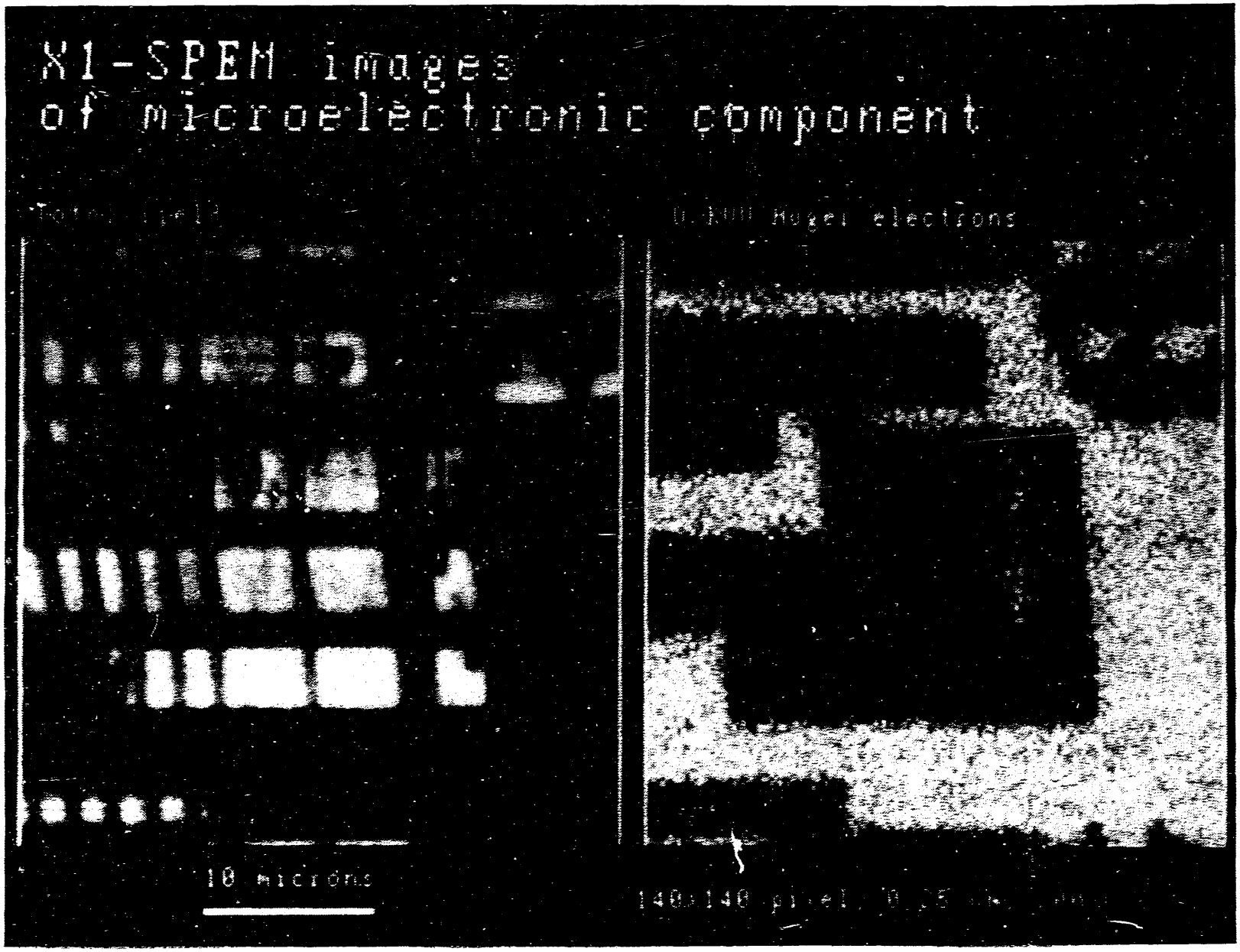
X1-SPEM images
of microelectronic component
10 microns

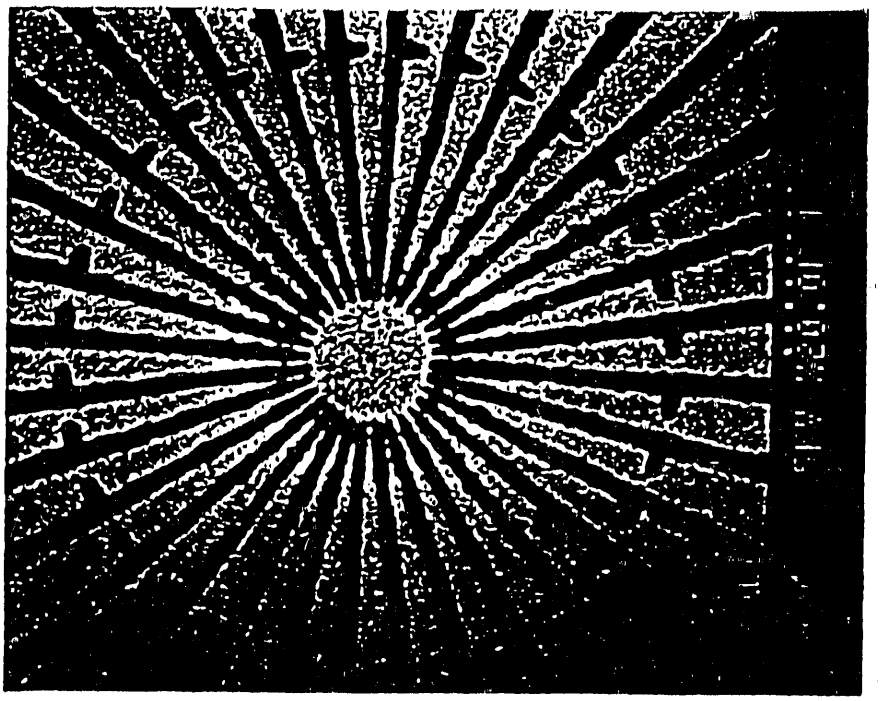

bright = transparent bright = transparent

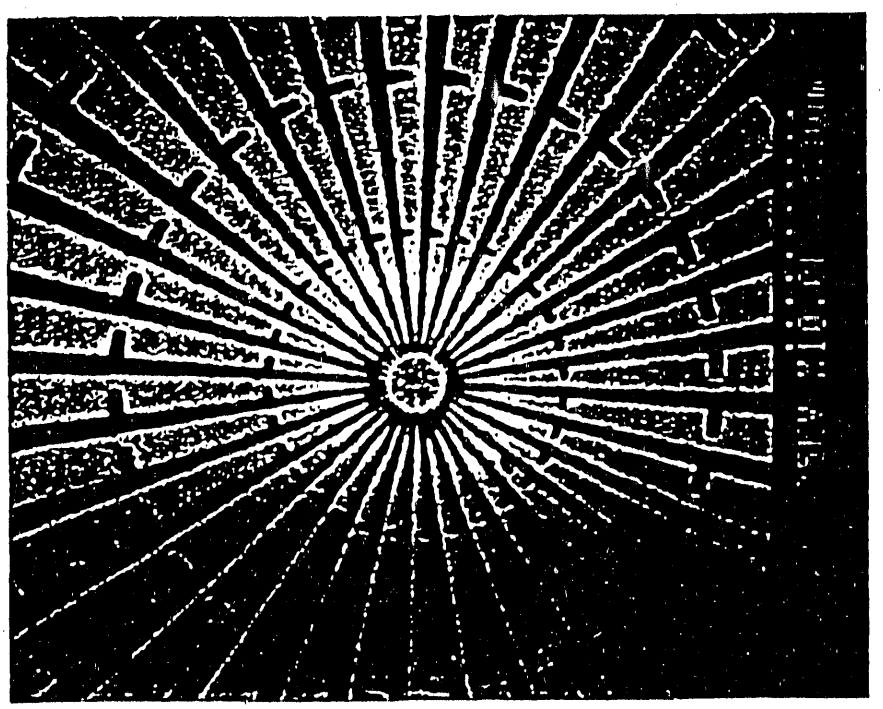

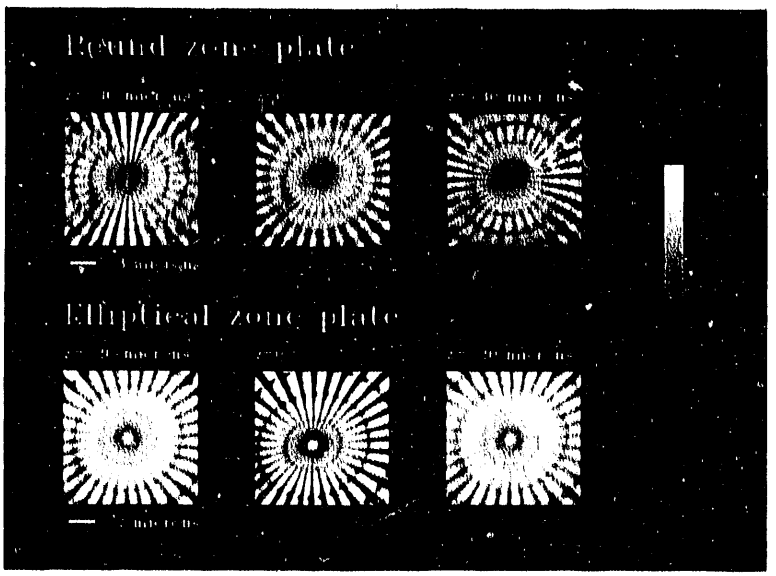
Round zone plate
Elliptical zone plate

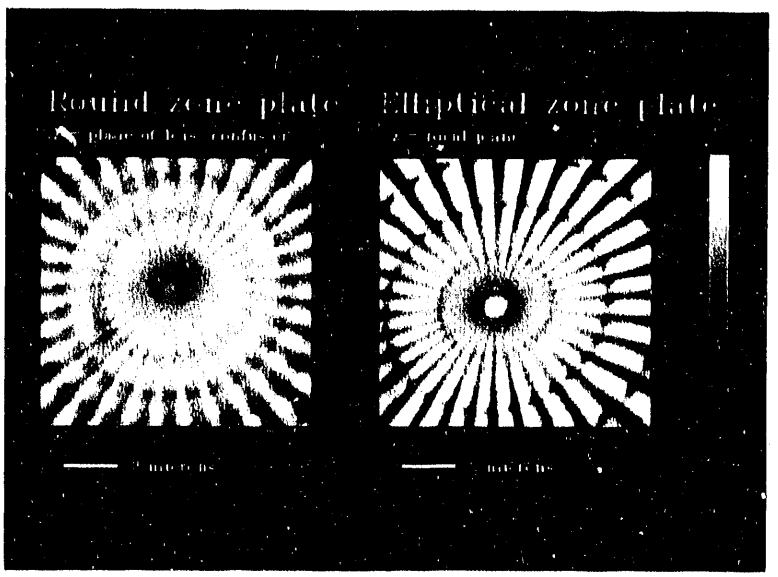
Round zone plate
Elliptical zone plate

Jacobsen, Zhang et al

GAWE

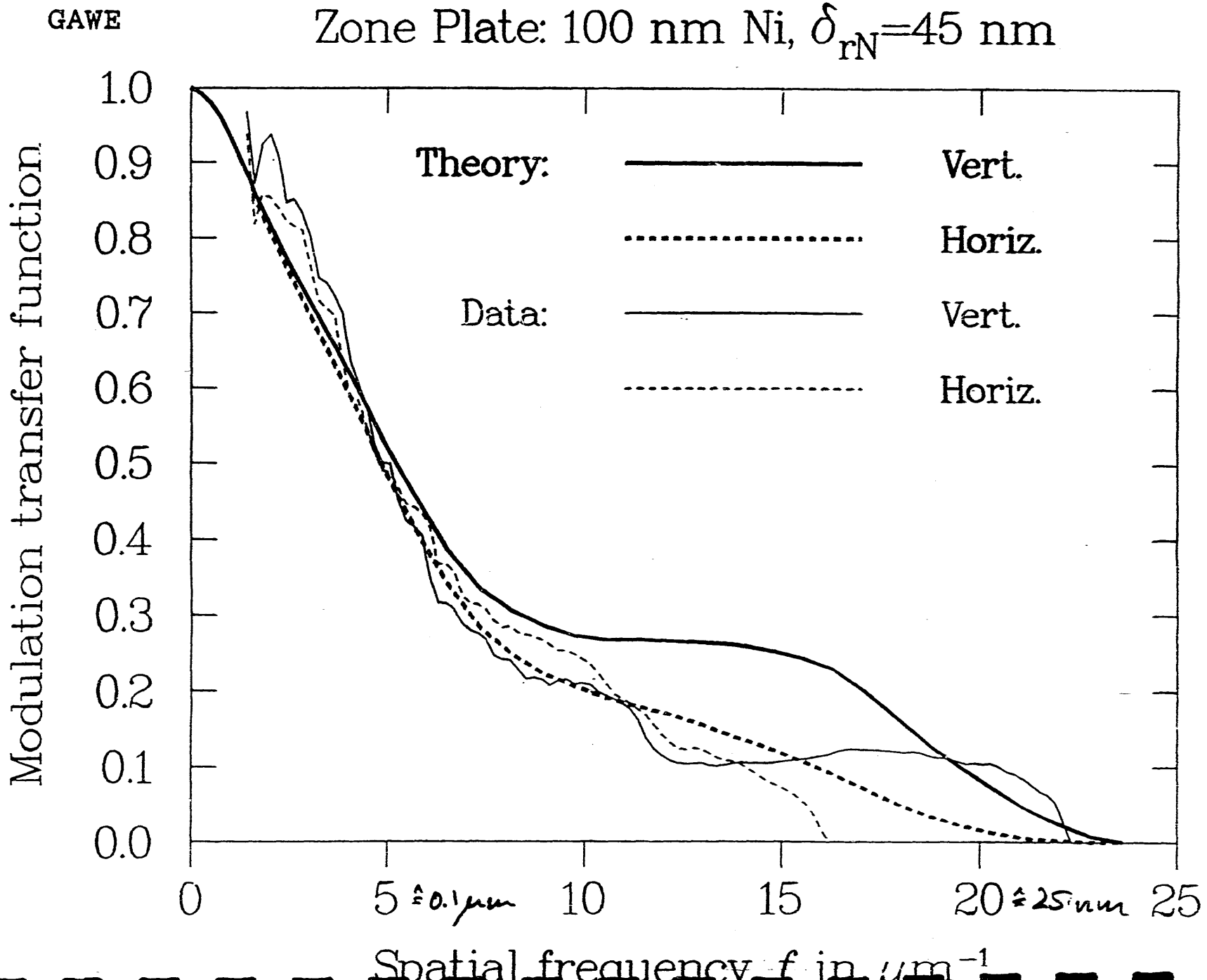

NI MTF_LIN.MAP

Possible Experiments

- Heterogeneous Alumina ($Al_2O_3 + \varepsilon H_2O$)
  - Catalyst or used as support for catalysts
  - Surface acidity depends strongly on binding energy of hydrogen in the hydroxyl group (alumina phase, local geometry)
  - Dosing with ammonia, various alcohols, CO, and CO_2

TEM Czanderna et al.

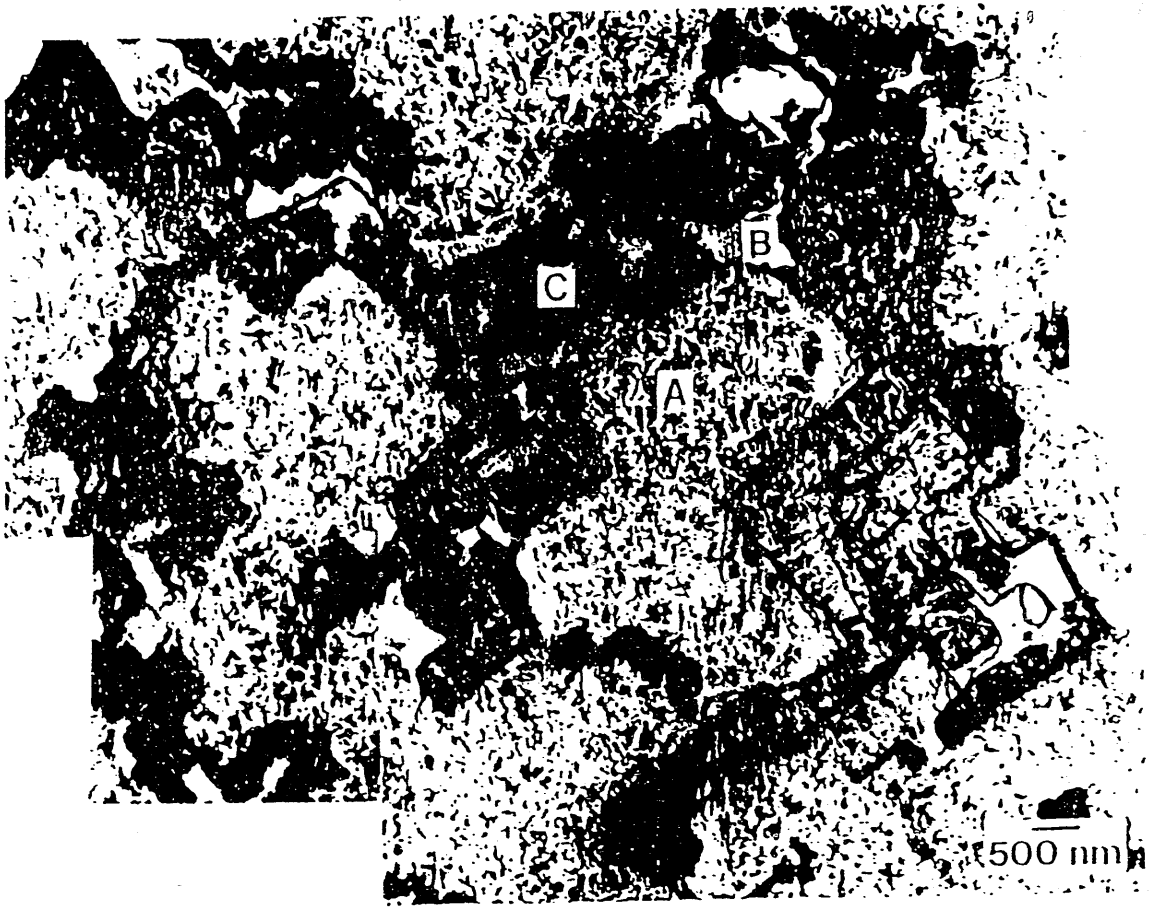

Growth habit observed on 5 9's pure, polished, polycrystalline coupon. Area A: crystalline matrix; B: amorphous; C: piled up amorphous material.

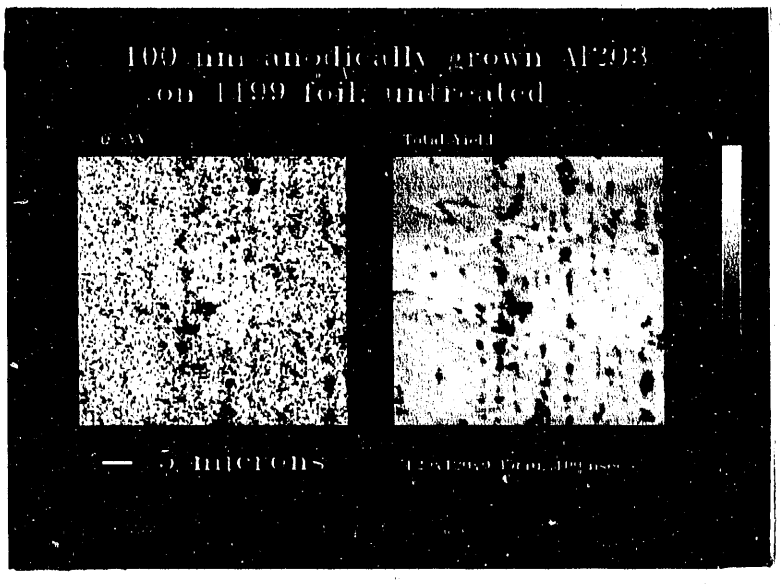
100 nm anodically grown Al2O3
on 1199 foil, untreated
— 5 microns

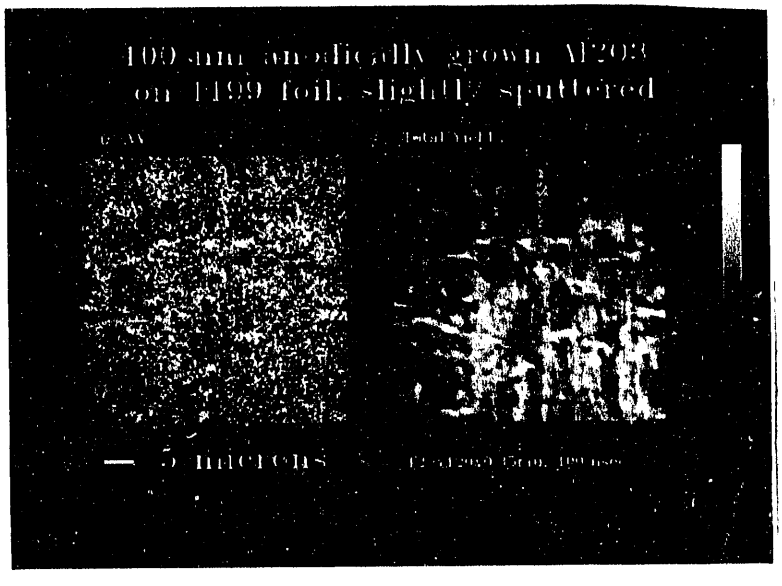
100 nm anodically grown Al2O3
on 1199 foil, slightly sputtered
— 5 microns

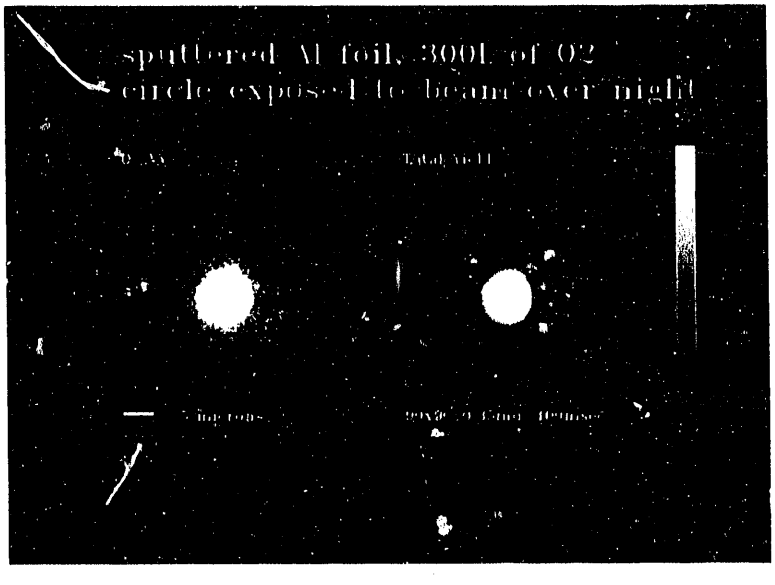
sputtered Al foil, 300L of O2
circle exposed to beam over night

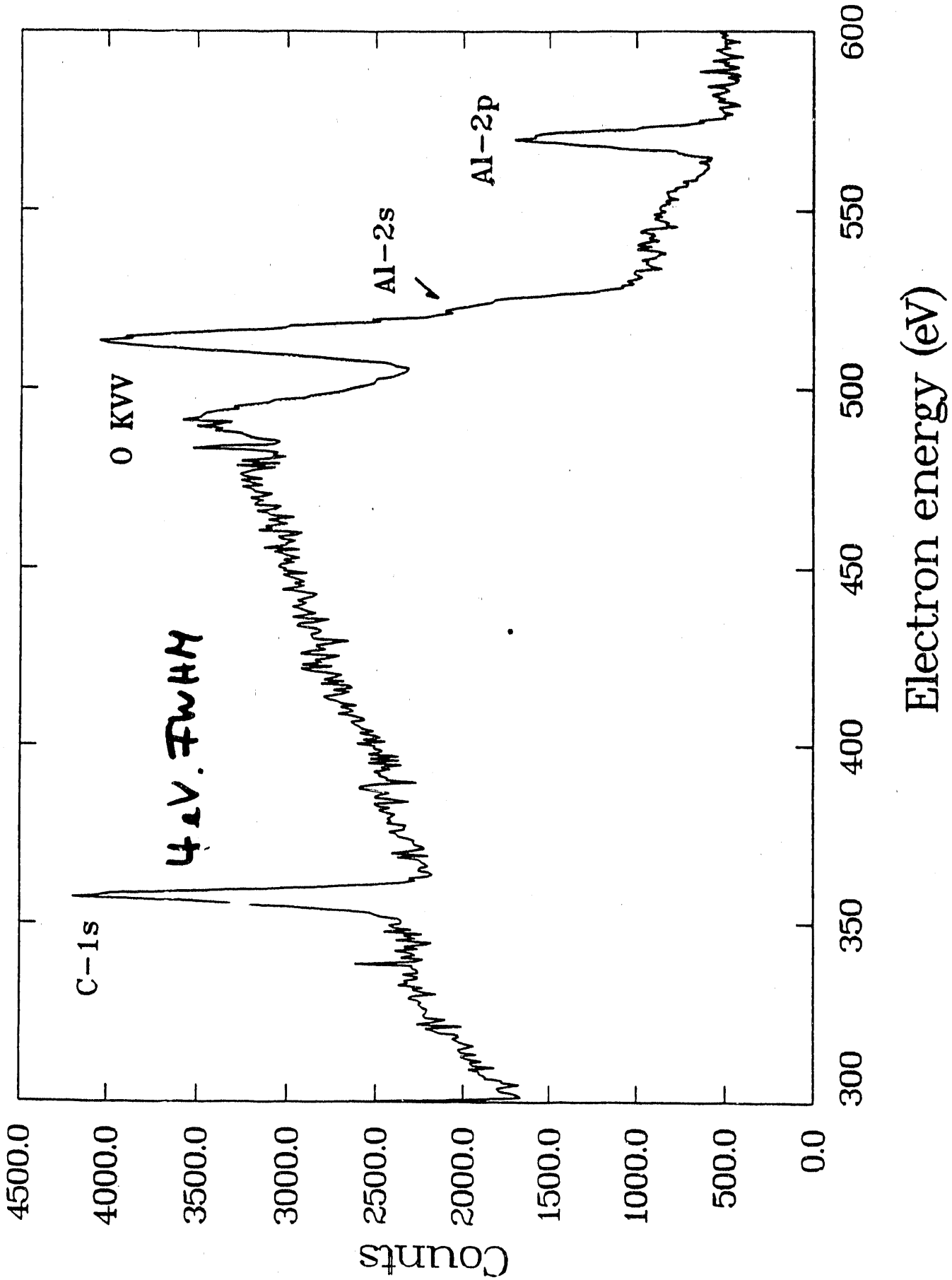
C-1s
4.2V. FWHM
O KVV
Al-2s
Al-2p
Counts
4500.0
4000.0
3500.0
3000.0
2500.0
2000.0
1500.0
1000.0
500.0
0.0
300
350
400
450
500
550
600
Electron energy (eV)

Summary of Present X1-SPEM Capabilities

- First and Only Submicron Images with Primary Photoelectrons
- Spatial Resolution Approaching 100 nm
- 3–6 eV Energy Resolution with Primary Photoelectrons
- 5–9 $\times 10^8$ photons/(sec, 0.29% BW) @ 650 eV
- Simultaneous TY and CMA Images
- Feasibility Studies on Alumina Under Way

Instrumental Improvements of the X1–SPEM

- Add XANES Mode with 0.3–1.0 eV Photon Energy Resolution
- Higher Spatial Resolution (few months: sub-100 nm; one year: 50 nm; few years: 20 nm)
- More Efficient Grating (gain of 2–5 in flux)
- Ni Phase Zone Plates (gain of factor 2 in flux)
- Commercial Spectrometer (gain of >10 peak count rate, simultaneously factor 2 in energy resolution, or <1 eV energy resolution)
- Multiple Energy (16 channel) Detection over 5–20 eV Window
- Alternate Signals (PSD, fluorescence [ALS], scattering)

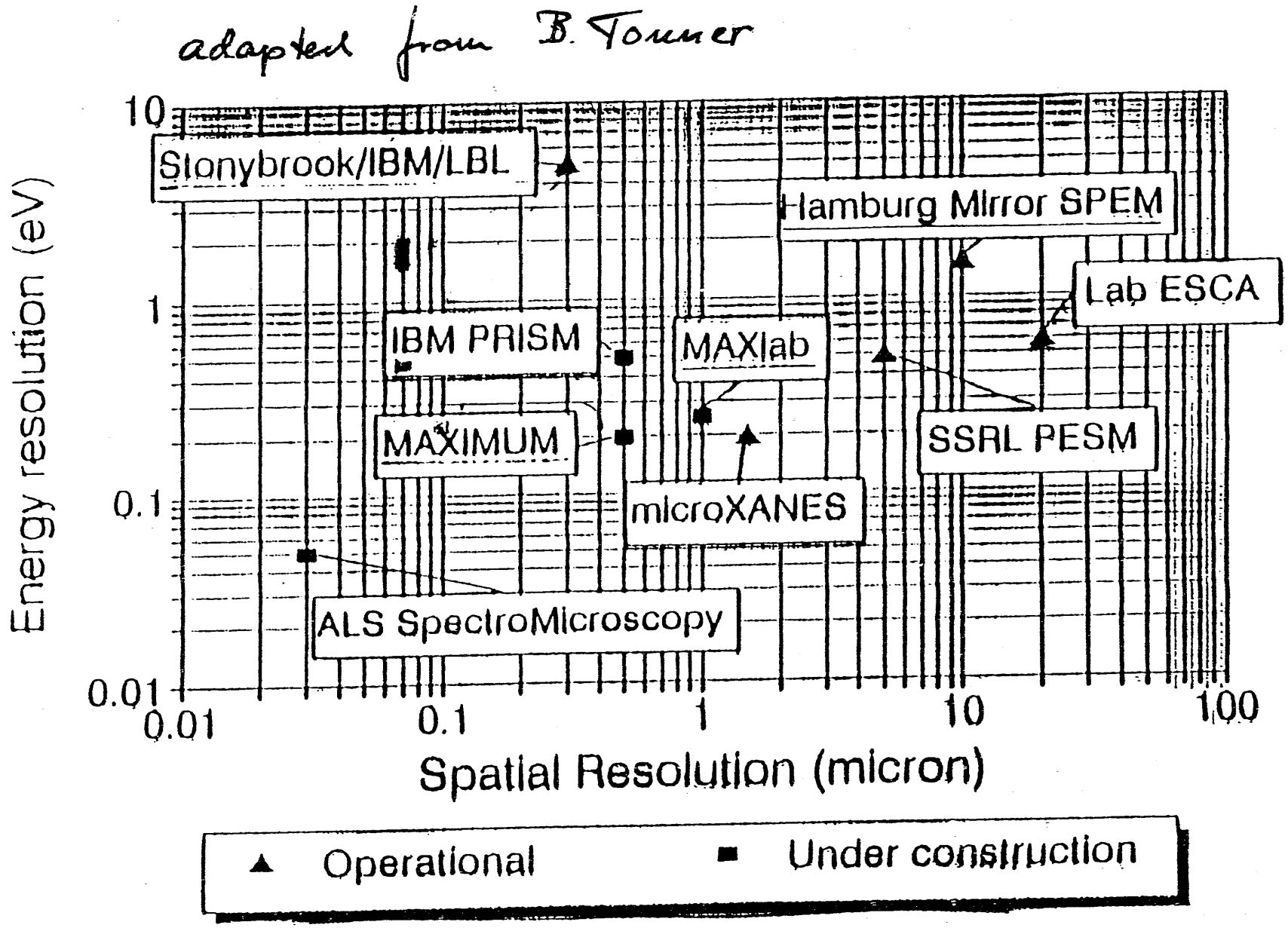
adapted from B. Tonner
Energy resolution (eV)
10
1
0.1
0.01
0.01
0.1
1
10
100
Spatial Resolution (micron)
Stonybrook/IBM/LBL
Hamburg Mirror SPEM
Lab ESCA
IBM PRISM
MAXlab
MAXIMUM
SSRL PESM
microXANES
ALS SpectroMicroscopy
▲ Operational
■ Under construction

Comments on Scanning Versus E-Imaging

- Spatial Resolution: E-Imaging May Be the Winner (XANES)
- Energy Resolution: Scanning and Imaging at Par
- Detection Efficiency: Scanning $\Omega/2\pi > 10\%$ and Multichannel Detection, E-Imaging (XPS mode) $\Omega/2\pi \leq 0.1\%$ (depends on ∂_r)
- Time Resolution: Since Undulator Output Is Coherent, Time Resolution Determined by the Detection Efficiency (i.e., E-imaging loses its advantage as a parallel imaging system)
- Damage: If Thermal, Need E-Imaging, Otherwise Scanning (detection efficiency)

Alternate Signals:

- Scanning: Fluorescence, SA Diffraction/Scattering, Neutral Ions
- E-Imaging: Compatible with LEED, Photoelectron Holography

Both techniques have a bright future and complement each other.

END

DATE
FILMED
4/16/92